DEVELOPMENT OF A METHODOLOGY FOR THE CHARACTERIZATION OF MAFIC ROCKS WITH RESPECT TO THEIR USE FOR MINERAL CARBONATION: THE MINERALOGY, PETROLOGY, AND GEOCHEMISTRY OF THE PORTAGE LAKE VOLCANICS IN THE KEWEENAW PENINSULA, MICHIGAN

By

Patrizia Bolz

RECOMMENDED:

Dr. Margaret Darrow

Dr. Rainer Newberry

Dr. Paul Metz, Advisory Committee Chair

Dr. Rajive Ganguli
Chair, Department of Mining and Geological Engineering

APPROVED:

Dr. Doug Goering
Dean, College of Engineering and Mines

Dr. John Eichelberger
Dean of the Graduate School

4/21/14
Date

DEVELOPMENT OF A METHODOLOGY FOR THE CHARACTERIZATION OF MAFIC ROCKS WITH RESPECT TO THEIR USE FOR MINERAL CARBONATION: THE MINERALOGY, PETROLOGY, AND GEOCHEMISTRY OF THE PORTAGE LAKE VOLCANICS IN THE KEWEENAW PENINSULA, MICHIGAN

A

THESIS

Presented to the Faculty

of the University of Alaska Fairbanks

in Partial Fulfillment of the Requirements

for the Degree of

MASTER OF SCIENCE

By

Patrizia Bolz, B.S.

Fairbanks, Alaska

May 2014

ABSTRACT

Mineral carbonation of basalt has been proposed by various researchers to reduce anthropogenic CO_2 output without necessitating considerable reduction of fossil fuel usage. The feasibility of any mafic rock for mineral carbonation depends on the present mineralogy, texture, grain size, and alteration. The purpose of this research is the development of a methodology for the characterization of mafic rocks regarding their susceptibility for mineral carbonation, based on samples from mine tailings in the Keweenaw Peninsula, Michigan. Samples were characterized using petrographic examination, microprobe analyses, whole rock data, and thermodynamic modeling.

Thin section analyses revealed several alteration assemblages ranging from relatively fresh samples to extremely altered samples. End-members of minerals present in the study area were used for thermodynamic modeling. Based on thermodynamics, anorthite, prehnite, and diopside are the most feasible minerals for carbonation, minerals potentially viable include forsterite, enstatite, talc, clinochlore, and phengite. To determine feasible minerals for carbonation, kinetic modeling should be conducted to establish minerals with realistic reaction rates.

The approach outlined in this study can be used as an inexpensive and expeditious method to determine mafic samples most feasible for mineral carbonation based on thermodynamic modeling. Not all mafic rocks should be treated as basalts, nor are all mafic rocks equally feasible for mineral carbonation.

TABLE OF CONTENTS

Page

SIGNATURE PAGE i

TITLE PAGE iii

ABSTRACT v

TABLE OF CONTENTS vii

LIST OF FIGURES xi

LIST OF TABLES xvii

LIST OF APPENDICES xxi

ACKNOWLEDGEMENTS xxiii

CHAPTER 1: INTRODUCTION 1

1.1 Purpose 3

1.2 Brief Background on Mineral Carbonation 3

1.3 Regional Geology 4

CHAPTER 2: METHODS 9

2.1 Field Work and Laboratory Analyses 9

2.2 Microprobe Work 9

2.3 Classification of Samples using Whole Rock Data 19

2.4 Thermodynamic Modeling 20

CHAPTER 3: THIN SECTION AND MICROPROBE ANALYSIS 25

3.1 Olivine 32

3.2 Amphibole 37

3.3 Feldspar 37
3.4 Pyroxene 49
3.5 Chlorite 52
3.6 Mica Group 60
3.7 Epidote 62
3.8 Pumpellyite 68
3.9 Prehnite 68
3.10 Copper Minerals 73
3.11 Quartz 73
3.12 Carbonate 73
3.13 Zeolites 77
3.14 Sphene 77
3.15 Apatite 81
3.16 Summary and Discussion 81
CHAPTER 4: CLASSIFICATION OF SAMPLES USING WHOLE ROCK DATA 85
4.1 Study of Original Compositions Based on Immobile Elements 86
4.1.1 Zr/TiO2-Nb/Y Diagrams 86
4.1.2 Nb-Zr-Y Ternary Diagrams 86
4.1.3 REE Diagrams 90
4.2 Study of Alteration Based on Mobile Elements 95
4.2.1 TAS System 95
4.2.2 Bivariate Diagrams 101
4.2.3 ACF Diagrams 107
4.2.4 AFM Diagrams 110
4.3 Summary and Discussion 115

CHAPTER 5: THERMODYNAMIC MODELING 119

5.1 Olivine Group 122

5.2 Anorthite 124

5.3 Pyroxene Group 128

5.4 Chlorite Group 134

5.5 Phengite 147

5.6 Epidote 147

5.7 Prehnite 147

5.8 Summary and Discussion 154

CHAPTER 6: MINERAL CARBONATION AND WHOLE ROCK DATA 159

CHAPTER 7: CONCLUSIONS 167

REFERENCES 171

APPENDICES 177

LIST OF FIGURES

Page

Figure 1.1: Distribution of major "basalt" formations in the western United States. .. 2
Figure 1.2: Location and geology of the MRS. ... 5
Figure 1.3: Schematic of a typical PLV flow interior. ... 6
Figure 2.1: Map of sample station locations. ... 10
Figure 2.2: Chlorite measurements, JEOL JXA-8530F vs. CAMECA SX-50. ... 18
Figure 2.3: Map of Keweenaw sample stations by location. ... 21
Figure 3.1: Locations of thin section samples used for microprobe analysis. ... 26
Figure 3.2: Coarse-grained olivine with fresh plagioclase and pyroxene. ... 33
Figure 3.3: Diagram of forsterite contents in olivine grains in sample 10SC004. ... 36
Figure 3.4: Diagram of forsterite contents in olivine grains in sample 10SG001. ... 36
Figure 3.5: Amphibole in PPL (a) and under crossed polarizers (b) in sample 10SC004. ... 38
Figure 3.6: Compositional classification of amphiboles based on EDS microprobe analysis. ... 40
Figure 3.7: Sericite and calcite alteration of plagioclase. ... 42
Figure 3.8: Prehnite alteration of former plagioclase core. ... 43
Figure 3.9: Chlorite and pumpellyite alteration of former plagioclase cores. ... 44
Figure 3.10: Feldspar ternary diagrams for samples of alteration assemblage 1 (a) and 2 (b). ... 46
Figure 3.11: Feldspar ternary diagrams for samples of alteration assemblage 3. ... 47
Figure 3.12: Feldspar ternary diagrams for samples of alteration assemblage 4. ... 48
Figure 3.13: BSE image of typical plagioclase zoning in relatively fresh samples. ... 50
Figure 3.14: Example of pyroxene surrounding plagioclase. ... 51
Figure 3.15: Pyroxene quadrilateral with all data. ... 54
Figure 3.16: Pyroxene quadrilaterals for samples of alteration assemblages 1 (a) and 2 (b). ... 55

Figure 3.17: Pyroxene quadrilaterals for samples of alteration assemblages 3 (a) and 4 (b). 56
Figure 3.18: Example of different chlorite textures. 57
Figure 3.19: Classification of chlorite analyses for all samples. 59
Figure 3.20: Classification of chlorite analyses for Caledonia samples. 61
Figure 3.21: Compositions of mica group minerals. 64
Figure 3.22: Coarse-grained epidote with pumpellyite and quartz in amygdule. 65
Figure 3.23: Histogram of "pistacite" component in analyzed epidote. 67
Figure 3.24: Coarse-grained pumpellyite with chlorite in amygdule. 69
Figure 3.25: Fe, Mg, and Al ternary plot of all pumpellyite analyses. 71
Figure 3.26: Interstitial prehnite and pumpellyite in gabbroic sample. 72
Figure 3.27: Al, Fe, and Ca ternary diagram for prehnite analyses. 75
Figure 3.28: BSE image of copper sulfide in carbonate vein (sample 10TR004). 76
Figure 3.29: Ternary diagram of Ca, Fe, and Mg for carbonate minerals. 78
Figure 4.1: Zr/TiO_2-Nb/Y diagram for samples by location. 87
Figure 4.2: Zr/TiO_2-Nb/Y diagram for Caledonia samples. 87
Figure 4.3: Zr/TiO_2-Nb/Y diagrams for samples by texture. 88
Figure 4.4: Nb–Zr–Y diagram for samples by location. 89
Figure 4.5: Nb-Zr-Y diagram for Caledonia samples. 89
Figure 4.6: Nb-Zr-Y diagram for samples by texture. 91
Figure 4.7: REE diagram by location. 92
Figure 4.8: REE diagram for Caledonia samples. 92
Figure 4.9: REE diagrams by grain size. 93
Figure 4.10: REE diagrams for amygdaloidal (a) and brecciated (b) samples. 93
Figure 4.11: REE diagrams for ophitic (a), subophitic (b), and porphyritic (c) samples. 94
Figure 4.12: TAS classification diagram with field labels. 97
Figure 4.13: TAS diagram for samples by loss on ignition (LOI). 97
Figure 4.14: TAS diagram for samples by location. 98

Figure 4.15: TAS diagram by location for samples with LOI < 5%. 98
Figure 4.16: TAS diagram for samples by grain size. 99
Figure 4.17: TAS diagram for amygdaloidal and brecciated samples. 99
Figure 4.18: TAS diagram for ophitic, subophitic, and porphyritic samples. 100
Figure 4.19: Bivariate diagram for samples by LOI. 102
Figure 4.20: Bivariate diagram for samples by location. 103
Figure 4.21: Bivariate diagram for samples by grain size. 104
Figure 4.22: Bivariate diagram for amygdaloidal and brecciated samples. 105
Figure 4.23: Bivariate diagram for ophitic, subophitic, and porphyritic samples. 106
Figure 4.24: Bivariate diagrams for CO_2 vs. Na_2O differentiated by location and texture. 108
Figure 4.25: ACF diagram for samples by loss on ignition (LOI). 109
Figure 4.26: ACF diagram for Caledonia samples. 109
Figure 4.27: ACF diagram for samples by location 111
Figure 4.28: ACF diagram for samples by grain size. 111
Figure 4.29: ACF diagram for amygdaloidal and brecciated samples 112
Figure 4.30: ACF diagram for ophitic, subophitic, and porphyritic samples. 112
Figure 4.31: AFM diagram for all samples by LOI 113
Figure 4.32: AFM diagram for Caledonia samples 113
Figure 4.33: AFM diagram for samples by location. 114
Figure 4.34: AFM diagram for samples by grain size. 114
Figure 4.35: AFM diagram for amygdaloidal and brecciated samples. 116
Figure 4.36: AFM diagram for ophitic, subophitic, and porphyritic samples. 116
Figure 5.1: Stability of forsterite decomposition products at standard conditions. 120
Figure 5.2: Stability of forsterite at standard conditions. 120
Figure 5.3: Stability of forsterite decomposition products with temperature and fCO_2. 123
Figure 5.4: Stability of forsterite with temperature and fCO_2. 123

Figure 5.5: Log fCO_2 at equilibrium between forsterite products at varying temperatures. 125
Figure 5.6: Stability of fayalite decomposition products at standard conditions. 126
Figure 5.7: Stability of fayalite at standard conditions. 126
Figure 5.8: Stability of siderite with varying fCO_2 and fO_2 at standard conditions. 127
Figure 5.9: Stability of anorthite decomposition products at standard conditions. 129
Figure 5.10: Stability of anorthite at standard conditions. 129
Figure 5.11: Stability of anorthite decomposition products with temperature and fCO_2. 130
Figure 5.12: Stability of anorthite with temperature and fCO_2. 130
Figure 5.13: Log fCO_2 at equilibrium between anorthite products at varying temperatures. 131
Figure 5.14: Stability of diopside at standard conditions. 132
Figure 5.15: Stability of diopside with temperature and fCO_2. 132
Figure 5.16: Log fCO_2 at equilibrium between diopside products at varying temperatures. 133
Figure 5.17: Stability of enstatite decomposition products at standard conditions. 135
Figure 5.18: Stability of enstatite at standard conditions 135
Figure 5.19: Stability of enstatite decomposition products with temperature and fCO_2. 136
Figure 5.20: Stability of enstatite with temperature and fCO_2. 136
Figure 5.21: Log fCO_2 at equilibrium between enstatite products at varying temperatures. 137
Figure 5.22: Stability of ferrosilite decomposition products at standard conditions. 138
Figure 5.23: Stability of ferrosilite at standard conditions. 138
Figure 5.24: Stability of clinochlore decomposition products at standard conditions. 139

Figure 5.25: Stability of clinochlore at standard conditions. 139
Figure 5.26: Stability of clinochlore decomposition products with temperatures and fCO_2. 141
Figure 5.27: Stability of clinochlore with varying temperatures and fCO_2. 141
Figure 5.28: Log fCO_2 at equilibrium between clinochlore products at varying temperatures. 142
Figure 5.29: Stability of ripidolite decomposition products at standard conditions. 143
Figure 5.30: Stability of ripidolite at standard conditions. 143
Figure 5.31: Stability of ripidolite decomposition products with temperature and fCO_2. 144
Figure 5.32: Stability of ripidolite with temperature and fCO_2. 144
Figure 5.33: Log fCO_2 at equilibrium between ripidolite products at varying temperatures. 145
Figure 5.34: Stability of daphnite at standard conditions. 146
Figure 5.35: Stability of phengite at standard conditions. 148
Figure 5.36: Stability of phengite with temperature and fCO_2. 148
Figure 5.37: Log fCO_2 at equilibrium between phengite products at varying temperatures. 149
Figure 5.38: Stability of epidote decomposition products at standard conditions. 150
Figure 5.39: Stability of epidote at standard conditions. 150
Figure 5.40: Stability of epidote decomposition products with temperature and fCO_2. 151
Figure 5.41: Stability of epidote with temperature and fCO_2. 151
Figure 5.42: Log fCO_2 at equilibrium between epidote products at varying temperatures. 152
Figure 5.43: Stability of prehnite decomposition products at standard conditions. 153
Figure 5.44: Stability of prehnite at standard conditions. 153

Figure 5.45: Stability of prehnite decomposition products with temperature and fCO_2. 155
Figure 5.46: Stability of prehnite with temperature and fCO_2. 155
Figure 5.47: Log fCO_2 at equilibrium between prehnite products at varying temperatures. 156
Figure 6.1: Bivariate diagrams for samples by thermodynamic category. 161
Figure 6.2: LOI (%) vs. Na_2O (%) for samples by thermodynamic category. 163
Figure 6.3: H_2O (%) vs. Na_2O (%) for samples by thermodynamic category. 163
Figure 6.4: Bivariate diagrams for samples potentially feasible for mineral carbonation. 165
Figure B-1: Flow chart used for site occupancy of cations of pyroxenes 213
Figure H-1: REE diagrams by station for samples from the northern fissures 304
Figure H-2: REE diagrams by station for samples from the middle section 305
Figure H-3: REE diagrams by station for samples from the southern section 308
Figure J-1: Stability diagram of forsterite 323
Figure J-2: Stability diagram of forsterite, suppressing one mineral. 323
Figure J-3: Stability diagram of forsterite, suppressing two minerals. 324
Figure J-4: Stability diagram of forsterite, suppressing three minerals. 324
Figure J-5: Stability diagram of forsterite, suppressing four minerals. 325
Figure J-6: Stability diagram of forsterite, suppressing five minerals. 325
Figure J-7: Stability diagram of forsterite, supressing six minerals. 326

LIST OF TABLES

Page

Table 2.1: Textures observed and their definitions. 11
Table 2.2: Sample station abbreviations for Keweenaw samples. 12
Table 2.3: Whole rock analyses performed by ALS Minerals. 13
Table 2.4: List of thin sections selected for microprobe analysis. 15
Table 2.5: Plagioclase standard compositions and EDS measurements. 17
Table 2.6: Albite standard compositions and EDS measurements 17
Table 2.7: Olivine standard compositions and EDS measurements. 17
Table 2.8: Typical values for log activity of SiO_2 in mine waters in the Keweenaw. 23
Table 2.9: Typical values for log fugacity of CO_2 (gas) of flue gas and atmosphere 23
Table 3.1: Samples and approximate abundances (%) of main minerals. 27
Table 3.2: Description of samples used for microprobe analysis. 29
Table 3.3: Electron microprobe analyses of olivine grains 1-3 (sample 10SC004) 34
Table 3.4: Electron microprobe analyses of olivine grains 4-6 (sample 10SC004) 34
Table 3.5: Electron microprobe analyses of olivine grains 1-2 (sample 10SG001) 35
Table 3.6: Electron microprobe analyses of olivine grain 3 (sample 10SG001). 35
Table 3.7: Electron microprobe analyses of amphibole (sample 10SC004). 39
Table 3.8: Electron microprobe analyses of selected feldspar group minerals 45
Table 3.9: Electron microprobe analyses of selected pyroxene samples. 53
Table 3.10: Electron microprobe analyses of selected chlorite group samples. 58
Table 3.11: Electron microprobe analyses of mica group minerals. 63
Table 3.12: Electron microprobe analyses of selected epidote group minerals. 66
Table 3.13: Electron microprobe analyses of selected pumpellyite minerals. 70
Table 3.14: Electron microprobe analyses of selected prehnite samples. 74
Table 3.15: Electron microprobe analyses of copper sulfide minerals. 76
Table 3.16: Electron microprobe analyses of carbonate minerals 79
Table 3.17: Electron microprobe analyses of zeolite minerals in sample 10DE006. 79

Table 3.18: Electron microprobe analyses of sphene. 80
Table 3.19: Electron microprobe analyses of apatite. 82
Table 4.1: Summary of results based on immobile elements. 117
Table 5.1: Summary of minimum log fCO_2 values for carbonation of minerals. 157
Table 6.1: Thermodynamic categories used for plotting of samples on bivariate diagrams. 160
Table 6.2: Samples potentially feasible for mineral carbonation. 164
Table A-1: Major element, C, and S analyses. 177
Table A-2: Base metal analyses. 185
Table A-3: Trace element analyses. 190
Table A-4: REE analyses. 198
Table A-5: Volatile element analyses. 205
Table F-1: Samples and approximate abundances (%) of all minerals observed in thin section. 224
Table G-1: Electron microprobe analyses of feldspar group minerals. 228
Table G-2: Electron microprobe analyses of pyroxene group minerals. 253
Table G-3: Electron microprobe analyses of chlorite group minerals. 271
Table G-4: Electron microprobe analyses of epidote group minerals. 287
Table G-5: Electron microprobe analyses of epidote group mineral with REE. 291
Table G-6: Electron microprobe analyses of pumpellyite minerals. 292
Table G-7: Electron microprobe analyses of prehnite minerals. 296
Table I-1: Data used for modeling of forsterite decomposition products. 309
Table I-2: Equilibrium constants with temperature for forsterite decomposition products. 309
Table I-3: Data used for modeling of forsterite. 310
Table I-4: Equilibrium constants with temperature for forsterite. 310
Table I-5: Data used for modeling of anorthite decomposition products. 311
Table I-6: Equilibrium constants with temperature for anorthite decomposition products. 311

Table I-7: Data used for modeling of anorthite. 312
Table I-8: Equilibrium constants with temperature for anorthite. 312
Table I-9: Data used for modeling of diopside. 313
Table I-10: Equilibrium constants with temperature for diopside. 313
Table I-11: Data used for modeling of enstatite. 314
Table I-12: Equilibrium constants with temperature for enstatite. 314
Table I-13: Data used for modeling of clinochlore decomposition products. 315
Table I-14: Equilibrium constants with temperature for clinochlore decomposition products. 315
Table I-15: Data used for modeling of clinochlore. 316
Table I-16: Equilibrium constants with temperature for for clinochlore. 316
Table I-17: Data used for modeling of ripidolite. 317
Table I-18: Equilibrium constants with temperature for ripidolite. 317
Table I-19: Data used for modeling of phengite. 318
Table I-20: Equilibrium constants with temperature for phengite. 318
Table I-21: Data used for modeling of epidote. 319
Table I-22: Equilibrium constants with temperature for epidote. 319
Table I-23: Data used for modeling of prehnite decomposition products. 320
Table I-24: Equilibrium constants with temperature for prehnite decomposition products. 320
Table I-25: Data used for modeling of prehnite. 321
Table I-26: Equilibrium constants with temperature for prehnite. 321

LIST OF APPENDICES

Page

APPENDIX A: WHOLE ROCK DATA. 177

APPENDIX B: DATA PROCESSING. 211

APPENDIX C: CONSTRUCTION OF ACF DIAGRAMS 217

APPENDIX D: CONSTRUCTION OF AFM DIAGRAMS 219

APPENDIX E: CALCULATION OF AQUEOUS SILICA IN KEWEENAW MINE.....

WATERS. 221

APPENDIX F: ABUNDANCES OF MINERALS OBSERVED IN THIN SECTION 223

APPENDIX G: COMPLETE ELECTRON MICROPROBE ANALYSES. 227

APPENDIX H: REE DIAGRAMS BY SAMPLE STATION 303

APPENDIX I: DATA USED FOR THERMODYNAMIC MODELING. 309

APPENDIX J: SUPPRESSING MINERALS IN THERMODYNAMIC MODELING. 323

APPENDIX K: REFERENCES USED IN APPENDIX. 327

ACKNOWLEDGEMENTS

First and foremost, I thank my advisor Paul Metz for his expertise, advice, patience, and financial support throughout my undergraduate and graduate studies. Thank you for giving me the chance to work on various research projects as a student assistant. I highly enjoyed working on these projects, especially the ones that got me out of the office and into the field. My studies in Alaska would not have been possible without this support.

I also owe a great debt of gratitude to my committee members Margaret Darrow and Rainer Newberry. Thank you for taking me on as "one of your own", for making time for me and my questions, and for your help and advice every step along the way. Your relentless efforts of improving this thesis will never be forgotten, for better or worse.

I thank the Department of Energy for providing funding for large portions of this research. I also thank Ken Severin at the Advanced Instrumentation Laboratory at UAF for teaching me how to use a microprobe, and for letting me call him whenever the dragon was upset. I thank Ted Bornhorst and Bob Barron at Michigan Tech for teaching me about Michigan's geology, and Ted Bornhorst for reviewing my section on regional geology in this thesis. I further thank Tim Eisele at Michigan Tech for providing laboratory space for sample processing.

Thanks to John Dezelski and Danford Moore for helping me sample those mine tailing piles, and for adventuring about in the Keweenaw. I have a lot of copper in my cabin thanks to you.

Finally, thank you to Kari Pile, Jolie & Matt Billings, and Lyle Croft for keeping me sane, providing moral support whenever needed, and for sharing this adventure with me!

DANKE SCHÖN!

CHAPTER 1: INTRODUCTION

Many authors have mentioned basalt in general as potential host rock for in situ mineral carbonation (e.g., McGrail et al., 2006; Goldberg et al., 2008; Matter et al., 2009; Rosenbauer et al., 2012); numerous aqueous phase studies for pure minerals and CO_2 have been conducted (e.g., Wogelius and Walther, 1991; Guthrie et al., 2001; Oelkers and Gíslason, 2001; Gerdemann et al., 2003; Gíslason and Oelkers, 2003; Béarat et al., 2006; Chen et al., 2006; Krevor and Lackner, 2009); and studies on thermodynamics and kinetics of mineral carbonation have been performed (e.g., Königsberger et al., 1999; Marini, 2007; Krupka et al., 2010; Aradóttir et al., 2012; Rosenbauer et al., 2012). Most of the work mentioned above is based on either specific basalts, or basalt compositions assumed to be typical. Often, any mafic rock is referred to as "basalt", disregarding classification systems for mafic rocks. Maps showing the distribution of such "basalts" have been presented (e.g., Figure 1.1), with the inference that the presence of "basalt" equals carbonation potential.

A first step in evaluating the feasibility of specific mafic rocks for mineral carbonation should involve determining the mineralogy, petrology, and geochemistry of these rocks. The thermodynamics and kinetics of reactions between calcium and magnesium silicate minerals with CO_2 depend on many factors, but especially on their mineralogy and texture. The mineralogy of mafic rocks can vary widely due to depositional environment and the presence and extent of chemical alteration. Naturally occurring alteration due to hydrothermal fluids or metamorphism can cause carbonation, may deplete the rocks in calcium and magnesium, or form silicate minerals that are less likely to react with CO_2 to form carbonates. All of these can decrease the potential for mineral carbonation. In this thesis, samples will be studied regarding these issues and special attention will be paid to the primary mineralogy and alteration products of the rocks in the study area.

Figure 1.1: Distribution of major "basalt" formations in the western United States. Map modified from McGrail and others (2006). The study area is shown in red.

1.1 Purpose

The purpose of this research was the development of a methodology for the characterization of mafic rocks with respect to their susceptibility for mineral carbonation, based on samples from the Keweenaw Peninsula in Michigan. The samples were characterized using standard petrographic examination, EDS microprobe analyses, and whole rock data. Thermodynamic modeling was conducted for minerals of interest observed, and whole rock data was used in conjunction with microprobe and thermodynamic modeling results to determine trends in whole rock data regarding carbonation feasibility. Kinetic modeling was not attempted as part of this study, but results from this research should be used for kinetic modeling to further study the feasibility of these mafic rocks for mineral carbonation. Material considered for mineral carbonation should be evaluated based on the mineralogy, petrology, and texture before further, more expensive studies are conducted.

1.2 Brief Background on Mineral Carbonation

With the attempt of limiting anthropogenic carbon emissions as part of international efforts to reduce global warming, several carbon sequestration options have been proposed, and are currently being studied (e.g., Beecy and Kuuskraa, 2001; Aradóttir et al., 2011; McGrail et al., 2011; Zevenhoven et al., 2011). Successful carbon sequestration could reduce anthropogenic carbon emissions, without necessitating a substantial decrease of fossil fuel usage. One type of geologic sequestration is generally referred to as mineral carbonation. Mineral carbonation is defined as the reaction of certain calcium and magnesium bearing silicate minerals with carbon dioxide to form thermodynamically stable carbonates such as calcite, magnesite, and dolomite (Lackner et al., 1995). The mineral carbonation process occurs naturally, commonly through metamorphism, hydrothermal alteration, or weathering. Ultramafic rocks are typically rich in magnesium silicates (e.g., olivine), while mafic rocks contain calcium and magnesium silicates (e.g., calcic

plagioclase, pyroxene, and sometimes olivine). Both have been studied by numerous authors with respect to their potential for mineral carbonation (e.g., Lackner et al., 1997; Gerdemann et al., 2003; Béarat et al., 2006; Chen et al., 2006; Oelkers et al., 2008; Brown et al., 2010). Alteration products of ultramafic rocks include hydrous silicates (e.g., serpentine), which are known to react with atmospheric CO_2 to form hydrous carbonates such as nesquehonite, dypingite, hydromagnesite, and lansfordite on mine tailings (Wilson et al., 2006; 2009).

1.3 Regional Geology

The Portage Lake Volcanics (PLV) are part of the Keweenawan Supergroup, which formed as part of a midcontinent rift system (MRS) during the Mesoproterozoic in the North American craton (Cannon and Nicholson, 1992). The MRS extends 2,200 km from Kansas to Lake Superior from where it continues southeastward to southern Michigan (Figure 1.2). Most of the MRS is buried by Phanerozoic sedimentary deposits, but MRS rocks (including the PLV) crop out in the vicinity of Lake Superior. The MRS is filled with more than 25 km of volcanic rocks near its center, of which about 10 km are part of the PLV (Cannon et al., 1993; Bornhorst and Lankton, 2009). The PLV dip towards the center of the MRS and the exposed base is truncated by the reverse Keweenaw Fault in the Keweenaw Peninsula. The exposed part of the PLV is up to 5 km thick (Cannon and Nicholson, 1992) consisting of up to 95% tholeiitic subaerial basalt lava flows, 3% interbedded sandy conglomerate, and less than 2% interbedded intermediate and felsic rocks (Paces, 1988). The PLV are made up of more than 200 flows (Paces, 1988). The thickness of different flows varies from less than a meter to over 400 m, with an average thickness of 10 to 20 m (Paces, 1988). Some flows can be traced along strike for more than 100 km, with persistent thickness of individual flows over 30-50 km along strike (White, 1968; Paces, 1988). Individual flows generally can be divided into four parts (from bottom to top; Figure 1.3): a thin, somewhat amygdaloidal, basal chill zone with dark chlorite in amygdules; a massive, fresh appearing zone

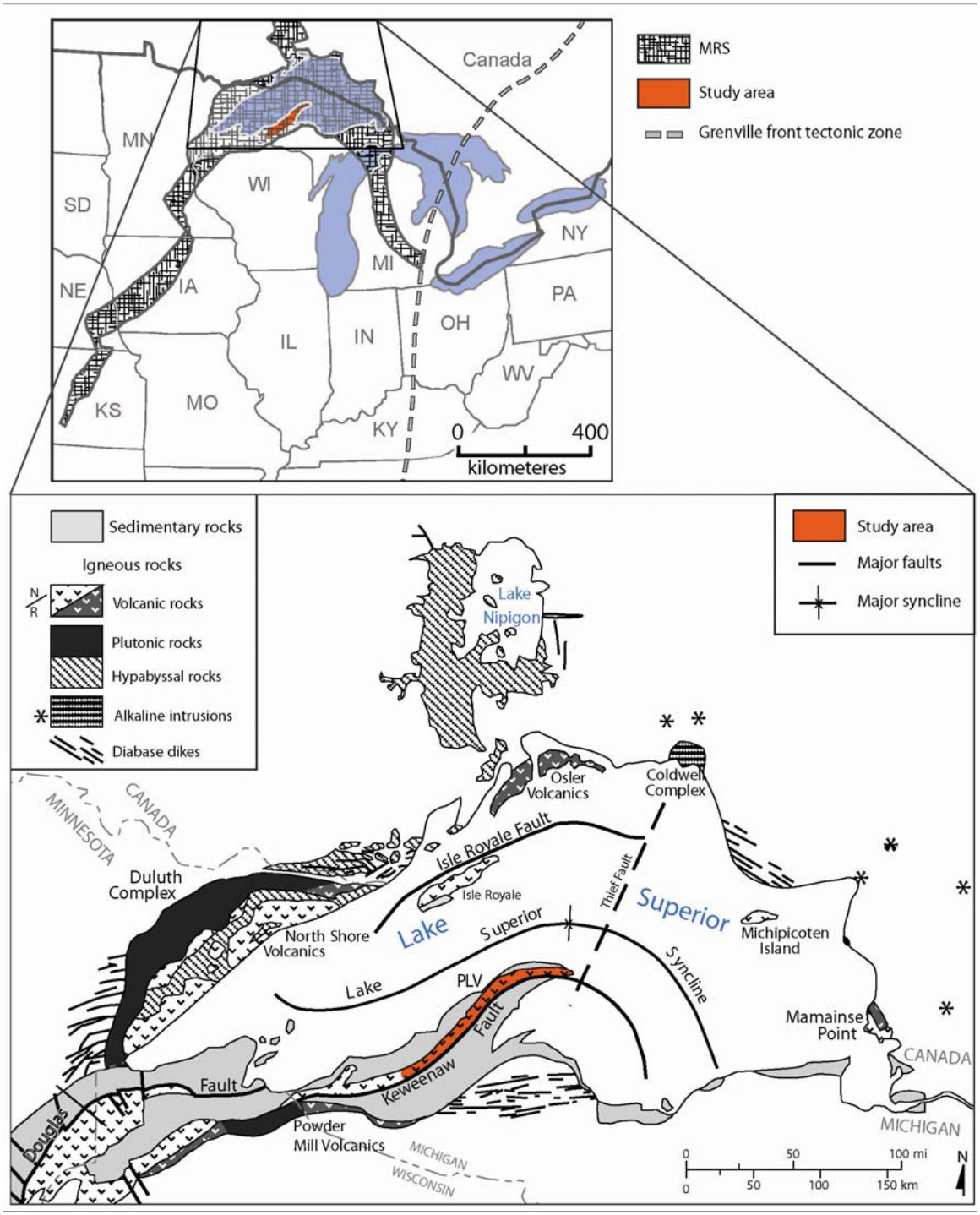

Figure 1.2: Location and geology of the MRS.
The orange area shows the location of the Keweenaw study area. Mamainse Bay samples were collected near Mamainse Point. Modified from Ojakangas et al. (2001), and Bornhorst and Lankton (2009).

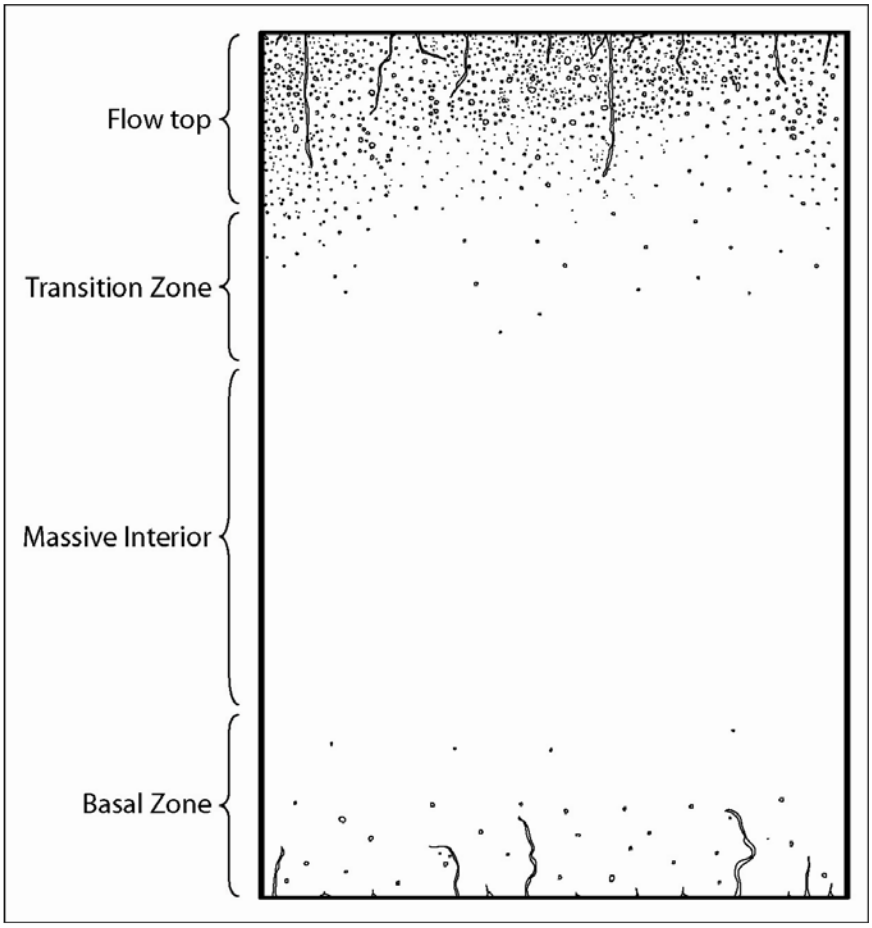

Figure 1.3: Schematic of a typical PLV flow interior.
Created after Jolly and Smith (1972) and Paces (1988).

without vesicles that is often increasingly ophitic towards the center; a transition zone with few, dark-chlorite filled amygdules; and a flow top that is brecciated and/or amygdaloidal (Jolly and Smith, 1972; Paces, 1988; Pueschner, 2001; Bornhorst and Barron, 2011). U-Pb analyses of zircons yielded PLV ages of 1096 ± 2 Ma for the Copper City Flow (one third above exposed fault-truncated base of the PLV), and 1094 ± 2 Ma for the Greenstone Flow (one third below the exposed top of the PLV; Paces and Davis, 1988).

The Keweenaw Peninsula native copper district has been studied extensively, especially since Douglass Houghton brought the district to the attention of miners with his reports on the geology in 1841 (Butler and Burbank, 1929; White, 1968; Bornhorst, 1997; Bornhorst and Lankton, 2009; Bornhorst and Barron, 2011, and references therein). The study area is part of the largest known native copper accumulation in the world. Between 1845 and 1968, 5 billion kg of refined copper were produced in the Keweenaw Peninsula native copper district (Weege and Pollock, 1972; Bornhorst and Barron, 2011). Several factors came together in the formation of this deposit. For one, the volcanic lavas in the MRS were deposited subaerially, facilitating the degassing of volatiles and with that the formation of sulfur-deficient basalts, ultimately leading to the precipitation of native copper instead of copper sulfides (Bornhorst and Lankton, 2009). Further, hydrothermal fluids were generated through the heating of the rift-filling basalts due to a combination of burial metamorphism and basal heat flow (Jolly and Smith, 1972). The hydrothermal fluids are believed to have dissolved copper from basalt strata underlying the present ore horizons (Stoiber and Davidson, 1959; White, 1968; Jolly and Smith, 1972; Bornhorst, 1997). The copper-bearing fluids moved upward through permeable tops of lava flows and interflow sedimentary layers, as well as fractures and faults generated by late rift compression (Bornhorst, 1997). The brecciated tops of lava flows and interflow conglomerates host most of the economic copper deposits (Bornhorst and Barron, 2011). Copper and associated minerals were likely precipitated due to the cooling of the copper-bearing fluid, and

fluid mixing (Bornhorst, 1997). Native copper deposits and related minerals formed at temperatures of about 225°C and low, poorly-defined pressures (Bornhorst and Barron, 2011). Native copper mineralization in the Keweenaw occurred at 1,060-1,047 Ma (Bornhorst et al., 1988).

While the overall chemical compositions of the PLV are believed to represent original igneous compositions (Paces, 1988), the mineralogy is dominated by hydrothermal-metamorphic minerals that accompanied the burial and formation of the native copper deposits (Butler and Burbank, 1929; White, 1968; Jolly and Smith, 1972; Livnat, 1983; Pueschner, 2001). The suite of secondary minerals ranges from very low (zeolite facies) to low grade (greenschist facies) metamorphic conditions. In general, higher metamorphic grades are associated with the area of abundant native copper deposits and stratigraphically deeper parts of the MRS section (Stoiber and Davidson, 1959).

CHAPTER 2: METHODS

2.1 Field Work and Laboratory Analyses

Samples were collected from mine tailings along the Keweenaw Peninsula and from outcrops near Mamainse Point during the field seasons of 2010 and 2011 by P. Bolz, P. Metz, and J. Dezelski (Figure 2.1). Additionally, 13 samples were collected from two stopes in the Caledonia Mine in 2011 by P. Metz. For each sample station, four to six samples were collected to represent the main textures present at the location. Textures observed included: aphanitic, very fine-grained, fine-grained, gabbroic, amygdaloidal, brecciated, subophitic, ophitic, and porphyritic (Table 2.1).

Figure 2.1 shows the sample station locations of all samples, former mine or lode names for samples from the Keweenaw are included. Sample names were based on year, location, and sample number. Locations of sample stations were recorded in UTM coordinates using a handheld GPS. Mine and lode names were verified in ArcGIS, using mine and lode locations compiled by Cannon et al. (1999). Some missing lode names were assigned using Butler and Burbank (1929). The sample station abbreviations, verified mine and lode names, and GPS coordinates of Keweenaw sample stations are listed in Table 2.2. Samples collected near Mamainse Point were: 10SG001, 10MB001, and 10MB002.

Overall, 216 samples were collected, of which 206 were submitted to *ALS Minerals* for whole rock analyses (included in Appendix A). The ALS "*Complete Characterization Package*" was chosen for all samples, analyzing for major elements, base metals, trace elements, rare earth elements (REE), volatiles, carbon, and sulfur (Table 2.3). Thin sections were available for 54 of these samples, of which 17 samples were selected for microprobe analysis.

2.2 Microprobe Work

Microprobe analysis was conducted using Energy Dispersive X-ray Spectroscopy (EDS) at the Advanced Instrumentation Laboratory (AIL) at the University of Alaska

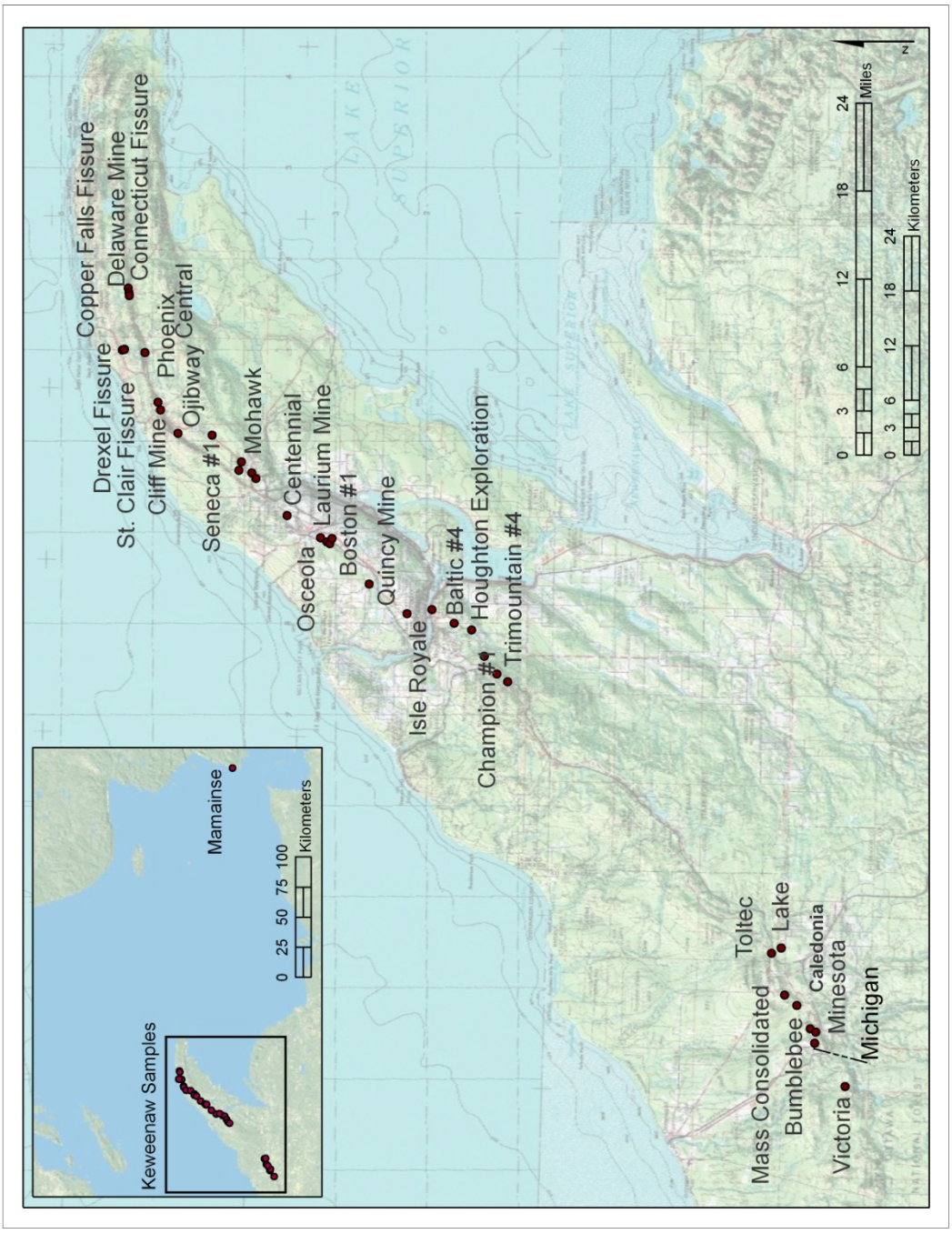

Figure 2.1: Map of sample station locations.

Table 2.1: Textures observed and their definitions.

Texture	Definition
aphanitic	no mineral grains visible by naked eye or hand lens
very fine-grained	average size of mineral grains ~ 1 mm, not identifiable by hand lens
fine-grained	mineral grains ~ 1-5 mm, some minerals identifiable by hand lens
gabbroic	mineral grains > 5 mm, mineral grains identifiable by hand lens, sometimes even by naked eye
amygdaloidal	few to abundant amygdules in groundmass
brecciated	brecciated by veins, causing angular clasts
ophitic	pyroxene surrounding plagioclase grains, causing "mottled" looking texture
subophitic	pyroxene partially surrounding plagioclase grains
porphyritic	few larger grains set in fine-grained groundmass

Table 2.2: Sample station abbreviations for Keweenaw samples.

Sample	Mine	Lode	UTM Zone: 16T	
			Northing	Easting
BA	Baltic #4	Baltic Amygdaloid	5,213,657	376,437
BB	Bumblebee	N/A	5,178,023	335,590
CC	Mohawk #6	Kearsarge Amygdaloid	5,238,639	395,919
CE	Central	Fissure	5,250,807	409,721
CF	Copper Falls Fissure	Fissure	5,253,261	410,018
CH	Champion #1	Baltic Amygdaloid	5,211,127	373,617
CL	Cliff Mine	Fissure	5,247,189	400,866
CN	Centennial	Calumet & Hecla Conglomerate	5,235,262	391,861
CO	Connecticut Fissure	Fissure	5,252,538	416,292
DE	Delaware Mine	Allouez Conglomerate	5,252,635	416,814
DR	Drexel Fissure	Fissure	5,252,490	415,977
FJ	Boston #1	Allouez Conglomerate	5,226,257	384,365
FU	Mohawk #5	Kearsarge Amygdaloid	5,239,116	396,519
GR	Mohawk #1	Kearsarge Amygdaloid	5,240,236	397,742
HE	Houghton Exploration	Baltic Amygdaloid	5,215,044	379,318
IR	Isle Royale #1	Isle Royale Amygdaloid	5,219,401	381,553
	Isle Royale #4	Isle Royale Amygdaloid	5,216,962	380,034
LA	Lake	Lake Amygdaloid *	5,181,192	344,416
MC	Mass Consolidated	N/A	5,180,802	339,252
MG	Michigan	Branch vein, Calico Amygdaloid, Evergreen series *	5,177,421	335,191
MI	Minesota (?)	Minesota Fissure	5,177,546	333,999
OC	Osceola #4	Osceola Amygdaloid	5,230,894	388,987
	Osceola #5	Osceola Amygdaloid	5,230,554	388,755
	Osceola # 13	Osceola Amygdaloid	5,231,570	389,440
OJ	Ojibway	Kearsarge Amygdaloid	5,243,453	400,679
PH	Phoenix	Fissure	5,249,104	403,419
QU	Quincy Mine	Pewabic Amygdaloidal	5,222,120	381,102
SC	St. Clair Fissure	Fissure	5,249,381	404,285
SE	Seneca #1	Iroquois & Houghton?	5,240,534	396,833
TO	Laurium Mine	Kearsarge Amygdaloid (?)	5,230,346	389,342
TR	Trimountain #4	Baltic Amygdaloid	5,212,289	374,483
TT	Toltec	N/A	5,182,240	343,842
VI	Victoria	N/A	5,174,214	329,226
CBF	Caledonia stope #1	N/A	5,179,700	337,622
CLD	Caledonia stope #2	N/A	5,179,700	337,622

* From Butler and Burbank, 1929

Table 2.3: Whole rock analyses performed by ALS Minerals.

Analyses	Description
Major Elements: Na, Mg, Al, Si, P, K, Ca, Ti, Mn, Fe, LOI	Lithium metaborate fusion, ICP-AES
C, S	Leco
Base Metals: Co, Ni, Cu, Zn, Mo, Ag, Cd, Pb	Four Acid, ICP-AES
Trace Elements: V, Cr, Ga, Rb, Sr, Y, Zr, Nb, Sn, Cs, Ba, Hf, Ta, W, Tl REEs: La, Ce, Pr, Nd, Sm, Eu, Gd, Tb, Dy, Ho, Er, Tm, Yb, Lu, Th, U	Lithium borate fusion, ICP-MS
Volatiles: As, Se, Sb, Te, Hg, Bi	Aqua regia, ICP-MS

Fairbanks (UAF). EDS analyses were used instead of more precise and accurate wavelength dispersive spectrometry (WDS) for the purpose of this research. EDS has a higher detection limit than WDS, but it was determined sufficient for this study. The advantage of EDS is that data collection can be achieved faster (and cheaper) than by WDS analyses.

The CAMECA SX-50 Electron Microprobe was used for EDS analysis of samples from the Caledonia Mine in 2012 and the JEOL JXA-8530F was used for EDS analysis of all other samples in 2013. Unidentified minerals were analyzed and compositions of minerals of interest were determined. The thin sections selected for microprobe analysis are listed in Table 2.4 with corresponding mine names.

The beam current, voltage, and collection time were specified as shown below:

- 10nA, 20kV, and 20 live seconds for the CAMECA SX-50, and
- 40nA, 20kV, and 30 live seconds for the JEOL JXA-8530F.

A higher current was used with the JEOL microprobe since it enabled better imaging and easier navigation of the thin sections. Sodium counts were affected by this higher current, but aluminum (Al) to silica (Si) ratios were used instead to calculate the anorthite content (X_{an}) of the plagioclase (Equation 1):

$$X_{An}(\%) = 100 \times \left(\frac{3 - \left(\frac{Si}{Al}\right)}{1 + \left(\frac{Si}{Al}\right)} \right) \quad (1)$$

At the beginning of each microprobe session, several standards were used to ensure proper working conditions of the microprobe. For that purpose, data were collected and compared for three locations of a standard mineral grain. Standards used included:

- chlorite (St 612, P177CHLR),
- albite (St 615, TALBITE),

Table 2.4: List of thin sections selected for microprobe analysis.

Sample #	Mine
11CBF004	Caledonia, stope #1
11CBF006	
11CLD001	Caledonia, stope #2
11CLD003	
11CLD005	
11CLD007	
10BA004	Baltic #4
10BB001	Bumblebee
10CN002	Centennial
10DE003	Delaware Mine
10DE006	
10FJ005	Boston #1
10QU006	Quincy Mine
10SC004	St. Clair Fissure
10SG001	Mamainse Bay
10TR004	Trimountain #4
10VI002	Victoria

- augite (St 204, USNM 122142, Kakanui New Zealand),
- plagioclase (St 228, labradorite, USNM 115900, Lake County, Oregon),
- olivine (St 303, OLIV1), and
- orthoclase (St 302, OR10 CT, Taylor Orthoclase).

The chlorite, albite, and augite standards were used before all measurements. Additionally, the plagioclase, olivine, and orthoclase standards were used prior to measurements made with the JEOL JXA-8530F microprobe. For each standard, three points on one grain were selected for analyses and compared. Examples of standard measurements are included in Tables 2.5, 2.6, and 2.7. Typically, analyses were within +/- 0.5 weight percent of the known standard composition, although some measurements deviated more from the actual composition. All analyses in this thesis are reported to one decimal point.

Of the 54 thin sections used for petrographic examination, 17 were selected for microprobe analyses. In general, elements were included in EDS analyses if they were expected to be present in a certain mineral. The spectrum based on EDS counts then was checked for other elements, which were included in the analyses if their peaks were significant. Zero values for elements thus can be due to the elements not being analyzed, or due to the measured values being below the detection limit of EDS. Either reason for zero values is designated in the data tables.

In order to compare data collected by the two microprobes, the JEOL JXA-8530F was used to create spectrum maps for two sample areas previously analyzed using the CAMECA SX-50. The spectrum maps were utilized to extract quantitative results for small areas at approximately the same locations where data were collected using the CAMECA SX-50. The results for three chlorite measurements from the JEOL JXA-8530F and the CAMECA SX-50 are shown in Figure 2.2, indicating that

Table 2.5: Plagioclase standard compositions and EDS measurements.
Example from measurements on 10-4-2013.

	weight %								
	Na_2O	MgO	Al_2O_3	SiO_2	K_2O	CaO	TiO_2	MnO	FeO
Standard	3.45	0.14	30.89	51.21	0.18	13.63	0.05	0.01	0.45
Point #1	3.49	0.15	30.26	52.02	-*	13.65	-*	-*	0.43
Point #2	3.32	0.16	30.26	52.06	-*	13.70	-*	-*	0.51
Point #3	3.43	0.15	30.43	51.74	0.04	13.74	-*	-*	0.48
Average	3.41	0.15	30.32	51.94	0.01	13.70	-*	-*	0.47
Absolute Error	0.03	-0.01	0.57	-0.73	0.17	-0.07	0.05	0.01	-0.02

*below detection limit

Table 2.6: Albite standard compositions and EDS measurements.
Example from measurements on 10-29-2013.

	weight %			
	Na_2O	Al_2O_3	SiO_2	K_2O
Standard	11.77	19.92	68.29	0.02
Point #1	10.75	19.51	69.74	-*
Point#2	10.53	19.44	70.03	-*
Point #3	10.73	19.43	69.83	-*
Average	10.67	19.46	69.87	-*
Absolute Error	1.10	0.46	1.57	0.02

*below detection limit

Table 2.7: Olivine standard compositions and EDS measurements.
Example from measurements on 10-24-2013.

	weight %					
	MgO	SiO_2	Cr_2O_3	MnO	FeO	NiO
Standard	50.79	41.18	0.02	0.10	7.62	0.29
Point #1	51.18	40.55	-*	0.17	7.70	0.40
Point #2	50.94	40.69	-*	0.23	7.72	0.42
Point #3	51.02	40.93	-*	0.18	7.56	0.31
Average	51.05	40.72	-*	0.19	7.67	0.38
Absolute Error	-0.26	0.46	0.02	-0.09	-0.05	-0.09

*below detection limit

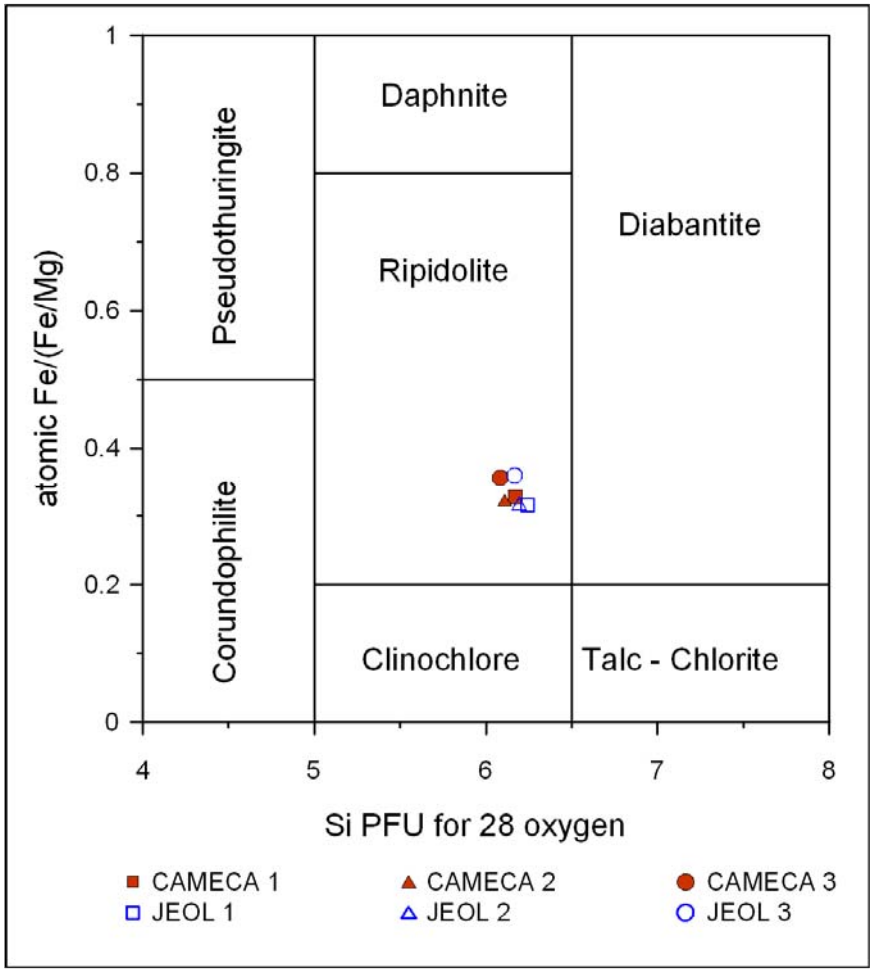

Figure 2.2: Chlorite measurements, JEOL JXA-8530F vs. CAMECA SX-50.

measurements from both microprobes produce similar results. Based on this comparison and standard analyses, it was concluded that EDS measurements from both microprobes could be used for the purpose of this research. Microprobe analyses of minerals were verified and classified using cation recalculation procedures and classification systems as described in Appendix B.

2.3 Classification of Samples using Whole Rock Data

Whole rock data (Appendix A) was used to examine the samples from the study area using various methods. The studied rocks have undergone low-grade metamorphism (Jolly and Smith, 1972; Livnat, 1983; Pueschner, 2001) likely leading to the migration of mobile elements. Thus, in order to determine the original composition of these rocks, classification systems based on immobile elements were used. Immobile element classification systems utilized included Zr/TiO_2-Nb/Y diagrams (Winchester and Floyd, 1977) and Nb-Zr-Y ternary diagrams (Meschede, 1986). Chondrite normalized rare earth element (REE) graphs were further employed to detect anomalous samples.

Changes in whole rock compositions due to alteration were visualized using the *Total Alkali Silica* (TAS) system (Le Bas et al., 1986; Le Maitre, 2002), bivariate diagrams, ACF ternary diagrams, and AFM diagrams. Descriptions of the construction of ACF and AFM diagrams are included in Appendix C and D, respectively.

In any diagram, data was plotted:

- for the Caledonia Mine only,
- differentiated by location, and
- differentiated by texture.

Additionally, diagrams based on mobile elements were used to plot the data by loss on ignition (LOI), which represents the sum of the H_2O and CO_2 content of the rocks.

In order to plot samples by location, the sample area was divided into several sections. Samples collected from the Keweenaw Peninsula were divided using a rough north-south differentiation: one group to the north mostly containing lodes within fissures, one group for the samples from the middle section with lodes mostly in amygdaloidal parts of the flows, and one group for the samples to the south (Figure 2.3). Samples collected from Mamainse Bay were plotted separately. Samples are color-coded on the map and in the diagrams.

2.4 Thermodynamic Modeling

Thermodynamic modeling was done using *Act2, Rxn*, and *Tact* from the *Geochemist's Work Bench*® (Bethke, 2000) for minerals available in the integrated *thermo.dat* database that most resembled minerals observed in the study area. Stability fields of minerals with respect to fugacity of CO_2 gas [fCO_2 (g)] and activity of aqueous SiO_2 [$aSiO_2$ (aq)] at standard conditions (25°C, 1.013 bar) were constructed in *Act2*. Since the minerals of interest often are not stable at standard conditions, the stable decomposition products were plotted first. In order to plot minerals of interest instead of decomposition products, more stable minerals had to be suppressed. The plotted minerals were then used to write balanced reactions and to determine the equilibrium constants (K) at various temperatures (T) in *Rxn*. The polynomial fit for the log of the equilibrium constant versus the temperature was used to rewrite the equilibrium equation, solving for fCO_2 (g) necessary for the minerals to be at equilibrium at various temperatures. All calculations were performed assuming quartz and H_2O activity of one. The fCO_2 (g) needed for equilibrium was plotted versus the temperature. The change of mineral stability with temperatures between 0 and 150 °C at 1 bar pressure in the presence of quartz was plotted in *Tact*.

Typical values for log $aSiO_2$ (aq) found in the study area were calculated from published Keweenaw mine water measurements as described in Appendix E. Ranges of log $aSiO_2$ (aq) were calculated from values published by Crisman (1982), Kelly et al. (1986), and Metz and Bolz (2013). Calculated log $aSiO_2$ (aq) and original

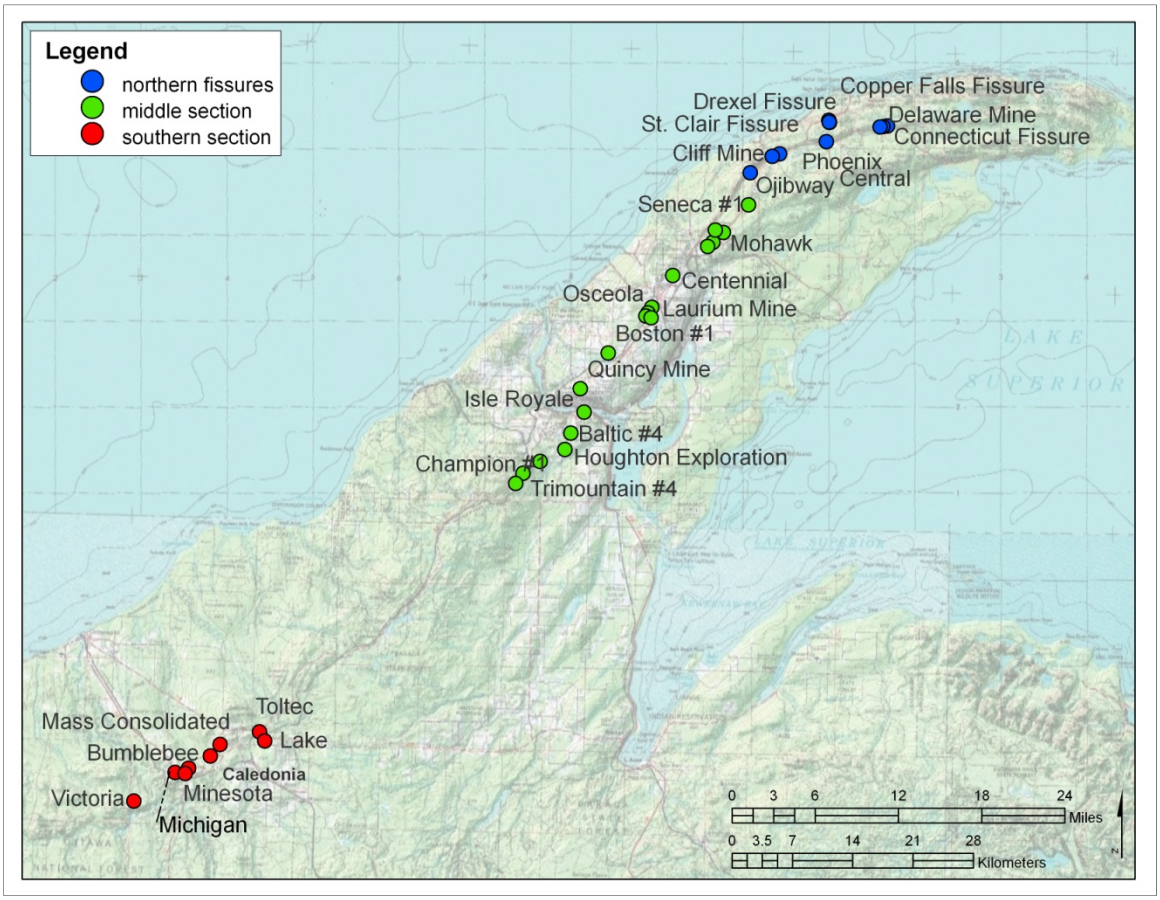

Figure 2.3: Map of Keweenaw sample stations by location.
Map does not show location of Mamainse samples to the east.

.

values published are shown in Table 2.8.

Values for flue gas from a power plant using Powder River basin coal were taken from Nogueira and Mamora (2008). Atmospheric CO_2 values from 1965 and 2013, measured at Mauna Loa Observatory and published by the Earth Systems Research Laboratory (ESRL, 2013) were included for atmospheric CO_2. Values were given in mole fraction of CO_2 in dry air.

The fugacity of a gas is defined as the partial pressure multiplied by the total pressure and a fugacity coefficient that equals one for an ideal gas. For the purpose of this research, the fugacity coefficient of CO_2 was assumed to be one. Original values and calculated fCO_2 are shown in Table 2.9.

Table 2.8: Typical values for log activity of SiO_2 in mine waters in the Keweenaw. Data was compiled from literature.

Source	Sample	Value given	SiO_2 (ppm)	log $aSiO_2$** (mol/kg)
Crisman (1982)	low value in near surface waters	Si^{4+}: 6 mg/L	13*	-3.7
Crisman (1982)	high value in near surface waters	Si^{4+}: 9 mg/L	19*	-3.5
Kelly et al. (1986)	Yellowknife	SiO_2: 8 ppm	8	-3.9
Metz and Bolz (2013)	Caledonia Mine, CMW1	Silicon: 6.6 mg/L	14*	-3.6
Metz and Bolz (2013)	Caledonia Mine, CMW2	Silicon: 8.5 mg/L	18*	-3.5
Metz and Bolz (2013)	Caledonia Mine, CMW3	Silicon: 6.7 mg/L	14*	-3.6
Metz and Bolz (2013)	Caledonia Mine, CMW4	Silicon: 4.4 mg/L	9*	-3.8
Metz and Bolz (2013)	Caledonia Mine, CMW5	Silicon: 6.4 mg/L	14*	-3.6
Metz and Bolz (2013)	Caledonia Mine, CMW6	Silicon: 5.1 mg/L	11*	-3.7
Metz and Bolz (2013)	Caledonia Mine, CMW7	Silicon: 6.3 mg/L	13*	-3.7

* assuming pure water at 4°C with density of 1000g/L

** assuming activity coefficient of 1.0

Table 2.9: Typical values for log fugacity of CO_2 (gas) of flue gas and atmosphere.

Source	Sample	Value given	fCO_2 (bar)	log fCO_2 (bar)
Nogueira and Mamora (2008)	Flue gas A	CO_2, mol % 11.95	0.12	-0.92
Nogueira and Mamora (2008)	Flue gas B	CO_2, mol % 13.57	0.14	-0.85
ESRL (2013)	2013	CO_2, ppm 400	0.0004	-3.4
ESRL (2013)	1965	CO_2, ppm 320	0.00032	-3.5

CHAPTER 3: THIN SECTION AND MICROPROBE ANALYSIS

As mentioned in the introduction of this thesis, unaltered mafic rocks (basalts) are being studied by various researchers regarding mineral carbonation (see Chapter 1). Typical basalts contain Ca-rich plagioclase, pyroxene, and sometimes olivine, of which both Ca-rich plagioclase and olivine show potential for mineral carbonation based on previous studies. However, the rocks in the sample area have undergone low-grade metamorphism and the mineralogy of these rocks has likely changed. Thus, the resulting mineralogy was studied in order to investigate the potential of these rocks for mineral carbonation. Special attention was paid to types and abundances of (Ca,Mg)-silicates.

Thin sections of 54 samples were examined using a petrographic microscope; 17 of the 54 available thin sections were then selected for microprobe analysis [including samples from Caledonia Mine (CLD, CBF), Mamainse Point (SG), St. Clair Fissure (SC), Victoria Mine (VI), Bumblebee (BB), Delaware Mine (DE), Baltic #4 (BA), Boston #1 (FJ), Trimountain (TR), Centennial Mine (CN), and Quincy Mine (QU)]. Locations of the Keweenaw thin section samples used for microprobe analyses are shown in Figure 3.1. For the location of the Mamainse samples refer to Figure 2.1.

Standard petrographic techniques were employed to determine minerals and their textures, approximate abundances, and alteration. Table 3.1 summarizes the main minerals and their approximate abundances (a complete table is included in Appendix F). Additional petrographic notes for samples selected for microprobe analyses are included in Table 3.2.

Microprobe analysis was used to collect data for minerals of interest identified under the petrographic microscope, as well as to help identify minerals that could not be positively classified using the microscope alone. In general, data for feldspars pyroxenes, and any alteration products were collected. Olivine and orthopyroxene minerals were confirmed in two thin sections, and prehnite and amphibole were,

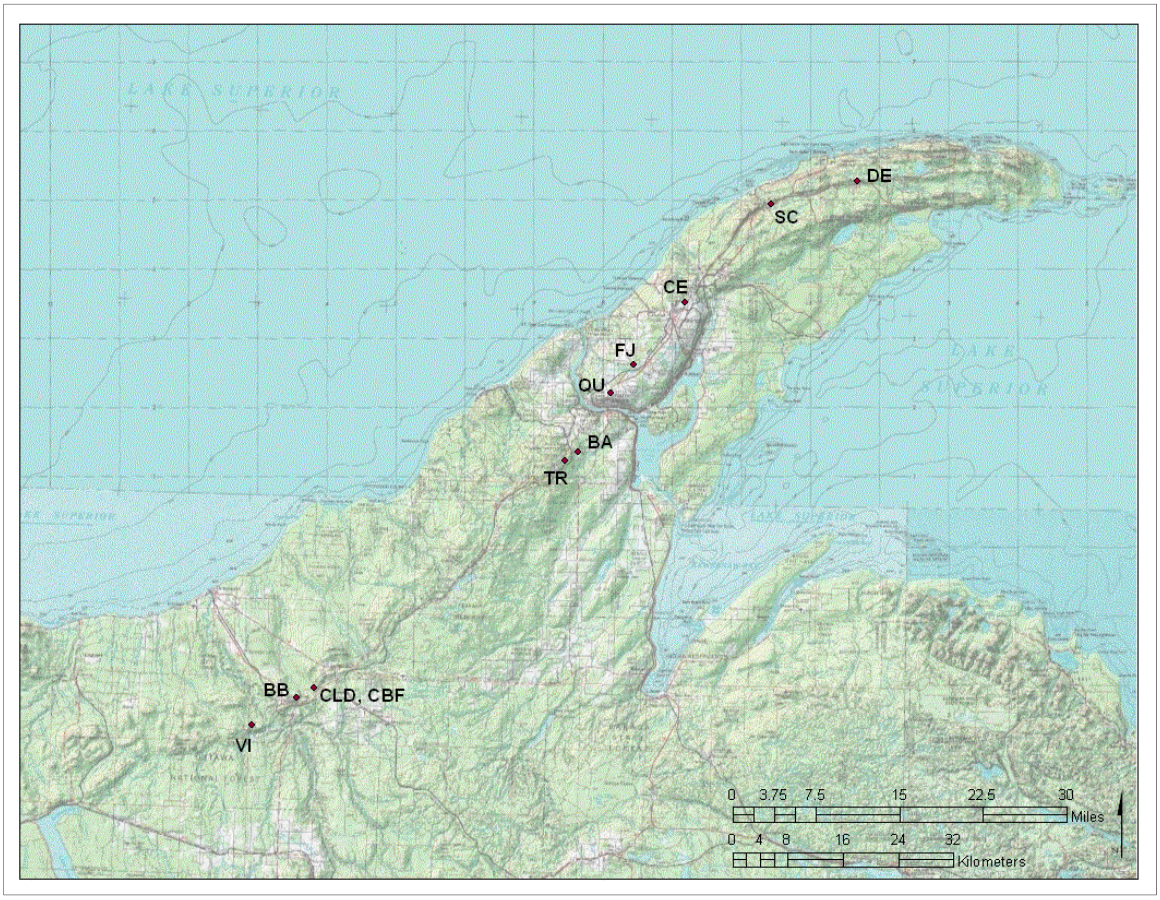

Figure 3.1: Locations of thin section samples used for microprobe analysis.

Table 3.1: Samples and approximate abundances (%) of main minerals.

alteration	sample #	plg	cpx	opx	ol	amph	chl	epi	prn	pp	ser	cc
1	10SG001	50	15	5	5	-	10	-	-	-	0.5	-
	10SC004	30	30	5	5	2	15	-	-	-	0.1	-
2a	10MI003	35	35	-	-	-	20	-	-	-	2	2
	10OC002	36	30	-	-	-	15	-	-	-	3	1
	10VI002	25	30	-	-	-	-	-	-	-	5	10
	10CC006	25	30	-	-	-	18	-	-	-	15	-
	10CH001	20	30	-	-	-	30	-	-	-	5	-
	10DE006	25	25	-	-	-	35	-	-	-	3	1
	10BB001	20	30	-	-	-	45	-	-	-	-	2
	10OC006	17	30	-	-	-	25	-	-	-	10	2
	10DR004	24	20	-	-	-	40	-	-	-	4	1
	10OC011	20	20	-	-	-	40	-	-	-	1	0.1
	10MG003	8	30	-	-	-	20	-	-	-	35	-
2b	10HE004	25	-	-	-	-	30	-	-	-	10	10
	10BA005	20	-	-	-	-	15	-	-	-	20	10
	10FJ006	20	-	-	-	-	30	-	-	-	5	20
	10FJ005	5	1	-	-	-	57	-	-	-	-	-
	10HE003	5	-	-	-	-	28	-	-	-	25	5
	10TR004	-	-	-	-	-	5	-	-	-	25	63
2c	10OC014	31	25	-	-	-	10	3	-	-	10	8
	10FU004	13	15	-	-	-	30	0.1	-	-	25	5
3a	10TT005	25	20	-	-	-	30	3	3	5	2	-
	10QU002	31	3	-	-	-	30	1	3	25	-	-
	10TT002	10	-	-	-	-	23	5	5	35	5	10
	10PH005	26	20	-	-	-	20	-	10	2	-	2
	10IR001	2	25	-	-	-	15	0.1	8	35	-	3
	10CF004	35	2	-	-	-	15	0.1	15	15	-	-
	10DR005	7	3	-	-	-	15	3	28	24	-	-
	10CL006	2	3	-	-	-	10	5	30	29	-	15
3b	10DE007	16	15	-	-	-	-	2	25	35	-	2
	10CN002	40	15	-	-	-	-	1	20	20	-	1
	10QU006	2	2	-	-	-	-	10	46	5	-	20

Table 3.1 (continued): Samples and approximate abundances (%) of main minerals.

alteration	sample #	plg	cpx	opx	ol	amph	chl	epi	prn	pp	ser	cc
4a	10OJ005	38	25	-	-	-	5	-	-	15	1	1
	10CE002	5	38	-	-	-	15	2	-	30	-	-
	10PH004	15	30	-	-	-	20	-	-	5	15	0.1
	10CF006	20	20	-	-	-	30	0.1	-	25	-	-
	10LA001	17	20	-	-	-	20	3	-	30	-	-
	10MC005	24	15	-	-	-	30	-	-	15	5	-
	10FU003	14	15	-	-	-	19	4	-	20	1	-
	10GR003	5	15	-	-	-	15	2	-	35	2	-
	11CBF006	30	10	-	-	-	25	5	-	20	-	-
	11CBF004	25	10	-	-	-	30	0.1	-	20	-	-
4b	10CF005	42	5	-	-	-	30	1	-	5	2	5
	10MC003	10	3	-	-	-	25	8	-	30	-	10
	11CLD003	29	-	-	-	-	30	10	-	25	-	-
	10CC002	26	2	-	-	-	15	15	-	10	1	-
	10CE001	25	-	-	-	-	25	1	-	5	6	10
	11CLD001	21	-	-	-	-	30	10	-	1	-	1
	10SE002	10	-	-	-	-	10	5	-	0.1	-	10
	10DE003	5	-	-	-	-	25	0.1	-	45	-	2
	11CLD007	2	-	-	-	-	20	1	-	24	1	-
N/A	10TO004	1	-	-	-	-	-	15	-	1	-	-
	11CLD005	-	-	-	-	-	-	25	-	-	-	-

Table 3.2: Description of samples used for microprobe analysis. Minerals present in small amounts are shown in parentheses.

Sample #	Notes	Alteration products	Alteration
10SG001	Fresh, porphyritic sample with slightly altered plagioclase. Some coarse-grained relict olivine present.	(chlorite)	1
10SC004	Fresh, massive sample with slightly altered plagioclase, often surrounded by coarse pyroxene. Relict olivine present.	(chlorite)	1
10VI002	Relatively fresh, massive sample with abundant opaque minerals. Few plagioclase grains with cores altered to calcite (and some sericite).	calcite, (sericite)	2a
10BB001	Somewhat fresh, massive sample with moderately altered plagioclase, often surrounded by pyroxene. Some plagioclase cores altered to granular chlorite. Chlorite also sheety, w. few coarse fibrous chlorite grains.	chlorite, calcite	2a
10DE006	Moderately altered, massive sample with plagioclase altered to chlorite and sericite.	chlorite, sericite, (calcite)	2a
10BA005	Extremely altered, massive sample with extremely altered plagioclase, no pyroxene, abundant sericite and calcite.	chlorite, calcite, sericite	2b
10FJ005	Highly amygdaloidal sample with dark greenish-yellow chlorite in amygdules sometimes with quartz along rim. Moderately cloudy, medium-grained plagioclase, few subhedral, moderately altered pyroxene grains.	chlorite	2b
10TR004	Brecciated sample with abundant calcite, some muscovite, and chlorite. Plagioclase extremely altered, no pyroxene.	calcite, muscovite, chlorite	2b
10CN002	Moderately altered, gabbroic sample with extremely cloudy plagioclase, some moderately altered pyroxene, and abundant interstitial pumpellyite, prehnite, and some epidote. No chlorite.	pumpellyite, prehnite, epidote	3b
10QU006	Brecciated sample with abundant prehnite, calcite, and quartz with some pumpellyite and epidote mostly in matrix and as alteration of original minerals throughout.	prehnite, calcite, quartz, epidote, pumpellyite	3b

Table 3.2 (continued): Description of samples used for microprobe analysis. Minerals present in small amounts are shown in parentheses.

Sample #	Notes	Alteration Products	Alteration
11CBF006	Slightly amygdaloidal sample with extremely altered, dusty plagioclase, with moderately altered, interstitial pyroxene. Interstitial chlorite throughout. Coarse epidote with acicular pumpellyite, quartz in vuggs.	chlorite, pumpellyite, epidote, quartz	4a
11CBF004	Moderately altered, gabbroic sample with plagioclase cores altered to chlorite and pumpellyite, some epidote interstitial with chlorite. Some relict, moderately altered pyroxene.	chlorite, pumpellyite, (epidote)	4a
11CLD003	Slightly amygdaloidal sample, with plagioclase replaced by pumpellyite and chlorite; no pyroxene. Epidote in amygdules with chlorite.	chlorite, pumpellyite, epidote	4b
11CLD001	Fine-grained sample with amygdules. Extremely altered plagioclase, and no pyroxene. Epidote as plagioclase alteration and with interstitial chlorite. Coarse epidote with chlorite and fine, acicular pumpellyite in large amygdule (~1.5 cm diameter).	chlorite, epidote, quartz, (pumpellyite)	4b
10DE003	Amygdaloidal sample, with cloudy plagioclase, abundant pumpellyite in amygdules, no pyroxene.	pumpellyite, chlorite, calcite	4b
11CLD007	Slightly amygdaloidal sample with extremely cloudy, fine-grained plagioclase throughout. No pyroxene. Pumpellyite, and chlorite in amygdules. Few specks of epidote in former plagioclase.	pumpellyite, chlorite, (kspar, epidote)	4b
11CLD005	Extremely fine-grained sample, somewhat vesicular with abundant quartz and epidote in vuggs.	epidote, quartz	N/A

identified using microprobe analysis. For all minerals, the collected microprobe data were used to determine mineral compositions and to classify the minerals.

In relatively unaltered samples, the primary basaltic minerals are present including plagioclase (plg), clinopyroxene (cpx), and some orthopyroxene (opx), olivine (ol), and amphibole (amph). Alteration minerals observed in the various thin sections include chlorite (chl), epidote (epi), pumpellyite (pp), prehnite (prn), copper (cu), quartz (qtz), sericite (ser), calcite (cc), potassium feldspar (ksp), and various zeolites (zeol). Greenish-brown olivine alteration was assumed to be iddingsite (id), and extremely fine-grained, high relief, brownish alteration was simply classified as alteration (altn). Opaque minerals without copper (op), sphene (sph), and holes were also included in the mineral abundance approximations. The thin sections described in Table 3.2 are organized by different alteration assemblages (referred to as "alteration"):

1. Relatively fresh samples with some chlorite alteration of few plagioclase grains. Some relict olivine, orthopyroxene (and amphibole) present.
2. Moderately altered samples with chlorite and sericite alteration of plagioclase (often with interstitial calcite);
    a. with plagioclase and clinopyroxene,
    b. with little plagioclase and very little (if any) clinopyroxene,
    c. with plagioclase, clinopyroxene, and little epidote.
3. Altered samples with prehnite and pumpellyite (sometimes epidote) alteration of plagioclase;
    a. with chlorite, and
    b. without chlorite.

4. Altered samples with chlorite, pumpellyite, and often epidote alteration of plagioclase;
    c. with plagioclase and clinopyroxene, and
    d. with less plagioclase, with no to very little clinopyroxene.

Brief descriptions of optical properties of the minerals observed are included below, along with microprobe results. All microprobe results are given in weight percent and recalculated cations where appropriate. For mineral groups with few data points, the data is included with the text. For mineral groups with abundant data, a set of representative samples is shown with the text and the complete analyses are included in Appendix G.

3.1 Olivine

Relict olivine was observed in the two freshest samples 10SG001 and 10SC004. Olivine ranges in size from relatively fine (~0.1 mm) to coarse (~1.5 mm) grains. Fresher olivine may be surrounded by orthopyroxene, which in turn is often surrounded by clinopyroxene. Most olivine is surrounded by green to red-brown (in plane polarized light, PPL) alteration products. Olivine appears clear in PPL, with moderate to high positive relief and poor cleavage. Third order interference colors are common. An example of coarse-grained olivine in sample 10SG001 is shown in Figure 3.2.

The presence of olivine was confirmed by microprobe analysis; cations were recalculated based on four oxygen atoms per formula unit (PFU). Six olivine grains were analyzed in sample 10SC004 (Tables 3.3 and 3.4), and three grains were analyzed in sample 10SG001 (Tables 3.5 and 3.6). Olivine grains are fine-grained in 10SC004 (0.1-0.3 mm) and coarse-grained in 10SG001 (up to 2 mm). Analyzed olivine grains contain between 53 and 61% forsterite (Fo, Figures 3.3 and 3.4). No zoning within grains is apparent; compositions appear to vary between grains. For

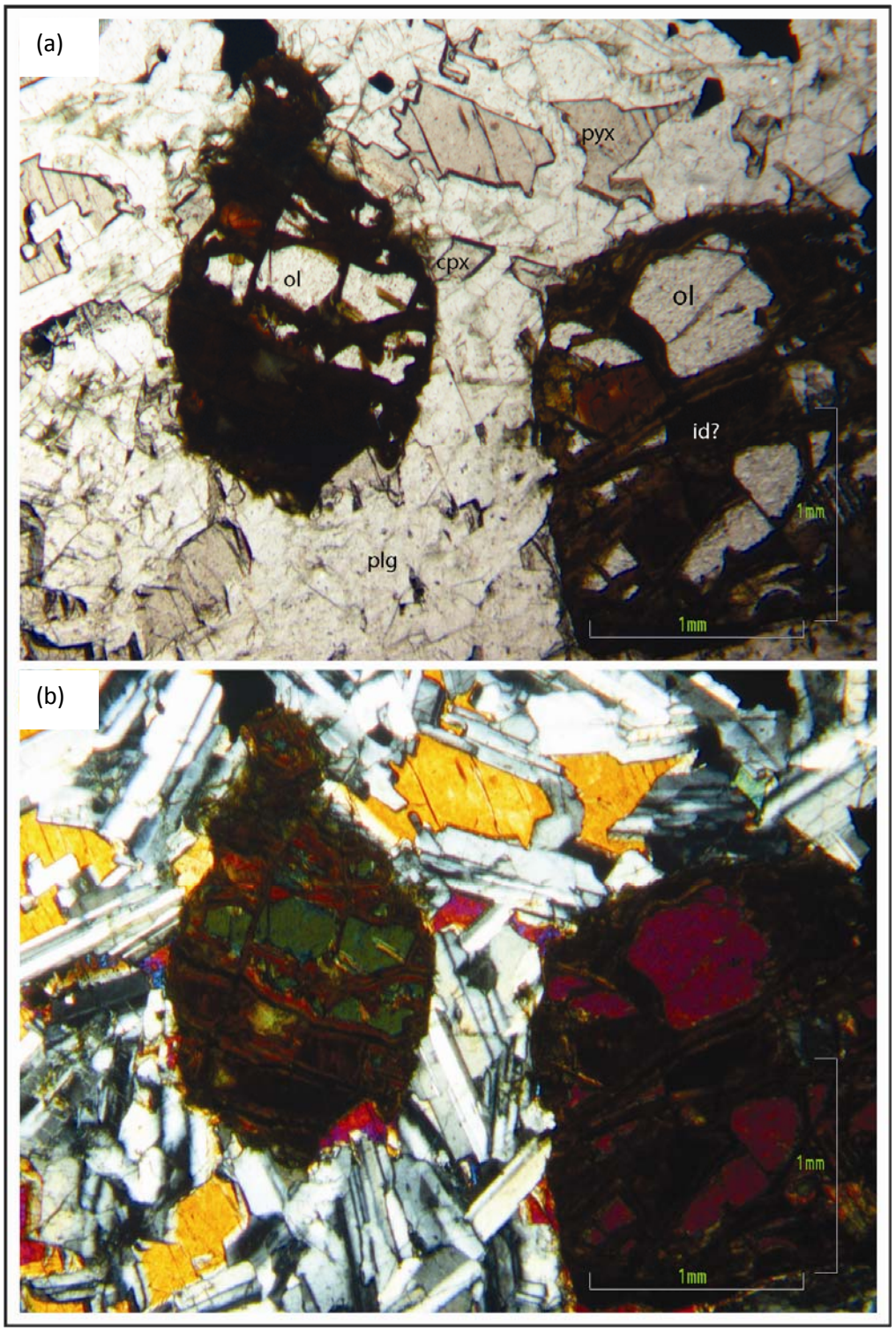

Figure 3.2: Coarse-grained olivine with fresh plagioclase and pyroxene. As seen in PPL (a) and under crossed polarizers (b) in sample 10SG001 (alteration assemblage 1). Iddingsite (?) alteration of olivine visible.

Table 3.3: Electron microprobe analyses of olivine grains 1-3 (sample 10SC004).
Table shows analyses for grains one through three.
Cation recalculations based on 4 oxygen atoms PFU.

Sample	-4-1-1	-4-1-2	-4-1-3	-4-2-1	-4-2-2	-4-2-3	-4-2-4	-7-1-1	-7-1-2	-7-1-3
	Grain 1			Grain 2				Grain 3		
MgO	28.6	28.8	28.8	27.6	27.3	27.5	27.5	28.8	28.3	28.5
SiO_2	37.1	37.3	37.2	36.8	36.7	36.5	36.6	35.9	36.2	36.4
CaO	0.1	0.1	0.2	0.2	0.1	0.1	0.1	0.2	0.2	0.2
MnO	0.6	0.6	0.6	0.6	0.5	0.7	0.6	0.7	0.7	0.8
FeO	33.6	33.1	33.3	34.9	35.3	35.2	35.2	34.5	34.7	34.2
∑	100.0	99.9	100.1	100.1	100.0	100.0	100.0	100.1	100.1	100.1
Si	1.0	1.0	1.0	1.0	1.0	1.0	1.0	1.0	1.0	1.0
Mg	1.2	1.2	1.2	1.1	1.1	1.1	1.1	1.2	1.2	1.2
Fe^{2+}	0.8	0.8	0.8	0.8	0.8	0.8	0.8	0.8	0.8	0.8
Mn	-	-	-	-	-	-	-	-	-	-
Ca	-	-	-	-	-	-	-	-	-	-
∑	3.0	3.0	3.0	2.9	2.9	2.9	2.9	3.0	2.9	3.0
Mg/(Mg+Fe)	0.60	0.61	0.60	0.58	0.58	0.58	0.58	0.60	0.59	0.60

Table 3.4: Electron microprobe analyses of olivine grains 4-6 (sample 10SC004).
Table shows analyses for grains four through six.
Cation recalculations based on 4 oxygen atoms PFU.

Sample	-7-2-1	-7-2-2	-7-2-3	-8-1-1	-8-1-2	-8-1-3
	Grain 4	Grain 5		Grain 6		
MgO	27.1	27.0	26.6	27.1	27.1	27.2
SiO_2	35.5	35.8	36.0	36.0	35.6	36.1
CaO	0.2	0.1	0.1	0.2	0.1	0.2
MnO	0.8	0.6	0.6	0.5	0.7	0.7
FeO	36.5	36.6	36.6	36.3	36.4	35.9
∑	100.1	100.0	99.9	100.1	99.9	100.1
Si	1.0	1.0	1.0	1.0	1.0	1.0
Mg	1.1	1.1	1.1	1.1	1.1	1.1
Fe^{2+}	0.9	0.9	0.9	0.9	0.9	0.8
Mn	-	-	-	-	-	-
Ca	-	-	-	-	-	-
∑	3.0	3.0	3.0	3.0	3.0	2.9
Mg/(Mg+Fe)	0.60	0.57	0.56	0.57	0.57	0.57

Table 3.5: Electron microprobe analyses of olivine grains 1-2 (sample 10SG001).
Table shows analyses for grains one and two.
Cation recalculations based on 4 oxygen atoms PFU.

Sample point	-7-1-1	-7-1-2	-7-1-3	-7-5-1	-7-5-2	-7-5-3	-7-6-1	-7-6-2	-7-6-3
	Grain 1			Grain 2					
MgO	25.1	25.0	25.4	25.0	25.1	25.2	24.8	24.9	25.2
SiO_2	35.7	35.4	35.5	35.7	35.4	35.4	35.4	35.5	35.6
CaO	0.1	0.2	0.2	0.3	0.2	0.2	0.2	0.2	0.3
MnO	0.7	0.7	0.8	0.8	0.7	0.8	0.8	0.8	0.7
FeO	38.4	38.7	38.2	38.3	38.6	38.5	38.8	38.7	38.3
∑	100.0	100.0	100.1	100.1	100.0	100.1	100.0	100.1	100.1
Si	1.0	1.0	1.0	1.0	1.0	1.0	1.0	1.0	1.0
Mg	1.1	1.1	1.1	1.1	1.1	1.1	1.1	1.1	1.1
Fe^{2+}	0.9	0.9	0.9	0.9	0.9	0.9	0.9	0.9	0.9
Mn	-	-	-	-	-	-	-	-	-
Ca	-	-	-	-	-	-	-	-	-
∑	3.0	3.0	3.0	3.0	3.0	3.0	3.0	3.0	3.0
Mg/(Mg+Fe)	0.54	0.54	0.54	0.54	0.54	0.54	0.53	0.53	0.54

Table 3.6: Electron microprobe analyses of olivine grain 3 (sample 10SG001).
Table shows analyses for grain three.
Cation recalculations based on 4 oxygen atoms PFU.

Sample point	10SG001 -9-1-1	10SG001 -9-1-2	10SG001 -9-1-3	10SG001 -9-1-4	10SG001 -9-2-1	10SG001 -9-2-2	10SG001 -9-2-3
	Grain 3						
MgO	27.9	28.3	28.1	27.8	28.4	28.0	28.1
SiO_2	36.1	36.2	35.9	36.0	36.1	36.1	36.2
CaO	0.1	0.2	0.2	0.2	0.3	0.3	0.3
MnO	0.7	0.7	0.6	0.7	0.7	0.8	0.7
FeO	35.1	34.6	35.1	35.3	34.6	34.9	34.7
∑	99.9	100.0	99.9	100.0	100.1	100.1	100.0
Si	1.0	1.0	1.0	1.0	1.0	1.0	1.0
Mg	1.2	1.2	1.2	1.2	1.2	1.2	1.2
Fe^{2+}	0.8	0.8	0.8	0.8	0.8	0.8	0.8
Mn	-	-	-	-	-	-	-
Ca	-	-	-	-	-	-	-
∑	3.0	3.0	3.0	3.0	3.0	3.0	3.0
Mg/(Mg+Fe)	0.59	0.59	0.59	0.58	0.59	0.59	0.59

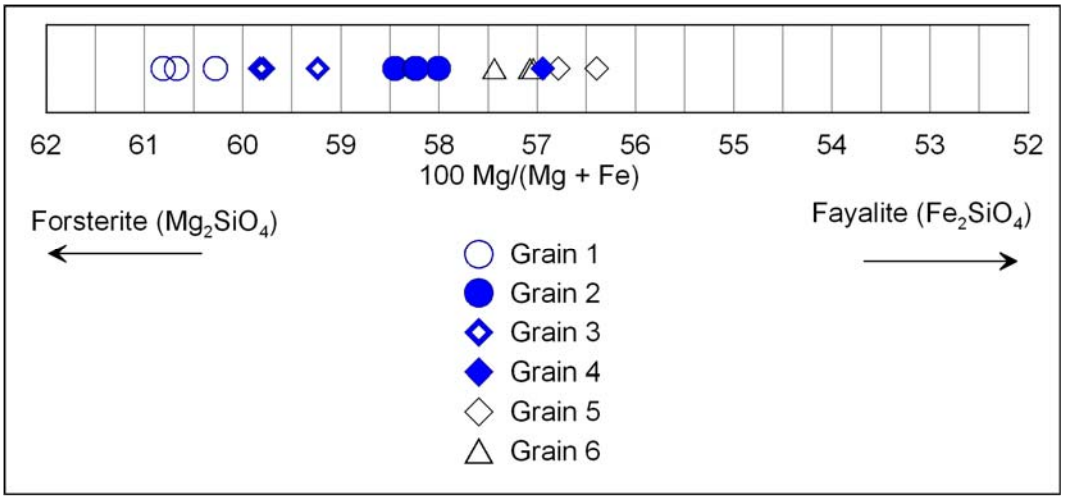

Figure 3.3: Diagram of forsterite contents in olivine grains in sample 10SC004.

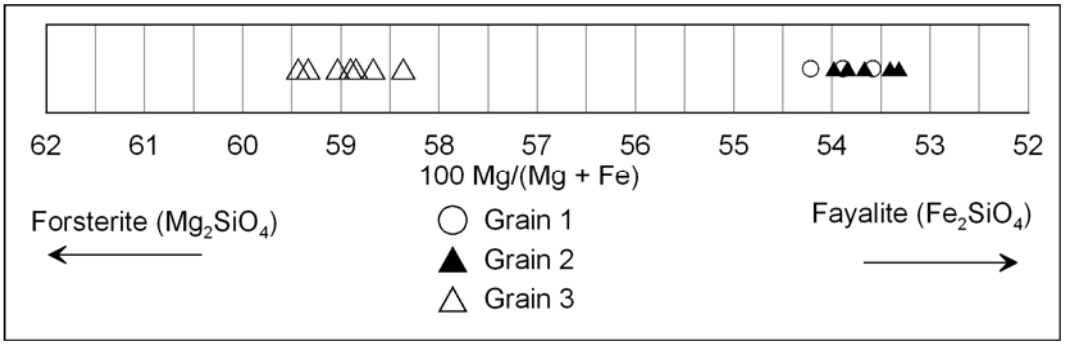

Figure 3.4: Diagram of forsterite contents in olivine grains in sample 10SG001.

example, 10SG001 contains two higher iron (Fo_{53-54}) grains, and one lower iron (Fo_{58-60}) grain, with no compositional overlap.

3.2 Amphibole

Clove brown, radial minerals up to 0.1 mm long were observed interstitial to plagioclase and pyroxene in 10SC004. These minerals are believed to be amphibole minerals. A typical example of one of these minerals is shown in Figure 3.5. The relief of these mineral ranges from moderate to high positive, birefringence appears to be moderate first order, and the optical sign could not be distinguished due to the extremely fine, needle-like habit.

The minerals were confirmed to be amphiboles by microprobe analysis (Table 3.7); cation recalculations were based on 23 oxygen atoms PFU. Since no fluorine or chlorine was detected, and Na^+ and K^+ in the A site (see Appendix B) summed up to less than 0.5, the silica PFU was plotted against the $Mg/(Mg+Fe^{2+})$ in order to classify the minerals (Leake et al., 1997). Analyses 10SC004-2-1-1 and 10SC004-6-1-1 plot identically in the magnesiohornblende field; and the other four analyses plot in the ferrohornblende field (Table 3.7 and Figure 3.6).

3.3 Feldspar

Feldspars occur as predominant minerals (up to 50%) in the groundmass of samples, and as phenocrysts in porphyritic samples. Groundmass feldspar varies between <0.1 mm (in very fine-grained samples) to 4 mm (in gabbroic samples). Phenocrysts range from 1 mm to 2 cm. Feldspars range from unaltered plagioclase with a fresh appearance, to relatively fresh plagioclase with altered cores, to moderately altered (former) plagioclase with brownish color, to extremely altered (former) plagioclase with brown, extremely fine-grained, often high relief alteration products replacing most of the former plagioclase. The different alteration assemblages introduced at the beginning of this chapter were observed in the alteration of plagioclase, ranging from chlorite/sericite/calcite to prehnite, to

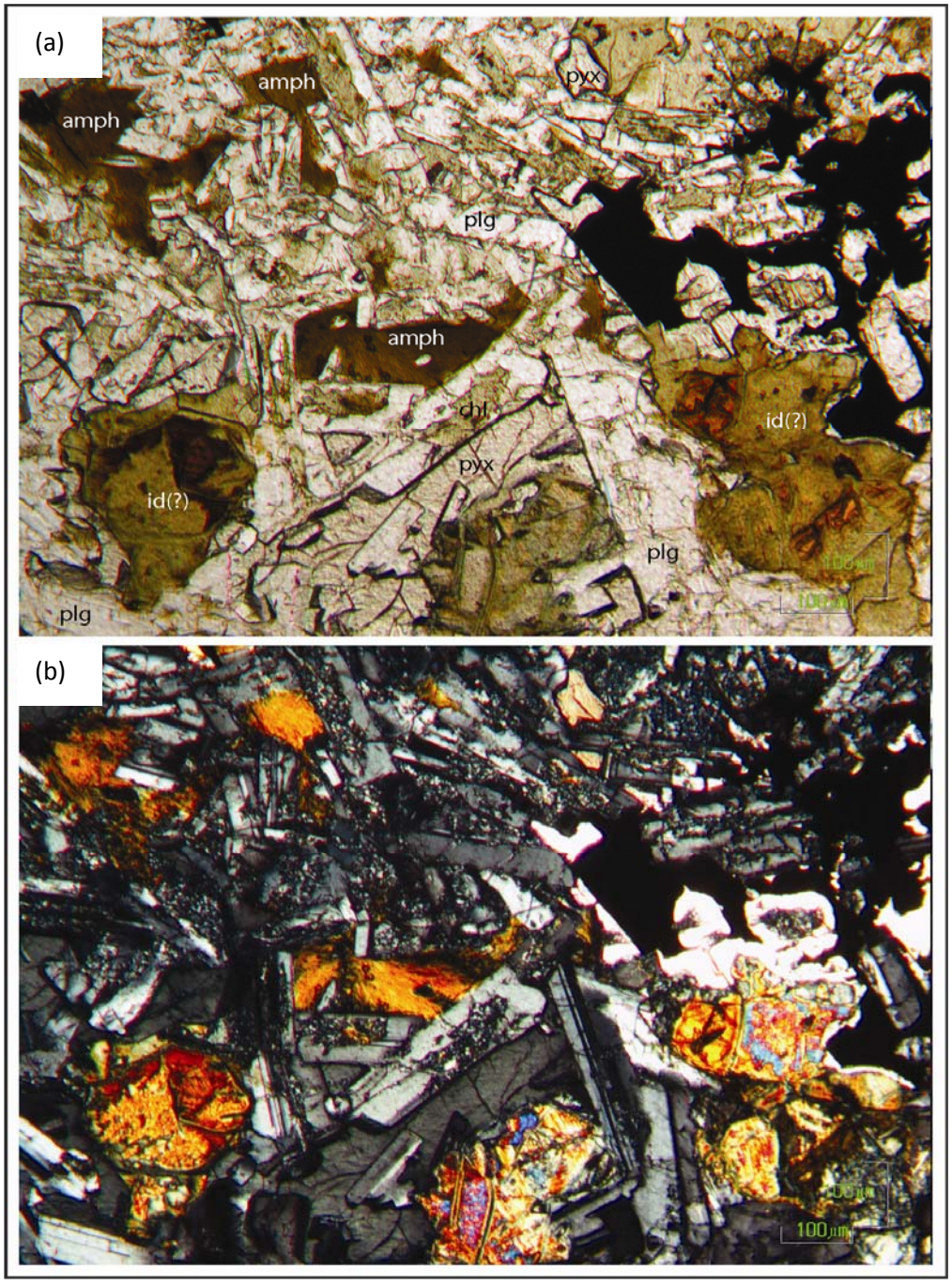

Figure 3.5: Amphibole in PPL (a) and under crossed polarizers (b) in sample 10SC004. Note chlorite alteration of plagioclase and iddingsite replacing olivine (?). Sample is considered alteration assemblage 1.

Table 3.7: Electron microprobe analyses of amphibole (sample 10SC004). Cation recalculations based on 23 oxygen atoms PFU.

Sample point	10SC004 -2-1-1	10SC004 -2-1-2	10SC004 -2-1-4	10SC004 -6-1-1	10SC004 -6-1-2	10SC004 -6-1-3
Na_2O	0.3	0.3	0.1	0.3	0.2	0.2
MgO	8.6	7.5	7.0	9.3	8.4	8.0
Al_2O_3	8.3	7.5	7.3	9.0	8.0	8.4
SiO_2	46.8	48.3	49.4	46.6	48.5	48.2
K_2O	-*	0.2	-*	0.1	0.2	-*
CaO	10.5	12.2	14.0	11.7	14.2	14.2
MnO	0.2	0.2	0.2	0.3	0.2	0.2
FeO	25.3	23.9	21.9	22.7	20.5	20.8
∑	100.0	99.9	100.0	100.0	100.2	100.0
Si	6.7	7.1	7.3	6.7	7.1	7.1
Al	1.3	0.9	0.7	1.3	0.9	0.9
∑	8.0	8.0	8.0	8.0	8.0	8.0
Al	0.1	0.4	0.6	0.2	0.5	0.6
Mg	1.8	1.7	1.5	2.0	1.8	1.8
Mn	-	-	-	-	-	-
Fe^{2+}	1.3	2.4	2.7	1.4	2.5	2.6
Fe^{3+}	1.8	0.6	-	1.4	-	-
∑	5.0	5.0	4.8	5.0	4.8	5.0
Ca	1.6	1.9	2.2	1.8	2.2	2.3
Na	0.1	0.1	-	0.1	-	-
∑	1.7	2.0	2.2	1.9	2.2	2.3
Na	-	-	-	-	0.1	0.1
K	-	-	-	-	-	-
∑	-	-	-	-	0.1	0.1
$Mg/(Mg+Fe^{2+})$	0.6	0.4	0.4	0.6	0.4	0.4

*below detection limit

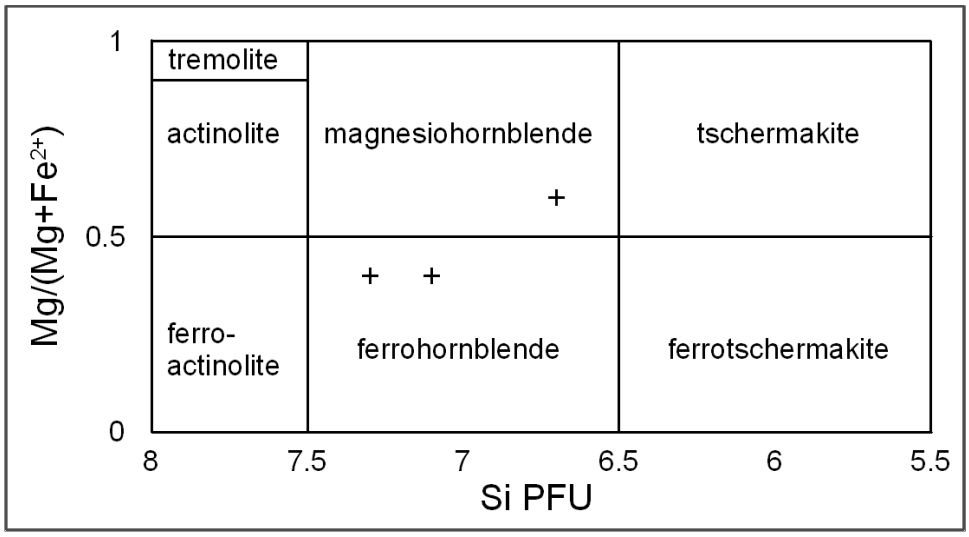

Figure 3.6: Compositional classification of amphiboles based on EDS microprobe analysis. All data are from thin section 10SC004.

pumpellyite/albite/(epidote). Examples of fresh plagioclase are shown in Figure 3.2; relatively fresh plagioclase with chlorite alteration is shown in Figure 3.5. An example of plagioclase with sericite and calcite alteration is included in Figure 3.7, and prehnite alteration of a former plagioclase core is shown in Figure 3.8. Here, the rim of the former plagioclase grain is completely altered to albite. Figure 3.9 shows an example of former plagioclase with chlorite, pumpellyite, and albite alteration.

In PPL, fresh plagioclase appears colorless, with low relief. More altered plagioclase has a cloudy appearance, with higher relief minerals replacing parts of the grains. Plagioclase shows low first order birefringence, with twinning visible even in more altered samples.

Potassium feldspar was mostly identified by microprobe analysis as very fine-grained plagioclase alteration. Some potassium feldspar is present along rims of amygdules with specks of epidote, surrounding chlorite and fine acicular pumpellyite. Potassium feldspar in amygdules has a cloudy appearance and is clear to slightly reddish-brownish in PPL. It has low relief, and low first order birefringence.

Feldspars were analyzed using EDS for all thin sections other than 10FJ005 and 10TR004. A total of 266 analyses for feldspar group minerals were performed. Cations were recalculated based on eight oxygen atoms PFU. Representative analyses are shown in Table 3.8 with alteration assemblages. Remaining analyses are included in Appendix G.

Analyses are plotted on Albite (Ab) - Anorthite (An) - Orthoclase (Or) ternary diagrams for classification purposes (Figures 3.10, 3.11, and 3.12). Si:Al ratios were used to determine X_{an} as described in Chapter 2. Listed with increasing alteration assemblage, diagrams for samples of alteration assemblage 1 (10SG001, 10SC004), and alteration assemblage 2 (10VI002, 10BB001, 10DE006, and 10BA005) are shown in Figure 3.10; diagrams for alteration assemblage 3 (10CN002, 10QU006)

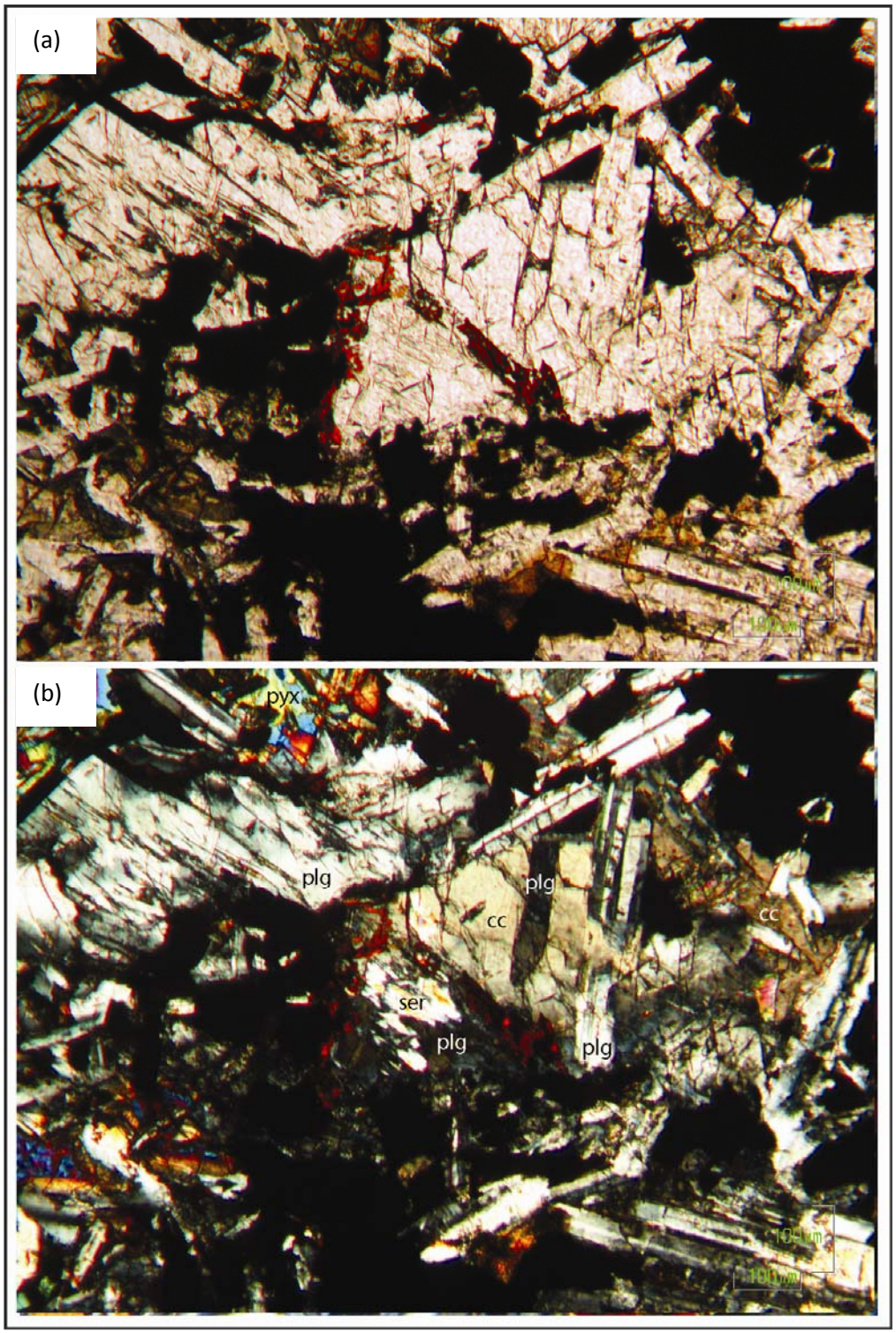

Figure 3.7: Sericite and calcite alteration of plagioclase.
As seen in PPL (a) and under crossed polarizers (b) in sample 10VI002 (alteration assemblage 2).

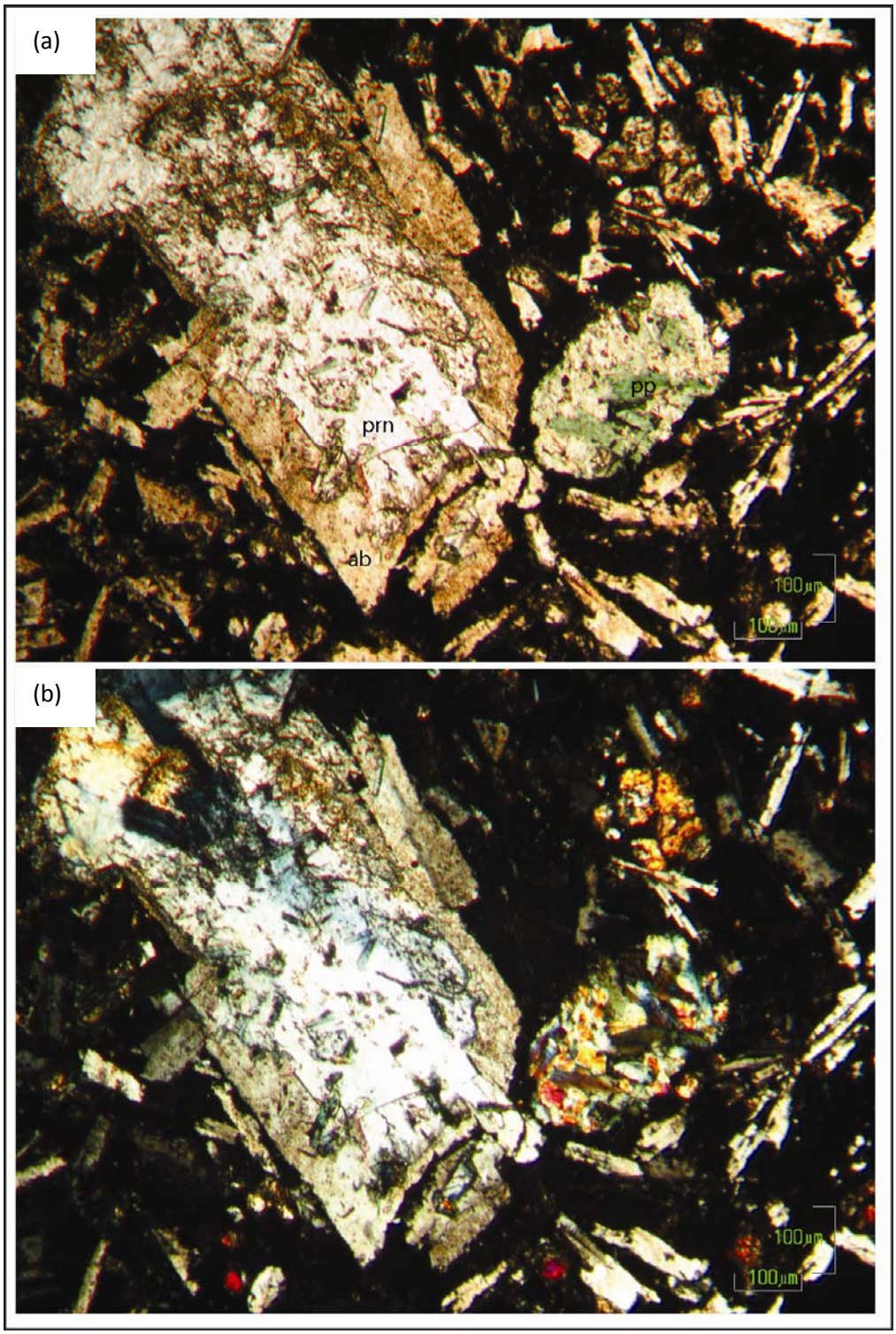

Figure 3.8: Prehnite alteration of former plagioclase core.
Rim is replaced by albite. As seen in PPL (a) and under crossed polarizers (b) in sample 10QU006 (alteration assemblage 3).

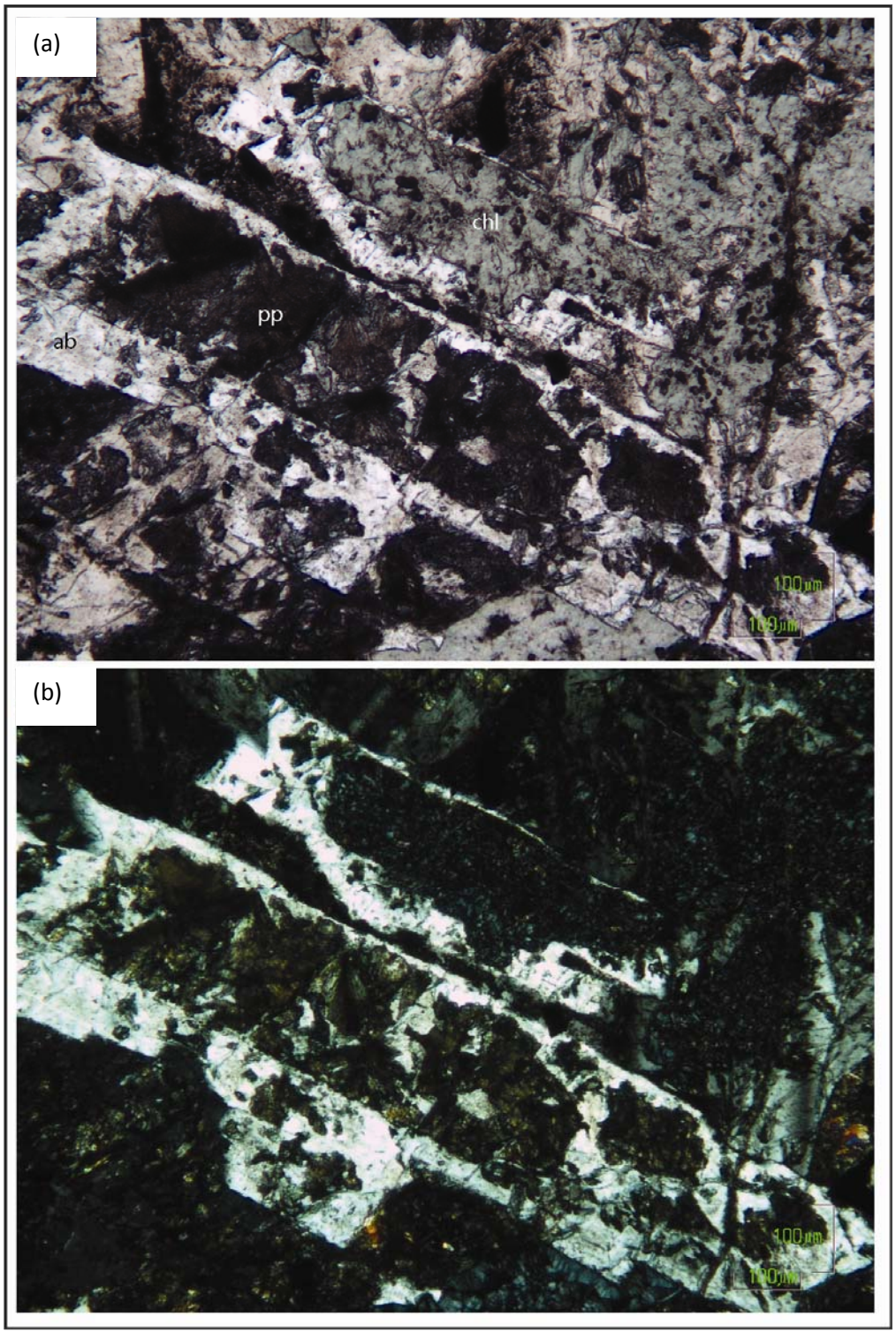

Figure 3.9: Chlorite and pumpellyite alteration of former plagioclase cores. As seen in PPL (a) and under crossed polarizers (b) in sample 11CBF004 (alteration assemblage 4).

Table 3.8: Electron microprobe analyses of selected feldspar group minerals. Analyses are shown with increasing alteration assemblage. Cation recalculations based on 8 oxygen atoms PFU.

Sample	10SC004 -7-1-8	10SC004 -4-2-11	10BB001 -6-1-12	10BA005 -6-1-6	11CLD001 10-29-45	11CLD007 -7-1-4
Assemblage	1	1	2a	2b	4b	4b
Na_2O	2.2	5.0	6.3	8.7	5.1	-*
MgO	-**	-**	-**	-**	1.2	-**
Al_2O_3	31.8	28.4	25.6	20.8	18.8	18.6
SiO_2	49.6	55.1	59.8	69.3	65.7	67.5
K_2O	-*	-*	-*	-*	9.2	14.0
CaO	15.6	10.7	7.6	1.2	-*	-*
TiO_2	-**	0.1	-**	-**	-**	-**
FeO	0.8	0.7	0.7	-**	-**	-**
∑	100.0	100.0	100.0	100.0	100.0	100.1
Si	2.3	2.5	2.7	3.0	3.0	3.1
Al	1.7	1.5	1.3	1.1	1.0	1.0
∑	4.0	4.0	4.0	4.1	4.0	4.1
Na	0.2	0.4	0.6	0.7	0.5	-
Ca	0.8	0.5	0.4	0.1	-	-
K	-	-	-	-	0.5	0.8
Mg	-	-	-	-	0.1	-
Fe^{2+}	-	-	-	-	-	-
∑	1.0	0.9	1.0	0.8	1.1	0.81
Xan	72	51	34	4	0	0
Xab	28	49	66	96	46	0
Xor	0	0	0	0	54	100

*below detection limit. ab = anorthite, an = anorthite, or = orthoclase

** not analyzed.

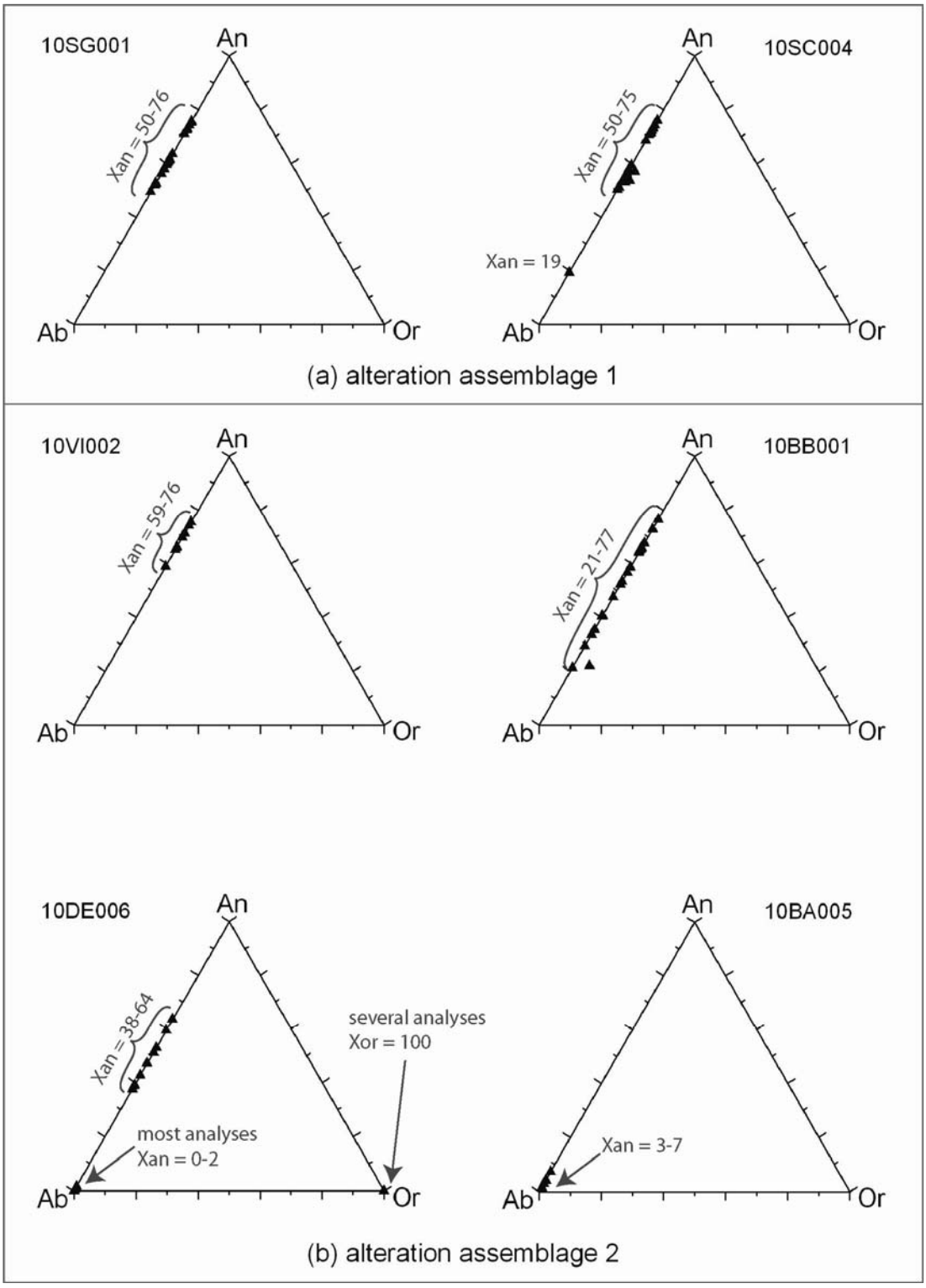

Figure 3.10: Feldspar ternary diagrams for samples of alteration assemblage 1 (a) and 2 (b).

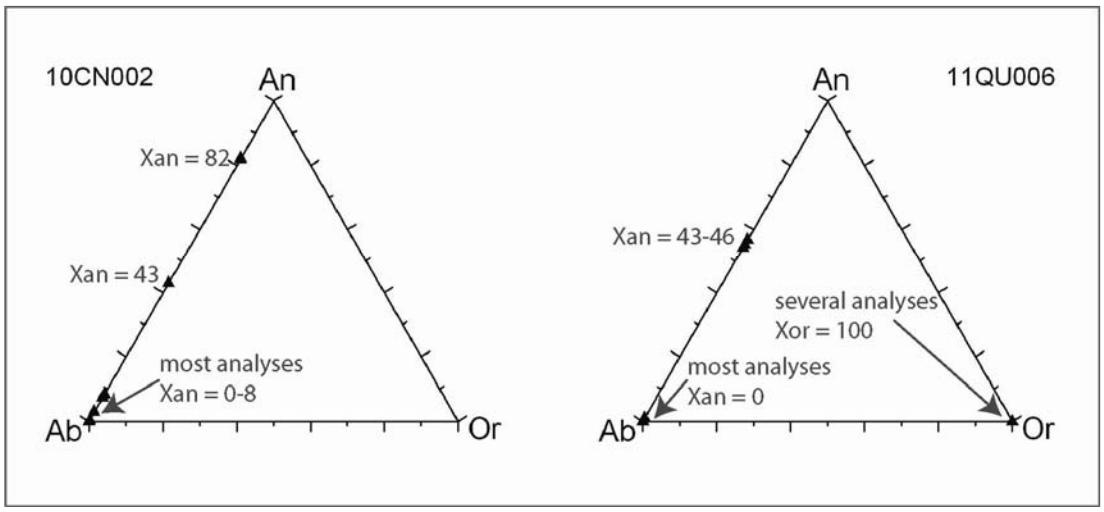

Figure 3.11: Feldspar ternary diagrams for samples of alteration assemblage 3.

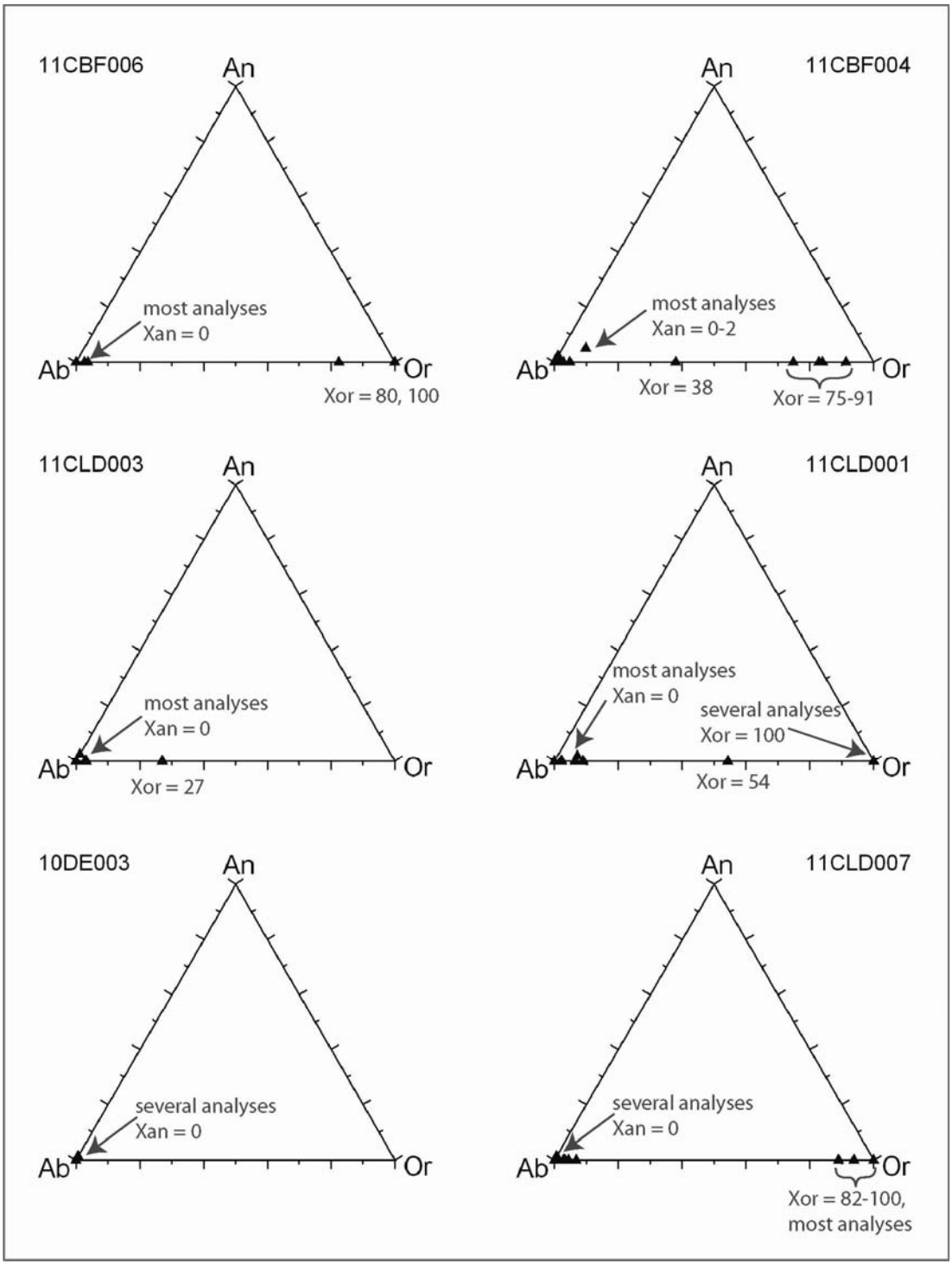

Figure 3.12: Feldspar ternary diagrams for samples of alteration assemblage 4.

are shown in Figure 3.11; and diagrams for samples of alteration assemblage 4 (five Caledonia samples and 10DE003) are included in Figure 3.12. Zoning of plagioclase grains with anorthite-rich cores and albite-rich rims could be observed in some less altered samples, mostly in coarse grains. An example of typical zoning observed in sample 10SG001 in a back scatter electron (BSE) image is shown in Figure 3.13. Lighter elements (i.e., Na^{+} in albite) appear darker than heavier elements (i.e., Ca^{2+} in anorthite) in BSE images. Spectral mapping was done on this grain, and the expected zoning was confirmed by analyses of several small areas in the core and along the rim of the sample as shown in Figure 3.13.

3.4 Pyroxene

Both orthopyroxene and clinopyroxene minerals were observed in thin section. Orthopyroxene occurs in the least altered samples, often surrounding relict olivine. The predominant pyroxene observed is clinopyroxene and is often present as part of the groundmass, interstitial to plagioclase. Grains (ranging from 0.5 to 2 mm) are often much larger than plagioclase grains, effectively surrounding several plagioclase grains (Figure 3.14). A few pyroxene phenocryst glomerations were noted. Intensely altered, brecciated, and many amygdaloidal samples either contain very fine fragments of relict clinopyroxene or none at all.

Clinopyroxene appears clear to light brown in PPL, sometimes showing two cleavage directions intersecting at approximately 90°. It is biaxial positive with up to high second order interference colors. The clinopyroxene observed displays inclined extinction with extinction angles of approximately 50°. Orthopyroxene can appear very similar to clinopyroxene under the microscope and was positively identified using microprobe analysis.

Pyroxenes were analyzed using EDS analyses in ten samples: 10SG001, 10SC004, 10VI002, 10BB001, 10DE006, 10FJ005, 11CBF006, 11CBF004, 10CN002, and 10QU006. They were classified using the pyroxene quadrilateral (Morimoto et al., 1988) as described in Appendix B.

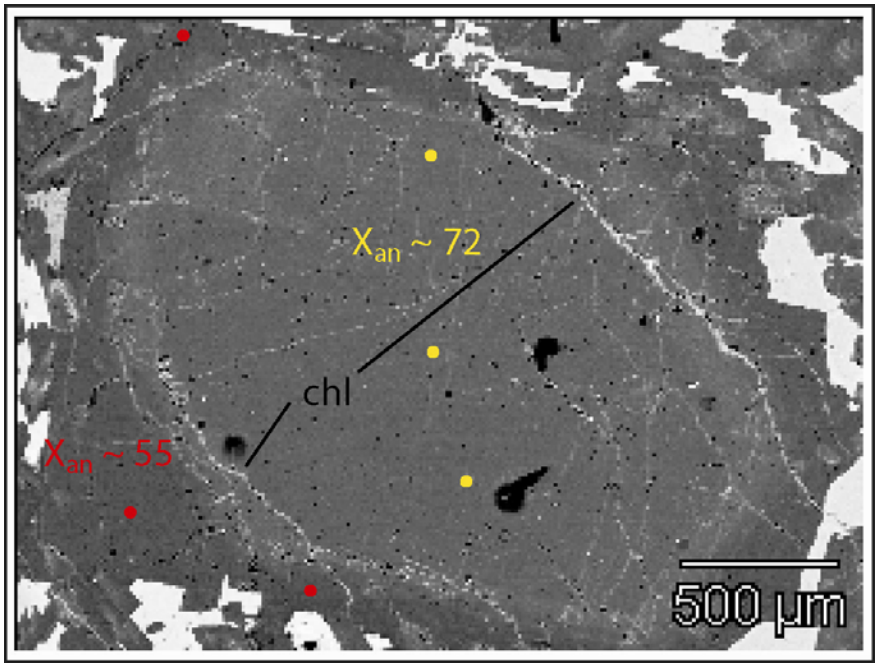

Figure 3.13: BSE image of typical plagioclase zoning in relatively fresh samples. Example from sample 10SG001. Note the albite-rich rim and anorthite-rich core. Chlorite (chl) is present along cracks in the grain.

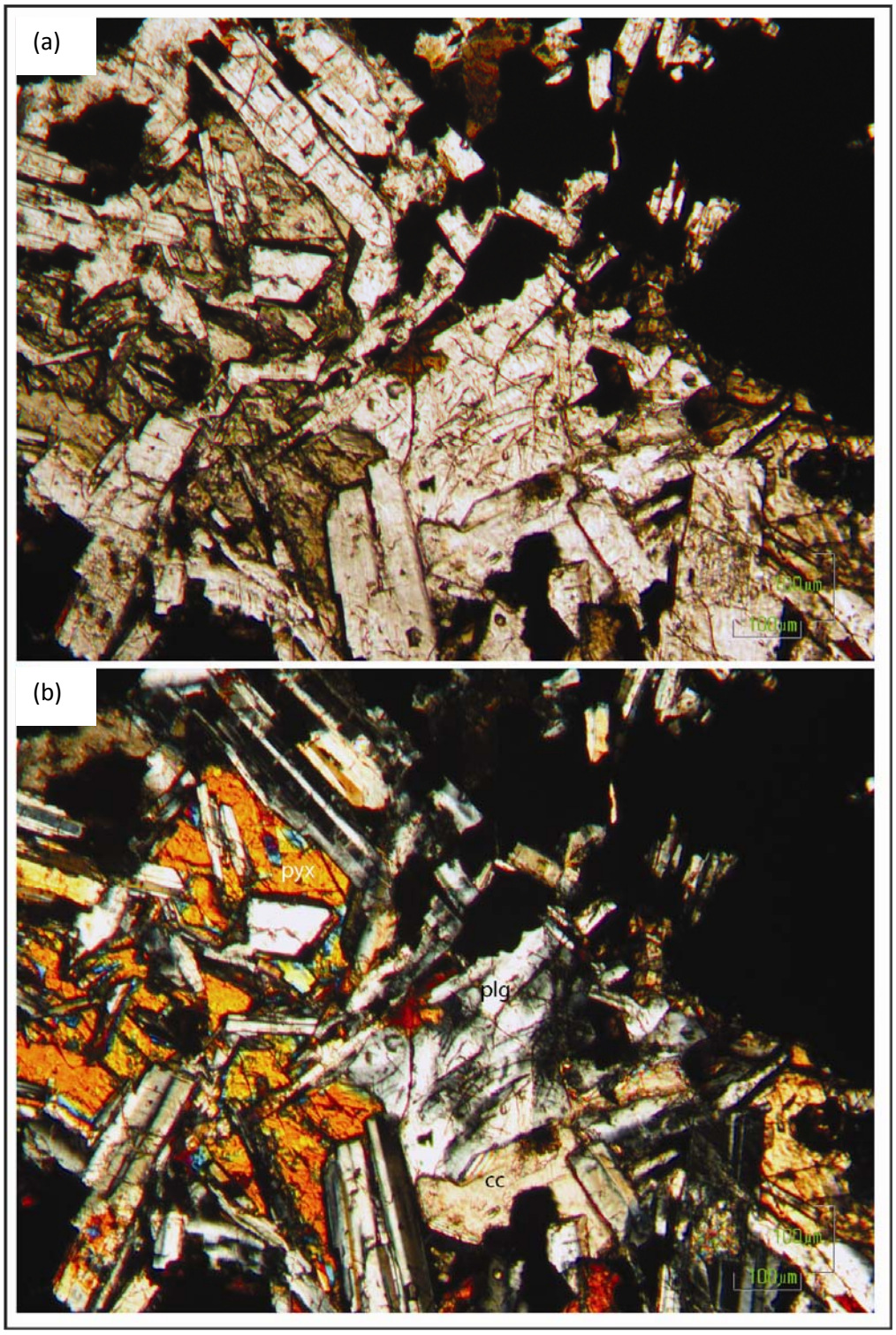

Figure 3.14: Example of pyroxene surrounding plagioclase.
As seen in PPL (a) and under crossed polarizers (b) in sample 10VI002 (alteration assemblage 2). Identifiers included in (b) to distinguish different minerals.

Electron microprobe raw data with recalculated cations and atomic percentages of Ca, Mg, and ∑Fe are shown for selected samples in Table 3.9. All other results are included in Appendix G. Cations were recalculated based on six oxygen atoms PFU. The classification diagram with all pyroxene data is shown in Figure 3.15. Diagrams by sample are shown in Figures 3.16 and 3.17 in order of progressing alteration assemblage. The two freshest appearing samples contain orthopyroxene and pigeonite; in more altered samples only augite is present.

3.5 Chlorite

Chlorite is the most common alteration product in these rocks. It occurs as replacement of former olivine grains, plagioclase grains, pyroxene grains, and as amygdule fillings. It can appear feathery to fibrous, spherulitic, granular, and sheety. It often contains small specks of sphene, and sheety varieties replacing former olivine (?) commonly surround dark reddish iddingsite (?) located along cracks. Chlorite forms along cracks in plagioclase, and characteristically replaces the plagioclase core or entire grains in more altered samples. Figure 3.18 shows sheety, fibrous, and granular chlorite in a single microprobe sample area.

In PPL, colors range from light to very dark green. Some chlorite in amygdules appears yellowish-green. Anomalous blue interference colors under crossed polarizers are common. The relief is moderate, and chlorite occurs as biaxial positive and negative varieties.

Chlorite is present in most samples. Only some extremely carbonated samples (11CLD005, 10QU006, and 10TR004) lack chlorite. Selected electron microprobe analyses with recalculated cations and Fe/(Fe+Mg) PFU are given in Table 3.10. Cations were recalculated based on 28 oxygen atoms PFU. A complete table of chlorite analyses is included in Appendix G. Chlorite classifications are plotted in Figure 3.19 for all thin sections by alteration assemblage. Samples from the Caledonia Mine are grouped together as “Caledonia”. Most chlorites classify as

Table 3.9: Electron microprobe analyses of selected pyroxene samples. Cation recalculations based on 6 oxygen atoms PFU.

	Sample	10SC004 -2-2-1	10SG001 -3-1-10	10BB001 -3-2-7	11CBF006 11-06_041
	Assemblage	1	1	2a	4a
	Na_2O	-**	-**	0.8	-**
	MgO	20.8	14.8	14.2	15.7
	Al_2O_3	0.4	0.3	2.4	2.2
	SiO_2	54.0	51.0	50.2	52.4
	CaO	1.9	3.4	18.3	18.4
	TiO_2	0.3	0.3	1.7	0.7
	Cr_2O_3	-**	-**	-**	0.6
	MnO	0.6	0.8	0.4	-**
	FeO	22.0	29.3	12.0	10.0
	∑	100.0	100.0	100.0	100.0
	Si	2.0	2.0	1.9	1.9
	Al	-	-	0.1	0.1
	∑	2.0	2.0	2.0	2.0
	Al	-	-	-	-
	Fe^{3+}	-	-	0.1	-
	Ti	-	-	0.1	-
M1	Cr	-	-	-	-
	Mg	1.0	0.9	0.8	0.9
	Fe^{2+}	-	0.1	0.1	0.1
	Mn	-	-	-	-
	∑	1.0	1.0	1.1	1.0
	Mg	0.2	-	-	-
	Fe^{2+}	0.7	0.8	0.2	0.3
	Mn	-	-	-	-
M2	Ca	0.1	0.1	0.7	0.7
	Na	-	-	0.1	-
	K	-	-	-	-
	∑	1.0	0.9	1.0	1.0
	Atomic percentages				
	Mg	60	43	41	46
	∑Fe*	36	49	20	16
	Ca	4	7	38	38

*$\sum Fe = Fe^{2+} + Fe^{3+} + Mn$

** not analyzed

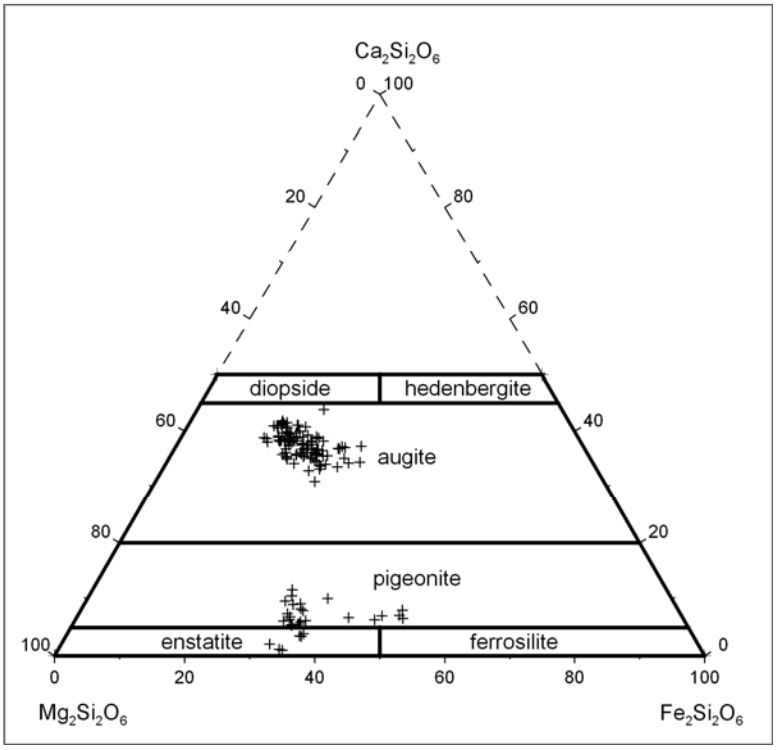

Figure 3.15: Pyroxene quadrilateral with all data.

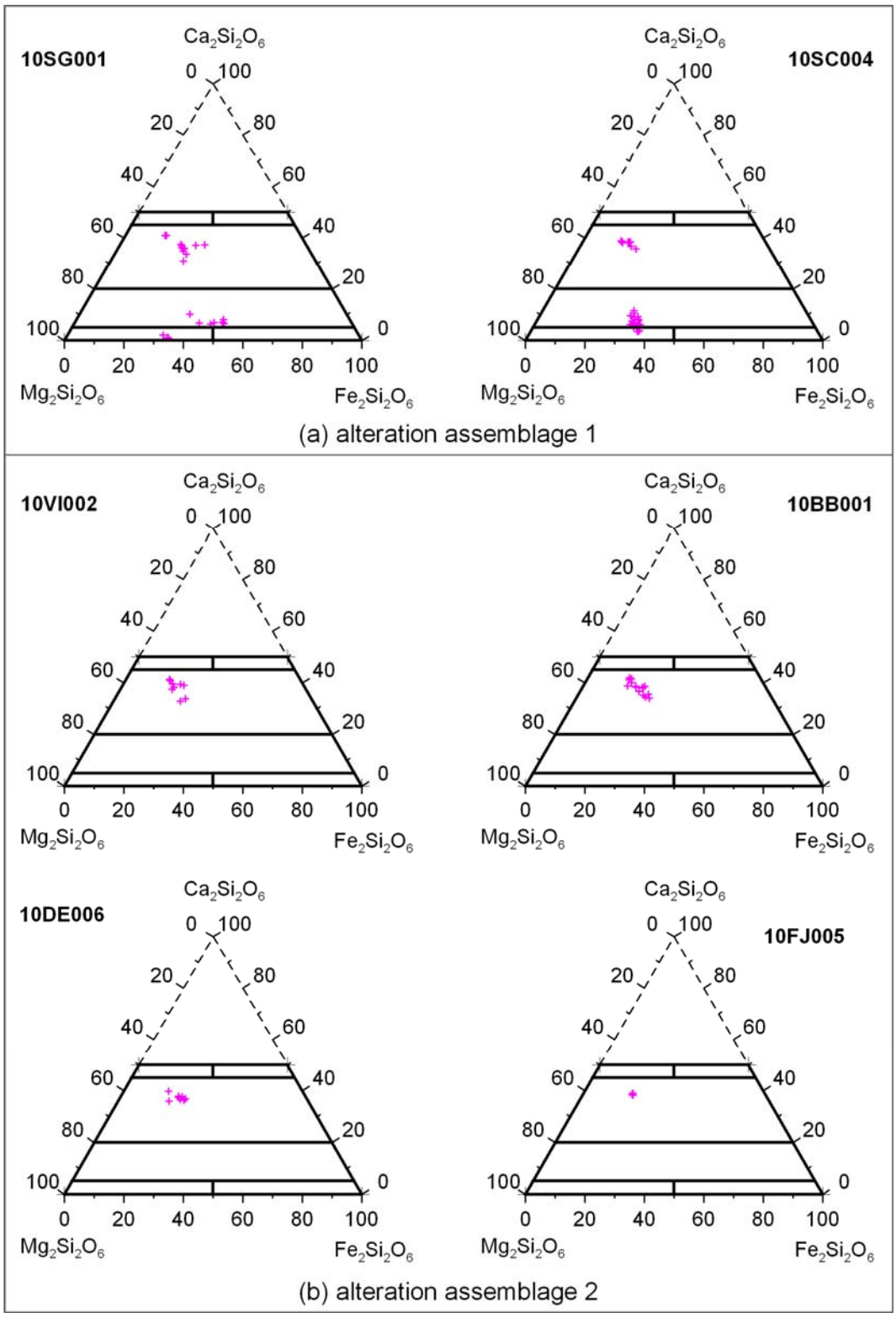

Figure 3.16: Pyroxene quadrilaterals for samples of alteration assemblages 1 (a) and 2 (b).

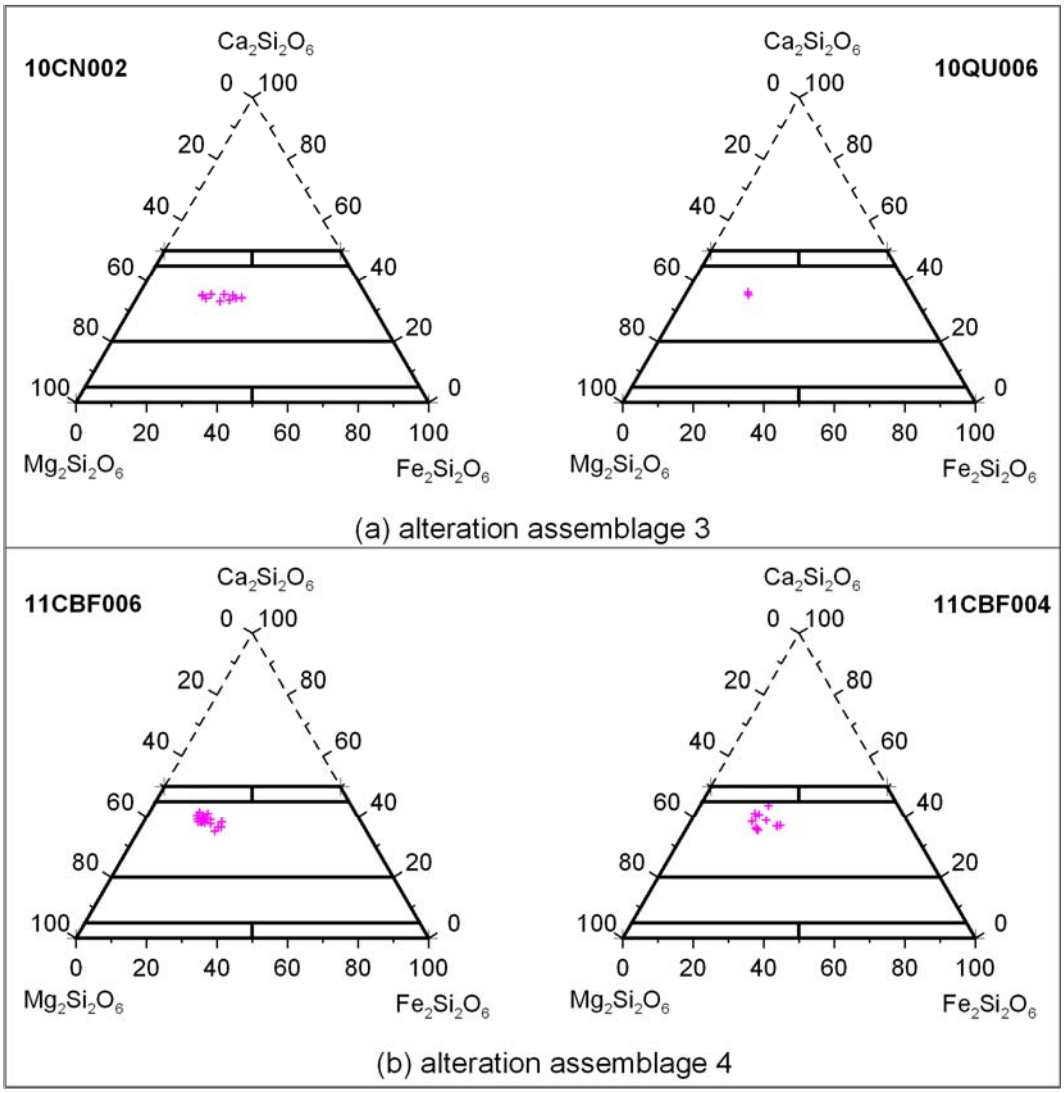

Figure 3.17: Pyroxene quadrilaterals for samples of alteration assemblages 3 (a) and 4 (b).

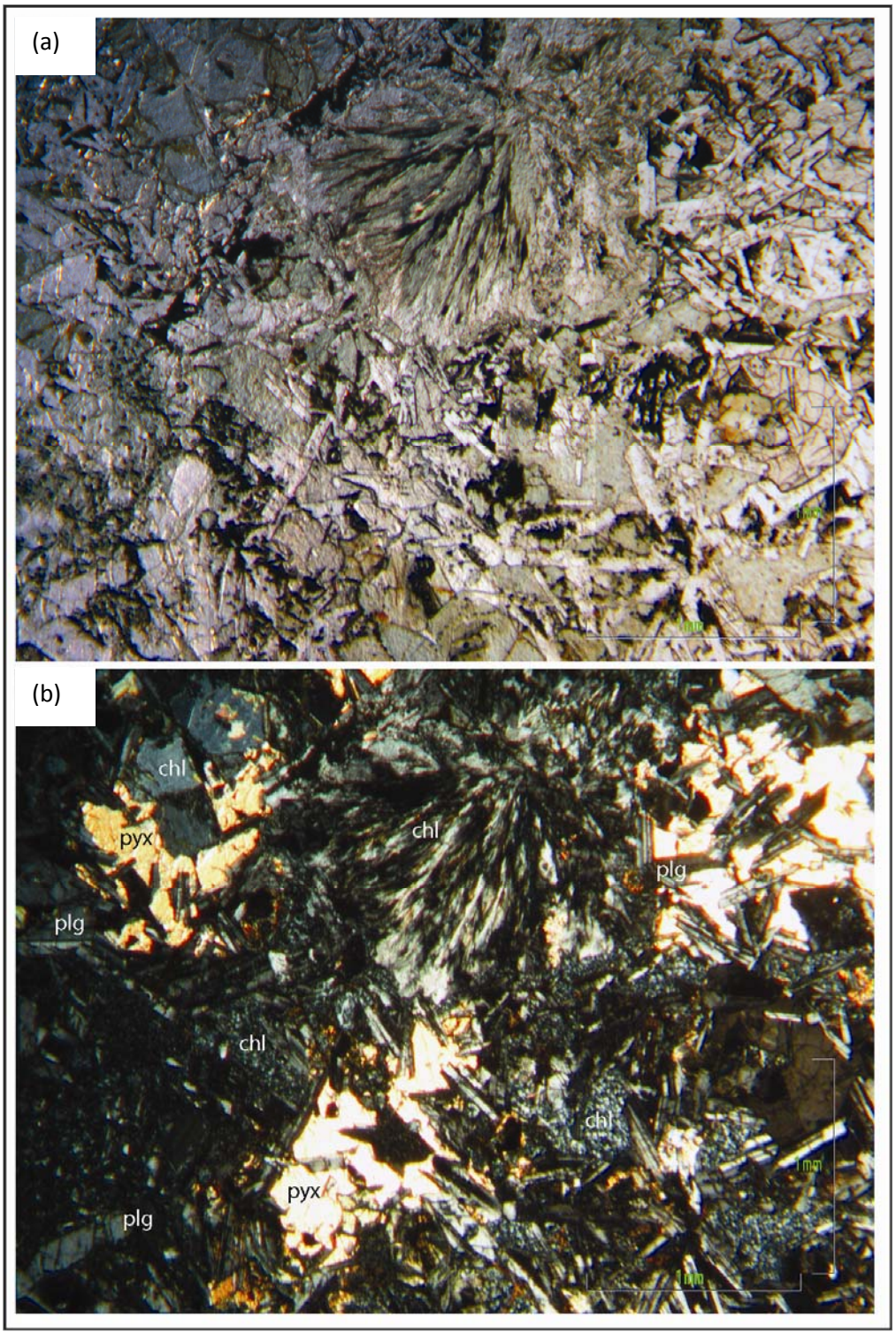

Figure 3.18: Example of different chlorite textures.
As seen in PPL (a) and under crossed polarizers (b) in sample 10BB001 (alteration assemblage 2).

Table 3.10: Electron microprobe analyses of selected chlorite group samples.
Cation recalculations based on 28 oxygen atoms PFU.

Sample	10SG001 -1-3-3	10SC004 -2-2-4	10BB001 -1-1-1	10DE006 -5-2-5	10BA005 -6-1-7	10DE003 -2-1-4	11CLD001 10-22_023
MgO	10.9	14.2	20.4	25.6	24.1	27.8	23.2
Al_2O_3	13.6	17.1	15.7	18.0	19.6	15.4	18.8
SiO_2	35.6	35.8	36.0	37.8	36.6	42.7	33.6
CaO	1.2	1.7	0.4	0.6	0.3	0.9	-**
MnO	0.4	0.5	0.9	0.6	-**	0.5	-**
FeO	38.4	30.9	26.6	17.6	19.4	12.7	24.4
∑	100.1	100.2	100.0	100.2	100.0	100.0	100.0
Si	6.9	6.7	6.6	6.6	6.4	7.3	6.1
Al	1.1	1.3	1.4	1.4	1.6	0.7	2.0
∑	8.0	8.0	8.0	8.0	8.0	8.0	8.1
Al	2.1	2.5	2.0	2.3	2.4	2.4	2.1
Fe*	6.3	4.9	4.1	2.6	2.8	1.8	3.7
Mg	3.2	4.0	5.6	6.7	6.3	7.0	6.2
Mn	0.1	0.1	0.1	0.1	-	0.1	-
Ca	0.2	0.3	0.1	0.1	0.1	0.2	-
∑	11.9	11.8	11.9	11.8	11.6	11.5	12.0
Fe/(Fe+Mg)	0.66	0.55	0.42	0.28	0.31	0.20	0.37

*all Fe as Fe^{2+}

** not analyzed

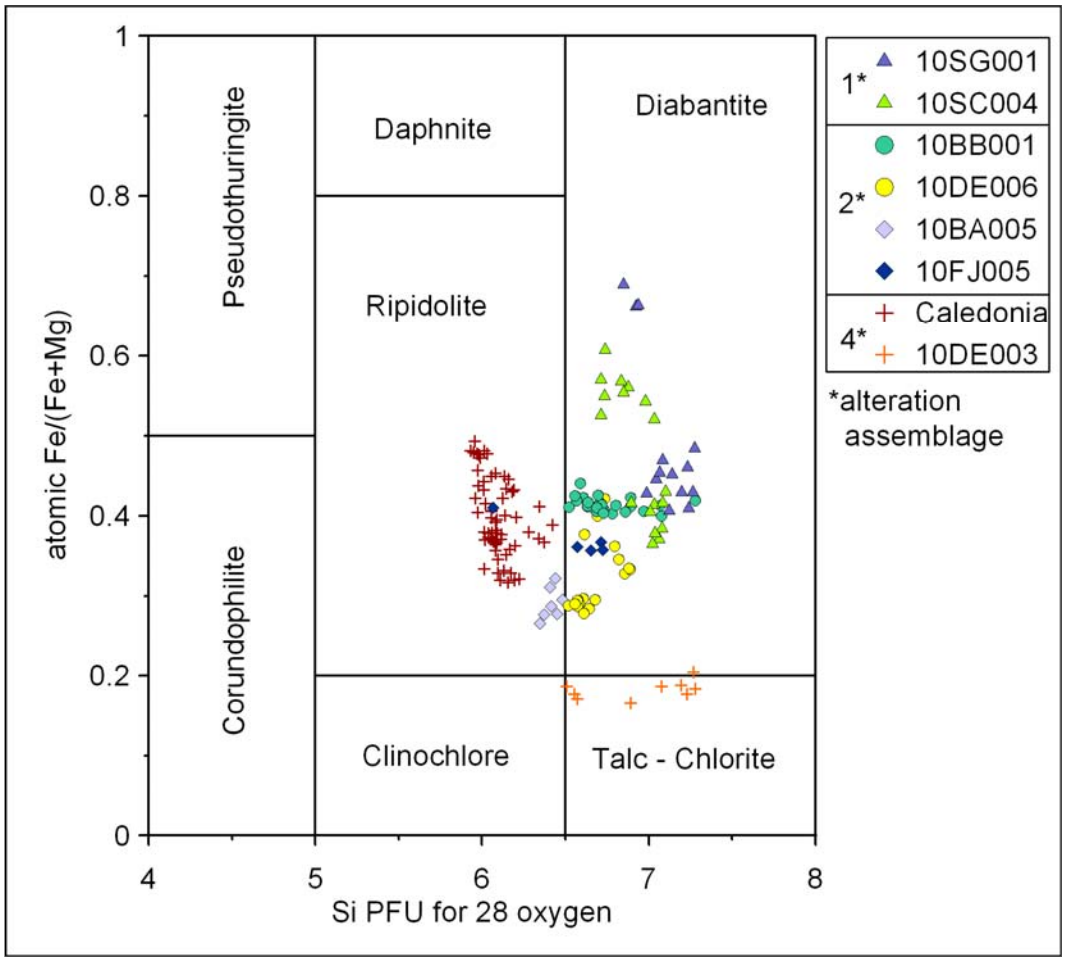

Figure 3.19: Classification of chlorite analyses for all samples.
Data are separated by alteration assemblage.

diabantite, ripidolite, and some as talc chlorite. The two freshest samples (10SC004 and 10SG001) have two chlorite populations: one with higher atomic Fe/(Fe+Mg) values and slightly lower silica PFU and one population with lower atomic Fe/(Fe+Mg) and slightly higher silica PFU. The chlorite with higher Fe/(Fe+Mg) was found interstitial to other minerals, whereas the chlorite with lower Fe/(Fe+Mg) was found as plagioclase alteration.

Overall, the Fe/(Fe+Mg) content in diabantite appears to decrease with increasing alteration assemblage (between stages 1 and 2b). With the appearance of pumpellyite, the Fe/(Fe+Mg) content in chlorites increases and the Si PFU decreases, yielding ripidolite. In 10FJ005, chlorite occurs in amygdules with most amygdules filled with diabantite, some containing ripidolite in the center. The chlorite in 10DE003 is present as alteration of pumpellyite in amygdules, and along rims of these amygdules surrounding pumpellyite.

Chlorite classifications for the different samples of the Caledonia Mine are plotted separately in Figure 3.20. The CBF samples contain pyroxene, the CLD samples do not contain pyroxene. Again, the overall trend of the samples shows a decrease in Fe/(Fe+Mg) with increasing alteration assemblage, with the exception of 11CBF004, which shows lower Fe/(Fe+Mg) values and higher Si PFU than all other Caledonia samples.

3.6 Mica Group

Sericite is extremely fine-grained muscovite that occurs in slightly altered samples as alteration of plagioclase cores (e.g., Figure 3.7). Sericite alteration is commonly accompanied by interstitial calcite. Some coarser grained muscovite was observed in an extremely altered sample (10TR004) as replacement of former pyroxene (?). Sericite is colorless in PPL and shows low moderate relief. It often exhibits first to third order interference colors. An optic sign could not be determined due to the very small size of the grains.

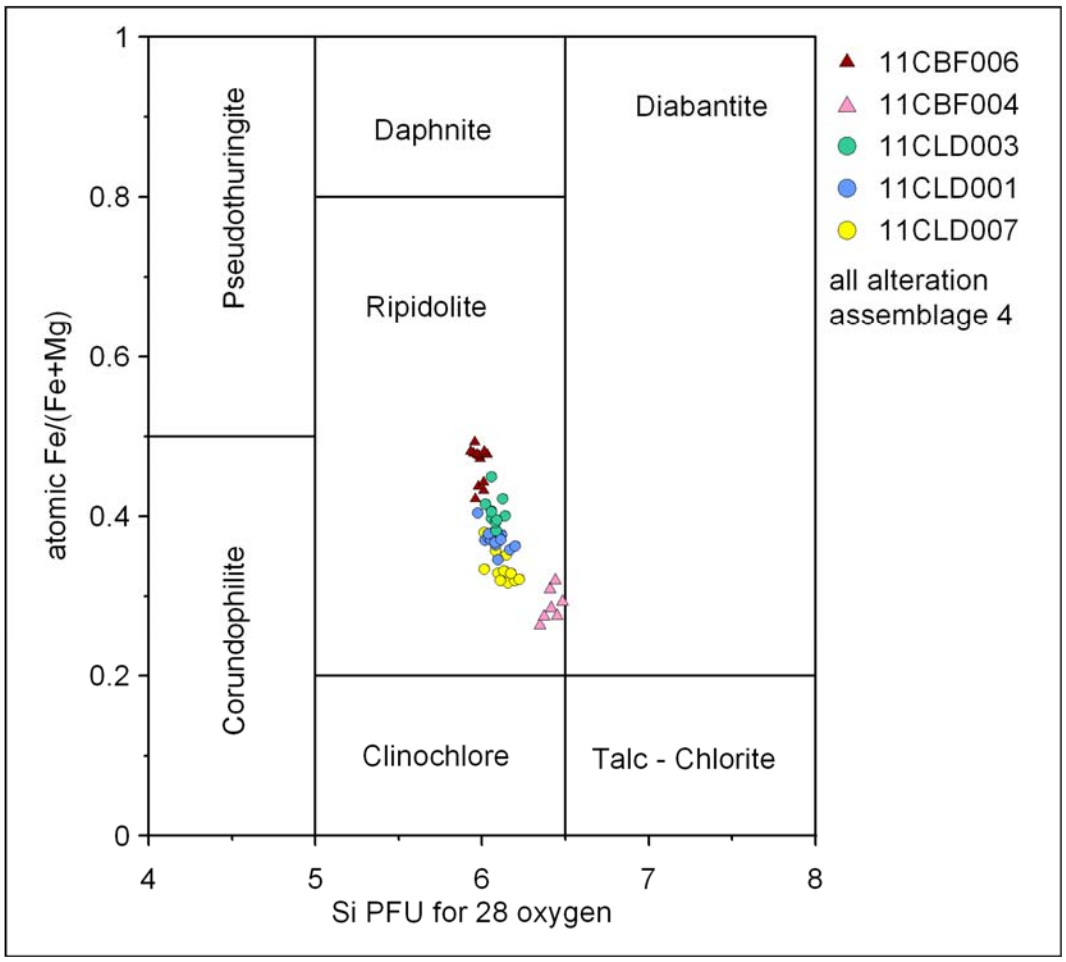

Figure 3.20: Classification of chlorite analyses for Caledonia samples.

Only few sericite grains could be analyzed using the microprobe due to the extremely fine-grained nature of the mineral. Analyses were collected for sericite alteration of a plagioclase grain in 10DE006, and for muscovite in 10TR004 (Table 3.11). Cation recalculations were based on 22 oxygen atoms PFU. Values for K^+ and Na^+ were likely underestimated due to the large beam current used. The chemical formula for pure muscovite is $K_2Al_4[Si_6Al_2O_{20}](OH,F)_4$ for which a coupled substitution [2 Al^{3+} <=> 1 (Mg, Fe^{2+}) + 1 Si^{4+}] can occur. The muscovite analyses contain far too little Al^{3+} (<< 6 PFU) and too much Si^{4+} relative to ($Mg+Fe^{2+}$), which probably reflects the poor quality of these analyses and not strange mineral chemistry (Figure 3.21).

3.7 Epidote

Epidote occurs as very fine grains replacing plagioclase cores, and as fine (< 0.01 mm) to coarse (1 mm), subhedral to euhedral minerals in amygdules where it commonly lines the rims of the amygdule. It occurs with pumpellyite, chlorite, quartz, and sometimes with copper. Figure 3.22 shows coarse epidote intergrown with pumpellyite and surrounded by quartz.

Epidote is slightly pleochroic in PPL with colors ranging from pistachio green to pale yellow. Epidote shows high positive relief, has second to third order interference colors, and is biaxial negative.

Epidote was analyzed using the microprobe in seven samples: 11CLD001, 11CLD003, 11CLD005, 11CBF006, 10CN002, 10QU006, and 10DE003. Recalculated cations (based on 12.5 oxygen PFU) were used to calculate the “pistacite” component $Fe^{3+}/(Al+Fe^{3+})$. Selected analyses are shown in Table 3.12; the complete set of analyses is included in Appendix G. The calculated pistacite component was plotted on a histogram for all data (Figure 3.23). The REEs lanthanum and cerium were identified in one sample (10QU006). The pistacite component of analyzed epidote ranges from 17 to 40, with most analyses close to the theoretical

Table 3.11: Electron microprobe analyses of mica group minerals.
Cation recalculations based on 22 oxygen atoms PFU.

Sample	10DE006 -8-2-1	10DE006 -8-2-2	10TR004 -3-1-1	10TR004 -3-1-2	10TR004 -3-1-3	10TR004 -4-1-1	10TR004 -4-1-2	10TR004 -4-1-3	10TR004 -4-1-4
Na_2O	-**	-**	-**	-**	-**	-**	0.4	-**	-**
MgO	-**	1.8	0.6	0.6	0.4	0.4	0.7	0.6	0.6
Al_2O_3	38.6	31.1	35.8	35.5	35.7	35.9	35.5	35.8	36.1
SiO_2	51.6	55.2	54.9	54.6	55.2	54.5	53.5	54.0	53.7
K_2O	8.9	8.6	7.0	7.3	6.8	7.5	7.9	7.8	7.4
FeO	1.0	3.3	1.8	2.0	1.9	1.8	2.0	1.9	2.2
∑	100.1	100.0	100.1	100.0	100.0	100.1	100.0	100.0	100.0
Si	6.4	7.0	6.8	6.8	6.8	6.7	6.7	6.7	6.7
Al	1.6	1.0	1.2	1.2	1.2	1.3	1.3	1.3	1.3
∑	8.0	8.0	8.0	8.0	8.0	8.0	8.0	8.0	8.0
Al	4.1	3.6	4.0	4.0	4.0	4.0	3.9	4.0	4.0
Mg	-	0.3	0.1	0.1	0.1	0.1	0.1	0.1	0.1
Fe*	0.1	0.4	0.2	0.2	0.2	0.2	0.2	0.2	0.2
∑	4.2	4.3	4.3	4.3	4.3	4.3	4.2	4.3	4.3
Na	-	-	-	-	-	-	0.1	-	-
K	1.4	1.4	1.1	1.2	1.1	1.2	1.3	1.2	1.2
∑	1.4	1.4	1.1	1.2	1.1	1.2	1.4	1.2	1.2
Fe+Mg	0.1	0.7	0.3	0.3	0.3	0.3	0.3	0.3	0.3

*all Fe as Fe^{2+}

** not analyzed

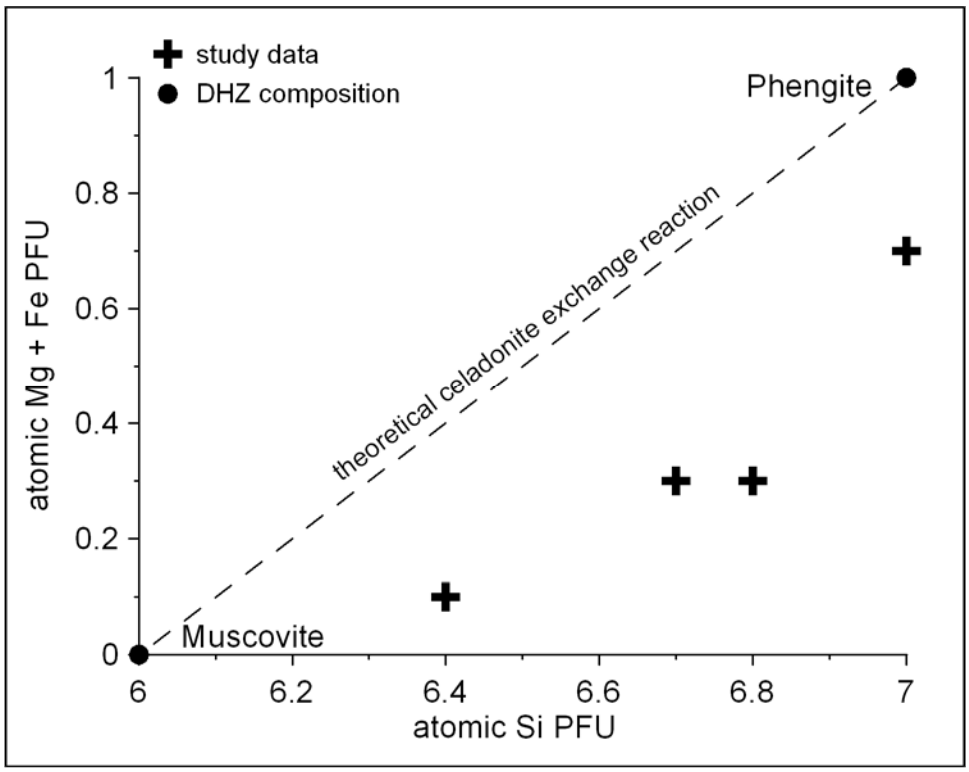

Figure 3.21: Compositions of mica group minerals.
With theoretical minerals from Deer et al. (DHZ, 1992).

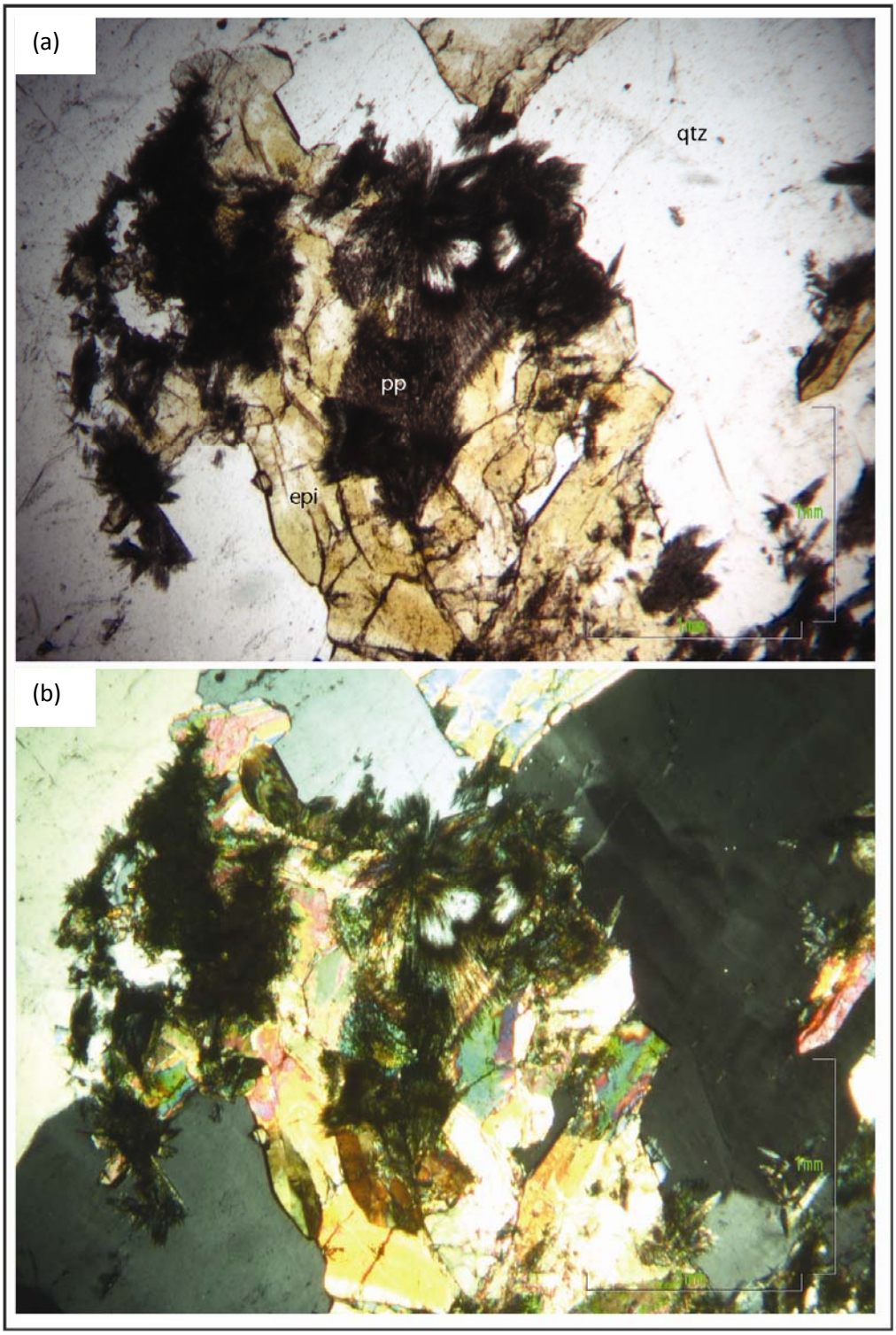

Figure 3.22: Coarse-grained epidote with pumpellyite and quartz in amygdule. As seen in PPL (a) and under crossed polarizers (b) in sample 11CBF004 (alteration assemblage 4).

Table 3.12: Electron microprobe analyses of selected epidote group minerals. Cation recalculations based on 12.5 oxygen atoms PFU.

Sample	10QU006 -5-2-2	11CBF006 -5-1-10	11CLD003 10-29_01	11CLD001 10-22_041	10DE003 -4-1	11CLD005 02-25-008
Al_2O_3	20.6	21.0	19.7	21.3	23.0	25.9
SiO_2	39.6	39.5	38.9	39.4	39.8	40.2
CaO	19.6	23.6	22.6	22.9	23.2	23.3
MnO	0.5	-*	-*	-*	0.5	-*
FeO	15.1	16.0	18.8	16.4	13.5	10.7
La_2O_3	1.6	-*	-*	-*	-*	-*
Ce_2O_3	3.0	-*	-*	-*	-*	-*
∑	100.0	100.0	100.0	100.0	100.0	100.1
Si	3.2	3.1	3.0	3.1	3.1	3.1
Al	-	-	-	-	-	-
∑	3.2	3.1	3.0	3.1	3.1	3.1
Al	2.0	1.9	1.8	2.0	2.1	2.3
Fe^{3+}	0.6	0.9	1.2	0.9	0.7	0.5
MnO	-	-	-	-	-	-
Fe^{2+}	0.5	0.1	-	0.1	0.1	0.2
∑	3.1	2.9	3.1	3.0	2.9	3.0
Fe^{2+}	-	-	-	-	-	-
Ca	1.7	2.0	1.8	1.9	1.9	1.9
La^{3+}	0.1	-	-	-	-	-
Ce^{3+}	0.1	-	-	-	-	-
∑	1.9	2.0	1.8	1.9	1.9	1.9
$Fe^{3+}/(Fe^{3+}+Al)$	0.23	0.32	0.40	0.31	0.25	0.18

*not analyzed

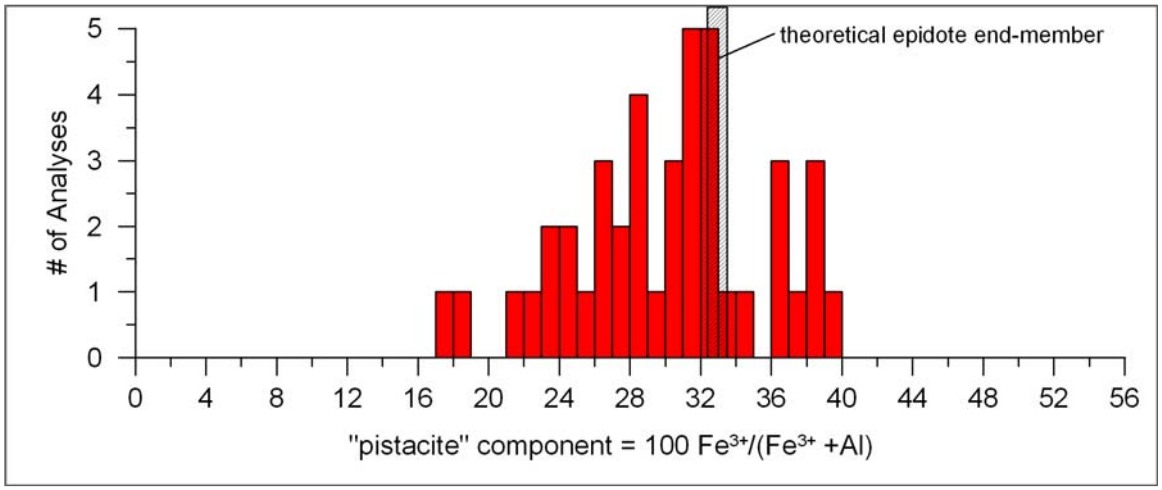

Figure 3.23: Histogram of "pistacite" component in analyzed epidote.
Theoretical epidote end-member is shown at 33% pistacite component.

end-member epidote (pistacite component = 33%) with the formula $Ca_2Fe^{3+}Al_2Si_3O_{11}(OH)$.

3.8 Pumpellyite

Pumpellyite commonly occurs as plagioclase alteration, interstitially in gabbroic samples, and in amygdules. It can be acicular (e.g., Figure 3.22), and appear cloudy where extremely fine-grained. As plagioclase replacement, it can appear radiating. It ranges between <0.1 mm to 1.5 mm. Figure 3.24 shows coarse-grained pumpellyite with chlorite in an amygdule.

Pumpellyite is pleochroic, ranging from clear (oriented with elongation along north-south) to distinctly dark green or sometimes slight brown (elongation along east-west) in PPL. It has extremely high relief and low birefringence, and commonly displays anomalous interference colors.

Pumpellyite was analyzed using microprobe analysis in seven samples: 10CN002, 10QU006, 11CBF004, 11CLD003, 11CLD001, 10DE003, and 11CLD007. Selected analyses are shown in Table 3.13 with increasing Fe content; the complete analyses are included in Appendix G. Cation recalculations were based on three silica atoms PFU. Pumpellyite analyses show relatively consistent compositions (Figure 3.25).

3.9 Prehnite

Prehnite occurs in extremely altered, massive, amygdular, or brecciated samples. It often occurs with pumpellyite and chlorite, and sometimes with epidote. The matrix in brecciated samples commonly consists of prehnite and calcite. Prehnite can range from <0.1 mm to 2 mm. It occurs as interstitial fillings, breccia matrix, and plagioclase replacement (Figure 3.8). Figure 3.26 shows fine- and coarse-grained prehnite in one microprobe sample area. Prehnite is clear in PPL with moderate positive relief. It has up to higher second order interference colors, and in certain orientations displays anomalous blue-gray interference colors. Prehnite commonly appears bladed in radiating leaves and is biaxial positive.

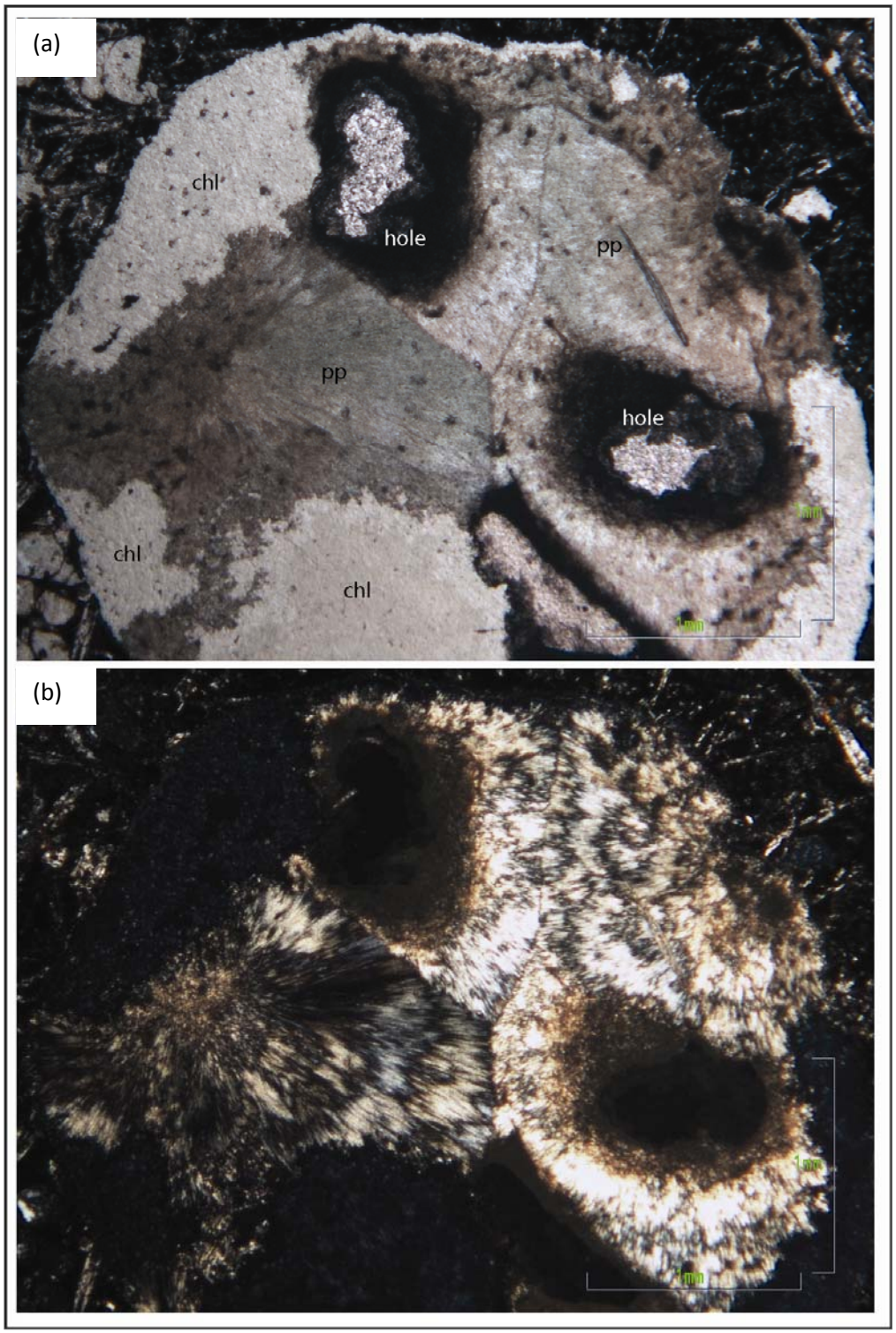

Figure 3.24: Coarse-grained pumpellyite with chlorite in amygdule.
As seen in PPL (a) and under crossed polarizers (b) in sample 11CLD007 (alteration assemblage 4).

Table 3.13: Electron microprobe analyses of selected pumpellyite minerals. Cation recalculations based on 3.0 silica atoms PFU.

Sample	10CN002 -4-2-1	10CN002 -5-1-6	10QU006 -6-1-2	11CLD007 -7-1-9
MgO	2.8	3.2	2.2	2.7
Al_2O_3	20.2	18.4	21.4	23.7
SiO_2	41.2	41.1	40.7	41.2
CaO	23.3	23.1	23.4	23.8
FeO	12.5	14.2	12.3	8.7
∑	100.0	100.0	100.0	100.1
Si	3.0	3.0	3.0	3.0
Al	-	-	-	-
∑	3.0	3.0	3.0	3.0
Al	1.7	1.6	1.9	2.0
∑	1.7	1.6	1.9	2.0
Al	-	-	-	-
Mg	0.3	0.4	0.2	0.3
Fe*	0.8	0.9	0.8	0.5
∑	1.1	1.3	1.0	0.8
Ca	1.8	1.8	1.8	1.9
∑	1.8	1.8	1.8	1.9
Al	62	57	65	71
Fe	27	31	27	19
Mg	11	12	8	10

* all Fe as Fe^{2+}

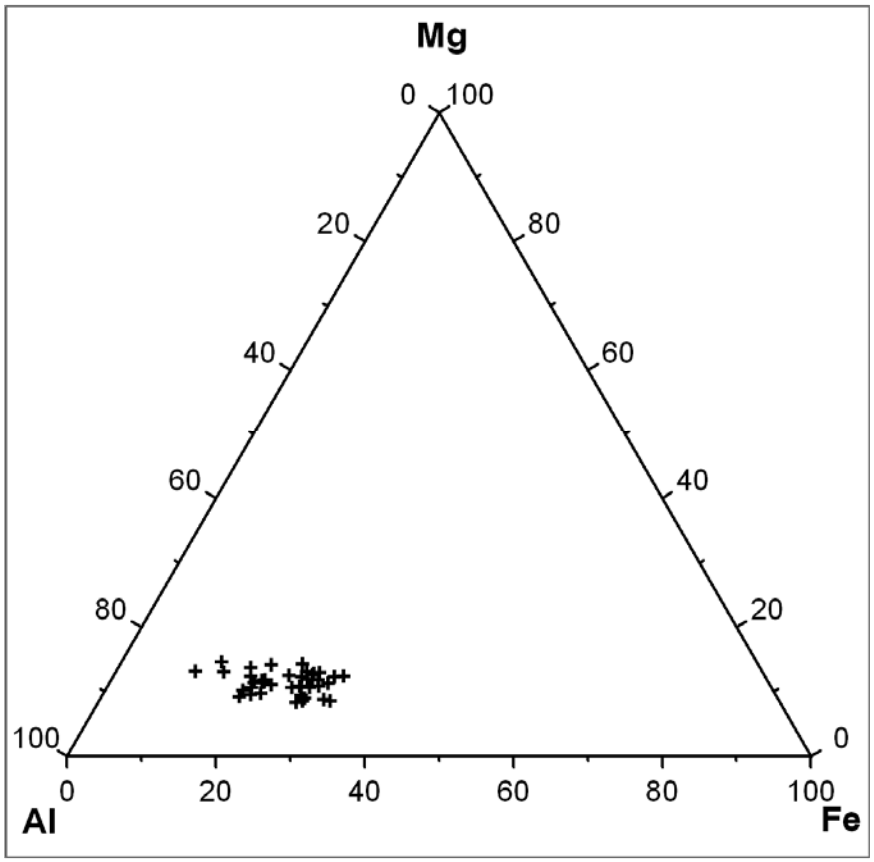

Figure 3.25: Fe, Mg, and Al ternary plot of all pumpellyite analyses.

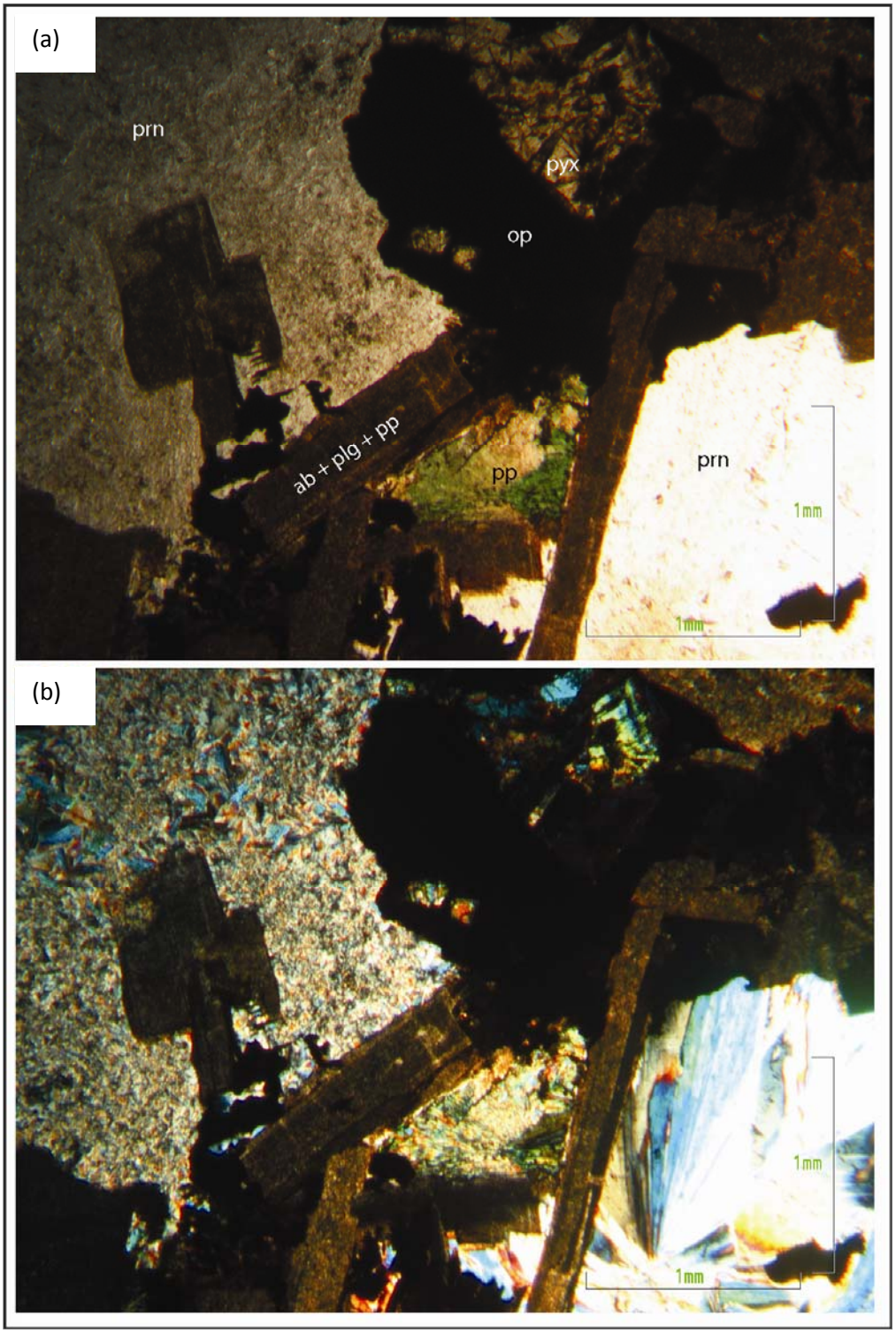

Figure 3.26: Interstitial prehnite and pumpellyite in gabbroic sample.
As seen in PPL (a) and under crossed polarizers (b) in 10CN002 (alteration assemblage 3).

The microprobe was used to analyze prehnite in samples 10CN002 and 10QU006. Table 3.14 shows selected analyses; remaining analyses are included in Appendix G. Cations recalculations were based on eleven oxygen atoms PFU. The amount of Al^{3+} and Fe^{3+} cations in the X site (see Appendix B) can vary, so analyses were plotted on a ternary diagram with Al^{3+}, Fe^{3+}, and Ca^{2+} (Figure 3.27). Analyses were not differentiated by alteration assemblage since both samples are from alteration assemblage 3.

3.10 Copper Minerals

Native copper was observed as extremely fine specks (<0.01 mm) in many samples throughout, with coarser copper (up to 0.5 cm) commonly present in amygdules or the matrix of brecciated samples. Copper appears opaque in PPL and bright copper-red under reflected light.

10TR004 was the only sample containing copper sulfides (Figure 3.28 and Table 3.15), present along a carbonate vein containing ankerite and calcite. Both chalcocite and covellite occur, apparently as alteration and not as weathering minerals.

3.11 Quartz

Quartz occurs as amygdule fillings and in some samples in veinlets. It can be subhedral to euhedral, and commonly occurrs with epidote. Quartz is colorless in PPL, has very low relief, and first order interference colors.

3.12 Carbonate

Carbonate occurs interstitially or as plagioclase alteration, commonly with sericite. Coarse-grained carbonate is present in interstices, in breccia matrix with prehnite, or in amygdules. Carbonate in amygdules is subhedral to euhedral, either filling the entire amygdule, or with other minerals.

Carbonate has low to moderate relief, which varies with orientation. It appears clear in PPL and is biaxially negative with inclined extinction angles and extremely high

Table 3.14: Electron microprobe analyses of selected prehnite samples. Cation recalculations based on 11 oxygen atoms PFU.

Sample	10CN002 -1-1-1	10QU006 -2-1-3
Al_2O_3	19.1	20.0
SiO_2	47.1	46.6
CaO	25.8	26.0
FeO	8.0	7.4
∑	100.0	100.0
Si	3.1	3.1
Al	0.9	0.9
∑	4.0	4.0
Al	0.6	0.7
Fe^{3+}	0.4	0.4
∑	1.0	1.1
Ca	1.8	1.9
∑	1.8	1.9
Atomic percentages		
Al	22	23
Fe	15	14
Ca	63	63

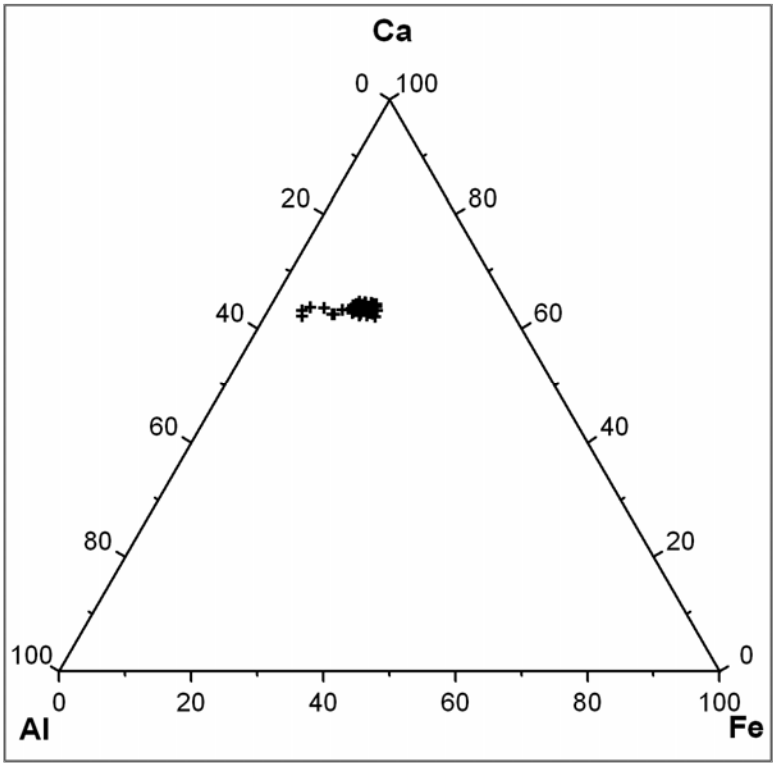

Figure 3.27: Al, Fe, and Ca ternary diagram for prehnite analyses. Only Al^{3+} and Fe^{3+} cations assigned to the X site are included.

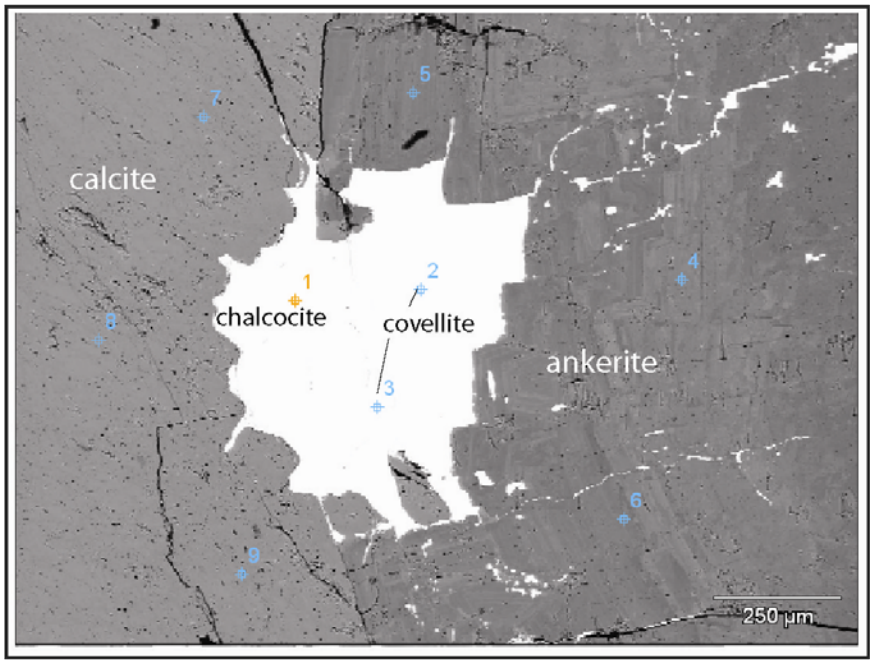

Figure 3.28: BSE image of copper sulfide in carbonate vein (sample 10TR004). Numbers refer to analyses given in Table 3.15 for the light colored copper sulfide, and in Table 3.16 for the surrounding, gray carbonates.

Table 3.15: Electron microprobe analyses of copper sulfide minerals.

Sample #	weight %		mol		ions in formula		mineral
	S	Cu	S	Cu	S	Cu	
10TR004-2-1-1	21.7	78.3	0.7	1.2	1	2	chalcocite
10TR004-2-1-2	33.5	66.5	1.1	1.1	1	1	covellite
10TR004-2-1-3	33.7	66.3	1.1	1.0	1	1	covellite

interference colors. Two perfect cleavage planes intersect at 60/120°.

Carbonate minerals identified petrographically were analyzed by EDS electron microprobe. Carbon was not measured because thin sections were carbon coated prior to analysis. Carbonate classifications for the samples are shown in Figure 3.29. Most carbonate minerals analyzed were calcite ($CaCO_3$); ankerite $Ca(Mg,Fe^{2+},Mn)(CO_3)_2$ is much less common and was only present in sample 10TR004 (e.g., Figure 3.28). Microprobe analyses are included in Table 3.16.

3.13 Zeolites

Only one zeolite was identified petrographically: it occurs along veins in a massive sample (10DE006). Zeolites may occur in other thin sections and may have been mistaken for quartz, although the distinctive shapes and negative relief of zeolite minerals make such unlikely.

The mineral identified as a zeolite appears pinkish to clear in PPL, has low to moderate negative relief, and low first order interference colors. The habit is somewhat feathery and elongate. Microprobe analysis was used to confirm the presence of zeolite. During the analyses, holes appeared where the beam was located on the sample, indicating sample vaporization. More volatile elements such as Na^+ were lost in this process, hence underestimated in the analyses. Zeolite analyses yielded mostly SiO_2 and Al_2O_3, with Na_2O, and very little CaO and FeO (Table 3.17). No cation recalculations were attempted due to the obvious sample degradation. The acicular appearance, combined with the lack of CaO and K_2O, and a Si:Al ratio of roughly 3:2 indicate the mineral is most likely natrolite.

3.14 Sphene

Sphene (theoretically $CaTiSiO_5$) commonly occurs in chlorite as small, <0.1 mm specks. It has extremely high relief with very high interference colors. Sphene was recognized in BSE images as small, bright specks, mostly in plagioclase or chlorite. Electron microprobe analyses and cation recalculations in Table 3.18 show analyzed

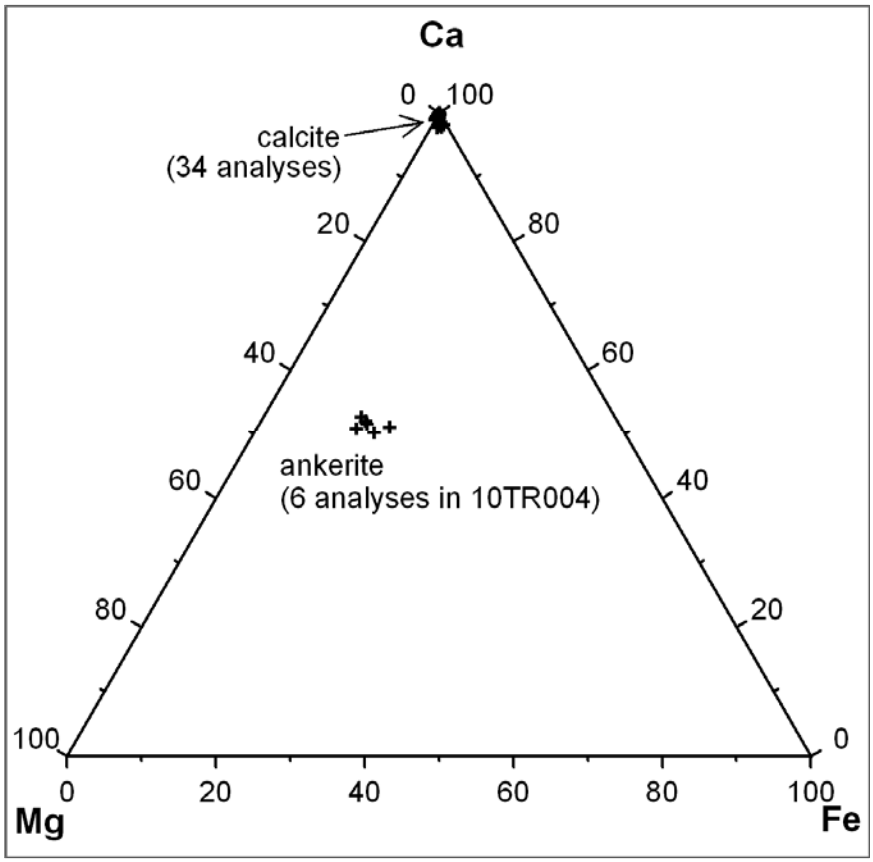

Figure 3.29: Ternary diagram of Ca, Fe, and Mg for carbonate minerals.

Table 3.16: Electron microprobe analyses of carbonate minerals.
No cation recalculations were attempted.

Sample	10DE006 -6-1-3	10TR004 -2-1-4	10TR004 -2-1-5	10TR004 -2-1-6	10TR004 -2-1-7	10TR004 -2-1-8	10TR004 -2-1-9	10TR004 -3-3-1	10TR004 -3-3-2	10TR004 -3-3-3
MgO	0.2	25.4	23.0	27.4	0.6	0.6	0.4	25.5	25.5	25.7
CaO	96.7	52.8	52.5	54.3	97.4	97.9	97.7	54.2	54.6	55.4
MnO	3.1	-*	1.0	-*	0.7	-*	0.7	0.8	1.0	1.2
FeO	-*	21.8	23.5	18.3	1.3	1.5	1.2	19.4	18.9	17.7
Total	100.0	100.0	100.0	100.0	100.0	100.0	100.0	99.9	100.0	100.0

*not analyzed

Table 3.17: Electron microprobe analyses of zeolite minerals in sample 10DE006.
No cation recalculations were attempted.

Sample point	1-1-1	1-1-2	1-1-3	2-1-1	2-1-2	2-1-3	2-1-10	2-1-11	3-1-4	3-1-5	3-1-6
Na_2O	10.2	9.6	10.3	10.3	10.4	10.3	8.4	9.8	9.5	9.6	9.7
MgO	-*	-*	-*	-*	-*	-*	0.3	-*	-*	0.5	-*
Al_2O_3	31.4	31.4	31.2	31.2	31.0	31.2	31.1	31.3	31.1	31.2	31.2
SiO_2	58.3	58.8	58.4	58.3	58.4	58.2	59.6	58.6	58.6	58.1	58.9
CaO	0.2	0.2	0.2	0.3	0.2	0.2	0.6	0.3	0.2	0.2	0.3
FeO	-*	-*	-*	-*	-*	-*	-*	-*	0.6	0.4	-*
Total	100.1	100.0	100.1	100.1	100.0	99.9	99.9	100.0	100.0	100.0	100.0

* not analyzed

Table 3.18: Electron microprobe analyses of sphene.
Cation recalculations based on 4 silica atoms PFU.

Sample point	11CLD001 10-22_029	11CLD001 10-22_031	11CLD003 10-29_10	11CLD007 11-06_077	11CLD007 11-06_095	11CBF004 -010	11CBF004 -017	11CBF004 -027	11CBF004 -029	11CBF004 -035
Na_2O	-*	-*	-*	-*	-*	-*	-*	0.7	-*	-*
MgO	3.2	3.3	0.5	*	-*	3.5	1.0	1.5	3.2	1.1
Al_2O_3	4.4	4.4	4.7	4.9	5.4	5.8	3.9	3.9	5.0	3.6
SiO_2	32.0	33.3	33.6	34.1	33.1	32.3	33.6	33.0	33.3	33.3
CaO	24.3	24.6	27.8	28.4	28.0	24.0	26.7	27.0	24.6	27.5
TiO_2	28.3	29.1	30.2	30.1	30.4	28.1	30.7	30.8	28.3	30.9
FeO*	7.9	5.3	3.1	2.5	3.2	6.3	4.1	3.2	5.6	3.6
∑	100.1	100.0	99.9	100.0	100.1	100.0	100.0	100.1	100.0	100.0
Si	4.0	4.0	4.0	4.0	4.0	4.0	4.0	4.0	4.0	4.0
Al	0.7	0.6	0.7	0.7	0.8	0.8	0.5	0.6	0.7	0.5
Fe	0.8	0.5	0.3	0.2	0.3	0.7	0.4	0.3	0.6	0.4
Ti	2.7	2.6	2.7	2.7	2.8	2.6	2.8	2.8	2.6	2.8
∑	4.1	3.8	3.7	3.6	3.9	4.1	3.7	3.7	3.9	3.7
Mg	0.6	0.6	0.1	-	-	0.7	0.2	0.3	0.6	0.2
Na	-	-	0.0	-	-	-	-	0.2	-	-
Ca	3.3	3.2	3.6	3.6	3.6	3.2	3.4	3.5	3.2	3.5
∑	3.9	3.8	3.6	3.6	3.6	3.8	3.6	4.0	3.7	3.7

*not analyzed

minerals are reasonably similar to the ideal composition of sphene, with some magnesium substitution for calcium, and iron and aluminum substitution for titanium. Cation recalculations were based on 4 silica atoms PFU.

3.15 Apatite

Apatite was not identified petrographically, but few specks with high mean atomic numbers were observed in BSE in amphibole and along rims of former plagioclase. EDS microprobe analyses indicated the presence of mainly calcium and phosphorus, hence apatite. Two analyses from extremely fine-grained specks near former plagioclase contained elements from nearby minerals and are not listed here. Analyses from three apatite grains surrounded by amphibole are shown in Table 3.19.

3.16 Summary and Discussion

Petrographic examination followed by EDS microprobe analyses proved extremely useful for mineral identification. Alteration assemblages identified petrographically were confirmed using the microprobe, and minerals that could not be positively identified using petrographic examination alone were quickly recognized using the microprobe. Furthermore, the classification of minerals would not have been possible without microprobe analysis, since most classification schemes rely heavily on mineral compositions.

During the analyses, special attention was paid to (Ca,Mg)-silicates and alteration products in former plagioclase cores. Less altered samples could easily be identified as such by the clear appearance of plagioclase, and sometimes the presence of olivine and orthopyroxene. Extremely altered samples were identified by the cloudy appearance of plagioclase, as well as the presence of pumpellyite, and sometimes epidote.

Based on other studies, minerals of interest regarding mineral carbonation consist of certain (Ca,Mg)-silicates including the magnesium end-member of olivine

Table 3.19: Electron microprobe analyses of apatite.

Sample point	10SC004 -1-1-10	10SC004 -2-1-5	10SC004 -2-1-6
Na_2O	0.2	0.2	0.3
MgO	0.1	-*	-
SiO_2	0.9	0.4	0.3
P_2O_5	41.4	42.8	42.9
CaO	56.5	56.0	56.0
FeO	0.8	0.6	0.6
Total	99.9	100.0	100.1

*Not analyzed

(forsterite), orthopyroxene, anorthite-rich plagioclase, and the olivine alteration product serpentine. Of the samples studied for this thesis, only the two freshest, most basalt-like samples contain olivine, orthopyroxene, and anorthite-rich plagioclase. In these samples, olivine contains 53 to 61% forsterite component, and plagioclase contains up to ~80% anorthite.

Most samples from the study area are moderately to extremely altered (mineralogically), and contain alteration products such as chlorite, mica, prehnite, epidote, pumpellyite, copper, quartz, carbonate and zeolites. Additionally, although most of these samples are variedly altered, no serpentine minerals were identified. The anorthite content decreases with alteration, and the most altered samples contain albite and orthoclase but little, if any, anorthite. Pyroxene grains in these more altered samples consist of augite. Chlorite is present in all samples except for those extremely carbonated.

In the least altered samples magnesium occurs in olivine, orthopyroxene, and clinopyroxene, and calcium is present in anorthite-rich plagioclase and clinopyroxene. With alteration, the magnesium remains in clinopyroxene, is abundantly present in chlorite, and somewhat in pumpellyite; the calcium occurs in prehnite, pumpellyite, epidote, carbonate, and zeolite. Thus, instead of olivine or orthopyroxene altering to serpentine, the assemblage of olivine, orthopyroxene, clinopyroxene, and anorthite-rich plagioclase is altered to mostly chlorite and various calcium minerals.

Based on their mineralogy, most of the studied samples do not classify as basalt. Typical basalt contains Ca-rich plagioclase, pyroxene, and sometimes olivine, but none of the alteration minerals observed. The least altered samples studied have more “basalt-like” mineralogies; with increasing alteration assemblage, the minerals in the samples become less “basalt-like”. Since these samples do not contain the same mineralogy as basalt, thermodynamic and kinetic modeling should be used to determine the feasibility of the present (Ca,Mg)-silicates for mineral carbonation.

CHAPTER 4: CLASSIFICATION OF SAMPLES USING WHOLE ROCK DATA

Whole rock data for 206 samples were used to characterize the collected samples based on immobile and mobile element concentrations. Immobile elements were used to characterize the original composition of the rocks, while mobile element diagrams were used to study potential alteration trends.

The rocks in the study area have undergone low-grade metamorphism and mobile elements potentially migrated. Immobile element concentrations are less affected by alteration processes, hence immobile element classification systems such as Zr/TiO2-Nb/Y diagrams (Winchester and Floyd, 1977) and Nb-Zr-Y ternary diagrams (Meschede, 1986) were used to estimate the original composition of these rocks. Chondrite normalized rare earth element (REE) graphs were then used to detect variations in original composition among samples.

Mobile element diagrams were used to detect changes of the bulk composition of samples due to alteration. Mineralogical changes with alteration were studied in Chapter 3; these can occur with little compositional changes due small additions of water during low-grade metamorphism. Thus, mineralogical changes may not lead to detectable changes of the overall sample chemistry. On the other hand, compositional changes such as the depletion or enrichment of certain elements may be indicative of mineralogical changes. To study the chemical alteration of the given samples using whole rock data, several mobile element systems were applied, including Total Alkali Silica (TAS) plots (Le Bas et al., 1986; Le Maitre, 2002), bivariate diagrams, AFM ternary diagram (Irvine and Barager, 1971), and ACF diagrams (after Blatt et al., 2006).

4.1 Study of Original Compositions Based on Immobile Elements

4.1.1 *Zr/TiO2-Nb/Y Diagrams*

A Zr/TiO_2-Nb/Y diagram for all samples by location is shown in Figure 4.1, and Figure 4.2 is a diagram for samples from the Caledonia Mine. According to these Zr/TiO_2-Nb/Y diagrams, most samples classify as subalkaline basalts; only four samples classify as andesites. Andesite samples consist of one sample from the *Caledonia Mine* in the southern section (11CLD005), and three samples from the sample site *Houghton Exploration* in the middle section (10HE002, 10HE004, and 10HE005).

Two of the Mamainse samples plot away from the bulk of the samples with relatively lower Nb/Y values (10MB001, 10MB002). Other samples that stand out include two samples with relatively lower Nb/Y values (10CF001 from the northern fissures and 10HE003 from the middle section), and one sample with relatively lower Zr/TiO_2 values (10OC010 from the middle section).

Data by texture is plotted on an enlarged version of the Zr/TiO_2-Nb/Y diagram (Figure 4.3). Amygdaloidal and brecciated samples scatter more than samples with all other textures. Gabbroic, ophitic, and subophitic samples appear to scatter the least.

4.1.2 *Nb-Zr-Y Ternary Diagrams*

The Nb-Zr-Y ternary diagram was introduced by Meschede (1986) to distinguish between normal mid-ocean ridge basalts (N-type MORB), plume-influenced region mid-ocean ridge basalts (P-type MORB), within-plate tholeiites (WPT), within-plate alkali basalts (WPA), and volcanic arc basalts (VAB). Since these diagrams were created strictly for basalts, samples previously classified as andesite (i.e., 11CLD005, 10HE002, 10HE004, and 10HE005) were excluded from this classification.

Results for all samples by location are shown in Figure 4.4; and data for samples from the Caledonia Mine are shown in Figure 4.5. Most samples plot in field C as

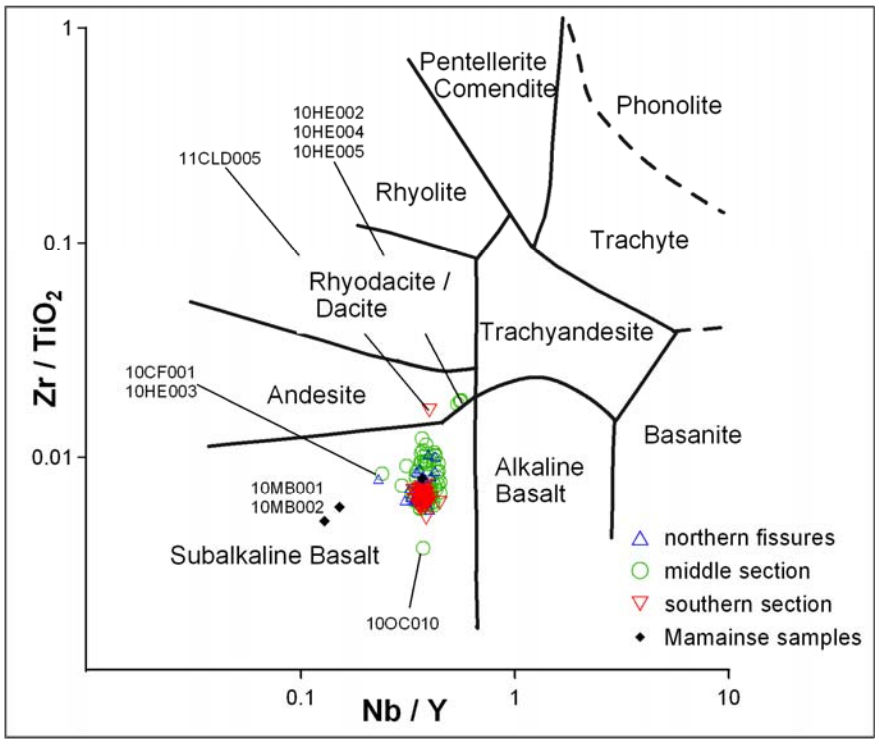

Figure 4.1: Zr/TiO_2-Nb/Y diagram for samples by location.
Samples from the Caledonia Mine are included with southern section samples.

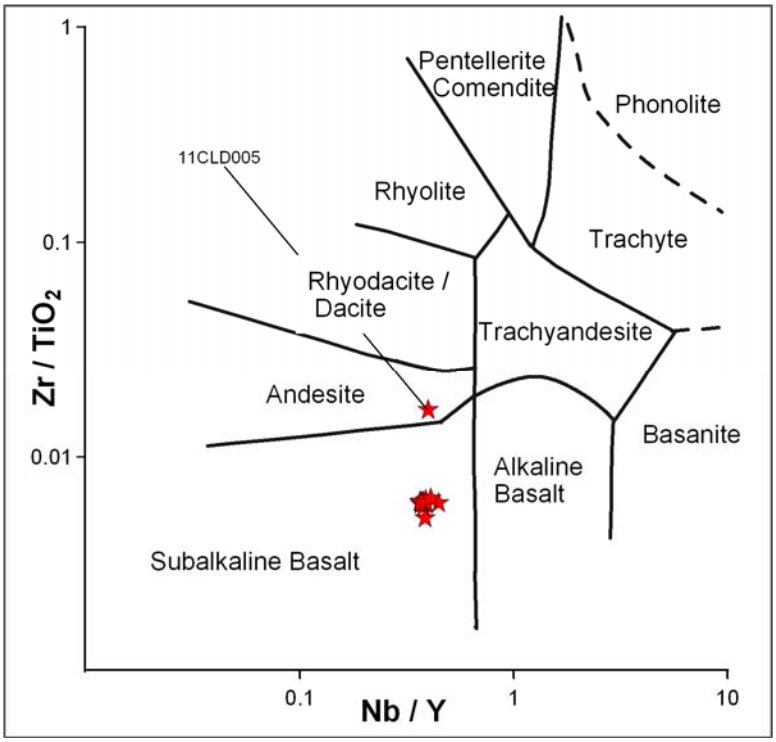

Figure 4.2: Zr/TiO_2-Nb/Y diagram for Caledonia samples.

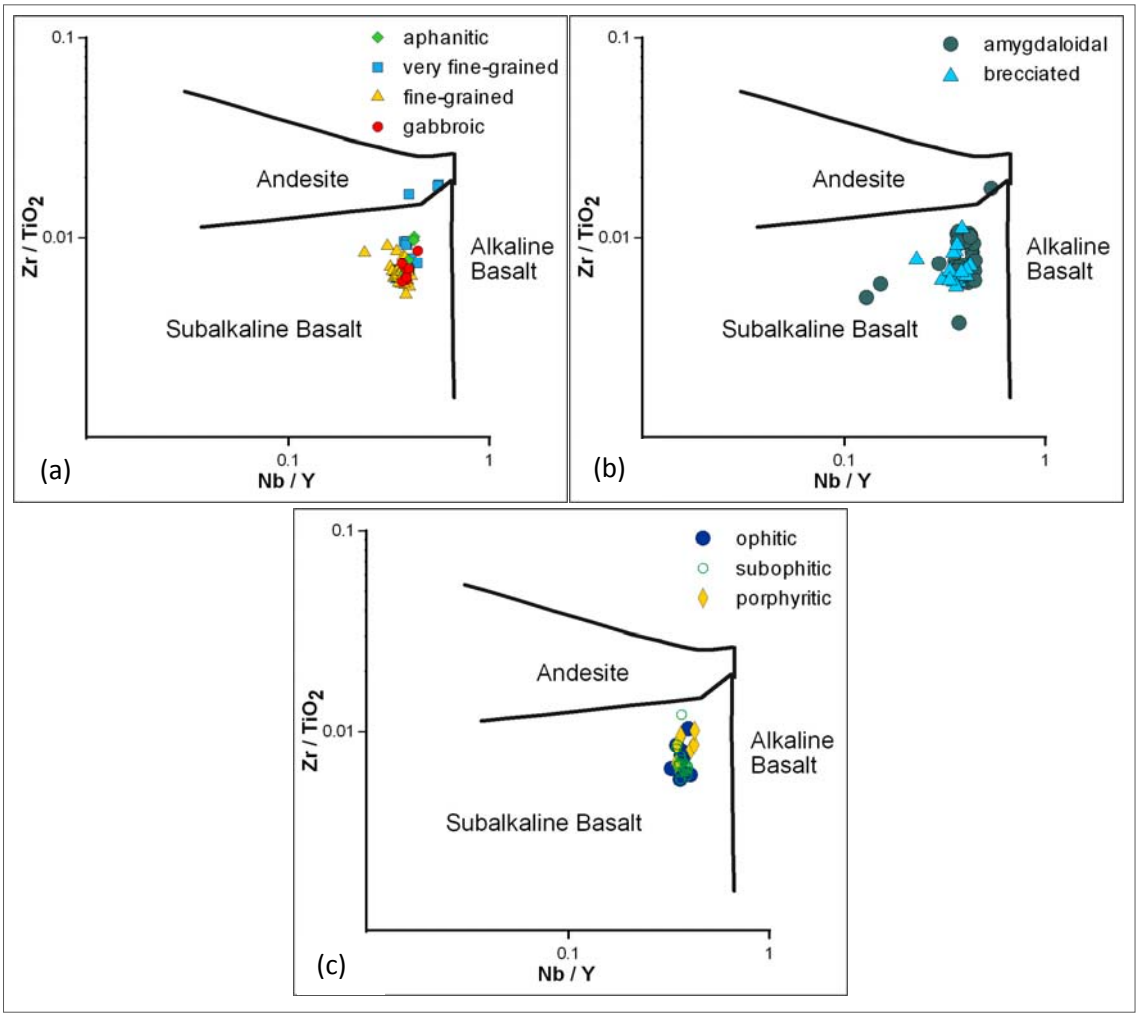

Figure 4.3: Zr/TiO_2-Nb/Y diagrams for samples by texture.
Figures are shown separately for aphanitic, very fine-grained, fine-grained, and gabbroic samples (a), amygdaloidal and brecciated samples (b), and for ophitic, subophitic, and porphyritic samples (c).

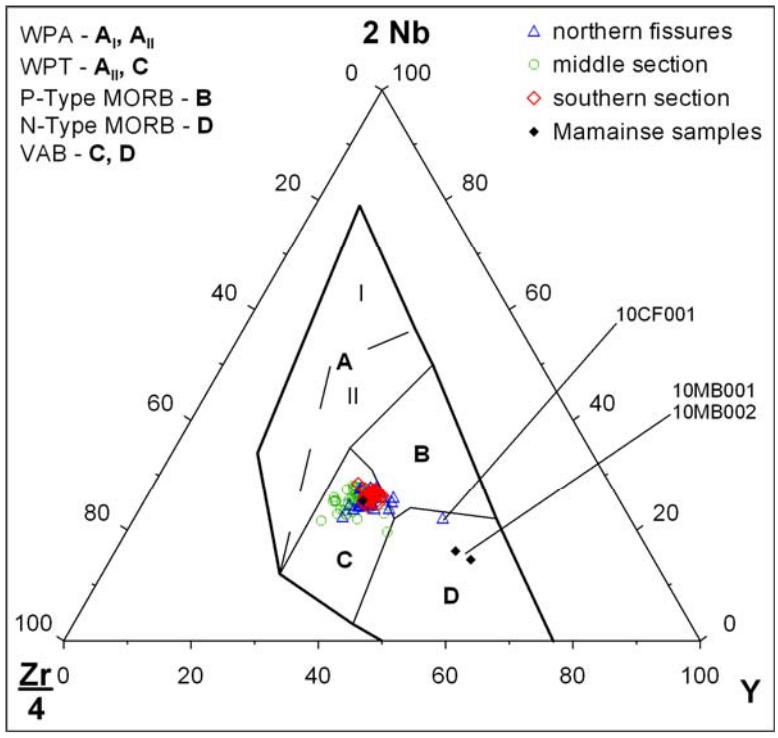

Figure 4.4: Nb–Zr–Y diagram for samples by location.

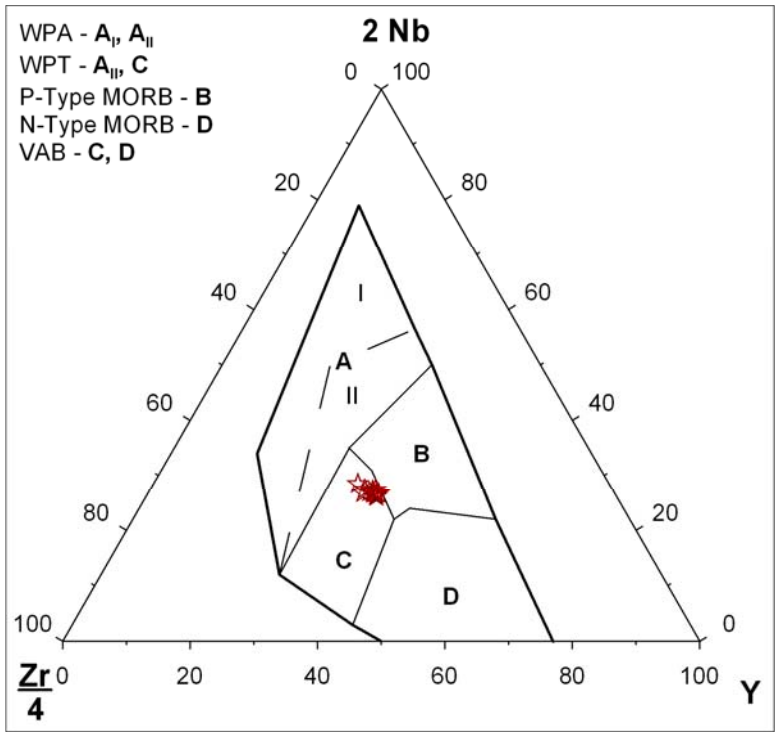

Figure 4.5: Nb-Zr-Y diagram for Caledonia samples.

WPT, and three samples plot in field D as N-type MORB (10CF001, 10MB001, 10MB002). All Caledonia samples plot closely together near the dividing line between C and B as WPT. Plots for samples by texture are included in Figure 4.6. Again, amygdaloidal and brecciated samples appear to scatter the most, while gabbroic, ophitic, and subophitic samples scatter the least.

4.1.3 *REE Diagrams*

The REE data were normalized using chondrite C1 data from Sun and McDonough (1989). Figure 4.7 shows graphs for all data by location. Most plots are strongly clustered with similar trends, yet five samples stand out: three with elevated REE element concentrations and different trends (10HE002, 10HE004, and 10HE005), and two with lower light REE element concentrations (10MB001, 10MB002). Overall, southern section samples form a relatively tight cluster while REE plots for middle section and northern fissure samples have a wider spread.

REE data for Caledonia samples were plotted separately (Figure 4.8). Most data for samples from the Caledonia Mine plot similarly, except 11CLD005 and 11CBF006. The data for 11CBF006 display a trend similar to the others with slightly elevated REE values. 11CLD005 displays a different trend with a negative europium (Eu) anomaly. The Eu anomaly for 11CLD005 is consistent with fractionation of andesite.

REE plots by grain size are included in Figure 4.9. Both aphanitic and very fine-grained samples appear to be split into two clusters (excluding samples 10HE002, 10HE004, and 10 HE005). Fine-grained samples span the entire range of REE plots, and gabbroic REE concentrations cluster between the two groups for aphanitic and very fine-grained samples. Amygdaloidal and brecciated samples appear to span the entire range of REE concentrations typical for the sample area (Figure 4.10). Data for samples with ophitic, subophitic, and porphyritic textures are plotted in Figure 4.11. Plots for ophitic and subophitic samples cover similar ranges of REE concentrations. The one subophitic sample that has seemingly higher REE

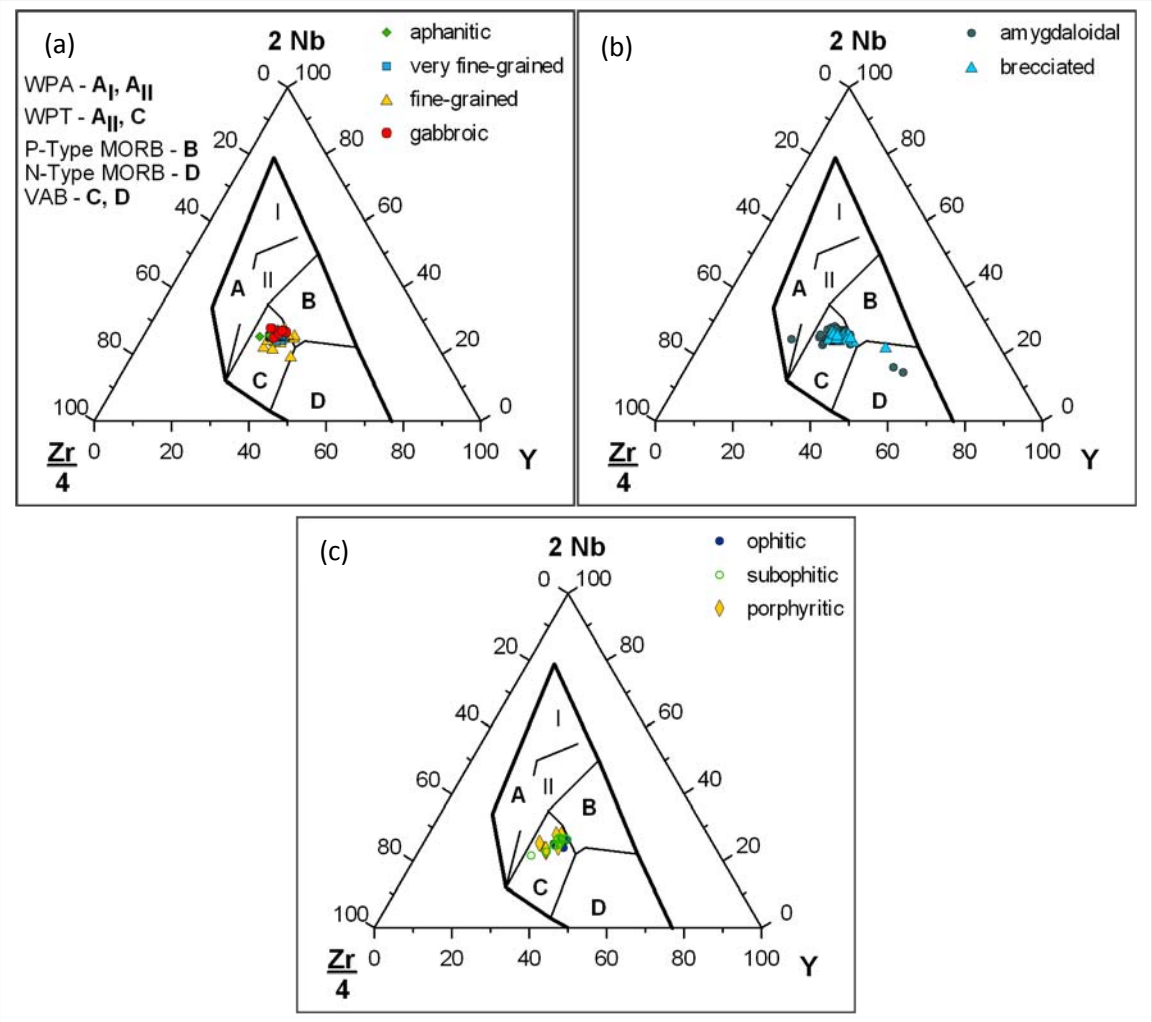

Figure 4.6: Nb-Zr-Y diagram for samples by texture.
Figures are shown separately for aphanitic, very fine-grained, fine-grained, and gabbroic samples (a), amygdaloidal and brecciated samples (b), and for ophitic, subophitic, and porphyritic samples (c).

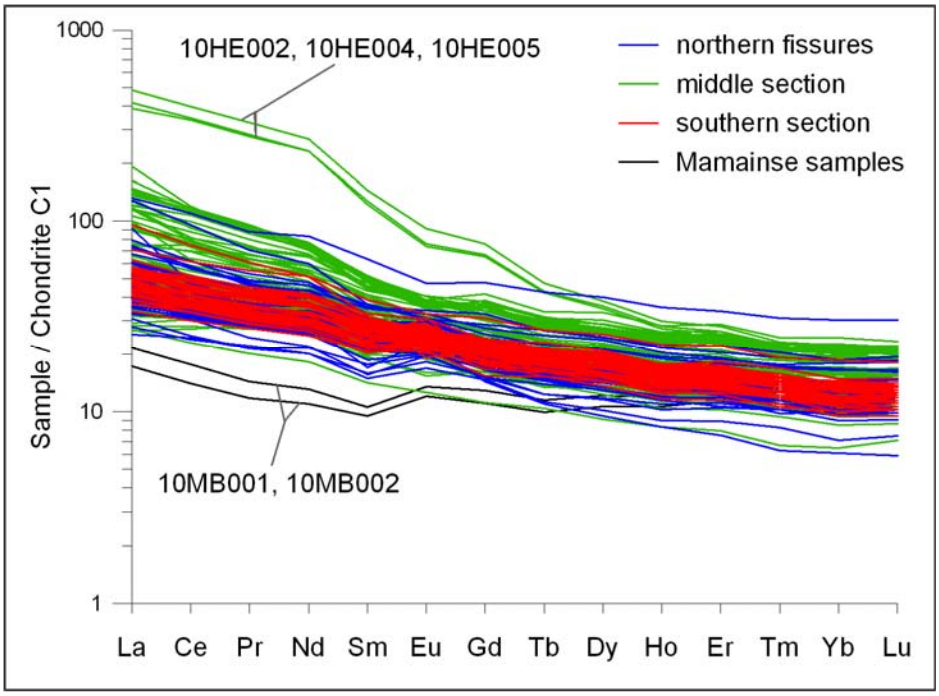

Figure 4.7: REE diagram by location.

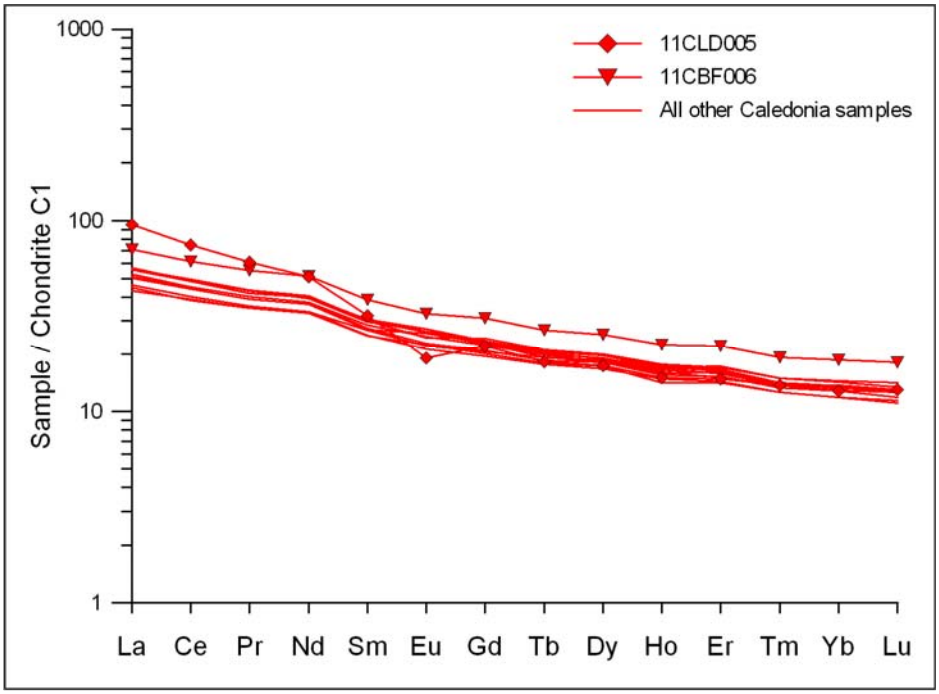

Figure 4.8: REE diagram for Caledonia samples.

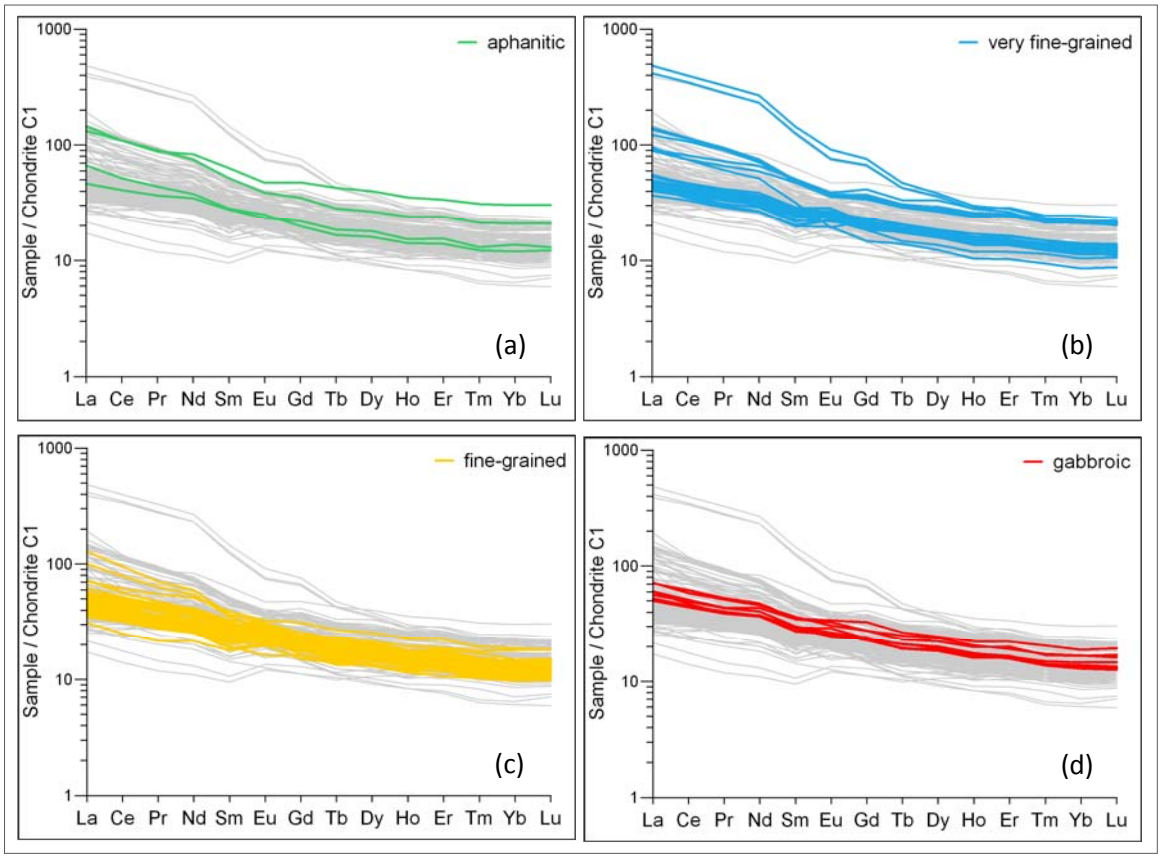

Figure 4.9: REE diagrams by grain size.
Figures show aphanitic (a), very fine-grained (b), fine-grained (c), and gabbroic samples (d).

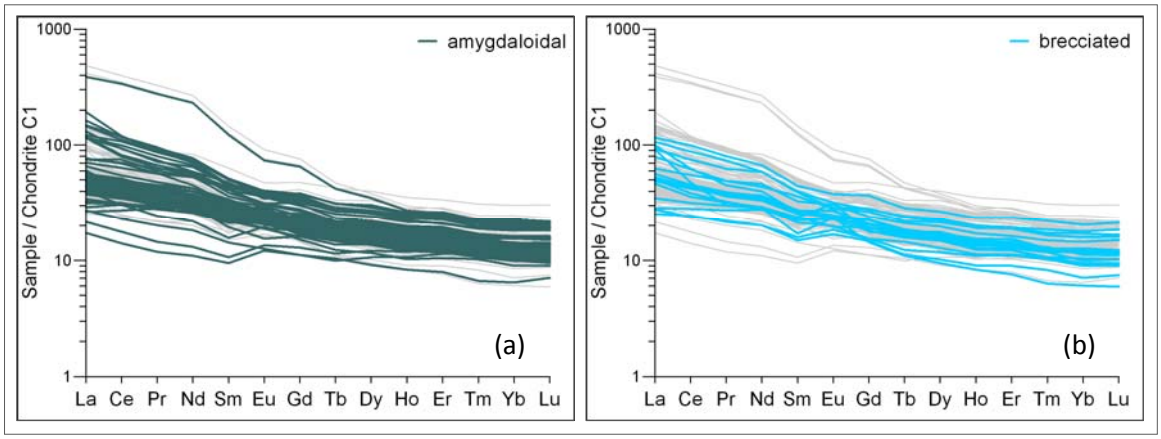

Figure 4.10: REE diagrams for amygdaloidal (a) and brecciated (b) samples.

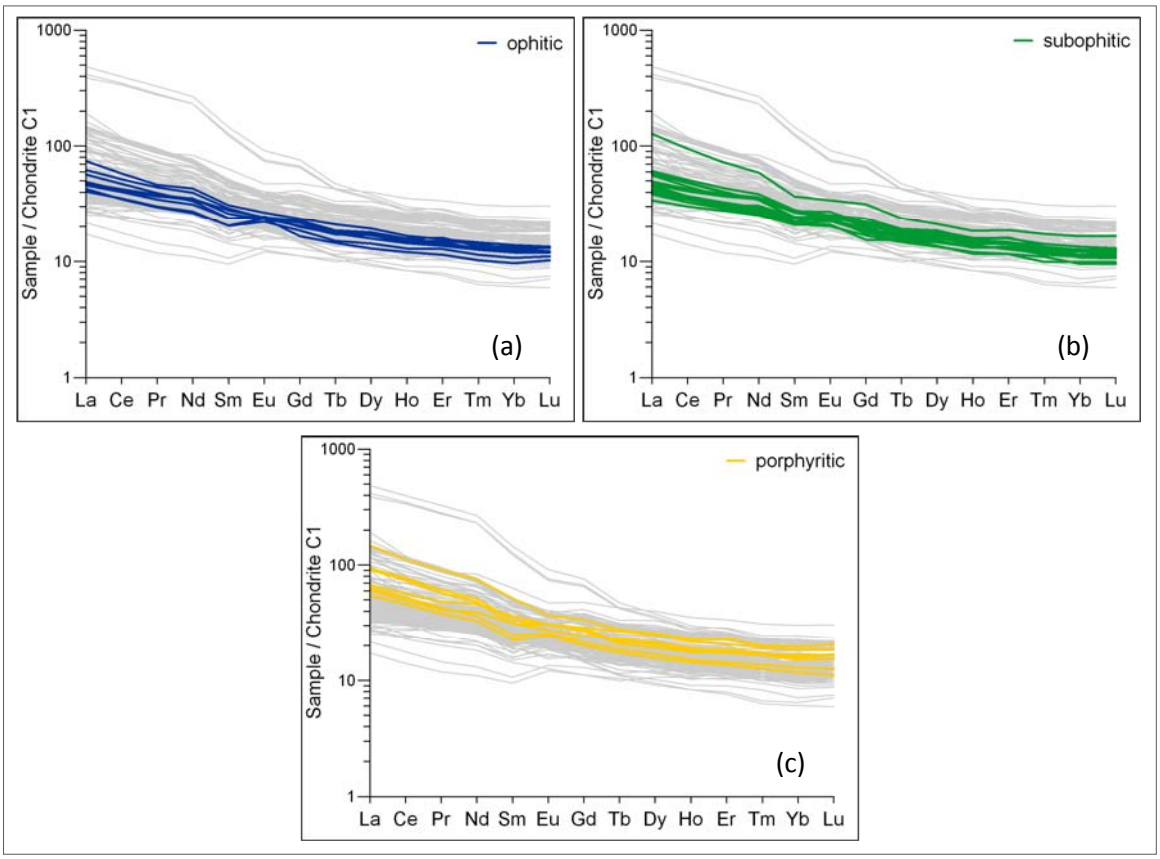

Figure 4.11: REE diagrams for ophitic (a), subophitic (b), and porphyritic (c) samples.

concentrations than other subophitic samples, contains a few phenocrysts as well, and could be classified as a porphyritic sample.

To visualize any potential variation with location on a smaller scale, REE diagrams were additionally created for samples by sample station. Plots are included in Appendix H. Most REE plots for a given station have similar trends with varying REE concentrations. Few plots have vastly different slopes. REE plots appear to vary by flow rather than by geographic location. Overall, the slopes of plots are mostly parallel to each other.

4.2 Study of Alteration Based on Mobile Elements

Unaltered mafic rocks can be studied using diagrams and classification systems based on mobile elements. Since rocks in the study area are known to have undergone low grade metamorphism, mobile elements were used to detect variations and general trends due to alteration. Mobile element systems used include the TAS diagram, bivariate diagrams, ACF diagrams, and AFM diagrams.

4.2.1 *TAS System*

The TAS classification system is based solely on the normalized weight percents of SiO_2, Na_2O, and K_2O of volcanic rocks. The *International Union of Geological Sciences Subcommission on the Systematics of Igneous Rocks* recommended that the TAS classification be used if samples are considered volcanic, the mineral mode cannot be determined, and chemical analyses are available (Le Maitre, 2002). The original TAS diagram was developed using fresh rocks with $H_2O < 2\%$ and $CO_2 < 0.5\%$ (Le Bas et al., 1986). The samples in the study area are variedly metamorphosed for which the classification "should be used with caution". Le Maitre (2002) further suggested that only samples with $H_2O < 2\%$ and $CO_2 < 0.5\%$ be used.

Values for samples from the study area were recalculated to 100%, without H_2O and CO_2 (=loss on ignition, LOI) before plotting the data. A TAS diagram with field labels

is shown for reference in Figure 4.12; the following figures exclude labels to show the data points more clearly.

Based on immobile elements, the samples from the study area should plot in the (subalkaline) basalt field. The expected compositions based on immobile elements are included on the TAS diagrams. To identify potential trends with LOI, the original LOI values for the data were divided into several classes and plotted separately (Figure 4.13). Classes used were: LOI > 10%, LOI between 5 and 10%, LOI between 2.5 and 5%, and LOI < 2.5%. Most samples cluster in the "basalt" and "trachy-basalt" fields, with few, sporadic samples plotting in the "basaltic trachy-andesite", "basaltic andesite", and "basanite" fields. Seven samples with near zero alkali contents are shown near the x-axis: 10CE003, 10CN005, 10FU005, 10OJ002, 10TO004, 10TO006, and 11CLD005. These samples will be referred to as *low alkali samples*.

Only eight samples have original LOI values of less than 2.5%; 110 samples have LOI values between 2.5 and 5%; 66 samples have LOI values between 5 and 10%; and 22 samples have LOI values above 10%. No correlation between low alkali samples and LOI values appears to exist. The low alkali content appears to be due to both hydrous and anhydrous alteration of these samples. Overall, the samples with LOI < 5% are more clustered than samples with higher LOI values.

Figure 4.14 shows a TAS diagram of all samples by location. Another graph by location was completed for selected samples with LOI < 5% (Figure 4.15) in an attempt to visualize any differences due to location without influence of excessive alteration. None of these diagrams show obvious location-based trends.

TAS diagrams for samples by texture are shown in Figures 4.16, 4.17, and 4.18. Aphanitic and very fine-grained samples contain variable silica and alkalis, whereas the silica contents in fine-grained samples are more consistent, and the alkali contents vary more. Gabbroic samples form a cluster in the trachy-basalt and basalt fields. Alkali and silica contents of gabbroic samples vary less than those of other

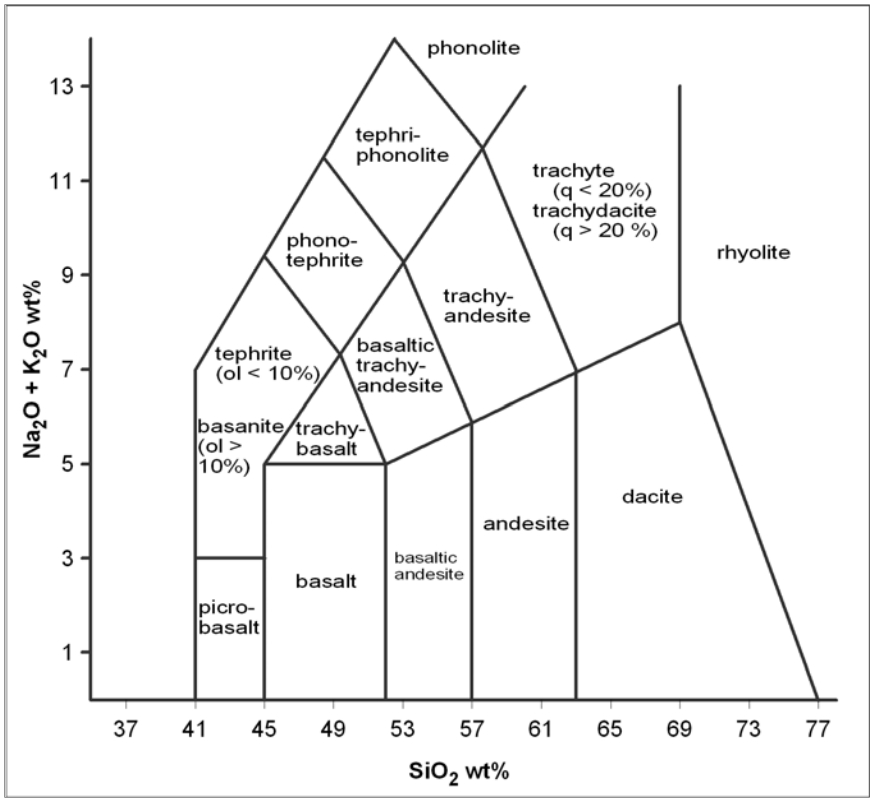

Figure 4.12: TAS classification diagram with field labels.

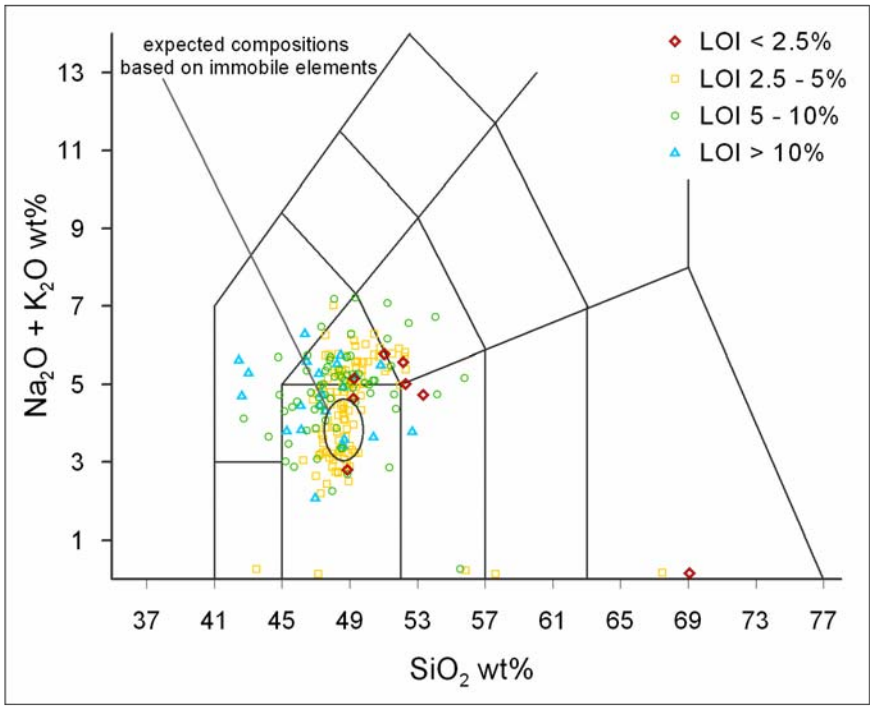

Figure 4.13: TAS diagram for samples by loss on ignition (LOI).

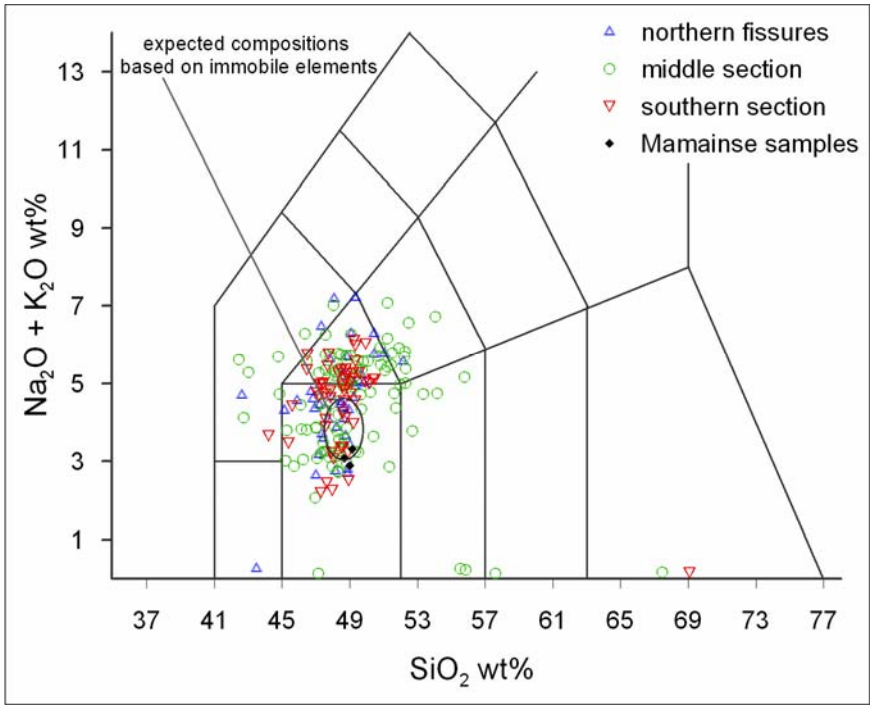

Figure 4.14: TAS diagram for samples by location.

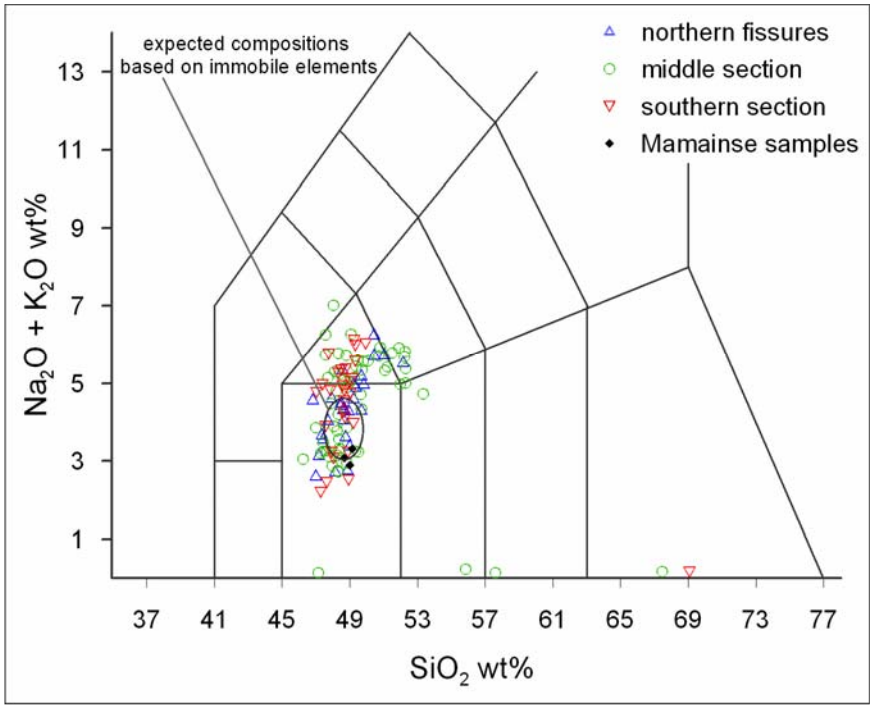

Figure 4.15: TAS diagram by location for samples with LOI < 5%.

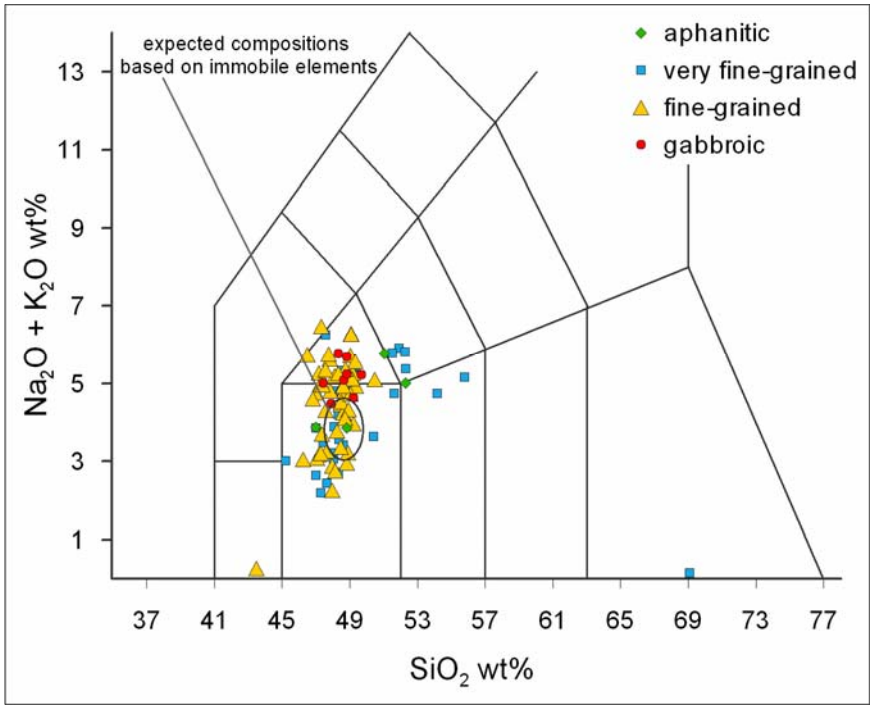

Figure 4.16: TAS diagram for samples by grain size.

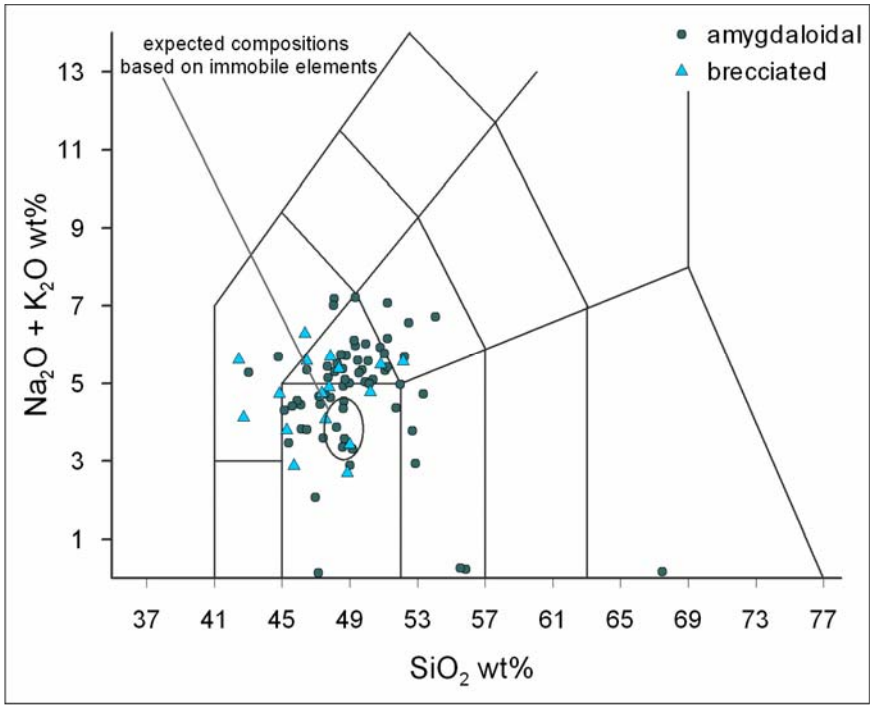

Figure 4.17: TAS diagram for amygdaloidal and brecciated samples.

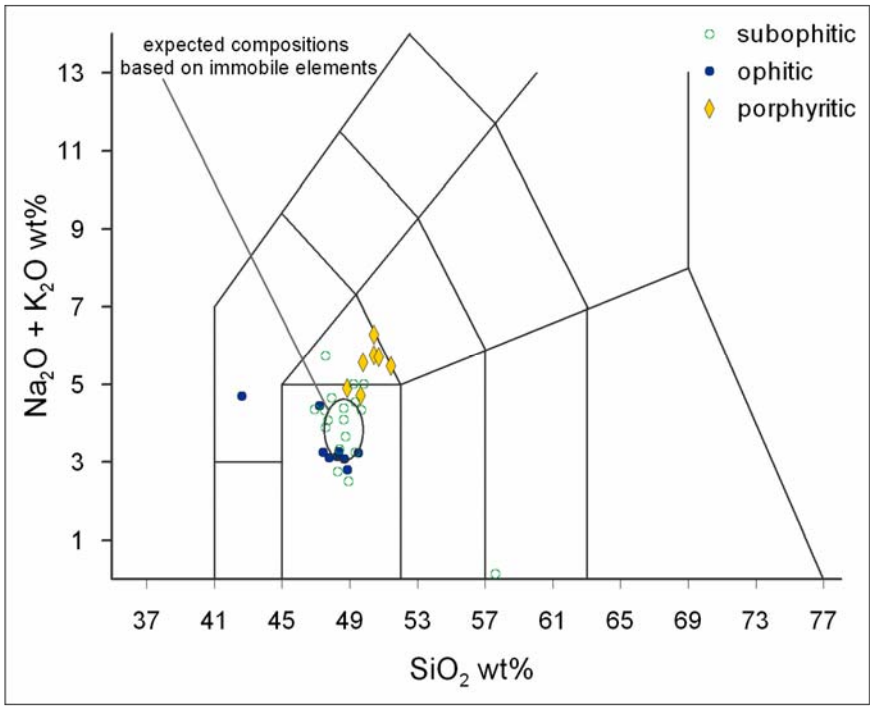

Figure 4.18: TAS diagram for ophitic, subophitic, and porphyritic samples.

samples (Figure 4.16). Amygdaloidal and brecciated samples show large variations in both their silica and alkali contents (Figure 4.17), whereas ophitic, subophitic and porphyritic samples show similar silica contents and somewhat varying alkali contents (Figure 4.18). Subophitic samples vary most in their alkali contents, while ophitic samples form a cluster with lower alkali contents (~3 weight %), and porphyritic samples form a cluster with slightly higher alkali contents (~5-7 weight %). Overall, alkali and silica contents of amygdaloidal and brecciated samples tend to vary the most while alkali and silica contents of gabbroic, ophitic, subophitic, and fine-grained samples vary the least. Samples from the middle section also show a wide spread of compositions, while southern section samples tend to form clusters.

4.2.2 *Bivariate Diagrams*

Bivariate diagrams were produced for major elements and CO_2, and plotted versus Na_2O content (Figures 3.19 through 3.24). Major element values, normalized to a total of 100% without LOI are displayed in weight percent. CO_2 values are also shown in weight percent, but were not normalized. Na_2O content was chosen for the x-axis, as unaltered basalt should contain around 3 weight % Na_2O, whereas most analyses contained more than 3 weight % Na_2O, likely due to chemical alteration. The average composition of 3,500 (unaltered) basalt analyses is included in these figures for reference and designated “basalt” (from Best, 2002).

Major element oxides in samples with LOI values below 5% vary somewhat less than in samples with LOI values above 5% (Figure 4.19). As expected, there is a direct correlation between CO_2 content and LOI, with higher LOI values corresponding to higher CO_2 values.

Samples from the middle section show lower Al_2O_3 contents, higher CO_2 contents, and generally more variation than other samples (Figure 4.20). For diagrams by texture (Figures 4.21, 4.22, and 4.23), major elements vary less in massive samples than in amygdaloidal or brecciated samples. Ophitic and porphyritic samples show

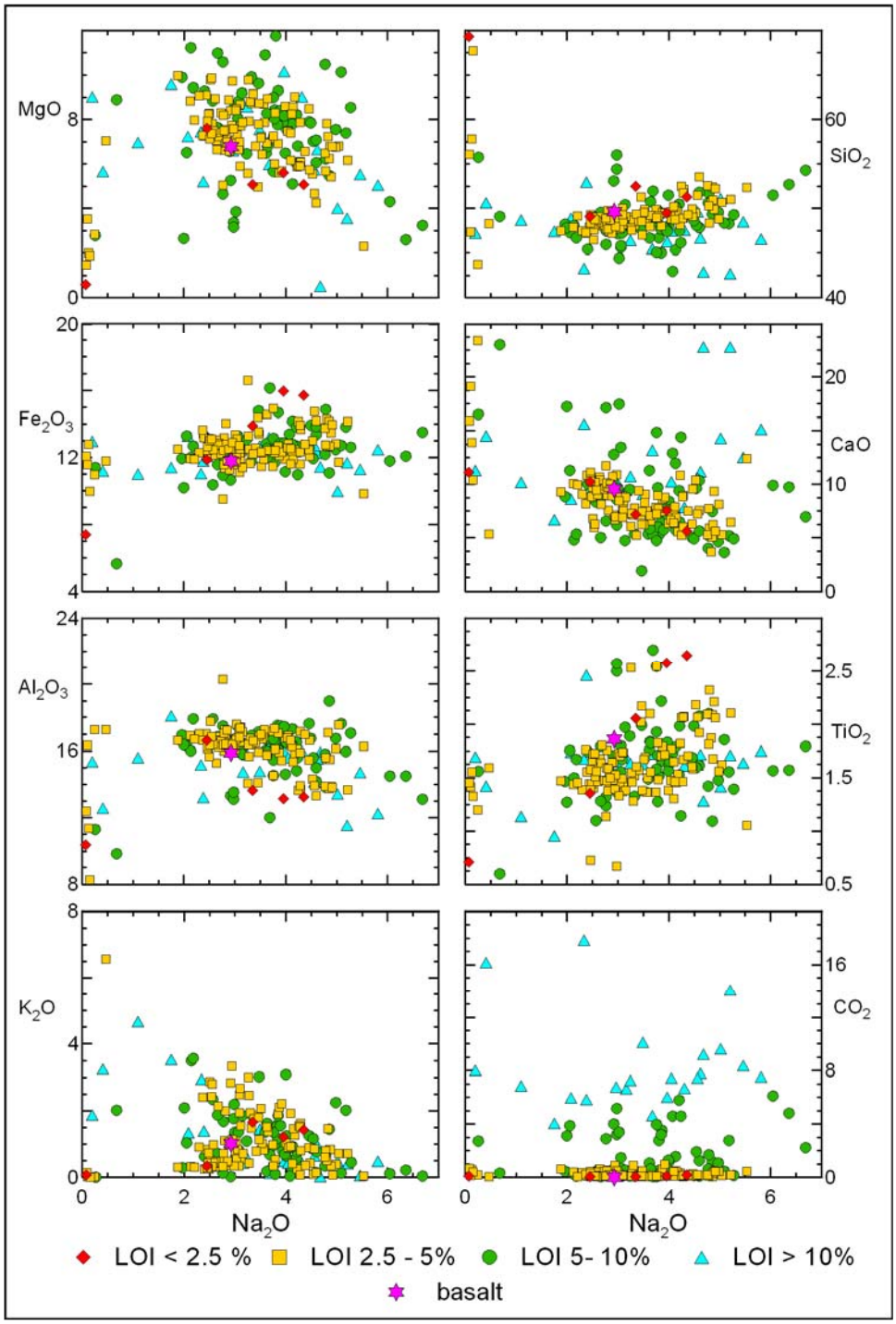

Figure 4.19: Bivariate diagram for samples by LOI.
Values for major elements were normalized to 100% without LOI, values for CO_2 were not normalized. All values are shown in weight %.

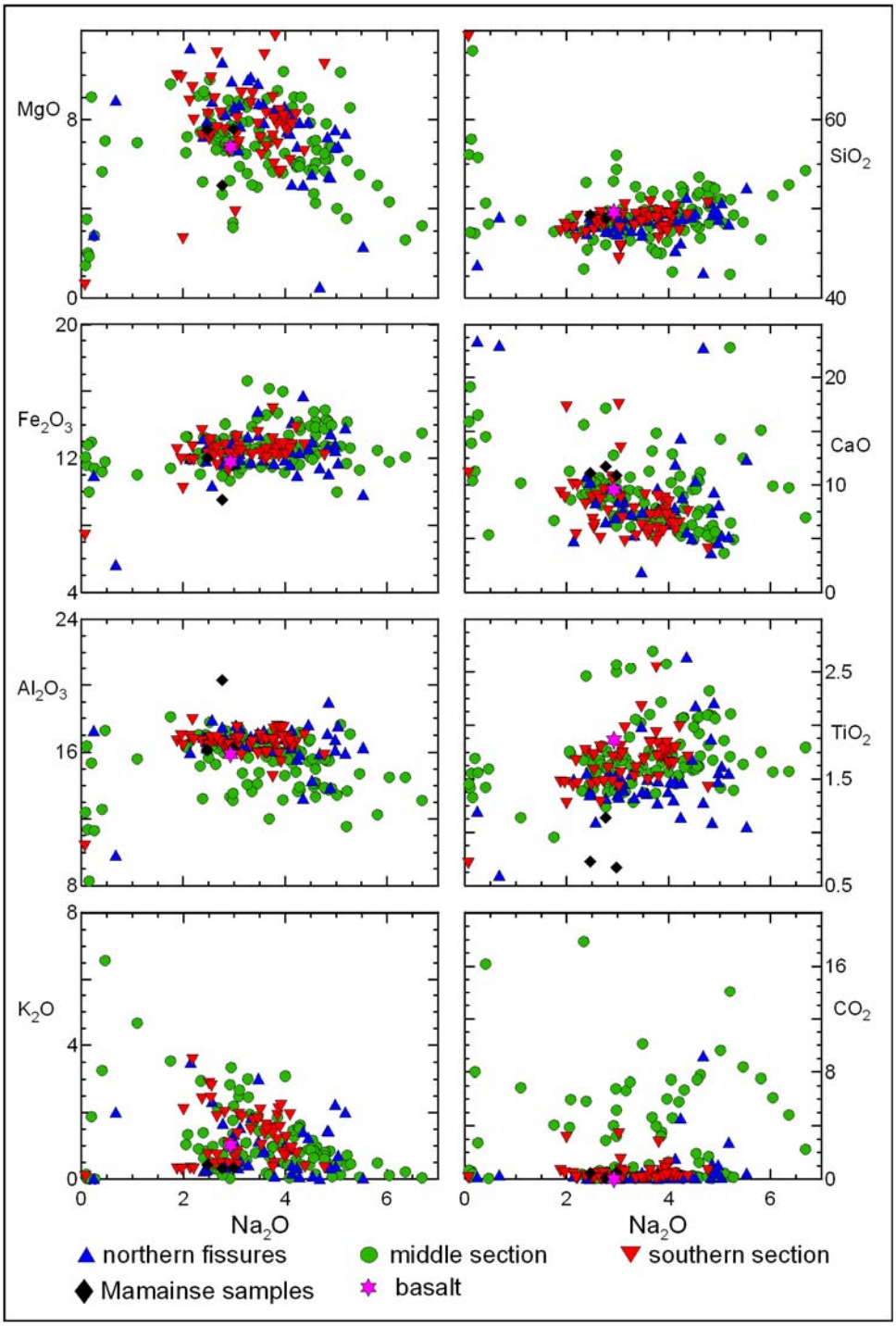

Figure 4.20: Bivariate diagram for samples by location.
Values for major elements were normalized to 100% without LOI, values for CO_2 were not normalized. All values are shown in weight %.

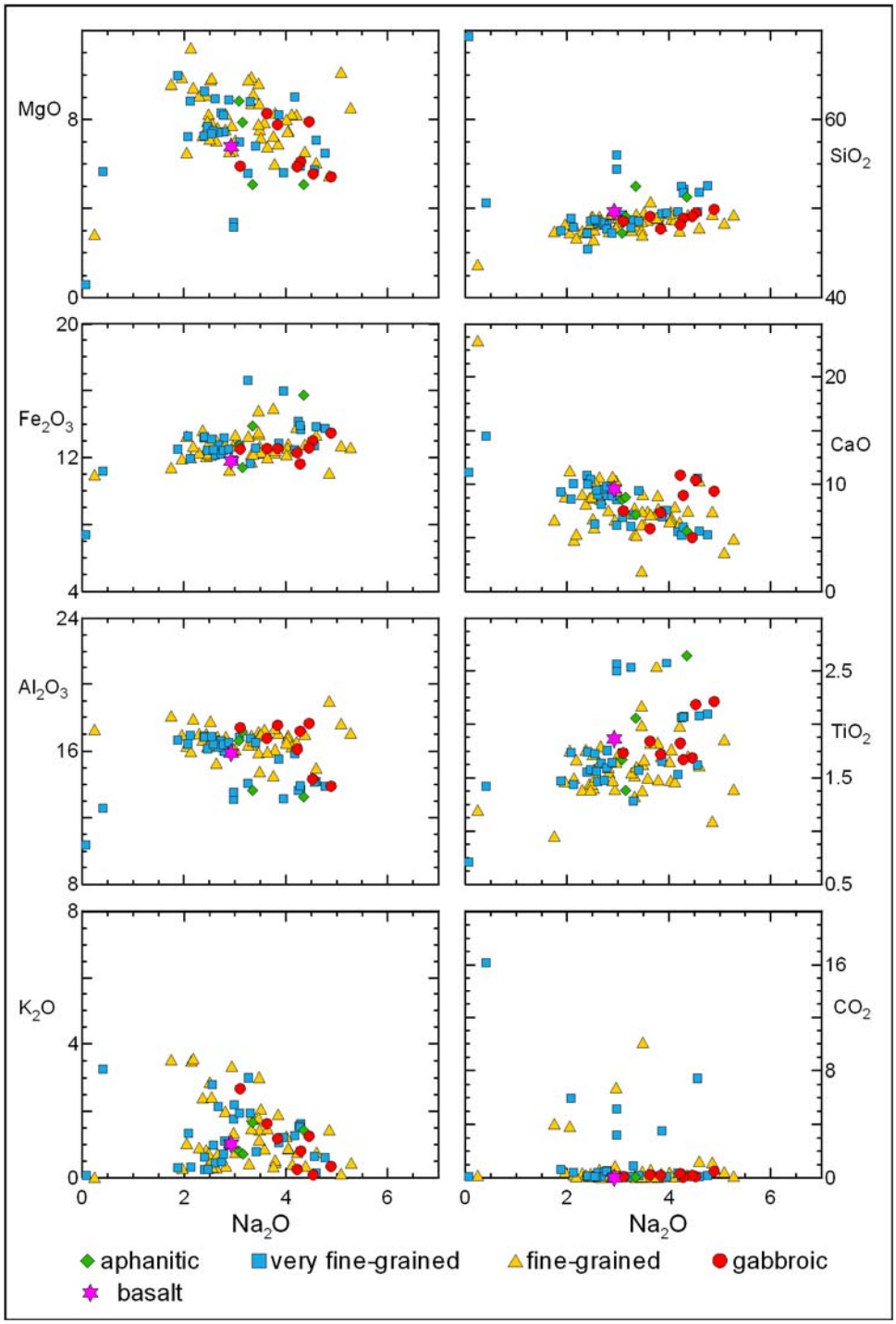

Figure 4.21: Bivariate diagram for samples by grain size.
Values for major elements were normalized to 100% without LOI, values for CO_2 were not normalized. All values are shown in weight %.

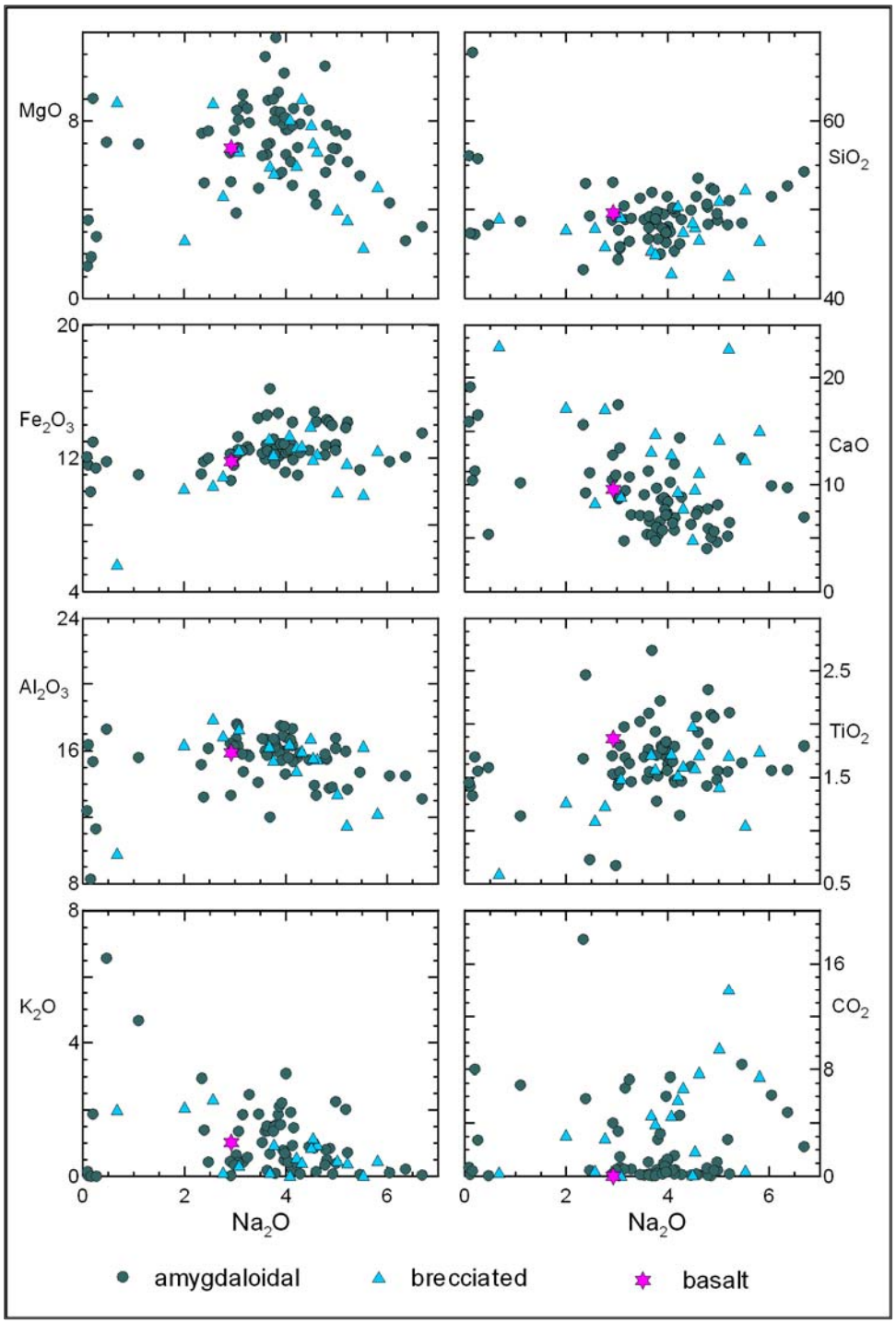

Figure 4.22: Bivariate diagram for amygdaloidal and brecciated samples. Values for major elements were normalized to 100% without LOI, values for CO_2 were not normalized. All values are shown in weight %.

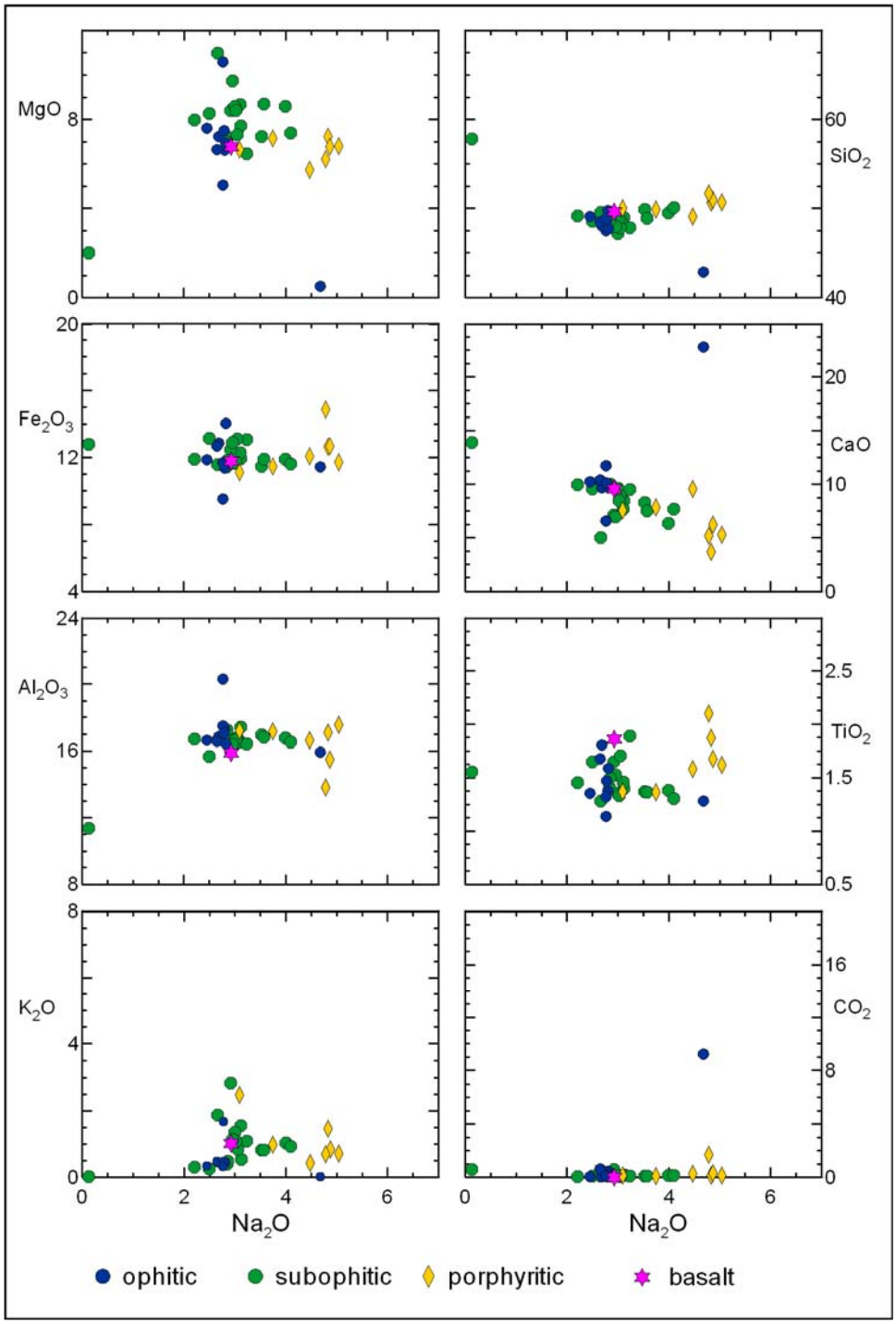

Figure 4.23: Bivariate diagram for ophitic, subophitic, and porphyritic samples. Values for major elements were normalized to 100% without LOI, values for CO_2 were not normalized. All values are shown in weight %.

the least variation and compositions most similar to the average basalt analysis. Porphyritic samples demonstrate more variation, and contain more Na_2O and SiO_2 and less CaO than the ophitic and subophitic samples. One ophitic sample (10CL005) has a high CO_2 content and an extremely high CaO content compared to other ophitic samples. Amygdaloidal and brecciated samples show the most variation throughout. Brecciated samples contain especially high amounts of CaO.

In order to compare variations with texture directly, bivariate diagrams showing CO_2 vs. Na_2O were created (Figure 4.24). Unaltered basalts should not contain any CO_2 or more than 3 weight % Na_2O; thus greater contents of either are considered to be indicative of alteration. Samples from the middle section, the northern fissures, a few very fine-grained and fine-grained samples, as well as amygdaloidal and brecciated samples show the most variation in CO_2 and Na_2O content. Samples from the southern section, as well as gabbroic, ophitic, and subophitic samples vary the least.

4.2.3 *ACF Diagrams*

ACF ternary diagrams were constructed from whole rock data to show changes in calcium, alkali, and magnesium contents due to alteration. FeO was calculated from Fe_2O_3 as described in Appendix C. CaO contents are shown after subtracting calcite and apatite. Thus, in this diagram, CaO depletion refers to CaO depletion in the silicates not in the samples per se (i.e., *CaO depleted* samples commonly contain significant amounts of calcite).

The ACF diagram for samples by LOI is shown in Figure 4.25, data for Caledonia samples are plotted in Figure 4.26. As indicated in the diagram, the data can be divided into three groupings: *CaO enriched* samples, relatively *unaltered* samples, and *CaO depleted* samples (all regarding relative proportions of CaO, MgO, and FeO in silicates). All categories of LOI contents plot in the *unaltered* and *CaO enriched* fields, whereas only samples with LOI > 5% plot in the *CaO depleted* field. Caledonia

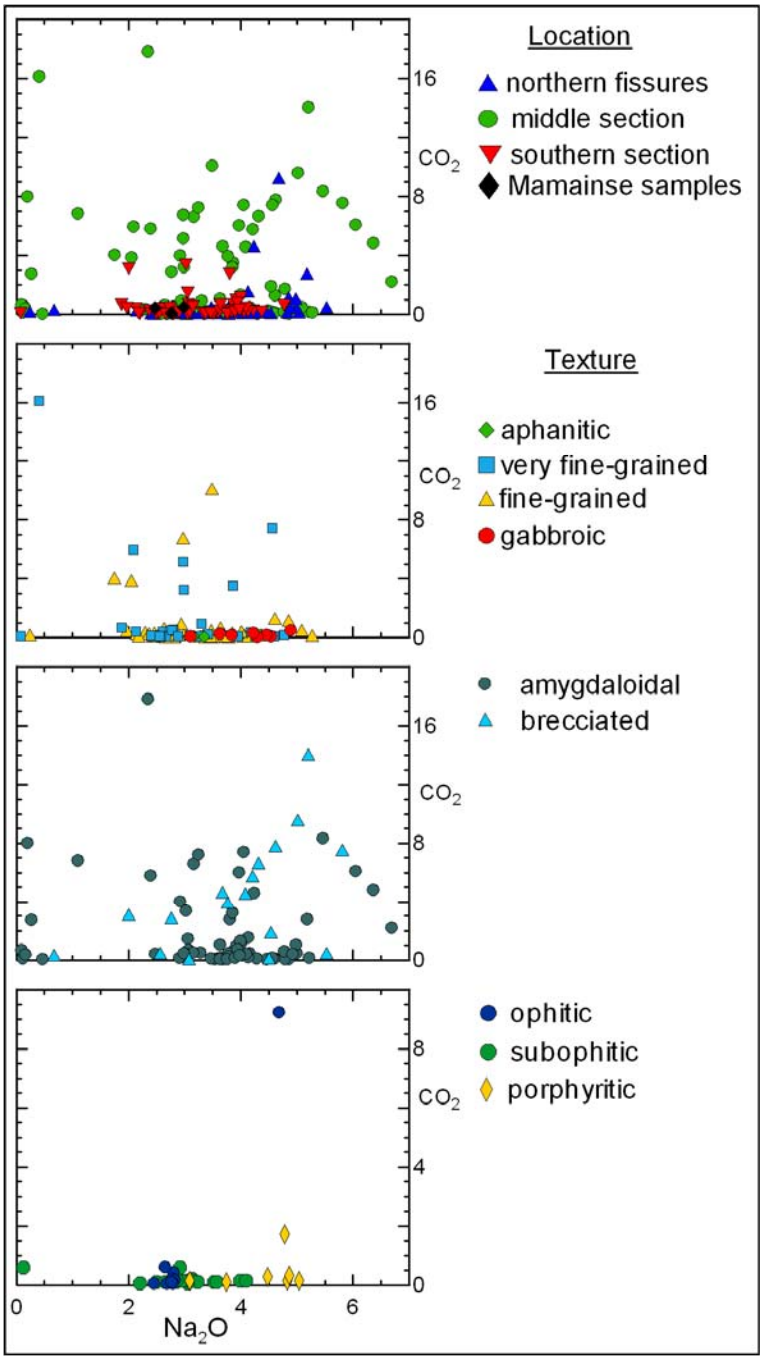

Figure 4.24: Bivariate diagrams for CO_2 vs. Na_2O differentiated by location and texture. Values for Na_2O were normalized to 100% without LOI, values for CO_2 were not normalized. All values are shown in weight %.

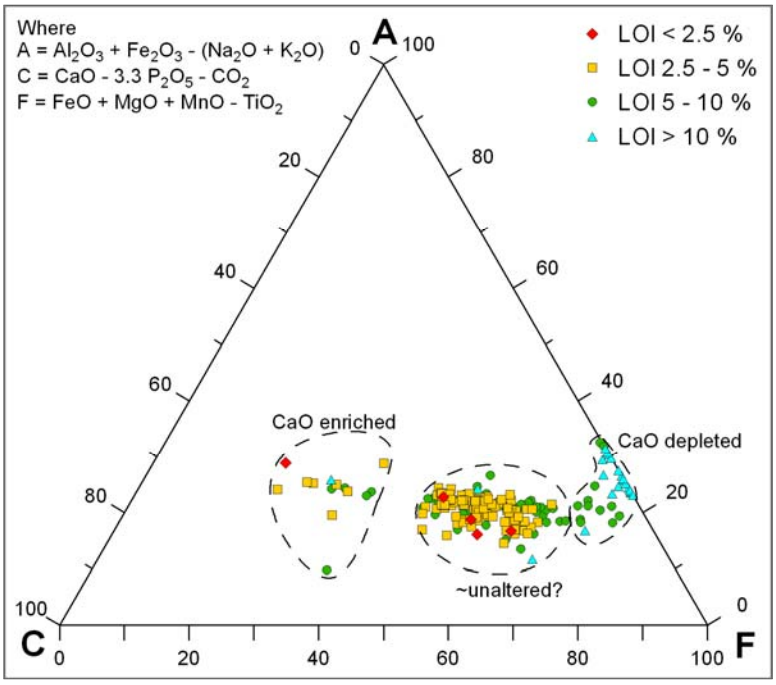

Figure 4.25: ACF diagram for samples by loss on ignition (LOI).

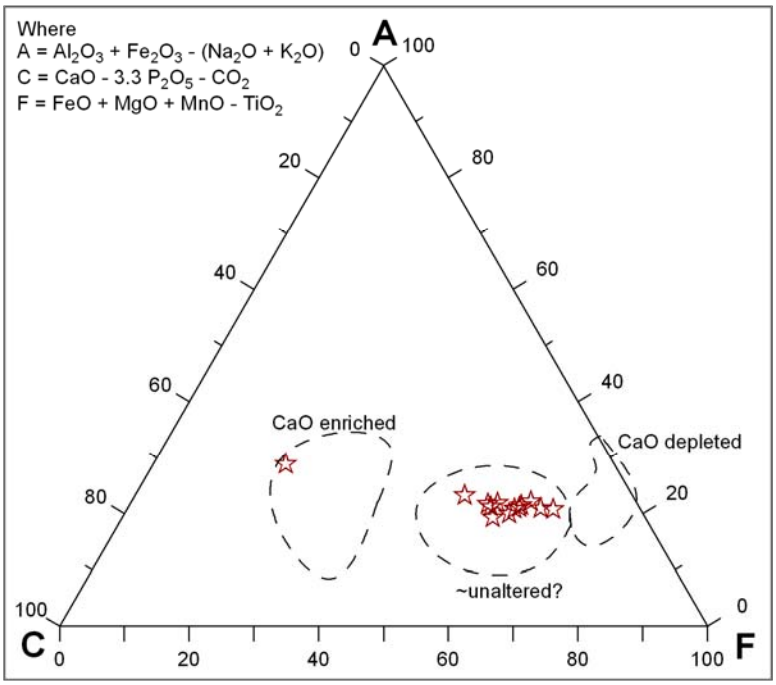

Figure 4.26: ACF diagram for Caledonia samples.

samples plotted in the *unaltered* group, with the exception of one sample (11CLD005), which plotted in the *CaO enriched* group.

Other ACF diagrams were constructed for data by location (Figure 4.27), grain size (Figure 4.28), for amygdaloidal and brecciated samples (Figure 4.29), and for ophitic, subophitic, and porphyritic samples (Figure 4.30). Samples from all locations plot in the *unaltered* and *CaO enriched* fields, and most samples in the *CaO depleted* field were collected in the middle section. Gabbroic and aphanitic samples all plot in the *unaltered* field. Brecciated and amygdaloidal samples are scattered in all fields, and most ophitic, subophitic, and porphyritic samples plot in the *unaltered* field as well, with the following exceptions: 10FU005 (subophitic), 10CL005, and 10SG001 (ophitic) plot in the *CaO enriched* field, and 10GR006 (porphyritic) plots in the *CaO depleted* field.

4.2.4 *AFM Diagrams*

AFM diagrams show relative abundances of alkalis ($Na_2O + K_2O$), iron oxide (total Fe as FeO), and magnesium oxide (MgO). The AFM diagrams were constructed as discussed in Appendix D.

An AFM diagram for all data by LOI is shown in Figure 4.31 and Caledonia samples are plotted in Figure 4.32. Low alkali samples are the same anomalous samples that stood out in the TAS diagram. The dashed line represents the dividing line between tholeiitic (above line) and calc-alkaline (below line) compositions after Irvine and Barager (1971) and is included in all figures for reference. Most samples plot near the dividing line, with few samples plotting as low alkali samples (10CE003, 10CN005, 10FU005, 10OJ002, 10TO004, 10T006, and 11CLD005), one sample as low magnesium (10CL005) and one sample as high magnesium (10CF001).

No trends are obvious for samples plotted by location (Figure 4.33). Samples by grain size are included in Figure 4.34. Gabbroic samples appear to cluster, while aphanitic samples appear to parallel the dividing line. Most amygdaloidal and

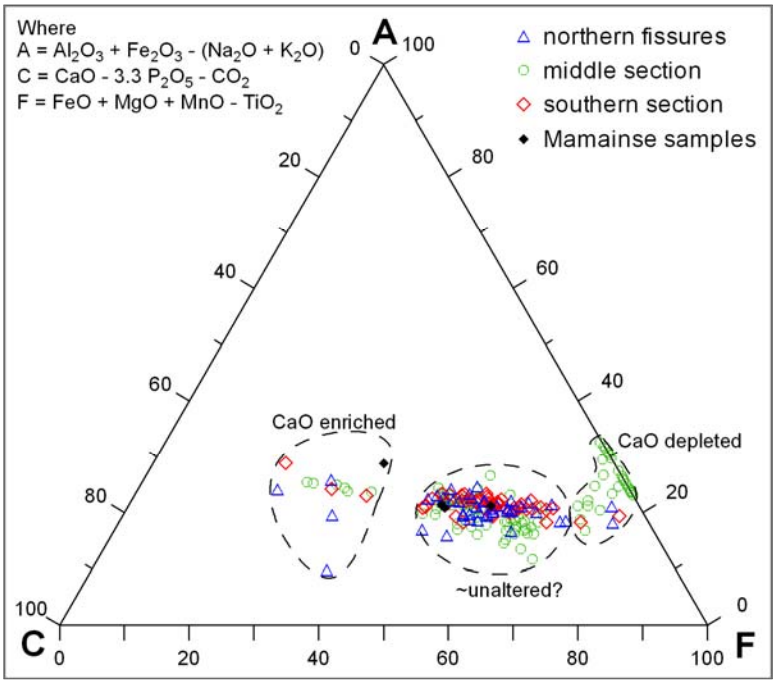

Figure 4.27: ACF diagram for samples by location.

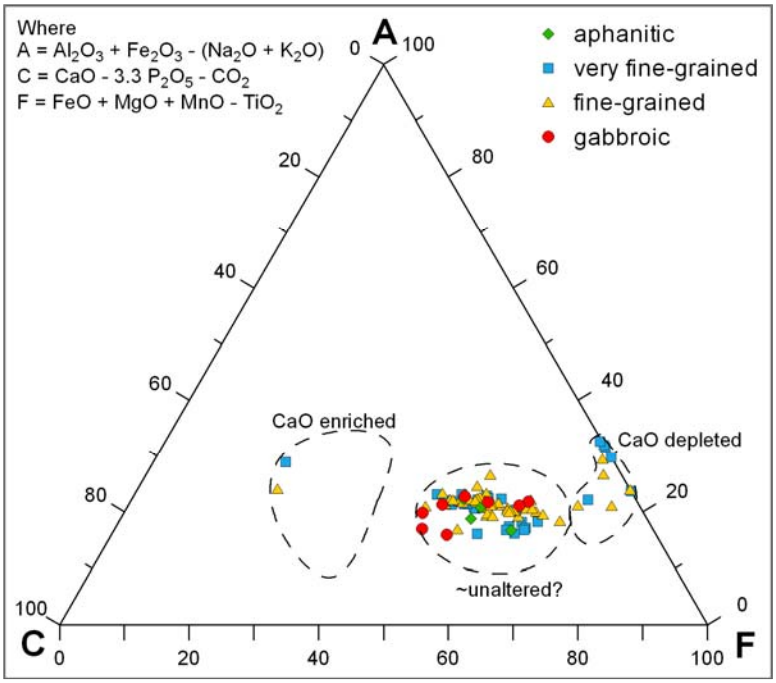

Figure 4.28: ACF diagram for samples by grain size.

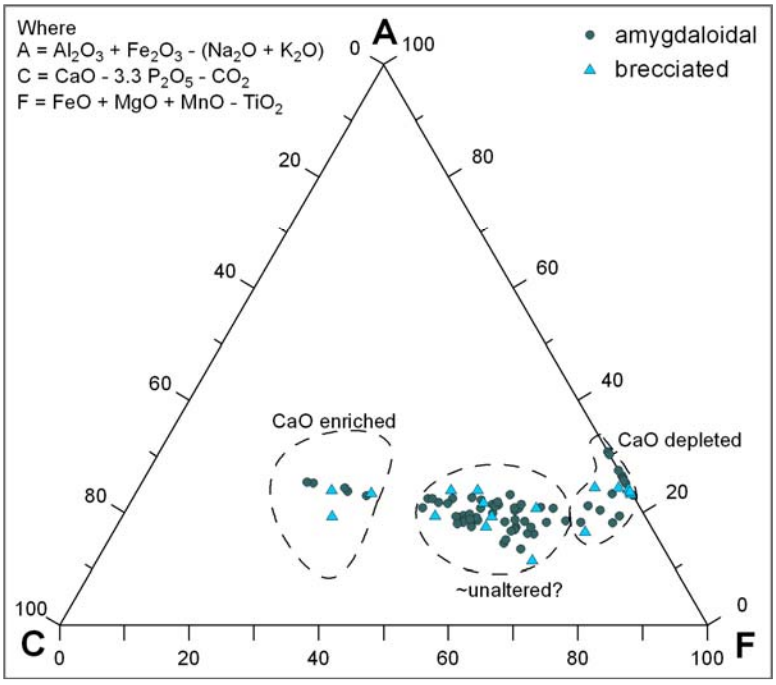

Figure 4.29: ACF diagram for amygdaloidal and brecciated samples.

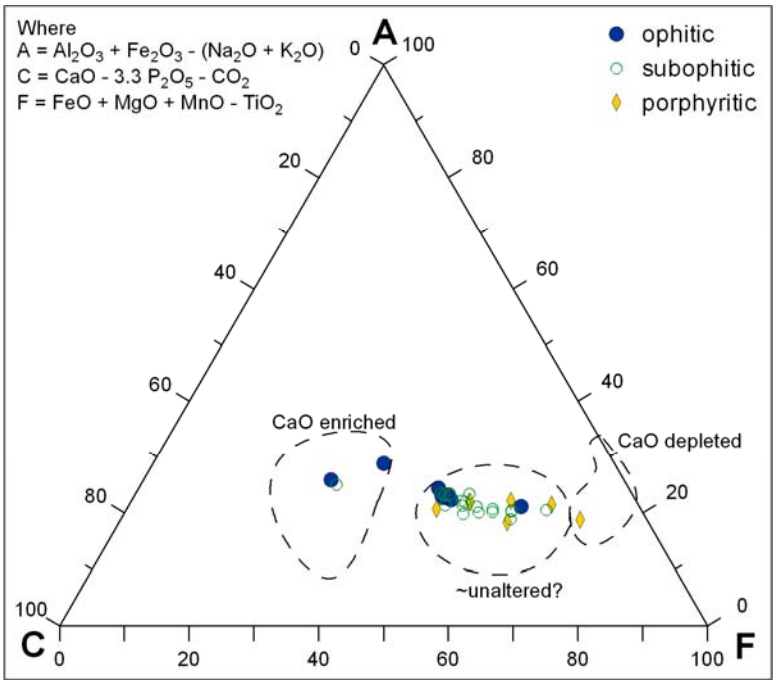

Figure 4.30: ACF diagram for ophitic, subophitic, and porphyritic samples.

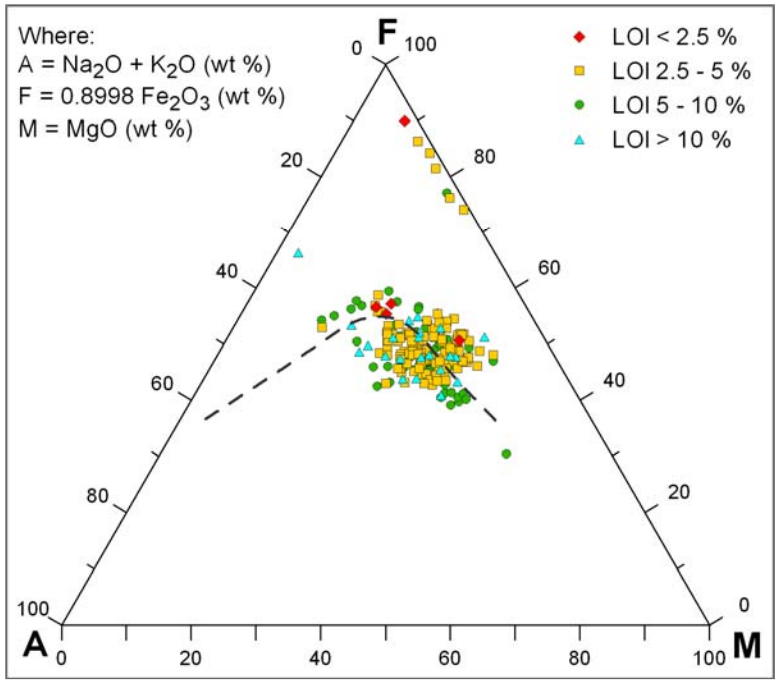

Figure 4.31: AFM diagram for all samples by LOI.

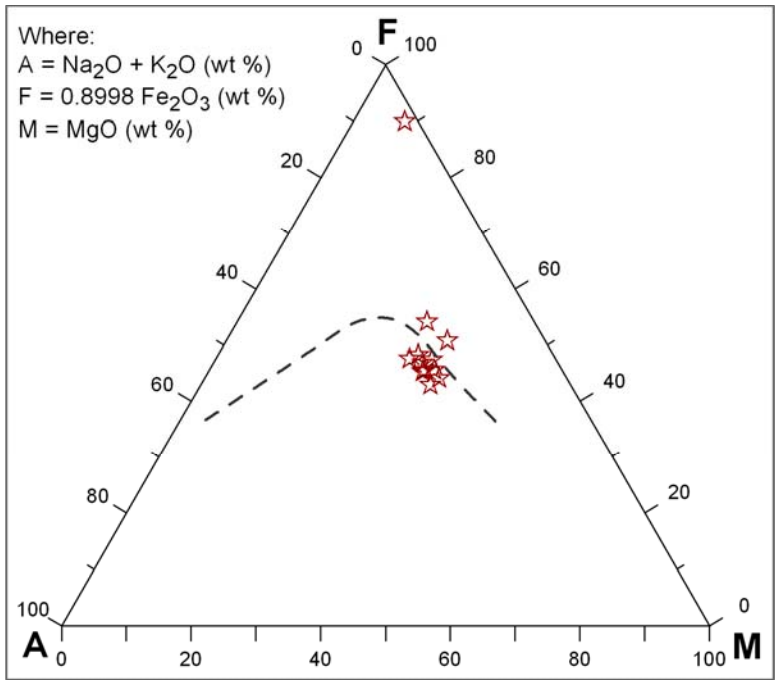

Figure 4.32: AFM diagram for Caledonia samples.

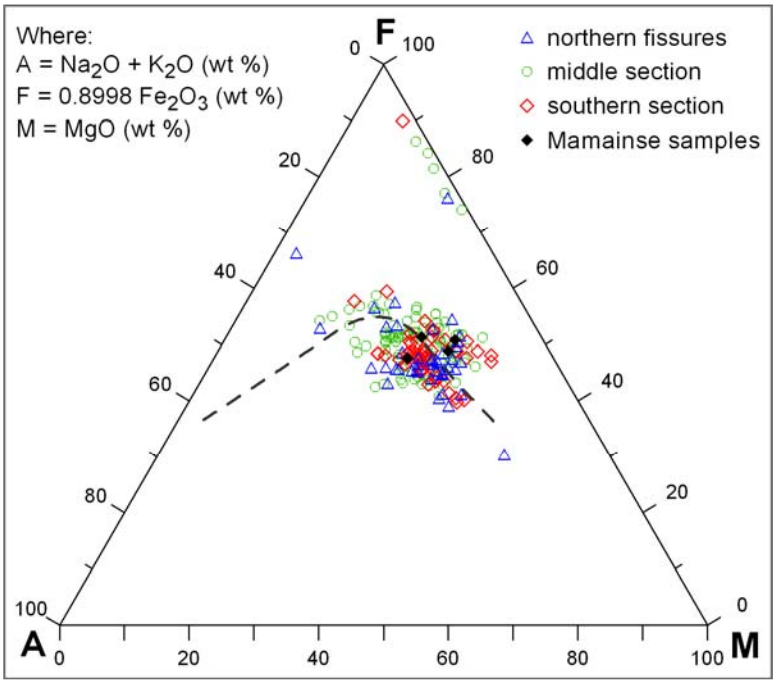

Figure 4.33: AFM diagram for samples by location.

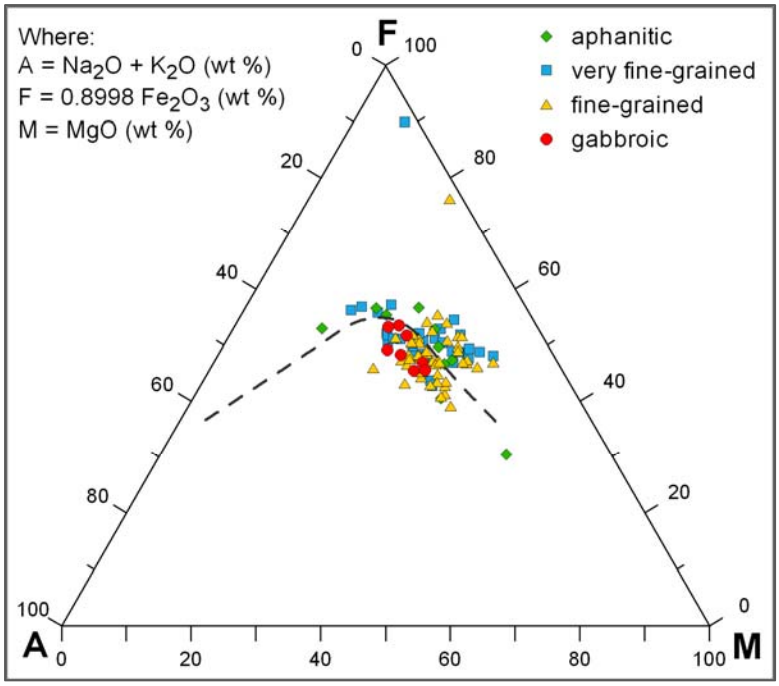

Figure 4.34: AFM diagram for samples by grain size.

brecciated samples are scattered throughout, with four amygdaloidal samples plotting as low alkali samples (Figure 4.35). Subophitic, ophitic, and porphyritic samples (Figure 4.36) mostly plot as higher magnesium samples along the dividing line. One subophitic sample plots as a low alkali sample, and one ophitic sample plots as a low magnesium sample.

4.3 Summary and Discussion

Classification systems based on immobile and mobile elements were used to characterize samples regarding their original composition, alteration, and trends with location and texture. Based on immobile element classification systems, the original composition of most samples is similar, with few outliers (Table 4.1): The majority of samples classifies as *subalkaline basalt*, and five samples classify as *andesite* based on Zr/TiO_2-Nb/Y diagrams. REE graphs were used to further characterize samples previously classified as andesite: The REE europium (Eu) becomes more depleted than other REE with fractionation, thus andesite samples should show a characteristic negative Eu anomaly. Sample 11CLD005 was confirmed to be an andesite using REE graphs, other "andesite" samples from *Houghton Exploration* (10HE002, 10HE004, and 10HE005) did not show an Eu low. These samples are likely extremely altered, leading to the mobilization of even the "immobile" elements. The Nb-Zr-Y ternary diagrams show some of the same outliers as detected using the Zr/TiO_2-Nb/Y diagrams. Overall, the Zr/TiO_2-Nb/Y proved to be most useful for the characterization of samples regarding their original composition. REE was helpful to verify andesite samples, and Nb-Zr-Y ternary diagrams could confirm some of the outlier samples. Any of the outliers should be disregarded for further mineral carbonation studies of the PLV, as they are not representative of most rocks in the study area.

The mobile element diagrams were used to detect trends of chemical alteration with location or texture. The TAS and AFM ternary diagrams help detect extremely low alkali samples, and an increasing scatter of data with increasing LOI while the ACF

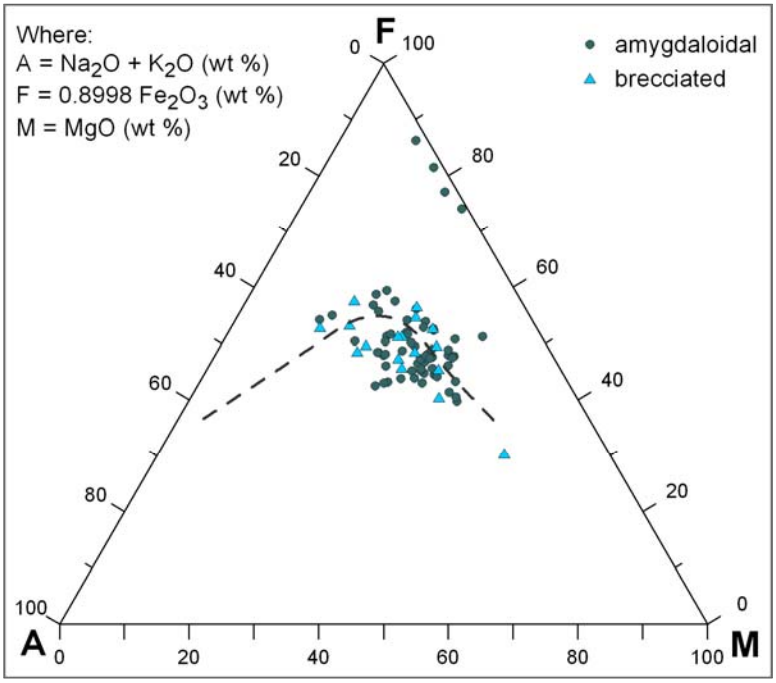

Figure 4.35: AFM diagram for amygdaloidal and brecciated samples.

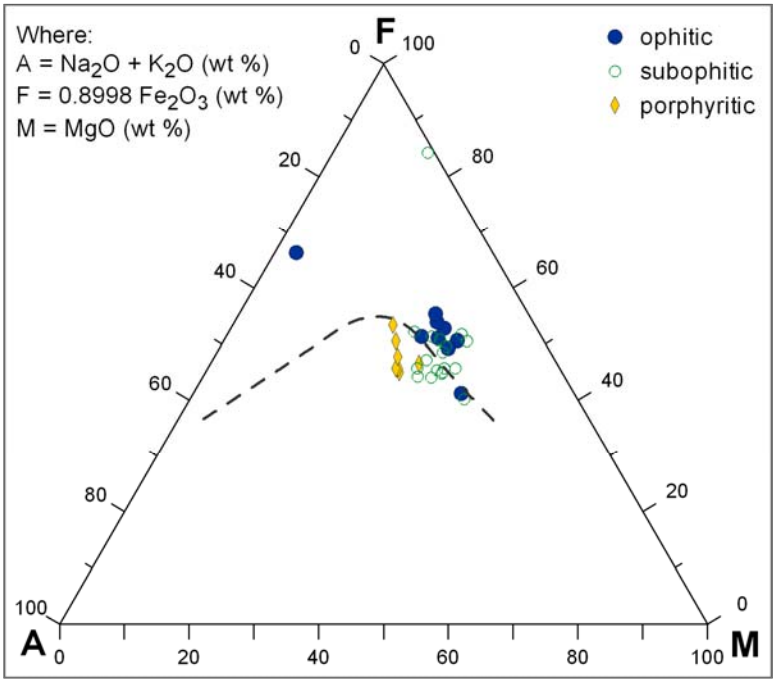

Figure 4.36: AFM diagram for ophitic, subophitic, and porphyritic samples.

Table 4.1: Summary of results based on immobile elements.

Diagram	Most samples classified as	Outliers classified as	Outlier samples
Zr/TiO_2-Nb/Y	Subalkaline Basalt	Andesite	10HE002, 10HE004, 10HE005, 11CLD005
Nb-Zr-Y	Within-plate Tholeiites	Within-plate Alkali Basalts	10HE002, 10HE004, 10HE005
		Normal mid ocean ridge basalts	10CF001, 10MB001, 10MB002
REE	N/A	higher values	10HE002, 10HE004, 10HE005
		lower values	10MB001, 10MB002

diagrams indicate samples with *CaO enriched*, *unaltered*, and *CaO depleted* silicate minerals; and bivariate diagrams reveal several trends: massive samples vary most in Na_2O, K_2O, and CaO content; high LOI samples contain highest amounts of CO_2; and brecciated samples contain highest amounts of K_2O.

Based on all mobile element diagrams, the following trends could be observed:

- compositions of southern section, gabbroic, ophitic, and subophitic samples vary the least, and
- compositions of middle section, amygdaloidal, and brecciated samples vary the most.

Thus, mobile element variations with texture show more variable compositions in the more permeable parts of flows (see Chapter 1) and less compositional variations in the less permeable parts of flows.

Overall, most samples display compositions very different from basalt. Compositional variations of most elements are likely due to hydrothermal alteration. Specifically, elevated percents CO_2, Na_2O, and K_2O are believed to be indicative of chemical alteration, but the lack of chemical alteration does not preclude mineralogical alteration. High LOI values likely reflect chemical alteration, yet samples with low LOI values are also potentially altered (e.g., the samples with extremely low alkali contents are likely chemically altered, yet some display low LOI values). Major element data can be used to identify chemically altered samples (that are likely mineralogically altered). Yet, samples without any apparent chemical alteration may also be mineralogically altered.

CHAPTER 5: THERMODYNAMIC MODELING

Thermodynamic modeling was used to determine reactions that should occur between (Ca,Mg)-silicates and CO_2. The rate of a given reaction ultimately determines the feasibility of a mineral for mineral carbonation, and kinetic modeling should be used to further study the thermodynamically feasible minerals. Any mineral that is thermodynamically unstable with respect to CO_2 (i.e., thermodynamically feasible for mineral carbonation), might not be feasible based on kinetics (i.e., the rate of reaction is too slow). Thermodynamic modeling can be used to determine what reactions should occur, kinetic modeling can then reveal the reactions that occur at reasonable rates. The thermodynamics and kinetics of some common (Ca,Mg)-silicates in basalts and ultramafic rocks have been studied by various authors with respect to mineral carbonation (see Chapter 1), whereas little information is available on many calcium- and magnesium-bearing alteration minerals found in the study area. For the purpose of this thesis, the thermodynamics of the reactions between (Ca,Mg)-silicate minerals present in the study area and CO_2-gas were determined.

Several programs from Geochemist's Workbench (Bethke, 2000) were used for thermodynamic modeling. Stability fields of minerals with respect to fCO_2 and $aSiO_2(aq)$ at standard conditions and assuming the presence of H_2O were constructed in *Act2* for mineral group end-members best representing minerals found in the study area. For some minerals, the presence of kaolinite, hematite, or potassium-feldspar (kspar) was assumed in order to accommodate Al^{3+}, Fe^{3+}, or K^{+}, respectively. These minerals were allowed to speciate over x and y. The stability of kaolinite and kspar is shown on diagrams where applicable. Often, minerals of interest are not stable at standard conditions, and their decomposition products were plotted instead (e.g., talc in Figure 5.1). For minerals not stable at standard conditions (e.g. forsterite, Figure 5.2), decomposition minerals were suppressed in

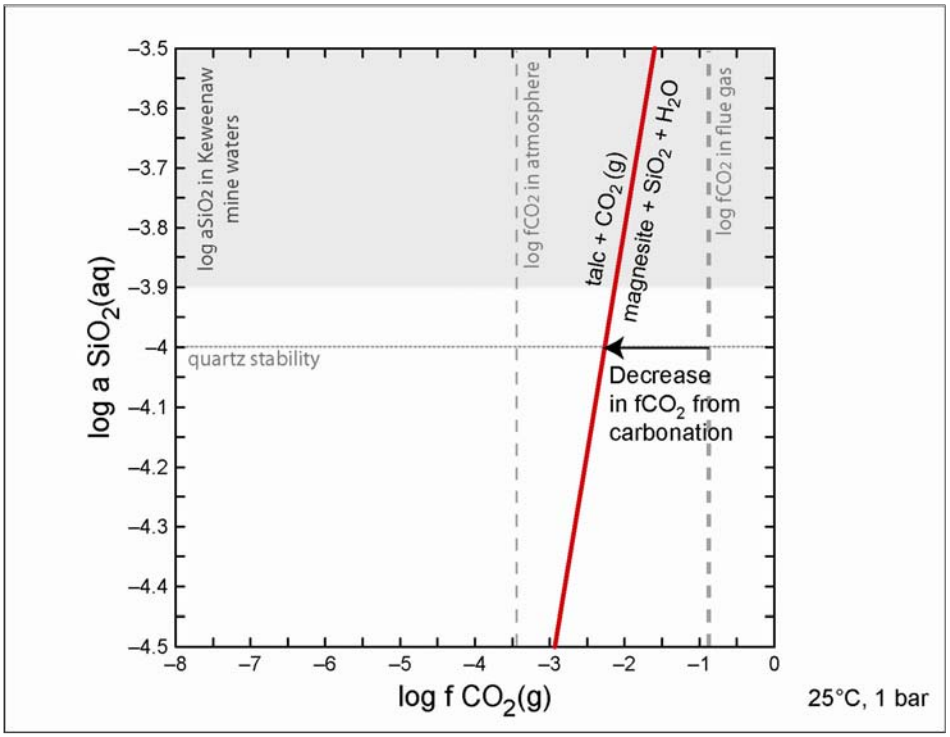

Figure 5.1: Stability of forsterite decomposition products at standard conditions.

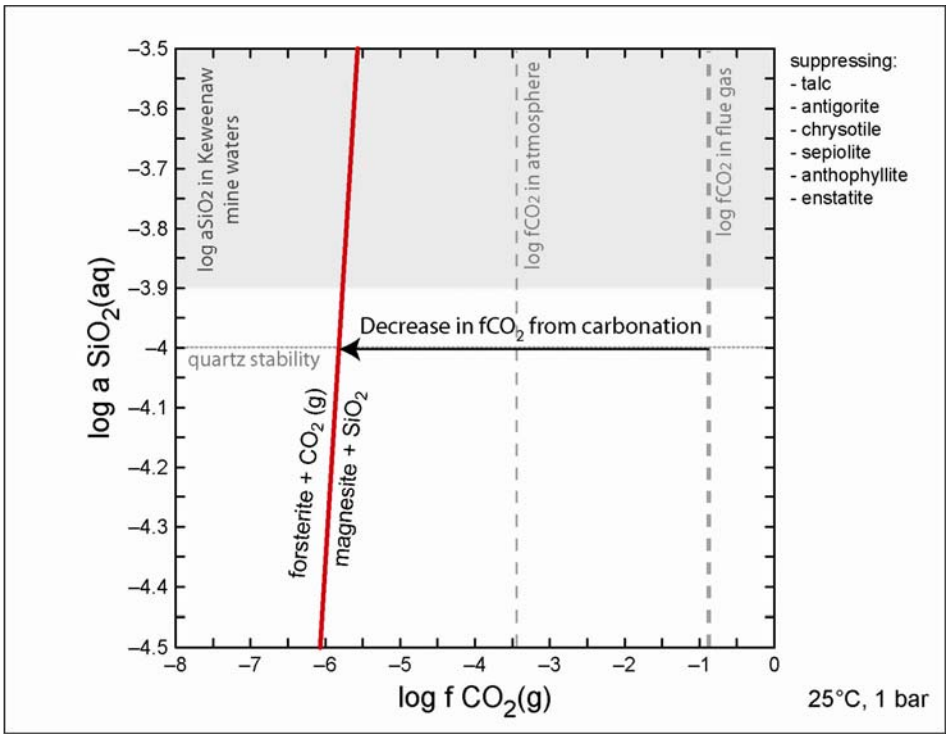

Figure 5.2: Stability of forsterite at standard conditions.

Act2 until a plot containing the mineral of interest was created. Any mineral formulas provided in this chapter reflect the chemical formulas used by *Geochemist's Workbench* (Bethke, 2000).

The plotted minerals then were used to write balanced reactions and to determine the equilibrium constants at various temperatures in *Rxn*. The log fCO_2 needed for equilibrium was calculated assuming an activity of H_2O of one, if present. Log fCO_2 needed for equilibrium was plotted with varying temperature for the given reactions. This step was completed for minerals stable at standard conditions and those minerals that could only be plotted through suppressing more stable minerals (i.e., minerals not technically in equilibrium). Balanced equations, equilibrium constants at varying temperatures for the given reactions, and the derived equations for fCO_2 needed for minerals to be at equilibrium are included in Appendix I. Mineral stability fields and plots of fCO_2 needed for minerals to be at equilibrium at varying temperatures are included with the text. The change of mineral stability with temperatures between 0° and 150 °C at one bar pressure and varying fCO_2 was visualized in *Tact* for mineral assemblages stable at standard conditions, and for minerals of interest, plotted by suppressing the stable minerals.

Minerals were not modeled using different pressures, as raising the total pressure (P_{total}) decreases the mole fraction of CO_2 (X_{CO2}) in the gas phase, while not affecting the fugacity of CO_2 (see Equation 2).

$$fCO_2 \approx X_{CO_2} * P_{total} \quad (2)$$

The aim of mineral carbonation is the removal of CO_2 from flue gas by reaction with minerals. The tendency of CO_2 to be removed is given by the log fCO_2 value at equilibrium for a given assemblage. If the fCO_2 at equilibrium is below that of flue gas, fCO_2 should decrease until equilibrium conditions are met. Using the example of forsterite (Figure 5.2), fCO_2 would decrease from log -1 (0.1 bar) to log -6 (10^{-6} bar), at quartz stability, essentially stripping CO_2 from the CO_2 bearing phase.

5.1 Olivine Group

Olivine group minerals in the study area had a forsterite (Mg_2SiO_4) content of roughly 50 to 60% (see Chapter 3), so both the magnesium end-member forsterite and the iron end-member fayalite (Fe_2SiO_4) were used for thermodynamic modeling. A diagram with stability fields for the decomposition products of forsterite with varying log fCO_2 at standard conditions and in the presence of H_2O, is shown in Figure 5.1. Forsterite is not stable at standard conditions and talc is plotted instead. In order to create a diagram showing forsterite and magnesite, the minerals talc, antigorite, chrysotile, sepiolite, anthopyllite, and enstatite had to be suppressed (Figure 5.2). A progression of diagrams between modeling decomposition products of forsterite (without suppressing more stable minerals) and forsterite (by suppressing more stable minerals) is included in Appendix J. For all other minerals modeled, the progression of diagrams is not included in this thesis; only the first and last diagrams are included.

The log fCO_2 values required for equilibrium between forsterite and magnesite are between -5.5 and -6, yet the instability of forsterite with respect to talc ultimately dictates CO_2 that can be sequestered using forsterite. Since talc is thermodynamically stable up to a log fCO_2 of about -2.5 at quartz stability, any of the magnesite shown in Figure 5.2 should combine with SiO_2, and form talc while releasing CO_2, until a log fCO_2 of -2.5 is reached. The stability of forsterite with varying temperatures, assuming quartz stability was plotted for one bar pressure. Again, since forsterite is not stable at standard conditions, talc was plotted when no minerals were suppressed for modeling (see Figure 5.3). In order to plot forsterite, the minerals talc, antigorite, chrysotile, sepiolite, anthopyllite, and enstatite were suppressed (see Figure 5.4).

Balanced chemical reactions for talc, CO_2, H_2O, and magnesite, as well as forsterite, CO_2, and magnesite are included in Appendix I with equilibrium constants. The

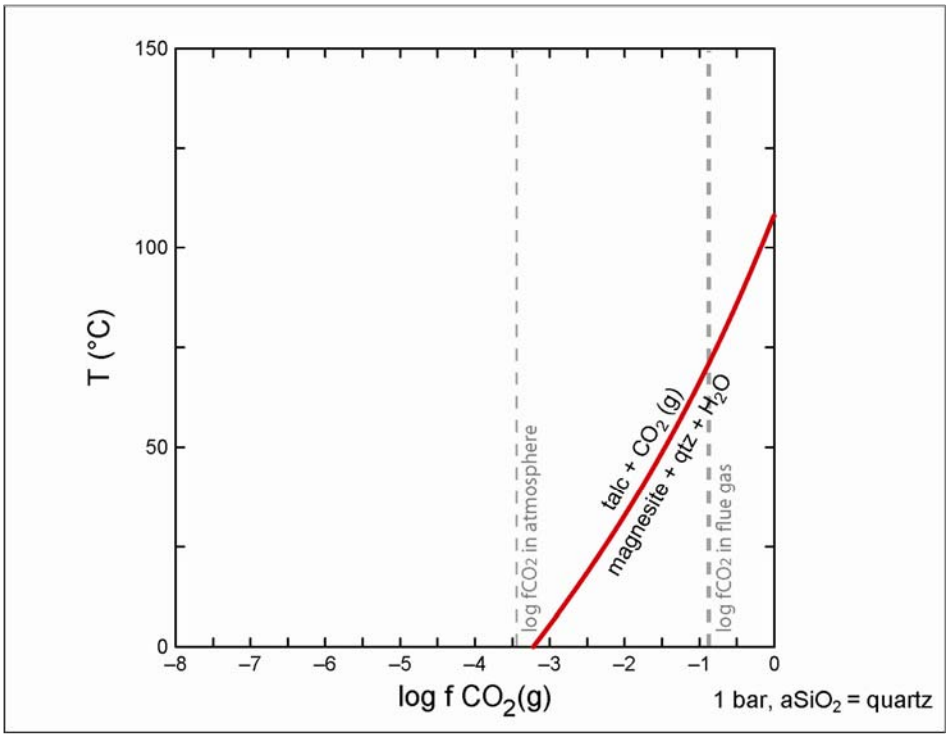

Figure 5.3: Stability of forsterite decomposition products with temperature and fCO_2.

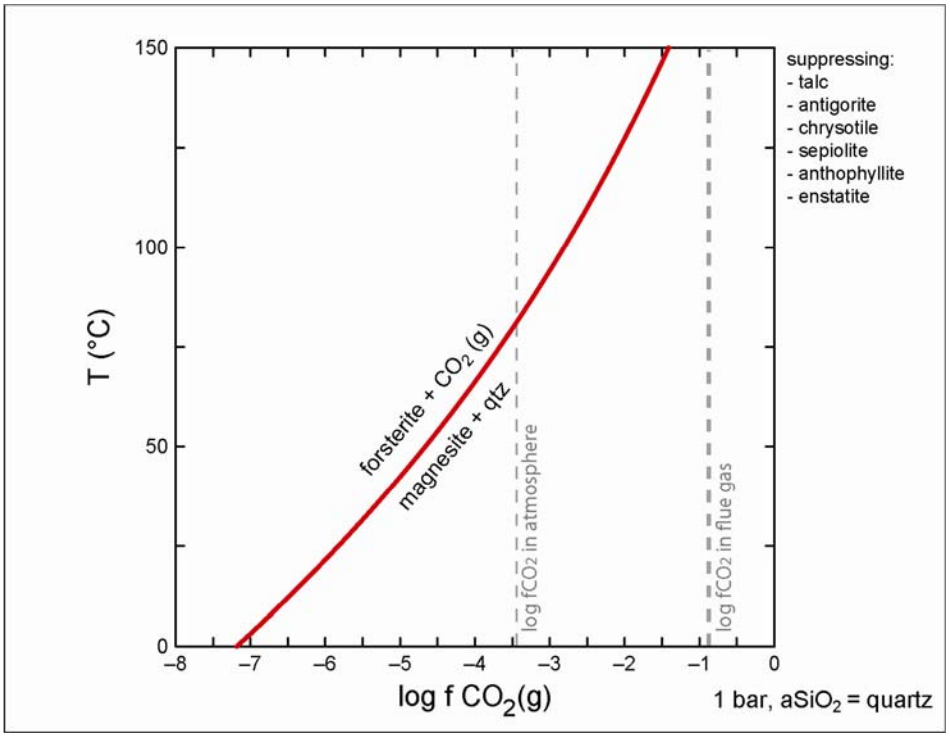

Figure 5.4: Stability of forsterite with temperature and fCO_2.

equilibrium constants for the given chemical equations at varying temperatures were used to calculate the log fCO_2 needed for equilibrium, an example of which is shown in Figure 5.5. For example, if forsterite reacts with CO_2 at 25°C and reaches equilibrium, CO_2 is stripped from the flue gas until log fCO_2 values reach -6.

The iron end-member of olivine, fayalite, was modeled in the presence of H_2O at standard conditions. Fayalite is not stable at standard conditions and instead minnesotaite and greenalite were plotted (Figure 5.6). In order to plot fayalite and siderite, minnesotaite, greenalite, FeO(c) and ferrosilite had to be suppressed for modeling (Figure 5.7).

The formation of the iron carbonate siderite requires the presence of Fe^{2+} and an essentially oxygen-free environment, which is unrealistic for the purpose of CO_2 sequestration. The stability of siderite at standard conditions was plotted in A*ct*, assuming the presence of H_2O, with varying fCO_2 and fO_2 (Figure 5.8). The dashed line at log fO_2 ~ -83 represents the stability limits of water. The log fCO_2 for atmosphere and flue gas, as well as log fO_2 of the atmosphere, are shown in the figure for reference. As can be seen, the stability field of siderite requires far lower log fO_2 values than are found in the atmosphere. No further modeling was completed for fayalite due to the requirement of extremely low fO_2 for the stability of siderite.

5.2 Anorthite

Since Na- and K-carbonates are soluble in water and thus not suitable for mineral carbonation (Metz et al., 2005), only the calcium end-member of the feldspar group was used for thermodynamic modeling. Anorthite contents (X_{an}) of up to 0.82 were found in plagioclase minerals of less altered samples in the study area (see Chapter 3). The stability of anorthite with varying fCO_2 and $aSiO_2(aq)$ at standard conditions was modeled in the presence of H_2O and kaolinite [$Al_2Si_2O_5(OH)_4$]. Resulting stability fields for decomposition products of anorthite are shown in

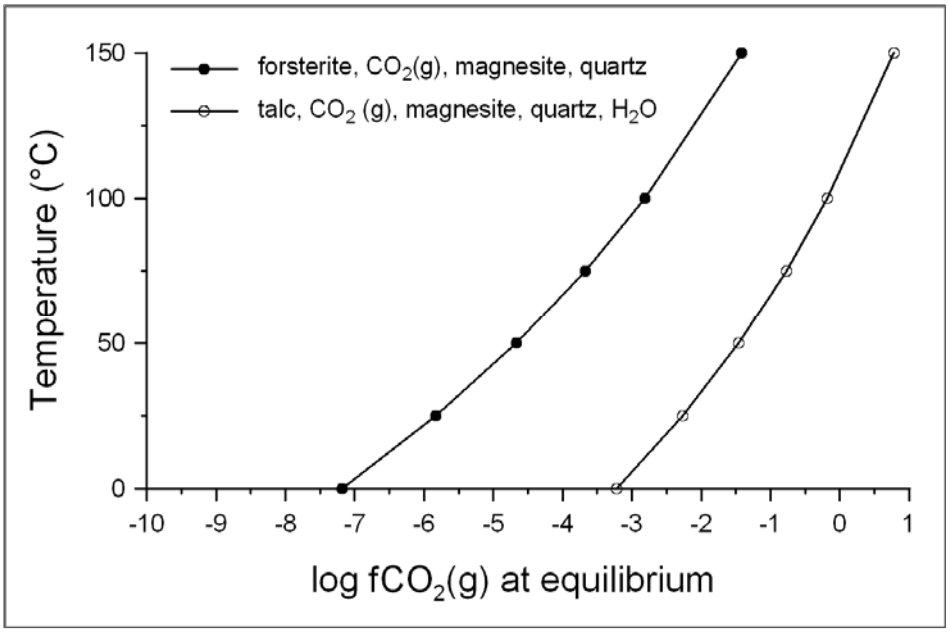

Figure 5.5: Log fCO_2 at equilibrium between forsterite products at varying temperatures.

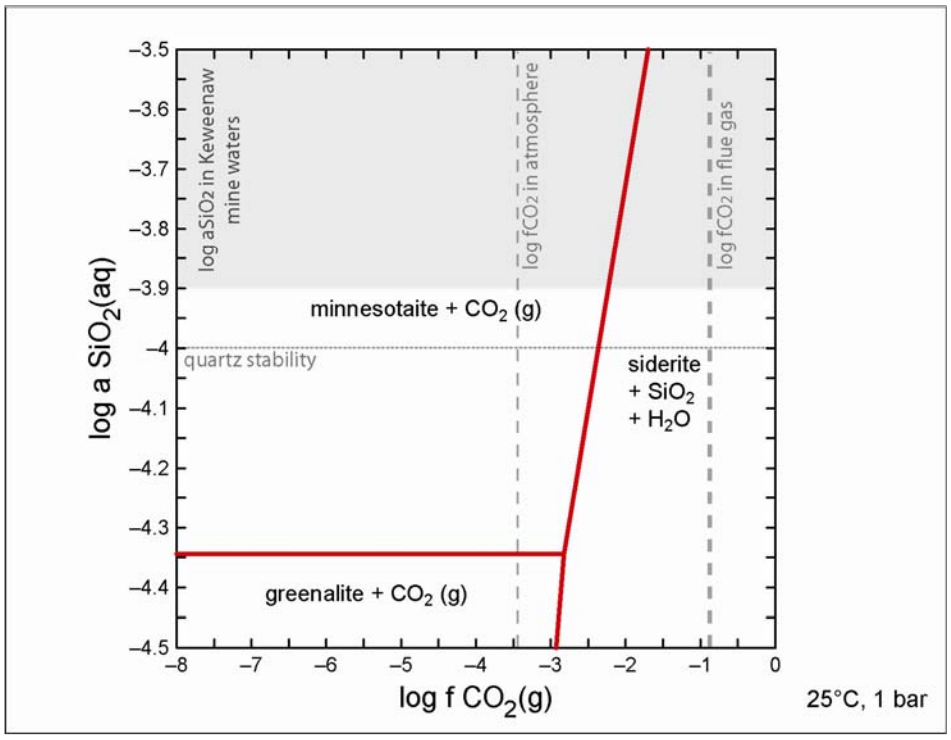

Figure 5.6: Stability of fayalite decomposition products at standard conditions.

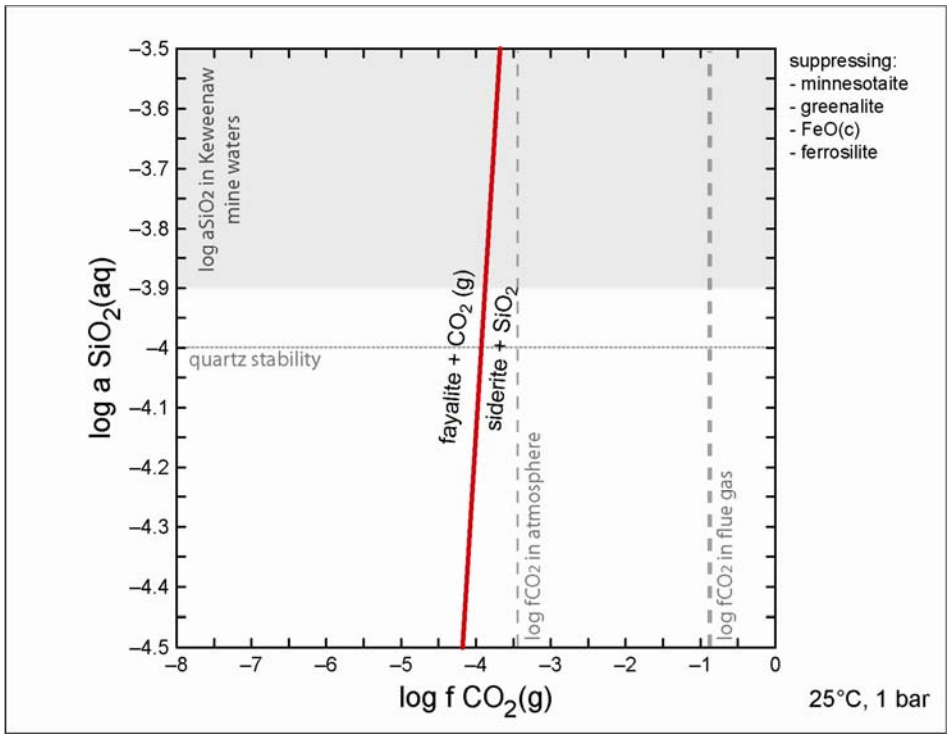

Figure 5.7: Stability of fayalite at standard conditions.

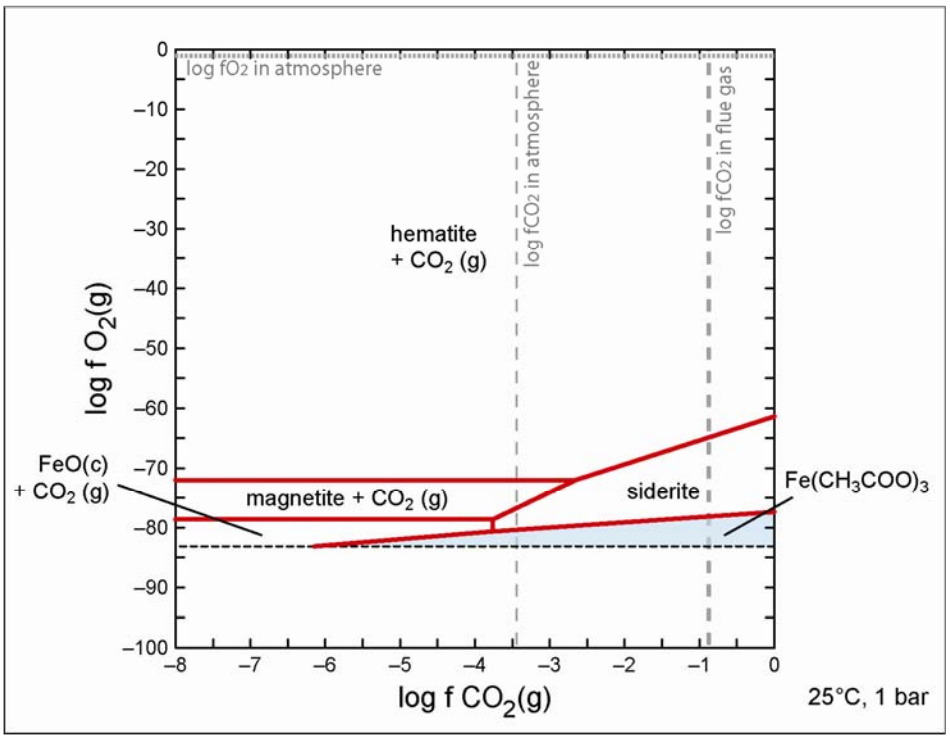

Figure 5.8: Stability of siderite with varying fCO_2 and fO_2 at standard conditions.

Figure 5.9. In order to plot anorthite and calcite without any of the decomposition products, 20 minerals had to be suppressed (Figure 5.10). Minerals suppressed included: clinoptilolite-Ca, laumontite, heulandite, beidellite-Ca, prehnite, lawsonite, grossular, clinozoisite, zoisite, $Ca_2Si_3O_8 \cdot 5/2\ H_2O$, $Ca_5Si_6O_{17} \cdot 21/2\ H_2O$, $CaSi_2O_5 \cdot 2\ H_2O$, wollastonite, $Ca_5Si_6O_{17} \cdot 11/2\ H_2O$, pseudowollastonite, $Ca_5Si_6O_{17} \cdot 3H_2O$, wairakite, margarite, $Ca_4Si_3O_{10} \cdot 3/2\ H_2O$, and $Ca_6Si_6O_{18} \cdot H_2O$. Figure 5.11 shows the stability of decomposition products of anorthite with temperatures between 0 and 150°C, varying fCO_2, and at quartz stability. Figure 5.12 shows anorthite, calcite, rankinite ($Ca_3Si_2O_7$), and kaolinite at varying temperatures, fCO_2, and at quartz stability without the suppressed decomposition products. The log fCO_2 values needed for equilibrium of the reactions at quartz stability were calculated and are shown for both reactions in Figure 5.13 at varying temperatures.

5.3 Pyroxene Group

Most pyroxene group minerals could be classified as Fe-poor augite, for which diopside ($CaMgSi_2O_6$) was used as the closest approximation for thermodynamic modeling. In fresher samples, orthopyroxene was observed, mostly with compositions between the magnesium and iron end-members, enstatite ($MgSiO_3$) and ferosillite ($FeSiO_3$), respectively, for which thermodynamic modeling was performed as well.

The stability of diopside with varying fCO_2 and $aSiO_2$ (aq) at standard conditions is shown in Figure 5.14, assuming the presence of H_2O. Diopside is stable at standard conditions and no minerals had to be suppressed in order to plot diopside and dolomite. The stability of diopside at varying temperatures, log fCO_2, 1 bar pressure, and quartz stability is shown in Figure 5.15. The log of fCO_2 needed for equilibrium for the balanced reaction was calculated for quartz stability and plotted with varying temperatures (Figure 5.16). Equilibrium constants and equations are included in Appendix I.

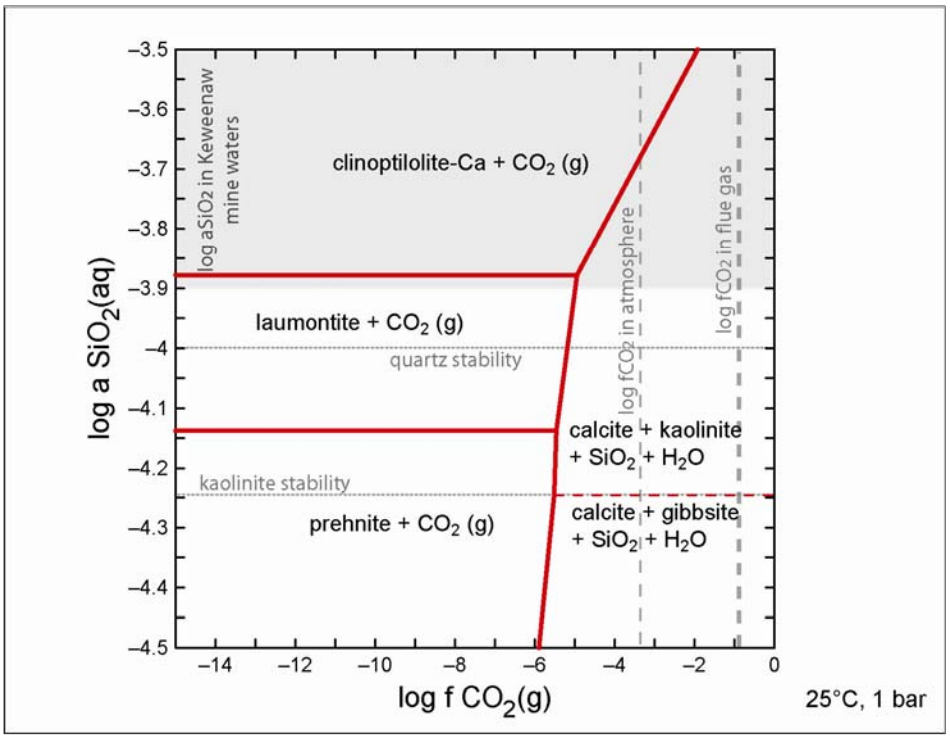

Figure 5.9: Stability of anorthite decomposition products at standard conditions.

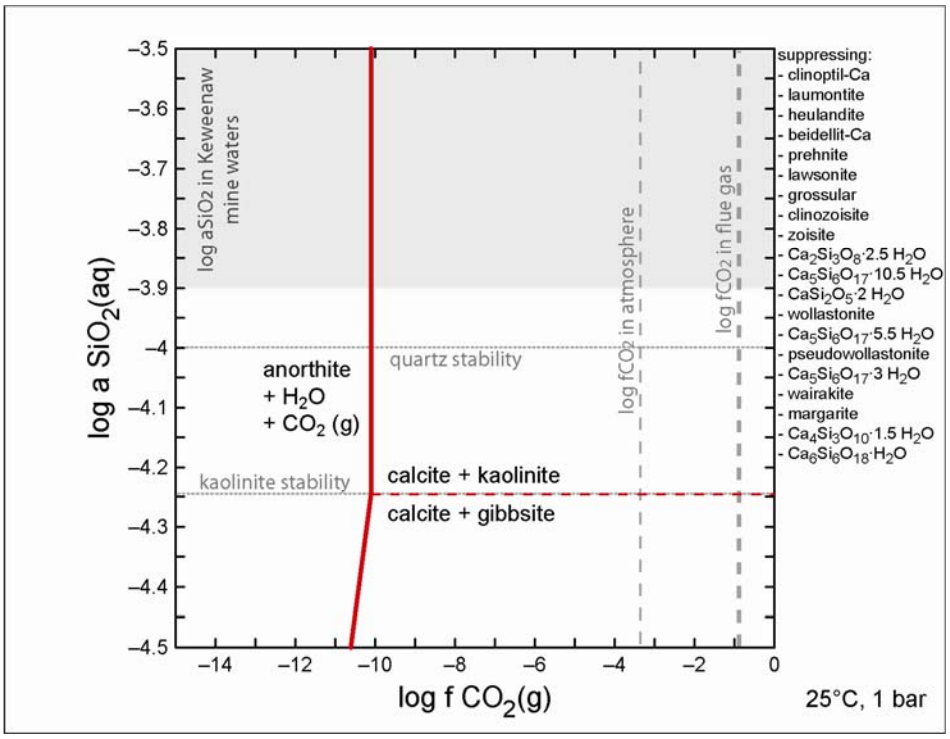

Figure 5.10: Stability of anorthite at standard conditions.

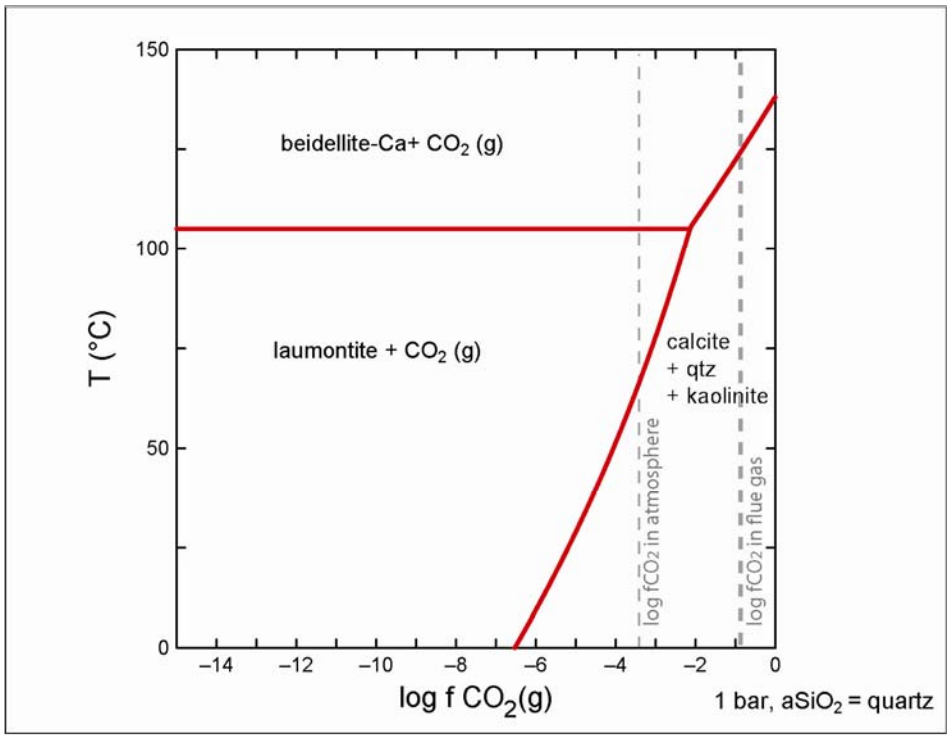

Figure 5.11: Stability of anorthite decomposition products with temperature and fCO_2.

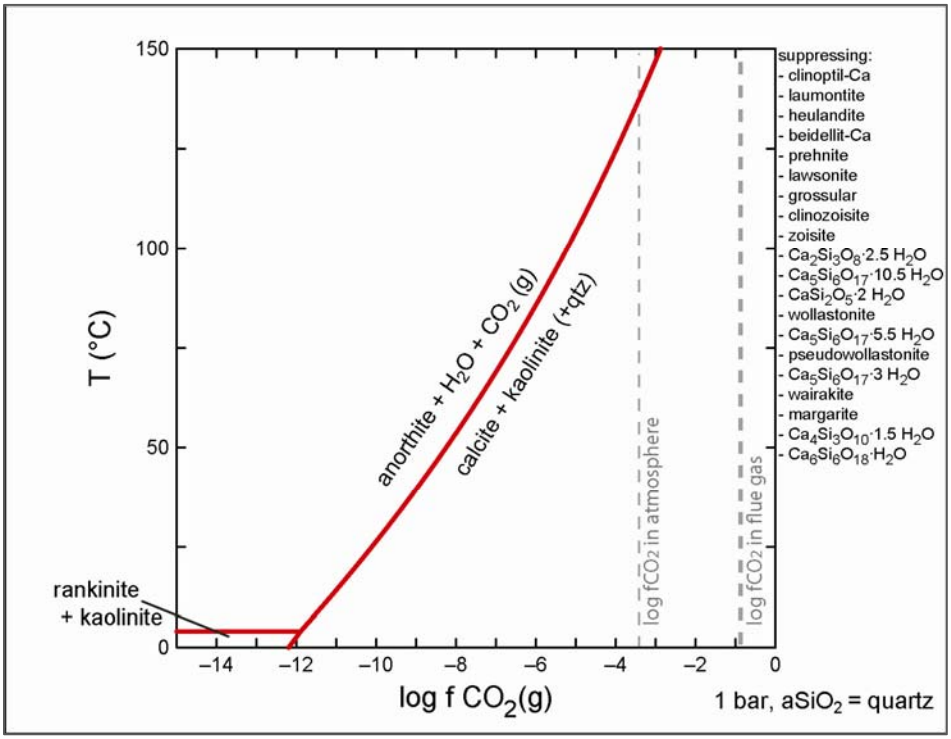

Figure 5.12: Stability of anorthite with temperature and fCO_2.

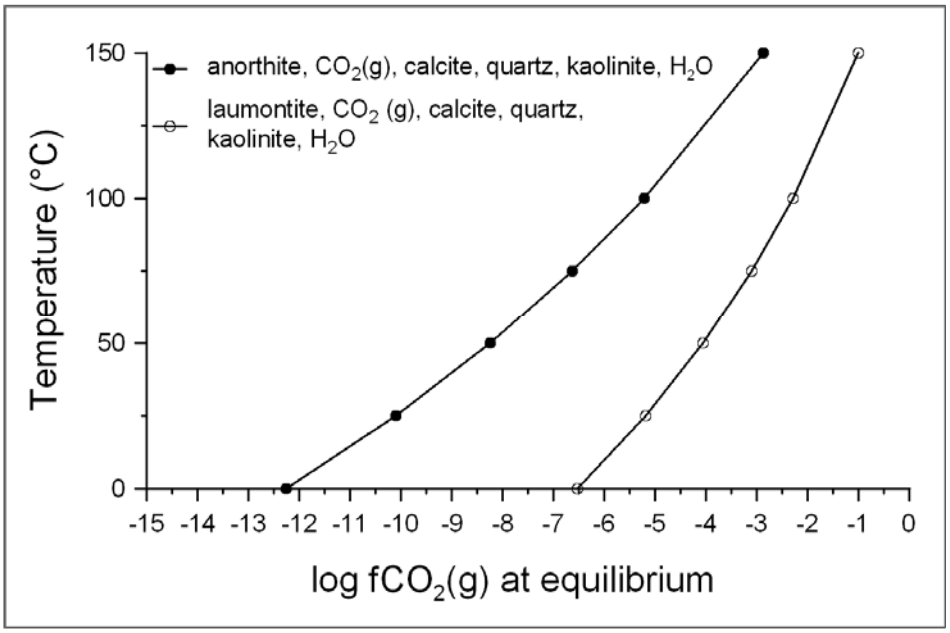

Figure 5.13: Log fCO_2 at equilibrium between anorthite products at varying temperatures.

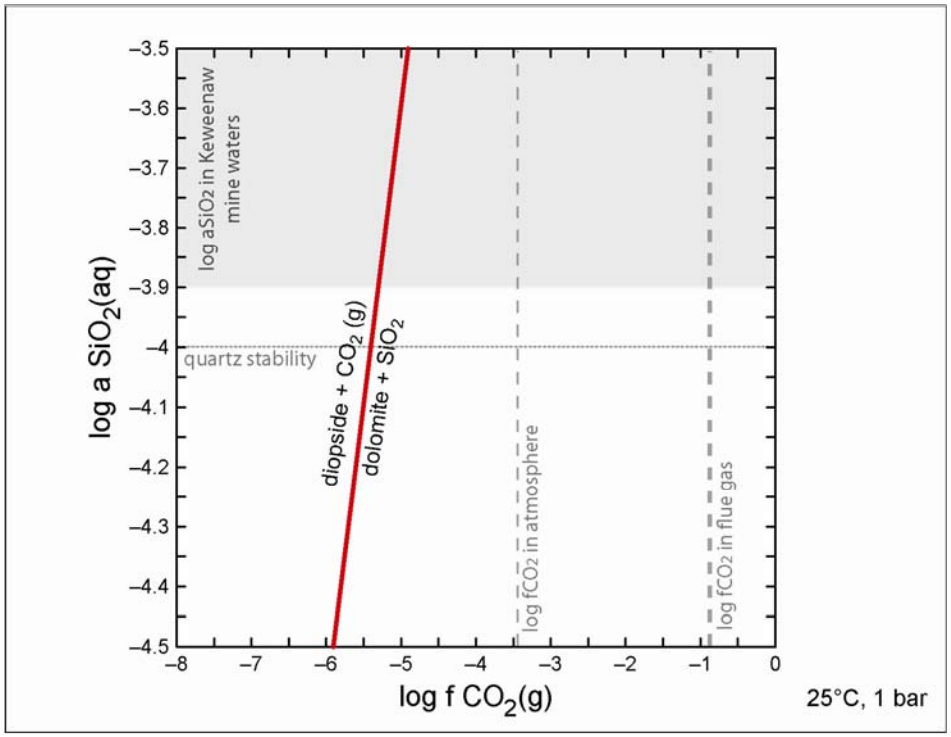

Figure 5.14: Stability of diopside at standard conditions.

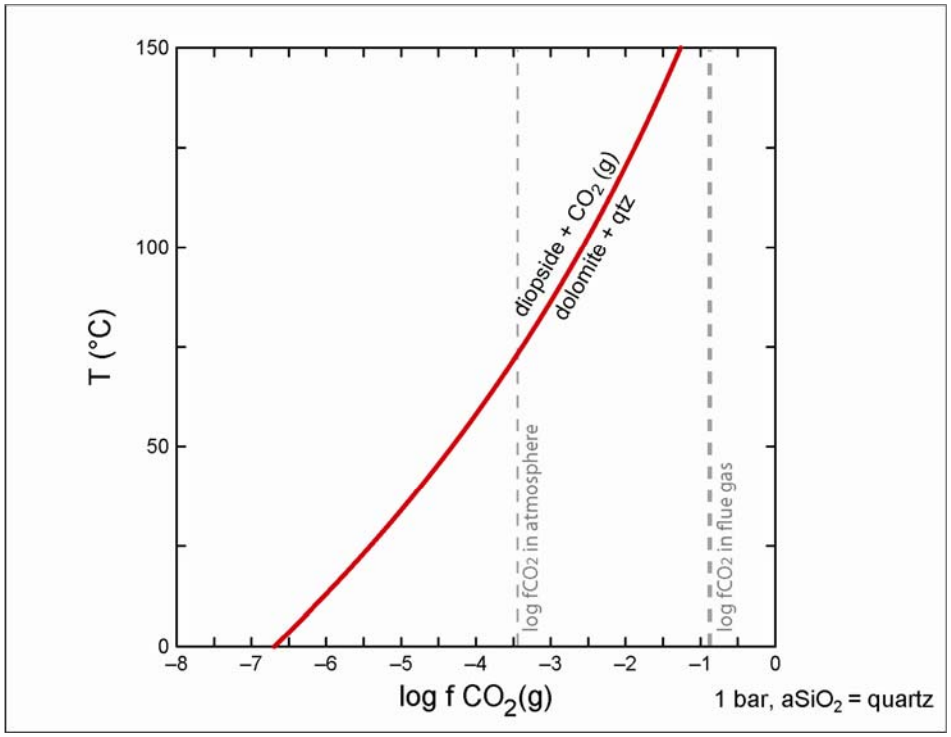

Figure 5.15: Stability of diopside with temperature and fCO_2.

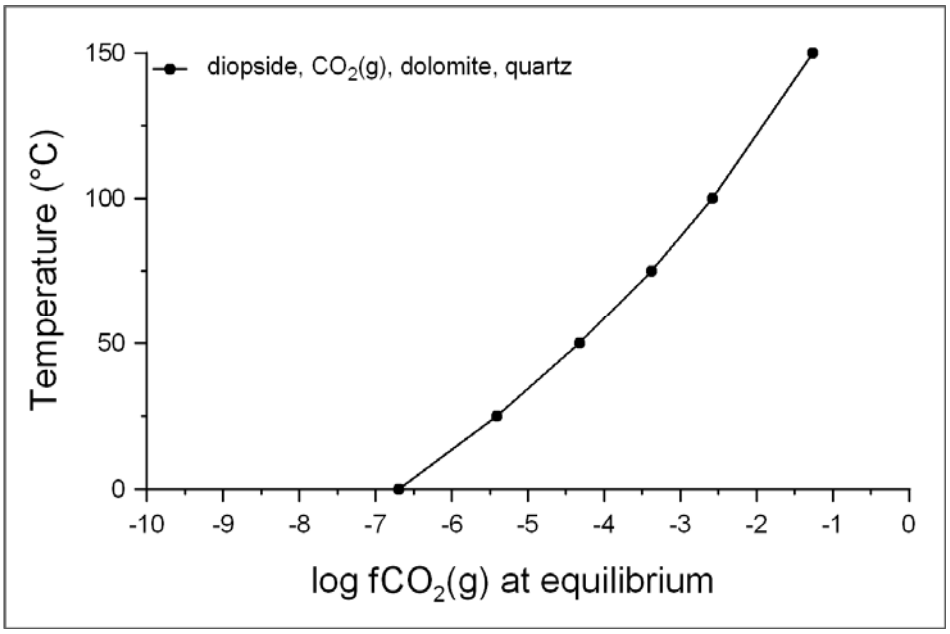

Figure 5.16: Log fCO_2 at equilibrium between diopside products at varying temperatures.

The stability of enstatite with varying log fCO_2 and log $aSiO_2$ (aq), at standard conditions, and in the presence of H_2O, produces the same stability diagram as for the decomposition products of forsterite. Since enstatite is not stable at low temperatures, talc, antigorite, and magnesite are plotted instead (Figure 5.17). In order to plot enstatite and magnesite, the minerals talc, antigorite, chrysotile, sepiolite, and anthopyllite had to be suppressed (Figure 5.18). The stability of enstatite decomposition products with varying temperatures is included in Figure 5.19; and Figure 5.20 shows the stability of enstatite with varying temperatures. The log fCO_2 needed for equilibrium of the balanced chemical reactions were calculated for quartz stability and are shown in Figure 5.21.

The iron end-member of pyroxene, ferrosilite, was modeled in the presence of H_2O at standard conditions. Ferrosilite is not stable at standard conditions and instead minnesotaite, siderite, and greenalite were plotted, just as for the iron end-member of olivine, fayalite (Figure 5.22). Ferrosilite and siderite were plotted in Figure 5.23, suppressing minnesotaite, greenalite, and FeO (c). As mentioned for modeling of fayalite, the formation of the iron carbonate siderite requires the presence of Fe^{2+} and an essentially oxygen free environment, which is unrealistic for the purpose of CO_2 sequestration. No further modeling was completed for ferrosilite due to the requirement of extremely low fO_2.

5.4 Chlorite Group

For the chlorite group minerals, the end-members clinochlore ($Mg_5Al_2Si_3O_{10}$), ripidolite [$Fe_2Mg_3Al_2Si_3O_{10}(OH)_8$], and daphnite [$Fe_5Al_2Si_3O_{10}(OH)_8$] were used to represent chlorites found in the rocks of the study area. Clinochlore was modeled as "clinochlore-14A" in the presence of kaolinite and H_2O. At standard conditions clinochlore is not stable, and saponite-Mg is shown instead (Figure 5.24). Figure 5.25 shows the stability of clinochlore, when suppressing the stable minerals saponite-Mg, talc, saponite-H, and antigorite. The decomposition products of clinochlore in the presence of kaolinite and quartz at varying temperatures and fCO_2

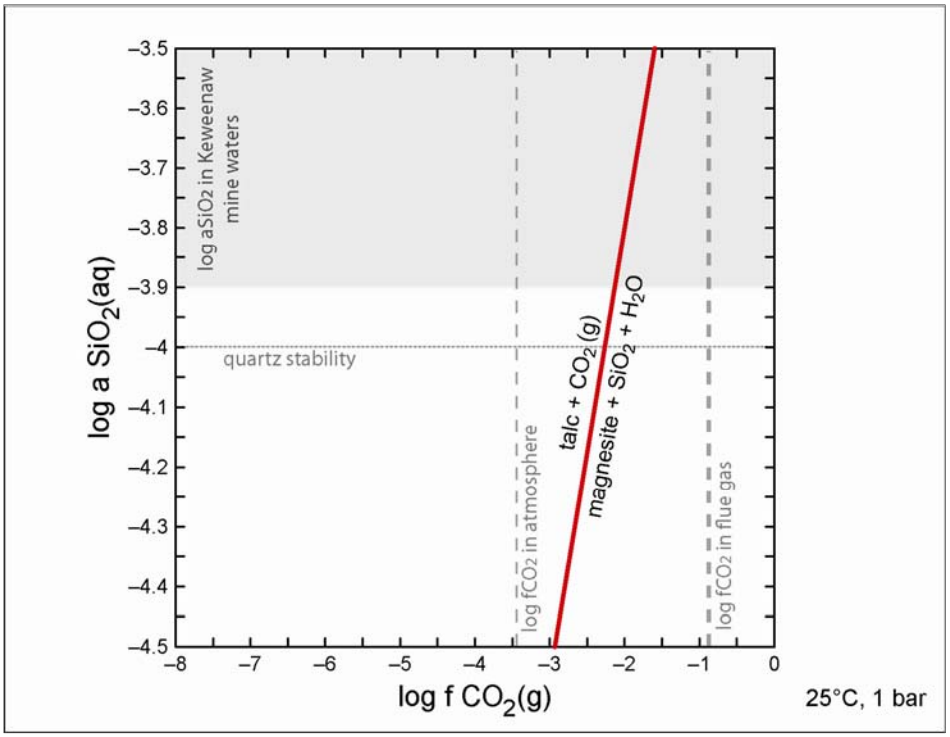

Figure 5.17: Stability of enstatite decomposition products at standard conditions.

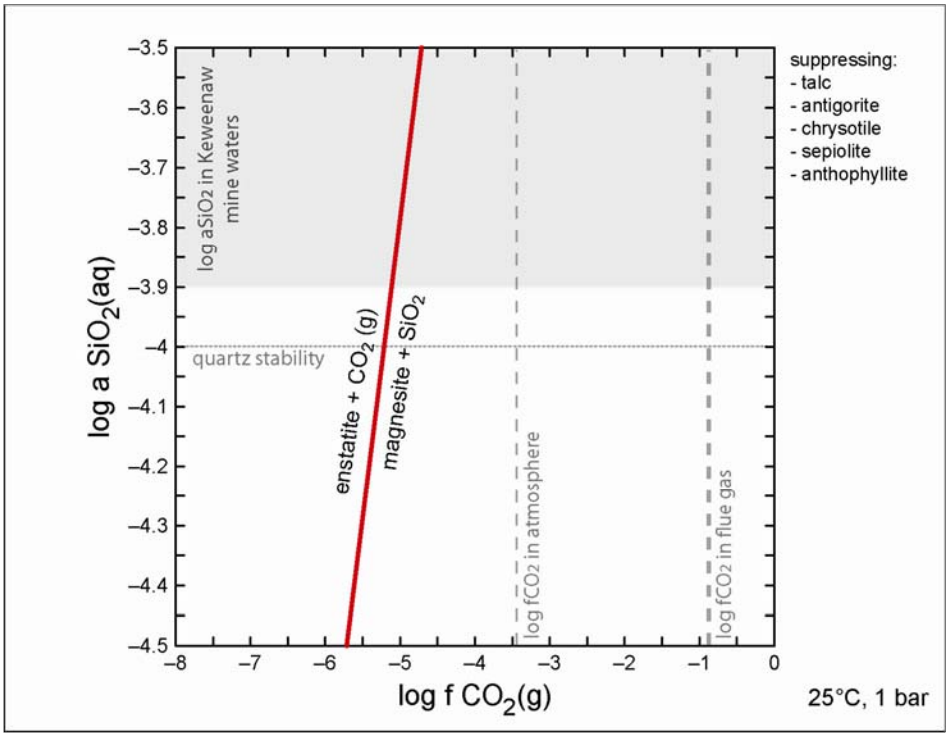

Figure 5.18: Stability of enstatite at standard conditions.

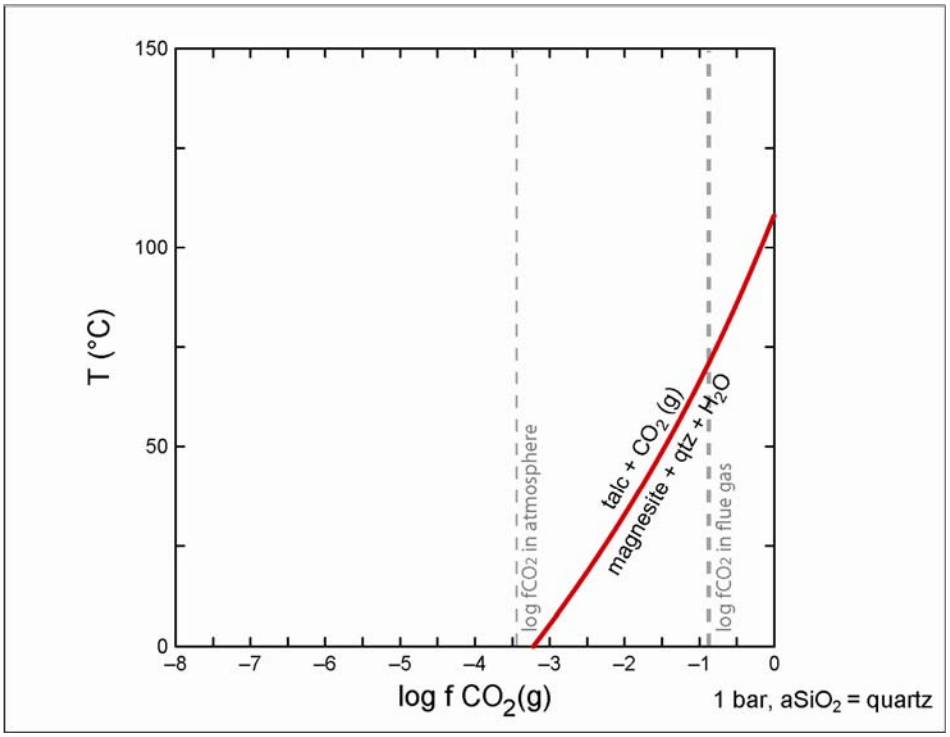

Figure 5.19: Stability of enstatite decomposition products with temperature and fCO_2.

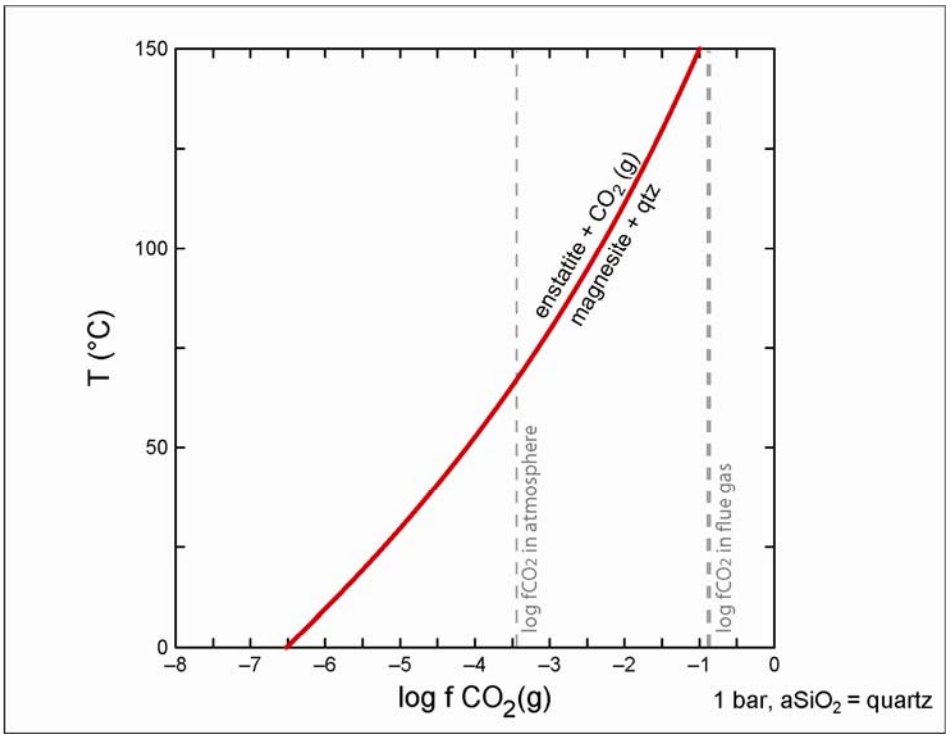

Figure 5.20: Stability of enstatite with temperature and fCO_2.

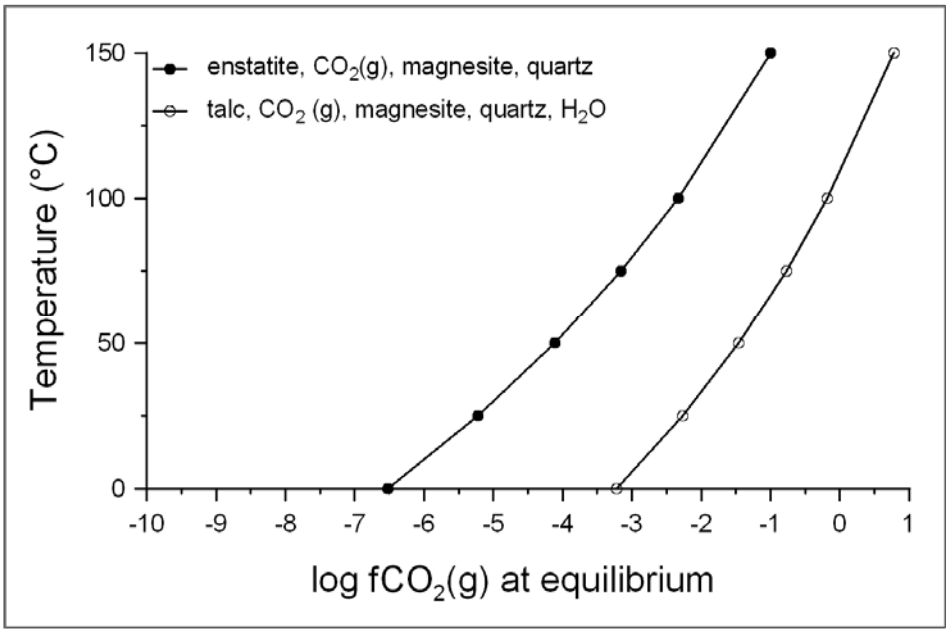

Figure 5.21: Log fCO_2 at equilibrium between enstatite products at varying temperatures.

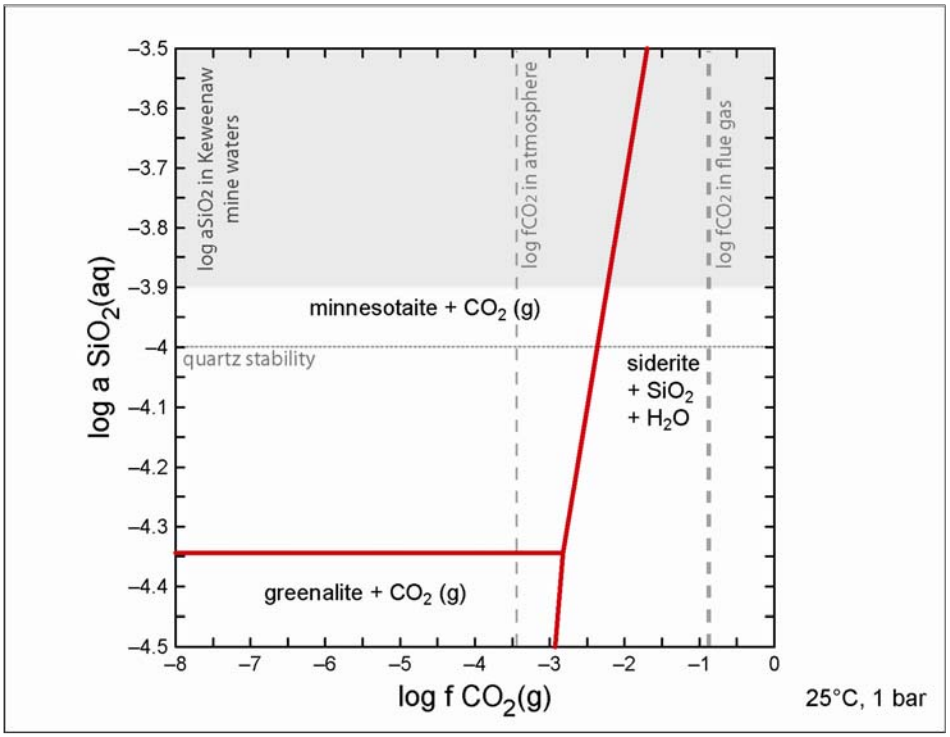

Figure 5.22: Stability of ferrosilite decomposition products at standard conditions.

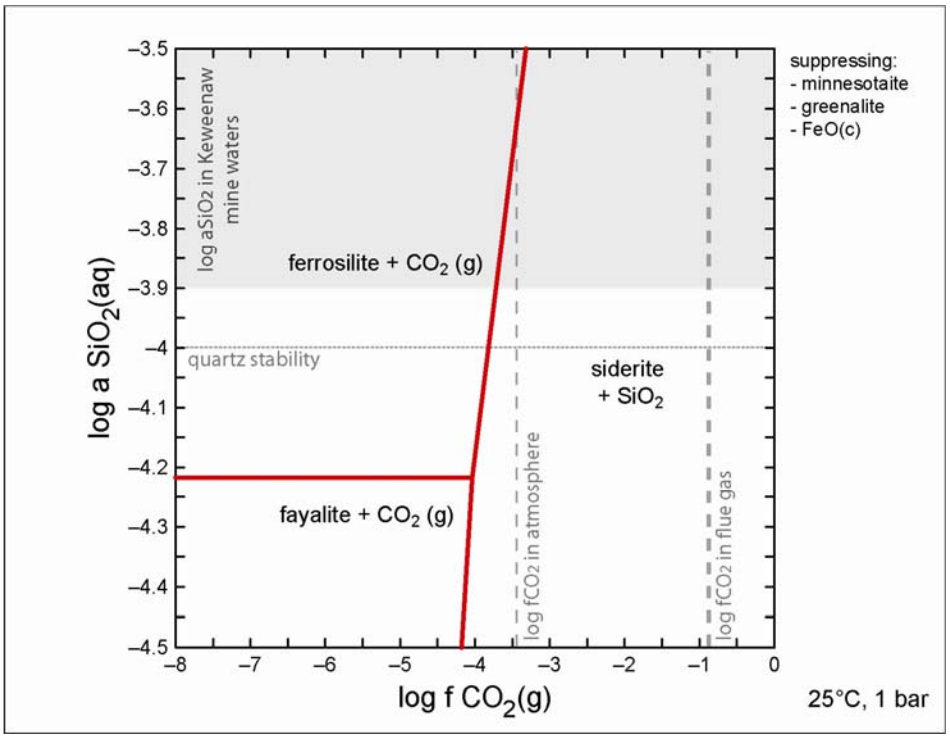

Figure 5.23: Stability of ferrosilite at standard conditions.

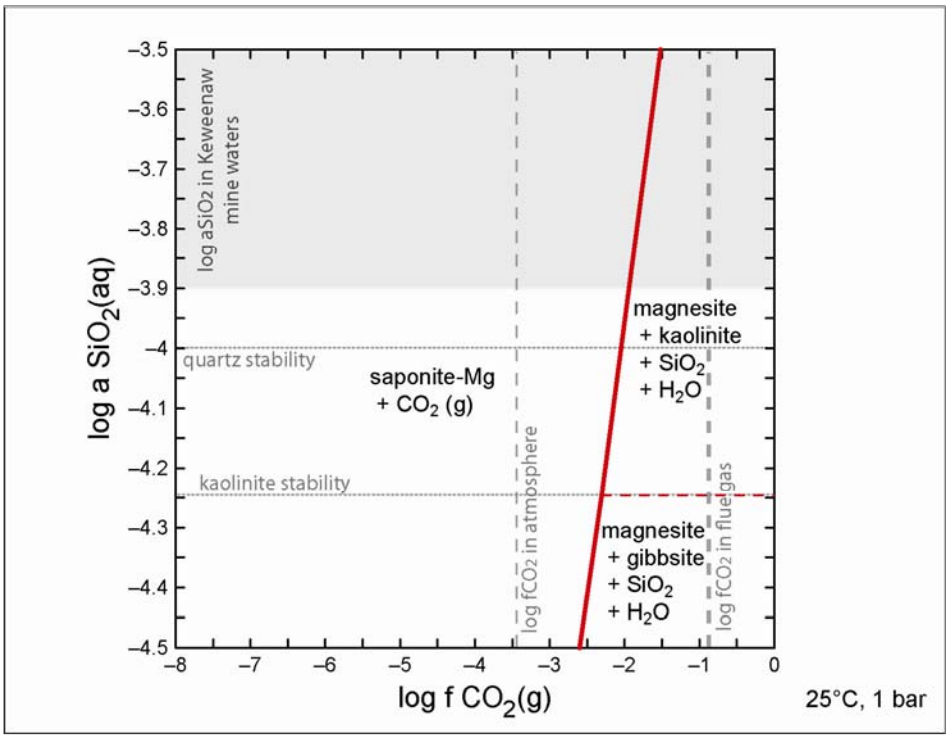

Figure 5.24: Stability of clinochlore decomposition products at standard conditions.

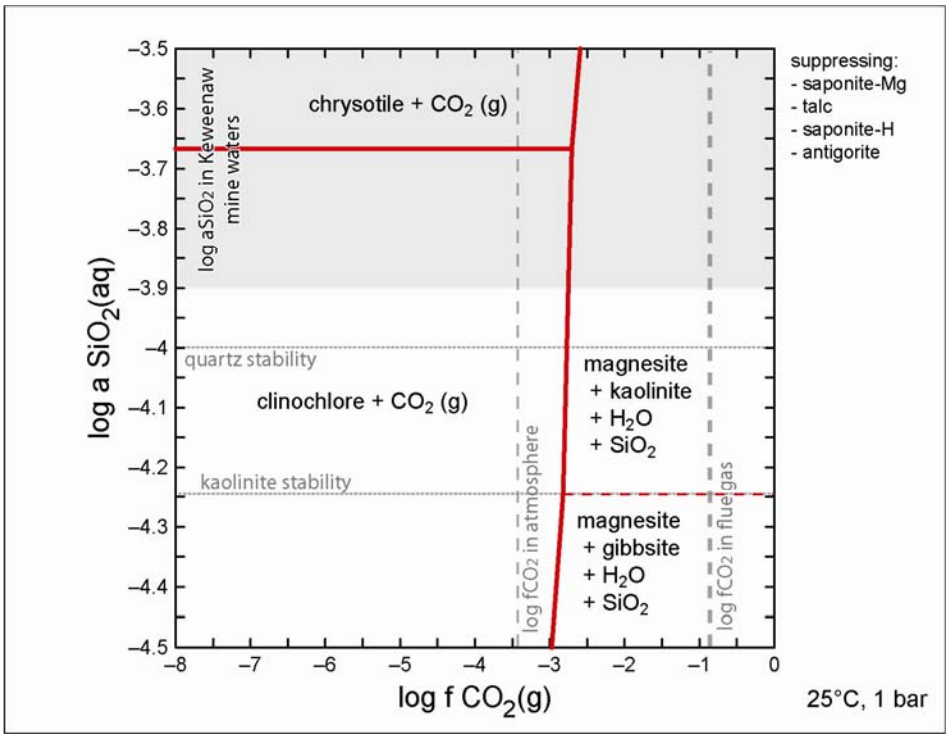

Figure 5.25: Stability of clinochlore at standard conditions.

are shown in Figure 5.26. Figure 5.27 shows the graph of clinochlore at varying temperatures and fCO_2 at quartz stability after suppressing more stable minerals. The balanced reactions were used to calculate the fCO_2 needed for equilibrium for the given reaction at varying temperatures (Figure 5.28). Chemical formulas and equilibrium constants used are included in Appendix I.

Ripidolite was modeled in the presence of H_2O, kaolinite, and hematite. In order to force the Fe^{2+} from ripidolite into Fe^{3+} to be accommodated by hematite, $fO_2(g)$ was set to 0.2, which roughly represents the fO_2 in the atmosphere at standard conditions. Ripidolite is not stable at standard conditions, and the smectites nontronite-Mg and saponite-Mg were plotted with magnesite instead (see Figure 5.29). In order to plot ripidolite with magnesite, 22 minerals and two aqueous species had to be suppressed (Figure 5.30). Suppressed minerals included: nontronite-Mg, saponite-Mg, talc, saponite-H, antigorite, clinochlore-14A, chrysotile, sepiolite, amesite-14A, clinochlore-7A, anthophyllite, enstatite, forsterite, brucite, artinite, beidellite-Mg, clinoptilolite-Mg, cordierite-hydrated, ferrite-Mg, MgH_2SiO_4 (aq), cordierite-anhydrated, hydromagnesite, spinel, and $Mg(H_3SiO_4)_2$ (aq). At quartz stability, the plot for decomposition products of ripidolite at varying temperatures and fCO_2 shows no reaction (Figure 5.31). When suppressing decomposition products, the stability fields of ripidolite and magnesite vary with temperature and fCO_2 as shown in Figure 5.32. Since there is no reaction at quartz stability, no equilibrium constants for the decomposition of ripidolite were calculated. The calculated log fCO_2 needed for the reaction between ripidolite, CO_2, O_2, magnesite, H_2O, quartz, kaolinite, and hematite is shown in Figure 5.33.

Daphnite was modeled in the presence of kaolinite and H_2O at standard conditions (Figure 5.34). Daphnite is stable at standard conditions and no minerals had to be suppressed. Again, as with fayalite and ferrosilite, the Fe^{2+}-carbonate siderite was produced, which is unstable at atmospheric fO_2, making it unrealistic for CO_2 sequestration. No further diagrams for daphnite are included.

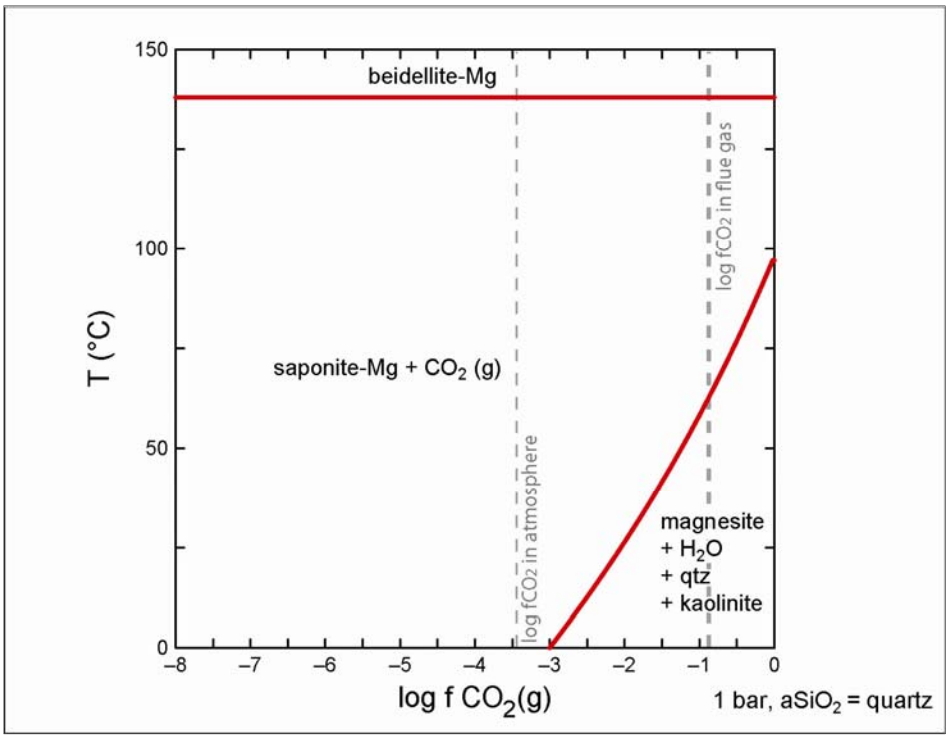

Figure 5.26: Stability of clinochlore decomposition products with temperatures and fCO_2.

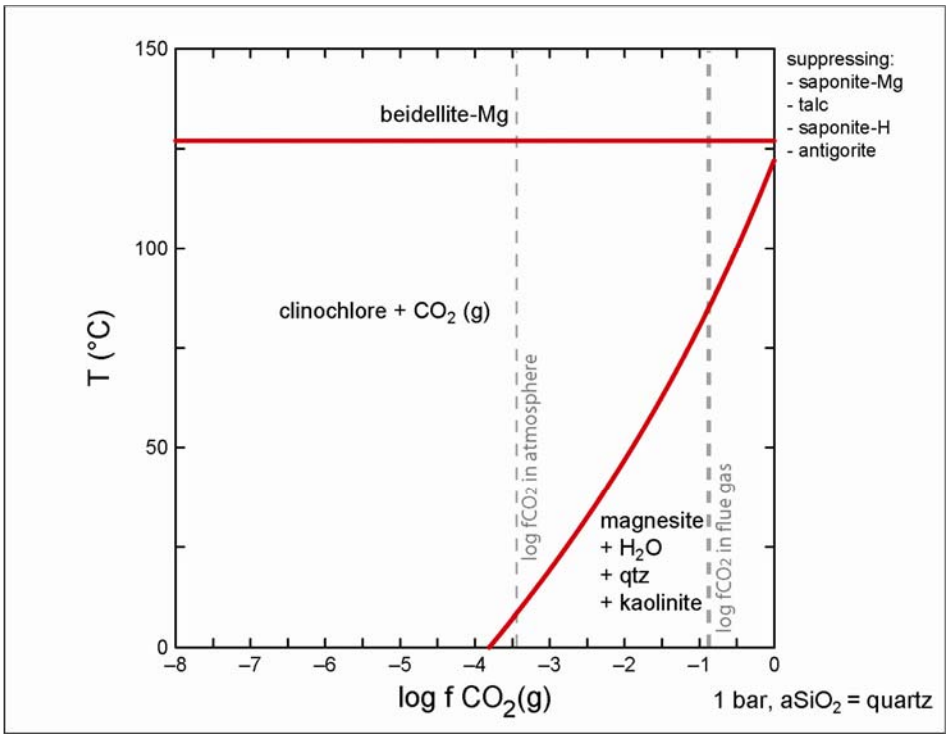

Figure 5.27: Stability of clinochlore with varying temperatures and fCO_2.

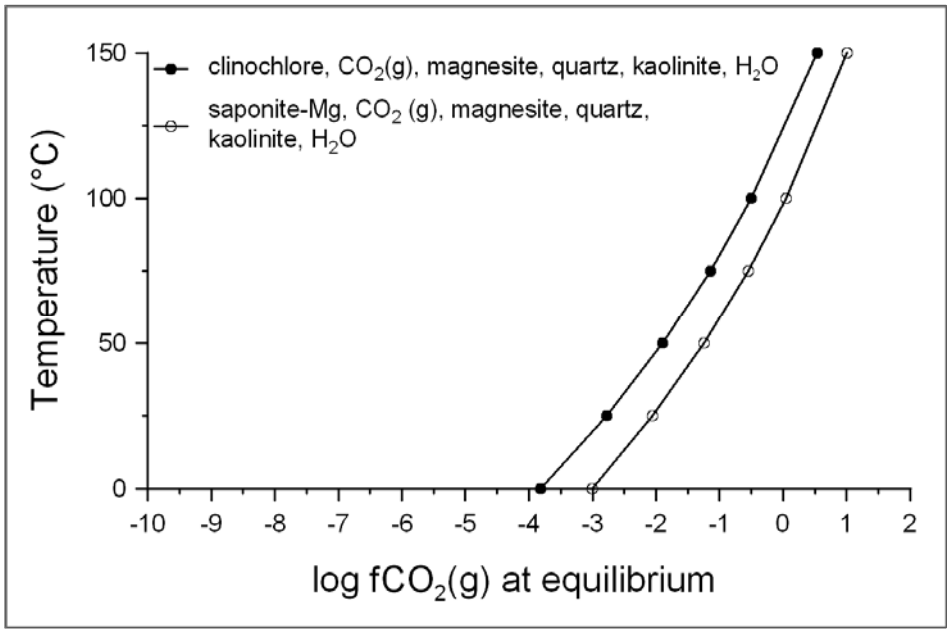

Figure 5.28: Log fCO_2 at equilibrium between clinochlore products at varying temperatures.

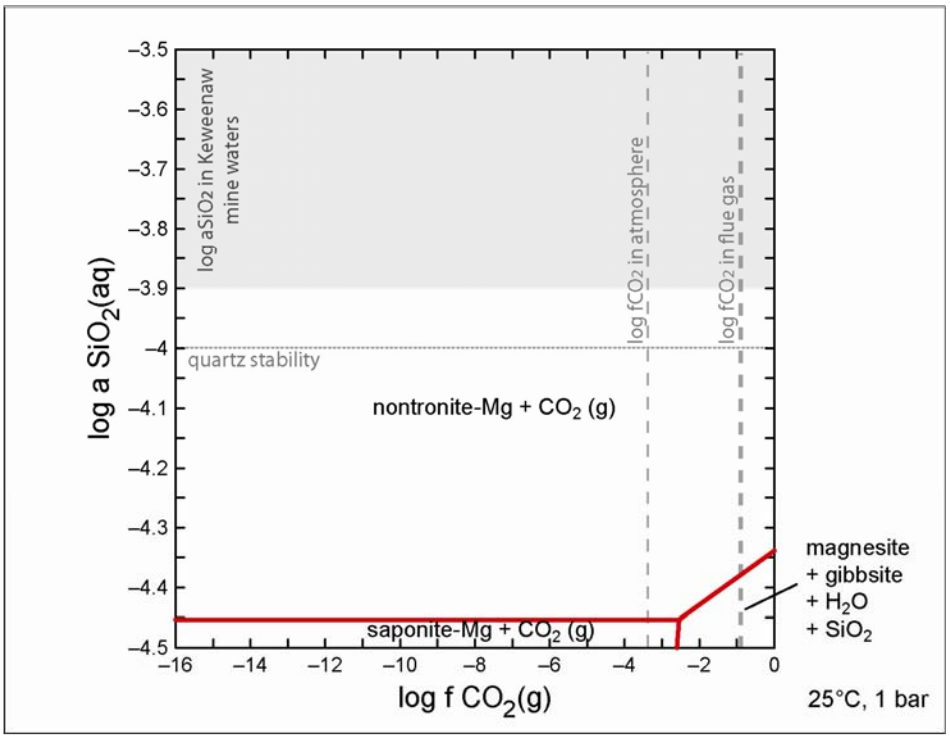

Figure 5.29: Stability of ripidolite decomposition products at standard conditions.

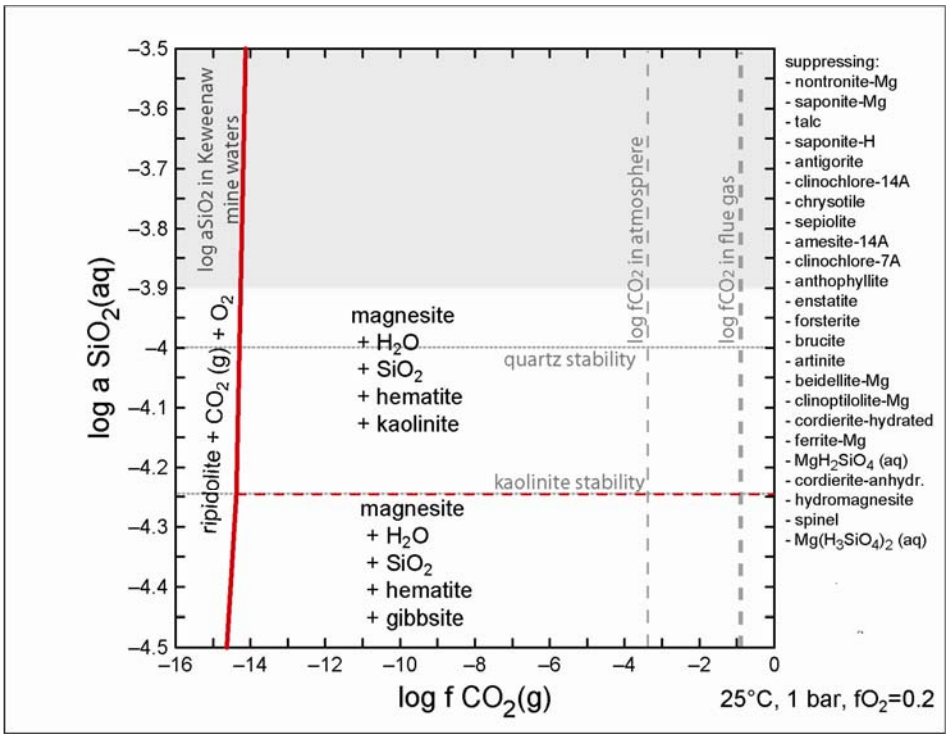

Figure 5.30: Stability of ripidolite at standard conditions.

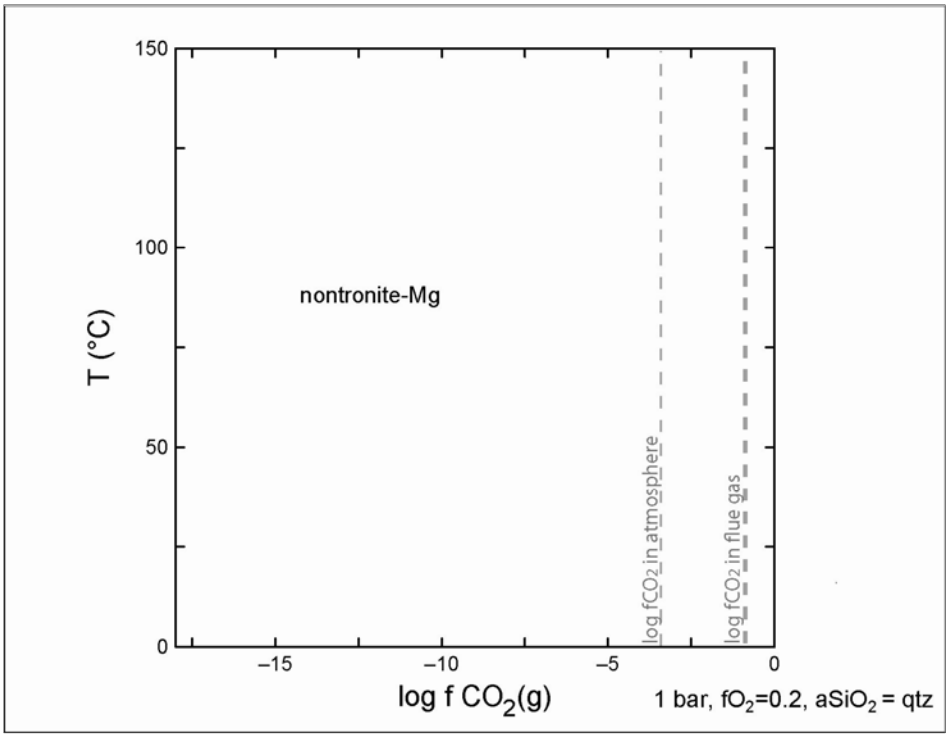

Figure 5.31: Stability of ripidolite decomposition products with temperature and fCO_2.

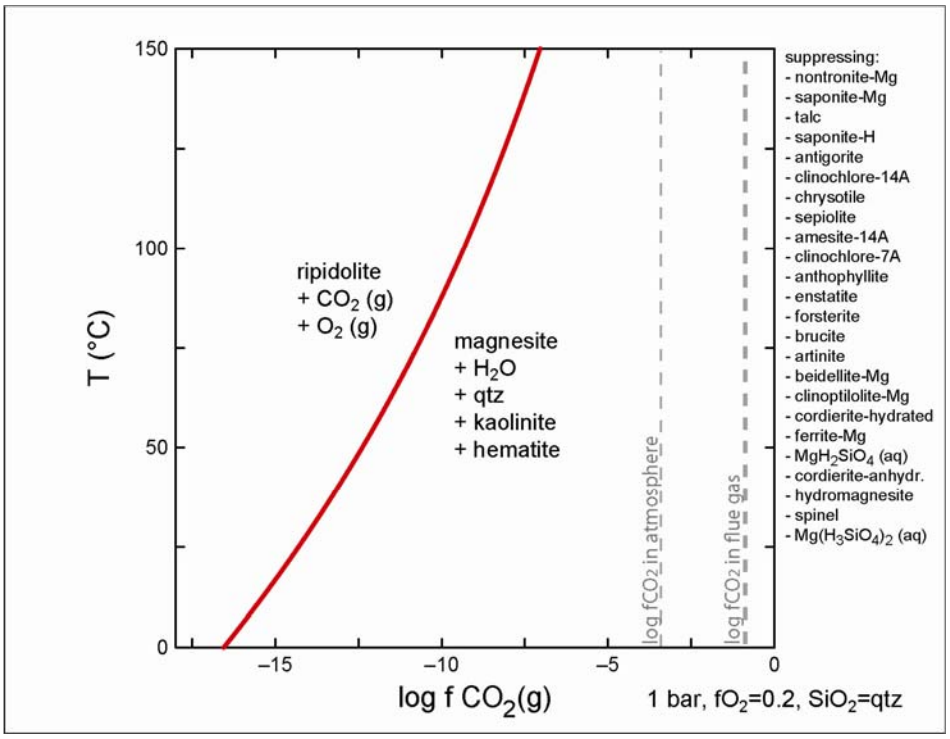

Figure 5.32: Stability of ripidolite with temperature and fCO_2.

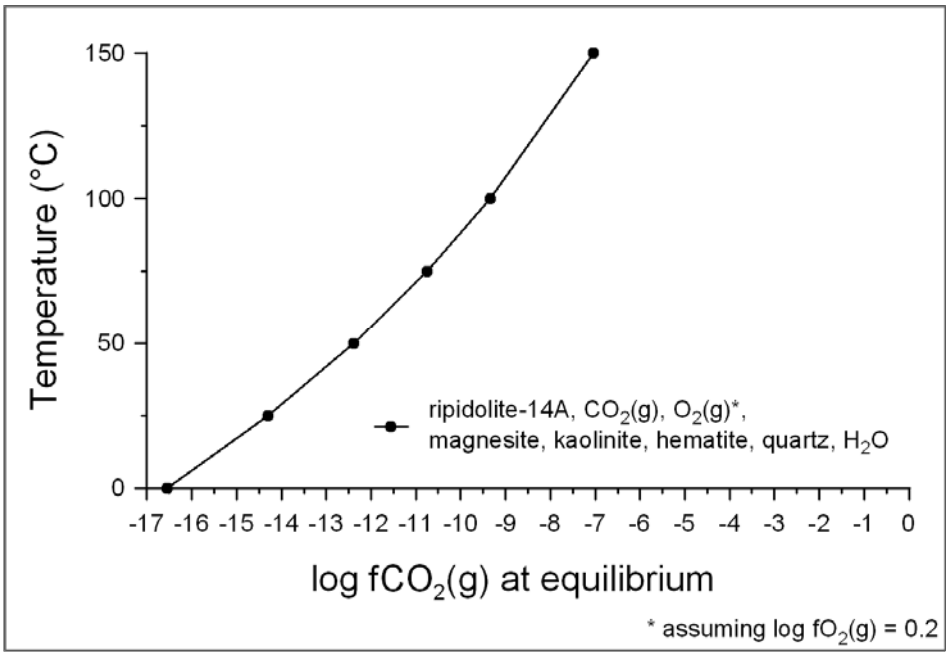

Figure 5.33: Log fCO_2 at equilibrium between ripidolite products at varying temperatures.

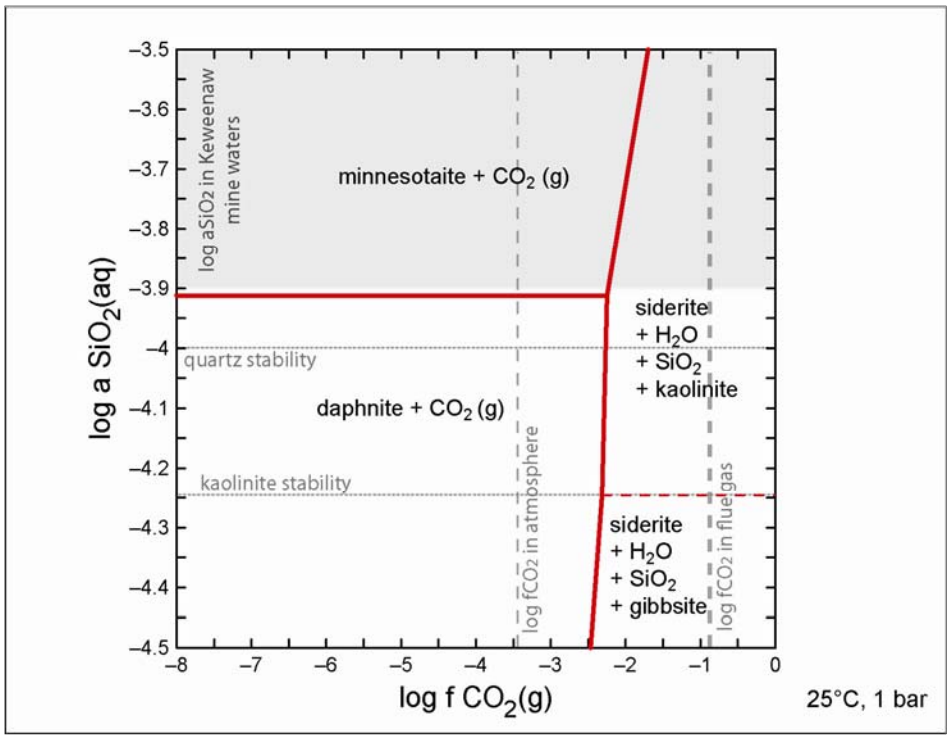

Figure 5.34: Stability of daphnite at standard conditions.

5.5 Phengite

Mica group minerals with compositions similar to phengite were identified in the studied samples. Thus, phengite was used for thermodynamic modeling. Phengite was modeled at standard conditions and in the presence of kspar and H_2O. Stability fields of phengite at standard conditions with varying log $aSiO_2$ (aq) and log fCO_2 are shown in Figure 5.35. The stability of phengite in the presence of kspar at varying temperatures and at one bar pressure is shown in Figure 5.36. The reaction between phengite, magnesite, quartz, kspar, and CO_2 with its equilibrium constants is given in Appendix I. The log fCO_2 needed for equilibrium of the reaction at varying temperatures is plotted in Figure 5.37.

5.6 Epidote

Most epidote group minerals found in the study area have compositions close to the end-member epidote, which was used for thermodynamic modeling. Epidote was modeled in the presence of kaolinite, hematite and H_2O. At standard conditions epidote is not stable, and nontronite-Ca (smectite) is plotted instead (Figure 5.38). Figure 5.39 shows the stability of epidote, when suppressing nontronite-Ca and laumontite. When plotting decomposition products of epidote at quartz stability with varying temperatures and fCO_2, no reaction occurs (Figure 5.40). The stability fields for epidote and calcite at varying temperatures and log fCO_2 were created by suppressing minerals listed above (Figure 5.41). Since no reaction occurs between decomposition products at standard conditions and quartz stability, only the log fCO_2 needed for "equilibrium" between epidote, CO_2, H_2O, calcite, kaolinite, hematite, and quartz is included (Figure 5.42). The balanced chemical reaction and equilibrium constants used are included in Appendix I.

5.7 Prehnite

For modeling the stability of prehnite in the presence of kaolinite and H_2O, the same diagram as for the decomposition of anorthite at standard conditions was created (Figure 5.43). Figure 5.44 shows a plot of prehnite versus calcite at quartz stability,

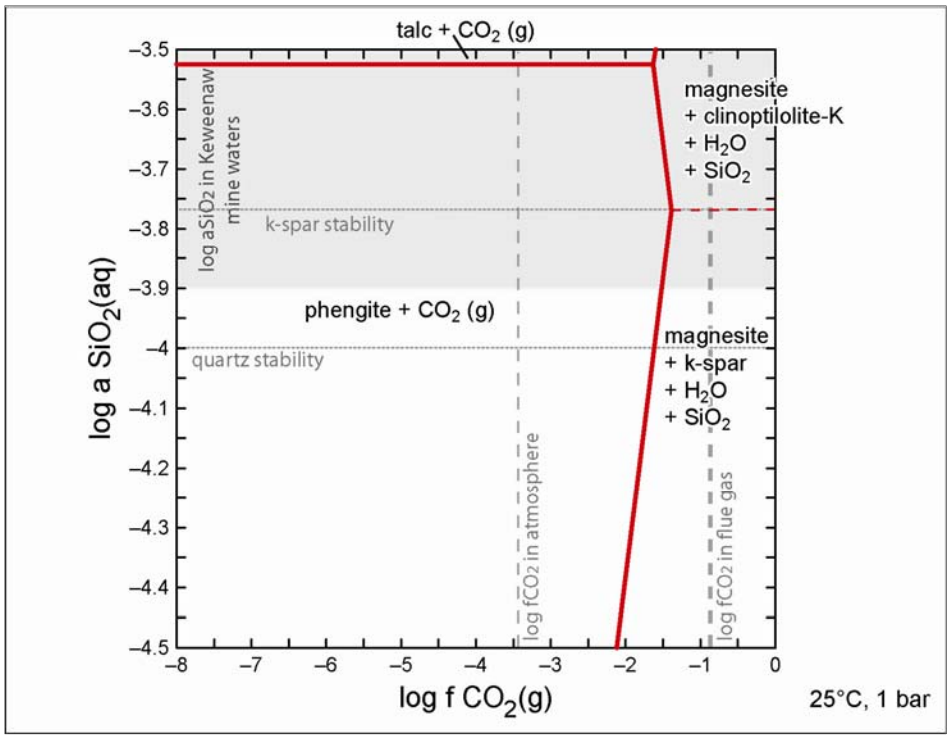

Figure 5.35: Stability of phengite at standard conditions.

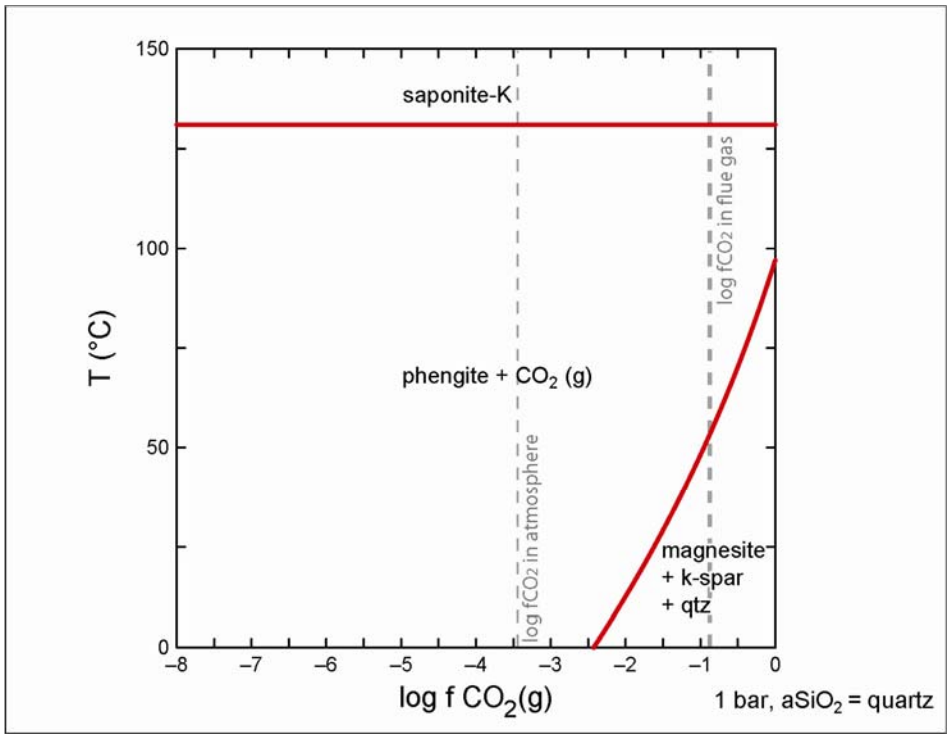

Figure 5.36: Stability of phengite with temperature and fCO_2.

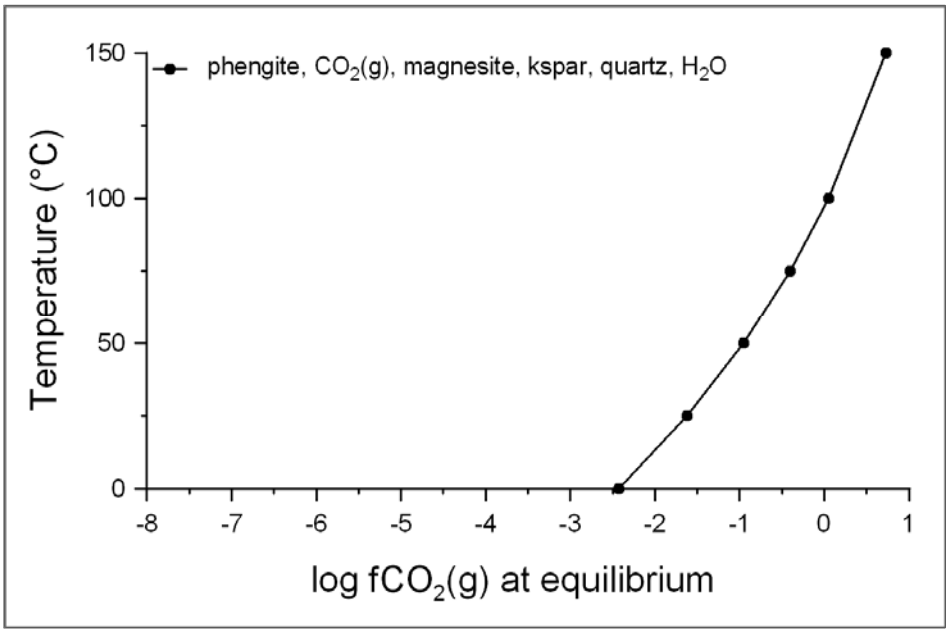

Figure 5.37: Log fCO_2 at equilibrium between phengite products at varying temperatures.

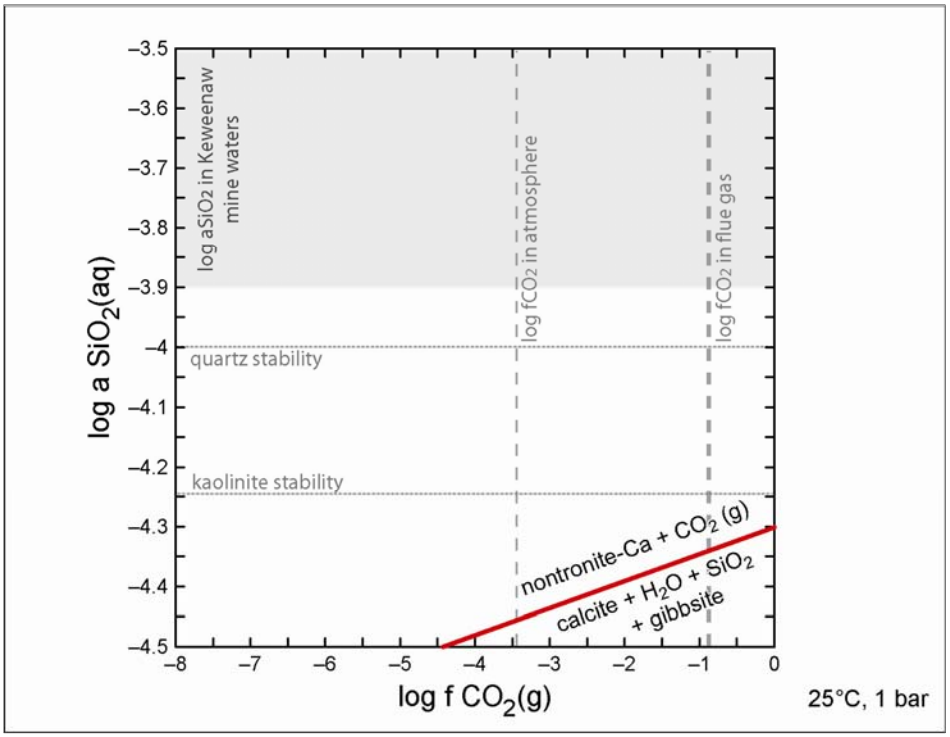

Figure 5.38: Stability of epidote decomposition products at standard conditions.

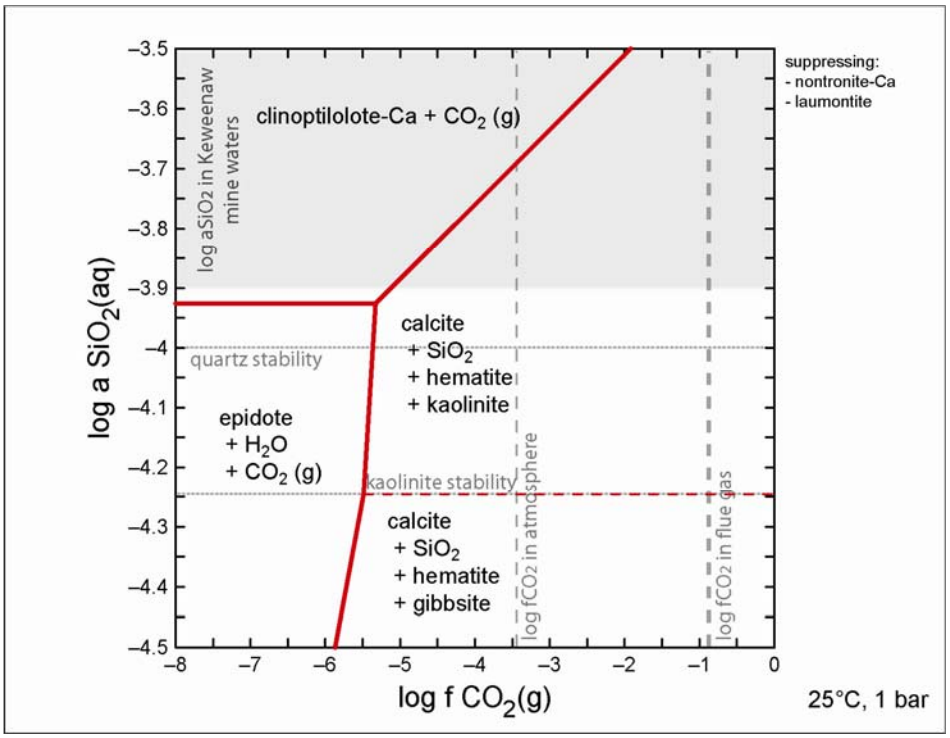

Figure 5.39: Stability of epidote at standard conditions.

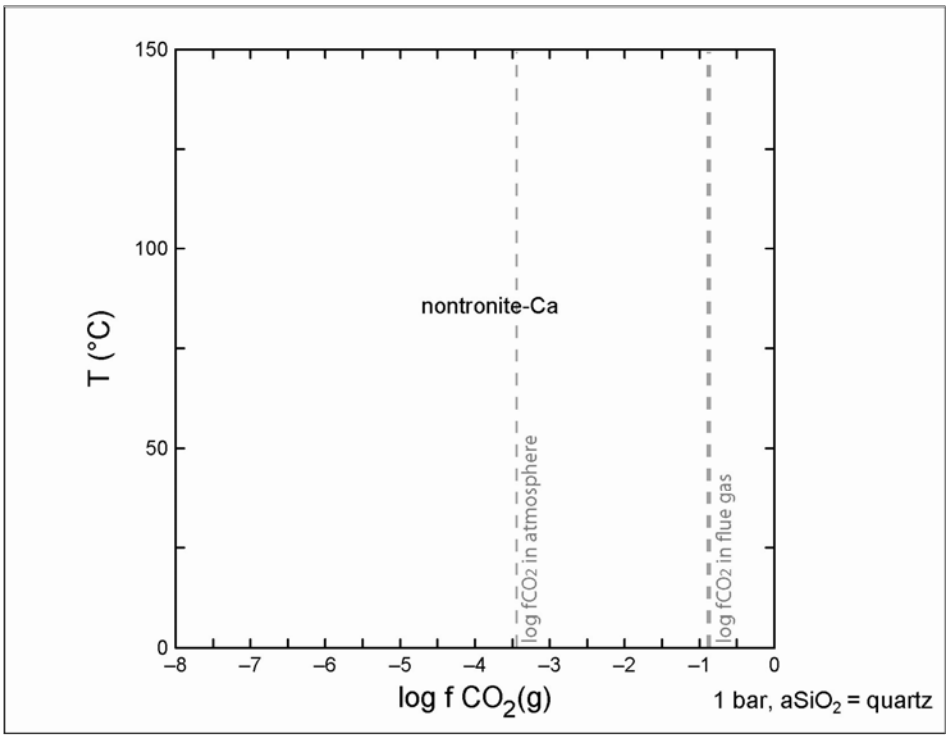

Figure 5.40: Stability of epidote decomposition products with temperature and fCO_2.

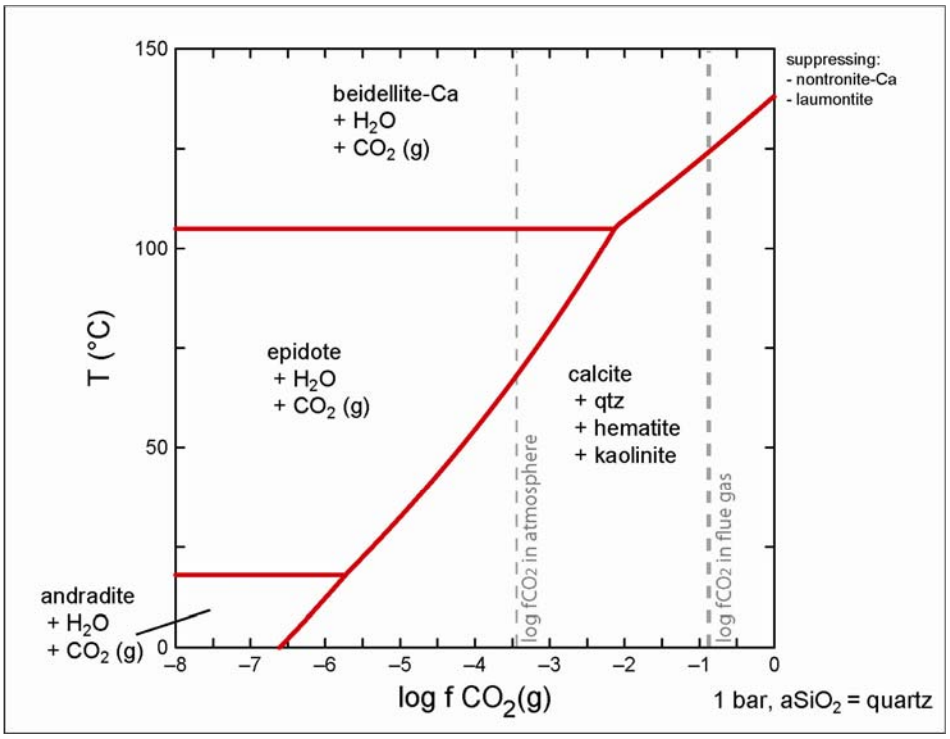

Figure 5.41: Stability of epidote with temperature and fCO_2.

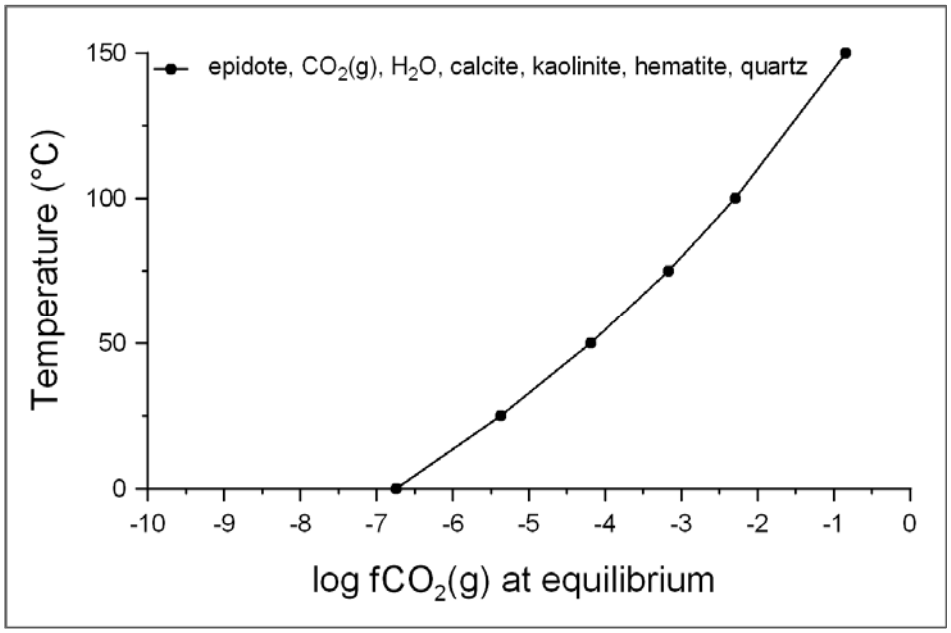

Figure 5.42: Log fCO_2 at equilibrium between epidote products at varying temperatures.

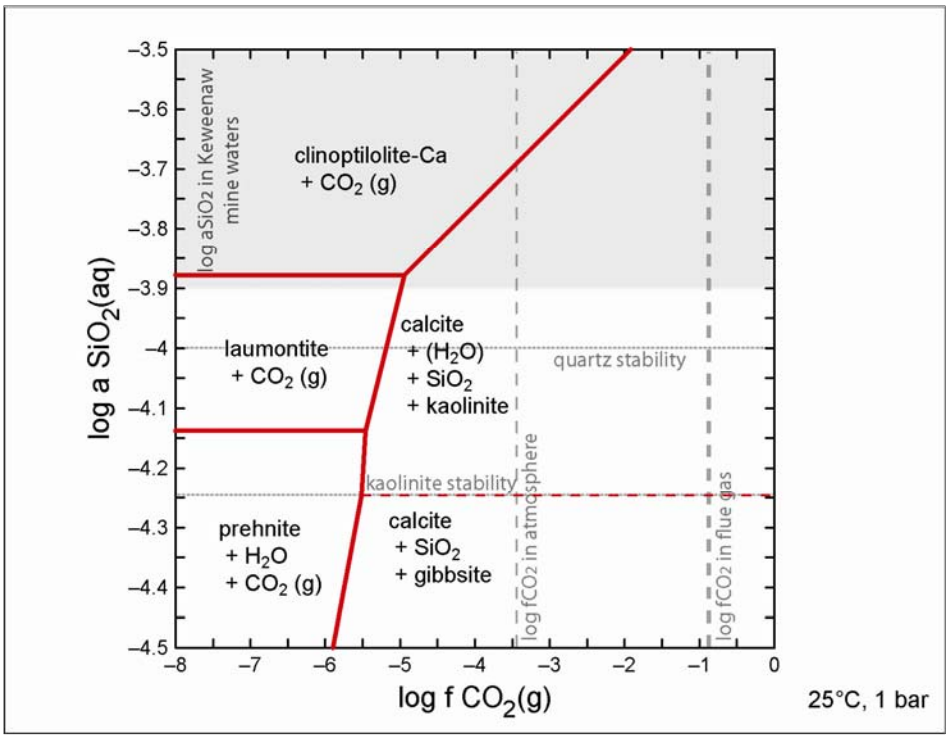

Figure 5.43: Stability of prehnite decomposition products at standard conditions.

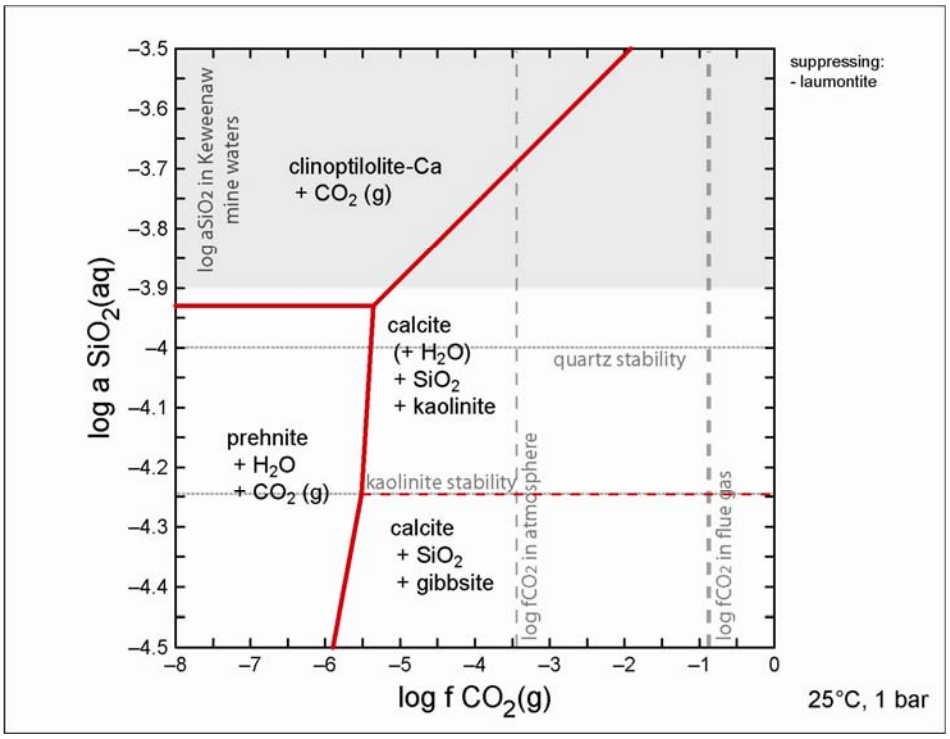

Figure 5.44: Stability of prehnite at standard conditions.

suppressing laumontite. Plots for prehnite decomposition products and for prehnite while suppressing laumontite are shown with varying temperatures in Figures 5.45 and 5.46.

When modeling the reaction between prehnite, laumontite, and calcite in the presence of kaolinite, a different chemical reaction was the result (Appendix I). The fCO_2 needed for equilibrium for the reaction between prehnite, laumontite, and calcite is plotted in Figure 5.47.

5.8 Summary and Discussion

Thermodynamic modeling was performed for minerals available in Geochemist's Workbench *thermo.dat* database (Bethke, 2000), best resembling minerals found in the study area. Many of the modeled minerals are not stable at standard conditions and decomposition products were plotted instead. The plot showing the assemblage stable at standard conditions should be used to determine mineral carbonation potential based on thermodynamics. Any carbonate theoretically formed from the unstable mineral should revert back to the decomposition products until fCO_2 values shown in the diagram for minerals stable are reached. For example, carbonate formed directly from forsterite is unstable with respect to talc and should react with H_2O and SiO_2 until the stable mineral assemblage is achieved at a much higher log fCO_2 value, consequently releasing CO_2. Thermodynamic modeling for siderite with fO_2 shows that iron silicates forming the Fe-carbonate siderite should not be further considered, as the Fe-carbonate itself is highly unstable at realistic fO_2 values.

Log fCO_2 values resulting from the carbonation of minerals by flue gas at standard conditions and quartz stability are summarized in Table 5.1. All minerals shown in Table 5.1 for which reactions should occur based on thermodynamics at standard conditions should be considered for kinetic modeling (excluding siderite forming minerals). Although log fCO_2 values resulting from carbonation are sometimes larger than found in the atmosphere, all fCO_2 values resulting from carbonation are

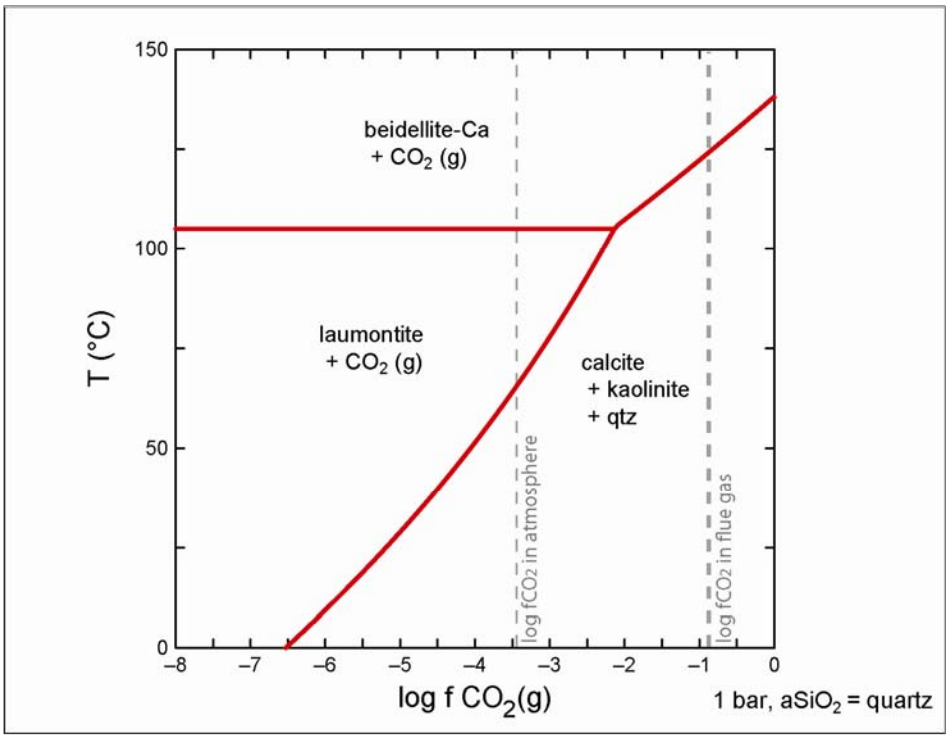

Figure 5.45: Stability of prehnite decomposition products with temperature and fCO_2.

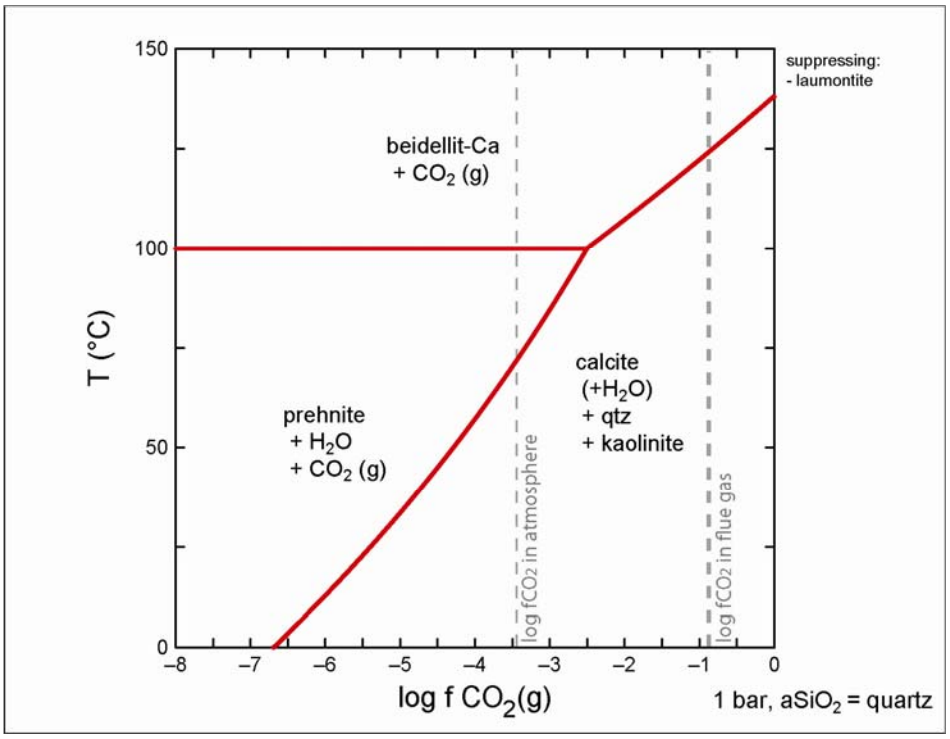

Figure 5.46: Stability of prehnite with temperature and fCO_2.

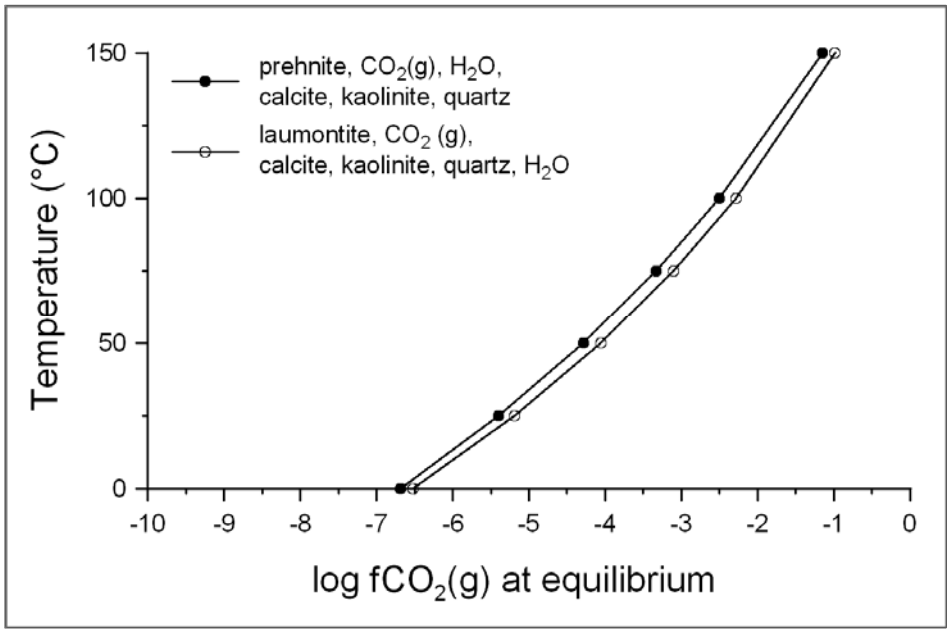

Figure 5.47: Log fCO_2 at equilibrium between prehnite products at varying temperatures.

Table 5.1: Summary of minimum log fCO_2 values for carbonation of minerals.

Log fCO_2 resulting from reaction with flue gas*	Original mineral	Decomposition products
no reaction	ripidolite	nontronite-Mg
-1.6	phengite	phengite, magnesite, kspar, quartz, H_2O
-2.0	clinochlore	saponite-Mg, magnesite, kaolinite, quartz, H_2O
-2.3	forsterite, enstatite	talc, magnesite, quartz
-2.5	fayalite, ferrosilite	minnesotaite, *siderite***, H_2O, quartz
-2.7	daphnite	daphnite, *siderite***, kaolinite, quartz, H_2O
-5.2	anorthite, prehnite	laumontite, calcite, kaolinite, quartz, H_2O
-5.4	diopside	diopside, dolomite, quartz

* at $aSiO_2(aq)$=-4 and standard conditions

** not stable at fO_2 of atmosphere

smaller than those found in flue gas. Thus, thermodynamically, these minerals should react with flue gas to form carbonates.

Since no thermodynamic data is available for solid solution minerals, end-members of mineral series were plotted. None of the minerals found in the study area directly resemble the pure end-members used for modeling. When reducing the end-member content, the minerals become more stable, and the equilibrium moves to higher fCO_2 values. Since no end-member diopside or anorthite was encountered in the study area, more specific thermodynamic modeling using augite and plagioclase with anorthite contents of up to 80% should be conducted. Additionally, pumpellyite should be included for modeling.

In general, elevated temperatures lead to larger log fCO_2 values at equilibrium and thus decrease the amount of CO_2 that could potentially be sequestered using this method. Decreasing end-member contents in minerals also decrease the carbonation potential of minerals.

Overall, thermodynamic modeling results suggest that the minerals anorthite, prehnite, and diopside are most feasible for mineral carbonation. Although not much anorthite could be found in the study area, diopside-rich clinopyroxene minerals were present in most samples, with relative abundances of up to ~25%. If diopside proves to be feasible for mineral carbonation based on kinetic modeling, the samples in the study area might be feasible for mineral carbonation. Chlorite end-members (ripidolite, clinochlore, and daphnite), forsterite, and enstatite (orthopyroxene) do not appear feasible for mineral carbonation based on thermodynamic modeling, but could prove to be viable using kinetic modeling. The feasibility of any of these minerals for mineral carbonation ultimately depends on the rates of the reactions (kinetics) that should occur based on thermodynamics. Overall, highly altered mafic rocks with basaltic chemical compositions, but lacking basaltic mineralogy appear not very feasible for mineral carbonation.

CHAPTER 6: MINERAL CARBONATION AND WHOLE ROCK DATA

Whole rock data was available for 206 samples. In order to determine the feasibility of samples for mineral carbonation based on this data alone, several approaches were tested. First, an attempt was made to determine the relative abundances of minerals based on whole rock data and typical mineral compositions found in the study area. While the abundance of calcite, ankerite, and apatite could reasonably be estimated based on the amounts of CO_2, CaO, and P_2O_5 present, no further abundances of minerals could be estimated based on whole rock data alone.

Next, trends of major element concentrations with alteration assemblages were studied: the thin sections analyzed using EDS were assigned to different thermodynamic categories (see Table 6.1), and plotted on bivariate diagrams (Figure 6.1), along with the average basalt composition from Best (2002). Major element data was normalized to 100% without LOI; the weight percent of CO_2 was not normalized.

Based on results from thermodynamic modeling, thin sections containing anorthite, prehnite, olivine, orthopyroxene, and clinopyroxene are of interest for mineral carbonation. The samples 10SC004 and 10SG001 were plotted as the "category I" samples, containing olivine, Mg-pyroxene, clinopyroxene, and plagioclase with X_{an}=50-80. The samples 10VI002, 10BB001, and 10DE006 were plotted as "category II" samples containing plagioclase with X_{an}=20-80, and clinopyroxene. The sample 10CN002 was plotted as a "category III" sample, containing prehnite, clinopyroxene, and plagioclase with X_{an}=0-50. Sample 10QU006 was not included in the "category III" category, since it is a brecciated sample. Samples 11CLD003, 11CLD001, 10DE003, and 11CLD007 were plotted as "category IV" samples, representing samples likely not feasible for mineral carbonation based on their mineral assemblage. Samples 11CBF006 and 11CBF004 were not included within "category IV", since they contained some clinopyroxene.

Table 6.1: Thermodynamic categories used for plotting of samples on bivariate diagrams.

category	sample #	thermodynamically feasible minerals
I	10SC004 10SG001	• olivine • orthopyroxene • plagioclase (X_{an}=50-80) • clinopyroxene
II	10VI002 10BB001 10DE006	• plagioclase (X_{an}=20-80) • clinopyroxene
III	10CN002	• prehnite • clinopyroxene
IV	11CLD003 11CLD001 10DE003 11CLD007	N/A

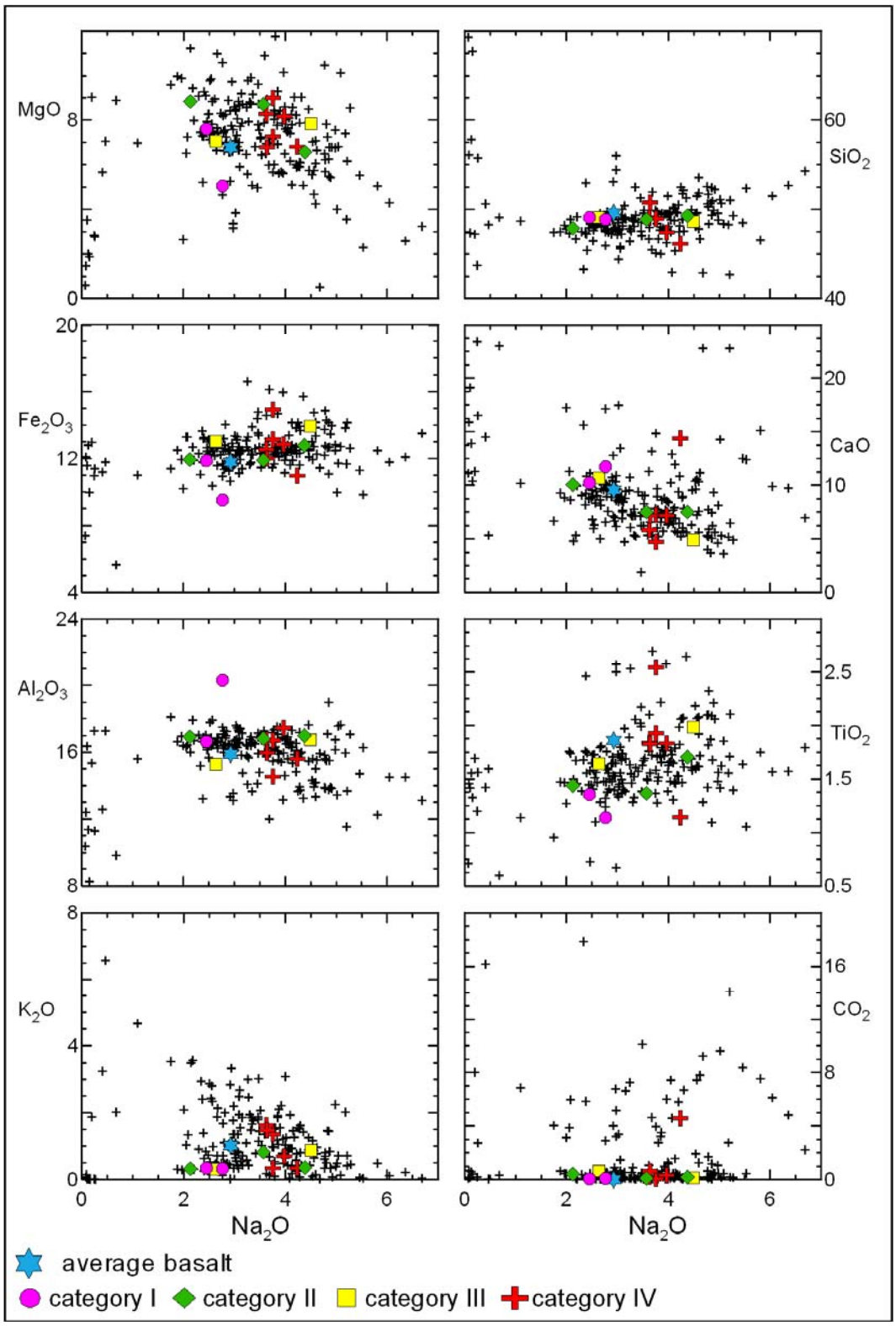

Figure 6.1: Bivariate diagrams for samples by thermodynamic category.

The original Na_2O contents were also plotted against LOI (Figure 6.2) and calculated H_2O (Figure 6.3). The H_2O contents were calculated from LOI, subtracting CO_2 (%). Based on these diagrams, potential indicators for feasible samples appear to be Na_2O, K_2O, LOI, H_2O, and CO_2: Less feasible samples contain less than 1% Na_2O or more than 3% Na_2O, as well as more than 0.5% K_2O. Based on LOI, the more feasible samples have generally lower LOI values, and less feasible samples contain more than 4% LOI. Additionally, H_2O contents >4%, as well as a CO_2 contents >1% indicate less feasible samples. When applying the requirements:

- 1 < normalized Na_2O (%) < 3.0,
- normalized K_2O (%) < 0.5,
- H_2O (%) < 4.0, and
- CO_2 (%) < 1.0

to all whole rock data, 20 samples appear to be feasible for mineral carbonation (listed with textures in Table 6.2). Two of these samples were outliers in immobile element classification diagrams (10MB001 and 10MB002) and were excluded in the bivariate diagrams in Figure 6.4. Interestingly, the plotted samples contain constant normalized CaO values of 10 weight percent, although no restrictions were placed on CaO itself.

18 samples of the 206 whole rock data samples were determined to be potentially feasible for mineral carbonation using this approach. Based on whole rock data alone, these results appear to be reasonable, yet should be verified by thin section and microprobe analysis.

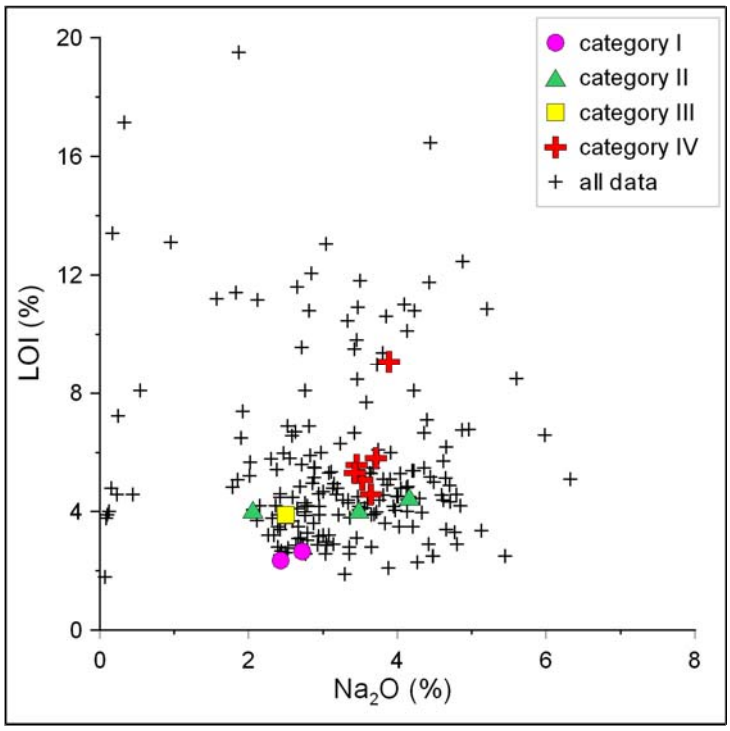

Figure 6.2: LOI (%) vs. Na_2O (%) for samples by thermodynamic category.

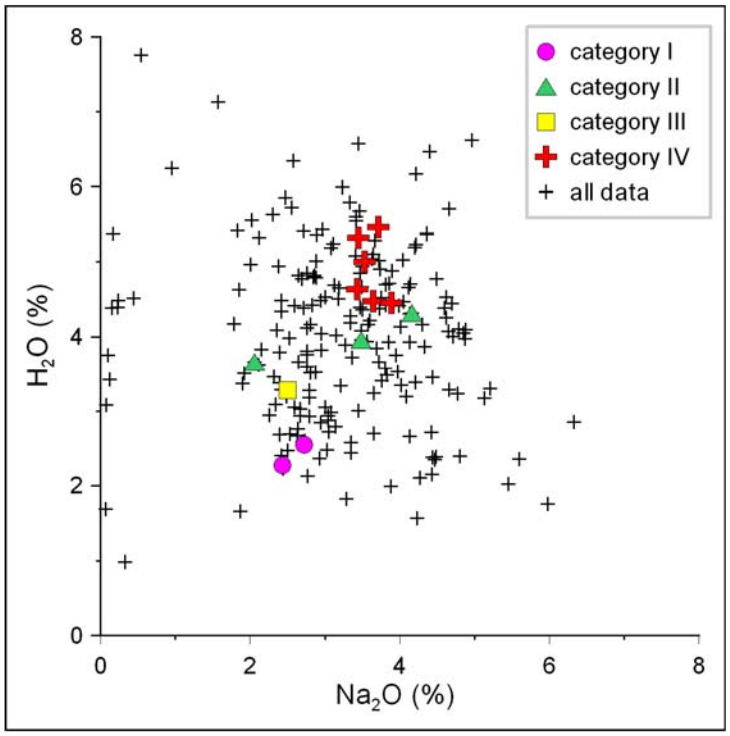

Figure 6.3: H_2O (%) vs. Na_2O (%) for samples by thermodynamic category.

Table 6.2: Samples potentially feasible for mineral carbonation.

Sample #	Texture
10BB001	very fine-grained
10CC003	subophitic
10CC004	ophitic
10CE004	very fine-grained
10CE005	fine-grained
10CN002	fine-grained
10CN006	subophitic
10IR011	ophitic
10MB001*	amygdaloidal
10MB002*	amygdaloidal
10MI001	subophitic
10MI004	very fine-grained
10MI005	very fine-grained
10OC002	fine-grained
10OC003	very fine-grained
10OJ006	ophitic
10PH006	fine-grained
10SC004	ophitic
10SE003	subophitic
10SG001	porphyritic

*outliers in immobile element plots

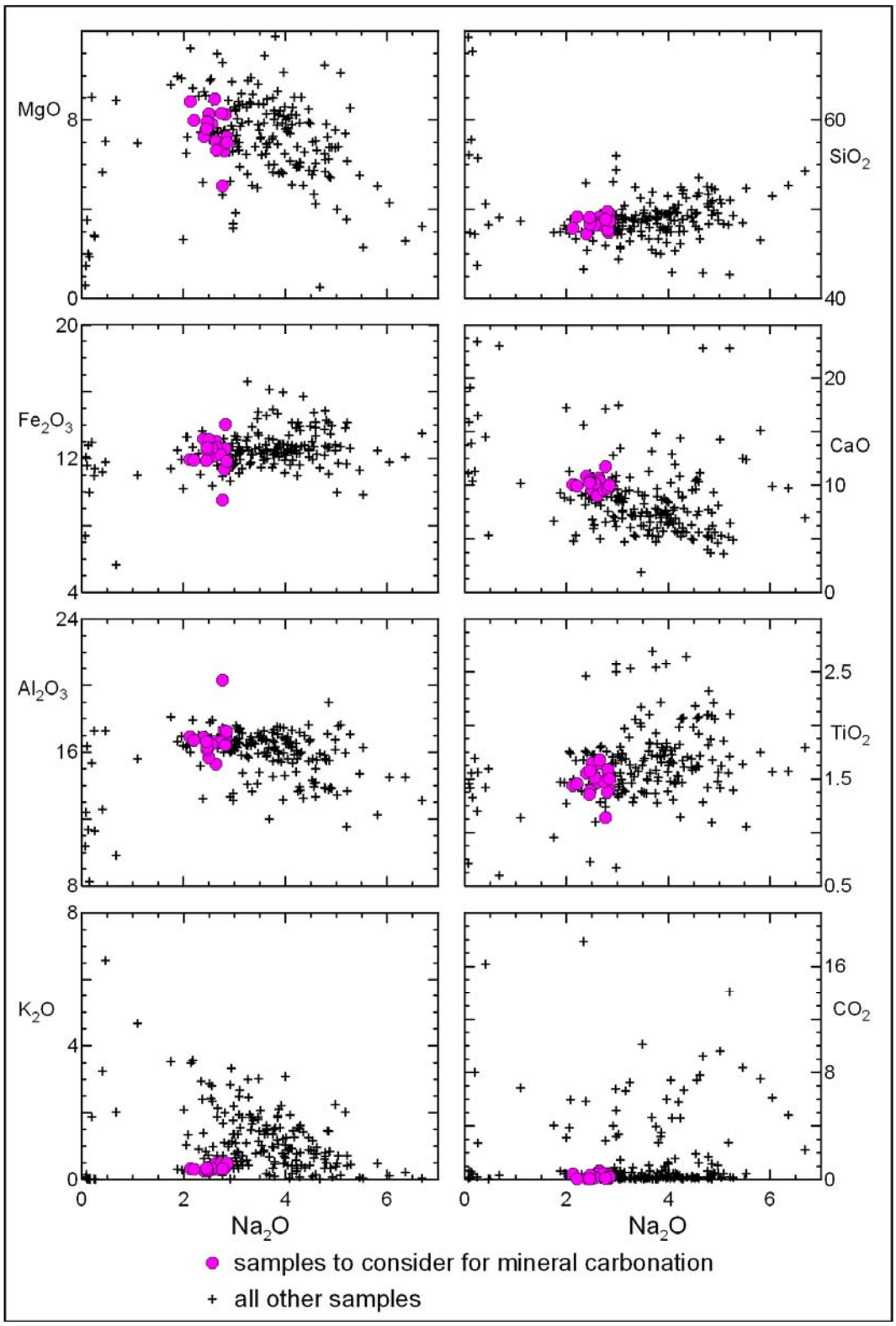

Figure 6.4: Bivariate diagrams for samples potentially feasible for mineral carbonation.

CHAPTER 7: CONCLUSIONS

Based on the steps completed as part of this research, a methodology was developed that could be applied to any mafic rock material considered for mineral carbonation. Overall, it appears that a combination of thin section and microprobe analyses of samples would be more helpful than trying to determine mineral carbonation feasibility using whole rock data alone (although whole rock data should be used if original compositions of the rocks in question are known to vary). The following steps should be completed to characterize mafic rocks regarding mineral carbonation.

1. *Compile literature research on mafic rocks of interest.*
   In this step, special attention should be paid to any mention of alteration or metamorphism of the rock unit of interest. Any prior research on mineral carbonation or studies on weathering of the rocks of interest should be included as well.
2. *Collect representative samples from all parts of the study area.*
   Samples should be large enough to produce: a hand sample, at least one plug to make thin sections, and 1–2 kg of crushed material for autoclave experiments.
3. *Obtain covered thin sections of all samples collected.*
4. *Analyze samples using thin section analysis*.
   Identify type, size, and relative amounts of minerals present. Pay special attention to calcium and magnesium bearing minerals. Note alteration and condition of plagioclase grains. Select representative and unusual samples for microprobe analysis.
5. *Analyze samples using microprobe analysis.*
   Use EDS to analyze minerals of interest using feasible beam conditions. Select beam conditions that should work best on minerals of interest and test beam

and analyzing conditions on standards available that are similar to minerals of interest.

6. *Perform cation recalculations to confirm minerals analyzed.*
7. *Classify minerals.*
8. *Conduct thermodynamic modeling based on minerals observed.*
9. *Determine minerals feasible for mineral carbonation based on thermodynamic modeling.*
10. *Conduct kinetic modeling on minerals feasible for mineral carbonation based on thermodynamic modeling.*
11. *Determine temperature and pressure conditions yielding best results based on kinetic and thermodynamic modeling.*
12. *Determine samples potentially feasible for mineral carbonation based on the minerals they contain and thermodynamic and kinetic modeling of these minerals.*
13. *Use samples from step 12 for autoclave experiments at temperatures and pressures determined in step 11.*

In order to develop this methodology, samples from the Keweenaw Peninsula in Michigan were studied using thin section analysis, microprobe analysis, whole rock data, and thermodynamic modeling. The sampled rocks have undergone low-grade metamorphism and have been variably altered, which proved to be an advantage for the development of the methodology.

Petrographic examination was first used to determine the general mineralogy, as well as texture, size, and alteration of minerals in 54 thin sections. Several alteration assemblages were determined petrographically:

(1) relatively “fresh” samples containing olivine and orthopyroxene with some chlorite alteration of fresh appearing plagioclase grains,

(2) moderately altered samples with chlorite, sericite, and sometimes calcite alteration of plagioclase cores,

(3) altered samples with prehnite, pumpellyite, and sometimes epidote alteration of plagioclase, and

(4) altered samples with chlorite, pumpellyite, and often epidote alteration of plagioclase.

Microprobe analyses of 17 thin sections were conducted next to classify the minerals and to detect potential compositional trends with alteration assemblages. Variations in feldspar group mineral compositions confirm the alteration assemblages listed above. Available whole rock data for 206 samples was used to study the original compositions and chemical alterations of samples, based on concentrations of immobile and mobile elements, respectively. Nearest end-members to the minerals identified in the studied samples were modeled regarding their thermodynamic stability in the presence of CO_2-gas and water. Anorthite, prehnite, and diopside appear the most feasible for mineral carbonation based on thermodynamic modeling, other minerals thermodynamically unstable with respect to CO_2 at standard conditions include forsterite, enstatite, talc, clinochlore, saponite-Mg, and phengite.

The feasibility of mineral carbonation as an artificial process to reduce anthropogenic CO_2 output hinges on the kinetics of specific, mixed mineral reactions. Although dissolution and reaction rates were not discussed in this research, an approach was developed to characterize mafic rocks regarding mineral carbonation based on their mineralogy, texture, geochemistry, and thermodynamic stability of minerals of interest.

Most samples for this study were collected from mine tailings in the Keweenaw Peninsula, likely creating a bias towards more altered rocks. Samples have undergone variable, low grade metamorphism; and hydrothermal alteration is expected to be more intense in and near areas of copper precipitation (i.e., copper mines). Thus, other parts of the MRS should be studied independently regarding their mineral carbonation potential, using the methodology developed in this thesis.

All of the samples from the study area show signs of alteration, with only very few "least altered" samples. These "least altered" samples might be feasible for mineral carbonation due to their relatively higher anorthite contents in plagioclase. Other samples contain little Ca-rich plagioclase, but considerable amounts of clinopyroxene. Thermodynamic modeling of diopside (clinopyroxene), anorthite, and prehnite revealed that these minerals are thermodynamically most feasible for mineral carbonation and kinetic modeling should be completed to determine the mineral carbonation potential of these minerals.

The potential for mineral carbonation of mafic rocks largely depends on their mineralogy, texture, and alteration. Petrographic examination combined with microprobe analysis and thermodynamic modeling appears to be a good first step in the determination of potentially viable samples. Kinetic modeling should be used next to determine the carbonation feasibility of these rocks. Autoclave experiment conditions and samples for autoclave experiments should be selected based on results from thermodynamic and kinetic modeling.

Overall, it is important to note that not all mafic rocks are basalts, and thus not all mafic rocks are equally feasible for mineral carbonation. Variations in original composition, mineralogy, grain size, and alteration can lead to great differences in mineral carbonation feasibility. The approach outlined above can be used as a relatively inexpensive and expeditious method to determine the samples most feasible for mineral carbonation or autoclave experiments.

REFERENCES

Aradóttir, E.S.P., Sigurdardóttir, H., Sigfússon, B., and Gunnlaugsson, E., 2011, CarbFix: A CCS pilot project imitating and accelerating natural CO_2 sequestration: Greenhouse Gases: Science and Technology, v. 1, no. 2, p. 105-118.

Aradóttir, E.S.P., Sonnenthal, E.L., and Jónsson, H., 2012, Development and evaluation of a thermodynamic dataset for phases of interest in CO_2 mineral sequestration in basaltic rocks: Chemical Geology, v. 304-305, p. 26-38.

Béarat, H., McKelvy, M.J., Chizmeshya, A.V.G., Gormley, D., Nunez, R., Carpenter, R.W., Squires, K., and Wolf, G.H., 2006, Carbon sequestration via aqueous olivine mineral carbonation: role of passivating layer formation: Environmental Science Technology, v. 40, p. 4802 - 4808.

Beecy, D.J., and Kuuskraa, V.A., 2001, Status of U.S. Geologic Carbon Sequestration Research and Technology: Environmental Geosciences, v. 8, no. 3, p. 152-159.

Best, M.G., 2002, Igneous and metamorphic petrology (2nd ed.), Wiley-Blackwell.

Bethke, C., 2000, The Geochemist's Workbench Release 3.1: A user's guide to Rxn, Act2, Tact, React, and GtPlot: University of Illinois, Urbana-Champaign.

Blatt, H., Tracy, R.J., and Owens, B.E., 2006, Petrology. Igneous, sedimentary, and metamorphic (3rd ed.): New York, W.H. Freeman and Company.

Bornhorst, T.J., 1997, Tectonic context of native copper deposits of the North American midcontinent rift system: Geological Society of America Bulletin, v. 312, p. 127-136.

Bornhorst, T.J., and Barron, R.J., 2011, Copper deposits of the western Upper Peninsula of Michigan: The Geological Society of America, Field Guide 24.

Bornhorst, T.J., and Lankton, L.D., 2009, Copper mining: a billion years of geologic and human history, Michigan Geology and Geography, p. 150-173.

Bornhorst, T.J., Paces, J.B., Grant, N.K., Obradovich, J.D., and Huber, N.K., 1988, Age of native copper mineralization, Keweenaw Peninsula, Michigan: Economic Geology, v. 83, no. 3, p. 619-625.

Brown, G.E.J., Bird, D.K., Kendelewicz, T., Maher, K., Mao, W., Johnson, N., Rosenbauer, R.J., and Real, P.G.D., 2010, Geological Sequestration of CO_2: An

Exploratory Study of the Mechanisms and Kinetics of CO_2 Reaction with Mg-Silicates: Stanford University.

Butler, B.S., and Burbank, W.S., 1929, The copper deposits of Michigan: U.S. Geological Survey.

Cannon, W.F., McRae, M.E., and Nicholson, S.W., 1999, Geology and mineral deposits of the Keweenaw Peninsula and vicinity, Michigan: U.S. Geological Survey Open-File Report 99-149.

Cannon, W.F., and Nicholson, S.W., 1992, Revisions of stratigraphic nomenclature within the Keweenawan Supergroup of Northern Michigan and geochemistry, petrography, and volcanology of rhyolites of the Portage Lake Volcanics, Keweenaw Peninsula, Michigan.

Cannon, W.F., Peterman, Z.E., and Sims, P.K., 1993, Crustal-scale thrusting and origin of the Montreal River monocline. A 35-km-thick cross section of the midcontinent rift in northern Michigan and Wisconsin: Tectonics, v. 12, no. 3, p. 728-744.

Chen, Z.-Y., O'Connor, W.K., and Gerdemann, S.J., 2006, Chemistry of aqueous mineral carbonation for carbon sequestration and explanation of experimental results: Environmental Progress, v. 25, no. 2, p. 161-166.

Crisman, D.P., 1982, Groundwater geochemistry in the Portage Lake Volcanics, Hancock, Michigan and implications for native copper stability: Houghton, Michigan Technological University, M.S., 95 p.

Deer, W.A., Howie, R.A., and Zussman, J., 1992, An introduction to the rock-forming minerals (2nd ed.), Pearson - Prentice Hall.

ESRL, 2013, Trends in atmospheric carbon dioxide, Earth Systems Research Laboratory, 2013, accessed: 12/31/2013.

Gerdemann, S.J., Dahlin, D.C., O'Connor, W.K., and Penner, L.R., 2003, Carbon dioxide sequestration by aqueous mineral carbonation of magnesium silicate minerals, in Second Annual Conference on Carbon Sequestration, Alexandria, VA, National Energy Technology Laboratory, NETL.

Gíslason, S.R., and Oelkers, E.H., 2003, Mechanism, rates, and consequences of basaltic glass dissolution: II. An experimental study of the dissolution rates of basaltic glass as a function of pH and temperature: Geochimica et Cosmochimica Acta, v. 67, no. 20, p. 3817-3832.

Goldberg, D.S., Takahashi, T., and Slagle , A.L., 2008, Carbon dioxide sequestration in deep-sea basalt: Proceedings of the National Academy of Sciences.

Guthrie, G.D.J., Carey, J.W., Bergfeld, D., Byler, D., Chipera, S., and Ziock, H.-J., 2001, Geochemical aspects of the carbonation of magnesium silicates in an aqueous medium, in First National Conference on Carbon Sequestration, National Energy Technology Laboratory, NETL.

Irvine, T.N., and Barager, W.R.A., 1971, A guide to the chemical classification of the common volcanic rocks: Canadian Journal of Earth Sciences, v. 8, p. 523-548.

Jolly, W.T., and Smith, R.E., 1972, Degradation and metamorphic differentiation of the Keweenawan tholeiitic lavas of Northern Michigan, U.S.A: Journal of Petrology, v. 13, no. 2, p. 273-309.

Kelly, W.C., Rye, R.O., and Livnat, A., 1986, Saline minewaters of the Keweenaw Peninsula, northern Michigan; their nature, origin, and relation to similar deep waters in Precambrian crystalline rocks of the Canadian Shield: American Journal of Science, v. 286, no. 4, p. 281-308.

Königsberger, E., Königsberger, L.-C., and Gamsjäger, H., 1999, Low-temperature thermodynamic model for the system Na_2CO_3-$MgCO_3$-$CaCO_3$-H_2O: Geochimica et Cosmochimica Acta, v. 63, no. 19-20, p. 3105-3119.

Krevor, S.C., and Lackner, K.S., 2009, Enhancing process kinetics for mineral carbon sequestration: Energy Procedia, v. 1, no. 1, p. 4867-4871.

Krupka, K.M., Cantrell, K.J., and McGrail, B.P., 2010, Thermodynamic data for geochemical modeling of carbonate reactions associated with CO_2 sequestration - literature review: Pacific Northwest National Laboratory.

Lackner, K.S., Butt, D.P., and Wendt, C.H., 1997, Progress on binding CO_2 in mineral substrates: Energy Conversion and Management, v. 38, no. Supplement 1, p. S259-S264.

Lackner, K.S., Wendt, C.H., Butt, D.P., Joyce, E.L., and Sharp, D.H., 1995, Carbon dioxide disposal in carbonate minerals: Energy, v. 20, no. 11, p. 1153-1170.

Le Bas, M.J., Le Maitre, R.W., Streckeisen, A., and Zanettin, B., 1986, A chemical classification of volcanic rocks based on the total alkali-silica diagram: Journal of Petrology, v. 27, no. 3, p. 745-750.

Le Maitre, R.W., 2002, Igneous rocks: a classification and glossary of terms: recommendations of the International Union of Geological Sciences, Subcomission on the Systematics of Igneous Rocks, Cambridge University Press, 236 p.

Leake, B.E., Wolley, A.R., Arps, C.E.S., Birch, W.D., Gilbert, M.C., Grice, J.D., Hawthorne, F.C., Kato, A., Kisch, H.J., Krivovichev, V.G., Linthout, K., Laird, J., Mandarino, J.A., Maresch, W.V., Nickel, E.H., Rock, N.M.S., Schumacher, J.C., Smith, D.C., Stephenson, N.C.N., Ungaretti, L., Whittaker, E.J.W., and Youzhi, G., 1997, Nomenclature of amphiboles: report of the Subcommittee on Amphiboles of the International Mineralogical Association, Commision on New Minerals and Mineral Names: The Canadian Mineralogist, v. 35, p. 219-246.

Livnat, A., 1983, Metamorphism and copper mineralization of the Portage Lake lava series, Northern Michigan, University of Michigan, PhD, 225 p.

Marini, L., 2007, Geological sequestration of carbon dioxide: thermodynamics, kinetics, and reaction path modeling, Elsevier, Amsterdam.

Matter, J.M., Broecker, W.S., Stute, M., Gislason, S.R., Oelkers, E.H., Stefánsson, A., Wolff-Boenisch, D., Gunnlaugsson, E., Axelsson, G., and Björnsson, G., 2009, Permanent Carbon Dioxide Storage into Basalt: The CarbFix Pilot Project, Iceland: Energy Procedia, v. 1, no. 1, p. 3641-3646.

McGrail, B.P., Schaef, H.T., Ho, A.M., Chien, Y.-J., Dooley, J.J., and Davidson, C.L., 2006, Potential for carbon dioxide sequestration in flood basalts: J. Geophys. Res., v. 111, no. B12, p. B12201.

McGrail, B.P., Spane, F.A., Sullivan, E.C., Bacon, D.H., and Hund, G., 2011, The Wallula basalt sequestration pilot project: Energy Procedia, v. 4, p. 5653-5660.

Meschede, M., 1986, A method of discriminating between different types of mid-ocean ridge basalts and continental tholeiites with the Nb-Zr-Y diagram: Chemical Geology, v. 56, no. 3-4, p. 207-218.

Metz, B., Davidson, O., de Coninck, H., Loos, M., and Meyer, L., 2005, IPCC Special Report on carbon dioxide capture and storage: Cambridge University Press, New York.

Metz, P.A., and Bolz, P., 2013, Geological and geotechnical site invesitgation for the design of a CO_2 rich flue gas direct injection and storage facility: University of Alaska Fairbanks Final Contract Report, Department of Energy Grant No. FE0001833.

Morimoto, N., Fabries, J., Ferguson, A.K., Ginzburg, I.V., Ross, M., Seifert, F.A., Zussman, J., Aoki, K., and Gottardi, G., 1988, Nomenclature of pyroxenes: American Mineralogist, v. 73, no. 9-10, p. 1123-1133.

Nogueira, M., and Mamora, D.D., 2008, Effect of flue-gas impurities on the process of injection and storage of CO_2 in depleted gas reservoirs: Journal of Energy Resources Technology, v. 130, no. 1, p. 013301-013301.

Oelkers, E.H., and Gíslason, S.R., 2001, The mechanism, rates and consequences of basaltic glass dissolution: I. An experimental study of the dissolution rates of basaltic glass as a function of aqueous Al, Si and oxalic acid concentration at 25°C and pH = 3 and 11: Geochimica et Cosmochimica Acta, v. 65, no. 21, p. 3671-3681.

Oelkers, E.H., Gislason, S.R., and Matter, J., 2008, Mineral Carbonation of CO2: Elements, v. 4, no. 5, p. 333-337.

Ojakangas, R.W., Morey, G.B., and Green, J.C., 2001, The mesoproterozoic midcontinent rift system, Lake Superior region, USA: Sedimentary Geology, v. 141-142, p. 421-442.

Paces, J.B., 1988, Magmatic processes, evolution and mantle source characteristics contributing to the petrogenesis of midcontinent rift basalts: Portage Lake basalts, Keweenaw Peninsula, Michigan: Houghton, Michigan Technological University, Ph.D. dissertation, 413 p.

Paces, J.B., and Davis, D.W., 1988, Implications of high precision U-Pb age dates on zircons from Portage Lake Volcanic basalts on midcontinent rift subsidence rates, lava flow repose periods and magma production rates, in Institute on Lake Superior Geology, Marquette, p. 85-86.

Pueschner, U.R., 2001, Very low-grade metamorphism in the Portage Lake Volcanics on the Keweenaw Peninsula, Michigan, USA: Basel, Universitaet Basel, 163 p.

Rosenbauer, R.J., Thomas, B., Bischoff, J.L., and Palandri, J., 2012, Carbon sequestration via reaction with basaltic rocks: Geochemical modeling and experimental results: Geochimica et Cosmochimica Acta, v. 89, p. 116-133.

Stoiber, R.E., and Davidson, E.S., 1959, Amygdule mineral zoning in the Portage Lake Lava series, Michigan copper district; Part 1: Economic Geology, v. 54, no. 7, p. 1250-1277.

Sun, S.-S., and McDonough, W.F., 1989, Chemical and isotopic systematics of oceanic basalts: implications for mantle composition and processes: Geological Society, London, Special Publications, v. 42, p. 313-345.

Weege, R.J., and Pollock, J.P., 1972, The geology of two new mines in the native copper district of Michigan: Economic Geology, v. 67, no. 5, p. 622-633.

White, W.S., 1968, The native-copper deposits of Northern Michigan, Ore deposits of the United States, 1933-1967: Rocky Mountain Fund Series.

Wilson, S.A., Dipple, G.M., Power, I.M., Thom, J.M., Anderson, R.G., Raudsepp, M., Gabites, J.E., and Southam, G., 2009, Carbon dioxide fixation within mine wastes of ultramafic-hosted ore deposits: examples from the Clinton Creek and Cassiar Chrysotile deposits, Canada: Economic Geology, v. 104, no. 1, p. 95-112.

Wilson, S.A., Raudsepp, M., and Dipple, G.M., 2006, Verifying and quantifying carbon fixation in minerals from serpentine-rich mine tailings using the Rietveld method with X-ray powder diffraction data: American Mineralogist, v. 91, no. 8-9, p. 1331-1341.

Winchester, J.A., and Floyd, P.A., 1977, Geochemical discrimination of different magma series and their differentiation products using immobile elements: Chemical Geology, v. 20, p. 325-343.

Wogelius, R.A., and Walther, J.V., 1991, Olivine dissolution at 25°C: Effects of pH, CO_2, and organic acids: Geochimica et Cosmochimica Acta, v. 55, no. 4, p. 943-954.

Zevenhoven, R., Fagerlund, J., and Songok, J.K., 2011, CO2 mineral sequestration: developments toward large-scale application: Greenhouse Gases: Science and Technology, v. 1, no. 1, p. 48-57.

APPENDIX A: WHOLE ROCK DATA

Table A-1: Major element, C, and S analyses.

	weight (%)																
	Na_2O	MgO	Al_2O_3	SiO_2	P_2O_5	K_2O	CaO	TiO_2	MnO	Fe_2O_3	Cr_2O_3	SrO	BaO	LOI	Total	C	S
10BA001	2.81	7.75	13.10	43.50	0.17	0.38	8.41	1.50	0.16	11.10	0.02	0.01	0.01	10.80	99.72	1.81	0.01
10BA002	3.58	7.62	14.40	45.80	0.18	0.98	6.44	1.53	0.18	11.90	0.03	0.02	0.02	7.68	100.36	0.96	<0.01
10BA003	0.17	7.88	13.40	41.20	0.18	1.64	9.83	1.48	0.15	11.30	0.02	0.01	0.02	13.40	100.68	2.19	0.01
10BA004	3.04	6.60	12.90	42.60	0.15	1.26	7.91	1.42	0.17	11.05	0.02	0.01	0.06	13.05	100.24	2.76	0.01
10BA005	1.83	6.38	14.45	43.00	0.16	1.18	7.57	1.53	0.14	11.70	0.03	0.01	0.02	11.40	99.40	1.63	0.01
10BA006	3.47	8.86	13.95	40.50	0.16	0.42	7.48	1.57	0.17	10.80	0.02	0.01	0.01	10.90	98.32	1.65	<0.01
10BB001	2.06	8.56	16.40	46.40	0.14	0.31	9.75	1.39	0.24	11.55	0.03	0.03	0.01	4.07	100.94	0.11	0.01
10BB002	3.19	8.40	15.75	46.20	0.14	1.43	7.47	1.46	0.17	11.75	0.03	0.01	0.07	4.80	100.87	0.04	0.01
10BB003	3.46	10.70	14.85	42.50	0.13	1.41	4.76	1.38	0.28	11.40	0.03	0.03	0.04	8.47	99.44	0.76	0.01
10BB004	3.41	10.35	15.20	46.40	0.14	1.28	5.08	1.41	0.20	11.35	0.03	0.03	0.11	5.23	100.22	0.04	0.01
10BB005	1.78	9.44	15.75	45.00	0.11	0.30	8.78	1.39	0.25	11.85	0.03	0.02	0.01	4.83	99.54	0.18	0.01
10BB006	1.85	9.30	15.95	45.40	0.13	0.28	8.31	1.38	0.25	11.25	0.03	0.02	0.01	5.07	99.23	0.12	0.01
10CC001	3.45	7.10	16.60	48.90	0.15	0.81	8.11	1.34	0.17	11.25	0.02	0.03	0.03	3.12	101.08	0.03	0.02
10CC002	5.13	6.06	13.45	50.20	0.28	0.70	6.36	2.07	0.16	13.90	0.02	0.02	0.02	3.36	101.73	0.05	0.02
10CC003	2.79	7.12	16.70	48.70	0.15	0.40	9.55	1.38	0.15	11.25	0.02	0.03	0.02	3.04	101.30	0.03	0.01
10CC004	2.77	6.54	17.10	49.20	0.15	0.43	9.85	1.36	0.16	11.25	0.03	0.03	0.02	2.57	101.46	0.12	0.01
10CC005	3.05	6.57	16.95	49.30	0.16	2.45	7.42	1.35	0.16	10.95	0.02	0.03	0.15	2.87	101.43	0.04	0.02
10CC006	3.65	6.98	16.75	48.70	0.14	0.96	7.64	1.33	0.16	11.20	0.03	0.03	0.03	2.81	100.41	0.03	0.01
10CE001	3.23	8.95	15.95	44.30	0.25	2.80	1.77	1.85	0.17	13.75	0.02	0.02	0.07	6.29	99.42	0.08	0.01
10CE002	4.48	5.49	14.15	48.90	0.21	0.10	10.30	2.16	0.18	12.85	0.03	0.02	<0.01	2.50	101.37	0.03	0.01
10CE003	0.23	2.69	16.45	41.70	0.19	0.02	22.30	1.14	0.11	10.45	0.02	0.03	<0.01	4.58	99.91	0.05	0.01
10CE004	2.34	7.11	16.50	46.20	0.13	0.25	10.60	1.52	0.17	12.90	0.03	0.03	0.01	3.20	100.99	0.03	0.01
10CE005	2.76	8.07	16.50	46.40	0.15	0.35	9.49	1.52	0.24	12.30	0.03	0.02	0.02	3.87	101.72	0.03	<0.01
10CE006	3.91	4.83	16.40	43.00	0.13	0.18	11.35	1.40	0.15	13.40	0.03	0.01	<0.01	6.00	100.79	0.43	0.01
10CF001	0.54	7.14	7.90	39.40	0.06	1.62	18.45	0.48	0.10	4.52	0.01	0.01	0.01	8.09	88.33	0.09	0.01
10CF002	4.85	6.56	16.90	48.80	0.17	0.70	5.10	1.56	0.22	11.30	0.03	0.05	0.03	4.20	100.47	0.04	0.01

Table A-1 (continued): Major element, C, and S analyses.

	weight %																
	Na_2O	MgO	Al_2O_3	SiO_2	P_2O_5	K_2O	CaO	TiO_2	MnO	Fe_2O_3	Cr_2O_3	SrO	BaO	LOI	Total	C	S
10CF003	4.27	4.97	13.00	50.30	0.28	1.40	5.49	2.60	0.27	15.40	0.01	0.03	0.04	2.29	100.35	0.05	<0.01
10CF004	4.62	6.93	16.35	48.50	0.17	1.40	3.51	1.79	0.26	12.10	0.03	0.02	0.03	4.40	100.11	0.04	0.01
10CF005	4.62	5.21	18.10	47.00	0.09	1.37	7.11	1.04	0.12	10.55	0.03	0.02	0.01	5.70	100.97	0.32	<0.01
10CF006	4.20	7.44	16.60	46.20	0.15	1.17	4.72	1.59	0.18	11.85	0.03	0.02	0.01	5.38	99.54	0.05	0.01
10CH001	2.67	7.11	15.30	46.20	0.17	1.06	8.55	1.68	0.17	12.60	0.03	0.03	0.04	3.49	99.10	0.15	0.01
10CH002	2.63	4.75	12.00	47.90	0.14	0.03	11.55	1.38	0.15	9.62	0.02	0.01	<0.01	6.70	96.88	1.10	<0.01
10CH003	1.92	6.10	15.25	44.20	0.17	0.96	10.55	1.64	0.14	12.40	0.03	0.02	0.03	7.39	100.80	1.06	0.01
10CH004	3.73	7.40	15.00	39.30	0.15	0.04	11.80	1.58	0.17	12.25	0.02	0.02	<0.01	8.96	100.42	1.25	0.01
10CH005	2.84	7.50	13.80	40.60	0.15	0.51	9.38	1.43	0.16	11.10	0.02	0.01	0.01	12.05	99.56	1.98	0.01
10CH006	2.94	6.92	15.75	47.40	0.17	0.76	8.83	1.69	0.17	13.05	0.03	0.03	0.03	3.18	100.95	0.09	0.02
10CL001	3.08	7.63	17.20	48.40	0.16	0.54	8.35	1.38	0.17	11.80	0.03	0.03	0.03	3.20	102.00	0.06	<0.01
10CL002	3.47	7.63	16.75	47.20	0.14	0.86	7.23	1.45	0.18	11.90	0.03	0.03	0.05	4.50	101.42	0.03	<0.01
10CL003	3.00	8.38	15.95	46.50	0.16	1.50	7.41	1.41	0.20	11.85	0.03	0.02	0.13	4.68	101.22	0.04	<0.01
10CL004	2.87	8.04	16.65	45.10	0.13	0.53	8.18	1.37	0.18	11.50	0.03	0.03	0.02	3.60	98.23	0.02	<0.01
10CL005	4.23	0.48	14.40	38.80	0.19	0.03	20.60	1.16	0.09	10.35	0.02	0.14	<0.01	10.80	101.29	2.52	0.01
10CL006	3.03	6.54	17.05	48.50	0.18	0.34	8.83	1.47	0.17	12.30	0.02	0.03	0.02	2.59	101.07	0.03	<0.01
10CN001	2.52	4.24	15.40	41.90	0.16	0.11	15.60	1.13	0.13	9.96	0.02	0.01	0.01	6.88	98.07	0.79	0.01
10CN002	2.50	6.69	14.50	46.50	0.11	0.30	10.10	1.56	0.12	12.35	0.03	0.03	0.01	3.90	98.70	0.17	<0.01
10CN003	2.76	7.96	15.10	45.20	0.17	2.68	6.73	1.56	0.23	11.80	0.03	0.02	0.28	4.19	98.71	0.16	<0.01
10CN004	3.21	7.76	15.35	48.00	0.11	2.40	7.00	1.43	0.17	12.25	0.03	0.02	0.14	3.89	101.76	0.15	<0.01
10CN005	0.10	3.36	15.60	45.20	0.14	0.03	18.25	1.35	0.20	11.05	0.03	0.10	<0.01	3.90	99.31	0.04	0.01
10CN006	2.39	7.94	15.00	46.50	0.11	0.25	9.17	1.58	0.19	12.60	0.03	0.03	0.01	2.80	98.60	0.03	<0.01
10DE001	3.81	8.20	16.00	47.20	0.13	0.98	6.03	1.32	0.23	11.35	0.03	0.04	0.09	4.57	99.98	0.04	0.01
10DE002	4.87	6.96	15.00	45.40	0.14	1.90	4.88	1.46	0.16	13.00	0.01	0.02	0.21	6.76	100.77	0.76	<0.01
10DE003	3.89	6.27	14.35	42.40	0.12	0.31	13.25	1.05	0.13	10.10	0.03	0.01	<0.01	9.07	100.98	1.26	0.02
10DE004	5.45	2.26	16.05	51.60	0.08	0.04	12.20	1.04	0.09	9.68	0.02	<0.01	<0.01	2.50	101.01	0.13	0.01
10DE005	4.79	6.49	15.50	46.90	0.16	0.39	7.81	1.50	0.17	12.30	0.03	0.01	<0.01	4.58	100.63	0.13	0.01
10DE006	3.48	8.49	16.40	47.70	0.15	0.81	7.32	1.33	0.20	11.60	0.03	0.04	0.03	4.07	101.65	0.03	<0.01
10DE007	4.80	5.33	13.65	49.00	0.24	0.34	9.17	2.17	0.19	13.20	0.02	0.02	0.01	2.91	101.05	0.14	0.01

Table A-1 (continued): Major element, C, and S analyses.

	weight %																
	Na_2O	MgO	Al_2O_3	SiO_2	P_2O_5	K_2O	CaO	TiO_2	MnO	Fe_2O_3	Cr_2O_3	SrO	BaO	LOI	Total	C	S
10DR001	2.88	8.26	16.05	45.30	0.13	1.31	9.25	1.30	0.19	11.20	0.03	0.04	0.10	5.16	101.20	0.04	0.01
10DR002	4.65	7.06	15.65	46.30	0.14	2.10	4.32	1.38	0.11	11.65	0.03	0.02	0.01	5.14	98.56	0.29	0.01
10DR003	2.58	9.86	16.30	44.20	0.12	1.57	6.11	1.23	0.21	10.90	0.03	0.01	0.02	6.57	99.71	0.06	0.01
10DR004	2.01	10.55	15.05	45.20	0.15	3.29	4.50	1.41	0.27	11.30	0.02	0.03	0.26	5.22	99.26	0.07	0.01
10DR005	2.38	8.21	16.65	44.60	0.10	2.17	7.75	1.02	0.27	9.64	0.02	0.01	0.02	5.42	98.26	0.13	0.01
10DR006	3.11	9.25	15.80	45.60	0.11	1.74	4.97	1.24	0.26	11.00	0.03	0.04	0.32	5.35	98.82	0.03	0.01
10FJ001	4.09	5.90	13.75	41.40	0.17	0.86	9.89	1.52	0.14	10.85	0.02	0.01	0.02	11.00	99.62	2.13	<0.01
10FJ002	4.49	7.32	14.50	45.20	0.24	0.48	5.48	2.17	0.20	13.35	0.02	0.01	0.01	5.00	98.47	0.06	0.01
10FJ003	3.88	5.51	12.90	48.60	0.17	1.19	7.44	2.53	0.23	15.65	0.01	0.06	0.05	2.10	100.32	0.03	0.01
10FJ004	4.13	5.90	16.55	47.10	0.17	0.77	8.61	1.61	0.16	11.20	0.02	0.05	0.04	4.00	100.31	0.02	<0.01
10FJ005	3.50	6.64	11.40	49.30	0.26	0.65	5.00	2.56	0.23	15.30	0.01	0.02	0.03	5.02	99.92	0.02	<0.01
10FJ006	3.45	8.34	14.40	40.40	0.20	1.66	5.89	1.99	0.19	13.15	0.01	0.03	0.02	9.80	99.53	0.88	0.01
10FU001	4.77	6.13	13.50	51.50	0.28	0.82	4.97	2.05	0.18	13.90	0.02	0.02	0.04	3.31	101.49	0.02	0.01
10FU002	4.71	6.55	15.00	49.30	0.22	0.82	6.05	1.62	0.14	12.25	0.02	0.01	0.02	4.34	101.05	0.09	0.01
10FU003	4.30	5.51	16.00	47.20	0.20	0.42	9.17	1.52	0.15	11.60	0.02	0.02	0.01	4.46	100.58	0.08	0.01
10FU004	3.15	8.39	15.95	46.40	0.12	1.86	6.79	1.22	0.19	11.10	0.03	0.03	0.14	4.94	100.31	0.25	0.01
10FU005	0.12	1.97	11.10	56.50	0.22	0.02	13.60	1.52	0.09	12.50	0.01	0.03	<0.01	4.01	101.69	0.16	0.02
10FU006	2.79	7.36	15.20	46.80	0.13	3.17	6.31	1.32	0.18	11.25	0.03	0.02	0.34	4.20	99.10	0.25	<0.01
10GR001	2.36	8.82	16.50	46.40	0.14	0.81	8.43	1.40	0.20	11.70	0.03	0.03	0.04	4.20	101.06	0.03	<0.01
10GR002	2.42	9.40	17.10	44.70	0.12	0.51	8.60	1.35	0.20	11.70	0.03	0.03	0.02	4.49	100.67	0.04	<0.01
10GR003	4.66	5.55	15.20	49.00	0.24	0.79	7.51	1.77	0.18	12.40	0.02	0.02	0.03	3.40	100.77	0.03	0.01
10GR004	4.44	3.03	9.84	36.40	0.21	0.35	19.45	1.46	0.11	9.95	0.01	0.01	0.01	16.45	101.72	3.84	0.01
10GR005	2.15	8.50	15.95	44.50	0.10	0.85	8.49	1.30	0.20	11.50	0.03	0.03	0.05	4.20	97.85	0.10	<0.01
10GR006	4.44	5.78	12.85	48.00	0.41	0.65	4.79	1.95	0.17	13.80	0.01	0.02	0.03	5.18	98.08	0.47	<0.01
10HE001	4.96	8.03	16.05	46.30	0.26	0.43	4.57	1.31	0.17	11.85	0.01	0.02	0.01	6.77	100.74	0.04	0.01
10HE002	2.12	4.64	11.75	47.10	1.05	1.24	8.19	2.19	0.14	10.50	<0.01	0.01	0.01	11.15	100.09	1.59	0.01
10HE003	1.57	8.62	16.25	42.60	0.13	3.17	6.00	0.86	0.22	10.25	0.01	0.02	0.12	11.20	101.02	1.11	0.01
10HE004	2.71	3.06	11.95	49.60	1.16	1.62	7.82	2.28	0.14	10.80	<0.01	0.01	0.02	9.55	100.72	1.41	<0.01
10HE005	2.76	2.92	12.55	51.90	1.20	2.03	5.71	2.38	0.12	11.00	<0.01	0.02	0.03	8.08	100.70	0.88	<0.01

Table A-1 (continued): Major element, C, and S analyses.

	weight %																
	Na_2O	MgO	Al_2O_3	SiO_2	P_2O_5	K_2O	CaO	TiO_2	MnO	Fe_2O_3	Cr_2O_3	SrO	BaO	LOI	Total	C	S
10HE006	0.95	6.06	13.55	42.30	0.11	4.05	8.85	0.99	0.20	9.57	0.01	0.01	0.22	13.10	99.97	1.87	<0.01
10IR001	4.05	5.65	15.45	46.20	0.19	0.25	10.40	1.75	0.17	11.80	0.03	0.03	0.01	4.80	100.78	0.09	0.01
10IR002	3.08	6.16	15.65	45.50	0.18	1.04	9.04	1.80	0.19	12.45	0.03	0.04	0.04	5.30	100.50	0.03	<0.01
10IR003	3.42	6.13	15.75	44.10	0.18	0.18	10.65	1.66	0.19	12.10	0.02	0.01	0.01	6.67	101.07	0.29	0.01
10IR004	2.59	6.99	16.25	46.30	0.17	0.42	9.31	1.74	0.18	12.40	0.03	0.03	0.02	4.49	100.92	0.02	<0.01
10IR005	3.33	5.41	14.75	41.20	0.14	0.12	11.90	1.56	0.16	11.95	0.02	0.01	<0.01	10.45	101.00	1.27	0.01
10IR006	4.88	4.93	13.15	43.30	0.06	0.05	11.20	1.46	0.14	10.10	0.03	0.01	<0.01	12.45	101.76	2.28	0.01
10IR007	4.66	9.27	16.15	44.30	0.20	0.11	3.33	1.70	0.21	11.65	0.03	0.01	<0.01	6.19	97.81	0.13	<0.01
10IR008	5.98	2.45	13.65	49.60	0.14	0.20	9.13	1.48	0.08	11.35	0.02	0.02	<0.01	6.59	100.69	1.32	<0.01
10IR009	3.80	5.44	13.40	45.60	0.12	0.52	8.46	1.38	0.15	11.45	0.02	0.01	0.01	9.37	99.73	1.58	<0.01
10IR010	2.65	5.89	14.40	42.70	0.23	1.21	9.22	1.47	0.16	11.35	0.02	0.01	<0.01	11.60	100.91	1.85	0.01
10IR011	2.59	6.50	16.20	47.40	0.15	0.48	10.15	1.64	0.18	12.40	0.03	0.03	0.01	3.68	101.44	0.17	<0.01
10IR012	5.60	3.99	13.45	47.70	0.14	0.11	9.15	1.45	0.13	10.95	0.02	0.01	<0.01	8.48	101.18	1.67	0.01
10LA001	4.04	7.88	15.85	45.50	0.18	0.74	6.17	1.90	0.22	13.25	0.03	0.02	0.02	5.28	101.08	0.07	0.01
10LA002	2.81	3.58	15.55	41.40	0.14	0.60	16.25	1.33	0.13	11.35	0.02	0.01	<0.01	6.89	100.06	0.92	<0.01
10LA003	2.83	6.31	15.10	42.30	0.12	0.39	12.45	1.44	0.15	11.60	0.02	0.01	<0.01	5.89	98.61	0.40	<0.01
10LA004	2.95	7.08	16.25	46.30	0.17	0.82	8.61	1.65	0.20	12.70	0.03	0.03	0.03	3.90	100.72	0.02	<0.01
10MB001	2.93	7.46	16.00	48.60	0.07	0.34	10.70	0.66	0.16	11.40	0.02	0.03	0.03	2.88	101.28	0.14	0.01
10MB002	2.44	7.48	15.95	48.70	0.07	0.42	11.00	0.72	0.17	11.85	0.02	0.03	0.03	2.67	101.55	0.12	0.02
10MC001	3.72	6.69	16.50	46.40	0.16	1.85	7.19	1.65	0.16	12.25	0.03	0.01	0.07	3.99	100.67	0.09	0.01
10MC002	3.65	5.29	14.95	46.70	0.16	1.99	8.10	1.69	0.17	11.40	0.03	0.02	0.06	3.90	98.11	0.18	0.01
10MC003	3.86	7.14	16.10	46.50	0.15	0.84	6.55	1.68	0.15	12.20	0.03	0.02	0.01	4.90	100.13	0.05	0.01
10MC004	2.26	6.95	15.85	45.10	0.15	2.29	7.77	1.68	0.16	13.00	0.03	0.02	0.11	3.20	98.57	0.07	<0.01
10MC005	2.42	9.40	16.00	45.40	0.13	2.32	5.67	1.51	0.18	12.10	0.03	0.02	0.15	4.60	99.93	0.03	<0.01
10MC006	3.76	5.46	14.80	47.50	0.15	2.12	8.42	1.65	0.17	11.85	0.03	0.01	0.07	4.40	100.39	0.27	<0.01
10MG001	1.90	2.52	15.60	45.50	0.12	1.98	16.40	1.21	0.12	9.70	0.02	0.04	0.02	6.49	101.62	0.85	<0.01
10MG002	3.60	5.72	16.50	46.50	0.22	0.44	8.52	1.74	0.17	11.70	0.03	0.02	0.01	4.29	99.46	0.02	0.01
10MG003	2.67	7.19	15.45	46.50	0.16	1.90	7.19	1.52	0.17	12.15	0.03	0.07	0.03	3.10	98.13	0.02	<0.01
10MG004	3.34	6.08	15.80	46.20	0.17	0.96	8.55	1.60	0.15	11.60	0.03	0.02	0.01	4.39	98.90	0.03	<0.01

Table A-1 (continued): Major element, C, and S analyses.

	weight %															
	Na_2O	MgO	Al_2O_3	SiO_2	P_2O_5	K_2O	CaO	TiO_2	MnO	Fe_2O_3	Cr_2O_3	SrO	BaO	LOI	Total	C	S
10MG005	3.74	7.13	15.70	45.00	0.19	0.61	7.86	1.52	0.19	11.55	0.02	0.02	0.02	6.08	99.63	0.32	0.01
10MG006	2.76	6.28	15.40	47.20	0.15	1.03	10.25	1.41	0.15	10.75	0.03	0.02	0.03	4.30	99.76	0.05	0.01
10MI001	2.11	7.64	16.00	47.10	0.13	0.30	9.51	1.39	0.15	11.40	0.03	0.03	0.01	3.70	99.50	0.02	0.01
10MI002	2.47	10.20	15.45	46.10	0.11	1.75	4.64	1.19	0.22	10.75	0.03	0.02	0.05	5.97	98.95	0.03	0.01
10MI003	2.39	7.96	15.80	47.30	0.16	0.71	8.51	1.39	0.18	11.80	0.03	0.02	0.03	3.49	99.77	0.03	<0.01
10MI004	2.49	8.54	15.90	46.10	0.13	0.44	8.61	1.40	0.19	11.60	0.03	0.02	0.02	3.60	99.07	0.11	<0.01
10MI005	2.65	8.06	16.10	46.70	0.15	0.47	9.27	1.43	0.18	11.85	0.03	0.03	0.02	4.10	101.04	0.12	<0.01
10MI006	4.40	9.66	14.60	46.70	0.12	0.31	3.69	1.31	0.17	11.25	0.03	0.01	0.01	7.09	99.35	0.17	<0.01
10OC001	4.33	8.24	15.00	48.50	0.15	0.87	6.10	1.56	0.16	12.10	0.03	0.03	0.03	3.98	101.08	0.03	0.01
10OC002	2.50	7.65	16.10	47.20	0.15	0.32	9.93	1.48	0.15	12.35	0.03	0.03	0.01	2.62	100.52	0.04	0.01
10OC003	2.42	7.56	15.85	47.70	0.14	0.25	10.25	1.55	0.20	12.20	0.03	0.03	0.01	2.55	100.74	0.04	0.01
10OC004	3.35	6.69	16.20	47.70	0.16	0.78	9.19	1.54	0.16	12.35	0.03	0.03	0.02	2.80	101.00	0.06	0.01
10OC005	2.64	7.33	16.05	47.90	0.16	2.12	8.04	1.62	0.19	12.60	0.03	0.03	0.16	2.87	101.74	0.03	0.01
10OC006	2.70	7.99	15.95	46.40	0.15	0.70	9.54	1.55	0.20	12.10	0.03	0.02	0.02	3.11	100.46	0.14	0.01
10OC007	4.01	8.65	15.20	47.60	0.13	1.22	5.31	1.47	0.23	11.95	0.03	0.03	0.12	4.50	100.45	0.10	<0.01
10OC008	3.56	8.75	15.45	48.10	0.15	1.34	6.38	1.52	0.19	12.15	0.03	0.03	0.09	4.12	101.86	0.05	<0.01
10OC009	2.53	7.36	16.10	47.70	0.15	0.97	9.26	1.53	0.18	12.25	0.03	0.03	0.03	2.77	100.89	0.02	0.01
10OC010	3.97	8.22	14.70	47.60	0.14	1.40	6.60	1.39	0.17	11.40	0.03	0.02	0.12	4.05	99.81	0.14	0.01
10OC011	2.79	8.59	15.95	45.70	0.17	0.95	8.63	1.59	0.19	12.10	0.03	0.02	0.04	3.29	100.04	0.03	0.01
10OC013	4.36	5.75	14.20	45.30	0.16	0.72	9.79	1.53	0.21	12.65	0.03	0.01	0.01	6.67	101.39	0.35	0.01
10OC014	2.30	8.87	16.10	43.50	0.18	0.60	9.57	1.67	0.20	12.70	0.03	0.02	0.02	5.78	101.54	0.04	0.01
10OC015	3.42	5.16	14.05	41.00	0.17	0.88	13.50	1.44	0.15	11.10	0.02	0.01	0.01	9.51	100.42	1.08	<0.01
10OC016	4.22	6.53	14.50	44.70	0.17	1.08	8.95	1.48	0.16	11.10	0.02	0.01	0.02	8.08	101.02	0.52	0.01
10OC017	3.75	6.08	13.70	48.30	0.10	2.90	6.88	1.47	0.16	10.45	0.03	0.01	0.04	5.84	99.71	0.36	<0.01
10OC018	2.89	8.31	15.60	44.40	0.15	0.76	8.03	1.57	0.21	11.95	0.03	0.04	0.04	5.47	99.45	0.03	<0.01
10OJ001	4.47	4.12	12.95	52.10	0.28	0.14	7.32	1.87	0.16	13.80	0.02	0.02	<0.01	2.50	99.75	0.04	<0.01
10OJ002	0.08	1.43	11.90	53.90	0.22	0.15	15.30	1.40	0.09	11.60	0.01	0.01	<0.01	3.78	99.87	0.19	<0.01
10OJ003	3.04	7.59	16.50	47.30	0.17	0.69	8.48	1.33	0.18	11.00	0.02	0.03	0.03	2.99	99.35	0.03	<0.01
10OJ004	3.35	4.81	13.65	49.70	0.39	1.82	6.91	1.96	0.18	13.95	0.02	0.05	0.08	2.59	99.46	0.04	0.01

Table A-1 (continued): Major element, C, and S analyses.

	weight %																
	Na_2O	MgO	Al_2O_3	SiO_2	P_2O_5	K_2O	CaO	TiO_2	MnO	Fe_2O_3	Cr_2O_3	SrO	BaO	LOI	Total	C	S
10OJ005	3.29	4.98	13.40	51.60	0.30	1.64	7.03	2.02	0.20	13.65	0.02	0.04	0.06	1.90	100.13	0.02	<0.01
10OJ006	2.73	6.72	15.90	46.20	0.12	0.43	9.45	1.54	0.14	13.60	0.03	0.03	0.02	2.79	99.70	0.05	<0.01
10PH001	3.27	8.23	15.90	44.30	0.20	1.07	7.01	1.30	0.19	12.60	0.02	0.03	0.04	4.40	98.56	0.14	<0.01
10PH002	3.49	7.79	14.95	44.70	0.17	0.09	8.91	1.18	0.14	10.80	0.03	0.02	<0.01	5.18	97.45	0.14	<0.01
10PH003	3.83	7.09	15.90	47.00	0.18	0.85	6.32	1.40	0.17	11.90	0.02	0.03	0.04	3.60	98.33	0.03	<0.01
10PH004	2.95	8.24	16.30	47.80	0.14	1.06	8.24	1.30	0.18	11.45	0.03	0.03	0.05	4.19	101.96	0.04	<0.01
10PH005	4.02	7.28	16.25	49.20	0.14	0.91	7.55	1.28	0.13	11.40	0.03	0.04	0.03	3.50	101.76	0.04	0.01
10PH006	2.32	7.48	15.35	45.60	0.13	0.28	9.69	1.31	0.13	11.90	0.03	0.03	0.01	3.79	98.05	0.09	<0.01
10QU001	0.44	6.72	16.45	46.00	0.17	6.26	5.07	1.52	0.26	11.25	0.01	0.06	1.10	4.59	99.90	0.02	<0.01
10QU002	2.94	5.58	16.45	46.00	0.19	2.53	7.10	1.64	0.18	11.85	0.01	0.03	0.19	4.60	99.29	0.03	<0.01
10QU003	3.14	5.39	13.55	46.10	0.30	2.89	5.83	2.44	0.26	16.00	0.01	0.04	0.44	2.90	99.29	0.03	<0.01
10QU004	3.48	6.65	15.10	46.00	0.22	1.46	6.76	2.01	0.21	13.95	0.01	0.01	0.04	4.19	100.09	0.03	<0.01
10QU005	4.42	4.54	13.50	49.90	0.22	0.84	6.98	2.00	0.18	14.30	0.01	0.02	0.04	2.90	99.85	0.05	<0.01
10QU006	4.22	7.38	15.70	45.60	0.24	0.83	4.60	1.86	0.24	13.05	0.01	0.03	0.05	5.38	99.19	0.04	<0.01
10SC001	2.86	9.42	15.90	46.50	0.14	1.10	6.75	1.48	0.22	12.50	0.02	0.04	0.05	4.97	101.95	0.04	0.01
10SC002	4.14	7.63	15.40	47.30	0.13	0.08	8.55	1.42	0.16	11.95	0.03	0.02	0.01	4.85	101.67	0.04	0.01
10SC003	3.13	9.35	15.65	45.50	0.12	0.41	6.98	1.48	0.21	12.70	0.02	0.04	0.02	4.80	100.41	0.03	0.01
10SC004	2.43	7.56	16.50	48.70	0.14	0.35	10.15	1.34	0.16	11.75	0.03	0.03	0.01	2.35	101.50	0.02	0.01
10SC005	3.99	7.99	15.75	47.20	0.13	0.40	7.61	1.42	0.20	12.00	0.03	0.04	0.04	4.53	101.33	0.03	0.01
10SC006	3.69	8.08	15.65	47.80	0.14	0.52	7.53	1.44	0.19	12.10	0.03	0.04	0.02	3.92	101.15	0.02	<0.01
10SE001	2.69	7.26	16.50	47.00	0.16	0.47	9.78	1.42	0.16	11.20	0.02	0.03	0.02	4.85	101.56	0.02	<0.01
10SE002	6.33	3.05	12.40	51.40	0.23	0.04	6.59	1.70	0.12	12.80	0.01	0.02	<0.01	5.09	99.78	0.61	<0.01
10SE003	2.76	6.78	16.70	47.10	0.19	0.47	9.66	1.45	0.16	11.45	0.03	0.03	0.03	3.99	100.80	0.05	<0.01
10SE004	4.36	6.72	13.45	49.20	0.30	0.14	5.33	1.97	0.20	13.15	0.02	0.01	0.01	5.48	100.34	0.03	0.01
10SE005	5.21	4.54	11.00	41.80	0.26	0.44	13.55	1.57	0.14	11.20	0.01	0.01	0.01	10.85	100.59	2.06	<0.01
10SE006	4.60	6.25	13.40	50.70	0.30	0.59	5.12	2.02	0.17	13.25	0.02	0.02	0.03	4.57	101.04	0.05	<0.01
10SG001	2.72	4.97	20.00	48.20	0.10	0.32	11.55	1.12	0.13	9.36	0.02	0.04	0.01	2.66	101.20	0.03	0.01
10TO001	4.21	5.98	13.45	51.10	0.34	1.59	5.58	2.03	0.20	13.40	0.02	0.03	0.09	3.50	101.52	0.03	0.01
10TO002	4.13	5.75	13.25	51.00	0.35	1.52	5.06	2.00	0.19	13.75	0.01	0.03	0.08	4.42	101.54	0.03	<0.01

Table A-1 (continued): Major element, C, and S analyses.

	weight %																
	Na_2O	MgO	Al_2O_3	SiO_2	P_2O_5	K_2O	CaO	TiO_2	MnO	Fe_2O_3	Cr_2O_3	SrO	BaO	LOI	Total	C	S
10TO003	4.70	6.48	13.20	49.90	0.36	0.07	5.37	1.97	0.16	13.35	0.01	0.01	<0.01	4.89	100.47	0.12	0.01
10TO004	0.15	1.80	7.97	65.20	0.20	0.01	10.00	1.28	0.09	9.60	0.01	0.01	<0.01	4.79	101.11	0.11	<0.01
10TO005	4.12	5.69	13.40	49.80	0.28	1.46	5.77	1.99	0.18	13.40	0.02	0.02	0.07	4.81	101.01	0.04	<0.01
10TO006	0.24	2.59	10.50	51.80	0.22	0.01	15.35	1.45	0.10	10.60	0.01	0.02	<0.01	7.23	100.12	0.75	<0.01
10TR001	4.43	3.53	11.85	45.10	0.15	0.43	12.60	1.25	0.11	8.82	0.02	0.01	0.01	11.75	100.06	2.62	0.01
10TR002	1.87	5.96	12.15	34.60	0.16	2.36	12.50	1.34	0.17	8.84	0.02	0.01	0.02	19.50	99.50	4.87	<0.01
10TR003	3.85	8.05	14.30	42.50	0.18	0.39	6.98	1.44	0.16	11.40	0.03	0.02	0.01	10.60	99.91	1.82	0.01
10TR004	0.33	4.62	10.25	41.30	0.13	2.64	11.85	1.16	0.12	9.14	0.02	0.01	0.01	17.15	98.73	4.41	0.13
10TR005	4.13	5.19	12.80	44.90	0.17	0.59	9.53	1.47	0.17	11.50	0.02	0.02	0.05	10.10	100.64	2.03	0.01
10TR006	3.50	6.62	13.50	41.10	0.16	0.37	8.85	1.44	0.14	10.80	0.02	0.01	0.01	11.80	98.32	2.03	0.02
10TT001	3.81	7.60	15.65	46.90	0.18	1.19	6.17	1.57	0.19	11.55	0.03	0.02	0.04	5.10	100.00	0.11	0.01
10TT002	2.71	6.15	15.35	45.60	0.17	0.43	9.74	1.59	0.15	11.45	0.03	0.01	0.01	5.60	98.99	0.05	0.01
10TT003	3.36	6.88	16.25	47.40	0.18	1.98	5.95	1.60	0.16	11.80	0.03	0.02	0.05	3.80	99.46	0.02	0.01
10TT004	3.90	7.37	15.40	47.40	0.17	0.87	5.38	1.69	0.16	12.10	0.03	0.02	0.02	5.10	99.61	0.06	<0.01
10TT005	3.18	8.67	15.70	46.70	0.16	1.67	4.96	1.52	0.21	11.55	0.03	0.03	0.19	4.58	99.15	0.02	<0.01
10TT006	2.88	7.58	16.40	43.10	0.16	1.28	8.26	1.69	0.14	12.50	0.03	0.01	0.01	5.49	99.53	0.19	<0.01
10VI001	2.39	6.79	15.60	46.70	0.16	2.73	6.47	1.64	0.20	12.40	0.03	0.06	0.12	3.90	99.19	0.03	<0.01
10VI002	4.16	6.23	16.15	46.80	0.18	0.34	7.12	1.62	0.17	12.15	0.02	0.02	0.02	4.50	99.48	0.05	<0.01
10VI003	3.00	6.81	16.35	47.90	0.20	1.90	6.67	1.69	0.21	12.35	0.02	0.07	0.05	3.20	100.42	0.04	0.01
10VI004	3.72	7.45	15.95	45.10	0.16	0.75	7.22	1.67	0.19	12.15	0.03	0.01	0.01	5.79	100.20	0.21	<0.01
10VI005	3.95	5.94	16.05	48.40	0.16	1.86	6.17	1.59	0.13	12.10	0.02	0.01	0.05	4.19	100.62	0.12	0.01
10VI006	2.42	7.00	16.00	46.30	0.17	2.66	5.97	1.64	0.20	12.45	0.03	0.08	0.08	3.40	98.40	0.03	<0.01

Table A-1 (continued): Major element, C, and S analyses.

	weight %															
	Na_2O	MgO	Al_2O_3	SiO_2	P_2O_5	K_2O	CaO	TiO_2	MnO	Fe_2O_3	Cr_2O_3	SrO	BaO	LOI	Total	C	S
11CBF001	3.64	7.36	16.60	45.20	0.15	1.11	6.96	1.63	0.17	11.90	0.03	0.01	0.02	5.29	100.07	0.05	0.02
11CBF002	3.63	7.73	15.95	47.80	0.17	1.44	5.76	1.64	0.11	11.75	0.02	0.02	<0.01	5.30	101.32	0.07	0.01
11CBF003	3.34	7.52	15.35	46.80	0.16	1.73	5.97	2.09	0.18	13.05	0.03	0.02	0.11	4.30	100.65	0.03	<0.01
11CBF004	3.45	7.87	15.95	46.70	0.17	1.55	5.55	1.75	0.16	11.95	0.02	0.01	0.03	5.58	100.74	0.07	0.01
11CBF005	2.55	7.33	16.15	46.70	0.16	0.68	8.27	1.72	0.16	12.10	0.03	0.01	0.01	5.80	101.67	0.02	<0.01
11CBF006	3.64	7.04	14.05	47.40	0.22	0.34	7.01	2.46	0.16	14.45	0.02	0.01	<0.01	4.59	101.39	0.03	0.01
11CLD001	3.53	8.46	15.70	46.00	0.15	1.27	4.45	1.81	0.18	12.35	0.03	0.02	0.01	5.08	99.04	0.02	<0.01
11CLD002	3.67	7.92	16.45	45.10	0.17	1.46	5.38	1.67	0.15	12.10	0.03	0.01	0.02	5.47	99.60	0.05	0.01
11CLD003	3.71	7.63	16.30	44.30	0.16	0.66	6.71	1.71	0.18	12.00	0.03	0.02	<0.01	5.80	99.21	0.09	0.01
11CLD004	2.02	8.74	16.60	43.30	0.15	3.30	4.95	1.55	0.18	11.75	0.03	0.01	0.08	5.67	98.33	0.03	0.01
11CLD005	0.07	0.58	10.10	67.60	0.08	0.08	10.85	0.69	0.08	7.21	0.01	0.18	<0.01	1.80	99.33	0.03	<0.01
11CLD006	2.97	8.68	14.95	47.60	0.19	1.75	4.47	1.86	0.18	11.75	0.03	0.01	0.01	5.99	100.44	0.15	<0.01
11CLD007	3.43	6.40	15.05	47.80	0.17	1.39	6.74	1.72	0.15	11.30	0.03	0.03	0.01	5.30	99.52	0.18	<0.01

Table A-2: Base metal analyses.

	ppm							
	Co	Ni	Cu	Zn	Mo	Ag	Cd	Pb
10BA001	49	158	1010	163	<1	<0.5	<0.5	5
10BA002	51	168	200	118	<1	<0.5	<0.5	3
10BA003	50	158	123	153	<1	<0.5	<0.5	3
10BA004	43	152	1535	91	<1	0.8	<0.5	4
10BA005	48	157	43	100	1	<0.5	<0.5	4
10BA006	52	154	99	126	<1	<0.5	<0.5	2
10BB001	56	194	120	85	<1	<0.5	<0.5	<2
10BB002	51	164	141	86	1	<0.5	0.7	12
10BB003	51	168	56	235	<1	<0.5	<0.5	5
10BB004	51	161	230	95	<1	<0.5	<0.5	5
10BB005	51	177	151	79	<1	<0.5	<0.5	4
10BB006	54	187	250	82	<1	0.6	<0.5	3
10CC001	45	161	56	86	<1	<0.5	<0.5	<2
10CC002	41	33	2130	130	<1	1.1	<0.5	10
10CC003	47	164	41	88	<1	<0.5	<0.5	<2
10CC004	44	163	35	79	<1	<0.5	<0.5	<2
10CC005	43	145	88	91	<1	<0.5	<0.5	3
10CC006	45	162	73	83	<1	<0.5	<0.5	<2
10CE001	52	153	706	113	<1	<0.5	<0.5	4
10CE002	38	64	613	98	<1	<0.5	<0.5	2
10CE003	18	61	98	30	<1	<0.5	<0.5	2
10CE004	48	178	33	93	<1	<0.5	<0.5	4
10CE005	49	186	31	102	<1	<0.5	<0.5	4
10CE006	48	161	1910	103	<1	1	<0.5	3
10CF001	17	36	524	63	<1	<0.5	<0.5	2
10CF002	37	56	210	111	<1	<0.5	<0.5	4
10CF003	37	39	318	147	<1	<0.5	<0.5	6
10CF004	39	56	198	129	<1	<0.5	<0.5	4
10CF005	31	121	1225	65	<1	1.4	<0.5	3
10CF006	40	75	207	95	<1	<0.5	<0.5	3
10CH001	48	166	121	105	<1	<0.5	<0.5	10
10CH002	36	190	>10000	87	<1	7.5	<0.5	8
10CH003	48	168	179	105	<1	<0.5	<0.5	8
10CH004	47	168	338	127	<1	0.5	<0.5	5
10CH005	47	165	148	123	<1	<0.5	<0.5	5
10CH006	47	161	122	99	<1	<0.5	<0.5	6
10CL001	46	172	52	94	<1	<0.5	<0.5	8
10CL002	46	158	36	96	<1	<0.5	<0.5	5
10CL003	51	197	50	128	<1	<0.5	<0.5	3
10CL004	48	176	72	92	<1	<0.5	<0.5	<2
10CL005	8	32	382	10	<1	<0.5	<0.5	8
10CL006	44	144	63	96	<1	<0.5	<0.5	<2
10CN001	30	107	6800	69	<1	1.5	<0.5	4
10CN002	49	158	312	93	<1	<0.5	<0.5	4

Table A-2 (continued): Base metal analyses.

	ppm							
	Co	Ni	Cu	Zn	Mo	Ag	Cd	Pb
10CN003	49	161	2710	113	1	<0.5	<0.5	8
10CN004	48	180	1420	174	1	<0.5	<0.5	8
10CN005	37	132	24	55	<1	<0.5	<0.5	<2
10CN006	54	175	145	105	<1	<0.5	<0.5	<2
10DE001	49	181	64	95	<1	<0.5	<0.5	6
10DE002	55	133	242	171	<1	1.1	<0.5	13
10DE003	35	132	2000	74	<1	<0.5	<0.5	4
10DE004	16	60	1770	18	<1	2.1	<0.5	7
10DE005	54	210	88	89	<1	<0.5	<0.5	<2
10DE006	49	178	49	84	<1	<0.5	<0.5	3
10DE007	39	94	201	94	<1	<0.5	0.7	6
10DR001	50	186	61	82	<1	<0.5	<0.5	10
10DR002	54	244	2780	98	<1	1.1	<0.5	9
10DR003	47	171	2380	125	<1	2.3	<0.5	13
10DR004	52	160	251	245	<1	<0.5	<0.5	18
10DR005	48	156	>10000	264	<1	3.6	<0.5	15
10DR006	53	197	92	94	<1	<0.5	<0.5	5
10FJ001	43	150	34	83	<1	<0.5	<0.5	<2
10FJ002	42	37	259	173	<1	<0.5	<0.5	<2
10FJ003	46	35	152	151	<1	<0.5	<0.5	4
10FJ004	42	88	70	98	<1	<0.5	<0.5	3
10FJ005	43	24	236	180	<1	<0.5	<0.5	<2
10FJ006	63	74	1080	284	<1	<0.5	<0.5	12
10FU001	39	33	1510	139	<1	0.8	<0.5	4
10FU002	42	72	3310	135	<1	1.6	<0.5	<2
10FU003	39	84	3370	121	<1	0.8	<0.5	2
10FU004	49	182	998	94	<1	<0.5	<0.5	<2
10FU005	36	22	377	70	<1	<0.5	<0.5	<2
10FU006	50	173	354	86	<1	<0.5	<0.5	5
10GR001	51	170	49	96	<1	<0.5	<0.5	3
10GR002	47	178	317	112	<1	<0.5	<0.5	5
10GR003	40	62	1075	140	<1	<0.5	<0.5	7
10GR004	36	34	1395	97	<1	1	<0.5	6
10GR005	49	185	154	105	<1	<0.5	<0.5	8
10GR006	36	27	275	119	<1	<0.5	<0.5	10
10HE001	48	112	250	110	<1	<0.5	<0.5	<2
10HE002	32	23	1490	226	1	<0.5	<0.5	7
10HE003	52	139	98	99	<1	<0.5	<0.5	4
10HE004	21	13	964	211	<1	0.9	<0.5	10
10HE005	22	17	661	149	<1	0.6	<0.5	16
10HE006	40	109	122	99	<1	<0.5	<0.5	10
10IR001	40	76	135	103	<1	<0.5	<0.5	2
10IR002	42	75	147	102	<1	<0.5	<0.5	3
10IR003	42	111	328	90	<1	<0.5	0.9	6

Table A-2 (continued): Base metal analyses.

	ppm							
	Co	Ni	Cu	Zn	Mo	Ag	Cd	Pb
10IR004	46	123	98	100	<1	<0.5	<0.5	<2
10IR005	42	108	61	82	<1	<0.5	0.9	6
10IR006	39	126	102	86	<1	<0.5	0.5	5
10IR007	47	80	3940	159	<1	3.4	<0.5	10
10IR008	32	130	474	57	<1	<0.5	<0.5	12
10IR009	41	110	146	98	<1	<0.5	<0.5	9
10IR010	42	115	694	91	<1	<0.5	<0.5	10
10IR011	45	117	128	97	<1	<0.5	<0.5	4
10IR012	35	106	430	77	<1	<0.5	<0.5	8
10LA001	41	65	175	118	<1	<0.5	<0.5	10
10LA002	28	83	1010	60	<1	0.7	<0.5	10
10LA003	44	154	763	89	<1	0.5	<0.5	5
10LA004	48	123	150	103	<1	<0.5	<0.5	13
10MB001	52	155	30	75	<1	<0.5	<0.5	4
10MB002	51	146	45	97	<1	<0.5	<0.5	3
10MC001	40	94	763	112	<1	0.8	<0.5	8
10MC002	42	90	2170	113	<1	1.9	<0.5	14
10MC003	45	107	303	104	<1	<0.5	<0.5	9
10MC004	47	150	244	95	<1	<0.5	<0.5	11
10MC005	46	153	219	114	<1	<0.5	<0.5	7
10MC006	42	75	2180	114	<1	1.8	<0.5	7
10MG001	25	91	4240	50	<1	1.5	<0.5	14
10MG002	38	63	91	107	<1	<0.5	<0.5	5
10MG003	49	154	252	101	<1	<0.5	<0.5	6
10MG004	40	71	2700	106	<1	1.1	<0.5	8
10MG005	42	87	160	125	<1	<0.5	<0.5	10
10MG006	38	88	153	86	<1	<0.5	<0.5	5
10MI001	49	195	118	88	<1	<0.5	<0.5	8
10MI002	49	190	119	170	<1	<0.5	<0.5	4
10MI003	48	176	150	92	<1	<0.5	<0.5	6
10MI004	49	175	130	89	<1	<0.5	<0.5	8
10MI005	47	166	37	91	<1	<0.5	<0.5	5
10MI006	45	146	402	136	<1	1.3	<0.5	10
10OC001	48	158	79	111	<1	<0.5	<0.5	<2
10OC002	51	202	35	95	<1	<0.5	<0.5	<2
10OC003	52	194	74	96	<1	<0.5	<0.5	<2
10OC004	51	180	63	81	<1	<0.5	<0.5	<2
10OC005	50	172	34	86	<1	<0.5	<0.5	<2
10OC006	48	158	50	85	<1	<0.5	<0.5	<2
10OC007	49	156	658	102	<1	<0.5	<0.5	<2
10OC008	49	171	159	100	<1	<0.5	<0.5	<2
10OC009	50	161	122	90	<1	<0.5	<0.5	<2
10OC010	51	191	633	90	<1	0.8	<0.5	<2
10OC011	49	160	2840	92	<1	1.1	<0.5	<2

Table A-2 (continued): Base metal analyses.

	ppm							
	Co	Ni	Cu	Zn	Mo	Ag	Cd	Pb
10OC013	46	157	409	107	<1	0.9	<0.5	3
10OC014	50	159	2170	116	<1	1	<0.5	5
10OC015	37	124	4100	90	<1	9.1	<0.5	2
10OC016	48	160	1205	126	<1	4.3	<0.5	3
10OC017	46	144	483	102	<1	2	0.5	6
10OC018	48	160	62	240	<1	<0.5	0.8	6
10OJ001	32	28	803	89	<1	0.6	<0.5	7
10OJ002	13	9	2140	38	<1	2.7	<0.5	10
10OJ003	46	163	63	102	<1	<0.5	<0.5	8
10OJ004	37	32	69	124	<1	<0.5	<0.5	11
10OJ005	39	31	93	140	<1	<0.5	<0.5	10
10OJ006	50	167	84	98	<1	<0.5	<0.5	<2
10PH001	54	163	45	102	<1	<0.5	<0.5	2
10PH002	44	164	241	117	<1	<0.5	<0.5	3
10PH003	46	149	128	101	<1	<0.5	<0.5	3
10PH004	49	186	67	95	<1	<0.5	<0.5	<2
10PH005	47	187	45	84	<1	<0.5	<0.5	2
10PH006	50	173	73	88	<1	<0.5	<0.5	<2
10QU001	38	65	462	163	<1	<0.5	<0.5	51
10QU002	40	64	171	121	<1	<0.5	<0.5	35
10QU003	43	39	167	162	<1	<0.5	<0.5	27
10QU004	32	49	5010	112	<1	1.9	<0.5	44
10QU005	30	37	1800	105	<1	0.9	<0.5	37
10QU006	42	61	672	181	<1	0.5	<0.5	33
10SC001	52	133	62	118	<1	<0.5	<0.5	<2
10SC002	53	155	357	99	<1	<0.5	<0.5	<2
10SC003	55	156	92	103	<1	<0.5	<0.5	<2
10SC004	52	179	97	91	<1	<0.5	<0.5	<2
10SC005	52	164	82	90	<1	<0.5	<0.5	<2
10SC006	52	159	26	93	<1	<0.5	<0.5	<2
10SE001	47	161	53	92	<1	<0.5	<0.5	3
10SE002	27	27	166	113	<1	<0.5	<0.5	11
10SE003	48	163	76	97	<1	<0.5	<0.5	3
10SE004	39	33	5170	181	<1	1.4	<0.5	7
10SE005	28	26	682	135	<1	<0.5	<0.5	9
10SE006	36	29	161	157	<1	<0.5	<0.5	9
10SG001	38	92	146	71	<1	<0.5	<0.5	<2
10TO001	44	37	264	166	<1	<0.5	<0.5	9
10TO002	40	32	395	132	<1	<0.5	<0.5	8
10TO003	37	29	1405	155	<1	1.9	<0.5	6
10TO004	24	20	50	57	<1	<0.5	1	8
10TO005	39	30	169	135	<1	<0.5	<0.5	8
10TO006	29	25	6330	71	<1	2.2	1.1	11
10TR001	31	128	1655	58	<1	0.5	<0.5	3

Table A-2 (continued): Base metal analyses.

	ppm							
	Co	Ni	Cu	Zn	Mo	Ag	Cd	Pb
10TR002	46	156	210	80	<1	<0.5	<0.5	6
10TR003	45	158	204	115	<1	<0.5	<0.5	9
10TR004	31	126	6100	53	<1	<0.5	<0.5	6
10TR005	53	186	41	98	<1	<0.5	<0.5	<2
10TR006	47	155	440	113	<1	<0.5	<0.5	<2
10TT001	43	85	647	122	<1	<0.5	<0.5	<2
10TT002	40	74	1305	99	<1	0.7	0.5	<2
10TT003	42	84	238	104	<1	<0.5	<0.5	<2
10TT004	45	77	269	131	<1	<0.5	<0.5	<2
10TT005	43	92	285	116	<1	<0.5	<0.5	3
10TT006	44	84	1190	105	<1	2.8	<0.5	2
10VI001	48	127	195	101	<1	<0.5	<0.5	<2
10VI002	44	90	66	113	<1	<0.5	<0.5	3
10VI003	43	90	113	105	<1	<0.5	<0.5	3
10VI004	47	90	326	137	<1	<0.5	<0.5	2
10VI005	42	87	584	121	<1	<0.5	<0.5	<2
10VI006	50	131	290	109	<1	<0.5	<0.5	<2
11CBF001	46	93	171	121	<1	<0.5	<0.5	5
11CBF002	41	90	123	78	<1	<0.5	<0.5	10
11CBF003	46	90	575	109	<1	0.5	<0.5	7
11CBF004	45	91	496	100	<1	0.5	<0.5	8
11CBF005	42	77	120	97	<1	<0.5	<0.5	7
11CBF006	41	49	331	104	<1	0.5	<0.5	9
11CLD001	42	75	3770	113	<1	1.7	<0.5	13
11CLD002	41	79	599	103	<1	0.5	<0.5	8
11CLD003	42	71	4370	110	<1	2.5	<0.5	11
11CLD004	44	88	409	122	<1	1.1	<0.5	5
11CLD005	3	10	1095	10	<1	1.7	<0.5	12
11CLD006	46	76	899	115	<1	4.5	<0.5	8
11CLD007	33	63	1585	83	<1	15.5	<0.5	15

Table A-3: Trace element analyses.

	ppm														
	V	Cr	Ga	Rb	Sr	Y	Zr	Nb	Sn	Cs	Ba	Hf	Ta	W	Tl
10BA001	161	180	17.7	12.5	95.5	21.9	106	8.7	1	0.26	62.7	2.8	0.6	<1	<0.5
10BA002	259	200	18.2	36.4	187.5	22.4	109	8.7	1	0.61	189.5	2.9	0.6	<1	<0.5
10BA003	225	190	17.0	55.7	82.1	22.2	105	8.5	1	1.26	151.0	2.9	0.5	1	<0.5
10BA004	225	190	15.4	34.0	111.0	19.9	96	7.8	1	1.60	480.0	2.7	0.5	1	<0.5
10BA005	249	200	19.3	46.7	121.0	23.1	109	8.9	1	2.07	134.0	2.9	0.6	<1	<0.5
10BA006	220	180	20.3	14.0	83.1	22.8	103	8.7	1	0.26	67.0	3.0	0.5	1	<0.5
10BB001	264	260	20.8	5.2	229.0	20.6	87	7.0	1	0.08	114.5	2.6	0.5	<1	<0.5
10BB002	274	250	21.9	26.9	103.5	21.8	98	7.5	1	0.22	591.0	2.9	0.5	<1	<0.5
10BB003	235	220	18.0	10.2	237.0	21.0	95	7.8	1	0.09	289.0	2.8	0.5	1	<0.5
10BB004	266	240	15.8	34.3	257.0	20.7	91	7.3	1	0.18	926.0	2.7	0.5	<1	<0.5
10BB005	265	250	19.6	5.6	198.0	20.7	93	7.1	1	0.21	88.1	2.9	0.5	<1	<0.5
10BB006	260	250	20.2	4.8	200.0	19.8	92	7.1	1	0.24	83.8	2.8	0.5	<1	<0.5
10CC001	232	190	21.0	16.4	275.0	21.3	115	7.4	1	0.97	252.0	3.3	0.4	<1	<0.5
10CC002	313	130	22.3	12.9	159.0	37.5	216	13.6	2	0.04	131.0	6.0	0.8	<1	<0.5
10CC003	233	180	20.3	4.9	287.0	21.2	113	7.3	1	0.14	198.5	3.3	0.5	<1	<0.5
10CC004	242	200	20.9	8.0	288.0	21.2	108	7.3	1	0.18	179.0	3.1	0.4	<1	<0.5
10CC005	222	170	20.3	78.3	235.0	21.4	115	7.4	1	1.60	1225.0	3.5	0.5	<1	<0.5
10CC006	217	190	19.6	17.9	280.0	20.1	92	6.9	1	1.43	260.0	2.8	0.4	<1	<0.5
10CE001	350	130	18.5	39.6	180.0	28.7	158	9.9	1	1.13	633.0	4.3	0.5	1	<0.5
10CE002	367	210	18.4	3.2	117.0	30.3	132	11.7	1	0.06	25.8	4.0	0.7	1	<0.5
10CE003	203	140	22.7	0.3	280.0	22.1	81	7.1	1	0.02	5.4	2.4	0.4	1	<0.5
10CE004	285	230	19.5	5.2	235.0	23.5	98	8.8	1	0.32	109.0	3.1	0.5	1	<0.5
10CE005	300	240	21.9	10.0	221.0	25.3	107	9.6	1	0.97	146.5	3.2	0.6	1	<0.5
10CE006	313	180	24.7	2.6	87.1	22.1	87	7.7	1	0.07	34.1	2.6	0.4	1	<0.5
10CF001	139	70	12.6	13.2	67.9	15.7	38	3.6	<1	0.57	66.3	1.1	0.2	1	<0.5
10CF002	291	180	19.9	23.5	434.0	28.8	127	11.7	1	0.77	274.0	3.7	0.7	1	<0.5
10CF003	397	60	22.9	44.5	258.0	54.2	262	22.9	2	0.40	373.0	7.8	1.4	1	<0.5
10CF004	308	210	21.8	30.9	163.5	32.4	154	13.7	1	0.56	278.0	4.6	0.8	1	<0.5
10CF005	258	200	22.0	11.8	122.0	17.9	65	6.0	1	3.02	56.6	1.9	0.3	1	<0.5
10CF006	319	200	23.3	7.9	143.5	26.5	111	10.1	1	0.44	64.9	3.3	0.6	1	<0.5

Table A-3 (continued): Trace element analyses.

	ppm														
	V	Cr	Ga	Rb	Sr	Y	Zr	Nb	Sn	Cs	Ba	Hf	Ta	W	Tl
10BA001	161	180	17.7	12.5	95.5	21.9	106	8.7	1	0.26	62.7	2.8	0.6	<1	<0.5
10BA002	259	200	18.2	36.4	187.5	22.4	109	8.7	1	0.61	189.5	2.9	0.6	<1	<0.5
10BA003	225	190	17.0	55.7	82.1	22.2	105	8.5	1	1.26	151.0	2.9	0.5	1	<0.5
10BA004	225	190	15.4	34.0	111.0	19.9	96	7.8	1	1.60	480.0	2.7	0.5	1	<0.5
10BA005	249	200	19.3	46.7	121.0	23.1	109	8.9	1	2.07	134.0	2.9	0.6	<1	<0.5
10BA006	220	180	20.3	14.0	83.1	22.8	103	8.7	1	0.26	67.0	3.0	0.5	1	<0.5
10BB001	264	260	20.8	5.2	229.0	20.6	87	7.0	1	0.08	114.5	2.6	0.5	<1	<0.5
10BB002	274	250	21.9	26.9	103.5	21.8	98	7.5	1	0.22	591.0	2.9	0.5	<1	<0.5
10BB003	235	220	18.0	10.2	237.0	21.0	95	7.8	1	0.09	289.0	2.8	0.5	1	<0.5
10BB004	266	240	15.8	34.3	257.0	20.7	91	7.3	1	0.18	926.0	2.7	0.5	<1	<0.5
10BB005	265	250	19.6	5.6	198.0	20.7	93	7.1	1	0.21	88.1	2.9	0.5	<1	<0.5
10BB006	260	250	20.2	4.8	200.0	19.8	92	7.1	1	0.24	83.8	2.8	0.5	<1	<0.5
10CC001	232	190	21.0	16.4	275.0	21.3	115	7.4	1	0.97	252.0	3.3	0.4	<1	<0.5
10CC002	313	130	22.3	12.9	159.0	37.5	216	13.6	2	0.04	131.0	6.0	0.8	<1	<0.5
10CC003	233	180	20.3	4.9	287.0	21.2	113	7.3	1	0.14	198.5	3.3	0.5	<1	<0.5
10CC004	242	200	20.9	8.0	288.0	21.2	108	7.3	1	0.18	179.0	3.1	0.4	<1	<0.5
10CC005	222	170	20.3	78.3	235.0	21.4	115	7.4	1	1.60	1225.0	3.5	0.5	<1	<0.5
10CC006	217	190	19.6	17.9	280.0	20.1	92	6.9	1	1.43	260.0	2.8	0.4	<1	<0.5
10CE001	350	130	18.5	39.6	180.0	28.7	158	9.9	1	1.13	633.0	4.3	0.5	1	<0.5
10CE002	367	210	18.4	3.2	117.0	30.3	132	11.7	1	0.06	25.8	4.0	0.7	1	<0.5
10CE003	203	140	22.7	0.3	280.0	22.1	81	7.1	1	0.02	5.4	2.4	0.4	1	<0.5
10CE004	285	230	19.5	5.2	235.0	23.5	98	8.8	1	0.32	109.0	3.1	0.5	1	<0.5
10CE005	300	240	21.9	10.0	221.0	25.3	107	9.6	1	0.97	146.5	3.2	0.6	1	<0.5
10CE006	313	180	24.7	2.6	87.1	22.1	87	7.7	1	0.07	34.1	2.6	0.4	1	<0.5
10CF001	139	70	12.6	13.2	67.9	15.7	38	3.6	<1	0.57	66.3	1.1	0.2	1	<0.5
10CF002	291	180	19.9	23.5	434.0	28.8	127	11.7	1	0.77	274.0	3.7	0.7	1	<0.5
10CF003	397	60	22.9	44.5	258.0	54.2	262	22.9	2	0.40	373.0	7.8	1.4	1	<0.5
10CF004	308	210	21.8	30.9	163.5	32.4	154	13.7	1	0.56	278.0	4.6	0.8	1	<0.5
10CF005	258	200	22.0	11.8	122.0	17.9	65	6.0	1	3.02	56.6	1.9	0.3	1	<0.5
10CF006	319	200	23.3	7.9	143.5	26.5	111	10.1	1	0.44	64.9	3.3	0.6	1	<0.5

Table A-3 (continued): Trace element analyses.

	ppm														
	V	Cr	Ga	Rb	Sr	Y	Zr	Nb	Sn	Cs	Ba	Hf	Ta	W	Tl
10CH001	243	200	20.5	19.3	246.0	24.0	106	9.3	2	0.69	337.0	3.4	0.6	1	<0.5
10CH002	205	150	14.7	0.6	125.5	17.8	85	7.4	1	0.05	12.7	2.7	0.5	1	<0.5
10CH003	238	200	20.1	29.9	188.5	23.1	103	8.9	1	1.43	247.0	3.2	0.5	1	<0.5
10CH004	189	160	20.0	0.7	133.5	22.6	97	8.4	1	0.03	23.5	3.1	0.5	1	<0.5
10CH005	177	170	18.5	16.0	75.2	20.1	92	7.8	1	1.31	51.8	2.8	0.5	1	<0.5
10CH006	241	200	20.6	17.6	245.0	23.3	102	9.1	1	0.63	249.0	3.3	0.6	1	<0.5
10CL001	254	200	20.6	10.5	262.0	22.7	103	8.2	1	1.19	238.0	3.1	0.5	1	<0.5
10CL002	269	210	21.0	23.4	281.0	24.8	116	9.2	1	2.32	486.0	3.5	0.5	1	<0.5
10CL003	242	240	18.7	62.6	185.5	21.9	91	8.2	1	5.05	1065.0	2.6	0.4	4	<0.5
10CL004	260	240	20.5	13.1	266.0	22.6	98	8.4	1	1.41	202.0	2.9	0.5	1	<0.5
10CL005	204	160	31.2	0.6	1245.0	25.9	120	10.2	1	0.04	19.6	3.5	0.6	1	<0.5
10CL006	276	170	21.5	6.6	291.0	26.6	129	9.5	1	1.74	200.0	3.7	0.5	1	<0.5
10CN001	255	140	30.3	2.3	136.0	21.0	97	7.3	1	0.08	66.2	2.9	0.4	1	<0.5
10CN002	229	210	19.6	6.4	236.0	21.7	97	8.4	1	0.34	119.0	3.0	0.5	4	<0.5
10CN003	246	240	19.7	92.7	186.0	22.6	99	8.5	1	2.21	2620.0	2.9	0.5	1	<0.5
10CN004	243	250	18.9	98.4	128.5	21.4	93	8.0	1	0.70	1315.0	2.7	0.5	1	<0.5
10CN005	279	230	30.8	1.3	893.0	20.3	86	7.2	1	0.03	27.7	2.6	0.4	1	<0.5
10CN006	240	220	21.5	5.3	239.0	22.9	102	8.9	1	0.43	109.5	3.2	0.6	1	<0.5
10DE001	239	250	18.3	31.6	316.0	19.9	90	7.0	1	1.01	752.0	2.6	0.4	<1	<0.5
10DE002	238	90	17.1	47.3	169.5	21.6	95	7.6	1	0.36	1725.0	2.8	0.5	<1	<0.5
10DE003	178	190	20.5	2.9	78.7	15.7	70	5.6	1	0.12	22.6	2.1	0.3	<1	<0.5
10DE004	146	170	22.0	0.7	42.1	13.6	66	4.9	1	0.05	17.0	2.0	0.3	<1	<0.5
10DE005	268	240	18.8	1.8	51.2	22.5	114	8.0	1	0.04	7.4	3.3	0.5	<1	<0.5
10DE006	235	240	19.2	18.6	289.0	19.6	89	6.9	1	1.74	229.0	2.6	0.4	<1	<0.5
10DE007	344	120	19.1	10.0	170.0	33.2	160	12.2	2	0.47	108.5	4.5	0.8	<1	<0.5
10DR001	253	260	18.3	30.9	290.0	18.2	81	6.5	1	0.94	851.0	2.2	0.4	<1	<0.5
10DR002	233	260	18.0	10.0	150.5	19.5	91	7.1	1	0.20	70.9	2.5	0.4	1	<0.5
10DR003	238	220	21.2	23.3	63.2	18.8	80	6.1	1	1.67	132.0	2.2	0.4	<1	<0.5
10DR004	276	160	19.8	84.3	266.0	19.0	86	6.9	1	1.09	2280.0	2.4	0.4	<1	<0.5
10DR005	223	140	33.3	18.5	79.6	17.0	64	5.2	1	0.25	172.0	1.8	0.3	<1	<0.5

Table A-3 (continued): Trace element analyses.

	ppm														
	V	Cr	Ga	Rb	Sr	Y	Zr	Nb	Sn	Cs	Ba	Hf	Ta	W	Tl
10DR006	222	240	17.9	48.5	320.0	18.5	83	6.4	1	1.04	2550.0	2.3	0.4	<1	<0.5
10FJ001	206	170	19.5	29.3	112.0	21.2	99	8.2	1	0.53	157.0	2.9	0.5	1	<0.5
10FJ002	319	160	23.7	8.7	106.0	33.9	157	13.7	2	0.08	122.5	4.8	0.8	1	<0.5
10FJ003	341	70	24.3	31.8	489.0	42.0	198	17.2	2	0.60	453.0	6.0	1.1	1	<0.5
10FJ004	237	160	21.8	23.9	437.0	24.4	112	9.7	1	0.16	338.0	3.4	0.6	1	<0.5
10FJ005	333	50	21.2	12.6	178.0	37.5	180	16.0	2	0.08	276.0	5.4	1.0	1	<0.5
10FJ006	326	100	20.7	44.6	282.0	27.4	121	10.8	1	0.89	153.0	3.6	0.7	1	<0.5
10FU001	320	120	23.0	17.3	158.0	36.7	207	13.7	2	0.11	286.0	5.5	0.8	<1	<0.5
10FU002	272	150	23.5	14.7	120.5	28.0	154	10.2	1	0.11	175.5	4.2	0.6	<1	<0.5
10FU003	255	150	26.0	7.4	129.5	26.6	144	9.6	1	0.04	91.1	4.0	0.6	<1	<0.5
10FU004	220	230	19.9	68.6	257.0	18.9	83	6.3	1	0.67	1115.0	2.3	0.4	<1	<0.5
10FU005	234	110	26.7	0.4	251.0	28.1	185	10.3	1	0.01	8.2	5.0	0.6	<1	<0.5
10FU006	241	240	19.2	116.0	173.5	20.1	89	6.6	1	0.82	2780.0	2.5	0.4	<1	0.6
10GR001	271	240	21.3	26.1	217.0	22.7	96	8.0	1	0.71	328.0	2.9	0.5	1	<0.5
10GR002	247	210	20.2	13.4	218.0	20.3	86	7.2	1	0.89	195.0	2.6	0.4	1	<0.5
10GR003	277	130	23.7	16.9	151.0	33.7	184	13.0	1	0.06	250.0	5.2	0.7	1	<0.5
10GR004	226	100	14.2	7.8	72.8	31.5	167	12.1	1	0.04	78.0	4.7	0.7	1	<0.5
10GR005	234	210	19.2	24.8	193.0	16.6	75	6.3	1	0.93	472.0	2.3	0.4	<1	<0.5
10GR006	327	110	20.0	13.7	116.0	33.0	197	14.0	2	0.13	263.0	5.4	0.9	<1	<0.5
10HE001	239	80	20.7	6.5	134.5	24.4	119	7.6	1	0.12	81.7	3.4	0.4	1	<0.5
10HE002	213	20	22.9	40.6	113.0	41.9	387	22.5	2	0.41	95.3	9.9	1.1	1	<0.5
10HE003	196	70	19.0	99.2	205.0	18.8	72	4.5	1	1.27	1075.0	2.2	0.3	1	0.5
10HE004	207	20	26.0	54.6	70.9	44.0	421	24.6	3	0.58	147.0	10.6	1.2	1	<0.5
10HE005	212	20	22.8	62.8	140.5	46.8	433	25.9	3	0.65	266.0	10.9	1.2	1	<0.5
10HE006	185	90	17.2	99.7	104.5	18.6	73	5.5	1	1.28	1905.0	2.2	0.3	1	<0.5
10IR001	236	190	23.1	5.1	237.0	24.2	109	9.2	1	0.07	87.7	3.3	0.6	1	<0.5
10IR002	268	220	21.8	25.5	337.0	23.2	108	9.0	1	1.20	330.0	3.3	0.5	1	<0.5
10IR003	238	190	22.3	3.2	79.5	23.0	101	8.3	1	0.03	71.1	3.0	0.5	1	<0.5
10IR004	240	180	21.9	7.8	263.0	23.5	108	8.9	2	0.29	173.0	3.3	0.6	1	<0.5
10IR005	206	180	22.8	2.3	67.6	22.5	96	7.9	1	0.12	12.4	2.9	0.5	1	<0.5

Table A-3 (continued): Trace element analyses.

	ppm														
	V	Cr	Ga	Rb	Sr	Y	Zr	Nb	Sn	Cs	Ba	Hf	Ta	W	Tl
10IR006	124	180	13.7	1.5	66.7	19.6	92	7.7	1	0.04	12.4	2.8	0.5	1	<0.5
10IR007	237	200	16.2	1.9	96.2	25.1	104	9.3	2	0.08	18.3	3.2	0.6	1	<0.5
10IR008	91	170	12.4	11.0	173.0	19.8	90	7.8	3	0.11	18.4	2.9	0.5	1	<0.5
10IR009	181	160	18.9	22.0	48.9	19.8	80	7.1	1	0.34	55.8	2.5	0.4	1	<0.5
10IR010	220	180	19.6	45.7	80.4	21.6	88	7.8	1	2.91	49.7	2.8	0.5	2	<0.5
10IR011	236	190	20.9	9.8	244.0	23.1	94	8.3	1	0.48	131.5	3.0	0.5	1	<0.5
10IR012	102	170	13.6	4.2	48.8	18.2	86	7.5	1	0.08	14.5	2.7	0.5	1	<0.5
10LA001	270	210	20.7	19.9	125.5	26.9	111	9.8	1	0.11	203.0	3.6	0.6	1	<0.5
10LA002	251	170	22.8	4.2	73.6	19.8	79	7.0	1	0.05	24.5	2.6	0.4	1	<0.5
10LA003	280	160	21.7	6.2	64.0	20.3	85	7.5	1	0.02	23.5	2.7	0.5	1	<0.5
10LA004	238	190	20.8	21.6	252.0	23.5	95	8.5	1	0.56	243.0	3.0	0.5	1	<0.5
10MB001	233	170	15.3	5.6	252.0	16.3	33	2.1	<1	1.61	204.0	1.1	0.1	<1	<0.5
10MB002	259	170	16.3	7.6	258.0	18.5	42	2.8	1	1.75	228.0	1.3	0.2	<1	<0.5
10MC001	269	200	20.4	37.0	113.0	23.7	98	8.7	1	0.07	644.0	3.0	0.5	1	<0.5
10MC002	266	210	19.5	42.9	204.0	25.4	108	9.8	1	0.07	529.0	3.4	0.6	2	<0.5
10MC003	261	220	22.0	14.7	168.5	24.3	104	9.2	1	0.10	119.0	3.4	0.6	1	<0.5
10MC004	248	220	22.2	93.4	203.0	24.9	103	9.2	1	0.52	1060.0	3.2	0.6	1	0.5
10MC005	230	220	19.1	80.2	204.0	22.4	89	7.9	1	0.33	1320.0	2.8	0.5	1	<0.5
10MC006	200	190	18.3	41.1	109.5	24.1	101	9.2	1	0.05	617.0	3.2	0.6	1	<0.5
10MG001	292	160	27.7	47.1	373.0	20.4	84	6.8	1	0.02	139.5	2.4	0.5	<1	<0.5
10MG002	284	220	23.1	11.1	171.5	27.9	128	10.7	1	0.09	79.3	3.6	0.7	<1	<0.5
10MG003	262	220	21.1	37.9	592.0	22.6	102	8.4	1	1.82	285.0	2.9	0.6	<1	<0.5
10MG004	293	210	21.6	19.8	128.0	24.3	111	9.1	1	0.04	90.6	3.1	0.6	<1	<0.5
10MG005	223	180	21.5	19.0	170.5	24.6	107	8.7	1	0.03	211.0	3.0	0.6	<1	<0.5
10MG006	247	250	20.7	31.8	201.0	22.7	102	8.3	1	0.34	228.0	2.8	0.6	<1	<0.5
10MI001	250	250	19.8	5.9	210.0	19.8	88	7.7	1	0.14	111.0	2.5	0.5	<1	<0.5
10MI002	228	260	18.1	53.4	139.0	18.2	81	6.9	1	0.39	468.0	2.2	0.5	<1	<0.5
10MI003	255	270	20.4	19.8	207.0	21.1	93	7.9	1	0.40	285.0	2.6	0.5	<1	<0.5
10MI004	255	270	21.6	10.6	190.0	21.3	94	8.1	1	0.33	159.5	2.6	0.5	<1	<0.5
10MI005	269	270	20.4	11.0	212.0	21.5	95	8.1	1	0.72	141.0	2.6	0.5	<1	<0.5

Table A-3 (continued): Trace element analyses.

	ppm														
	V	Cr	Ga	Rb	Sr	Y	Zr	Nb	Sn	Cs	Ba	Hf	Ta	W	Tl
10MI006	226	240	13.3	6.5	85.0	19.2	88	7.4	1	0.02	53.0	2.4	0.5	<1	<0.5
10OC001	269	200	16.2	29.8	273.0	22.5	95	7.9	1	0.31	270.0	2.9	0.5	<1	<0.5
10OC002	270	250	19.6	6.4	234.0	21.2	101	7.4	1	0.27	111.5	3.0	0.5	<1	<0.5
10OC003	271	250	19.8	4.7	250.0	22.5	107	8.0	1	0.64	97.8	3.2	0.5	<1	<0.5
10OC004	289	240	19.8	24.1	234.0	22.5	105	7.8	1	0.86	200.0	3.2	0.5	<1	<0.5
10OC005	284	220	20.0	71.3	215.0	23.8	102	8.4	1	2.76	1285.0	3.1	0.5	<1	0.5
10OC006	280	220	20.5	22.3	207.0	22.8	101	8.1	1	0.71	187.0	3.1	0.5	<1	<0.5
10OC007	267	210	19.5	34.8	260.0	21.8	95	7.7	1	0.62	959.0	2.8	0.5	<1	<0.5
10OC008	258	220	17.9	41.1	269.0	22.1	93	7.8	1	2.21	727.0	2.8	0.5	<1	<0.5
10OC009	260	210	20.5	30.8	222.0	22.9	99	8.2	2	0.75	243.0	2.9	0.5	<1	<0.5
10OC010	164	160	11.1	28.3	127.0	12.4	52	4.6	<1	0.19	643.0	1.3	0.3	<1	0.7
10OC011	282	220	19.7	25.2	203.0	22.1	96	8.1	1	0.86	321.0	2.6	0.6	<1	0.8
10OC013	133	200	18.6	13.5	120.0	20.5	99	8.2	1	0.02	120.5	3.0	0.5	1	<0.5
10OC014	253	210	21.8	16.6	199.5	22.8	101	8.7	1	0.72	183.5	3.1	0.5	1	<0.5
10OC015	173	180	19.8	16.9	108.0	23.0	90	7.7	1	0.03	129.0	2.6	0.5	1	<0.5
10OC016	154	180	18.8	23.0	93.3	19.8	97	8.0	1	0.03	168.0	2.9	0.5	1	<0.5
10OC017	136	210	12.9	53.3	47.5	18.4	100	8.2	1	0.05	323.0	3.1	0.5	1	<0.5
10OC018	250	220	20.7	20.4	312.0	23.3	104	8.8	4	0.76	366.0	3.3	0.5	1	<0.5
10OJ001	319	110	23.2	2.8	126.5	33.1	196	13.8	2	0.03	26.7	5.4	0.9	<1	<0.5
10OJ002	234	90	37.0	1.8	81.7	28.9	150	10.7	2	0.20	21.1	4.3	0.7	<1	<0.5
10OJ003	234	180	21.0	16.0	247.0	19.7	102	7.8	1	0.56	294.0	3.0	0.5	<1	<0.5
10OJ004	322	110	21.8	50.5	335.0	33.0	200	14.0	2	0.82	755.0	5.5	0.9	<1	<0.5
10OJ005	318	110	21.6	41.9	296.0	33.1	196	13.9	2	1.11	584.0	5.8	0.9	<1	<0.5
10OJ006	263	220	19.0	8.0	225.0	20.8	93	8.4	1	0.73	214.0	3.1	0.5	<1	<0.5
10PH001	255	140	18.7	37.7	253.0	18.4	80	7.0	1	2.94	378.0	2.5	0.5	<1	<0.5
10PH002	229	220	19.7	1.9	142.5	17.5	77	6.6	1	0.08	40.2	2.4	0.4	<1	<0.5
10PH003	257	170	19.7	29.2	280.0	21.1	111	8.0	1	2.29	341.0	3.2	0.5	<1	<0.5
10PH004	248	240	19.8	33.0	285.0	18.9	87	7.4	1	1.78	499.0	2.5	0.5	<1	<0.5
10PH005	238	230	18.0	31.3	312.0	18.3	84	7.2	1	2.14	299.0	2.6	0.5	<1	<0.5
10PH006	266	220	18.7	5.6	239.0	17.8	74	7.1	1	0.51	127.5	2.4	0.4	<1	<0.5

Table A-3 (continued): Trace element analyses.

	ppm														
	V	Cr	Ga	Rb	Sr	Y	Zr	Nb	Sn	Cs	Ba	Hf	Ta	W	Tl
10QU001	253	90	23.0	389.0	483.0	25.2	129	10.9	1	5.51	>10000	3.9	0.8	<1	1.8
10QU002	283	100	22.5	139.5	276.0	27.5	141	12.1	1	1.81	1965.0	4.3	0.8	<1	0.6
10QU003	353	60	18.8	125.0	286.0	35.9	181	15.7	2	0.51	4160.0	5.4	1.1	<1	0.7
10QU004	337	80	26.6	29.3	120.0	32.4	161	14.1	2	0.32	362.0	4.8	1.0	<1	<0.5
10QU005	405	60	19.5	25.2	135.0	29.7	153	13.3	2	0.16	343.0	4.5	0.9	<1	<0.5
10QU006	293	80	18.9	29.7	199.0	26.9	137	11.4	1	0.31	452.0	4.0	0.8	<1	<0.5
10SC001	249	130	19.4	23.7	345.0	21.3	102	7.6	1	1.16	389.0	2.9	0.5	<1	<0.5
10SC002	244	180	16.5	1.9	128.0	20.1	89	6.9	1	0.09	44.6	2.6	0.4	<1	<0.5
10SC003	263	130	19.3	8.5	308.0	21.4	94	7.3	1	1.33	140.5	2.7	0.4	<1	<0.5
10SC004	234	180	18.9	8.9	259.0	22.3	101	8.1	1	0.94	123.0	3.0	0.5	<1	<0.5
10SC005	263	180	18.8	8.7	300.0	20.2	89	7.1	1	0.93	352.0	2.5	0.4	<1	<0.5
10SC006	265	190	18.7	10.8	354.0	21.3	93	7.5	1	1.28	148.5	2.6	0.5	<1	<0.5
10SE001	205	180	21.1	8.1	274.0	21.3	104	7.9	1	0.23	217.0	3.1	0.5	1	<0.5
10SE002	197	100	18.3	0.7	133.0	26.4	159	11.6	2	0.02	16.9	4.6	0.7	1	<0.5
10SE003	211	190	21.4	9.6	279.0	21.3	104	7.8	1	0.18	224.0	3.0	0.5	1	<0.5
10SE004	310	120	25.2	3.3	86.8	37.3	188	14.0	2	0.04	47.0	4.8	0.8	<1	<0.5
10SE005	252	90	15.5	7.6	93.8	31.2	148	11.3	1	0.03	76.2	3.8	0.7	1	<0.5
10SE006	295	100	22.2	13.8	207.0	37.7	194	14.6	2	0.15	292.0	4.9	0.9	<1	<0.5
10SG001	199	140	21.1	6.8	311.0	19.0	89	7.0	1	1.28	105.0	2.6	0.4	<1	<0.5
10TO001	303	110	22.9	33.5	242.0	36.7	187	14.3	2	0.08	808.0	4.8	0.8	<1	<0.5
10TO002	310	110	22.2	31.7	255.0	37.6	191	14.5	2	0.08	814.0	4.9	0.9	<1	<0.5
10TO003	303	110	22.0	1.5	63.5	37.0	185	14.0	2	0.01	26.5	4.7	0.8	<1	<0.5
10TO004	210	80	21.3	0.3	123.5	23.3	123	9.3	2	0.01	7.7	3.0	0.5	<1	<0.5
10TO005	310	110	23.6	28.8	191.5	36.6	184	14.1	2	0.08	609.0	4.9	0.8	<1	<0.5
10TO006	276	80	29.3	0.3	176.5	28.5	138	10.4	1	<0.01	7.8	3.4	0.6	<1	<0.5
10TR001	119	160	13.6	17.2	54.2	17.6	88	7.1	1	0.24	56.9	2.4	0.5	<1	<0.5
10TR002	165	170	14.8	70.3	124.0	19.8	97	7.7	1	2.41	171.0	2.7	0.5	5	<0.5
10TR003	245	200	18.9	16.0	158.0	20.9	99	8.0	1	2.03	65.3	2.8	0.5	<1	<0.5
10TR004	145	130	15.0	79.3	102.0	16.5	80	6.6	1	1.60	105.0	2.2	0.4	15	<0.5
10TR005	224	190	16.5	18.2	144.0	21.4	103	8.3	1	1.76	421.0	2.9	0.6	1	<0.5

Table A-3 (continued): Trace element analyses.

	ppm														
	V	Cr	Ga	Rb	Sr	Y	Zr	Nb	Sn	Cs	Ba	Hf	Ta	W	Tl
10TR006	190	150	18.8	11.9	116.5	20.9	100	8.1	1	1.56	62.7	2.8	0.5	<1	<0.5
10TT001	251	210	19.6	26.5	131.0	24.1	108	8.9	1	0.16	354.0	3.0	0.6	<1	<0.5
10TT002	266	210	23.5	6.0	78.6	24.5	112	9.1	1	0.02	50.1	3.1	0.6	<1	<0.5
10TT003	266	210	20.4	54.2	176.5	23.9	109	8.9	1	0.31	421.0	3.0	0.6	<1	<0.5
10TT004	281	210	19.2	21.2	129.5	24.7	114	9.3	1	0.43	197.0	3.2	0.6	<1	<0.5
10TT005	237	200	18.3	46.8	271.0	21.5	98	8.1	1	0.39	1595.0	2.7	0.5	<1	<0.5
10TT006	319	220	25.3	8.1	97.7	26.1	115	9.4	1	0.07	56.8	3.3	0.7	<1	<0.5
10VI001	262	200	21.3	86.0	561.0	23.8	109	8.8	1	6.27	988.0	3.1	0.6	<1	<0.5
10VI002	265	190	20.9	8.0	134.5	24.1	109	8.8	1	0.13	137.5	3.1	0.6	<1	<0.5
10VI003	271	190	22.1	55.8	625.0	24.9	115	9.4	1	2.99	453.0	3.1	0.6	<1	<0.5
10VI004	294	260	19.5	12.4	102.5	24.4	111	8.9	1	0.09	117.5	3.1	0.6	<1	<0.5
10VI005	265	190	16.7	36.4	81.3	24.1	108	8.7	1	0.12	470.0	3.1	0.6	<1	<0.5
10VI006	270	210	22.7	80.5	707.0	24.8	113	9.2	1	9.86	727.0	3.1	0.6	<1	<0.5
11CBF001	239	190	21.5	20.9	114.5	24.0	98	8.8	1	0.09	197.0	3.2	0.5	1	<0.5
11CBF002	258	180	20.0	6.7	194.5	22.1	98	8.6	1	0.06	15.4	3.1	0.5	1	<0.5
11CBF003	300	200	20.3	45.3	178.0	25.7	108	9.9	1	0.19	946.0	3.5	0.6	1	<0.5
11CBF004	262	180	20.4	23.9	88.2	25.4	110	9.8	1	0.08	227.0	3.5	0.6	1	<0.5
11CBF005	337	200	22.3	10.7	57.5	25.4	106	9.2	1	0.13	50.7	3.4	0.6	1	<0.5
11CBF006	350	120	22.5	3.2	87.7	33.6	144	12.7	1	0.05	14.1	4.6	0.8	1	<0.5
11CLD001	255	200	20.2	26.9	139.0	26.3	112	9.9	1	0.14	125.0	3.6	0.6	1	<0.5
11CLD002	251	200	21.0	19.7	84.6	24.2	101	9.0	1	0.06	133.0	3.2	0.6	1	<0.5
11CLD003	247	190	23.7	4.8	172.0	25.3	106	9.3	1	0.06	18.0	3.4	0.6	1	<0.5
11CLD004	229	180	20.3	65.2	46.6	22.1	95	8.6	1	0.12	718.0	3.0	0.5	1	<0.5
11CLD005	71	70	19.6	1.5	1650.0	24.4	114	9.7	2	0.03	12.9	3.7	0.6	1	<0.5
11CLD006	250	200	19.3	17.1	93.8	23.0	113	10.2	1	0.05	70.1	3.6	0.6	1	<0.5
11CLD007	273	190	18.9	20.4	219.0	23.8	110	9.7	1	0.06	109.5	3.6	0.6	1	<0.5

Table A-4: REE analyses.

	ppm															
	La	Ce	Pr	Nd	Sm	Eu	Gd	Tb	Dy	Ho	Er	Tm	Yb	Lu	Th	U
10BA001	12.40	27.40	3.74	16.4	4.05	1.42	4.00	0.67	4.14	0.78	2.28	0.32	1.89	0.29	1.45	0.30
10BA002	11.80	26.10	3.59	16.2	4.10	1.42	3.85	0.70	4.17	0.80	2.35	0.33	2.00	0.30	1.26	0.31
10BA003	11.50	26.30	3.62	16.1	4.01	1.41	3.90	0.69	4.05	0.80	2.33	0.33	1.97	0.30	1.21	0.29
10BA004	10.00	22.80	3.19	14.5	3.72	1.27	3.59	0.63	3.76	0.73	2.14	0.30	1.83	0.28	1.03	0.24
10BA005	12.60	27.20	3.70	16.5	4.15	1.45	4.00	0.69	4.29	0.81	2.36	0.33	1.99	0.30	1.23	0.30
10BA006	13.40	30.50	4.28	19.8	5.02	1.71	5.02	0.66	4.29	0.82	2.42	0.33	2.15	0.31	1.13	0.30
10BB001	8.70	20.30	2.73	12.3	3.11	1.31	3.98	0.65	3.98	0.79	2.23	0.32	1.98	0.28	0.92	0.23
10BB002	9.10	21.20	2.90	13.1	3.39	1.32	4.08	0.67	4.09	0.82	2.28	0.33	2.05	0.29	0.92	0.25
10BB003	13.30	31.30	4.05	17.5	4.12	1.38	4.47	0.72	4.40	0.82	2.33	0.32	2.02	0.30	1.22	0.41
10BB004	9.20	21.20	2.86	12.7	3.28	1.26	3.98	0.64	4.03	0.81	2.24	0.31	1.96	0.29	0.92	0.24
10BB005	9.50	22.00	2.97	13.5	3.29	1.40	4.21	0.66	4.04	0.82	2.29	0.31	2.00	0.29	1.01	0.26
10BB006	9.10	20.40	2.77	12.3	3.13	1.22	3.87	0.62	3.90	0.78	2.17	0.31	1.92	0.29	0.90	0.24
10CC001	13.90	29.70	3.84	16.0	3.65	1.44	4.17	0.66	4.15	0.82	2.32	0.34	2.11	0.31	1.56	0.33
10CC002	28.70	65.50	8.20	33.6	7.01	2.35	7.77	1.17	7.30	1.44	4.05	0.56	3.62	0.55	4.37	0.82
10CC003	13.70	29.30	3.78	16.2	3.70	1.43	4.23	0.66	4.07	0.83	2.32	0.31	2.10	0.31	1.57	0.35
10CC004	13.40	28.80	3.74	15.6	3.62	1.42	4.06	0.65	4.00	0.81	2.24	0.32	2.02	0.30	1.45	0.31
10CC005	15.00	32.00	4.07	17.0	3.79	1.47	4.38	0.69	4.27	0.85	2.38	0.35	2.19	0.32	1.75	0.36
10CC006	12.90	27.90	3.63	15.3	3.42	1.41	4.10	0.65	3.95	0.81	2.24	0.32	1.99	0.28	1.43	0.29
10CE001	30.40	58.70	6.69	28.0	5.62	1.79	5.26	0.84	5.42	1.10	3.11	0.45	3.04	0.46	2.37	0.36
10CE002	14.30	31.20	4.16	20.3	5.32	1.89	5.65	0.93	6.00	1.16	3.15	0.44	2.84	0.41	1.24	0.30
10CE003	13.40	25.90	3.26	15.6	3.82	1.62	4.09	0.63	4.02	0.77	2.06	0.29	1.86	0.27	0.85	0.26
10CE004	11.30	24.50	3.23	15.9	4.19	1.55	4.42	0.72	4.60	0.88	2.44	0.34	2.29	0.33	0.98	0.23
10CE005	12.30	26.20	3.42	16.8	4.44	1.64	4.65	0.76	4.80	0.94	2.58	0.36	2.33	0.35	1.04	0.24
10CE006	11.90	25.00	3.17	15.1	3.88	1.46	4.10	0.66	4.14	0.83	2.22	0.31	2.00	0.29	0.82	0.38
10CF001	21.70	29.00	2.86	13.2	2.60	1.36	2.95	0.41	2.41	0.47	1.25	0.16	1.03	0.15	0.39	0.12
10CF002	14.40	30.30	3.91	18.3	4.80	1.57	4.98	0.84	5.42	1.07	2.94	0.43	2.81	0.42	1.51	0.37
10CF003	31.30	67.10	8.34	39.0	9.67	2.73	9.76	1.59	10.15	2.00	5.57	0.79	5.13	0.77	3.86	0.93
10CF004	15.90	35.00	4.58	21.5	5.57	1.78	5.88	1.00	6.26	1.22	3.39	0.49	3.15	0.47	1.89	0.45
10CF005	7.30	15.30	2.04	10.1	2.71	1.14	3.09	0.52	3.29	0.65	1.76	0.26	1.64	0.25	0.60	0.24
10CF006	14.20	28.80	3.69	17.5	4.49	1.67	4.83	0.79	5.06	0.99	2.71	0.38	2.47	0.37	1.18	0.34

Table A-4 (continued): REE analyses.

	ppm															
	La	Ce	Pr	Nd	Sm	Eu	Gd	Tb	Dy	Ho	Er	Tm	Yb	Lu	Th	U
10CH001	12.80	28.70	3.98	18.0	4.46	1.46	4.52	0.70	4.55	0.90	2.48	0.34	2.15	0.31	1.33	0.31
10CH002	7.50	18.80	2.79	13.1	3.35	1.09	3.28	0.57	3.65	0.69	1.99	0.27	1.70	0.24	1.12	0.26
10CH003	12.30	27.80	3.78	17.4	4.26	1.42	4.26	0.69	4.43	0.88	2.50	0.34	2.07	0.31	1.24	0.29
10CH004	11.90	26.80	3.69	16.9	4.12	1.56	4.26	0.68	4.38	0.83	2.38	0.32	2.04	0.30	1.13	0.42
10CH005	13.80	23.30	3.23	15.4	3.70	1.27	3.72	0.60	3.89	0.75	2.10	0.28	1.80	0.27	1.02	0.24
10CH006	12.70	28.40	3.87	17.7	4.19	1.47	4.39	0.72	4.56	0.88	2.39	0.34	2.07	0.30	1.20	0.28
10CL001	13.20	27.40	3.51	16.6	4.17	1.56	4.32	0.70	4.36	0.87	2.36	0.34	2.14	0.32	1.18	0.24
10CL002	14.80	30.80	3.94	18.4	4.55	1.72	4.88	0.78	4.90	0.97	2.66	0.37	2.41	0.36	1.35	0.34
10CL003	10.00	22.30	2.94	14.2	3.72	1.34	3.89	0.64	4.07	0.78	2.10	0.30	1.92	0.28	0.90	0.23
10CL004	11.50	24.80	3.23	15.5	3.95	1.51	4.18	0.69	4.35	0.85	2.36	0.33	2.13	0.31	1.00	0.23
10CL005	17.60	35.50	4.37	20.1	4.69	1.54	4.83	0.78	4.86	0.94	2.57	0.37	2.35	0.34	2.98	1.32
10CL006	18.80	37.90	4.66	21.6	4.98	1.77	4.93	0.79	5.00	0.97	2.69	0.38	2.46	0.38	1.62	0.30
10CN001	23.60	38.40	4.27	18.6	4.02	1.60	3.96	0.62	3.89	0.78	2.15	0.31	1.99	0.30	1.31	0.34
10CN002	10.90	24.40	3.36	15.1	4.13	1.26	4.19	0.64	4.21	0.79	2.34	0.32	2.02	0.26	0.95	0.23
10CN003	11.70	25.90	3.52	16.3	4.13	1.35	4.53	0.67	4.36	0.84	2.43	0.33	2.16	0.32	1.03	0.24
10CN004	10.70	24.10	3.29	15.1	3.85	1.27	4.30	0.67	4.18	0.84	2.41	0.31	2.12	0.29	0.96	0.27
10CN005	9.30	21.30	2.93	13.9	3.49	1.20	3.87	0.60	3.97	0.78	2.28	0.29	1.96	0.28	0.87	0.21
10CN006	11.00	25.00	3.51	16.2	4.07	1.40	4.52	0.71	4.69	0.88	2.66	0.34	2.14	0.33	1.03	0.25
10DE001	9.30	21.10	2.85	12.7	3.25	1.29	4.03	0.60	3.82	0.76	2.17	0.32	1.93	0.30	0.88	0.21
10DE002	10.10	22.50	3.09	13.9	3.57	1.42	4.43	0.65	4.26	0.84	2.47	0.35	2.13	0.31	0.84	0.40
10DE003	9.50	18.60	2.31	10.2	2.39	1.13	3.10	0.46	2.94	0.58	1.73	0.26	1.53	0.23	0.72	0.20
10DE004	6.60	14.60	2.09	9.4	2.28	0.98	3.01	0.42	2.58	0.51	1.48	0.21	1.20	0.19	0.62	0.25
10DE005	10.30	24.70	3.35	14.9	3.69	1.49	4.59	0.70	4.34	0.89	2.63	0.37	2.35	0.36	1.28	0.27
10DE006	9.60	21.80	2.89	13.1	3.19	1.31	4.02	0.59	3.81	0.74	2.21	0.31	1.88	0.30	0.89	0.22
10DE007	16.80	37.80	5.04	22.2	5.40	1.97	6.71	0.99	6.20	1.26	3.66	0.52	3.18	0.49	1.56	0.37
10DR001	9.10	20.00	2.73	12.1	3.19	1.17	3.44	0.55	3.40	0.68	1.91	0.25	1.69	0.25	0.74	0.17
10DR002	12.70	26.10	3.42	15.0	3.65	1.34	3.83	0.61	3.66	0.75	2.07	0.28	1.81	0.29	0.86	0.23
10DR003	10.10	21.30	2.81	12.3	3.13	1.36	3.38	0.54	3.27	0.68	1.88	0.26	1.63	0.26	0.82	0.18
10DR004	8.70	19.50	2.74	12.5	3.31	1.19	3.62	0.60	3.64	0.75	2.01	0.27	1.74	0.27	0.75	0.19
10DR005	6.00	14.90	2.04	9.4	2.43	1.06	3.15	0.46	2.99	0.62	1.83	0.26	1.53	0.23	0.55	0.15

Table A-4 (continued): REE analyses.

	ppm															
	La	Ce	Pr	Nd	Sm	Eu	Gd	Tb	Dy	Ho	Er	Tm	Yb	Lu	Th	U
10DR006	8.30	19.30	2.62	11.8	2.85	1.17	3.67	0.54	3.44	0.67	1.96	0.28	1.74	0.27	0.74	0.18
10FJ001	11.60	25.70	3.52	16.0	4.02	1.33	4.20	0.63	4.20	0.81	2.35	0.30	2.00	0.30	1.02	0.32
10FJ002	16.70	39.00	5.38	24.8	6.28	1.81	6.56	1.03	6.71	1.30	3.89	0.49	3.24	0.48	1.70	0.42
10FJ003	21.70	49.80	6.89	31.0	7.81	2.24	8.53	1.25	8.40	1.60	4.73	0.62	4.13	0.59	2.19	0.54
10FJ004	12.20	27.40	3.77	17.5	4.52	1.43	4.96	0.71	4.85	0.94	2.74	0.36	2.34	0.34	1.20	0.29
10FJ005	17.80	42.90	5.97	27.5	7.27	1.99	7.89	1.16	7.69	1.48	4.36	0.57	3.84	0.55	2.07	0.49
10FJ006	12.50	28.40	3.97	18.7	4.90	1.51	5.26	0.82	5.46	1.08	3.08	0.42	2.64	0.40	1.08	0.31
10FU001	27.50	60.70	7.60	31.5	6.77	2.19	7.53	1.06	6.75	1.32	3.89	0.56	3.48	0.54	4.22	0.84
10FU002	22.10	47.10	5.80	24.0	5.10	1.76	5.78	0.81	5.19	1.03	3.06	0.44	2.68	0.42	2.85	0.56
10FU003	21.70	44.90	5.48	22.6	4.73	1.76	5.51	0.77	4.88	0.99	2.85	0.42	2.55	0.39	2.64	0.52
10FU004	9.90	21.80	2.87	12.5	3.05	1.29	3.78	0.55	3.46	0.67	1.96	0.29	1.76	0.27	1.22	0.22
10FU005	30.10	58.10	6.89	27.6	5.61	1.97	6.45	0.88	5.36	1.04	3.07	0.44	2.80	0.42	3.38	0.62
10FU006	9.80	22.10	2.92	13.0	3.24	1.31	3.99	0.58	3.76	0.76	2.18	0.32	1.96	0.30	0.97	0.22
10GR001	11.90	25.20	3.29	15.7	4.03	1.54	4.24	0.70	4.37	0.86	2.34	0.33	2.19	0.33	1.06	0.24
10GR002	10.70	22.60	2.93	14.2	3.59	1.43	3.82	0.62	3.86	0.75	2.07	0.30	1.92	0.28	0.93	0.21
10GR003	27.50	57.10	6.86	30.3	6.91	2.18	6.49	1.02	6.49	1.26	3.44	0.48	3.24	0.49	3.49	0.73
10GR004	22.00	45.70	5.96	27.2	6.09	1.84	5.69	0.90	5.77	1.13	3.19	0.47	3.03	0.47	3.35	0.79
10GR005	9.80	20.90	2.85	12.6	3.30	1.25	3.37	0.52	3.35	0.67	1.95	0.26	1.73	0.26	0.96	0.19
10GR006	34.80	68.10	8.62	35.2	7.91	2.13	6.91	1.03	6.50	1.29	3.79	0.51	3.34	0.52	4.45	0.89
10HE001	23.70	48.40	6.02	25.4	5.36	1.59	4.85	0.71	4.62	0.91	2.67	0.36	2.46	0.37	1.73	0.26
10HE002	91.70	206.00	26.30	108.0	18.75	4.29	13.40	1.57	8.80	1.54	4.22	0.56	3.47	0.52	4.38	0.56
10HE003	8.90	19.60	2.67	12.0	2.93	0.93	3.30	0.50	3.36	0.69	2.12	0.29	1.92	0.28	0.64	0.16
10HE004	98.70	212.00	26.90	108.5	19.50	4.40	13.75	1.60	9.14	1.59	4.36	0.54	3.60	0.51	4.77	0.58
10HE005	115.00	242.00	31.00	125.0	22.10	5.30	15.60	1.76	9.66	1.68	4.64	0.59	3.79	0.56	5.03	0.67
10HE006	14.30	25.40	3.23	13.7	2.96	0.89	3.31	0.51	3.47	0.71	2.10	0.29	1.90	0.28	0.86	0.25
10IR001	12.40	27.80	3.85	17.3	4.38	1.42	4.74	0.73	4.64	0.90	2.66	0.35	2.31	0.33	1.24	0.26
10IR002	11.70	26.20	3.68	16.8	4.26	1.46	4.81	0.71	4.63	0.90	2.61	0.36	2.27	0.33	1.13	0.26
10IR003	11.40	25.80	3.56	16.5	4.06	1.39	4.47	0.67	4.52	0.86	2.51	0.34	2.20	0.33	1.01	0.22
10IR004	11.40	25.90	3.60	16.3	4.26	1.40	4.65	0.69	4.52	0.89	2.64	0.34	2.27	0.34	1.04	0.25
10IR005	11.50	26.70	3.65	17.1	4.17	1.42	4.60	0.66	4.43	0.84	2.55	0.32	2.06	0.29	0.97	0.34

Table A-4 (continued): REE analyses.

	ppm															
	La	Ce	Pr	Nd	Sm	Eu	Gd	Tb	Dy	Ho	Er	Tm	Yb	Lu	Th	U
10IR006	6.90	18.70	2.82	13.8	3.72	1.21	3.98	0.60	3.94	0.78	2.15	0.30	2.01	0.30	0.92	0.24
10IR007	10.50	26.20	3.82	18.1	4.47	1.44	4.76	0.76	4.90	0.96	2.69	0.36	2.34	0.34	1.28	0.28
10IR008	8.90	21.00	3.00	14.0	3.50	1.19	3.60	0.60	4.02	0.76	2.21	0.31	1.90	0.28	1.00	0.23
10IR009	6.70	17.20	2.58	13.0	3.42	1.32	3.67	0.59	3.76	0.70	2.01	0.27	1.76	0.26	0.85	0.23
10IR010	10.20	23.20	3.27	15.1	3.67	1.24	3.94	0.63	4.01	0.79	2.21	0.30	1.99	0.27	0.94	0.22
10IR011	11.10	25.20	3.49	16.4	3.95	1.35	4.17	0.67	4.37	0.86	2.44	0.32	2.13	0.31	1.02	0.23
10IR012	6.30	16.60	2.69	13.2	3.45	1.27	3.41	0.55	3.44	0.68	1.95	0.27	1.68	0.25	0.97	0.22
10LA001	13.50	30.40	4.16	19.4	4.81	1.56	4.96	0.80	5.21	1.01	2.90	0.39	2.41	0.35	1.42	0.32
10LA002	9.60	21.50	2.98	13.9	3.50	1.18	3.65	0.57	3.66	0.72	2.04	0.27	1.71	0.26	0.85	0.22
10LA003	10.40	23.20	3.21	14.9	3.46	1.27	3.75	0.60	3.84	0.76	2.15	0.30	1.91	0.27	0.97	0.23
10LA004	11.50	25.90	3.60	16.5	4.06	1.41	4.24	0.68	4.46	0.87	2.43	0.34	2.05	0.30	1.05	0.24
10MB001	4.10	8.60	1.12	5.1	1.45	0.70	2.28	0.37	2.71	0.60	1.89	0.30	1.85	0.29	0.46	0.12
10MB002	5.10	10.80	1.37	6.1	1.62	0.78	2.64	0.43	3.08	0.67	2.09	0.33	2.09	0.35	0.74	0.19
10MC001	13.70	30.10	4.01	17.3	4.42	1.39	4.43	0.70	4.24	0.90	2.51	0.35	2.26	0.36	1.23	0.30
10MC002	12.90	29.30	4.00	18.6	4.55	1.48	4.80	0.75	4.99	1.00	2.80	0.37	2.37	0.34	1.38	0.35
10MC003	13.40	29.30	3.95	17.7	4.24	1.45	4.63	0.73	4.83	0.94	2.70	0.37	2.29	0.33	1.94	0.33
10MC004	11.90	27.20	3.79	17.5	4.33	1.49	4.62	0.75	4.87	0.95	2.62	0.36	2.31	0.31	1.03	0.26
10MC005	10.50	23.90	3.31	15.5	3.81	1.35	4.20	0.65	4.32	0.83	2.37	0.31	2.06	0.29	0.93	0.22
10MC006	12.10	26.90	3.69	16.7	4.19	1.41	4.45	0.73	4.65	0.90	2.60	0.35	2.20	0.30	1.17	0.27
10MG001	11.00	21.90	3.04	13.6	3.62	1.81	3.63	0.61	3.81	0.72	2.09	0.30	1.69	0.26	0.97	0.36
10MG002	14.70	31.60	4.29	19.5	4.99	1.78	4.90	0.86	5.30	1.00	3.02	0.43	2.52	0.38	1.41	0.33
10MG003	11.30	24.80	3.39	15.2	4.01	1.48	4.03	0.71	4.27	0.82	2.41	0.34	1.99	0.31	0.99	0.23
10MG004	12.80	27.40	3.72	16.5	4.20	1.60	4.37	0.76	4.62	0.90	2.59	0.37	2.22	0.34	1.23	0.28
10MG005	13.20	28.10	3.80	17.2	4.40	1.57	4.37	0.75	4.54	0.87	2.62	0.37	2.16	0.33	1.21	0.33
10MG006	11.60	25.20	3.45	15.4	3.99	1.50	3.95	0.72	4.31	0.82	2.49	0.35	2.06	0.31	1.06	0.25
10MI001	9.80	21.40	2.91	13.2	3.55	1.36	3.56	0.62	3.87	0.74	2.19	0.31	1.83	0.27	0.91	0.23
10MI002	8.00	18.40	2.61	11.7	3.17	1.20	3.17	0.57	3.46	0.66	1.91	0.28	1.61	0.24	0.78	0.19
10MI003	10.30	22.30	3.09	13.9	3.66	1.38	3.74	0.66	4.00	0.77	2.27	0.32	1.93	0.29	0.96	0.22
10MI004	11.00	23.40	3.23	14.3	3.79	1.42	3.78	0.66	4.03	0.77	2.23	0.31	1.91	0.29	0.94	0.23
10MI005	10.50	22.80	3.15	14.2	3.77	1.42	3.78	0.67	4.02	0.78	2.27	0.33	1.93	0.29	0.93	0.23

Table A-4 (continued): REE analyses.

	ppm															
	La	Ce	Pr	Nd	Sm	Eu	Gd	Tb	Dy	Ho	Er	Tm	Yb	Lu	Th	U
10MI006	10.00	21.80	2.94	13.2	3.39	1.27	3.42	0.60	3.69	0.70	2.08	0.30	1.80	0.26	0.89	0.23
10OC001	11.20	25.20	3.37	14.7	3.68	1.37	4.43	0.72	4.46	0.89	2.55	0.35	2.25	0.33	1.06	0.25
10OC002	9.70	21.80	2.98	13.4	3.34	1.35	4.06	0.68	4.12	0.83	2.32	0.33	2.01	0.30	0.92	0.24
10OC003	10.20	23.20	3.18	14.2	3.65	1.35	4.38	0.70	4.39	0.88	2.46	0.34	2.16	0.31	0.96	0.25
10OC004	11.20	24.50	3.31	14.6	3.75	1.46	4.54	0.72	4.50	0.90	2.51	0.36	2.28	0.33	1.07	0.28
10OC005	11.60	26.00	3.45	15.3	3.81	1.51	4.76	0.77	4.70	0.96	2.70	0.38	2.38	0.35	1.15	0.27
10OC006	10.90	24.60	3.27	14.6	3.64	1.41	4.39	0.72	4.37	0.87	2.46	0.34	2.16	0.32	1.04	0.26
10OC007	11.20	24.50	3.25	13.9	3.43	1.26	4.15	0.67	4.21	0.84	2.37	0.34	2.09	0.31	1.01	0.23
10OC008	10.50	23.50	3.22	14.4	3.59	1.35	4.30	0.69	4.28	0.86	2.41	0.35	2.15	0.32	1.01	0.24
10OC009	11.00	24.80	3.33	14.6	3.69	1.43	4.38	0.70	4.43	0.89	2.49	0.35	2.17	0.32	1.04	0.26
10OC010	6.40	14.00	1.91	8.5	2.17	0.73	2.29	0.39	2.31	0.47	1.31	0.17	1.10	0.18	0.55	0.14
10OC011	11.80	25.10	3.37	14.9	3.68	1.40	4.30	0.70	4.19	0.84	2.31	0.34	2.05	0.32	1.08	0.24
10OC013	9.80	23.20	3.16	14.8	3.86	1.24	4.23	0.64	4.25	0.80	2.36	0.31	2.05	0.29	0.97	0.28
10OC014	11.10	25.30	3.50	15.8	4.07	1.37	4.56	0.70	4.61	0.86	2.52	0.34	2.26	0.33	1.02	0.23
10OC015	13.30	27.70	3.74	16.6	4.09	1.35	4.65	0.69	4.31	0.87	2.51	0.32	2.15	0.31	0.91	0.44
10OC016	8.20	19.30	2.84	13.3	3.61	1.13	3.99	0.59	3.96	0.76	2.25	0.30	2.00	0.29	0.96	0.54
10OC017	8.10	19.10	2.81	13.2	3.48	1.10	3.72	0.58	3.86	0.73	2.16	0.28	1.95	0.29	1.01	0.42
10OC018	11.00	25.00	3.47	16.2	4.21	1.35	4.49	0.69	4.55	0.86	2.56	0.33	2.33	0.33	1.04	0.23
10OJ001	38.60	71.50	8.95	36.0	7.82	2.33	7.20	1.04	6.58	1.32	3.80	0.53	3.43	0.52	4.42	0.80
10OJ002	45.80	73.20	8.43	33.0	6.78	2.07	6.29	0.87	5.55	1.12	3.21	0.43	2.74	0.41	3.43	0.65
10OJ003	15.80	31.70	4.15	17.6	4.31	1.45	4.08	0.62	4.04	0.80	2.30	0.31	2.02	0.31	1.70	0.32
10OJ004	34.60	68.00	8.54	34.9	7.82	2.23	6.98	1.04	6.56	1.33	3.84	0.53	3.44	0.52	4.51	0.88
10OJ005	34.20	67.40	8.60	34.9	7.93	2.24	7.19	1.05	6.76	1.36	3.95	0.54	3.54	0.53	4.60	0.90
10OJ006	11.60	25.40	3.54	15.8	4.31	1.39	4.15	0.64	4.28	0.86	2.38	0.33	2.21	0.33	1.09	0.28
10PH001	9.40	20.50	2.84	13.0	3.64	1.28	3.75	0.57	3.72	0.76	2.15	0.29	1.87	0.28	0.82	0.20
10PH002	7.80	18.60	2.66	12.1	3.26	1.22	3.53	0.55	3.59	0.73	2.11	0.28	1.79	0.26	0.84	0.19
10PH003	17.20	34.50	4.50	19.0	4.50	1.52	4.44	0.66	4.36	0.87	2.51	0.34	2.16	0.34	1.56	0.28
10PH004	10.60	22.60	3.10	13.7	3.73	1.30	3.85	0.58	3.77	0.75	2.17	0.29	1.86	0.28	0.95	0.21
10PH005	10.80	22.60	3.02	13.6	3.58	1.30	3.67	0.55	3.69	0.75	2.15	0.29	1.89	0.29	0.96	0.20
10PH006	9.20	20.60	2.84	12.9	3.60	1.19	3.68	0.56	3.67	0.72	2.05	0.29	1.80	0.27	0.79	0.19

Table A-4 (continued): REE analyses.

	ppm															
	La	Ce	Pr	Nd	Sm	Eu	Gd	Tb	Dy	Ho	Er	Tm	Yb	Lu	Th	U
10QU001	15.60	33.40	4.54	19.8	5.19	1.52	5.18	0.77	5.05	1.02	2.94	0.40	2.63	0.41	1.63	0.39
10QU002	16.90	35.80	4.86	21.3	5.54	1.77	5.67	0.86	5.63	1.12	3.30	0.43	2.81	0.43	1.83	0.45
10QU003	21.10	45.90	6.30	27.7	7.27	2.07	7.26	1.12	7.36	1.46	4.15	0.58	3.74	0.56	2.27	0.54
10QU004	27.90	50.30	6.38	27.0	6.59	2.19	6.64	1.00	6.55	1.32	3.74	0.50	3.33	0.49	2.08	0.48
10QU005	27.20	48.70	6.06	25.9	6.28	2.05	6.15	0.95	6.10	1.22	3.49	0.48	3.06	0.46	1.93	0.61
10QU006	14.80	33.60	4.67	20.4	5.51	1.63	5.45	0.82	5.42	1.09	3.11	0.42	2.70	0.41	1.79	0.46
10SC001	9.40	22.20	2.99	13.1	3.38	1.38	4.33	0.64	4.02	0.82	2.34	0.34	2.05	0.31	0.99	0.21
10SC002	7.70	19.30	2.65	12.3	3.23	1.29	4.11	0.59	3.90	0.79	2.24	0.32	1.90	0.30	0.80	0.22
10SC003	8.40	20.40	2.82	12.8	3.32	1.33	4.16	0.62	4.01	0.78	2.31	0.32	1.94	0.30	0.76	0.20
10SC004	10.80	24.50	3.28	14.6	3.62	1.37	4.51	0.67	4.23	0.84	2.48	0.36	2.16	0.34	1.14	0.28
10SC005	8.50	20.00	2.75	12.5	3.30	1.28	3.98	0.59	3.77	0.75	2.24	0.31	1.86	0.28	0.75	0.19
10SC006	8.90	21.60	2.87	12.8	3.29	1.36	4.07	0.61	3.95	0.78	2.28	0.32	1.97	0.31	0.79	0.20
10SE001	14.70	31.70	4.18	18.4	4.40	1.38	4.44	0.66	4.26	0.82	2.35	0.33	2.17	0.31	1.64	0.31
10SE002	17.80	45.80	5.67	25.0	5.50	1.77	5.52	0.82	5.24	1.04	2.96	0.39	2.64	0.38	3.34	0.56
10SE003	14.40	31.10	4.11	17.9	4.28	1.38	4.33	0.65	4.17	0.80	2.37	0.32	2.06	0.31	1.50	0.29
10SE004	28.90	65.80	8.58	33.1	7.51	2.09	7.22	1.12	7.03	1.41	3.99	0.56	3.65	0.54	4.16	0.70
10SE005	25.30	53.90	6.99	27.6	5.93	1.66	5.80	0.88	5.55	1.08	3.13	0.44	2.91	0.42	3.21	0.54
10SE006	33.00	70.10	8.99	35.0	7.59	2.17	7.57	1.15	7.27	1.42	4.13	0.57	3.74	0.55	4.34	0.70
10SG001	9.60	21.60	2.84	12.7	3.09	1.28	3.81	0.56	3.60	0.73	2.11	0.29	1.82	0.28	0.98	0.24
10TO001	32.40	69.20	8.90	33.9	7.59	2.07	6.99	1.08	6.75	1.35	4.01	0.55	3.63	0.53	4.10	0.69
10TO002	33.30	70.40	8.96	34.6	7.35	2.12	7.20	1.10	6.90	1.37	3.97	0.55	3.70	0.53	4.13	0.70
10TO003	35.00	71.80	9.06	34.5	7.66	2.20	6.99	1.08	6.87	1.39	3.93	0.54	3.62	0.50	4.07	0.69
10TO004	18.10	42.30	5.41	21.1	4.71	1.24	4.32	0.67	4.33	0.87	2.45	0.35	2.33	0.35	2.68	0.50
10TO005	32.80	69.50	8.80	33.8	7.42	2.12	7.35	1.09	6.84	1.37	3.98	0.55	3.58	0.52	4.10	0.70
10TO006	31.00	56.50	7.07	27.5	5.89	1.82	5.68	0.82	5.23	1.04	2.96	0.41	2.73	0.39	3.01	0.58
10TR001	12.00	23.50	3.07	13.4	3.24	1.15	3.15	0.54	3.25	0.64	1.86	0.27	1.60	0.24	0.91	0.22
10TR002	9.50	21.80	3.06	13.8	3.80	1.26	3.60	0.63	3.81	0.73	2.14	0.30	1.82	0.27	1.07	0.26
10TR003	12.40	26.70	3.42	15.5	3.88	1.40	3.86	0.67	4.04	0.78	2.27	0.33	1.90	0.28	1.13	0.30
10TR004	10.20	21.40	2.80	12.3	3.03	1.13	3.00	0.52	3.12	0.59	1.69	0.24	1.45	0.22	0.86	0.23
10TR005	11.60	25.50	3.50	15.7	3.94	1.47	4.08	0.69	4.15	0.81	2.36	0.33	2.02	0.29	1.19	0.30

Table A-4 (continued): REE analyses.

	ppm															
	La	Ce	Pr	Nd	Sm	Eu	Gd	Tb	Dy	Ho	Er	Tm	Yb	Lu	Th	U
10TR006	10.60	24.50	3.43	15.3	3.94	1.49	3.85	0.66	4.09	0.78	2.24	0.32	1.96	0.29	1.13	0.38
10TT001	12.60	27.30	3.71	16.6	4.24	1.56	4.24	0.73	4.55	0.86	2.55	0.37	2.20	0.32	1.17	0.29
10TT002	12.90	27.60	3.76	16.8	4.39	1.56	4.19	0.73	4.64	0.88	2.58	0.37	2.17	0.33	1.17	0.28
10TT003	12.90	27.50	3.77	16.7	4.28	1.56	4.15	0.74	4.52	0.86	2.57	0.37	2.14	0.32	1.19	0.27
10TT004	13.00	28.30	3.86	17.2	4.46	1.60	4.42	0.78	4.84	0.93	2.73	0.38	2.28	0.35	1.28	0.32
10TT005	11.50	24.60	3.35	15.1	3.91	1.39	3.73	0.65	3.94	0.78	2.28	0.32	1.87	0.29	1.03	0.24
10TT006	12.10	26.50	3.69	16.8	4.48	1.58	4.41	0.78	4.89	0.93	2.81	0.40	2.38	0.36	1.26	0.30
10VI001	12.60	27.20	3.73	16.7	4.35	1.61	4.31	0.76	4.54	0.89	2.59	0.37	2.19	0.33	1.08	0.25
10VI002	13.00	27.90	3.79	16.8	4.31	1.67	4.28	0.75	4.68	0.88	2.64	0.38	2.25	0.33	1.16	0.27
10VI003	13.10	28.10	3.81	17.1	4.38	1.65	4.39	0.76	4.70	0.90	2.71	0.38	2.25	0.34	1.18	0.28
10VI004	12.80	27.70	3.81	16.9	4.34	1.61	4.33	0.76	4.67	0.89	2.66	0.38	2.23	0.33	1.16	0.28
10VI005	13.00	27.50	3.78	16.9	4.30	1.69	4.28	0.76	4.59	0.88	2.56	0.37	2.18	0.32	1.11	0.25
10VI006	13.00	27.90	3.81	17.0	4.37	1.63	4.31	0.76	4.61	0.91	2.64	0.38	2.26	0.33	1.12	0.26
11CBF001	11.90	26.90	3.69	17.1	4.13	1.49	4.66	0.72	4.64	0.95	2.61	0.35	2.19	0.32	1.08	0.25
11CBF002	10.60	23.60	3.33	15.3	3.81	1.30	4.13	0.67	4.40	0.80	2.34	0.32	2.01	0.28	1.10	0.27
11CBF003	13.30	29.90	4.09	18.4	4.51	1.57	4.84	0.77	4.99	0.96	2.85	0.38	2.46	0.36	1.32	0.30
11CBF004	13.30	30.20	4.13	18.9	4.58	1.53	4.84	0.78	4.99	0.98	2.75	0.36	2.25	0.33	1.32	0.30
11CBF005	13.10	29.50	3.98	18.6	4.61	1.51	4.63	0.75	4.86	0.93	2.62	0.35	2.32	0.33	1.15	0.27
11CBF006	16.80	37.50	5.24	24.0	5.93	1.89	6.37	1.00	6.44	1.27	3.65	0.49	3.17	0.46	1.66	0.38
11CLD001	13.20	30.20	4.11	18.7	4.61	1.41	4.96	0.79	5.06	1.00	2.82	0.38	2.42	0.34	1.41	0.33
11CLD002	12.50	27.60	3.82	17.6	4.36	1.44	4.56	0.74	4.62	0.90	2.67	0.36	2.31	0.33	1.15	0.26
11CLD003	13.40	29.80	4.11	18.6	4.66	1.57	4.72	0.76	4.83	0.96	2.70	0.35	2.33	0.33	1.31	0.32
11CLD004	10.90	24.60	3.39	15.6	3.85	1.23	4.02	0.66	4.24	0.84	2.38	0.32	2.01	0.29	1.10	0.25
11CLD005	22.70	45.90	5.79	23.9	4.89	1.11	4.53	0.68	4.42	0.85	2.45	0.35	2.18	0.33	4.78	1.50
11CLD006	10.20	23.90	3.34	15.6	4.09	1.28	4.23	0.72	4.75	0.91	2.49	0.35	2.28	0.32	1.43	0.33
11CLD007	12.10	27.70	3.81	17.5	4.19	1.32	4.31	0.69	4.59	0.88	2.52	0.34	2.17	0.30	1.53	0.34

Table A-5: Volatile element analyses.

	ppm					
	As	Se	Sb	Te	Hg	Bi
10BA001	<0.1	0.5	<0.05	<0.01	0.020	0.01
10BA002	1.3	0.7	0.12	0.01	0.007	<0.01
10BA003	<0.1	0.5	0.11	<0.01	<0.005	<0.01
10BA004	1.8	0.5	0.51	<0.01	0.018	<0.01
10BA005	<0.1	0.5	0.83	<0.01	<0.005	<0.01
10BA006	<0.1	0.6	0.05	0.01	<0.005	<0.01
10BB001	0.1	0.5	<0.05	0.01	0.005	<0.01
10BB002	0.8	0.6	<0.05	0.01	<0.005	<0.01
10BB003	0.3	0.6	<0.05	0.01	<0.005	0.01
10BB004	0.4	0.6	<0.05	0.01	<0.005	<0.01
10BB005	1.4	0.5	0.05	0.01	<0.005	<0.01
10BB006	0.2	0.5	<0.05	0.01	0.007	<0.01
10CC001	0.1	0.5	<0.05	0.01	0.011	<0.01
10CC002	3.2	0.9	<0.05	<0.01	0.018	0.01
10CC003	0.1	0.5	<0.05	<0.01	0.009	<0.01
10CC004	0.2	0.6	<0.05	<0.01	0.008	0.01
10CC005	1.1	0.6	<0.05	<0.01	<0.005	<0.01
10CC006	0.2	0.5	<0.05	<0.01	<0.005	0.01
10CE001	1.1	1.0	<0.05	0.01	0.007	0.01
10CE002	0.2	0.8	<0.05	0.01	0.007	<0.01
10CE003	0.7	0.6	<0.05	0.02	0.011	0.01
10CE004	<0.1	0.8	<0.05	0.01	0.007	<0.01
10CE005	0.1	0.7	<0.05	0.01	0.005	<0.01
10CE006	0.6	1.0	<0.05	0.01	0.016	<0.01
10CF001	0.4	0.7	0.17	0.01	0.014	0.02
10CF002	0.3	1.0	<0.05	0.01	0.008	<0.01
10CF003	0.4	1.6	<0.05	0.01	0.011	0.01
10CF004	0.6	0.9	<0.05	0.01	0.012	<0.01
10CF005	1.2	0.7	0.05	0.01	0.121	0.01
10CF006	0.9	1.2	<0.05	0.01	0.016	0.01
10CH001	2.2	0.5	<0.05	0.01	<0.005	<0.01
10CH002	32.3	0.7	<0.05	0.01	0.262	<0.01
10CH003	1.5	0.7	0.16	<0.01	<0.005	<0.01
10CH004	5.8	0.7	0.06	0.10	0.011	0.01
10CH005	<0.1	0.5	0.46	<0.01	0.005	0.01
10CH006	2.5	0.5	0.12	<0.01	<0.005	<0.01
10CL001	0.2	0.7	0.07	0.01	0.008	0.01
10CL002	0.1	0.6	<0.05	0.01	<0.005	<0.01
10CL003	0.1	0.7	<0.05	0.01	0.009	<0.01
10CL004	0.2	0.5	<0.05	0.01	0.010	<0.01
10CL005	0.8	0.7	0.05	0.01	0.011	0.02
10CL006	0.1	0.6	<0.05	0.01	0.010	0.01
10CN001	0.9	0.8	<0.05	0.01	0.022	0.01
10CN002	<0.1	0.6	<0.05	<0.01	<0.005	<0.01

Table A-5 (continued): Volatile element analyses.

	ppm					
	As	Se	Sb	Te	Hg	Bi
10CN003	0.4	0.7	<0.05	<0.01	0.007	<0.01
10CN004	0.1	0.7	<0.05	0.01	<0.005	<0.01
10CN005	<0.1	0.6	0.07	<0.01	<0.005	<0.01
10CN006	<0.1	0.5	<0.05	<0.01	<0.005	<0.01
10DE001	<0.1	0.4	<0.05	<0.01	0.006	<0.01
10DE002	0.2	0.9	<0.05	<0.01	0.019	0.01
10DE003	<0.1	0.6	<0.05	<0.01	0.005	0.01
10DE004	0.5	0.4	<0.05	<0.01	0.030	<0.01
10DE005	<0.1	0.8	<0.05	<0.01	<0.005	<0.01
10DE006	<0.1	0.4	<0.05	<0.01	<0.005	<0.01
10DE007	<0.1	1.1	<0.05	<0.01	0.007	<0.01
10DR001	0.2	0.6	<0.05	<0.01	<0.005	<0.01
10DR002	0.9	0.9	<0.05	0.01	0.013	0.01
10DR003	0.6	0.8	<0.05	<0.01	0.018	<0.01
10DR004	0.2	0.7	<0.05	<0.01	<0.005	<0.01
10DR005	1.4	0.7	<0.05	<0.01	0.033	<0.01
10DR006	0.3	0.6	<0.05	<0.01	<0.005	<0.01
10FJ001	<0.1	0.5	0.28	0.01	<0.005	0.01
10FJ002	0.2	1.0	<0.05	<0.01	0.005	<0.01
10FJ003	0.2	0.9	<0.05	<0.01	<0.005	<0.01
10FJ004	<0.1	0.6	<0.05	<0.01	<0.005	<0.01
10FJ005	0.1	0.9	<0.05	<0.01	0.011	<0.01
10FJ006	0.7	1.1	<0.05	<0.01	<0.005	0.01
10FU001	1.5	1.1	<0.05	<0.01	0.006	0.01
10FU002	1.9	0.9	<0.05	<0.01	0.010	<0.01
10FU003	3.8	0.9	<0.05	0.01	0.006	0.01
10FU004	1.0	0.6	<0.05	<0.01	<0.005	<0.01
10FU005	2.8	0.9	0.05	<0.01	0.008	0.01
10FU006	2.0	0.6	<0.05	<0.01	<0.005	<0.01
10GR001	0.3	0.5	<0.05	0.01	0.009	<0.01
10GR002	0.8	0.7	<0.05	0.01	0.006	<0.01
10GR003	5.1	0.7	<0.05	0.01	0.010	0.01
10GR004	4.7	1.0	0.09	0.01	0.015	0.01
10GR005	1.9	0.6	<0.05	0.01	<0.005	<0.01
10GR006	1.3	1.1	<0.05	0.01	0.009	0.01
10HE001	1.5	0.8	<0.05	<0.01	0.010	0.01
10HE002	6.9	0.7	0.10	<0.01	0.028	0.02
10HE003	0.6	0.4	0.10	<0.01	<0.005	<0.01
10HE004	3.5	0.8	0.05	0.01	0.047	0.02
10HE005	0.6	0.8	0.08	<0.01	0.023	0.01
10HE006	<0.1	0.5	0.06	<0.01	0.006	0.01
10IR001	5.9	0.5	0.05	<0.01	0.056	<0.01
10IR002	2.3	0.5	<0.05	<0.01	<0.005	<0.01
10IR003	4.4	0.7	0.16	<0.01	<0.005	<0.01

Table A-5 (continued): Volatile element analyses.

	ppm					
	As	Se	Sb	Te	Hg	Bi
10IR004	3.5	0.5	<0.05	<0.01	<0.005	<0.01
10IR005	4.0	0.8	0.31	0.01	<0.005	0.01
10IR006	0.7	0.6	0.07	<0.01	<0.005	<0.01
10IR007	15	1.1	0.08	<0.01	0.136	<0.01
10IR008	11.2	0.6	0.33	<0.01	<0.005	<0.01
10IR009	1.9	0.7	0.11	0.01	<0.005	0.01
10IR010	28.4	0.7	0.11	<0.01	0.008	<0.01
10IR011	2.0	0.5	0.05	<0.01	<0.005	<0.01
10IR012	1.9	0.5	0.09	0.01	<0.005	0.01
10LA001	0.1	0.8	<0.05	<0.01	0.011	<0.01
10LA002	<0.1	1.9	<0.05	0.01	0.007	<0.01
10LA003	0.6	0.9	<0.05	<0.01	0.014	<0.01
10LA004	<0.1	0.7	<0.05	<0.01	<0.005	0.01
10MB001	0.3	0.4	<0.05	0.01	<0.005	<0.01
10MB002	0.6	0.4	0.05	0.01	<0.005	0.01
10MC001	1.8	0.9	<0.05	<0.01	0.006	0.01
10MC002	2.0	1.1	<0.05	<0.01	0.020	0.02
10MC003	0.1	1.0	<0.05	<0.01	0.008	0.01
10MC004	0.1	0.8	<0.05	<0.01	<0.005	<0.01
10MC005	0.3	0.7	<0.05	0.01	0.006	<0.01
10MC006	0.7	0.6	<0.05	<0.01	0.025	0.01
10MG001	0.9	0.7	<0.05	0.01	0.012	<0.01
10MG002	<0.1	0.8	<0.05	<0.01	0.006	<0.01
10MG003	<0.1	0.5	<0.05	<0.01	<0.005	<0.01
10MG004	0.6	0.8	<0.05	<0.01	0.008	<0.01
10MG005	0.9	0.8	<0.05	<0.01	0.007	0.01
10MG006	0.2	0.7	<0.05	<0.01	0.006	<0.01
10MI001	<0.1	0.6	<0.05	<0.01	<0.005	<0.01
10MI002	<0.1	0.6	<0.05	<0.01	0.007	<0.01
10MI003	<0.1	0.5	<0.05	<0.01	0.008	<0.01
10MI004	<0.1	0.7	0.08	<0.01	0.006	<0.01
10MI005	<0.1	0.6	<0.05	0.01	0.007	<0.01
10MI006	0.3	0.8	<0.05	<0.01	0.026	<0.01
10OC001	<0.1	0.7	<0.05	<0.01	<0.005	0.01
10OC002	<0.1	0.5	<0.05	<0.01	<0.005	0.01
10OC003	0.1	0.4	<0.05	0.01	0.006	<0.01
10OC004	<0.1	0.6	<0.05	<0.01	<0.005	0.01
10OC005	0.1	0.7	<0.05	<0.01	<0.005	<0.01
10OC006	<0.1	0.6	0.05	<0.01	<0.005	<0.01
10OC007	0.1	0.7	<0.05	<0.01	0.006	<0.01
10OC008	0.1	0.7	<0.05	<0.01	<0.005	<0.01
10OC009	<0.1	0.6	<0.05	0.01	0.006	<0.01
10OC010	0.5	0.6	<0.05	<0.01	0.008	<0.01
10OC011	<0.1	0.8	<0.05	<0.01	0.010	<0.01

Table A-5 (continued): Volatile element analyses.

	ppm					
	As	Se	Sb	Te	Hg	Bi
10OC013	0.6	0.7	0.06	<0.01	0.037	0.01
10OC014	<0.1	1.0	<0.05	<0.01	0.008	<0.01
10OC015	0.1	0.8	0.06	<0.01	0.349	<0.01
10OC016	0.4	0.8	<0.05	<0.01	0.034	<0.01
10OC017	0.1	0.7	<0.05	<0.01	0.023	<0.01
10OC018	<0.1	0.6	<0.05	<0.01	<0.005	<0.01
10OJ001	3.4	1.0	<0.05	0.01	0.010	0.02
10OJ002	3.8	0.7	<0.05	0.01	0.011	0.01
10OJ003	0.3	0.6	<0.05	0.01	0.007	0.01
10OJ004	1.7	1.0	<0.05	0.01	0.008	0.01
10OJ005	0.9	1.0	<0.05	0.01	0.009	0.01
10OJ006	1.6	0.7	<0.05	0.01	0.006	<0.01
10PH001	0.4	0.5	<0.05	0.01	<0.005	<0.01
10PH002	0.3	0.7	<0.05	0.01	<0.005	<0.01
10PH003	0.2	0.7	<0.05	0.01	0.009	<0.01
10PH004	0.2	0.5	<0.05	0.01	0.008	<0.01
10PH005	0.3	0.5	<0.05	0.01	<0.005	<0.01
10PH006	0.2	0.5	<0.05	0.01	0.005	<0.01
10QU001	0.3	0.9	<0.05	0.01	0.016	0.01
10QU002	0.3	1.1	<0.05	0.01	0.008	<0.01
10QU003	0.3	1.3	<0.05	0.01	0.011	0.01
10QU004	0.7	1.2	<0.05	0.02	0.208	0.06
10QU005	0.4	4.4	<0.05	0.01	0.038	0.01
10QU006	0.6	1.9	<0.05	0.02	0.025	0.01
10SC001	0.1	0.6	<0.05	<0.01	<0.005	<0.01
10SC002	0.3	0.8	<0.05	0.01	0.006	0.01
10SC003	0.1	0.7	<0.05	<0.01	<0.005	<0.01
10SC004	<0.1	0.2	<0.05	0.01	0.005	0.01
10SC005	<0.1	0.7	<0.05	<0.01	<0.005	<0.01
10SC006	<0.1	0.4	<0.05	0.01	<0.005	<0.01
10SE001	0.2	0.5	<0.05	<0.01	<0.005	<0.01
10SE002	1.9	0.7	<0.05	<0.01	0.011	0.01
10SE003	0.4	0.4	<0.05	<0.01	<0.005	<0.01
10SE004	3.5	0.9	<0.05	<0.01	0.011	<0.01
10SE005	4.2	0.8	<0.05	<0.01	0.015	0.01
10SE006	2.0	0.9	<0.05	<0.01	<0.005	0.01
10SG001	0.2	0.5	<0.05	<0.01	<0.005	<0.01
10TO001	0.5	0.9	<0.05	<0.01	0.006	0.01
10TO002	0.5	1.0	<0.05	<0.01	0.005	0.01
10TO003	1.0	1.0	0.16	<0.01	0.015	<0.01
10TO004	1.7	0.7	0.06	<0.01	0.022	<0.01
10TO005	0.5	1.0	<0.05	<0.01	<0.005	0.01
10TO006	2.5	0.7	<0.05	<0.01	0.021	0.01
10TR001	4.6	0.5	0.06	0.15	0.010	<0.01

Table A-5 (continued): Volatile element analyses.

	ppm					
	As	Se	Sb	Te	Hg	Bi
10TR002	<0.1	0.6	0.60	0.01	0.008	0.01
10TR003	0.6	0.4	0.74	0.01	0.008	<0.01
10TR004	1.0	0.4	0.32	0.01	0.009	0.01
10TR005	<0.1	0.5	0.12	<0.01	<0.005	<0.01
10TR006	<0.1	0.5	0.07	0.02	0.015	0.03
10TT001	1.0	0.7	<0.05	<0.01	0.019	<0.01
10TT002	0.5	0.7	<0.05	0.01	0.023	<0.01
10TT003	<0.1	0.6	0.08	<0.01	0.019	<0.01
10TT004	0.2	0.7	<0.05	0.01	0.008	0.01
10TT005	0.1	0.7	<0.05	<0.01	0.008	<0.01
10TT006	0.6	1.0	<0.05	<0.01	0.045	<0.01
10VI001	0.5	0.7	<0.05	<0.01	<0.005	<0.01
10VI002	1.0	0.9	<0.05	<0.01	0.005	<0.01
10VI003	0.2	0.7	<0.05	0.01	0.009	<0.01
10VI004	0.6	1.7	<0.05	0.01	0.010	<0.01
10VI005	3.0	1.1	<0.05	0.01	0.021	<0.01
10VI006	0.4	0.7	<0.05	0.01	0.006	<0.01
11CBF001	0.5	0.7	<0.05	<0.01	0.007	<0.01
11CBF002	0.7	0.9	<0.05	0.01	0.010	0.01
11CBF003	1.0	0.7	<0.05	<0.01	0.008	<0.01
11CBF004	0.3	0.8	<0.05	<0.01	0.008	<0.01
11CBF005	0.1	0.9	<0.05	<0.01	0.007	<0.01
11CBF006	0.4	0.8	<0.05	0.01	0.014	<0.01
11CLD001	0.9	1.0	<0.05	0.01	0.013	0.01
11CLD002	0.3	1.0	<0.05	0.01	0.010	<0.01
11CLD003	2.0	0.9	<0.05	0.01	0.029	0.01
11CLD004	0.3	0.9	<0.05	<0.01	0.009	<0.01
11CLD005	4.2	0.6	0.24	0.03	0.024	0.05
11CLD006	0.7	1.2	<0.05	0.01	0.055	0.01
11CLD007	1.4	1.1	<0.05	0.04	0.287	0.02

APPENDIX B: DATA PROCESSING

B-1 Olivine Group

Members of the (Mg,Fe)-olivine group have compositions between fayalite (Fe_2SiO_4) and forsterite (Mg_2SiO_4). For cation recalculations, the general formula X_2TO_4 was used, where Si^{4+} was assumed to occupy the T site, and Mg^{2+}, Fe^{2+}, and some Mn^{2+} and Ca^{2+} were assigned to the X site. Calculations were based on four oxygen atoms PFU. For classification purposes, the atomic Mg^{2+} was divided by the sum of Mg^{2+}, Fe^{2+}, and Mn^{2+}. Naming divisions as in Deer et al. (1992) were used for classification purposes.

B-2 Amphibole Group

Although amphibole group minerals are not very common in mafic rocks, some minerals identified by microscope analysis were believed to be amphiboles. In order to confirm this suspicion, the minerals were analyzed using microprobe analysis, and cation recalculations were performed in order to confirm and classify the mineral. The formula used for cation recalculations was $A_{0\text{-}1}B_2C_5T_8O_{22}(OH,F,Cl)_2$, where the A site could be vacant or contain Na^+ and K^+. All Si^{4+} was assigned to T, along with enough Al^{3+} to fill the site. Remaining Al^{3+}, as well as Fe^{2+}, Fe^{3+}, and enough Mg^{2+} to fill the site were assigned to C. Remaining Mg^{2+}, as well as Ca^{2+} were assigned to B. No Na^+ or K^+ was detected in the analyses, thus the Fe^{3+}/Fe^{2+} ratio was adjusted until a total of ~13 ions for the sum of Si^{4+}, Al^{3+}, Fe^{2+}, Fe^{3+}, Mg^{2+}, and Mn^{2+} was calculated. Cation recalculations were based on 23 oxygen atoms. Classification of amphiboles was based on the 1997 International Mineralogical Association (IMA) report on the nomenclature of amphiboles by Leake et al. (1997). Since no Na^+ or K^+ was detected, and Ca^{2+} was the dominant cation in the B site, the classification scheme for calcium amphiboles was used. The silica PFU and $Mg/(Mg+Fe^{2+})$ were used to classify the minerals.

B-3 Feldspar Group

The feldspar group can be classified using the ternary system $NaAlSi_3O_8$ (albite) – $KAlSi_3O_8$ (potassium feldspar) - $CaAl_2Si_2O_8$ (anorthite). The formula used for cation recalculation was $X[T_4O_8]$ where T = $Al_{1-2}Si_{2-3}$,Ti^{4+} and X=Ca^{2+}, Na^{+}, K^{+}, Mg^{2+}, Fe^{2+}, Ba^{2+}. Cations were recalculated based on eight oxygen atoms PFU, and all iron was left as FeO.

Na^{+} or K^{+} cations are replaced by cations with a 2+ charge through coupled substitution: exchange of X^{+} and T^{4+} with X^{2+} and T^{3+}. Thus the T^{4+} to T^{3+} ratio can be used to approximate the anorthite content (X_{an}) of the feldspars:

$$X_{An} = \left(\frac{3 - \left(\frac{Si}{Al}\right)}{1 + \left(\frac{Si}{Al}\right)}\right) \qquad \text{B-1}$$

B-4 Pyroxene Group

For pyroxene group minerals, the general formula $[(M2)(M1)(T)_2O_6]$ was used. The T site was filled with Si^{4+}, Al^{3+}, (and Fe^{3+}), M1 with Al^{3+}, Fe^{3+}, Ti^{4+}, Cr^{3+}, Mg^{2+}, Fe^{2+}, and Mn^{2+}; and M2 was filled with Mg^{2+}, Fe^{2+}, Mn^{2+}, Ca^{2+}, and Na^{+} following the flow chart in Figure B-1, as suggested by Morimoto et al. (1988). Additionally, K^{+} was allowed to fill the M2 site. Cations were recalculated based on six oxygen atoms. Since only FeO was determined with microprobe analyses, the Fe^{3+} to Fe^{2+} ratio was adjusted manually if the total number of cations was bigger than 4.0 (i.e., the Fe^{3+} to Fe^{2+} ratio was set to default to zero unless the number of cations was bigger than 4.0).

Ca-Mg-Fe pyroxenes can be classified using the pyroxene quadrilateral between end-members enstatite (En, $Mg_2Si_2O_6$), ferrosilite (FS, $Fe^{2+}{}_2Si_2O_6$), diopside (Di, $CaMgSi_2O_6$), and hedenbergite (Hd, $CaFe^{2+}Si_2O_6$). Diopside and hedenbergite would plot between wollastonite (Wo, Ca_2Si_2O6), and enstatite and hedenbergite, respectively, in a ternary diagram. As suggested by Morimoto et al. (1988), the

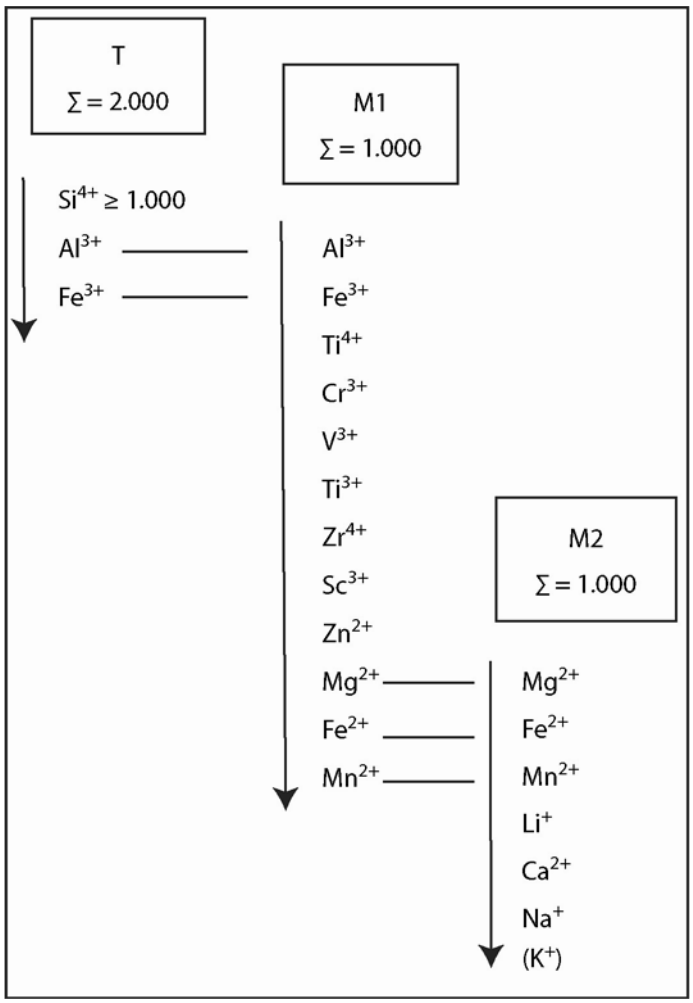

Figure B-1: Flow chart used for site occupancy of cations of pyroxenes. Modified from Morimoto et al. (1988).

atomic Ca, Mg, and the sum of Fe^{2+}, Fe^{3+}, and Mn^{2+}($\sum$Fe) contents were normalized to 100 and plotted on the ternary diagram to classify the pyroxene minerals.

B-5 Chlorite Group

Cation recalculations for chlorite group minerals were based on the formula $(R)_{12}[(Si,Al)_8O_{20}](OH)_{16}$ where R=Mg^{2+}, Fe^{2+}, Mn^{2+}, (Ca^{2+}, Na^{+}, K^{+}), Al^{3+}. Some Ti^{4+} was accepted in the octahedral site. The possibility of Fe^{3+} in the R site was ignored. Cations were recalculated based on 28 oxygen atoms PFU, using eight oxygen atoms instead of 16 OH^{-} in order to maintain charge balance. Chlorite was classified based on atomic Fe/(Fe+Mg) and silica atoms PFU as suggested by Hey (1954).

B-6 Mica Group

Both muscovite and sericite (very fine-grained muscovite) were observed in thin section and analyzed using the microprobe. For both, the general formula $X_2Y_4[Z_8O_{20}](OH,F)_4$ was used, where Z was set to consist of Si^{4+} and enough Al^{3+} to add to 8.0 ions. The Y site was made up of remaining Al^{3+}, as well as any Mg^{2+} and all Fe as Fe^{2+}. Na^{+} and K^{+} were accepted in the X site. A ternary diagram with total Al, total Si, and Mg^{2+} plus Fe^{2+} cations was used to classify the mica group minerals.

B-7 Epidote Group

Epidote cation recalculations were done following recommendations by Armbruster et al. (2006). The formula $A_2M_3(T_3O_{12})(OH)$ was used, and cation recalculations were based on 12.5 oxygen atoms. The T site was first filled by Si^{4+}, which was expected to remain at less than 3.1 atoms PFU. If necessary, enough Al^{3+} was added to the site to add up to 3.0 cations total. The M site was filled by remaining Al^{3+} and Fe^{3+}, as well as Ti^{4+}, Mn^{2+}, Mg^{2+}, and Fe^{2+} to add up to 3.0 cations. The A site was filled with any remaining Fe^{2+}, and Ca^{2+}, K^{+}, and La^{3+} and Ce^{3+} if present. All FeO was first converted into Fe_2O_3, the Fe^{3+}/Fe^{2+} ratio was then adjusted to achieve a total of 8.0 cations. For classification purposes, the “pistacite” component (X_{Fe}) was calculated using:

$$X_{Fe} = \frac{Fe^{3+}}{Fe^{3+} + Al} \qquad \text{A-1}$$

B-8 Pumpellyite

Cation recalculations for pumpellyite were based on the general formula $W_2XY_2Z_3(O,OH)_{14}$, where Si^{4+} was assigned to the Z site, Al^{3+}, and any Ti^{4+} were accepted in the Y site, remaining Al^{3+}, as well as Mg^{2+}, Mn^{2+}, and Fe^{2+} were assigned to the X site, and Ca^{2+}, Na^{+}, and K^{+} were assigned to the W site. All iron was left as FeO, and no attempts were made to adjust the Fe^{3+} to Fe^{2+} ratio. Since the number of oxygen in the formula is not constant, recalculations were based on 3.0 silica atoms PFU. Recalculation based on 16 cations as done by other authors was considered, but disregarded. According to Passaglia and Gottardi (1973), vacancies in the X site are common , and recalculation to 16 cations would distribute the potential error due to vacancies to all other cation sites. Pumpellyite data was analyzed by plotting Al^{3+}, Mg^{2+}, and total Fe as Fe^{2+} on a ternary diagram. No further classification of pumpellyite was attempted.

B-9 Prehnite Group

Prehnite group minerals consist of a solid solution series between the ideal end members $Ca_2Al_2Si_3O_{10}(OH)_2$ and $Ca_2Fe_2Si_3O_{10}(OH)_2$. Cation recalculations were based on the general formula $Y_2XZ_4O_{10}(OH)_2$, where the Z site was filled with Si^{4+}, and enough Al^{3+} to add to 4.0 ions. Remaining Al^{3+} was assigned to the X site, with all Fe as Fe^{3+}. Ti^{4+}, Ca^{2+}, and Mg^{2+} were accepted in the Y site. Cation recalculations were based on eleven oxygen atoms PFU. In order to visualize varying Al^{3+} and Fe^{3+} contents in the X site, the number of cations of Al^{3+} and Fe^{3+} of the X site were plotted in a ternary diagram with cations of Ca^{2+}.

B-10 Sphene

Sphene cation recalculations were based on the general formula $XYTO_4$, where all Si was assigned to T; Al, Fe^{3+}, and Ti were assigned to Y; and Ca, Mg, and Na were accepted in the X site. Calculations were based on 4 silica atoms PFU.

APPENDIX C: CONSTRUCTION OF ACF DIAGRAMS

The ACF diagrams were constructed as described by Blatt et al. (2006) from the mol proportions of Al_2O_3, Fe_2O_3, Na_2O, K_2O, CaO, P_2O_5, CO_2, FeO, MgO, MnO, and TiO_2, where:

- $A = Al_2O_3 + Fe_2O_3 – (Na_2O + K_2O)$,
- $C = CaO – 3.3\ P_2O_5 – CO_2$, and
- $F = FeO + MgO + MnO - (TiO_2)$.

Since whole rock data only provided a value for the weight percent of Fe_2O_3, amounts of Fe_2O_3 and FeO for this diagram were approximated using a Fe_2O_3 to FeO ratio of 0.15 as suggested by Brooks (1976). The given Fe_2O_3 weight percent value was first used to calculate mol proportions of Fe present. In order to achieve a ratio of 0.15, 0.15 mol of Fe_2O_3 had to be present for every one mol of FeO. The total mol of Fe was calculated to be 1.3 (one mol Fe from FeO, 0.3 mol Fe from 0.15 mol Fe_2O_3). The total Fe value thus was normalized to yield 1.3, and mol proportions of FeO and Fe_2O_3 were calculated.

APPENDIX D: CONSTRUCTION OF AFM DIAGRAMS

AFM diagrams were constructed as suggested by Irvine and Barager (1971), where:

- A = Na_2O + K_2O (wt %),
- F = total Fe as FeO (wt %) = 0.8998 Fe_2O_3 (wt %), and
- M = MgO (wt %).

All values were given in weight percent, with total iron expressed as FeO (wt %). Since the iron content was given in weight percent Fe_2O_3, it was converted to weight percent FeO using the relationship FeO (wt %) = 0.8998 Fe_2O_3 (wt %).

APPENDIX E: CALCULATION OF AQUEOUS SILICA IN KEWEENAW MINE WATERS

Conversions from mg/L to ppm were made using Equation D-1, assuming pure water at 4°C:

$$\frac{mg}{L} * \frac{L}{1\ kg} = \frac{mg}{kg} = ppm \qquad \text{D-1}$$

Conversions from Si (ppm) to SiO_2 (ppm) were made using Equation D-2:

$$SiO_2(ppm) = \ Si\ (ppm) * \frac{mol.weight\ SiO_2}{at.\ weight\ Si} = Si(ppm) * \frac{60.08}{28.08} \qquad \text{D-2}$$

Knowing that mg/kg = ppm, the log activity of SiO_2(aq) was then calculated using:

$$\log aSiO_2\left(aq, \frac{mol}{kg}\right) = \log SiO_2\left(\frac{mg}{kg}\right) * \frac{g}{1000\ mg} * \frac{mol}{60.08\ g} \qquad \text{D-3}$$

APPENDIX F: ABUNDANCES OF MINERALS OBSERVED IN THIN SECTION

In the main text of this thesis, the main minerals [plagioclase (plg), clinopyroxene (cpx), orthopyroxene (opx), olivine (ol), amphibole (amph), chlorite (chl), epidote (epi), prehnite (prn), pumpellyite (pp), sericite (ser), and calcite(cc)] observed in thin sections were included in tables. Additionally, relative amounts of potassium feldspar (kspar), quartz (qtz), copper (cu), opaque minerals (op), sphene (sph), zeolites (zeo), holes in the thin sections (holes), iddingsite (id), and other, not identified alteration (altn) were recorded, and are included here. Trace amounts are indicated as 0.1%, zero values denote minerals not observed.

Table F-1: Samples and approximate abundances (%) of all minerals observed in thin section.

stage	Sample	texture	plg	cpx	opx	ol	amph	chl	epi	pp	prn	ser	cc	ksp	qtz	cu	op	sph	zeo	holes	id	altn
1.	10SG001	porphyritic	50	15	5	5	-	10	-	-	-	-	-	-	-	-	5	-	-	-	10	-
	10SC004	ophitic	30	30	5	5	2	15	-	-	-	0.1	-	-	-	-	5	-	-	-	5	-
2a	10MI003	fine-grained	35	35	-	-	-	20	-	-	-	2	2	-	-	-	4	2	-	-	-	-
	10OC002	fine-grained	36	30	-	-	-	15	-	-	-	3	1	-	-	-	15	0.1	-	-	-	-
	10VI002	fine-grained	25	30	-	-	-	-	-	-	-	5	10	-	-	0.1	30	0.1	-	-	-	-
	10CC006	porphyritic	25	30	-	-	-	18	-	-	-	15	-	-	-	-	10	2	-	-	-	-
	10CH001	very fine-grained	20	30	-	-	-	30	-	-	-	5	-	-	-	0.1	10	5	-	-	-	-
	10DE006	subophitic	25	25	-	-	-	35	-	-	-	3	1	-	-	-	4	6	2	-	-	-
	10BB001	very fine-grained	20	30	-	-	-	45	-	-	-	-	2	-	-	-	3	-	-	-	-	-
	10OC006	very fine-grained	17	30	-	-	-	25	-	-	-	10	2	-	-	-	15	1	-	-	-	-
	10DR004	fine-grained	24	20	-	-	-	40	-	-	-	4	1	-	3	-	5	3	-	-	-	-
	10OC011	very fine-grained	20	20	-	-	-	40	-	-	-	1	0.1	-	-	4	10	4	-	-	-	-
	10MG003	fine-grained	8	30	-	-	-	20	-	-	-	35	-	-	-	5	5	2	-	-	-	-
2b	10HE004	very fine-grained	25	-	-	-	-	30	-	-	-	10	10	-	2	0.1	20	2	0.1	-	-	-
	10BA005	very fine-grained	20	-	-	-	-	15	-	-	-	20	10	-	5	-	5	-	10	-	-	15
	10FJ006	amygd.	20	-	-	-	-	30	-	-	-	5	20	0.1	0.1	0.1	10	5	0.1	-	-	-
	10FJ005	amygd.	5	1	-	-	-	57	-	-	-	-	-	-	-	-	15	2	-	-	-	20
	10HE003	fine-grained	5	-	-	-	-	28	-	-	-	25	5	-	-	0.1	5	2	-	-	-	30
	10TR004	very fine-grained	-	-	-	-	-	5	-	-	-	25	63	-	2	-	5	-	-	-	-	-
2c	10OC014	very fine-grained	31	25	-	-	-	10	3	-	-	10	8	-	0.1	-	7	1	-	-	-	5
	10FU004	very fine-grained	13	15	-	-	-	30	0.1	-	-	25	5	-	-	1	10	1	-	-	-	-

Table F-1 (continued): Samples and approximate abundances (%) of all minerals observed in thin section.

stage	Sample	texture	plg	cpx	opx	ol	amph	chl	epi	pp	prn	ser	cc	ksp	qtz	cu	op	sph	zeo	holes	id	altn
3a	10TT005	fine-grained	25	20	-	-	-	30	3	5	3	2	-	-	-	-	10	2	-	-	-	-
	10QU002	gabbroic	31	3	-	-	-	30	1	25	3	-	-	-	-	-	5	1	-	-	-	-
	10TT002	amygd.	10	-	-	-	-	23	5	35	5	5	10	-	0.1	0.1	15	2	-	-	-	-
	10PH005	subophitic	26	20	-	-	-	20	-	2	10	-	2	-	0.1	-	20	0.1	-	-	-	-
	10IR001	gabbroic	2	25	-	-	-	15	0.1	35	8	-	3	-	1	-	10	1	-	-	-	-
	10CF004	porphyritic	35	2	-	-	-	15	0.1	15	15	-	-	-	-	-	10	8	-	-	-	-
	10DR005	brecciated	7	3	-	-	-	15	3	24	28	-	-	-	5	3	5	0.1	-	7	-	-
	10CL006	brecciated	2	3	-	-	-	10	5	29	30	-	15	-	2	2	3	4	-	-	-	-
3b	10DE007	gabbroic	16	15	-	-	-	-	2	35	25	-	2	-	-	-	5	-	-	-	-	-
	10QU006	brecciated	2	2	-	-	-	-	10	5	46	-	20	-	15	-	-	-	-	-	-	-
	10CN002	fine-grained	40	15	-	-	-	-	1	20	20	-	1	-	0.1	-	3	-	-	-	-	-

Table F-1 (continued): Samples and approximate abundances (%) of all minerals observed in thin section.

stage	Sample	texture	plg	cpx	opx	ol	amph	chl	epi	pp	prn	ser	cc	ksp	qtz	cu	op	sph	zeo	holes	id	altn
4a	10OJ005	aphanitic	38	25	-	-	-	5	-	15	-	1	1	-	-	-	15	0.1	-	-	-	-
	10CE002	gabbroic	5	38	-	-	-	15	2	30	-	-	-	-	-	-	8	-	-	2	-	2
	10PH004	subophitic	15	30	-	-	-	20	-	5	-	15	0.1	2	0.1	-	12	1	-	-	-	-
	10CF006	gabbroic	20	20	-	-	-	30	0.1	25	-	-	-	-	-	-	5	0.1	-	-	-	-
	10LA001	fine-grained	17	20	-	-	-	20	3	30	-	-	-	-	-	-	8	2	-	-	-	-
	10MC005	fine-grained	24	15	-	-	-	30	-	15	-	5	-	-	-	-	10	1	-	-	-	-
	10FU003	porphyritic	14	15	-	-	-	19	4	20	-	1	-	-	2	6	15	3	-	-	-	-
	10GR003	amygd.	5	15	-	-	-	15	2	35	-	2	-	-	1	1	15	4	-	-	-	-
	11CBF006	fine-grained	30	10	-	-	-	25	5	20	-	-	-	-	5	-	5	1	-	-	-	-
	11CBF004	gabbroic	25	10	-	-	-	30	0.1	20	-	-	-	-	-	-	3	2	-	-	-	-
4b	10CF005	fine-grained	42	5	-	-	-	30	1	5	-	2	5	-	1	0.1	5	2	-	2	-	-
	10MC003	fine-grained	10	3	-	-	-	25	8	30	-	-	10	-	5	-	8	1	-	-	-	-
	11CLD003	amygd.	29	-	-	-	-	30	10	25	-	-	-	-	-	-	5	1	-	-	-	-
	10CC002	amygd.	26	2	-	-	-	15	15	10	-	1	-	-	-	1	10	-	-	-	-	20
	10CE001	fine-grained	25	-	-	-	-	25	1	5	-	6	10	-	1	0.1	20	3	-	10	-	-
	11CLD001	amygd.	21	-	-	-	-	30	10	1	-	-	1	-	9	3	25	-	-	-	-	-
	10SE002	amygd.	10	-	-	-	-	10	5	0.1	-	-	10	0.1	25	-	10	-	-	-	-	30
	10DE003	amygd.	5	-	-	-	-	25	0.1	45	-	-	2	-	-	-	20	1	-	-	-	-
	11CLD007	fine-grained	2	-	-	-	-	20	1	24	-	1	-	25	1	0.1	25	1	-	-	-	-
N/A	10TO004	amygd.	1	-	-	-	-	-	15	1	-	-	-	64	-	-	20	-	-	-	-	-
	11CLD005	very fine-grained	-	-	-	-	-	-	25	-	-	-	-	-	10	-	-	-	-	-	-	65

APPENDIX G: COMPLETE EDS MICROPROBE ANALYSES

Complete sets of electron microprobe analyses for olivine, amphibole, mica group minerals, copper sulfide minerals, zeolite minerals, sphene, and apatite are included in the text of this thesis. For minerals with abundant data points (i.e., feldspar, pyroxene, chlorite, epidote, pumpellyite, prehnite, and carbonate minerals), only a small set of representative analyses is included with the text and the complete set of analyses is included in this Appendix.

Table G-1: Electron microprobe analyses of feldspar group minerals.
Cation recalculations based on eight oxygen atoms PFU.

Sample	11CLD001 10-22_032	11CLD001 10-22_034	11CLD001 10-22_036	11CLD001 10-22_037	11CLD001 10-22_039	11CLD001 10-29_33	11CLD001 10-29_34	11CLD001 10-29_36	11CLD001 10-29_37	11CLD001 10-29_38
Na_2O	11.3	11.2	11.1	-*	11.4	10.4	-*	-*	10.7	-*
MgO	-**	-**	-**	-**	-**	-**	-**	0.6	-**	-**
Al_2O_3	19.6	19.6	19.7	18.3	19.4	19.6	18.4	18.4	20.0	18.2
SiO_2	69.1	68.3	69.2	65.8	69.2	68.9	65.8	65.2	68.9	65.7
K_2O	-*	0.3	-*	15.9	-*	1.1	15.8	15.8	0.4	16.2
CaO	-*	-*	-*	-*	-*	-*	-*	-*	-*	-*
TiO_2	-**	-**	-**	-**	-**	-**	-**	-**	-**	-**
FeO	-**	0.6	-**	-**	-**	-**	-**	-**	-**	-**
BaO	-**	-**	-**	-**	-**	-**	-**	-**	-**	-**
∑	100.0	100.0	100.0	100.0	100.0	100.0	100.0	100.0	100.0	100.1
Si	3.0	3.0	3.0	3.0	3.0	3.0	3.0	3.0	3.0	3.0
Al	1.0	1.0	1.0	1.0	1.0	1.0	1.0	1.0	1.0	1.0
∑	4.0	4.0	4.0	4.0	4.0	4.0	4.0	4.0	4.0	4.0
Na	1.0	1.0	0.9	-	1.0	0.9	-	-	0.9	-
Ca	-	-	-	-	-	-	-	-	-	-
K	-	-	-	0.9	-	0.1	0.9	0.9	-	1.0
Mg	-	-	-	-	-	-	-	-	-	-
Ba	-	-	-	-	-	-	-	-	-	-
Fe^{2+}	-	-	-	-	-	-	-	-	-	-
∑	1.0	1.0	0.9	0.9	1.0	1.0	0.9	0.9	0.9	1.0
Xan	0	0	0	0	0	0	0	0	0	0
Xab	100	98	100	0	100	93	0	0	98	0
Xor	0	2	0	100	0	7	100	100	2	100

*below detection limit, **not analyzed

Table G-1 (continued): Electron microprobe analyses of feldspar group minerals.
Cation recalculations based on eight oxygen atoms PFU.

Sample	11CLD001 10-29_41	11CLD001 10-29_42	11CLD001 10-29_45	11CLD001 10-29_49	11CLD001 10-29_50	11CLD001 10-29_51	11CLD001 10-29_53	11CLD001 10-29_54	11CLD003 10-29_11	11CLD003 10-29_12	11CLD003 10-29_13
Na_2O	11.1	10.3	5.1	-*	-*	11.2	10.2	11.0	11.3	11.0	10.6
MgO	-*	-*	1.2	-**	-**	-**	-**	-**	-**	-**	1.7
Al_2O_3	19.5	19.5	18.8	18.2	18.1	19.3	19.7	19.5	20.0	19.8	19.6
SiO_2	68.8	66.8	65.7	65.7	65.6	69.6	68.6	69.1	68.3	69.2	66.7
K_2O	-*	1.0	9.2	16.1	16.3	-*	1.5	0.3	-*	-*	-*
CaO	-*	0.5	-*	-*	-*	-*	-*	-*	0.3	-*	-*
TiO_2	-**	-**	-**	-**	-**	-**	-**	-**	-**	-**	-**
FeO	0.7	1.9	-**	-**	-**	-**	-**	-**	-**	-**	1.4
BaO	-*	-**	-**	-**	-**	-**	-**	-**	-**	-**	-**
∑	100.1	100.0	100.0	100.0	100.0	100.1	100.0	99.9	99.9	100.0	100.0
Si	3.0	3.0	3.0	3.0	3.0	3.0	3.0	3.0	3.0	3.0	2.9
Al	1.0	1.0	1.0	1.0	1.0	1.0	1.0	1.0	1.0	1.0	1.0
∑	4.0	4.0	4.0	4.0	4.0	4.0	4.0	4.0	4.0	4.0	4.0
Na	0.9	0.9	0.5	-	-	0.9	0.9	0.9	1.0	0.9	0.9
Ca	-	-	-	-	-	-	-	-	-	-	-
K	-	0.1	0.5	1.0	1.0	-	0.1	-	-	-	-
Mg	-	-	0.1	-	-	-	-	-	-	-	0.1
Ba		-	-	-	-	-	-	-	-	-	-
Fe^{2+}	-	0.1	-	-	-	-	-	-	-	-	0.1
∑	0.9	1.1	1.1	1.0	1.0	0.9	0.9	0.9	1.0	0.9	1.1
Xan	0	2	0	0	0	0	0	0	3	0	0
Xab	100	92	46	0	0	100	91	98	97	100	100
Xor	0	6	54	100	100	0	9	2	0	0	0

*below detection limit, **not analyzed

Table G-1 (continued): Electron microprobe analyses of feldspar group minerals.
Cation recalculations based on eight oxygen atoms PFU.

Sample	11CLD003 10-29_18	11CLD003 10-29_19	11CLD003 10-29_21	11CLD003 10-29_28	11CLD003 10-29_29	11CLD003 10-29_31	11CLD003 10-29_32	11CBF006 11-06_019	11CBF006 11-06_020	11CBF006 11-06_021	11CBF006 11-06_027
Na_2O	11.1	11.0	11.2	7.8	11.1	11.1	10.8	11.4	11.2	11.5	11.4
MgO	-**	-**	-**	-**	-**	-**	-**	-**	-**	-**	-**
Al_2O_3	19.7	19.4	19.6	19.5	19.3	19.8	19.8	19.7	19.6	19.3	19.6
SiO_2	69.3	69.0	68.8	68.4	68.6	69.2	69.4	68.9	69.2	69.2	69.0
K_2O	-*	0.6	-*	4.4	0.5	-*	-*	-*	-*	-*	-*
CaO	-*	-*	0.4	-*	0.6	-*	-*	-*	-*	-*	-*
TiO_2	-**	-**	-**	-**	-**	-**	-**	-**	-**	-**	-**
FeO	-**	-**	-**	-**	-**	-**	-**	-**	-**	-**	-**
BaO	-**	-**	-**	-**	-**	-**	-**	-**	-**	-**	-**
∑	100.1	100.0	100.0	100.1	100.1	100.1	100.0	100.0	100.0	100.0	100.0
Si	3.0	3.0	3.0	3.0	3.0	3.0	3.0	3.0	3.0	3.0	3.0
Al	1.0	1.0	1.0	1.0	1.0	1.0	1.0	1.0	1.0	1.0	1.0
∑	4.0	4.0	4.0	4.0	4.0	4.0	4.0	4.0	4.0	4.0	4.0
Na	0.9	0.9	1.0	0.7	0.9	0.9	0.9	1.0	0.9	1.0	1.0
Ca	-	-	-	-	-	-	-	-	-	-	-
K	-	-	-	0.3	-	-	-	-	-	-	-
Mg	-	-	-	-	-	-	-	-	-	-	-
Ba	-	-	-	-	-	-	-	-	-	-	-
Fe^{2+}	-	-	-	-	-	-	-	-	-	-	-
∑	0.9	0.9	1.0	1.0	0.9	0.9	0.9	1.0	0.9	1.0	1.0
Xan	0	0	0	0	0	0	0	0	0	0	0
Xab	100	97	100	73	97	100	100	100	100	100	100
Xor	0	3	0	27	3	0	0	0	0	0	0

*below detection limit, **not analyzed

Table G-1 (continued): Electron microprobe analyses of feldspar group minerals.
Cation recalculations based on eight oxygen atoms PFU.

Sample	11CBF006 11-06_030	11CBF006 11-06_032	11CBF006 11-06_038	11CBF006 11-06_039	11CBF006 11-06_040	11CBF006 11-06_042	11CBF006 11-06_047	11CBF006 11-06_048	11CBF006 11-06_051	11CBF006 11-06_052
Na_2O	11.2	-*	10.9	11.4	2.0	11.6	11.6	11.2	11.5	11.4
MgO	-**	-**	-**	-**	-**	-**	-**	-**	-**	-**
Al_2O_3	19.7	20.1	19.7	19.8	18.5	19.5	19.5	19.7	19.5	19.5
SiO_2	69.1	63.5	68.7	68.9	65.5	69.0	69.0	69.1	69.0	69.1
K_2O	-*	15.3	0.7	-*	14.0	-*	-*	-*	-*	-*
CaO	-*	-*	-*	-*	-*	-*	-*	-*	-*	-*
TiO_2	-**	-**	-**	-**	-**	-**	-**	-**	-**	-**
FeO	-**	1.1	-**	-**	-**	-**	-**	-**	-**	-**
BaO	-**	-**	-**	-**	-**	-**	-**	-**	-**	-**
∑	100.0	100.0	100.0	100.1	100.0	100.1	100.1	100.0	100.0	100.0
Si	3.0	2.9	3.0	3.0	3.0	3.0	3.0	3.0	3.0	3.0
Al	1.0	1.1	1.0	1.0	1.0	1.0	1.0	1.0	1.0	1.0
∑	4.0	4.0	4.0	4.0	4.0	4.0	4.0	4.0	4.0	4.0
Na	0.9	-	0.9	1.0	0.2	1.0	1.0	0.9	1.0	1.0
Ca	-	-	-	-	-	-	-	-	-	-
K	-	0.9	-	-	0.8	-	-	-	-	-
Mg	-	-	-	-	-	-	-	-	-	-
Ba	-	-	-	-	-	-	-	-	-	-
Fe^{2+}	-	-	-	-	-	-	-	-	-	-
∑	0.9	0.9	0.9	1.0	1.0	1.0	1.0	0.9	1.0	1.0
Xan	0	0	0	0	0	0	0	0	0	0
Xab	100	0	96	100	18	100	100	100	100	100
Xor	0	100	4	0	82	0	0	0	0	0

*below detection limit, **not analyzed

Table G-1 (continued): Electron microprobe analyses of feldspar group minerals.
Cation recalculations based on eight oxygen atoms PFU.

Sample	11CBF006 11-06_055	11CBF006 11-06_056	11CBF006 -5-1-4	11CBF006 -5-1-5	11CBF006 -5-1-6	11CLD007 11-06_060	11CLD007 11-06_061	11CLD007 11-06_062	11CLD007 11-06_064	11CLD007 11-06_068
Na_2O	11.4	11.3	9.3	8.7	9.6	10.9	-*	11.1	0.7	-*
MgO	-**	-**	-**	-**	-**	-**	-**	-**	-**	-**
Al_2O_3	19.4	19.4	19.9	20.0	19.5	19.6	18.5	19.6	18.4	18.6
SiO_2	69.2	69.2	70.1	71.0	70.7	67.3	65.7	69.3	65.3	65.7
K_2O	-*	-*	0.4	-*	-*	0.8	15.8	-*	15.7	15.7
CaO	-*	-*	0.2	0.3	-*	-*	-*	-*	-*	-*
TiO_2	-**	-**	-**	-**	-**	-**	-**	-**	-**	-**
FeO	-**	-**	-**	-**	0.2	1.4	-**	-**	-**	-**
BaO	-**	-**	-**	-**	-**	-**	-**	-**	-**	-**
∑	100.0	99.9	99.9	100.0	100.0	100.0	100.0	100.0	100.1	100.0
Si	3.0	3.0	3.0	3.1	3.1	3.0	3.0	3.0	3.0	3.0
Al	1.0	1.0	1.0	1.0	1.0	1.0	1.0	1.0	1.0	1.0
∑	4.0	4.0	4.0	4.1	4.1	4.0	4.0	4.0	4.0	4.0
Na	1.0	1.0	0.8	0.7	0.8	0.9	-	0.9	0.1	-
Ca	-	-	-	-	-	-	-	-	-	-
K	-	-	-	-	-	-	0.9	-	0.9	0.9
Mg	-	-	-	-	-	-	-	-	-	-
Ba	-	-	-	-	-	-	-	-	-	-
Fe^{2+}	-	-	-	-	-	0.1	-	-	-	-
∑	1.0	1.0	0.8	0.7	0.8	1.0	0.9	0.9	1.0	0.9
Xan	0	0	0	0	0	0	0	0	0	0
Xab	100	100	97	100	100	95	0	100	6	0
Xor	0	0	3	0	0	5	100	0	94	100

*below detection limit, **not analyzed

Table G-1 (continued): Electron microprobe analyses of feldspar group minerals.
Cation recalculations based on eight oxygen atoms PFU.

Sample	11CLD007 11-06_069	11CLD007 11-06_071	11CLD007 11-06_072	11CLD007 11-06_073	11CLD007 11-06_074	11CLD007 11-06_081	11LCD007 11-06_082	11CLD007 11-06_084	11CLD007 11-06_085	11CLD007 11-06_091
Na_2O	10.9	10.8	1.2	-*	10.9	-*	-*	11.2	-*	11.3
MgO	-**	-**	-**	-**	-**	-**	-**	-**	-**	-**
Al_2O_3	19.7	19.7	18.7	18.4	19.7	18.5	18.3	19.5	18.3	19.6
SiO_2	68.9	69.0	65.6	65.6	69.4	65.6	65.7	69.3	65.7	67.9
K_2O	0.6	0.5	14.6	16.0	-*	16.0	15.9	-*	16.0	-*
CaO	-*	-*	-*	-*	-*	-*	-*	-*	-*	0.5
TiO_2	-**	-**	-**	-**	-**	-**	-**	-**	-**	-**
FeO	-**	-**	-**	-**	-**	-**	-**	-**	-**	0.8
BaO	-**	-**	-**	-**	-**	-**	-**	-**	-**	-**
∑	100.1	100.0	100.1	100.0	100.0	100.1	99.9	100.0	100.0	100.0
Si	3.0	3.0	3.0	3.0	3.0	3.0	3.0	3.0	3.0	3.0
Al	1.0	1.0	1.0	1.0	1.0	1.0	1.0	1.0	1.0	1.0
∑	4.0	4.0	4.0	4.0	4.0	4.0	4.0	4.0	4.0	4.0
Na	0.9	0.9	0.1	-	0.9	-	-	0.9	-	1.0
Ca	-	-	-	-	-	-	-	-	-	-
K	-	-	0.9	0.9	-	0.9	0.9	-	0.9	-
Mg	-	-	-	-	-	-	-	-	-	-
Ba	-	-	-	-	-	-	-	-	-	-
Fe^{2+}	-	-	-	-	-	-	-	-	-	-
∑	0.9	0.9	1.0	0.9	0.9	0.9	0.9	0.9	0.9	1.0
Xan	0	0	0	0	0	0	0	0	0	1
Xab	97	97	11	0	100	0	0	100	0	99
Xor	3	3	89	100	0	100	100	0	100	0

*below detection limit, **not analyzed

Table G-1 (continued): Electron microprobe analyses of feldspar group minerals.
Cation recalculations based on eight oxygen atoms PFU.

Sample	11CLD007 11-06_092	11CLD007 11-06_094	11CLD007 11-06_097	11CLD007 11-06_098	11CLD007 -7-1-1	11CLD007 -7-1-2	11CLD007 -7-1-3	11CLD007 -7-1-4	11CLD007 -7-1-5	11CLD007 -7-1-6	11CBF004 -004
Na_2O	-*	-*	-*	-*	8.8	8.2	9.0	-*	-*	-*	10.6
MgO	-**	-**	-**	-**	-**	-**	-**	-**	-**	-**	-*
Al_2O_3	18.9	18.3	18.6	18.5	19.7	19.7	19.7	18.6	18.4	18.6	19.4
SiO_2	65.6	65.6	65.5	65.5	71.2	70.8	70.9	67.5	67.5	67.4	70.1
K_2O	15.5	16.0	15.9	16.0	-*	0.9	-*	14.0	13.9	13.6	-*
CaO	-*	-*	-*	-*	0.3	0.4	0.4	-*	-*	-*	-*
TiO_2	-**	-**	-**	-**	-**	-**	-**	-**	0.1	-**	-**
FeO	-**	-**	-**	-**	-**	-**	-**	-**	-**	-**	-**
BaO	-**	-**	-**	-**	-**	-**	-**	-**	-**	0.5	-**
∑	100.0	99.9	100.0	100.0	100.0	100.0	100.0	100.1	99.9	100.1	100.1
Si	3.0	3.0	3.0	3.0	3.1	3.1	3.1	3.1	3.1	3.1	3.0
Al	1.0	1.0	1.0	1.0	1.0	1.0	1.0	1.0	1.0	1.0	1.0
∑	4.0	4.0	4.0	4.0	4.1	4.1	4.1	4.1	4.1	4.1	4.0
Na	-	-	-	-	0.7	0.7	0.8	-	-	-	0.9
Ca	-	-	-	-	-	-	-	-	-	-	-
K	0.9	0.9	0.9	0.9	-	0.1	-	0.8	0.8	0.8	-
Mg	-	-	-	-	-	-	-	-	-	-	-
Ba	-	-	-	-	-	-	-	-	-	-	-
Fe^{2+}	-	-	-	-	-	-	-	-	-	-	-
∑	0.9	0.9	0.9	0.9	0.7	0.8	0.8	0.8	0.8	0.8	0.9
Xan	0	0	0	0	0	0	0	0	0	0	0
Xab	0	0	0	0	100	93	100	0	0	0	100
Xor	100	100	100	100	0	7	0	100	100	100	0

*below detection limit, **not analyzed

Table G-1 (continued): Electron microprobe analyses of feldspar group minerals.
Cation recalculations based on eight oxygen atoms PFU.

Sample	11CBF004-005	11CBF004-006	11CBF004-007	11CBF004-008	11CBF004-014	11CBF004-018	11CBF004-024	11CBF004-025	11CBF004-030	11CBF004-032	11CBF004-3-2-4
Na_2O	10.4	10.4	1.7	2.8	10.2	10.3	1.0	1.9	10.5	10.3	6.1
MgO	-**	-**	-**	-**	1.6	-**	-**	-**	-**	-**	-**
Al_2O_3	19.7	19.7	19.0	18.9	19.4	19.3	18.2	18.5	19.4	19.9	19.6
SiO_2	69.5	70.0	66.2	65.6	66.6	69.6	65.0	65.4	70.1	69.2	68.6
K_2O	-*	-*	13.2	12.8	-*	0.8	15.3	14.2	-*	-*	5.7
CaO	0.4	-*	-*	-*	0.5	-*	-*	-*	-*	0.6	-*
TiO_2	-**	-**	-**	-**	-**	-**	0.5	-**	-**	-**	-**
FeO	-**	-**	-**	-**	1.9	-**	-**	-**	-**	-**	-**
BaO	-**	-**	-**	-**	-**	-**	-**	-**	-**	-**	-**
∑	100.0	100.1	100.1	100.1	100.2	100.0	100.0	100.0	100.0	100.0	100.0
Si	3.0	3.0	3.0	3.0	2.9	3.0	3.0	3.0	3.0	3.0	3.0
Al	1.0	1.0	1.0	1.0	1.0	1.0	1.0	1.0	1.0	1.0	1.0
∑	4.0	4.0	4.0	4.0	3.9	4.0	4.0	4.0	4.0	4.0	4.0
Na	0.9	0.9	0.2	0.3	0.9	0.9	0.1	0.2	0.9	0.9	0.5
Ca	-	-	-	-	-	-	-	-	-	-	-
K	-	-	0.8	0.7	-	-	0.9	0.8	-	-	0.3
Mg	-	-	-	-	0.1	-	-	-	-	-	-
Ba	-	-	-	-	-	-	-	-	-	-	-
Fe^{2+}	-	-	-	-	0.1	-	-	-	-	-	-
∑	0.9	0.9	0.9	1.0	1.1	0.9	1.0	1.0	0.9	0.9	0.8
Xan	0	0	0	0	2	0	0	0	0	1	0
Xab	100	100	16	25	98	95	9	17	100	99	62
Xor	0	0	84	75	0	5	91	83	0	0	38

*below detection limit, **not analyzed

Table G-1 (continued): Electron microprobe analyses of feldspar group minerals.
Cation recalculations based on eight oxygen atoms PFU.

Sample	11CBF004 -3-2-5	11CBF004 -3-2-6	11CBF004 -8-1-7	11CBF004 -8-1-8	11CBF004 -8-1-9	10CN002 -1-2-1	10CN002 -1-2-2	10CN002 -1-2-3	10CN002 -1-5-1	10CN002 -1-5-2	10CN002 -1-5-3
Na_2O	7.6	8.6	8.7	8.5	8.4	8.8	8.9	9.6	8.7	9.4	8.9
MgO	-**	-**	-**	-**	-**	0.5	-**	-**	-**	-**	-**
Al_2O_3	21.1	20.0	20.2	20.0	20.3	20.9	19.8	19.8	21.6	20.1	20.7
SiO_2	69.6	70.9	70.5	70.7	70.3	66.3	70.4	70.3	69.4	70.4	70.3
K_2O	1.0	0.3	-*	0.4	-*	-*	-*	-*	-*	-*	-*
CaO	0.8	0.3	0.6	0.5	0.6	3.1	0.4	0.2	0.3	0.2	0.1
TiO_2	-**	-**	-**	-**	-**	-**	0.2	-**	-**	-**	-**
FeO	-**	-**	-**	-**	0.4	0.4	0.3	0.2	-**	-**	-**
BaO	-**	-**	-**	-**	-**	-**	-**	-**	-**	-**	-**
∑	100.1	100.1	100.0	100.0	100.0	100.0	100.0	100.1	100.0	100.1	100.0
Si	3.0	3.1	3.0	3.0	3.0	2.9	3.0	3.0	3.0	3.0	3.0
Al	1.1	1.0	1.0	1.0	1.0	1.1	1.0	1.0	1.1	1.0	1.1
∑	4.1	4.1	4.1	4.1	4.1	4.0	4.0	4.0	4.1	4.1	4.1
Na	0.6	0.7	0.7	0.7	0.7	0.8	0.7	0.8	0.7	0.8	0.7
Ca	-	-	-	-	-	0.2	-	-	-	-	-
K	0.1	-	-	-	-	-	-	-	-	-	-
Mg	-	-	-	-	-	-	-	-	-	-	-
Ba	-	-	-	-	-	-	-	-	-	-	-
Fe^{2+}	-	-	-	-	-	-	-	-	-	-	-
∑	0.7	0.7	0.8	0.8	0.7	1.0	0.7	0.8	0.7	0.8	0.7
Xan	5	0	0	0	1	8	0	0	7	0	3
Xab	88	98	100	97	99	92	100	100	93	100	97
Xor	7	2	0	3	0	0	0	0	0	0	0

*below detection limit, **not analyzed

Table G-1 (continued): Electron microprobe analyses of feldspar group minerals.
Cation recalculations based on eight oxygen atoms PFU.

Sample	10CN002 -2-1-9	10CN002 -2-1-10	10CN002 -2-1-11	10CN002 -2-2-4	10CN002 -2-2-5	10CN002 -2-2-6	10CN002 -2-2-7	10CN002 -2-2-8	10CN002 -2-2-9	10CN002 -4-3-4	10CN002 -4-3-5
Na_2O	10.2	10.2	10.7	1.5	-*	-*	9.3	9.4	9.3	9.4	10.0
MgO	-**	-**	-**	-**	1.5	0.7	-**	-**	-**	-**	0.0
Al_2O_3	19.6	19.8	19.5	24.4	30.3	30.5	19.6	19.8	20.0	19.8	19.7
SiO_2	70.0	69.8	69.6	51.5	42.7	43.2	70.7	70.7	70.3	70.7	70.0
K_2O	-*	-*	-*	-*	-*	-*	-*	-*	-*	-*	-*
CaO	0.1	0.2	0.2	21.7	23.1	23.0	0.2	0.1	0.2	0.1	0.2
TiO_2	-**	-**	-**	-**	-**	-**	-**	-**	-**	-**	-**
FeO	-**	-**	-**	1.0	2.4	2.6	0.2	-**	0.1	-**	-**
BaO	-**	-**	-**	-**	-**	-**	-**	-**	-**	-**	-**
∑	99.9	100.0	100.0	100.1	100.0	100.0	100.0	100.0	99.9	100.0	99.9
Si	3.0	3.0	3.0	2.4	2.0	2.1	3.1	3.1	3.0	3.1	3.0
Al	1.0	1.0	1.0	1.3	1.7	1.7	1.0	1.0	1.0	1.0	1.0
∑	4.0	4.0	4.0	3.7	3.7	3.8	4.1	4.1	4.0	4.1	4.0
Na	0.9	0.9	0.9	0.1	-	-	0.8	0.8	0.8	0.8	0.8
Ca	-	-	-	1.1	1.2	1.2	-	-	-	-	-
K	-	-	-	-	-	-	-	-	-	-	-
Mg	-	-	-	-	0.1	0.1	-	-	-	-	-
Ba	-	-	-	-	-	-	-	-	-	-	-
Fe^{2+}	-	-	-	-	0.1	0.1	-	-	-	-	-
∑	0.9	0.9	0.9	1.2	1.4	1.4	0.8	0.8	0.8	0.8	0.8
Xan	0	0	0	43	82	82	0	0	0	0	0
Xab	100	100	100	57	18	18	100	100	100	100	100
Xor	0	0	0	0	0	0	0	0	0	0	0

*below detection limit, **not analyzed

Table G-1 (continued): Electron microprobe analyses of feldspar group minerals.
Cation recalculations based on eight oxygen atoms PFU.

Sample	10CN002 -4-3-6	10CN002 -5-2-4	10CN002 -5-2-5	10CN002 -5-2-6	10CN002 -5-2-13	10CN002 -5-2-14	10CN002 -6-1-1	10CN002 -6-1-2	10CN002 -6-1-3	10CN002 -6-1-4	10CN002 -6-2-7
Na_2O	10.8	9.1	9.2	9.2	8.2	6.8	10.3	9.8	9.3	9.5	9.9
MgO	-*	-*	-*	-*	-*	-*	-*	-*	-*	-*	-*
Al_2O_3	19.7	19.9	20.1	20.1	19.6	19.7	19.6	19.7	20.0	19.8	19.7
SiO_2	69.4	70.8	70.6	70.6	71.3	73.3	70.2	70.5	70.6	70.8	70.4
K_2O	-*	-*	-*	-*	-*	-*	-*	-*	-*	-*	-*
CaO	0.2	0.2	0.2	0.2	0.4	0.2	-*	-*	-*	-*	-*
TiO_2	-**	-**	-**	-**	0.2	-**	-**	-**	-**	-**	-**
FeO	-**	-**	-**	-**	0.3	-**	-**	-**	-**	-**	-**
BaO	-**	-**	-**	-**	-**	-**	-**	-**	-**	-**	-**
∑	100.1	100.0	100.1	100.1	100.0	100.0	100.1	100.0	99.9	100.1	100.0
Si	3.0	3.1	3.0	3.0	3.1	3.1	3.0	3.0	3.0	3.1	3.0
Al	1.0	1.0	1.0	1.0	1.0	1.0	1.0	1.0	1.0	1.0	1.0
∑	4.0	4.1	4.0	4.0	4.1	4.1	4.0	4.0	4.0	4.1	4.0
Na	0.9	0.8	0.8	0.8	0.7	0.6	0.9	0.8	0.8	0.8	0.8
Ca	-	-	-	-	-	-	-	-	-	-	-
K	-	-	-	-	-	-	-	-	-	-	-
Mg	-	-	-	-	-	-	-	-	-	-	-
Ba	-	-	-	-	-	-	-	-	-	-	-
Fe^{2+}	-	-	-	-	-	-	-	-	-	-	-
∑	0.9	0.8	0.8	0.8	0.7	0.6	0.9	0.8	0.8	0.8	0.8
Xan	0	0	0	0	0	0	0	0	0	0	0
Xab	100	100	100	100	100	100	100	100	100	100	100
Xor	0	0	0	0	0	0	0	0	0	0	0

*below detection limit, **not analzyed

Table G-1 (continued): Electron microprobe analyses of feldspar group minerals.
Cation recalculations based on eight oxygen atoms PFU.

Sample	10CN002 -6-2-8	10CN002 -6-2-9	10QU006 -2-2-4	10QU006 -2-2-5	10QU006 -2-2-6	10QU006 -3-1-1	10QU006 -3-1-2	10QU006 -3-1-3	10QU006 -3-1-7	10QU006 -3-1-8	10QU006 -3-1-9
Na_2O	9.2	9.1	-*	-*	-*	11.1	11.0	9.6	-*	-*	-*
MgO	-**	-**	-**	-**	-**	-**	-**	-**	-**	-**	-**
Al_2O_3	19.8	19.8	25.5	25.6	26.0	19.6	19.8	20.0	19.0	18.8	18.9
SiO_2	70.7	70.6	47.9	47.7	47.5	69.2	69.0	70.1	66.7	66.7	65.8
K_2O	-*	-*	-*	-*	-*	-*	-*	-*	13.8	14.0	14.4
CaO	0.2	0.2	26.2	26.0	26.3	-*	-*	-*	-*	-*	-*
TiO_2	-**	-**	-**	-**	-**	-**	-**	-**	-**	-**	-**
FeO	-**	0.4	0.4	0.6	0.2	0.2	0.2	0.4	-**	-**	-**
BaO	-**	-**	-**	-**	-**	-**	-**	-**	0.6	0.5	0.9
∑	99.9	100.1	100.0	99.9	100.0	100.1	100.0	100.0	100.1	100.0	100.0
Si	3.1	3.0	2.3	2.3	2.2	3.0	3.0	3.0	3.0	3.0	3.0
Al	1.0	1.0	1.4	1.4	1.5	1.0	1.0	1.0	1.0	1.0	1.0
∑	4.1	4.0	3.7	3.7	3.7	4.0	4.0	4.0	4.0	4.0	4.0
Na	0.8	0.8	-	-	-	0.9	0.9	0.8	-	-	-
Ca	-	-	1.3	1.3	1.3	-	-	-	-	-	-
K	-	-	-	-	-	-	-	-	0.8	0.8	0.8
Mg	-	-	-	-	-	-	-	-	-	-	-
Ba	-	-	-	-	-	-	-	-	-	-	-
Fe^{2+}	-	-	-	-	-	-	-	-	-	-	-
∑	0.8	0.8	1.3	1.3	1.3	0.9	0.9	0.8	0.8	0.8	0.8
Xan	0	0	54	55	57	0	0	0	0	0	0
Xab	100	100	46	45	43	100	100	100	0	0	0
Xor	0	0	0	0	0	0	0	0	100	100	100

*below detection limit, **not analyzed

Table G-1 (continued): Electron microprobe analyses of feldspar group minerals.
Cation recalculations based on eight oxygen atoms PFU.

Sample	10QU006 -4-1-4	10QU006 -4-1-5	10QU006 -4-1-6	10QU006 -6-1-7	10QU006 -6-1-8	10QU006 -6-1-9	10SC004 -1-1-1	10SC004 -1-1-2	10SC004 -1-1-3	10SC004 -1-2-8	10SC004 -1-2-9
Na_2O	11.7	9.5	10.1	8.9	11.3	11.6	3.0	3.2	3.2	2.8	3.0
MgO	-**	-**	-**	-**	-**	-**	0.1	-**	0.1	-**	-**
Al_2O_3	19.4	19.7	19.7	19.8	19.8	19.5	31.8	31.7	31.7	32.1	31.8
SiO_2	68.9	70.8	70.2	71.0	68.8	68.7	49.9	50.1	50.2	49.8	50.1
K_2O	-*	-*	-*	-*	-*	-*	-*	-*	-*	-*	-*
CaO	-*	-*	-*	0.1	0.2	0.1	14.6	14.4	14.2	14.8	14.7
TiO_2	-**	-**	-**	-**	-**	-**	-**	-**	-**	-**	-**
FeO	-**	-**	-**	0.2	-**	-**	0.5	0.6	0.6	0.6	0.5
BaO	-**	-**	-**	-**	-**	-**	-**	-**	-**	-**	-**
∑	100.0	100.0	100.0	100.0	100.1	99.9	100.0	100.0	100.0	100.1	100.1
Si	3.0	3.1	3.0	3.1	3.0	3.0	2.3	2.3	2.3	2.3	2.3
Al	1.0	1.0	1.0	1.0	1.0	1.0	1.7	1.7	1.7	1.7	1.7
∑	4.0	4.1	4.0	4.1	4.0	4.0	4.0	4.0	4.0	4.0	4.0
Na	1.0	0.8	0.9	0.8	1.0	1.0	0.3	0.3	0.3	0.3	0.3
Ca	-	-	-	-	-	-	0.7	0.7	0.7	0.7	0.7
K	-	-	-	-	-	-	-	-	-	-	-
Mg	-	-	-	-	-	-	-	-	-	-	-
Ba	-	-	-	-	-	-	-	-	-	-	-
Fe^{2+}	-	-	-	-	-	-	-	-	-	-	-
∑	1.0	0.8	0.9	0.8	1.0	1.0	1.0	1.0	1.0	1.0	1.0
Xan	0	0	0	0	1	0	72	71	71	73	71
Xab	100	100	100	100	99	100	28	29	29	27	29
Xor	0	0	0	0	0	0	0	0	0	0	0

*below detection limit, **not analyzed

Table G-1 (continued): Electron microprobe analyses of feldspar group minerals.
Cation recalculations based on eight oxygen atoms PFU.

Sample	10SC004 -1-2-10	10SC004 -2-1-7	10SC004 -2-1-8	10SC004 -2-1-9	10SC004 -2-2-10	10SC004 -2-2-11	10SC004 -2-2-12	10SC004 -3-1-1	10SC004 -3-1-2	10SC004 -3-1-3	10SC004 -3-1-5
Na_2O	4.6	4.7	4.9	5.1	4.2	4.6	4.9	2.8	2.7	3.1	4.3
MgO	-**	-**	-**	-**	-**	-**	-**	-**	-**	-**	-**
Al_2O_3	29.2	29.4	28.4	28.4	29.3	28.5	28.7	32.2	32.5	31.9	30.0
SiO_2	54.0	54.1	55.4	55.1	53.8	55.7	54.4	49.7	49.5	50.0	53.4
K_2O	-*	-*	-*	-*	-*	-*	-*	-*	-*	-*	-*
CaO	11.7	11.3	10.6	10.6	12.0	10.7	11.4	14.8	14.9	14.5	12.4
TiO_2	-**	-**	-**	-**	-**	-**	-**	-**	-**	-**	-**
FeO	0.6	0.6	0.7	0.8	0.8	0.7	0.7	0.6	0.5	0.6	-**
BaO	-**	-**	-**	-**	-**	-**	-**	-**	-**	-**	-**
∑	100.1	100.1	100.0	100.0	100.1	100.2	100.1	100.1	100.1	100.1	100.1
Si	2.4	2.4	2.5	2.5	2.4	2.5	2.5	2.3	2.3	2.3	2.4
Al	1.6	1.6	1.5	1.5	1.6	1.5	1.5	1.7	1.8	1.7	1.6
∑	4.0	4.0	4.0	4.0	4.0	4.0	4.0	4.0	4.1	4.0	4.0
Na	0.4	0.4	0.4	0.4	0.4	0.4	0.4	0.2	0.2	0.3	0.4
Ca	0.6	0.6	0.5	0.5	0.6	0.5	0.6	0.7	0.7	0.7	0.6
K	-	-	-	-	-	-	-	-	-	-	-
Mg	-	-	-	-	-	-	-	-	-	-	-
Ba	-	-	-	-	-	-	-	-	-	-	-
Fe^{2+}	-	-	-	-	-	-	-	-	-	-	-
∑	1.0	1.0	0.9	0.9	1.0	0.9	1.0	0.9	0.9	1.0	1.0
Xan	56	56	50	51	56	50	53	74	75	72	59
Xab	44	44	50	49	44	50	47	26	25	28	41
Xor	0	0	0	0	0	0	0	0	0	0	0

*below detection limit, **not analyzed

Table G-1 (continued): Electron microprobe analyses of feldspar group minerals.
Cation recalculations based on eight oxygen atoms PFU.

Sample	10SC004 -3-1-6	10SC004 -3-1-7	10SC004 -4-1-10	10SC004 -4-1-11	10SC004 -4-1-12	10SC004 -4-2-10	10SC004 -4-2-11	10SC004 -4-2-12	10SC004 -5-1-7	10SC004 -5-1-8	10SC004 -5-1-9
Na_2O	4.7	4.5	4.5	4.8	4.2	4.5	5.0	4.7	4.7	4.5	5.8
MgO	-**	-**	-**	-**	-**	-**	-**	-**	-**	-**	0.2
Al_2O_3	29.1	29.5	29.0	28.8	29.6	29.2	28.4	28.7	29.2	29.2	23.3
SiO_2	53.8	53.5	54.5	54.6	53.5	53.7	55.1	54.4	54.2	53.6	64.5
K_2O	-*	-*	-*	-*	-*	-*	-*	0.2	-*	-*	-*
CaO	11.6	11.9	11.4	11.2	11.9	11.7	10.7	11.4	11.3	11.9	5.8
TiO_2	0.2	-**	-**	-**	-**	0.2	0.1	-**	-**	-**	-**
FeO	0.7	0.6	0.6	0.7	0.7	0.8	0.7	0.7	0.7	0.9	0.6
BaO	-**	-**	-**	-**	-**	-**	-**	-**	-**	-**	-**
∑	100.1	100.0	100.0	100.1	99.9	100.1	100.0	100.1	100.1	100.1	100.2
Si	2.4	2.4	2.5	2.5	2.4	2.4	2.5	2.5	2.5	2.4	2.8
Al	1.6	1.6	1.5	1.5	1.6	1.6	1.5	1.5	1.6	1.6	1.2
∑	4.0	4.0	4.0	4.0	4.0	4.0	4.0	4.0	4.1	4.0	4.0
Na	0.4	0.4	0.4	0.4	0.4	0.4	0.4	0.4	0.4	0.4	0.5
Ca	0.6	0.6	0.6	0.5	0.6	0.6	0.5	0.6	0.6	0.6	0.3
K	-	-	-	-	-	-	-	-	-	-	-
Mg	-	-	-	-	-	-	-	-	-	-	-
Ba	-	-	-	-	-	-	-	-	-	-	-
Fe^{2+}	-	-	-	-	-	-	-	-	-	-	-
∑	1.0	1.0	1.0	0.9	1.0	1.0	0.9	1.0	1.0	1.0	0.8
Xan	56	58	54	53	58	56	51	53	55	56	19
Xab	44	42	46	47	42	44	49	46	45	44	81
Xor	0	0	0	0	0	0	0	1	0	0	0

*below detection limit, **not analyzed

Table G-1 (continued): Electron microprobe analyses of feldspar group minerals.
Cation recalculations based on eight oxygen atoms PFU.

Sample	10SC004 -6-1-10	10SC004 -6-1-11	10SC004 -6-1-12	10SC004 -6-1-14	10SC004 -7-1-7	10SC004 -7-1-8	10SC004 -7-1-9	10SG001 -1-2-4	10SG001 -1-2-5	10SG001 -1-2-6	10SG001 -2-1-4
Na_2O	4.3	3.4	4.7	2.4	4.1	2.2	3.9	4.5	3.5	3.5	2.9
MgO	-**	-**	-**	-**	-**	-**	-**	0.2	-**	0.1	0.1
Al_2O_3	29.5	31.3	29.1	32.6	28.6	31.8	29.2	28.4	30.0	30.2	31.4
SiO_2	53.6	50.7	54.1	48.9	54.0	49.6	53.4	54.5	52.2	51.6	49.6
K_2O	-*	-*	-*	-*	0.3	-*	0.4	-*	-*	-*	-*
CaO	12.0	14.0	11.5	15.5	12.2	15.6	12.4	11.7	13.4	13.9	15.6
TiO_2	-**	-**	-**	-**	-**	-**	-**	-**	-**	-**	-**
FeO	0.6	0.6	0.6	0.7	0.8	0.8	0.8	0.8	0.9	0.7	0.4
BaO	-**	-**	-**	-**	-**	-**	-**	-**	-**	-**	-**
∑	100.0	100.0	100.0	100.1	100.0	100.0	100.1	100.1	100.0	100.0	100.0
Si	2.4	2.3	2.4	2.2	2.5	2.3	2.4	2.5	2.4	2.4	2.3
Al	1.6	1.7	1.6	1.8	1.5	1.7	1.6	1.5	1.6	1.6	1.7
∑	4.0	4.0	4.0	4.0	4.0	4.0	4.0	4.0	4.0	4.0	4.0
Na	0.4	0.3	0.4	0.2	0.4	0.2	0.3	0.4	0.3	0.3	0.3
Ca	0.6	0.7	0.6	0.8	0.6	0.8	0.6	0.6	0.7	0.7	0.8
K	-	-	-	-	-	-	-	-	-	-	-
Mg	-	-	-	-	-	-	-	-	-	-	-
Ba	-	-	-	-	-	-	-	-	-	-	-
Fe^{2+}	-	-	-	-	-	-	-	-	-	-	-
∑	1.0	1.0	1.0	1.0	1.0	1.0	0.9	1.0	1.0	1.0	1.1
Xan	58	69	55	76	54	72	57	52	62	63	71
Xab	42	31	45	24	44	28	41	48	38	37	29
Xor	0	0	0	0	2	0	2	0	0	0	0

*below detection limit, **not analyzed

Table G-1 (continued): Electron microprobe analyses of feldspar group minerals.
Cation recalculations based on eight oxygen atoms PFU.

Sample	10SG001 -2-1-5	10SG001 -2-1-6	10SG001 -2-1-7	10SG001 -2-1-8	10SG001 -2-3-4	10SG001 -2-3-5	10SG001 -2-3-6	10SG001 -3-1-4	10SG001 -3-1-5	10SG001 -3-1-6	10SG001 -3-2-5
Na_2O	2.4	2.4	2.3	2.2	4.3	4.1	4.2	4.1	3.7	3.8	1.7
MgO	0.1	0.2	0.2	0.2	0.1	-**	-**	-**	-**	-**	-**
Al_2O_3	32.2	32.3	31.7	32.1	28.4	28.6	28.5	29.4	29.8	29.7	31.5
SiO_2	48.7	48.6	49.1	49.0	54.5	54.4	54.5	53.0	52.7	52.3	49.1
K_2O	-*	-*	-*	-*	-*	-*	-*	-*	-*	-*	-*
CaO	16.1	16.0	16.3	16.0	12.0	12.2	12.2	12.7	13.3	13.4	16.6
TiO_2	-**	-**	-**	-**	-**	-**	-**	-**	-**	-**	-**
FeO	0.5	0.5	0.5	0.5	0.8	0.7	0.7	0.7	0.6	0.8	1.1
BaO	-**	-**	-**	-**	-**	-**	-**	-**	-**	-**	-**
∑	100.0	100.0	100.1	100.0	100.1	100.0	100.1	99.9	100.1	100.0	100.0
Si	2.2	2.2	2.3	2.2	2.5	2.5	2.5	2.4	2.4	2.4	2.3
Al	1.7	1.7	1.7	1.7	1.5	1.5	1.5	1.6	1.6	1.6	1.7
∑	3.9	3.9	4.0	3.9	4.0	4.0	4.0	4.0	4.0	4.0	4.0
Na	0.2	0.2	0.2	0.2	0.4	0.4	0.4	0.4	0.3	0.3	0.2
Ca	0.8	0.8	0.8	0.8	0.6	0.6	0.6	0.6	0.7	0.7	0.8
K	-	-	-	-	-	-	-	-	-	-	-
Mg	-	-	-	-	-	-	-	-	-	-	-
Ba	-	-	-	-	-	-	-	-	-	-	-
Fe^{2+}	-	-	-	-	-	-	-	-	-	-	-
∑	1.0	1.0	1.0	1.0	1.0	1.0	1.0	1.0	1.0	1.0	1.0
Xan	75	76	73	74	52	53	53	58	60	60	72
Xab	25	24	27	26	48	47	47	42	40	40	28
Xor	0	0	0	0	0	0	0	0	0	0	0

*below detection limit, **not analyzed

Table G-1 (continued): Electron microprobe analyses of feldspar group minerals.
Cation recalculations based on eight oxygen atoms PFU.

Sample	10SG001 -3-2-7	10SG001 -3-2-8	10SG001 -3-2-9	10SG001 -4-2-7	10SG001 -4-2-8	10SG001 -4-2-9	10SG001 -5-1-7	10SG001 -5-1-8	10SG001 -5-1-9	10BB001 -1-2-10	10BB001 -1-2-11
Na_2O	3.5	4.3	3.8	3.6	4.2	4.9	2.7	3.0	4.0	3.9	3.1
MgO	-**	-**	-**	0.1	0.1	-**	-**	-**	-**	-**	0.2
Al_2O_3	29.9	28.5	29.4	29.9	29.1	28.0	31.8	31.4	29.6	29.5	30.9
SiO_2	52.3	54.3	53.1	52.1	53.4	55.2	49.4	49.6	52.6	52.8	50.5
K_2O	-*	-*	-*	-*	-*	-*	-*	-*	-*	-*	-*
CaO	13.5	12.0	12.8	13.6	12.5	11.2	15.5	15.2	13.2	13.0	14.7
TiO_2	-**	-**	-**	-**	-**	-**	-**	-**	-**	-**	-**
FeO	0.8	0.9	0.9	0.8	0.7	0.6	0.6	0.7	0.6	0.8	0.7
BaO	-**	-**	-**	-**	-**	-**	-**	-**	-**	-**	-**
∑	100.0	100.0	100.0	100.1	100.0	99.9	100.0	99.9	100.0	100.0	100.1
Si	2.4	2.5	2.4	2.4	2.4	2.5	2.3	2.3	2.4	2.4	2.3
Al	1.6	1.5	1.6	1.6	1.6	1.5	1.7	1.7	1.6	1.6	1.7
∑	4.0	4.0	4.0	4.0	4.0	4.0	4.0	4.0	4.0	4.0	4.0
Na	0.3	0.4	0.3	0.3	0.4	0.4	0.2	0.3	0.4	0.4	0.3
Ca	0.7	0.6	0.6	0.7	0.6	0.5	0.8	0.8	0.6	0.6	0.7
K	-	-	-	-	-	-	-	-	-	-	-
Mg	-	-	-	-	-	-	-	-	-	-	-
Ba	-	-	-	-	-	-	-	-	-	-	-
Fe^{2+}	-	-	-	-	-	-	-	-	-	-	-
∑	1.0	1.0	0.9	1.0	1.0	0.9	1.0	1.1	1.0	1.0	1.0
Xan	61	53	58	61	56	50	73	71	59	59	68
Xab	39	47	42	39	44	50	27	29	41	41	32
Xor	0	0	0	0	0	0	0	0	0	0	0

*below detection limit, **not analyzed

Table G-1 (continued): Electron microprobe analyses of feldspar group minerals.
Cation recalculations based on eight oxygen atoms PFU.

Sample	10BB001 -1-2-12	10BB001 -3-2-1	10BB001 -3-2-2	10BB001 -3-2-3	10BB001 -3-2-4	10BB001 -4-1-4	10BB001 -4-1-5	10BB001 -4-1-6	10BB001 -5-2-4	10BB001 -5-2-5	10BB001 -5-2-6
Na_2O	2.4	4.5	4.0	5.6	3.5	4.5	3.3	5.6	2.9	3.1	3.0
MgO	-**	0.2	-**	-**	0.2	0.1	0.3	0.1	0.2	0.2	0.2
Al_2O_3	32.4	28.6	29.2	26.7	30.3	28.4	30.4	26.6	30.7	30.7	30.5
SiO_2	48.4	54.1	53.5	57.7	51.5	54.5	50.9	57.8	51.3	51.3	51.5
K_2O	-*	-*	-*	-*	-*	-*	-*	-*	-*	-*	-*
CaO	16.3	11.9	12.7	9.4	13.8	11.8	14.3	9.3	14.4	14.1	14.2
TiO_2	-**	-**	-**	-**	-**	-**	-**	-**	-**	0.1	-**
FeO	0.6	0.8	0.6	0.7	0.8	0.7	0.8	0.6	0.5	0.5	0.6
BaO	-**	-**	-**	-**	-**	-**	-**	-**	-**	-**	-**
∑	100.1	100.1	100.0	100.1	100.1	100.0	100.0	100.0	100.0	100.0	100.0
Si	2.2	2.5	2.4	2.6	2.3	2.5	2.3	2.6	2.3	2.3	2.3
Al	1.8	1.5	1.6	1.4	1.6	1.5	1.6	1.4	1.7	1.6	1.6
∑	4.0	4.0	4.0	4.0	3.9	4.0	3.9	4.0	4.0	3.9	3.9
Na	0.2	0.4	0.4	0.5	0.3	0.4	0.3	0.5	0.3	0.3	0.3
Ca	0.8	0.6	0.6	0.5	0.7	0.6	0.7	0.5	0.7	0.7	0.7
K	-	-	-	-	-	-	-	-	-	-	-
Mg	-	-	-	-	-	-	-	-	-	-	-
Ba	-	-	-	-	-	-	-	-	-	-	-
Fe^{2+}	-	-	-	-	-	-	-	-	-	-	-
∑	1.0	1.0	1.0	1.0	1.0	1.0	1.0	1.0	1.0	1.0	1.0
Xan	77	54	57	41	64	52	65	41	66	65	65
Xab	23	46	43	59	36	48	35	59	34	35	35
Xor	0	0	0	0	0	0	0	0	0	0	0

*below detection limit, **not analyzed

Table G-1 (continued): Electron microprobe analyses of feldspar group minerals.
Cation recalculations based on eight oxygen atoms PFU.

Sample	10BB001 -5-2-7	10BB001 -5-2-8	10BB001 -5-2-9	10BB001 -6-1-1	10BB001 -6-1-2	10BB001 -6-1-3	10BB001 -6-1-10	10BB001 -6-1-11	10BB001 -6-1-12	10DE003 -4-2-1	10DE003 -4-2-2
Na_2O	5.1	5.9	6.3	2.5	3.2	3.2	6.8	4.9	6.3	8.4	8.5
MgO	0.2	-**	-**	0.2	0.2	0.2	-**	0.1	-**	-**	-**
Al_2O_3	25.9	23.8	24.9	31.9	30.6	30.6	23.4	27.6	25.6	19.9	19.8
SiO_2	59.4	64.3	61.2	49.4	51.0	51.3	62.7	55.6	59.8	70.8	71.2
K_2O	-*	-*	-*	-*	-*	-*	0.7	-*	-*	-*	-*
CaO	8.5	5.3	6.9	15.5	14.3	14.2	5.5	10.9	7.6	0.6	0.2
TiO_2	0.2	0.2	-**	-**	-**	-**	0.2	-**	-**	-**	-**
FeO	0.8	0.6	0.7	0.4	0.6	0.5	0.7	0.9	0.7	0.4	0.3
BaO	-**	-**	-**	-**	-**	-**	-**	-**	-**	-**	-**
∑	100.1	100.1	100.0	99.9	99.9	100.0	100.0	100.0	100.0	100.1	100.0
Si	2.6	2.8	2.7	2.3	2.3	2.3	2.8	2.5	2.7	3.1	3.1
Al	1.4	1.2	1.3	1.7	1.7	1.6	1.2	1.5	1.3	1.0	1.0
∑	4.0	4.0	4.0	4.0	4.0	3.9	4.0	4.0	4.0	4.1	4.1
Na	0.4	0.5	0.5	0.2	0.3	0.3	0.6	0.4	0.6	0.7	0.7
Ca	0.4	0.3	0.3	0.8	0.7	0.7	0.3	0.5	0.4	-	-
K	-	-	-	-	-	-	-	-	-	-	-
Mg	-	-	-	-	-	-	-	-	-	-	-
Ba	-	-	-	-	-	-	-	-	-	-	-
Fe^{2+}	-	-	-	-	-	-	-	-	-	-	-
∑	0.8	0.8	0.8	1.0	1.0	1.0	0.9	0.9	1.0	0.7	0.7
Xan	36	21	29	73	66	65	22	48	34	0	0
Xab	64	79	71	27	34	35	73	52	66	100	100
Xor	0	0	0	0	0	0	5	0	0	0	0

*below detection limit, **not analyzed

Table G-1 (continued): Electron microprobe analyses of feldspar group minerals.
Cation recalculations based on eight oxygen atoms PFU.

Sample	10DE003 -4-2-3	10DE003 -4-2-4	10DE003 -7-1-1	10DE003 -7-1-2	10DE003 -7-1-3	10DE003 -7-1-4	10DE003 -8-1-1	10DE003 -8-1-3	10DE003 -8-1-4	10DE006 -1-1-7	10DE006 -1-1-8
Na_2O	8.5	10.6	9.1	9.2	9.0	8.6	9.4	8.5	8.5	5.8	6.0
MgO	-**	0.1	0.4	-**	0.5	0.3	0.7	-**	0.9	-**	-**
Al_2O_3	19.8	19.6	19.7	20.2	19.7	20.4	19.8	20.0	19.6	26.1	26.3
SiO_2	71.1	69.2	70.3	70.1	70.4	70.3	68.9	71.1	69.9	58.5	58.3
K_2O	-*	-*	-*	-*	-*	-*	-*	-*	-*	-*	-*
CaO	0.3	0.2	0.5	0.6	0.3	0.4	0.3	0.4	0.4	8.8	8.7
TiO_2	-**	-**	-**	-**	-**	-**	-**	-**	-**	-**	-**
FeO	0.4	0.3	-**	-**	-**	-**	1.0	-**	0.8	0.8	0.7
BaO	-**	-**	-**	-**	-**	-**	-**	-**	-**	-**	-**
∑	100.1	100.0	100.0	100.1	99.9	100.0	100.1	100.0	100.1	100.0	100.0
Si	3.1	3.0	3.0	3.0	3.0	3.0	3.0	3.1	3.0	2.6	2.6
Al	1.0	1.0	1.0	1.0	1.0	1.0	1.0	1.0	1.0	1.4	1.4
∑	4.1	4.0	4.0	4.0	4.0	4.0	4.0	4.1	4.0	4.0	4.0
Na	0.7	0.9	0.8	0.8	0.8	0.7	0.8	0.7	0.7	0.5	0.5
Ca	-	-	-	-	-	-	-	-	-	0.4	0.4
K	-	-	-	-	-	-	-	-	-	-	-
Mg	-	-	-	-	-	-	-	-	0.1	-	-
Ba	-	-	-	-	-	-	-	-	-	-	-
Fe^{2+}	-	-	-	-	-	-	-	-	-	-	-
∑	0.7	0.9	0.8	0.8	0.8	0.7	0.8	0.7	0.8	0.9	0.9
Xan	0	0	0	1	0	1	1	0	0	38	39
Xab	100	100	100	99	100	99	99	100	100	62	61
Xor	0	0	0	0	0	0	0	0	0	0	0

*below detection limit, **not analyzed

Table G-1 (continued): Electron microprobe analyses of feldspar group minerals.
Cation recalculations based on eight oxygen atoms PFU.

Sample	10DE006 -1-1-9	10DE006 -1-3-1	10DE006 -1-3-2	10DE006 -1-3-3	10DE006 -1-3-4	10DE006 -1-3-5	10DE006 -1-3-6	10DE006 -2-1-4	10DE006 -2-1-5	10DE006 -2-1-6	10DE006 -2-1-7
Na_2O	5.4	8.2	8.3	7.9	-*	-*	-*	8.4	8.3	8.1	-*
MgO	-**	-**	-**	-**	0.2	-**	-**	-**	-**	-**	-**
Al_2O_3	26.9	20.2	20.2	20.2	18.7	18.6	18.6	20.5	20.3	20.4	18.9
SiO_2	57.1	71.1	71.1	71.4	67.0	67.5	67.7	70.6	71.0	70.9	67.4
K_2O	-*	-*	-*	-*	12.7	13.3	13.1	-*	-*	-*	13.2
CaO	9.9	0.6	0.4	0.5	-*	-*	-*	0.6	0.5	0.6	-*
TiO_2	-**	-**	-**	-**	-**	-**	-**	-**	-**	-**	-**
FeO	0.8	-**	-**	-**	0.6	-**	-**	-**	-**	-**	-**
BaO	-**	-**	-**	-**	0.8	0.7	0.6	-**	-**	-**	0.6
∑	100.1	100.1	100.0	100.0	100.0	100.1	100.0	100.1	100.1	100.0	100.1
Si	2.6	3.1	3.1	3.1	3.0	3.1	3.1	3.0	3.1	3.0	3.1
Al	1.4	1.0	1.0	1.0	1.0	1.0	1.0	1.0	1.0	1.0	1.0
∑	4.0	4.1	4.1	4.1	4.0	4.1	4.1	4.0	4.1	4.0	4.1
Na	0.5	0.7	0.7	0.7	-	-	-	0.7	0.7	0.7	-
Ca	0.5	-	-	-	-	-	-	-	-	-	-
K	-	-	-	-	0.7	0.8	0.8	-	-	-	0.8
Mg	-	-	-	-	-	-	-	-	-	-	-
Ba	-	-	-	-	-	-	-	-	-	-	-
Fe^{2+}	-	-	-	-	-	-	-	-	-	-	-
∑	1.0	0.7	0.7	0.7	0.7	0.8	0.8	0.7	0.7	0.7	0.8
Xan	43	0	0	0	0	0	0	2	0	1	0
Xab	57	100	100	100	0	0	0	98	100	99	0
Xor	0	0	0	0	100	100	100	0	0	0	100

*below detection limit, **not analyzed

Table G-1 (continued): Electron microprobe analyses of feldspar group minerals.
Cation recalculations based on eight oxygen atoms PFU.

Sample	10DE006 -2-1-8	10DE006 -2-1-9	10DE006 -4-1-4	10DE006 -4-1-5	10DE006 -4-1-6	10DE006 -4-1-7	10DE006 -4-1-8	10DE006 -4-1-9	10DE006 -6-1-7	10DE006 -6-1-8	10DE006 -6-1-9
Na_2O	-*	-*	4.2	-*	3.5	7.9	8.4	8.1	4.0	4.8	5.9
MgO	-**	-**	-**	-**	-**	-**	-**	-**	-**	-**	-**
Al_2O_3	18.7	18.9	28.7	19.2	30.3	20.2	20.1	20.2	29.6	28.3	26.4
SiO_2	67.2	66.8	54.6	68.4	51.7	71.3	70.8	71.3	52.7	54.8	58.1
K_2O	13.5	13.7	-*	12.5	-*	-*	-*	-*	-*	-*	-*
CaO	-*	-*	11.8	-*	13.8	0.6	0.5	0.4	13.0	11.4	9.0
TiO_2	-**	-**	-**	-**	-**	-**	-**	-**	-**	-**	-**
FeO	-**	-**	0.7	-**	0.7	-**	0.2	-**	0.7	0.8	0.7
BaO	0.6	0.6	-**	-**	-**	-**	-**	-**	-**	-**	-**
∑	100.0	100.0	100.0	100.1	100.0	100.0	100.0	100.0	100.0	100.1	100.1
Si	3.1	3.0	2.5	3.1	2.35	3.06	3.0	3.1	2.4	2.5	2.6
Al	1.0	1.0	1.5	1.0	1.63	1.02	1.0	1.0	1.6	1.5	1.4
∑	4.1	4.0	4.0	4.1	3.98	4.08	4.0	4.1	4.0	4.0	4.0
Na	-	-	0.4	-	0.31	0.66	0.7	0.7	0.4	0.4	0.5
Ca	-	-	0.6	-	0.67	0.03	-	-	0.6	0.6	0.4
K	0.8	0.8	-	0.7	-	-	-	-	-	-	-
Mg	-	-	-	-	-	-	-	-	-	-	-
Ba	-	-	-	-	-	-	-	-	-	-	-
Fe^{2+}	-	-	-	-	0.03	-	-	-	-	-	-
∑	0.8	0.8	1.0	0.7	1.01	0.68	0.7	0.7	1.0	1.0	0.9
Xan	0	0	53	0	64	0	0	0	59	51	39
Xab	0	0	47	0	36	100	100	100	41	49	61
Xor	100	100	0	100	0	0	0	0	0	0	0

*below detection limit, **not analyzed

Table G-1 (continued): Electron microprobe analyses of feldspar group minerals.
Cation recalculations based on eight oxygen atoms PFU.

Sample	10DE006 -7-2-2	10DE006 -7-2-3	10BA005 -6-1-4	10BA005 -6-1-5	10BA005 -6-1-6	10BA005 -2-2-4	10BA005 -2-2-5	10BA005 -2-2-6	10VI002 -3-2-4	10VI002 -3-2-5	10VI002 -3-2-6
Na_2O	8.4	4.9	8.4	8.2	8.7	8.3	8.4	7.9	3.4	3.7	2.4
MgO	-**	-**	-**	-**	-**	-**	-**	-**	-**	-**	-**
Al_2O_3	20.3	27.6	20.6	20.9	20.8	21.3	20.4	20.9	30.6	29.7	32.2
SiO_2	70.4	55.8	70.0	69.8	69.3	68.6	70.5	69.8	51.2	53.0	48.6
K_2O	-*	-*	-*	-*	-*	-*	-*	-*	-*	-*	-*
CaO	0.9	10.8	1.0	1.2	1.2	1.8	0.8	1.4	14.2	13.0	16.0
TiO_2	-**	-**	-**	-**	-**	-**	-**	-**	-**	-**	-**
FeO	-**	0.9	-**	-**	-**	-**	-**	-**	0.7	0.6	0.7
BaO	-**	-**	-**	-**	-**	-**	-**	-**	-**	-**	-**
∑	100.0	100.0	100.0	99.9	100.0	100.0	100.1	100.0	100.1	100.0	99.9
Si	3.0	2.5	3.0	3.0	3.0	3.0	3.0	3.0	2.3	2.4	2.2
Al	1.0	1.5	1.1	1.1	1.1	1.1	1.0	1.1	1.6	1.6	1.7
∑	4.0	4.0	4.1	4.1	4.1	4.1	4.0	4.1	3.9	4.0	3.9
Na	0.7	0.4	0.7	0.7	0.7	0.7	0.7	0.7	0.3	0.3	0.2
Ca	-	0.5	0.1	0.1	0.1	0.1	-	0.1	0.7	0.6	0.8
K	-	-	-	-	-	-	-	-	-	-	-
Mg	-	-	-	-	-	-	-	-	-	-	-
Ba	-	-	-	-	-	-	-	-	-	-	-
Fe^{2+}	-	-	-	-	-	-	-	-	-	-	-
∑	0.7	0.9	0.8	0.8	0.8	0.8	0.7	0.8	1.0	0.9	1.0
Xan	1	47	3	4	4	7	2	4	65	59	76
Xab	99	53	97	96	96	93	98	96	35	41	24
Xor	0	0	0	0	0	0	0	0	0	0	0

*below detection limit, **not analyzed

Table G-1 (continued): Electron microprobe analyses of feldspar group minerals. Cation recalculations based on eight oxygen atoms PFU.

Sample	10VI002 -4-1-4	10VI002 -4-1-5	10VI002 -4-1-6	10VI004 -6-2-4	10VI004 -6-2-5	10VI004 -6-2-6
Na_2O	3.5	3.8	3.3	2.9	2.6	2.7
MgO	0.1	-**	-**	-**	0.3	-**
Al_2O_3	30.7	30.7	30.8	31.5	31.9	31.3
SiO_2	51.0	50.9	51.3	49.6	48.8	50.0
K_2O	-*	-*	-*	-*	-*	-*
CaO	14.1	14.2	14.2	15.4	15.8	15.2
TiO_2	-**	-**	-**	-**	-**	-**
FeO	0.6	0.4	0.5	0.6	0.7	0.8
BaO	-**	-**	-**	-**	-**	-**
∑	100.0	100.0	100.1	100.0	100.1	100.0
Si	2.3	2.3	2.3	2.27	2.2	2.3
Al	1.7	1.7	1.7	1.70	1.7	1.7
∑	4.0	4.0	4.0	3.97	3.9	4.0
Na	0.3	0.3	0.3	0.26	0.2	0.2
Ca	0.7	0.7	0.7	0.76	0.8	0.8
K	-	-	-	-	-	-
Mg	-	-	-	-	-	-
Ba	-	-	-	-	-	-
Fe^{2+}	-	-	-	0.02	-	-
∑	1.0	1.0	1.0	1.04	1.0	1.0
Xan	66	66	66	71	74	70
Xab	34	34	34	29	26	30
Xor	0	0	0	0	0	0

*below detection limit, **not analyzed

Table G-2: Electron microprobe analyses of pyroxene group minerals.
Cation recalculations based on six oxygen atoms PFU.

Sample	11CBF006 11-06-011	11CBF006 11-06_013	11CBF006 11-06_014	11CBF006 11-06_015	11CBF006 11-06_016	11CBF006 11-06_017	11CBF006 11-06_024
Na_2O	-**	-**	0.8	-**	-**	-**	-**
MgO	14.8	15.4	15.5	15.1	15.1	13.6	15.8
Al_2O_3	2.2	2.5	2.4	2.9	3.3	2.8	2.6
SiO_2	51.7	52.2	52.4	51.6	51.2	50.6	52.2
CaO	16.9	18.3	18.2	19.4	18.7	18.3	18.8
TiO_2	1.0	1.0	0.8	1.0	0.9	1.2	0.8
Cr_2O_3	-**	-**	-**	0.7	0.8	-**	0.6
MnO	-**	-**	-**	-**	-**	-**	-**
FeO	13.4	10.8	10.0	9.5	9.9	13.6	9.2
∑	100.0	100.2	100.1	100.2	99.9	100.1	100.0
Si	1.9	1.9	1.9	1.9	1.9	1.9	1.9
Al	0.1	0.1	0.1	0.1	0.1	0.1	0.1
∑	2.0	2.0	2.0	2.0	2.0	2.0	2.0
Al	-	-	-	-	0.1	-	-
Fe^{3+}	-	-	-	-	-	-	-
Ti	-	-	-	-	-	-	-
Cr	-	-	-	-	-	-	-
Mg	0.8	0.9	0.9	0.8	0.8	0.8	0.9
Fe^{2+}	0.1	0.1	0.1	0.1	0.1	0.2	0.1
Mn	-	-	-	-	-	-	-
∑	0.9	1.0	1.0	0.9	1.0	1.0	1.0
Mg	-	-	-	-	-	-	-
Fe^{2+}	0.3	0.3	0.2	0.2	0.2	0.3	0.2
Mn	-	-	-	-	-	-	-
Ca	0.7	0.7	0.7	0.8	0.8	0.7	0.8
Na	-	-	0.1	-	-	-	-
K	-	-	-	-	-	-	-
∑	1.0	1.0	1.0	1.0	1.0	1.0	1.0
			Atomic percentages				
Mg	43	45	45	44	44	40	46
∑Fe*	22	17	16	16	16	22	15
Ca	35	38	38	41	39	38	39

*$\sum Fe = Fe^{2+} + Fe^{3+} + Mg$

**not analyzed

Table G-2 (continued): Electron microprobe analyses of pyroxene group minerals. Cation recalculations based on six oxygen atoms PFU.

Sample	11CBF006 11-06_025	11CBF006 11-06_029	11CBF006 11-06_033	11CBF006 11-06_041	11CBF006 11-06_044	11CBF006 11-06_045	11CBF006 11-06_046
Na_2O	-**	0.9	1.1	-**	-**	-**	0.9
MgO	15.9	14.3	14.1	15.7	15.3	15.7	14.6
Al_2O_3	2.4	3.7	2.3	2.2	2.4	2.4	3.3
SiO_2	52.3	50.1	50.9	52.4	52.2	51.5	51.1
CaO	18.3	18.4	17.4	18.4	18.9	18.5	18.8
TiO_2	0.7	1.3	0.8	0.7	0.8	0.9	1.0
Cr_2O_3	0.8	-**	-**	0.6	-**	0.5	-**
MnO	-**	-**	-**	-**	-**	-**	-**
FeO	9.6	11.3	13.4	10.0	10.5	10.4	10.5
∑	100.0	100.0	100.0	100.0	100.1	99.9	100.2
Si	1.9	1.9	1.9	1.9	1.9	1.9	1.9
Al	0.1	0.1	0.1	0.1	0.1	0.1	0.1
∑	2.0	2.0	2.0	2.0	2.0	2.0	2.0
Al	-	-	-	-	-	-	-
Fe^{3+}	-	0.1	0.2	-	-	-	0.1
Ti	-	-	-	-	-	-	-
Cr	-	-	-	-	-	-	-
Mg	0.9	0.8	0.8	0.9	0.9	0.9	0.8
Fe^{2+}	-	-	-	0.1	0.1	0.1	0.1
Mn	-	-	-	-	-	-	-
∑	0.9	0.9	1.0	1.0	1.0	1.0	1.0
Mg	-	-	-	-	-	-	-
Fe^{2+}	0.3	0.2	0.2	0.3	0.2	0.3	0.2
Mn	-	-	-	-	-	-	-
Ca	0.7	0.7	0.7	0.7	0.8	0.7	0.7
Na	-	0.1	0.1	-	-	-	0.1
K	-	-	-	-	-	-	-
∑	1.0	1.0	1.0	1.0	1.0	1.0	1.0
Atomic percentages							
Mg	46	42	41	46	44	45	43
∑Fe*	16	19	22	16	17	17	17
Ca	38	39	37	38	39	38	40

*$\sum Fe = Fe^{2+} + Fe^{3+} + Mg$

**not analyzed

Table G-2 (continued): Electron microprobe analyses of pyroxene group minerals. Cation recalculations based on six oxygen atoms PFU.

Sample	11CBF004 -013	11CBF004 -019	11CBF004 -020	11CBF004 -022	11CBF004 -3-2-10	11CBF004 -3-2-11	11CBF004 -3-2-12
Na_2O	-**	0.9	0.9	-**	0.8	0.9	0.8
MgO	15.3	14.3	14.3	12.8	15.0	15.1	15.1
Al_2O_3	2.1	3.3	3.5	3.1	1.5	1.4	1.3
SiO_2	52.3	50.4	50.6	49.2	52.4	52.2	52.3
CaO	18.6	18.8	19.4	21.3	16.8	17.3	17.1
TiO_2	1.0	1.1	1.1	1.4	1.1	1.1	1.1
Cr_2O_3	-**	0.6	-**	-**	-**	-**	-**
MnO	-**	-**	-**	-**	-**	0.3	0.3
FeO	10.9	10.7	10.3	12.1	12.5	11.7	11.9
∑	100.2	100.1	100.1	99.9	100.1	100.0	99.9
Si	1.9	1.9	1.9	1.9	2.0	1.9	2.0
Al	0.1	0.1	0.1	0.1	0.1	0.1	0.1
∑	2.0	2.0	2.0	2.0	2.1	2.0	2.1
Al	-	-	-	-	-	-	-
Fe^{3+}	-	0.1	0.1	0.1	-	0.1	-
Ti	-	-	-	-	-	-	-
Cr	-	-	-	-	-	-	-
Mg	0.9	0.8	0.8	0.7	0.8	0.8	0.8
Fe^{2+}	0.1	0.1	0.1	0.2	0.1	0.1	0.1
Mn	-	-	-	-	-	-	-
∑	1.0	1.0	1.0	1.0	0.9	1.0	0.9
Mg	-	-	-	-	-	-	-
Fe^{2+}	0.3	0.2	0.2	0.1	0.3	0.2	0.3
Mn	-	-	-	-	-	-	-
Ca	0.7	0.8	0.8	0.9	0.7	0.7	0.7
Na	-	0.1	0.1	-	0.1	0.1	0.1
K	-	-	-	-	-	-	-
∑	1.0	1.1	1.1	1.0	1.1	1.0	1.1
Atomic percentages							
Mg	44	42	42	37	44	44	44
∑Fe*	18	18	17	19	21	20	20
Ca	38	40	41	44	35	36	36

*$\sum Fe = Fe^{2+} + Fe^{3+} + Mg$

**not analyzed

Table G-2 (continued): Electron microprobe analyses of pyroxene group minerals. Cation recalculations based on six oxygen atoms PFU.

Sample	11CBF004 -8-1-1	11CBF004 -8-1-2	11CBF004 -8-1-3	10CN002 -1-3-1	10CN002 -1-3-2	10CN002 -1-3-3	10CN002 -5-1-7
Na_2O	1.0	1.0	0.8	-**	-**	-**	-**
MgO	12.3	12.7	12.7	12.5	12.7	11.9	14.6
Al_2O_3	1.3	1.1	1.3	1.2	1.2	1.1	1.2
SiO_2	51.7	51.8	52.0	52.9	52.7	52.5	52.8
CaO	17.3	17.2	17.3	15.9	16.5	16.0	15.8
TiO_2	1.0	1.0	0.9	0.9	0.8	0.9	0.9
Cr_2O_3	-**	-**	-**	-**	-**	-**	-**
MnO	0.4	0.5	0.4	0.4	0.5	0.6	0.5
FeO	15.1	14.7	14.7	16.2	15.7	17.0	14.2
∑	100.1	100.0	100.1	100.0	100.1	100.0	100.0
Si	2.0	2.0	2.0	2.0	2.0	2.0	2.0
Al	-	-	-	-	-	-	-
∑	2.0	2.0	2.0	2.0	2.0	2.0	2.0
Al	-	-	-	0.1	-	-	-
Fe^{3+}	0.1	0.1	-	-	-	-	-
Ti	-	-	-	-	-	-	-
Cr	-	-	-	-	-	-	-
Mg	0.7	0.7	0.7	0.7	0.7	0.7	0.8
Fe^{2+}	0.2	0.2	0.2	0.2	0.2	0.3	0.1
Mn	-	-	-	-	-	-	-
∑	1.0	1.0	0.9	1.0	0.9	1.0	0.9
Mg	-	-	-	-	-	-	-
Fe^{2+}	0.2	0.2	0.2	0.3	0.3	0.3	0.3
Mn	-	-	-	-	-	-	-
Ca	0.7	0.7	0.7	0.6	0.7	0.7	0.6
Na	0.1	0.1	0.1	-	-	-	-
K	-	-	-	-	-	-	-
∑	1.0	1.0	1.0	0.9	1.0	1.0	0.9
				Atomic percentages			
Mg	37	38	38	38	38	36	43
∑Fe*	26	25	25	28	27	30	24
Ca	37	37	37	34	35	34	33

*$\sum Fe = Fe^{2+} + Fe^{3+} + Mg$

**not analyzed

Table G-2 (continued): Electron microprobe analyses of pyroxene group minerals. Cation recalculations based on six oxygen atoms PFU.

Sample	10CN002 -5-1-8	10CN002 -5-1-9	10CN002 -6-3-1	10CN002 -6-3-2	10CN002 -6-3-3	10CN002 -6-3-4	10QU006 -4-1-1
Na_2O	-**	-**	0.8	0.9	-**	0.8	-**
MgO	13.6	13.5	15.6	14.9	16.2	16.1	16.0
Al_2O_3	1.5	1.3	2.7	1.9	1.4	1.3	2.2
SiO_2	52.4	52.2	51.4	51.8	53.4	52.9	52.8
CaO	16.8	15.9	16.2	16.8	17.0	16.8	17.0
TiO_2	1.1	1.0	1.5	1.3	0.8	0.9	1.0
Cr_2O_3	-**	-**	-**	-**	-**	-**	-**
MnO	0.4	0.5	0.4	0.4	0.4	0.5	-**
FeO	14.1	15.6	11.5	12.1	10.8	10.7	11.0
∑	99.9	100.0	100.1	100.1	100.0	100.0	100.0
Si	2.0	2.0	1.9	1.9	2.0	2.0	2.0
Al	-	-	0.1	0.1	-	-	0.1
∑	2.0	2.0	2.0	2.0	2.0	2.0	2.1
Al	-	-	-	-	-	-	0.1
Fe^{3+}	-	-	-	0.1	-	-	-
Ti	-	-	-	-	-	-	-
Cr	-	-	-	-	-	-	-
Mg	0.8	0.8	0.9	0.8	0.9	0.9	0.9
Fe^{2+}	0.2	0.2	-	0.1	0.1	-	-
Mn	-	-	-	-	-	-	-
∑	1.0	1.0	0.9	1.0	1.0	0.9	1.0
Mg	-	-	-	-	-	-	-
Fe^{2+}	0.3	0.3	0.3	0.3	0.3	0.3	0.3
Mn	-	-	-	-	-	-	-
Ca	0.7	0.6	0.6	0.7	0.7	0.7	0.7
Na	-	-	0.1	0.1	-	0.1	-
K	-	-	-	-	-	-	-
∑	1.0	0.9	1.0	1.1	1.0	1.1	1.0
				Atomic percentages			
Mg	40	40	46	44	47	47	47
∑Fe*	24	27	20	21	18	18	18
Ca	36	34	34	36	35	35	35

*$\sum Fe = Fe^{2+} + Fe^{3+} + Mg$

**not analyzed

Table G-2 (continued): Electron microprobe analyses of pyroxene group minerals. Cation recalculations based on six oxygen atoms PFU.

Sample	10QU006 -4-1-2	10QU006 -4-1-3	10SC004 -1-1-7	10SC004 -1-1-8	10SC004 -1-1-9	10SC004 -1-2-1	10SC004 -1-2-2
Na_2O	0.8	0.8	-**	-**	-**	-**	-**
MgO	15.9	16.0	20.3	20.6	21.0	21.1	20.3
Al_2O_3	1.8	1.8	0.8	0.6	0.6	0.7	0.9
SiO_2	52.5	52.5	53.6	53.9	53.6	53.9	53.7
CaO	17.3	17.4	5.7	4.4	2.7	3.4	5.2
TiO_2	1.0	0.9	0.4	0.4	0.4	0.4	0.6
Cr_2O_3	-**	-**	-**	-**	-**	-**	-**
MnO	0.4	0.3	0.5	0.7	0.5	0.4	0.6
FeO	10.3	10.4	18.7	19.4	21.2	20.0	18.8
∑	100.0	100.1	100.0	100.0	100.0	99.9	100.1
Si	1.9	1.9	2.0	2.0	2.0	2.0	2.0
Al	0.1	0.1	-	-	-	-	-
∑	2.0	2.0	2.0	2.0	2.0	2.0	2.0
Al	-	-	-	-	-	-	-
Fe^{3+}	-	0.1	-	-	-	-	-
Ti	-	-	-	-	-	-	-
Cr	-	-	-	-	-	-	-
Mg	0.9	0.9	1.0	1.0	1.0	1.0	1.0
Fe^{2+}	-	-	-	-	-	-	-
Mn	-	-	-	-	-	-	-
∑	0.9	1.0	1.0	1.0	1.0	1.0	1.0
Mg	-	-	0.2	0.2	0.2	0.2	0.2
Fe^{2+}	0.3	0.2	0.6	0.6	0.7	0.6	0.6
Mn	-	-	-	-	-	-	-
Ca	0.7	0.7	0.2	0.2	0.1	0.1	0.2
Na	0.1	0.1	-	-	-	-	-
K	-	-	-	-	-	-	-
∑	1.1	1.0	1.0	1.0	1.0	0.9	1.0
			Atomic percentages				
Mg	46	46	58	59	60	60	58
∑Fe*	17	17	31	32	35	33	31
Ca	36	36	12	9	6	7	11

*$\sum Fe = Fe^{2+} + Fe^{3+} + Mg$

**not analyzed

Table G-2 (continued): Electron microprobe analyses of pyroxene group minerals. Cation recalculations based on six oxygen atoms PFU.

Sample	10SC004 -1-2-3	10SC004 -2-2-1	10SC004 -2-2-2	10SC004 -2-2-3	10SC004 -3-1-8	10SC004 -3-1-9	10SC004 -3-1-10
Na_2O	-**	-**	-**	-**	0.7	0.7	0.7
MgO	21.3	20.8	21.1	21.2	16.7	16.7	16.9
Al_2O_3	0.5	0.4	0.4	0.4	2.3	2.3	2.2
SiO_2	54.0	54.0	53.9	54.0	52.5	52.6	52.6
CaO	2.6	1.9	1.7	1.7	18.8	18.4	18.9
TiO_2	0.4	0.3	0.3	0.3	0.9	1.0	0.8
Cr_2O_3	-**	-**	-**	-**	-**	-**	-**
MnO	0.6	0.6	0.6	0.5	0.3	0.3	0.3
FeO	20.5	22.0	22.0	21.9	7.9	8.2	7.7
∑	99.9	100.	100.0	100.0	100.1	100.2	100.1
Si	2.0	2.0	2.0	2.0	1.9	1.9	1.9
Al	-	-	-	-	0.1	0.1	0.1
∑	2.0	2.0	2.0	2.0	2.0	2.0	2.0
Al	-	-	-	-	-	-	-
Fe^{3+}	-	-	-	-	0.1	-	0.1
Ti	-	-	-	-	-	-	-
Cr	-	-	-	-	-	-	-
Mg	1.0	1.0	1.0	1.0	0.9	0.9	0.9
Fe^{2+}	-	-	-	-	-	-	-
Mn	-	-	-	-	-	-	-
∑	1.0	1.0	1.0	1.0	1.0	0.9	1.0
Mg	0.2	0.2	0.2	0.2	-	-	-
Fe^{2+}	0.6	0.7	0.7	0.7	0.2	0.2	0.2
Mn	-	-	-	-	-	-	-
Ca	0.1	0.1	0.1	0.1	0.7	0.7	0.7
Na	-	-	-	-	0.1	0.1	0.1
K	-	-	-	-	-	-	-
∑	1.1	1.0	1.0	1.0	1.0	1.0	1.0
Atomic percentages							
Mg	61	60	60	61	48	48	48
∑Fe*	34	36	36	36	13	14	13
Ca	5	4	3	4	39	38	39

*$\sum Fe = Fe^{2+} + Fe^{3+} + Mg$

**not analyzed

Table G-2 (continued): Electron microprobe analyses of pyroxene group minerals. Cation recalculations based on six oxygen atoms PFU.

Sample	10SC004 -4-1-7	10SC004 -4-1-8	10SC004 -4-1-9	10SC004 -4-2-8	10SC004 -4-2-9	10SC004 -5-1-10	10SC004 -5-1-11
Na_2O	-**	-**	-**	-**	-**	-**	-**
MgO	21.8	21.1	21.2	20.9	20.1	20.3	20.3
Al_2O_3	0.5	0.7	0.6	0.4	0.5	0.4	0.5
SiO_2	54.0	53.6	54.1	53.9	53.7	53.8	53.7
CaO	3.0	4.8	3.7	2.7	4.5	3.9	4.1
TiO_2	0.4	0.6	0.4	0.4	0.5	0.3	0.4
Cr_2O_3	-**	-**	-**	-**	-**	-**	-**
MnO	0.6	0.5	0.6	0.6	0.6	0.5	0.5
FeO	19.6	18.8	19.5	21.2	20.1	20.8	20.6
∑	99.9	100.1	100.1	100.1	100.0	100.0	100.1
Si	2.0	2.0	2.0	2.0	2.0	2.0	2.0
Al	-	-	-	-	-	-	-
∑	2.0	2.0	2.0	2.0	2.0	2.0	2.0
Al	-	-	-	-	-	-	-
Fe^{3+}	-	-	-	-	-	-	-
Ti	-	-	-	-	-	-	-
Cr	-	-	-	-	-	-	-
Mg	1.0	1.0	1.0	1.0	1.0	1.0	1.0
Fe^{2+}	-	-	-	-	-	-	-
Mn	-	-	-	-	-	-	-
∑	1.0	1.0	1.0	1.0	1.0	1.0	1.0
Mg	0.2	0.2	0.2	0.2	0.2	0.2	0.2
Fe^{2+}	0.6	0.6	0.6	0.7	0.6	0.7	0.6
Mn	-	-	-	-	-	-	-
Ca	0.1	0.2	0.2	0.1	0.2	0.2	0.2
Na	-	-	-	-	-	-	-
K	-	-	-	-	-	-	-
∑	0.9	1.0	1.0	1.0	1.0	1.1	1.0
				Atomic percentages			
Mg	62	60	60	60	58	58	58
∑Fe*	32	31	32	35	33	34	34
Ca	6	10	7	6	9	8	8

*$\sum Fe = Fe^{2+} + Fe^{3+} + Mg$

**not analyzed

Table G-2 (continued): Electron microprobe analyses of pyroxene group minerals. Cation recalculations based on six oxygen atoms PFU.

Sample	10SC004 -5-1-12	10SC004 -6-1-7	10SC004 -6-1-8	10SC004 -6-1-9	10SC004 -6-2-7	10SC004 -6-2-8	10SC004 -6-2-9
Na_2O	-**	-**	-**	-**	-**	0.7	0.9
MgO	20.8	21.4	21.3	20.3	15.7	16.0	15.5
Al_2O_3	0.4	0.5	0.7	0.4	1.3	1.8	1.6
SiO_2	53.6	53.7	53.8	53.9	52.8	52.0	52.3
CaO	2.9	2.7	3.1	3.0	17.3	17.8	17.2
TiO_2	0.4	0.4	0.4	0.3	0.9	1.1	0.8
Cr_2O_3	-**	-**	-**	-**	-**	-**	-**
MnO	0.6	0.6	0.6	0.4	0.4	0.3	0.5
FeO	21.2	20.7	20.0	21.7	11.6	10.3	11.4
∑	99.9	100.0	99.9	100.0	100.0	100.0	100.2
Si	2.0	2.0	2.0	2.0	2.0	1.9	1.9
Al	-	-	-	-	-	0.1	0.1
∑	2.0	2.0	2.0	2.0	2.0	2.0	2.0
Al	-	-	-	-	-	-	-
Fe^{3+}	-	-	-	-	-	0.1	0.1
Ti	-	-	-	-	-	-	-
Cr	-	-	-	-	-	-	-
Mg	1.0	1.0	1.0	1.0	0.9	0.9	0.9
Fe^{2+}	-	-	-	-	0.1	-	-
Mn	-	-	-	-	-	-	-
∑	1.0	1.0	1.0	1.0	1.0	1.0	1.0
Mg	0.2	0.2	0.2	0.2	-	-	-
Fe^{2+}	0.7	0.6	0.6	0.7	0.3	0.2	0.2
Mn	-	-	-	-	-	-	-
Ca	0.1	0.1	0.1	0.1	0.7	0.7	0.7
Na	-	-	-	-	-	0.1	0.1
K	-	-	-	-	-	-	-
∑	1.0	0.9	0.9	1.0	1.0	1.0	1.0
Atomic percentages							
Mg	59	61	61	58	45	46	45
∑Fe*	35	34	33	36	19	17	19
Ca	6	6	6	6	36	37	36

*$\sum Fe = Fe^{2+} + Fe^{3+} + Mg$

**not analyzed

Table G-2 (continued): Electron microprobe analyses of pyroxene group minerals. Cation recalculations based on six oxygen atoms PFU.

Sample	10SC004 -7-1-4	10SC004 -7-1-5	10SC004 -7-1-6	10SG001 -2-3-1	10SG001 -2-3-2	10SG001 -2-3-3	10SG001 -3-1-1
Na_2O	0.8	0.8	0.7	-**	-**	0.8	-**
MgO	15.9	16.1	16.3	15.5	14.5	14.7	17.9
Al_2O_3	1.7	2.0	1.5	1.7	2.1	1.9	0.6
SiO_2	51.8	51.7	52.4	51.4	51.3	50.7	51.9
CaO	18.8	18.7	18.8	15.0	17.2	17.4	3.3
TiO_2	1.0	1.0	0.8	1.1	1.2	1.3	0.3
Cr_2O_3	-**	-**	-**	-**	-**	-**	-**
MnO	0.3	0.3	0.4	0.5	0.5	0.4	0.8
FeO	9.8	9.5	9.2	14.8	13.3	12.8	25.2
∑	100.1	100.1	100.1	100.0	100.1	100.0	100.0
Si	1.9	1.9	1.9	1.9	1.9	1.9	2.0
Al	0.1	0.1	0.1	0.1	0.1	0.1	-
∑	2.0	2.0	2.0	2.0	2.0	2.0	2.0
Al	-	-	-	-	-	-	-
Fe^{3+}	0.1	0.1	0.1	-	-	0.1	-
Ti	-	-	-	-	-	-	-
Cr	-	-	-	-	-	-	-
Mg	0.9	0.9	0.9	0.9	0.8	0.8	1.0
Fe^{2+}	-	-	-	0.1	0.1	-	-
Mn	-	-	-	-	-	-	-
∑	1.0	1.0	1.0	1.0	0.9	0.9	1.0
Mg	-	-	-	-	-	-	-
Fe^{2+}	0.2	0.2	0.2	0.4	0.3	0.3	0.8
Mn	-	-	-	-	-	-	-
Ca	0.7	0.7	0.7	0.6	0.7	0.7	0.1
Na	0.1	0.1	0.1	-	-	0.1	-
K	-	-	-	-	-	-	-
∑	1.0	1.0	1.0	1.0	1.0	1.1	0.9
Atomic percentages							
Mg	45	46	46	45	42	42	51
∑Fe*	16	16	15	24	22	21	42
Ca	38	38	38	31	36	36	7

*$\sum Fe = Fe^{2+} + Fe^{3+} + Mg$

**not analyzed

Table G-2 (continued): Electron microprobe analyses of pyroxene group minerals. Cation recalculations based on six oxygen atoms PFU.

Sample	10SG001 -3-1-2	10SG001 -3-1-3	10SG001 -3-1-10	10SG001 -3-1-11	10SG001 -3-3-2	10SG001 -3-3-3	10SG001 -3-3-4
Na_2O	-**	0.8	-**	-**	-**	-**	-**
MgO	14.8	14.5	14.8	16.4	14.7	13.0	11.8
Al_2O_3	1.7	2.0	0.3	0.4	1.5	0.8	0.7
SiO_2	51.5	50.8	51.0	51.6	51.6	51.6	51.6
CaO	18.2	17.8	3.4	3.0	16.4	18.1	17.9
TiO_2	1.1	1.3	0.3	0.4	0.8	0.6	0.4
Cr_2O_3	-**	-**	-**	-**	-**	-**	-**
MnO	0.4	0.4	0.8	0.8	0.4	0.4	0.4
FeO	12.3	12.5	29.3	27.5	14.5	15.5	17.1
∑	100.0	100.1	99.9	100.1	99.9	100.0	99.9
Si	1.9	1.9	2.0	2.0	2.0	2.0	2.0
Al	0.1	0.1	-	-	0.1	-	-
∑	2.0	2.0	2.0	2.0	2.1	2.0	2.0
Al	-	-	-	-	-	-	-
Fe^{3+}	-	0.1	-	-	-	-	-
Ti	-	-	-	-	-	-	-
Cr	-	-	-	-	-	-	-
Mg	0.8	0.8	0.9	0.9	0.8	0.7	0.7
Fe^{2+}	0.1	0.1	0.1	-	0.1	0.2	0.3
Mn	-	-	-	-	-	-	-
∑	0.9	1.0	1.0	0.9	0.9	0.9	1.0
Mg	-	-	-	-	-	-	-
Fe^{2+}	0.3	0.2	0.8	0.8	0.3	0.3	0.2
Mn	-	-	-	-	-	-	-
Ca	0.7	0.7	0.1	0.1	0.7	0.7	0.7
Na	-	0.1	-	-	-	-	-
K	-	-	-	-	-	-	-
∑	1.0	1.0	0.9	0.9	1.0	1.0	0.9
Atomic percentages							
Mg	42	42	43	48	42	37	34
∑Fe*	20	21	49	46	24	26	28
Ca	37	37	7	6	34	37	37

*$\sum Fe = Fe^{2+} + Fe^{3+} + Mg$

**not analyzed

Table G-2 (continued): Electron microprobe analyses of pyroxene group minerals. Cation recalculations based on six oxygen atoms PFU.

Sample	10SG001 -3-3-5	10SG001 -3-3-6	10SG001 -3-3-7	10SG001 -5-1-4	10SG001 -5-1-5	10SG001 -5-1-6	10SG001 -8-2-4
Na_2O	-**	-**	-**	0.7	0.8	-**	0.7
MgO	14.5	15.9	14.8	14.7	14.4	18.7	16.0
Al_2O_3	0.3	0.4	0.3	1.5	1.9	0.6	1.7
SiO_2	51.1	51.3	51.0	51.4	50.6	52.0	52.0
CaO	3.8	3.4	3.2	16.8	17.4	5.0	20.2
TiO_2	0.1	0.3	0.2	1.0	1.2	0.4	0.8
Cr_2O_3	-**	-**	-**	-**	-**	-**	-**
MnO	0.8	0.8	0.7	0.4	0.5	0.7	0.3
FeO	29.3	28.0	29.9	13.5	13.3	22.6	8.3
∑	99.9	100.1	100.1	100.0	100.1	100.0	100.0
Si	2.0	2.0	2.0	1.9	1.9	2.0	1.9
Al	-	-	-	0.1	0.1	-	0.1
∑	2.0	2.0	2.0	2.0	2.0	2.0	2.0
Al	-	-	-	-	-	-	-
Fe^{3+}	-	-	-	0.1	0.1	-	0.1
Ti	-	-	-	-	-	-	-
Cr	-	-	-	-	-	-	-
Mg	0.8	0.9	0.9	0.8	0.8	1.0	0.9
Fe^{2+}	0.2	0.1	0.1	0.1	-	-	-
Mn	-	-	-	-	-	-	-
∑	1.0	1.0	1.0	1.0	0.9	1.0	1.0
Mg	-	-	-	-	-	0.1	-
Fe^{2+}	0.8	0.8	0.8	0.3	0.3	0.7	0.2
Mn	-	-	-	-	-	-	-
Ca	0.2	0.1	0.1	0.7	0.7	0.2	0.8
Na	-	-	-	0.1	0.1	-	0.1
K	-	-	-	-	-	-	-
∑	1.0	0.9	0.9	1.1	1.1	1.0	1.1
Atomic percentages							
Mg	42	46	43	43	42	53	45
∑Fe*	49	47	50	23	22	37	14
Ca	8	7	7	35	36	10	41

*$\sum Fe = Fe^{2+} + Fe^{3+} + Mg$

**not analyzed

Table G-2 (continued): Electron microprobe analyses of pyroxene group minerals. Cation recalculations based on six oxygen atoms PFU.

Sample	10SG001 -8-2-5	10SG001 -8-3-1	10SG001 -8-3-2	10SG001 -8-3-3	10BB001 -1-2-7	10BB001 -1-2-8	10BB001 -1-2-9
Na_2O	0.6	-**	-**	-**	0.6	-	0.7
MgO	16.1	23.2	23.6	23.8	15.2	15.3	15.2
Al_2O_3	1.7	0.5	0.6	0.9	2.9	3.2	2.7
SiO_2	52.5	53.3	52.9	53.4	51.2	51.3	50.8
CaO	20.0	0.5	0.6	1.0	20.1	19.7	20.2
TiO_2	0.8	0.4	0.3	0.3	1.2	1.2	1.1
Cr_2O_3	-**	-**	-**	-**	-**	0.6	-**
MnO	0.4	0.4	0.5	0.5	-**	-**	0.3
FeO	7.9	21.7	21.5	20.1	8.7	8.8	9.0
∑	100.0	100.0	100.0	100.0	99.9	100.1	100.0
Si	1.9	2.0	2.0	2.0	1.9	1.9	1.9
Al	0.1	-	-	-	0.1	0.1	0.1
∑	2.0	2.0	2.0	2.0	2.0	2.0	2.0
Al	-	-	-	-	-	-	-
Fe^{3+}	0.1	-	-	-	0.1	-	0.1
Ti	-	-	-	-	-	-	-
Cr	-	-	-	-	-	-	-
Mg	0.9	1.0	1.0	1.0	0.8	0.8	0.8
Fe^{2+}	-	-	-	-	-	0.1	-
Mn	-	-	-	-	-	-	-
∑	1.0	1.0	1.0	1.0	0.9	0.9	0.9
Mg	-	0.3	0.3	0.3	-	-	-
Fe^{2+}	0.2	0.7	0.6	0.6	0.2	0.2	0.2
Mn	-	-	-	-	-	-	-
Ca	0.8	-	-	-	0.8	0.8	0.8
Na	-	-	-	-	0.1	-	0.1
K	-	-	-	-	-	-	-
∑	1.0	1.0	0.9	0.9	1.1	1.0	1.1
Atomic percentages							
Mg	46	65	65	66	44	44	44
∑Fe*	13	35	34	32	14	14	15
Ca	41	1	1	2	42	41	42

*$\sum Fe = Fe^{2+} + Fe^{3+} + Mg$

**not analyzed

Table G-2 (continued): Electron microprobe analyses of pyroxene group minerals. Cation recalculations based on six oxygen atoms PFU.

Sample	10BB001 -3-2-5	10BB001 -3-2-6	10BB001 -3-2-7	10BB001 -4-1-1	10BB001 -4-1-2	10BB001 -4-1-3	10BB001 -5-2-10
Na_2O	0.9	-**	0.8	0.7	0.7	0.8	0.8
MgO	13.8	14.3	14.2	16.3	15.2	14.6	14.1
Al_2O_3	2.2	1.3	2.4	1.5	2.4	2.1	1.7
SiO_2	50.1	51.6	50.2	52.5	50.7	50.5	50.9
CaO	18.4	16.5	18.3	19.1	18.5	16.8	17.0
TiO_2	1.8	1.1	1.7	0.7	1.3	1.6	1.3
Cr_2O_3	-**	-**	-**	-**	-**	-**	-**
MnO	0.3	0.4	0.4	0.3	0.4	0.4	0.5
FeO	12.4	14.8	12.0	9.1	10.8	13.1	13.9
∑	99.9	100.0	100.0	100.1	100.0	99.9	100.2
Si	1.9	2.0	1.9	1.9	1.9	1.9	1.9
Al	0.1	0.1	0.1	0.1	0.1	0.1	0.1
∑	2.0	2.1	2.0	2.0	2.0	2.0	2.0
Al	-	-	-	-	-	-	-
Fe^{3+}	0.1	-	0.1	0.1	0.1	0.1	0.1
Ti	0.1	-	0.1	-	-	0.1	-
Cr	-	-	-	-	-	-	-
Mg	0.8	0.8	0.8	0.9	0.8	0.8	0.8
Fe^{2+}	0.1	0.2	0.1	-	-	0.1	0.1
Mn	-	-	-	-	-	-	-
∑	1.1	1.0	1.1	1.0	0.9	1.1	1.0
Mg	-	-	-	-	-	-	-
Fe^{2+}	0.2	0.3	0.2	0.2	0.2	0.3	0.3
Mn	-	-	-	-	-	-	-
Ca	0.7	0.7	0.7	0.8	0.7	0.7	0.7
Na	0.1	-	0.1	0.1	0.1	0.1	0.1
K	-	-	-	-	-	-	-
∑	1.0	1.0	1.0	1.0	1.0	1.1	1.1
Atomic percentages							
Mg	40	41	41	46	44	43	41
∑Fe*	21	25	20	15	18	22	24
Ca	39	34	38	39	38	35	36

*$\sum Fe = Fe^{2+} + Fe^{3+} + Mg$

**not analyzed

Table G-2 (continued): Electron microprobe analyses of pyroxene group minerals. Cation recalculations based on six oxygen atoms PFU.

Sample	10BB001 -5-2-11	10BB001 -5-2-12	10BB001 -6-1-7	10BB001 -6-1-8	10BB001 -6-1-9	10DE006 -1-1-4	10DE006 -1-1-5
Na_2O	0.8	-**	0.8	0.7	0.7	0.8	0.8
MgO	14.2	14.9	15.0	15.4	15.0	14.7	14.7
Al_2O_3	2.2	1.1	2.1	2.5	2.4	1.8	2.0
SiO_2	50.5	51.7	50.9	51.1	50.9	51.2	50.8
CaO	18.2	16.8	17.7	19.4	18.7	17.7	17.6
TiO_2	1.6	1.1	1.3	1.2	1.3	1.4	1.6
Cr_2O_3	-**	-**	-**	-**	-**	-**	-**
MnO	0.3	0.5	0.5	-**	0.3	0.4	0.4
FeO	12.2	13.9	11.8	9.8	10.7	12.0	12.2
∑	100.0	100.0	100.1	100.1	100.0	99.8	100.1
Si	1.9	2.0	1.9	1.9	1.9	1.9	1.9
Al	0.1	0.1	0.1	0.1	0.1	0.1	0.1
∑	2.0	2.1	2.0	2.0	2.0	2.0	2.0
Al	-	-	-	-	-	-	-
Fe^{3+}	0.1	-	0.1	0.1	0.1	0.1	0.1
Ti	0.1	-	-	-	-	-	-
Cr	-	-	-	-	-	-	-
Mg	0.8	0.8	0.8	0.9	0.8	0.8	0.8
Fe^{2+}	0.1	0.1	-	-	0.1	0.1	-
Mn	-	-	-	-	-	-	-
∑	1.1	0.9	0.9	1.0	1.0	1.0	0.9
Mg	-	-	-	-	-	-	-
Fe^{2+}	0.2	0.3	0.2	0.2	0.2	0.2	0.2
Mn	-	-	-	-	-	-	-
Ca	0.7	0.7	0.7	0.8	0.7	0.7	0.7
Na	0.1	-	0.1	0.1	0.1	0.1	0.1
K	-	-	-	-	-	-	-
∑	1.0	1.0	1.0	1.1	1.0	1.0	1.0
Atomic percentages							
Mg	41	42	43	44	43	43	43
∑Fe*	21	23	20	16	18	20	21
Ca	38	35	37	40	39	37	37

*$\sum Fe = Fe^{2+} + Fe^{3+} + Mg$

**not analyzed

Table G-2 (continued): Electron microprobe analyses of pyroxene group minerals. Cation recalculations based on six oxygen atoms PFU.

Sample	10DE006 -1-1-6	10DE006 -4-1-1	10DE006 -4-1-2	10DE006 -4-1-3	10DE006 -5-2-1	10DE006 -5-2-2	10DE006 -5-2-3
Na_2O	0.9	0.8	0.9	0.9	0.2	0.7	0.8
MgO	14.8	14.4	14.3	14.1	15.7	16.4	14.8
Al_2O_3	2.1	1.7	2.0	1.7	2.5	2.2	1.9
SiO_2	50.5	51.0	50.6	50.9	51.5	51.3	50.7
CaO	18.0	17.3	18.0	17.5	19.2	17.4	18.3
TiO_2	1.6	1.4	1.5	1.4	1.2	1.2	1.6
Cr_2O_3	-**	-**	-**	-**	0.4	-**	-**
MnO	0.4	0.5	0.4	0.5	0.3	0.4	0.4
FeO	11.6	12.9	12.4	13.1	9.1	10.3	11.6
∑	99.9	100.0	100.1	100.1	100.1	99.9	100.1
Si	1.9	1.9	1.9	1.9	1.9	1.9	1.9
Al	0.1	0.1	0.1	0.1	0.1	0.1	0.1
∑	2.0	2.0	2.0	2.0	2.0	2.0	2.0
Al	-	-	-	-	-	-	-
Fe^{3+}	0.1	0.1	0.1	0.1	-	0.1	0.1
Ti	0.1	-	-	-	-	-	-
Cr	-	-	-	-	-	-	-
Mg	0.8	0.8	0.8	0.8	0.9	0.9	0.8
Fe^{2+}	-	0.1	-	0.1	0.1	-	-
Mn	-	-	-	-	-	-	-
∑	1.0	1.0	0.9	1.0	1.0	1.0	0.9
Mg	-	-	-	-	-	-	-
Fe^{2+}	0.2	0.2	0.23	0.2	0.2	0.2	0.2
Mn	-	-	0.01	-	-	-	-
Ca	0.7	0.7	0.72	0.7	0.8	0.7	0.7
Na	0.1	0.1	0.06	0.1	-	0.1	0.1
K	-	-	-	-	-	-	-
∑	1.0	1.0	1.02	1.0	1.0	1.0	1.0
Atomic percentages							
Mg	43	42	42	41	45	47	43
∑Fe*	19	22	21	22	15	17	19
Ca	38	36	38	37	40	36	38

*$\sum Fe = Fe^{2+} + Fe^{3+} + Mg$

**not analyzed

Table G-2 (continued): Electron microprobe analyses of pyroxene group minerals. Cation recalculations based on six oxygen atoms PFU.

Sample	10FJ005 -3-1-1	10FJ005 -3-1-2	10FJ005 -3-1-3	10VI002 -3-2-1	10VI002 -3-2-2	10VI002 -3-2-3	10VI002 -4-1-1
Na_2O	0.7	0.7	0.7	0.7	-**	0.8	0.7
MgO	15.3	15.6	15.6	15.3	15.0	13.8	14.2
Al_2O_3	2.7	2.7	2.8	2.4	3.2	2.0	2.5
SiO_2	51.1	50.8	50.8	51.3	51.4	50.7	50.3
CaO	18.8	18.5	18.8	19.7	19.7	18.6	18.8
TiO_2	1.2	1.2	1.1	1.2	1.2	1.5	1.8
Cr_2O_3	-**	-**	-**	-**	0.7	-**	-**
MnO	0.3	0.5	0.3	-**	-**	0.4	0.4
FeO	9.9	10.2	10.0	9.4	8.9	12.3	11.4
∑	100.0	100.2	100.1	100.0	100.1	100.1	100.1
Si	1.9	1.9	1.9	1.9	1.9	1.9	1.9
Al	0.1	0.1	0.1	0.1	0.1	0.1	0.1
∑	2.0	2.0	2.0	2.0	2.0	2.0	2.0
Al	-	-	-	-	-	-	-
Fe^{3+}	0.1	0.1	0.1	0.1	-	0.1	0.1
Ti	-	-	-	-	-	-	0.1
Cr	-	-	-	-	-	-	-
Mg	0.9	0.9	0.9	0.8	0.8	0.8	0.8
Fe^{2+}	-	-	-		0.1	0.1	0.1
Mn	-	-	-	-	-	-	-
∑	1.0	1.0	1.0	0.9	0.9	1.0	1.1
Mg	-	-	-	-	-	-	-
Fe^{2+}	0.2	0.2	0.2	0.2	0.2	0.2	0.2
Mn	-	-	-	-	-	-	-
Ca	0.8	0.7	0.7	0.8	0.8	0.8	0.8
Na	0.1	0.1	0.1	0.1	-	0.1	0.1
K	-	-	-	-	-	-	-
∑	1.1	1.0	1.0	1.1	1.0	1.1	1.1
Atomic percentages							
Mg	44	45	45	44	44	40	41
∑Fe*	17	17	17	15	15	21	19
Ca	39	38	39	41	41	39	39

*$\sum Fe = Fe^{2+} + Fe^{3+} + Mg$

**not analyzed

Table G-2 (continued): Electron microprobe analyses of pyroxene group minerals. Cation recalculations based on six oxygen atoms PFU.

Sample	10VI002 -4-1-2	10VI002 -4-1-3	10VI004 -6-2-1	10VI004 -6-2-2	10VI004 -6-2-3
Na_2O	0.7	0.9	0.8	0.7	0.8
MgO	15.1	14.6	15.2	15.8	15.5
Al_2O_3	2.5	2.1	2.3	1.3	1.7
SiO_2	51.1	50.3	51.0	52.2	50.6
CaO	19.1	16.3	18.4	18.3	16.0
TiO_2	1.4	1.4	1.4	1.0	1.4
Cr_2O_3	-**	-**	-**	-**	-**
MnO	0.3	0.4	0.4	0.5	0.5
FeO	9.8	14.1	10.5	10.3	13.6
∑	100.0	100.1	100.0	100.1	100.1
Si	1.9	1.9	1.9	1.9	1.9
Al	0.1	0.1	0.1	0.1	0.1
∑	2.0	2.0	2.0	2.0	2.0
Al	-	-	-	-	-
Fe^{3+}	0.1	0.1	0.1	0.1	0.1
Ti	-	-	-	-	-
Cr	-	-	-	-	-
Mg	0.8	0.8	0.8	0.9	0.9
Fe^{2+}	0.1	-	-	-	-
Mn	-	-	-	-	-
∑	1.0	0.9	0.9	1.0	1.0
Mg	-	-	-	-	-
Fe^{2+}	0.2	0.3	0.2	0.2	0.3
Mn	-	-	-	-	-
Ca	0.8	0.7	0.7	0.7	0.6
Na	0.1	0.1	0.1	0.1	0.1
K	-	-	-	-	-
∑	1.1	1.1	1.0	1.0	1.0
Atomic percentages					
Mg	44	42	44	45	44
∑Fe*	16	24	18	17	23
Ca	40	34	38	37	33

*$\sum Fe = Fe^{2+} + Fe^{3+} + Mg$

**not analyzed

Table G-3: Electron microprobe analyses of chlorite group minerals.
Cation recalculations based on eight oxygen atoms PFU.

Sample	11CLD001 10-22-007	11CLD001 10-22-008	11CLD001 10-22-009	11CLD001 10-22-010	11CLD001 10-22-021	11CLD001 10-22-022	11CLD001 10-22-023	11CLD001 10-22-035	11CLD001 10-22-044	11CLD001 10-29-39
Na_2O	-**	-**	-**	-**	-**	-**	-**	-**	-**	-**
MgO	22.8	23.0	22.9	22.1	23.2	22.8	23.2	23.5	23.4	23.1
Al_2O_3	18.5	18.5	18.9	17.8	19.0	18.7	18.8	18.7	18.4	19.4
SiO_2	33.6	33.5	33.3	33.1	33.7	33.8	33.6	34.5	34.6	33.9
CaO	-**	-**	-**	-**	-**	-**	-**	-**	-**	-**
TiO_2	-**	-**	-**	-**	-**	-**	-**	-**	-**	-**
MnO	-**	-**	0.6	-**	-**	-**	-**	-**	-**	-**
FeO	25.1	25.0	24.3	27.0	24.1	24.8	24.4	23.3	23.7	23.6
∑	100.0	100.0	100.0	100.0	100.0	100.1	100.0	100.0	100.1	100.0
Si	6.1	6.1	6.0	6.1	6.1	6.1	6.1	6.2	6.2	6.1
Ti	-	-	-	-	-	-	-	-	-	-
Al	1.9	1.9	2.0	2.0	1.9	1.9	2.0	1.8	1.8	1.9
∑	8.0	8.0	8.0	8.1	8.0	8.0	8.1	8.0	8.0	8.0
Al	2.0	2.0	2.1	1.9	2.1	2.1	2.1	2.1	2.1	2.2
Fe*	3.8	3.8	3.7	4.1	3.6	3.7	3.7	3.5	3.6	3.5
Mg	6.1	6.2	6.2	6.0	6.2	6.1	6.2	6.3	6.2	6.2
Mn	-	-	0.1	-	-	-	-	-	-	-
Na	-	-	-	-	-	-	-	-	-	-
Ca	-	-	-	-	-	-	-	-	-	-
∑	11.9	12.0	12.1	12.0	11.9	11.9	12.0	11.9	11.9	11.9
Fe/(Fe+Mg)	0.38	0.38	0.37	0.41	0.37	0.38	0.37	0.36	0.36	0.36

*all Fe as Fe^{2+}

**not analyzed

Table G-3 (continued): Electron microprobe analyses of chlorite group minerals.
Cation recalculations based on eight oxygen atoms PFU.

Sample	11CLD001 10-29-43	11CLD001 10-29-44	11CLD001 10-29-52	11CLD001 10-29-55	11CLD001 10-29-57	11CLD003 10-29-04	11CLD003 10-29-05	11CLD003 10-29-06	11CLD003 10-29-14	11CLD003 10-29-15
Na_2O	-**	-**	-**	-**	-**	-**	-**	-**	-**	0.6
MgO	23.9	23.2	23.0	22.8	22.1	20.8	19.9	21.4	22.3	21.6
Al_2O_3	19.0	18.6	18.4	18.7	18.4	19.1	17.6	18.4	19.3	18.5
SiO_2	34.0	33.6	33.7	33.2	32.7	32.8	32.4	33.4	33.8	32.8
CaO	-**	-**	-**	-**	-**	-**	-**	0.4	-**	0.3
TiO_2	-**	-**	-**	-**	-**	-**	-**	-**	-**	-**
MnO	0.6	0.7	0.7	0.6	-**	0.9	1.1	1.0	-**	0.7
FeO	22.6	24.0	24.2	24.7	26.8	26.4	29.0	25.5	24.6	25.4
∑	100.1	100.1	100.0	100.0	100.0	100.0	100.0	100.1	100.0	99.9
Si	6.1	6.1	6.1	6.0	6.0	6.0	6.1	6.1	6.1	6.1
Ti	-	-	-	-	-	-	-	-	-	-
Al	1.9	1.9	1.9	2.0	2.0	2.0	1.9	1.9	1.9	2.0
∑	8.0	8.0	8.0	8.0	8.0	8.0	8.0	8.0	8.0	8.1
Al	2.1	2.0	2.1	2.0	1.9	2.2	1.9	2.1	2.2	2.1
Fe*	3.4	3.6	3.7	3.8	4.1	4.1	4.5	3.9	3.7	3.9
Mg	6.4	6.3	6.2	6.2	6.0	5.7	5.6	5.9	6.0	5.9
Mn	0.1	0.1	0.1	0.1	-	0.1	0.2	0.2	-	0.1
Na	-	-	-	-	-	-	-	-	-	0.2
Ca	-	-	-	-	-	-	-	0.1	-	0.1
∑	12.0	12.0	12.1	12.1	12.0	12.1	12.2	12.2	11.9	12.0
Fe/(Fe+Mg)	0.35	0.37	0.37	0.38	0.40	0.42	0.45	0.40	0.38	0.40

*all Fe as Fe^{2+}

**not analyzed

Table G-3 (continued): Electron microprobe analyses of chlorite group minerals.
Cation recalculations based on eight oxygen atoms PFU.

Sample	11CLD003 10-29-16	11CLD003 10-29-25	11CLD003 10-29-26	11CLD003 10-29-27	11CBF006 11-06-018	11CBF006 11-06-022	11CBF006 11-06-023	11CBF006 11-06-026	11CBF006 11-06-037	11CBF006 11-06-043
Na_2O	0.8	0.8	0.8	-**	-**	-**	-**	-**	-**	-**
MgO	21.7	21.7	21.2	20.8	18.9	18.1	18.6	18.8	20.9	18.5
Al_2O_3	18.7	18.5	18.6	18.1	18.3	18.7	18.5	18.1	18.9	18.5
SiO_2	33.1	33.1	32.8	33.3	32.0	31.9	31.7	31.9	32.3	31.5
CaO	-**	-**	-**	-**	-**	-**	-**	-**	-**	-**
TiO_2	-**	-**	-**	-**	-**	-**	-**	-**	-**	-**
MnO	0.7	0.7	0.8	0.7	0.8	-**	0.8	0.7	0.7	0.9
FeO	25.0	25.2	25.9	27.1	30.1	31.3	30.5	30.5	27.2	30.6
∑	100.0	100.0	100.1	100.0	100.1	100.0	100.1	100.0	100.0	100.0
Si	6.1	6.1	6.1	6.1	6.0	6.0	6.0	6.0	6.0	5.9
Ti	-	-	-	-	-	-	-	-	-	-
Al	1.9	1.9	1.9	1.9	2.0	2.0	2.1	2.0	2.0	2.1
∑	8.0	8.0	8.0	8.0	8.0	8.0	8.1	8.0	8.0	8.0
Al	2.1	2.1	2.1	2.0	2.0	2.1	2.0	2.0	2.1	2.0
Fe*	3.8	3.9	4.0	4.2	4.7	4.9	4.8	4.8	4.2	4.8
Mg	5.9	5.9	5.8	5.7	5.3	5.0	5.2	5.3	5.7	5.2
Mn	0.1	0.1	0.1	0.1	0.1	-	0.1	0.1	0.1	0.1
Na	0.3	0.3	0.3	-	-	-	-	-	-	-
Ca	-	-	-	-	-	-	-	-	-	-
∑	12.2	12.3	12.3	12.0	12.1	12.0	12.1	12.2	12.1	12.1
Fe/(Fe+Mg)	0.39	0.40	0.41	0.42	0.47	0.49	0.48	0.48	0.42	0.48

*all Fe as Fe^{2+}

**not analyzed

Table G-3 (continued): Electron microprobe analyses of chlorite group minerals.
Cation recalculations based on eight oxygen atoms PFU.

Sample	11CBF006 11-06-049	11CBF006 11-06-053	11CBF006 11-06-058	11CBF006 -5-1-7	11CBF006 -5-1-8	11CBF006 -5-1-9	11CLD007 11-06-066	11CLD007 11-06-067	11CLD007 11-06-070	11CLD007 11-06-076
Na_2O	-**	-**	-**	-**	-**	-**	-**	-**	-**	-**
MgO	20.3	18.4	18.6	20.2	19.7	18.2	25.0	24.7	24.3	25.0
Al_2O_3	18.5	18.7	18.3	18.9	19.2	18.7	19.0	19.0	19.6	18.7
SiO_2	32.2	31.9	32.2	32.6	32.6	32.1	34.6	34.1	33.6	34.8
CaO	-**	-**	-**	-**	-**	0.2	-**	-**	-**	-**
TiO_2	-**	-**	-**	-**	-**	-**	-**	-**	-**	-**
MnO	0.8	0.9	0.7	0.8	0.6	0.7	0.7	0.8	0.7	0.7
FeO	28.2	30.1	30.2	27.5	27.9	30.1	20.7	21.5	21.7	20.9
∑	100.0	100.0	100.0	100.0	100.0	100.0	100.0	100.1	99.9	100.1
Si	6.0	6.0	6.0	6.0	6.0	6.0	6.2	6.1	6.0	6.2
Ti	-	-	-	-	-	-	-	-	-	-
Al	2.0	2.0	2.0	2.0	2.0	2.0	1.8	1.9	2.0	1.8
∑	8.0	8.0	8.0	8.0	8.0	8.0	8.0	8.0	8.0	8.0
Al	2.0	2.1	2.1	2.1	2.2	2.1	2.1	2.1	2.2	2.1
Fe*	4.4	4.7	4.7	4.3	4.3	4.7	3.1	3.2	3.3	3.1
Mg	5.6	5.2	5.2	5.6	5.4	5.1	6.6	6.6	6.5	6.6
Mn	0.1	0.1	0.1	0.1	0.1	0.1	0.1	0.1	0.1	0.1
Na	-	-	-	-	-	-	-	-	-	-
Ca	-	-	-	-	-	-	-	-	-	-
∑	12.1	12.1	12.1	12.1	12.0	12.0	11.9	12.0	12.1	11.9
Fe/(Fe+Mg)	0.44	0.48	0.48	0.43	0.44	0.48	0.32	0.33	0.33	0.32

*all Fe as Fe^{2+}

**not analyzed

Table G-3 (continued): Electron microprobe analyses of chlorite group minerals.
Cation recalculations based on eight oxygen atoms PFU.

Sample	11CLD007 11-06-078	11CLD007 11-06-080	11CLD007 11-06-083	11CLD007 11-06-086	11CLD007 11-06-087	11CLD007 11-06-089	11CLD007 11-06-093	11CLD007 11-06-100	11CBF004 -001	11CBF004 -002
Na_2O	-**	-**	-**	-**	-**	-**	-**	-**	-**	-**
MgO	24.7	22.8	23.7	24.9	24.6	25.1	23.7	23.2	20.0	19.5
Al_2O_3	19.0	18.5	18.4	18.4	18.6	19.0	19.0	19.0	17.4	18.8
SiO_2	34.5	33.0	34.1	34.9	34.5	34.2	33.9	33.9	33.0	32.3
CaO	-**	-**	-**	-**	-**	-**	-**	-**	0.9	-**
TiO_2	-**	-**	-**	-**	-**	-**	-**	-**	0.6	-**
MnO	-**	0.6	0.8	0.8	0.7	0.7	-**	-**	0.7	-**
FeO	21.8	24.9	23.0	21.0	21.5	21.1	23.4	23.9	27.4	29.3
∑	100.0	99.8	100.0	100.0	99.9	100.1	100.0	100.0	100.0	99.9
Si	6.1	6.0	6.1	6.2	6.2	6.1	6.1	6.1	6.1	6.0
Ti	-	-	-	-	-	-	-	-	0.1	-
Al	1.9	2.0	1.9	1.8	1.8	1.9	1.9	1.9	1.8	2.0
∑	8.0	8.0	8.0	8.0	8.0	8.0	8.0	8.0	8.0	8.0
Al	2.1	2.0	2.1	2.1	2.1	2.1	2.1	2.1	2.1	2.1
Fe*	3.2	3.8	3.5	3.1	3.2	3.1	3.5	3.6	4.3	4.5
Mg	6.5	6.2	6.4	6.6	6.6	6.7	6.3	6.2	5.6	5.4
Mn	-	0.1	0.1	0.1	0.1	0.1	-	-	0.1	-
Na	-	-	-	-	-	-	-	-	-	-
Ca	-	-	-	-	-	-	-	-	0.2	-
∑	11.8	12.1	12.1	11.9	12.0	12.0	11.9	11.9	12.3	12.0
Fe/(Fe+Mg)	0.33	0.38	0.35	0.32	0.33	0.32	0.36	0.37	0.43	0.46

*all Fe as Fe^{2+}

**not analyzed

Table G-3 (continued): Electron microprobe analyses of chlorite group minerals.
Cation recalculations based on eight oxygen atoms PFU.

Sample	11CBF004 -003	11CBF004 -015	11CBF004 -016	11CBF004 -028	11CBF004 -034	11CBF004 -3-2-7	11CBF004 -3-2-8	11CBF004 -3-2-9	11CBF004 -8-1-4	11CBF004 -8-1-5
Na_2O	-**	-**	-**	0.7	-**	-**	-**	-**	-**	-**
MgO	20.6	19.9	20.5	19.8	19.5	21.8	22.6	22.5	20.6	21.5
Al_2O_3	17.1	17.7	17.8	17.5	18.1	18.9	18.1	17.9	18.2	17.7
SiO_2	33.3	33.3	33.8	33.1	32.8	34.8	35.5	35.2	34.9	35.5
CaO	0.5	-**	-**	0.5	-**	0.2	0.2	0.2	-**	0.4
TiO_2	-**	-**	-**	-**	-**	-**	-**	-**	-**	-**
MnO	0.7	-**	-**	-**	0.7	0.6	0.4	0.5	0.6	0.6
FeO	27.8	29.1	27.9	28.4	28.9	23.8	23.3	23.7	25.7	24.4
∑	100.0	100.0	100.0	100.0	100.0	100.1	100.1	100.0	100.0	100.0
Si	6.2	6.1	6.2	6.2	6.1	6.3	6.4	6.3	6.3	6.4
Ti	-	-	-	-	-	-	-	-	-	-
Al	1.8	1.9	1.8	1.8	1.9	1.7	1.6	1.7	1.7	1.6
∑	8.0	8.0	8.0	8.0	8.0	8.0	8.0	8.0	8.0	8.0
Al	1.9	2.0	2.0	2.0	2.0	2.3	2.2	2.1	2.2	2.2
Fe*	4.3	4.5	4.3	4.4	4.5	3.6	3.5	3.6	3.9	3.7
Mg	5.7	5.5	5.6	5.5	5.4	5.9	6.0	6.0	5.6	5.8
Mn	0.1	-	-	-	0.1	0.1	0.1	0.1	0.1	0.1
Na	-	-	-	0.3	-	-	-	-	-	-
Ca	0.1	-	-	0.1	-	-	0.1	-	-	0.1
∑	12.1	12.0	11.9	12.3	12.0	11.8	11.9	11.8	11.8	11.9
Fe/(Fe+Mg)	0.43	0.45	0.43	0.45	0.45	0.38	0.37	0.37	0.41	0.39

*all Fe as Fe^{2+}

**not analyzed

Table G-3 (continued): Electron microprobe analyses of chlorite group minerals.
Cation recalculations based on eight oxygen atoms PFU.

Sample	11CBF004 -8-1-6	10SC004 -1-1-5	10SC004 -1-1-6	10SC004 -2-1-10	10SC004 -2-1-11	10SC004 -2-1-12	10SC004 -2-2-4	10SC004 -2-2-5	10SC004 -2-2-6	10SC004 -3-1-4
Na_2O	-**	-**	-**	-**	-**	-**	-**	-**	-**	-**
MgO	21.3	21.1	21.6	22.3	22.1	22.1	14.2	13.0	14.2	19.3
Al_2O_3	18.7	12.9	12.9	14.0	13.8	14.8	17.1	18.1	15.6	14.3
SiO_2	34.2	38.6	39.1	39.5	39.1	39.2	35.8	35.6	36.5	39.0
CaO	0.2	0.8	1.4	0.8	0.8	1.0	1.7	2.0	1.3	1.2
TiO_2	-**	-**	1.1	-**	-**	-**	-**	-**	-**	-**
MnO	0.4	-**	-**	-**	0.3	0.3	0.5	0.4	0.4	0.3
FeO	25.1	26.6	24.0	23.4	24.0	22.7	30.9	30.9	32.2	25.9
∑	99.9	100.0	100.1	100.0	100.1	100.1	100.2	100.0	100.2	100.0
Si	6.2	7.0	7.1	7.1	7.0	7.0	6.7	6.7	6.9	7.1
Ti	-	-	0.1	-	-	-	-	-	-	-
Al	1.8	1.0	0.8	0.9	1.0	1.0	1.3	1.3	1.1	0.9
∑	8.0	8.0	8.0	8.0	8.0	8.0	8.0	8.0	8.0	8.0
Al	2.2	1.8	2.0	2.0	2.0	2.1	2.5	2.7	2.3	2.2
Fe*	3.8	4.1	3.6	3.5	3.6	3.4	4.9	4.9	5.1	4.0
Mg	5.7	5.7	5.8	5.9	5.9	5.9	4.0	3.7	4.0	5.2
Mn	0.1	-	-	-	0.1	-	0.1	0.1	0.1	-
Na	-	-	-	-	-	-	-	-	-	-
Ca	-	0.2	0.3	0.2	0.2	0.2	0.3	0.4	0.3	0.2
∑	11.8	11.8	11.7	11.6	11.8	11.7	11.8	11.8	11.8	11.6
Fe/(Fe+Mg)	0.40	0.41	0.38	0.37	0.38	0.37	0.55	0.57	0.56	0.43

*all Fe as Fe^{2+}

**not analyzed

Table G-3 (continued): Electron microprobe analyses of chlorite group minerals.
Cation recalculations based on eight oxygen atoms PFU.

Sample	10SC004 -5-1-1	10SC004 -5-1-2	10SC004 -5-1-3	10SC004 -5-1-4	10SC004 -5-1-5	10SC004 -5-1-6	10SC004 -6-1-4	10SC004 -6-1-5	10SC004 -6-1-6	10SG001 -1-3-1
Na_2O	-**	-**	-**	-**	-**	-**	-**	-**	-**	-**
MgO	14.2	13.6	12.0	19.0	21.5	20.9	15.2	15.0	15.9	10.0
Al_2O_3	16.1	16.4	17.1	16.5	13.2	13.0	17.1	14.7	14.3	14.0
SiO_2	36.4	36.3	35.2	37.8	38.7	39.0	35.9	37.2	37.7	34.8
CaO	1.5	1.4	2.0	2.2	0.6	0.7	1.7	1.4	1.3	1.3
TiO_2	-**	-**	-**	-**	-**	-**	-**	-**	-**	-**
MnO	0.3	0.3	0.5	0.4	-**	-**	-**	-**	-**	0.5
FeO	31.5	32.0	33.2	24.2	26.0	26.5	30.1	31.7	30.8	39.5
∑	100.0	100.0	100.0	100.1	100.0	100.1	100.1	100.0	100.0	100.1
Si	6.9	6.8	6.7	6.9	7.0	7.1	6.7	7.0	7.0	6.9
Ti	-	-	-	-	-	-	-	-	-	-
Al	1.2	1.2	1.3	1.1	1.0	0.9	1.3	1.0	1.0	1.2
∑	8.1	8.0	8.0	8.0	8.0	8.0	8.0	8.0	8.0	8.1
Al	2.4	2.5	2.6	2.5	1.8	1.9	2.5	2.2	2.2	2.1
Fe*	5.0	5.1	5.3	3.7	4.0	4.0	4.7	5.0	4.8	6.5
Mg	4.0	3.8	3.4	5.2	5.8	5.7	4.2	4.2	4.4	2.9
Mn	0.1	0.1	0.1	0.1	-	-	-	-	-	0.1
Na	-	-	-	-	-	-	-	-	-	-
Ca	0.3	0.3	0.4	0.4	0.1	0.1	0.4	0.3	0.3	0.3
∑	11.7	11.8	11.8	11.9	11.7	11.7	11.8	11.7	11.7	11.9
Fe/(Fe+Mg)	0.55	0.57	0.61	0.42	0.40	0.42	0.53	0.54	0.52	0.69

*all Fe as Fe^{2+}

**not analyzed

Table G-3 (continued): Electron microprobe analyses of chlorite group minerals.
Cation recalculations based on eight oxygen atoms PFU.

Sample	10SG001 -1-3-2	10SG001 -1-3-3	10SG001 -2-1-1	10SG001 -2-1-2	10SG001 -2-1-3	10SG001 -3-1-7	10SG001 -3-1-8	10SG001 -3-1-9	10SG001 -3-3-8	10SG001 -3-3-9
Na_2O	-**	-**	-**	-**	-**	-**	-**	-**	-**	-**
MgO	10.9	10.9	18.8	20.0	19.4	21.4	20.7	21.8	20.0	20.6
Al_2O_3	13.8	13.6	13.3	14.0	13.5	11.6	11.5	11.9	11.1	11.1
SiO_2	35.5	35.6	38.9	38.3	38.5	39.9	39.3	39.2	37.9	39.6
CaO	1.2	1.2	1.0	0.7	0.9	0.6	0.7	0.7	1.0	1.0
TiO_2	-**	-**	-**	-**	-**	-**	-**	-**	-**	-**
MnO	0.5	0.4	0.3	0.3	-**	-**	0.2	-**	0.4	-**
FeO	38.1	38.4	27.7	26.7	27.8	26.4	27.7	26.5	29.6	27.6
∑	100.0	100.1	100.0	100.0	100.1	99.9	100.1	100.1	100.0	99.9
Si	6.9	6.9	7.1	7.0	7.0	7.2	7.2	7.1	7.1	7.3
Ti	-	-	-	-	-	-	-	-	-	-
Al	1.1	1.1	0.9	1.0	1.0	0.8	0.8	0.9	0.9	0.7
∑	8.0	8.0	8.0	8.0	8.0	8.0	8.0	8.0	8.0	8.0
Al	2.1	2.1	2.0	2.0	2.0	1.7	1.7	1.7	1.5	1.7
Fe*	6.2	6.3	4.2	4.1	4.3	4.0	4.2	4.0	4.6	4.2
Mg	3.2	3.2	5.2	5.4	5.3	5.8	5.6	5.9	5.6	5.6
Mn	0.1	0.1	-	0.1	-	-	-	-	0.1	-
Na	-	-	-	-	-	-	-	-	-	-
Ca	0.3	0.2	0.2	0.1	0.2	0.1	0.1	0.1	0.2	0.2
∑	11.9	11.9	11.7	11.7	11.8	11.6	11.6	11.7	12.0	11.7
Fe/(Fe+Mg)	0.66	0.66	0.45	0.43	0.45	0.41	0.43	0.41	0.45	0.43

*all Fe as Fe^{2+}

**not analyzed

Table G-3 (continued): Electron microprobe analyses of chlorite group minerals.
Cation recalculations based on eight oxygen atoms PFU.

Sample	10SG001 -5-1-1	10SG001 -5-1-2	10SG001 -5-1-3	10BB001 -1-1-1	10BB001 -1-1-2	10BB001 -1-1-3	10BB001 -1-2-4	10BB001 -1-2-5	10BB001 -1-2-6	10BB001 -3-1-1
Na_2O	-**	-**	-**	-**	-**	-**	-**	-**	-**	-**
MgO	18.3	19.3	19.2	20.4	20.8	20.7	20.4	20.1	19.2	20.6
Al_2O_3	11.2	11.3	11.7	15.7	15.9	16.7	14.9	14.3	14.3	16.0
SiO_2	39.2	39.3	38.2	36.0	36.3	35.8	37.8	39.0	40.3	37.5
CaO	0.8	0.6	0.6	0.4	0.4	0.3	0.8	0.7	1.0	0.6
TiO_2	-**	-**	-**	-**	-**	-**	-**	-**	-**	-**
MnO	-**	-**	-**	0.9	0.9	0.7	0.7	0.6	0.6	0.6
FeO	30.5	29.5	30.3	26.6	25.9	25.8	25.4	25.3	24.6	24.8
∑	100.0	100.0	100.0	100.0	100.2	100.0	100.1	100.0	100.0	100.1
Si	7.3	7.2	7.1	6.6	6.6	6.5	6.9	7.1	7.3	6.8
Ti	-	-	-	-	-	-	-	-	-	-
Al	0.7	0.8	0.9	1.4	1.4	1.5	1.1	0.9	0.7	1.2
∑	8.0	8.0	8.0	8.0	8.0	8.0	8.0	8.0	8.0	8.0
Al	1.7	1.7	1.6	2.0	2.1	2.1	2.1	2.1	2.3	2.2
Fe*	4.7	4.5	4.7	4.1	4.0	3.9	3.9	3.8	3.7	3.8
Mg	5.1	5.3	5.3	5.6	5.7	5.6	5.5	5.4	5.2	5.6
Mn	-	-	-	0.1	0.1	0.1	0.1	0.1	0.1	0.1
Na	-	-	-	-	-	-	-	-	-	-
Ca	0.2	0.1	0.1	0.1	0.1	0.1	0.2	0.1	0.2	0.1
∑	11.8	11.6	11.7	11.9	12.0	11.8	11.8	11.5	11.5	11.8
Fe/(Fe+Mg)	0.48	0.46	0.47	0.42	0.41	0.41	0.41	0.41	0.42	0.40

*all Fe as Fe^{2+}

**not analyzed

Table G-3 (continued): Electron microprobe analyses of chlorite group minerals.
Cation recalculations based on eight oxygen atoms PFU.

Sample	10BB001 -3-1-2	10BB001 -3-1-3	10BB001 -4-1-7	10BB001 -4-1-8	10BB001 -4-1-9	10BB001 -5-1-1	10BB001 -5-1-2	10BB001 -5-1-3	10BB001 -5-1-4	10BB001 -5-1-5
Na_2O	-**	-**	-**	-**	-**	-**	-**	-**	-**	-**
MgO	20.4	20.7	20.3	20.4	19.9	20.6	20.1	21.1	20.5	20.6
Al_2O_3	15.8	16.1	15.1	14.9	16.2	16.1	16.4	14.9	15.7	15.9
SiO_2	37.9	36.8	38.5	39.2	36.6	35.8	35.7	36.8	36.8	36.4
CaO	0.6	0.5	0.7	0.8	1.4	0.4	0.3	0.6	0.4	0.5
TiO_2	-**	-**	-**	-**	-**	-**	-**	-**	-**	-**
MnO	0.5	0.7	0.7	0.6	0.6	0.8	0.9	0.8	0.8	0.8
FeO	24.7	25.2	24.7	24.2	25.3	26.4	26.6	25.9	25.8	25.8
∑	99.9	100.0	100.0	100.1	100.0	100.1	100.0	100.1	100.0	100.0
Si	6.9	6.7	7.0	7.1	6.7	6.6	6.6	6.7	6.7	6.7
Ti	-	-	-	-	-	-	-	-	-	-
Al	1.1	1.3	1.0	0.9	1.3	1.4	1.4	1.3	1.3	1.4
∑	8.0	8.0	8.0	8.0	8.0	8.0	8.0	8.0	8.0	8.1
Al	2.2	2.1	2.2	2.2	2.2	2.0	2.1	2.0	2.1	2.1
Fe*	3.7	3.8	3.7	3.6	3.9	4.1	4.1	4.0	3.9	3.9
Mg	5.5	5.6	5.5	5.5	5.4	5.6	5.5	5.8	5.6	5.6
Mn	0.1	0.1	0.1	0.1	0.1	0.1	0.1	0.1	0.1	0.1
Na	-	-	-	-	-	-	-	-	-	-
Ca	0.1	0.1	0.1	0.2	0.3	0.1	0.1	0.1	0.1	0.1
∑	11.6	11.7	11.6	11.6	11.9	11.9	11.9	12.0	11.8	11.8
Fe/(Fe+Mg)	0.40	0.41	0.41	0.40	0.42	0.42	0.43	0.41	0.41	0.41

*all Fe as Fe^{2+}

**not analyzed

Table G-3 (continued): Electron microprobe analyses of chlorite group minerals.
Cation recalculations based on eight oxygen atoms PFU.

Sample	10BB001 -5-1-6	10BB001 -5-1-7	10BB001 -5-2-1	10BB001 -5-2-2	10BB001 -5-2-3	10BB001 -6-1-4	10BB001 -6-1-5	10BB001 -6-1-6	10DE003 -1-1-4	10DE003 -1-1-5
Na_2O	-**	-**	-**	-**	-**	-**	-**	-**	-**	-**
MgO	20.1	20.7	20.0	19.4	19.2	20.8	19.8	20.9	31.1	30.6
Al_2O_3	15.8	16.0	16.5	16.4	16.4	15.6	15.1	15.6	17.9	18.0
SiO_2	37.4	36.3	36.2	36.4	35.7	36.7	37.9	37.0	38.8	38.2
CaO	0.6	0.3	1.1	1.4	1.1	0.5	0.6	0.6	0.2	0.2
TiO_2	-**	-**	-**	-**	-**	-**	-**	-**	-**	-**
MnO	0.8	0.9	0.7	0.7	0.7	0.7	0.6	0.7	0.6	0.5
FeO	25.3	25.8	25.5	25.7	26.9	25.8	26.0	25.3	11.5	12.5
∑	100.0	100.0	100.0	100.0	100.0	100.1	100.0	100.1	100.1	100.0
Si	6.8	6.6	6.6	6.7	6.6	6.7	6.9	6.7	6.6	6.5
Ti	-	-	-	-	-	-	-	-	-	-
Al	1.2	1.4	1.4	1.3	1.4	1.3	1.1	1.3	1.4	1.5
∑	8.0	8.0	8.0	8.0	8.0	8.0	8.0	8.0	8.0	8.0
Al	2.2	2.1	2.2	2.3	2.2	2.0	2.1	2.1	2.2	2.1
Fe*	3.9	4.0	3.9	3.9	4.2	3.9	4.0	3.8	1.6	1.8
Mg	5.5	5.6	5.5	5.3	5.3	5.7	5.4	5.7	7.9	7.8
Mn	0.1	0.1	0.1	0.1	0.1	0.1	0.1	0.1	0.1	0.1
Na	-	-	-	-	-	-	-	-	-	-
Ca	0.1	0.1	0.2	0.3	0.2	0.1	0.1	0.1	-	-
∑	11.8	11.9	11.9	11.9	12.0	11.8	11.7	11.8	11.8	11.8
Fe/(Fe+Mg)	0.41	0.41	0.42	0.43	0.44	0.41	0.42	0.40	0.17	0.19

*all Fe as Fe^{2+}

**not analyzed

Table G-3 (continued): Electron microprobe analyses of chlorite group minerals.
Cation recalculations based on eight oxygen atoms PFU.

Sample	10DE003 -1-1-6	10DE003 -2-1-4	10DE003 -2-1-5	10DE003 -2-1-6	10DE003 -5-1-7	10DE003 -5-1-8	10DE003 -5-1-9	10DE006 -1-2-1	10DE006 -1-2-2	10DE006 -1-2-3
Na_2O	-**	-**	-**	-**	-**	-**	-**	-**	-**	-**
MgO	30.8	27.8	28.5	28.8	29.0	28.4	30.4	20.0	25.5	21.7
Al_2O_3	18.0	15.4	15.9	16.6	15.7	15.7	17.0	17.2	16.8	16.4
SiO_2	38.6	42.7	42.5	41.9	42.9	43.1	40.9	36.6	37.4	37.6
CaO	0.3	0.9	0.8	0.7	0.9	1.0	0.6	1.9	0.6	1.7
TiO_2	-**	-**	-**	-**	-**	-**	-**	-**	-**	-**
MnO	0.5	0.5	0.5	0.4	0.5	0.4	0.4	0.7	0.6	0.6
FeO	11.8	12.7	11.8	11.7	11.1	11.4	10.8	23.7	19.2	22.0
∑	100.0	100.0	100.0	100.1	100.1	100.0	100.0	100.1	100.1	100.0
Si	6.6	7.3	7.2	7.1	7.2	7.3	6.9	6.7	6.6	6.8
Ti	-	-	-	-	-	-	-	-	-	-
Al	1.5	0.7	0.8	0.9	0.8	0.7	1.1	1.3	1.4	1.2
∑	8.1	8.0	8.0	8.0	8.0	8.0	8.0	8.0	8.0	8.0
Al	2.2	2.4	2.4	2.4	2.4	2.4	2.3	2.4	2.1	2.3
Fe*	1.7	1.8	1.7	1.7	1.6	1.6	1.5	3.6	2.8	3.3
Mg	7.8	7.0	7.2	7.2	7.3	7.2	7.6	5.4	6.7	5.8
Mn	0.1	0.1	0.1	0.1	0.1	0.1	0.1	0.1	0.1	0.1
Na	-	-	-	-	-	-	-	-	-	-
Ca	0.1	0.2	0.2	0.1	0.2	0.2	0.1	0.4	0.1	0.3
∑	11.9	11.5	11.6	11.5	11.6	11.5	11.6	11.9	11.8	11.8
Fe/(Fe+Mg)	0.18	0.20	0.19	0.19	0.18	0.18	0.17	0.40	0.30	0.36

*all Fe as Fe^{2+}

**not analyzed

Table G-3 (continued): Electron microprobe analyses of chlorite group minerals.
Cation recalculations based on eight oxygen atoms PFU.

Sample	10DE006 -1-3-7	10DE006 -1-3-8	10DE006 -1-3-9	10DE006 -2-2-1	10DE006 -2-2-2	10DE006 -2-2-3	10DE006 -3-1-7	10DE006 -3-1-8	10DE006 -3-1-9	10DE006 -5-2-4
Na_2O	-**	-**	-**	-**	-**	-**	-**	-**	-**	-**
MgO	24.4	25.1	25.5	22.7	22.5	19.4	26.1	24.8	25.0	26.1
Al_2O_3	13.8	13.9	17.6	16.9	17.0	16.6	16.4	17.5	18.0	16.8
SiO_2	38.0	38.5	38.0	39.0	38.9	36.8	37.3	38.0	37.5	37.3
CaO	0.3	0.2	0.4	0.6	0.8	1.4	0.3	0.7	0.7	0.5
TiO_2	-**	-**	-**	-**	-**	-**	-**	-**	-**	-**
MnO	0.5	0.5	0.5	0.6	0.6	0.5	0.5	0.5	0.6	0.5
FeO	23.1	21.8	18.0	20.2	20.2	25.2	19.4	18.5	18.3	18.7
∑	100.1	100.0	100.0	100.0	100.0	99.9	100.0	100.0	100.1	99.9
Si	6.8	6.9	6.6	6.9	6.9	6.7	6.6	6.7	6.6	6.6
Ti	-	-	-	-	-	-	-	-	-	-
Al	1.2	1.2	1.4	1.1	1.1	1.3	1.4	1.3	1.4	1.4
∑	8.0	8.1	8.0	8.0	8.0	8.0	8.0	8.0	8.0	8.0
Al	1.7	1.8	2.3	2.4	2.4	2.3	2.0	2.3	2.3	2.1
Fe*	3.5	3.3	2.6	3.0	3.0	3.9	2.9	2.7	2.7	2.8
Mg	6.5	6.7	6.6	6.0	5.9	5.3	6.9	6.5	6.6	6.9
Mn	0.1	0.1	0.1	0.1	0.1	0.1	0.1	0.1	0.1	0.1
Na	-	-	-	-	-	-	-	-	-	-
Ca	0.1	-	0.1	0.1	0.2	0.3	0.1	0.1	0.1	0.1
∑	11.9	11.0	11.7	11.6	11.6	11.8	12.0	11.7	11.8	12.0
Fe/(Fe+Mg)	0.35	0.33	0.28	0.33	0.33	0.42	0.29	0.30	0.29	0.29

*all Fe as Fe^{2+}

**not analyzed

Table G-3 (continued): Electron microprobe analyses of chlorite group minerals.
Cation recalculations based on eight oxygen atoms PFU.

Sample	10DE006 -5-2-5	10DE006 -5-2-6	10DE006 -6-1-4	10DE006 -6-1-5	10DE006 -6-1-6	10FJ005 -2-1-1	10FJ005 -2-1-2	10FJ005 -3-1-4	10FJ005 -3-1-5	10FJ005 -3-1-6
Na_2O	-**	-**	-**	-**	-**	-**	-**	-**	-**	-**
MgO	25.6	21.2	26.4	26.3	26.3	21.1	22.0	22.2	21.4	21.9
Al_2O_3	18.0	17.2	17.1	16.1	16.6	18.5	17.6	17.2	17.4	17.3
SiO_2	37.8	36.3	37.2	37.2	37.2	32.9	36.5	37.1	37.4	37.6
CaO	0.6	1.6	0.3	0.4	0.3	-**	-**	0.7	0.9	1.0
TiO_2	-**	-**	-**	-**	-**	-**	-**	-**	-**	-**
MnO	0.6	0.7	-**	0.5	0.5	1.3	1.0	0.7	0.7	0.6
FeO	17.6	22.9	19.0	19.6	19.1	26.2	22.2	22.0	22.2	21.7
∑	100.2	99.9	100.0	100.1	100.0	100.0	100.3	99.9	100.0	100.1
Si	6.6	6.6	6.5	6.6	6.6	6.1	6.6	6.7	6.7	6.7
Ti	-	-	-	-	-	-	-	-	-	-
Al	1.4	1.4	1.5	1.4	1.4	1.9	1.4	1.3	1.3	1.3
∑	8.0	8.0	8.0	8.0	8.0	8.0	8.0	8.0	8.0	8.0
Al	2.3	2.3	2.0	1.9	2.0	2.1	2.3	2.3	2.4	2.4
Fe*	2.6	3.5	2.8	2.9	2.8	4.0	3.4	3.3	3.3	3.2
Mg	6.7	5.8	6.9	6.9	6.9	5.8	5.9	5.9	5.7	5.8
Mn	0.1	0.1	-	0.1	0.1	0.2	0.1	0.1	0.1	0.1
Na	-	-	-	-	-	-	-	-	-	-
Ca	0.1	0.3	0.1	0.1	0.1	-	-	0.1	0.2	0.2
∑	11.8	12.0	11.8	11.9	11.9	12.1	11.7	11.7	11.7	11.7
Fe/(Fe+Mg)	0.28	0.38	0.29	0.29	0.29	0.41	0.36	0.36	0.37	0.36

*all Fe as Fe^{2+}

**not analyzed

Table G-3 (continued): Electron microprobe analyses of chlorite group minerals. Cation recalculations based on eight oxygen atoms PFU.

Sample	10BA005 -6-1-3	10BA005 -6-1-7	10BA005 -6-1-8	10BA005 -6-1-9	10BA005 -2-2-10	10BA005 -2-2-11	10BA005 -2-2-12
Na_2O	-**	-**	-**	-**	-**	-**	-**
MgO	26.2	24.1	23.1	25.8	24.4	24.7	23.9
Al_2O_3	19.8	19.6	20.2	19.4	20.6	20.5	20.2
SiO_2	36.6	36.6	36.8	36.6	37.0	37.3	37.2
CaO	0.3	0.3	0.3	0.2	0.2	0.3	0.3
TiO_2	-**	-**	-**	-**	-**	-**	-**
MnO	0.3	-**	-**	0.3	0.4	0.4	0.5
FeO	16.9	19.4	19.6	17.6	17.5	16.9	17.9
∑	100.1	100.0	100.0	99.9	100.1	100.1	100.0
Si	6.4	6.4	6.4	6.4	6.4	6.5	6.5
Ti	-	-	-	-	-	-	-
Al	1.7	1.6	1.6	1.6	1.6	1.6	1.5
∑	8.1	8.0	8.0	8.0	8.0	8.1	8.0
Al	2.4	2.4	2.6	2.4	2.6	2.6	2.6
Fe*	2.5	2.8	2.9	2.6	2.5	2.5	2.6
Mg	6.8	6.3	6.0	6.7	6.3	6.4	6.2
Mn	0.1	-	-	0.1	0.1	0.1	0.1
Na	-	-	-	-	-	-	-
Ca	0.1	0.1	0.1	-	-	0.1	0.1
∑	11.9	11.6	11.6	11.8	11.5	11.7	11.6
Fe/(Fe+Mg)	0.27	0.31	0.32	0.28	0.29	0.28	0.30

*all Fe as Fe^{2+}

**not analyzed

Table G-4: Electron microprobe analyses of epidote group minerals.
Cation recalculations based on 12.5 oxygen atoms PFU.

Sample	11CLD001 10-22-038	11CLD001 10-22-040	11CLD001 10-22-041	11CLD001 10-22-043	11CLD001 10-29-46	11CLD001 10-29-47	11CLD001 10-29-48	11CLD003 10-29-01	11CLD003 10-29-02	11CLD003 10-29-03
MgO	-*	-*	-*	-*	-*	-*	-*	-*	1.3	0.8
Al_2O_3	21.7	20.8	21.3	20.8	23.1	20.1	19.7	19.7	19.9	19.4
SiO_2	39.0	39.1	39.4	39.4	40.2	38.8	38.7	38.9	38.7	38.8
K_2O	-*	-*	-*	-*	0.4	-*	-*	-*	-*	-*
CaO	22.6	22.9	22.9	22.7	22.7	22.5	22.6	22.6	21.8	22.3
TiO_2	-*	0.6	-*	-*	-*	-*	-*	-*	-*	-*
MnO	-*	-*	-*	-*	-*	-*	-*	-*	-*	-*
FeO	16.7	16.6	16.4	17.1	13.7	18.7	19.0	18.8	18.3	18.7
∑	100.0	100.0	100.0	100.0	100.1	100.1	100.0	100.0	100.0	100.0
Si	3.0	3.1	3.1	3.1	3.1	3.0	3.0	3.1	3.0	3.0
Al	-	-	-	-	-	-	-	-	-	-
∑	3.0	3.1	3.1	3.1	3.1	3.0	3.0	3.1	3.0	3.0
Al	2.0	1.9	2.0	1.9	2.1	1.9	1.8	1.8	1.8	1.8
Fe^{3+}	0.9	0.9	0.9	1.0	0.7	1.1	1.1	1.1	1.2	1.2
Ti	-	-	-	-	-	-	-	-	-	-
MnO	-	-	-	-	-	-	-	-	-	-
Mg	-	-	-	-	-	-	-	-	0.2	0.1
Fe^{2+}	0.1	0.1	0.1	0.1	0.2	0.1	0.1	0.1	-	-
∑	3.0	2.9	3.0	3.0	3.0	3.1	3.0	3.0	3.1	3.1
Fe^{2+}	0.1	-	-	-	-	0.1	0.1	0.1	-	0.1
Ca	1.9	1.9	1.9	1.9	1.9	1.9	1.9	1.9	1.8	1.9
K	-	-	-	-	-	-	-	-	-	-
∑	2.0	1.9	1.9	1.9	1.9	2.0	2.0	2.0	1.8	2.0
$Fe^{3+}/(Fe^{3+}+Al)$	32.1	32.5	31.6	33.1	25.7	36.5	38.2	37.1	38.8	39.4

*not analyzed

Table G-4 (continued): Electron microprobe analyses of epidote group minerals.
Cation recalculations based on 12.5 oxygen atoms PFU.

Sample	11CLD003 10-29-22	11CLD003 10-29-24	11CBF006 11-06-001	11CBF006 11-06-002	11CBF006 11-06-003	11CBF006 11-06-007	11CBF006 11-06-028	11CBF006 11-06_057	11CBF006 -5-1-10	11CBF006 -5-1-11
MgO	0.8	-*	-*	-*	-*	-*	-*	-*	-*	-*
Al_2O_3	20.1	18.9	22.3	24.5	22.0	21.4	23.7	21.8	21.0	21.6
SiO_2	39.2	39.0	39.0	39.6	39.6	39.2	40.1	39.5	39.5	39.6
K_2O	-*	-*	-*	-*	-*	-*	-*	-*	-*	-*
CaO	22.0	22.2	21.7	22.7	21.8	23.1	22.6	22.3	23.6	23.8
TiO_2	-*	-*	-*	-*	-*	-*	-*	-*	-*	-*
MnO	-*	-*	1.0	-*	1.0	-*	-*	-*	-*	-*
FeO	17.8	19.9	15.9	13.2	15.6	16.2	13.7	16.4	16.0	15.0
∑	99.9	100.0	99.9	100.0	100.0	99.9	100.1	100.0	100.1	100.0
Si	3.1	3.1	3.0	3.1	3.1	3.1	3.1	3.1	3.1	3.1
Al	-	-	-	-	-	-	-	-	-	-
∑	3.1	3.1	3.0	3.1	3.1	3.1	3.1	3.1	3.1	3.1
Al	1.9	1.8	2.1	2.2	2.0	2.0	2.2	2.0	1.9	2.0
Fe^{3+}	1.0	1.1	0.9	0.7	0.8	0.9	0.7	0.9	0.9	0.9
Ti	-	-	-	-	-	-	-	-	-	-
MnO	-	-	0.1	-	0.1	-	-	-	-	-
Mg	0.1	-	-	-	-	-	-	-	-	-
Fe^{2+}	-	0.1	-	0.1	0.1	0.1	0.2	0.1	0.1	0.1
∑	3.0	3.0	3.1	3.0	3.0	3.0	3.1	3.0	2.9	3.0
Fe^{2+}	0.1	0.1	0.2	0.1	0.1	-	-	0.1	-	-
Ca	1.8	1.9	1.8	1.9	1.8	1.9	1.9	1.9	2.0	2.0
K	-	-	-	-	-	-	-	-	-	-
∑	1.9	2.0	2.0	2.0	1.9	1.9	1.9	1.9	2.0	2.0
$Fe^{3+}/(Fe^{3+}+Al)$	36.0	38.9	30.1	23.4	28.7	31.9	23.6	29.9	32.7	30.7

*not analyzed

Table G-4 (continued): Electron microprobe analyses of epidote group minerals.
Cation recalculations based on 12.5 oxygen atoms PFU.

Sample	11CBF006 -5-1-12	11CLD005 02-25-003	11CLD005 02-25-004	11CLD005 02-25-005	11CLD005 02-25-007	11CLD005 02-25-008	10CN002 -1-3-7	10CN002 -1-3-8	10CN002 -1-3-9	10CN002 -6-2-1
MgO	-*	-*	-*	-*	-*	-*	-*	-*	-*	-*
Al_2O_3	21.2	22.6	20.9	22.7	25.9	25.9	21.9	20.0	20.4	20.2
SiO_2	39.4	39.7	38.8	39.8	40.0	40.2	40.7	41.5	40.9	40.2
K_2O	-*	-*	-*	-*	-*	-*	-*	-*	-*	-*
CaO	24.0	23.1	23.2	23.2	22.8	23.3	22.7	22.6	22.9	23.1
TiO_2	-*	-*	-*	-*	-*	-*	0.3	-*	-*	-*
MnO	-*	-*	-*	-*	0.7	-*	-*	-*	-*	-*
FeO	15.4	14.6	17.2	14.3	10.6	10.7	14.4	16.0	15.9	16.5
∑	100.0	100.0	100.1	100.0	100.0	100.1	100.0	100.1	100.1	100.0
Si	3.1	3.1	3.0	3.1	3.1	3.1	3.2	3.2	3.2	3.1
Al	-	-	-	-	-	-	-	-	-	-
∑	3.1	3.1	3.0	3.1	3.1	3.1	3.2	3.2	3.2	3.1
Al	1.9	2.1	1.9	2.1	2.3	2.3	2.0	1.8	1.9	1.9
Fe^{3+}	0.9	0.8	1.0	0.8	0.5	0.5	0.7	0.7	0.7	0.9
Ti	-	-	-	-	-	-	-	-	-	-
MnO	-	-	-	-	0.1	-	-	-	-	-
Mg	-	-	-	-	-	-	-	-	-	-
Fe^{2+}	0.1	0.2	0.1	0.2	0.1	0.2	0.3	0.4	0.3	0.2
∑	2.9	3.1	3.0	3.1	3.0	3.0	3.0	2.9	2.9	3.0
Fe^{2+}	-	-	-	-	0.1	-	-	-	-	-
Ca	2.0	1.9	1.9	1.9	1.9	1.9	1.9	1.9	1.9	1.9
K	-	-	-	-	-	-	-	-	-	-
∑	2.0	1.9	1.9	1.9	2.0	1.9	1.9	1.9	1.9	1.9
$Fe^{3+}/(Fe^{3+}+Al)$	32.2	27.3	34.9	26.8	18.5	18.0	24.6	26.9	28.4	31.7

*not analyzed

Table G-4 (continued): Electron microprobe analyses of epidote group minerals.
Cation recalculations based on 12.5 oxygen atoms PFU.

Sample	10CN002 -6-2-2	10CN002 -6-2-3	10QU006 -5-1-9	10QU006 -5-1-10	10QU006 -5-2-1	10QU006 -5-2-4	10QU006 -5-2-5	10DE003 -4-1	10DE003 -4-2	10DE003 -4-3	10DE003 -4-4
MgO	-*	-*	-*	-*	2.1	-*	-*	-*	-*	-*	-*
Al_2O_3	22.5	21.0	21.2	20.0	20.5	20.1	20.5	23.0	19.7	22.2	22.4
SiO_2	41.0	40.3	41.3	40.4	41.1	40.5	40.3	39.8	39.3	40.0	39.7
K_2O	-*	-*	-*	-*	-*	-*	-*	-*	-*	-*	-*
CaO	22.6	22.8	22.8	23.0	23.4	22.9	22.9	23.2	23.7	23.2	23.5
TiO_2	0.3	0.3	-*	-*	-*	-*	-*	-*	-*	-*	-*
MnO	-*	-*	-*	-*	-*	-*	-*	0.5	-*	-*	-*
FeO	13.7	15.7	14.7	16.6	12.9	16.6	16.3	13.5	17.4	14.6	14.3
∑	100.1	100.1	100.0	100.0	100.1	100.1	100.0	100.0	100.1	100.0	99.9
Si	3.2	3.1	3.2	3.2	3.2	3.2	3.1	3.1	3.1	3.1	3.1
Al	-	-	-	-	-	-	-	-	-	-	-
∑	3.2	3.1	3.2	3.2	3.2	3.2	3.1	3.1	3.1	3.1	3.1
Al	2.1	1.9	1.9	1.8	1.9	1.8	1.9	2.1	1.8	2.0	2.1
Fe^{3+}	0.6	0.8	0.6	0.9	0.8	0.8	0.9	0.7	1.0	0.8	0.8
Ti	-	-	-	-	-	-	-	-	-	-	-
MnO	-	-	-	-	-	-	-	-	-	-	-
Mg	-	-	-	-	0.2	-	-	-	-	-	-
Fe^{2+}	0.3	0.3	0.3	0.2	-	0.3	0.2	0.1	0.1	0.2	0.1
∑	3.0	3.0	2.8	2.9	2.9	2.9	3.0	2.9	2.9	3.0	3.0
Fe^{2+}	-	-	-	-	-	-	-	-	-	-	-
Ca	1.9	1.9	1.9	1.9	1.9	1.9	1.9	1.9	2.0	1.9	2.0
K	-	-	-	-	-	-	-	-	-	-	-
∑	1.9	1.9	1.9	1.9	1.9	1.9	1.9	1.9	2.0	1.9	2.0
$Fe^{3+}/(Fe^{3+}+Al)$	21.9	28.5	24.8	32.1	30.9	31.1	31.2	26.2	36.5	27.2	28.2

*not analyzed

Table G-5: Electron microprobe analyses of epidote group mineral with REE.
Cation recalculations based on 12.5 oxygen atoms PFU.

Sample	10QU006
Al_2O_3	20.6
SiO_2	39.6
K_2O	-*
CaO	19.6
MnO	0.5
FeO	15.1
La_2O_3	1.6
Ce_2O_3	3.0
∑	100.0
Si	3.2
Al	-
∑	3.2
Al	2.0
Fe^{3+}	0.6
MnO	-
Fe^{2+}	0.5
∑	3.1
Fe^{2+}	-
Ca	1.7
K	-
La^{3+}	0.1
Ce^{3+}	0.1
∑	1.9
$Fe^{3+}/(Fe^{3+}+Al)$	22.3

*not analyzed

Table G-6: Electron microprobe analyses of pumpellyite minerals.
Cation recalculations based on three silica atoms PFU.

Sample	11CLD001 10-22_015	11CLD001 10-22_016	11CLD001 10-22_017	11CLD003 10-29-020	11CLD007 11-06_075	11CLD007 11-06_088	11CLD007 -7-1-9	11CBF004 -021	11CBF004 -023	10CN002 -2-1-4	10CN002 -2-1-5
Na_2O	-**	-**	-**	0.8	-**	-**	-**	-**	-**	-**	-**
MgO	2.9	3.7	3.0	3.9	2.9	3.4	2.7	2.5	3.2	3.1	3.3
Al_2O_3	22.3	21.7	21.7	22.7	24.2	23.8	23.7	24.6	24.1	20.0	19.4
SiO_2	39.6	40.5	40.2	41.3	40.5	40.3	41.2	40.9	40.0	41.2	41.4
CaO	23.0	21.3	22.6	21.5	23.0	23.7	23.8	23.3	23.2	23.2	23.3
TiO_2	-**	-**	-**	-**	-**	-**	-**	-**	-**	-**	-**
MnO	-**	-**	-**	-**	-**	-**	-**	-**	-**	-**	-**
FeO	12.1	12.8	12.5	9.9	9.5	8.9	8.7	8.8	9.5	12.5	12.5
∑	99.9	100.0	100.0	100.1	100.1	100.1	100.1	100.1	100.0	100.0	99.9
Si	3.0	3.0	3.0	3.0	3.0	3.0	3.0	3.0	3.0	3.0	3.0
Al	-	-	-	-	0.1	0.1	-	0.1	0.1	-	-
∑	3.0	3.0	3.0	3.0	3.1	3.1	3.0	3.1	3.1	3.0	3.0
Al	2.0	1.9	1.9	1.9	2.0	2.0	2.0	2.0	2.0	1.7	1.7
Ti	-	-	-	-	-	-	-	-	-	-	-
∑	2.0	1.9	1.9	1.9	2.0	2.0	2.0	2.0	2.0	1.7	1.7
Al	-	-	-	-	0.1	0.1	-	0.1	0.1	-	-
Mg	0.3	0.4	0.3	0.4	0.3	0.4	0.3	0.3	0.4	0.3	0.4
Mn	-	-	-	-	-	-	-	-	-	-	-
Fe*	0.8	0.8	0.8	0.6	0.6	0.6	0.5	0.5	0.6	0.8	0.8
∑	1.1	1.2	1.1	1.0	1.0	1.1	0.8	0.9	1.1	1.1	1.2
Ca	1.9	1.7	1.8	1.7	1.8	1.9	1.9	1.8	1.9	1.8	1.8
Na	-	-	-	0.1	-	-	-	-	-	-	-
∑	1.9	1.7	1.8	1.8	1.8	1.9	1.9	1.8	1.9	1.8	1.8
Atomic percentages											
Al	64.5	61.3	63.3	65.5	69.9	69.2	71.3	72.3	69.2	61.1	59.6
Fe	24.8	25.6	25.8	20.2	19.4	18.4	18.5	18.4	19.4	27.0	27.4
Mg	10.7	13.1	10.9	14.2	10.7	12.5	10.2	9.3	11.4	11.9	13.0

* all Fe as Fe^{2+}, **not analyzed

Table G-6 (continued): Electron microprobe analyses of pumpellyite minerals.
Cation recalculations based on three silica atoms PFU.

Sample	10CN002 -2-1-6	10CN002 -2-1-8	10CN002 -2-3-1	10CN002 -2-3-2	10CN002 -2-3-3	10CN002 -4-2-1	10CN002 -4-2-2	10CN002 -4-2-3	10CN002 -5-1-4	10CN002 -5-1-5	10CN002 -5-1-6
Na_2O	-**	-**	-**	-**	-**	-**	0.5	-**	-**	-**	-**
MgO	3.3	3.3	2.8	3.8	2.9	2.8	2.8	2.8	3.1	3.2	3.2
Al_2O_3	19.7	20.0	19.8	20.3	19.2	20.2	20.3	20.8	20.2	19.1	18.4
SiO_2	41.0	41.0	40.4	41.0	41.2	41.2	40.7	41.3	41.1	40.9	41.1
CaO	23.6	23.4	23.9	23.4	23.3	23.3	23.2	23.0	23.6	23.1	23.1
TiO_2	-**	-**	0.1	0.1	-**	-**	-**	-**	-**	-**	-**
MnO	-**	-**	-**	-**	-**	-**	-**	-**	-**	-**	-**
FeO	12.3	12.3	13.0	11.4	13.4	12.5	12.6	12.1	12.1	13.8	14.2
∑	99.9	100.0	100.0	100.0	100.0	100.0	100.1	100.0	100.1	100.1	100.0
Si	3.0	3.0	3.0	3.0	3.0	3.0	3.0	3.0	3.0	3.0	3.0
Al	-	-	-	-	-	-	-	-	-	-	-
∑	3.0	3.0	3.0	3.0	3.0	3.0	3.0	3.0	3.0	3.0	3.0
Al	1.7	1.7	1.7	1.8	1.7	1.7	1.8	1.8	1.7	1.7	1.6
Ti	-	-	-	-	-	-	-	-	-	-	-
∑	1.7	1.7	1.7	1.8	1.7	1.7	1.8	1.8	1.7	1.7	1.6
Al	-	-	-	-	-	-	-	-	-	-	-
Mg	0.4	0.4	0.3	0.4	0.3	0.3	0.3	0.3	0.3	0.4	0.4
Mn	-	-	-	-	-	-	-	-	-	-	-
Fe*	0.8	0.8	0.8	0.7	0.8	0.8	0.8	0.7	0.7	0.8	0.9
∑	1.2	1.2	1.1	1.1	1.1	1.1	1.1	1.0	1.0	1.2	1.3
Ca	1.9	1.8	1.9	1.8	1.8	1.8	1.8	1.8	1.8	1.8	1.8
Na	-	-	-	-	-	-	0.1	-	-	-	-
∑	1.9	1.8	1.9	1.8	1.8	1.8	1.9	1.8	1.8	1.8	1.8
Atomic percentages											
Al	60.4	60.7	60.7	61.2	59.3	62.1	62.1	63.2	61.8	57.9	56.6
Fe	26.7	26.6	28.3	24.4	29.3	27.3	27.3	26.1	26.2	29.7	30.9
Mg	12.9	12.7	11.0	14.4	11.3	10.7	10.7	10.7	12.0	12.4	12.4

* all Fe as Fe^{2+}, **not analyzed

Table G-6 (continued): Electron microprobe analyses of pumpellyite minerals.
Cation recalculations based on three silica atoms PFU.

Sample	10CN002 -5-2-7	10CN002 -6-2-4	10CN002 -6-2-5	10CN002 -6-2-6	10QU006 -1-1-10	10QU006 -1-1-11	10QU006 -1-1-12	10QU006 -6-1-1	10QU006 -6-1-2	10QU006 -6-1-3	10DE003 -1-1-1
Na_2O	-**	-**	-**	-**	-**	-**	-**	-**	-**	-**	-**
MgO	3.6	3.2	3.1	3.3	2.4	2.3	2.2	2.3	2.2	2.2	3.1
Al_2O_3	26.1	20.4	19.7	21.2	20.6	19.9	19.5	20.7	21.4	20.9	22.6
SiO_2	42.5	41.3	41.0	41.2	41.1	40.4	40.6	41.0	40.7	41.0	40.8
CaO	22.7	23.4	23.5	23.4	23.1	23.3	23.4	23.4	23.4	23.4	24.0
TiO_2	-**	-**	-**	-**	0.1	-**	-**	-**	-**	-**	-**
MnO	-**	-**	-**	-**	0.4	0.3	0.3	-**	-**	-**	-**
FeO	5.1	11.7	12.7	11.0	12.1	13.8	14.1	12.6	12.3	12.6	9.5
∑	100.0	100.0	100.0	100.1	99.8	100.0	100.1	100.0	100.0	100.1	100.0
Si	3.0	3.0	3.0	3.0	3.0	3.0	3.0	3.0	3.0	3.0	3.0
Al	0.2	-	-	-	-	-	-	-	-	-	-
∑	3.2	3.0	3.0	3.0	3.0	3.0	3.0	3.0	3.0	3.0	3.0
Al	2.0	1.8	1.7	1.8	1.8	1.7	1.7	1.8	1.9	1.8	2.0
Ti	-	-	-	-	-	-	-	-	-	-	-
∑	2.0	1.8	1.7	1.8	1.8	1.7	1.7	1.8	1.9	1.8	2.0
Al	0.2	-	-	-	-	-	-	-	-	-	-
Mg	0.4	0.4	0.3	0.4	0.3	0.3	0.2	0.3	0.2	0.2	0.3
Mn	-	-	-	-	-	-	-	-	-	-	-
Fe*	0.3	0.7	0.8	0.7	0.7	0.9	0.9	0.8	0.8	0.8	0.6
∑	0.9	1.1	1.1	1.1	1.0	1.2	1.1	1.1	1.0	1.0	0.9
Ca	1.7	1.8	1.8	1.8	1.8	1.9	1.9	1.8	1.8	1.8	1.9
Na	-	-	-	-	-	-	-	-	-	-	-
∑	1.7	1.8	1.8	1.8	1.8	1.9	1.9	1.8	1.8	1.8	1.9
Atomic percentages											
Al	76.2	62.3	60.3	63.9	63.9	61.1	60.4	63.6	65.1	64.0	67.9
Fe	10.6	25.3	27.8	23.5	26.6	30.0	31.1	27.4	26.6	27.3	20.3
Mg	13.2	12.4	11.9	12.6	9.4	8.8	8.6	9.0	8.3	8.6	11.8

* all Fe as Fe^{2+}, **not analyzed

Table G-6 (continued): Electron microprobe analyses of pumpellyite minerals.
Cation recalculations based on three silica atoms PFU.

Sample	10DE003 -1-1-2	10DE003 -1-1-3	10DE003 -2-1-7	10DE003 -2-1-8	10DE003 -2-1-9	10DE003 -5-1-2	10DE003 -5-1-3	10DE003 -5-1-4	10DE003 -5-1-5	10DE003 -5-1-6
Na_2O	-**	-**	-**	-**	-**	-**	-**	-**	-**	-**
MgO	3.1	2.9	4.0	3.2	3.7	3.6	3.1	2.6	2.5	2.5
Al_2O_3	23.0	22.2	24.5	22.7	23.2	25.9	24.9	22.9	23.1	23.5
SiO_2	40.6	40.7	41.2	41.2	40.6	41.0	40.7	40.0	40.2	40.4
CaO	23.6	24.0	23.9	23.2	24.1	23.9	24.4	24.6	24.2	24.3
TiO_2	-**	-**	-**	-**	-**	-**	-**	-**	-**	-**
MnO	-**	-**	-**	-**	-**	0.3	-**	-**	-**	-**
FeO	9.8	10.2	6.4	9.8	8.5	5.3	7.0	9.9	10.0	9.3
∑	100.1	100.0	100.0	100.1	100.1	100.0	100.0	100.0	100.0	100.0
Si	3.0	3.0	3.0	3.0	3.0	3.0	3.0	3.0	3.0	3.0
Al	-	-	0.1	-	-	0.2	0.2	-	-	0.1
∑	3.0	3.0	3.1	3.0	3.0	3.2	3.2	3.0	3.0	3.1
Al	2.0	1.9	2.0	2.0	2.0	2.0	2.0	2.0	2.0	2.0
Ti	-	-	-	-	-	-	-	-	-	-
∑	2.0	1.9	2.0	2.0	2.0	2.0	2.0	2.0	2.0	2.0
Al	-	-	0.1	-	-	0.2	0.2	-	-	0.1
Mg	0.3	0.3	0.4	0.3	0.4	0.4	0.3	0.3	0.3	0.3
Mn	-	-	-	-	-	-	-	-	-	-
Fe*	0.6	0.6	0.4	0.6	0.5	0.3	0.4	0.6	0.6	0.6
∑	0.9	0.9	0.9	0.9	0.9	1.0	0.9	0.9	0.9	1.0
Ca	1.9	1.9	1.9	1.8	1.9	1.9	1.9	2.0	1.9	1.9
Na	-	-	-	-	-	-	-	-	-	-
∑	1.9	1.9	1.9	1.8	1.9	1.9	1.9	2.0	1.9	1.9
Atomic percentages										
Al	68.0	67.0	71.9	67.5	68.5	75.6	73.6	69.1	69.3	70.6
Fe	20.5	21.9	13.4	20.6	17.8	11.1	14.7	21.1	21.2	19.9
Mg	11.5	11.1	14.7	11.9	13.8	13.3	11.7	9.8	9.5	9.5

* all Fe as Fe^{2+}, **not analyzed

Table G-7: Electron microprobe analyses of prehnite minerals.
Cation recalculations based on eleven oxygen atoms PFU.

Sample	10CN002 -1-1-1	10CN002 -1-1-2	10CN002 -1-1-3	10CN002 -1-4-1	10CN002 -1-4-2	10CN002 -1-4-3	10CN002 -1-4-4	10CN002 -2-1-7	10CN002 -3-1-1	10CN002 -3-1-2	10CN002 -3-1-3	10CN002 -3-2-1
MgO	-*	-*	-*	-*	-*	-*	-*	-*	-*	-*	0.3	-*
Al_2O_3	19.1	19.6	18.8	18.8	18.9	19.8	19.1	23.8	19.7	20.0	20.2	19.0
SiO_2	47.1	47.4	46.9	46.7	46.6	47.4	47.2	47.1	46.7	46.8	46.8	46.7
CaO	25.8	25.6	25.7	26.1	26.2	25.4	25.5	26.3	26.2	26.5	26.1	26.4
TiO_2	-*	-*	-*	-*	-*	-*	-*	-*	-*	-*	-*	-*
FeO	8.0	7.5	8.6	8.4	8.4	7.4	8.2	2.8	7.4	6.7	6.6	8.0
∑	100.0	100.1	100.0	100.0	100.1	100.0	100.0	100.0	100.0	100.0	100.0	100.1
Si	3.1	3.1	3.1	3.1	3.1	3.1	3.1	3.1	3.1	3.1	3.1	3.1
Al	0.9	0.9	0.9	0.9	0.9	0.9	0.9	0.9	0.9	0.9	0.9	0.9
∑	4.0	4.0	4.0	4.0	4.0	4.0	4.0	4.0	4.0	4.0	4.0	4.0
Al	0.6	0.7	0.6	0.6	0.6	0.7	0.6	0.9	0.6	0.7	0.7	0.6
Fe^{3+}	0.4	0.4	0.5	0.5	0.5	0.4	0.5	0.2	0.4	0.4	0.4	0.4
∑	1.0	1.1	1.1	1.1	1.1	1.1	1.1	1.1	1.1	1.1	1.1	1.0
Ti	-	-	-	-	-	-	-	-	-	-	-	-
Ca	1.8	1.8	1.8	1.9	1.9	1.8	1.8	1.8	1.9	1.9	1.9	1.9
Mg	-	-	-	-	-	-	-	-	-	-	-	-
∑	1.8	1.8	1.8	1.9	1.9	1.8	1.8	1.8	1.9	1.9	1.9	1.9
Atomic percentages												
Al	21.4	23.1	20.3	20.1	20.1	23.4	21.7	31.6	22.1	22.9	23.5	20.5
Fe	15.3	14.3	16.5	16.1	16.0	14.2	15.6	5.2	14.1	12.8	12.5	15.2
Ca	63.3	62.7	63.1	63.9	64.0	62.4	62.7	63.2	63.8	64.3	64.0	64.4

*not analyzed

Table G-7 (continued): Electron microprobe analyses of prehnite minerals.
Cation recalculations based on eleven oxygen atoms PFU.

Sample	10CN002 -3-2-2	10CN002 -3-2-3	10CN002 -4-1-1	10CN002 -4-1-2	10CN002 -4-1-3	10CN002 -4-3-1	10CN002 -4-3-2	10CN002 -4-3-3	10CN002 -5-1-1	10CN002 -5-1-2	10CN002 -5-1-3	10CN002 -5-2-10
MgO	0.2	0.1	0.1	0.1	-*	-*	-*	-*	-*	-*	-*	-*
Al_2O_3	20.4	19.7	19.2	18.7	19.1	22.2	20.4	20.8	19.7	19.5	20.3	23.6
SiO_2	46.6	46.7	47.4	47.4	47.0	47.1	46.9	47.3	46.8	47.0	47.2	47.7
CaO	26.2	26.3	25.2	25.1	25.5	26.4	26.1	26.0	26.4	26.1	25.7	25.7
TiO_2	-*	-*	-*	-*	-*	-*	-*	-*	-*	-*	-*	-*
FeO	6.6	7.3	8.0	8.7	8.4	4.4	6.6	5.9	7.2	7.4	6.8	3.0
∑	100.0	100.1	99.9	100.0	100.0	100.1	100.0	100.0	100.1	100.0	100.0	100.0
Si	3.1	3.1	3.1	3.2	3.1	3.1	3.1	3.1	3.1	3.1	3.1	3.1
Al	0.9	0.9	0.9	0.9	0.9	0.9	0.9	0.9	0.9	0.9	0.9	0.9
∑	4.0	4.0	4.0	4.1	4.0	4.0	4.0	4.0	4.0	4.0	4.0	4.0
Al	0.7	0.6	0.6	0.6	0.6	0.8	0.7	0.7	0.7	0.6	0.7	0.9
Fe^{3+}	0.4	0.4	0.4	0.5	0.5	0.2	0.4	0.3	0.4	0.4	0.4	0.2
∑	1.1	1.0	1.0	1.1	1.1	1.0	1.1	1.0	1.1	1.0	1.1	1.1
Ti	-	-	-	-	-	-	-	-	-	-	-	-
Ca	1.9	1.9	1.8	1.8	1.8	1.9	1.9	1.8	1.9	1.9	1.8	1.8
Mg	-	-	-	-	-	-	-	-	-	-	-	-
∑	1.9	1.9	1.8	1.8	1.8	1.9	1.9	1.8	1.9	1.9	1.8	1.8
Atomic percentages												
Al	23.5	22.0	22.3	21.1	21.3	28.1	24.0	25.5	22.1	22.1	24.2	32.2
Fe	12.5	13.8	15.4	16.8	16.1	8.3	12.5	11.2	13.7	14.1	13.0	5.6
Ca	64.0	64.2	62.3	62.1	62.7	63.7	63.5	63.3	64.2	63.8	62.8	62.2

*not analyzed

Table G-7 (continued): Electron microprobe analyses of prehnite minerals.
Cation recalculations based on eleven oxygen atoms PFU.

Sample	10CN002 -5-2-11	10CN002 -5-2-12	10CN002 -5-3-1	10CN002 -5-3-2	10CN002 -5-3-3	10CN002 -5-3-4	10QU006 -1-1-1	10QU006 -1-1-2	10QU006 -1-1-3	10QU006 -1-1-7	10QU006 -1-1-8
MgO	-*	-*	-*	-*	-*	-*	-*	-*	-*	-*	-*
Al_2O_3	23.0	21.8	20.2	19.9	19.9	20.0	21.5	19.0	19.2	19.8	20.6
SiO_2	47.1	47.0	47.1	46.4	46.7	46.6	47.5	46.3	46.6	46.2	46.4
CaO	26.2	25.8	25.8	26.2	26.2	26.3	25.7	26.4	26.1	26.7	26.3
TiO_2	0.4	-*	-*	-*	-*	-*	-*	-*	-*	-*	-*
FeO	3.2	5.5	6.8	7.5	7.1	7.0	5.3	8.4	8.1	7.4	6.8
∑	99.9	100.1	99.9	100.0	99.9	99.9	100.0	100.1	100.0	100.1	100.1
Si	3.1	3.1	3.1	3.1	3.1	3.1	3.1	3.1	3.1	3.1	3.1
Al	0.9	0.9	0.9	0.9	0.9	0.9	0.9	0.9	0.9	0.9	0.9
∑	4.0	4.0	4.0	4.0	4.0	4.0	4.0	4.0	4.0	4.0	4.0
Al	0.9	0.8	0.7	0.6	0.7	0.7	0.8	0.6	0.6	0.6	0.7
Fe^{3+}	0.2	0.3	0.4	0.4	0.4	0.4	0.3	0.5	0.5	0.4	0.4
∑	1.1	1.1	1.1	1.0	1.1	1.1	1.1	1.1	1.1	1.0	1.1
Ti	-	-	-	-	-	-	-	-	-	-	-
Ca	1.8	1.8	1.8	1.9	1.9	1.9	1.8	1.9	1.9	1.9	1.9
Mg	-	-	-	-	-	-	-	-	-	-	-
∑	1.8	1.8	1.8	1.9	1.9	1.9	1.8	1.9	1.9	1.9	1.9
Atomic percentages											
Al	30.1	27.1	24.0	22.0	22.6	22.7	27.4	19.8	20.8	21.4	23.5
Fe	6.1	10.3	13.0	14.3	13.5	13.2	10.1	15.9	15.4	13.9	12.8
Ca	63.8	62.6	63.0	63.7	63.9	64.0	62.5	64.3	63.8	64.7	63.8

*not analyzed

Table G-7 (continued): Electron microprobe analyses of prehnite minerals.
Cation recalculations based on eleven oxygen atoms PFU.

Sample	10QU006 -1-1-9	10QU006 -2-1-1	10QU006 -2-1-2	10QU006 -2-1-3	10QU006 -2-1-4	10QU006 -2-1-5	10QU006 -2-1-6	10QU006 -2-2-1	10QU006 -2-2-2	10QU006 -2-2-3	10QU006 -3-1-4
MgO	-*	-*	-*	-*	-*	-*	-*	-*	-*	-*	-*
Al_2O_3	19.4	20.2	19.1	20.0	21.6	20.1	19.7	20.7	20.7	21.1	20.7
SiO_2	46.2	46.2	46.3	46.6	47.4	46.5	46.3	47.1	46.7	47.3	47.0
CaO	26.5	26.8	26.4	26.0	25.7	26.2	26.6	25.9	26.2	26.0	25.9
TiO_2	-*	-*	-*	-*	-*	-*	-*	-*	-*	-*	-*
FeO	7.9	6.9	8.2	7.4	5.3	7.2	7.5	6.4	6.3	5.7	6.4
∑	100.0	100.1	100.0	100.0	100.0	100.0	100.1	100.1	99.9	100.1	100.0
Si	3.1	3.1	3.1	3.1	3.1	3.1	3.1	3.1	3.1	3.1	3.1
Al	0.9	0.9	0.9	0.9	0.9	0.9	0.9	0.9	0.9	0.9	0.9
∑	4.0	4.0	4.0	4.0	4.0	4.0	4.0	4.0	4.0	4.0	4.0
Al	0.6	0.7	0.6	0.7	0.8	0.7	0.6	0.7	0.7	0.8	0.7
Fe^{3+}	0.4	0.4	0.5	0.4	0.3	0.4	0.4	0.4	0.4	0.3	0.4
∑	1.0	1.1	1.1	1.1	1.1	1.1	1.0	1.1	1.1	1.1	1.1
Ti	-	-	-	-	-	-	-	-	-	-	-
Ca	1.9	1.9	1.9	1.9	1.8	1.9	1.9	1.8	1.9	1.8	1.8
Mg	-	-	-	-	-	-	-	-	-	-	-
∑	1.9	1.9	1.9	1.9	1.8	1.9	1.9	1.8	1.9	1.8	1.8
Atomic percentages											
Al	20.5	22.2	20.1	22.6	27.4	22.7	21.3	24.8	24.4	26.0	24.8
Fe	15.0	13.0	15.5	14.0	10.1	13.6	14.1	12.1	12.0	10.8	12.1
Ca	64.5	64.8	64.3	63.4	62.5	63.7	64.6	63.1	63.7	63.2	63.1

*not analyzed

Table G-7 (continued): Electron microprobe analyses of prehnite minerals.
Cation recalculations based on eleven oxygen atoms PFU.

Sample	10QU006 -3-1-5	10QU006 -3-1-6	10QU006 -5-1-1	10QU006 -5-1-2	10QU006 -5-1-3	10QU006 -5-1-4	10QU006 -5-1-5	10QU006 -5-1-6	10QU006 -6-1-4	10QU006 -6-1-5
MgO	-*	-*	-*	-*	-*	-*	-*	-*	-*	-*
Al_2O_3	21.3	20.8	20.5	19.3	20.9	21.5	19.9	19.1	20.3	19.2
SiO_2	46.7	46.6	46.5	46.2	46.9	46.7	46.5	46.1	46.7	46.7
CaO	26.5	26.3	26.8	26.5	26.0	26.4	26.2	26.5	26.3	25.9
TiO_2	-*	-*	-*	-*	-*	-*	-*	-*	-*	-*
FeO	5.5	6.3	6.2	8.1	6.2	5.4	7.4	8.4	6.8	8.3
∑	100.0	100.0	100.0	100.1	100.0	100.0	100.0	100.1	100.1	100.1
Si	3.1	3.1	3.1	3.1	3.1	3.1	3.1	3.1	3.1	3.1
Al	0.9	0.9	0.9	0.9	0.9	0.9	0.9	0.9	0.9	0.9
∑	4.0	4.0	4.0	4.0	4.0	4.0	4.0	4.0	4.0	4.0
Al	0.8	0.7	0.7	0.6	0.7	0.8	0.7	0.6	0.7	0.6
Fe^{3+}	0.3	0.4	0.3	0.5	0.3	0.3	0.4	0.5	0.4	0.5
∑	1.1	1.1	1.0	1.1	1.0	1.1	1.1	1.1	1.1	1.1
Ti	-	-	-	-	-	-	-	-	-	-
Ca	1.9	1.9	1.9	1.9	1.8	1.9	1.9	1.9	1.9	1.8
Mg	-	-	-	-	-	-	-	-	-	-
∑	1.9	1.9	1.9	1.9	1.8	1.9	1.9	1.9	1.9	1.8
Atomic percentages										
Al	25.6	24.4	23.5	20.3	25.1	25.9	22.1	19.7	23.3	20.9
Fe	10.4	11.9	11.6	15.3	11.7	10.2	14.1	15.9	12.9	15.8
Ca	64.0	63.7	64.9	64.4	63.3	63.9	63.8	64.4	63.8	63.3

*not analyzed

Table G-7 (continued): Electron microprobe analyses of prehnite minerals.
Cation recalculations based on eleven oxygen atoms PFU.

Sample	10QU006 -6-1-6	10QU006 -5-2-3
MgO	-*	-*
Al_2O_3	20.4	22.4
SiO_2	46.7	47.7
CaO	26.4	25.7
TiO_2	-*	-*
FeO	6.5	4.2
∑	100.0	100.0
Si	3.1	3.1
Al	0.9	0.9
∑	4.0	4.0
Al	0.7	0.9
Fe^{3+}	0.4	0.2
∑	1.1	1.1
Ti	-	-
Ca	1.9	1.8
Mg	-	-
∑	1.9	1.8
	Atomic percentages	
Al	23.6	29.7
Fe	12.3	7.9
Ca	64.1	62.4

*not analyzed

APPENDIX H: REE DIAGRAMS BY SAMPLE STATION

Sample stations of the northern fissures include from north to south: Central, Drexel Fissure, Copper Falls Fissure, Phoenix, Cliff Mine, St. Claire Fissure, and Delaware Mine (see Figure H-1). Sample stations of the middle section include from north to south: Baltic #4, Boston #1, Mohawk #6, Mohawk #5, Champion #1, Mohawk #1, Centennial, Houghton Exploration, Isle Royale #1, Osceola #5, Isle Royale #4, Ojibway, Osceola #13, Quincy Mine, Osceola #4, Seneca #1, Laurium Mine, and Trimountain #4 (see Figure H-2). Sample stations for the southern section, from north to south were: Bumblebee, Michigan, Caledonia, Minesota, Lake, Toltec, Mass Consolidated, and Victoria (see Figure H-3).

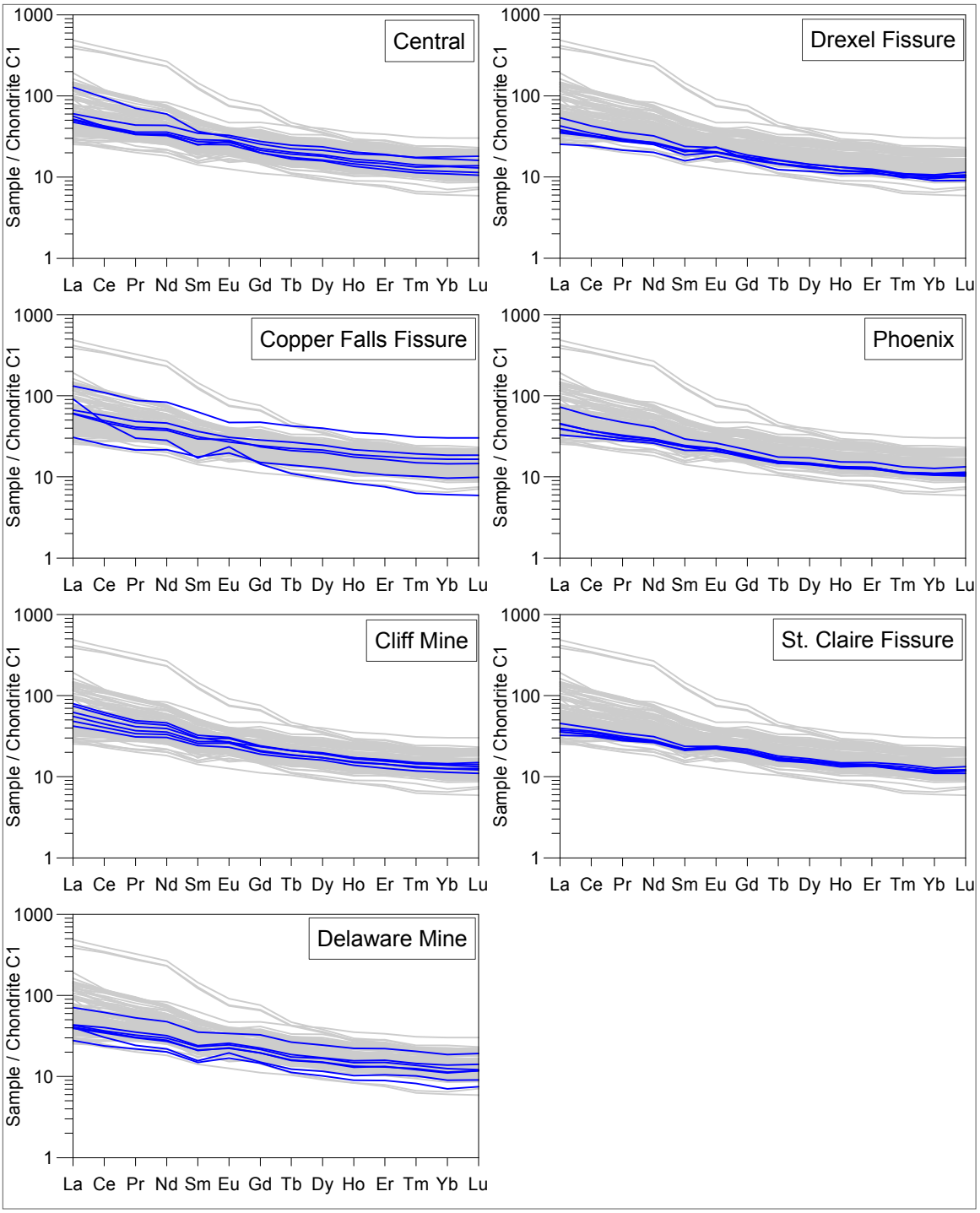

Figure H-1: REE diagrams by station for samples from the northern fissures. Sample stations are listed from north to south.

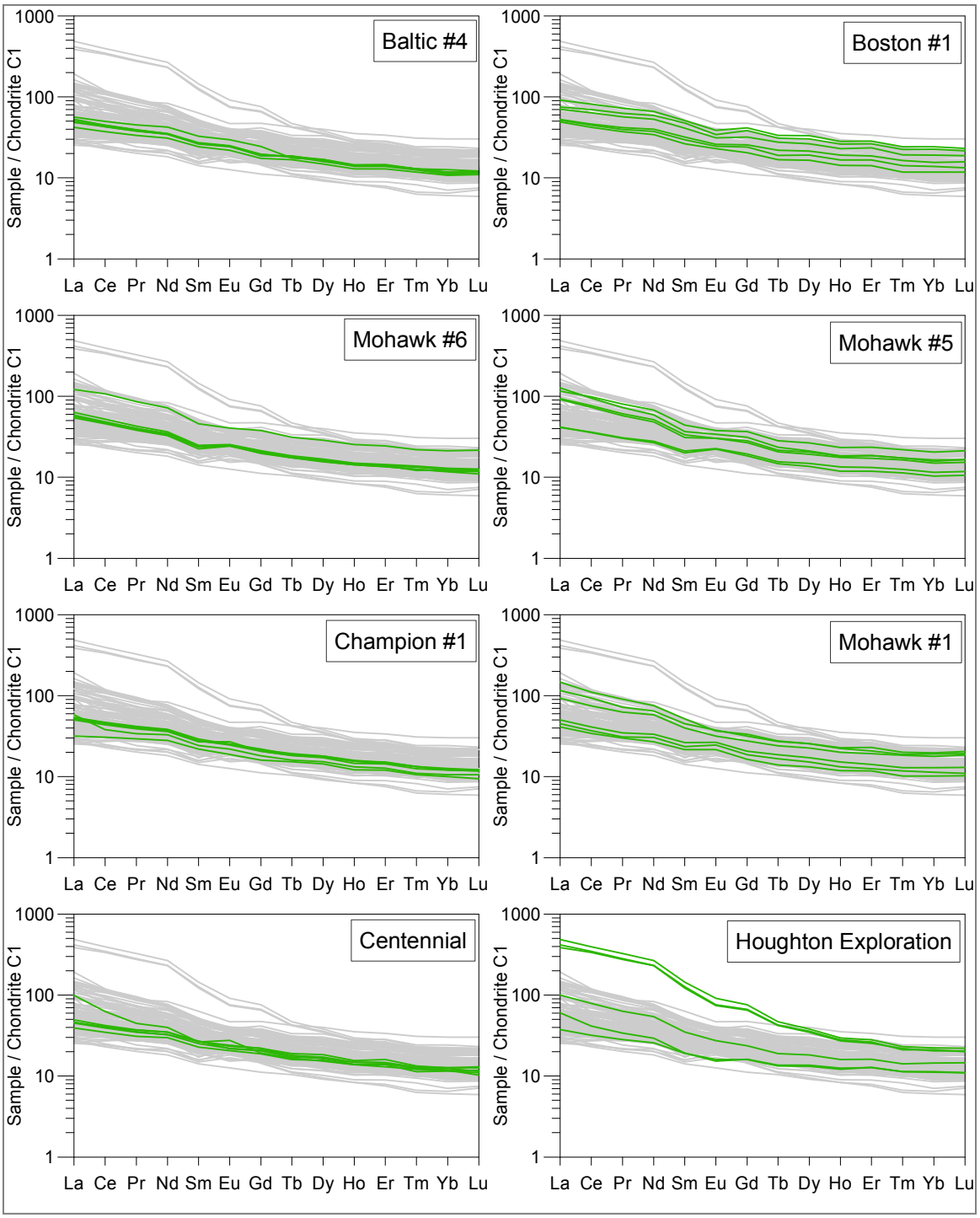

Figure H-2: REE diagrams by station for samples from the middle section. Sample stations are listed from north to south.

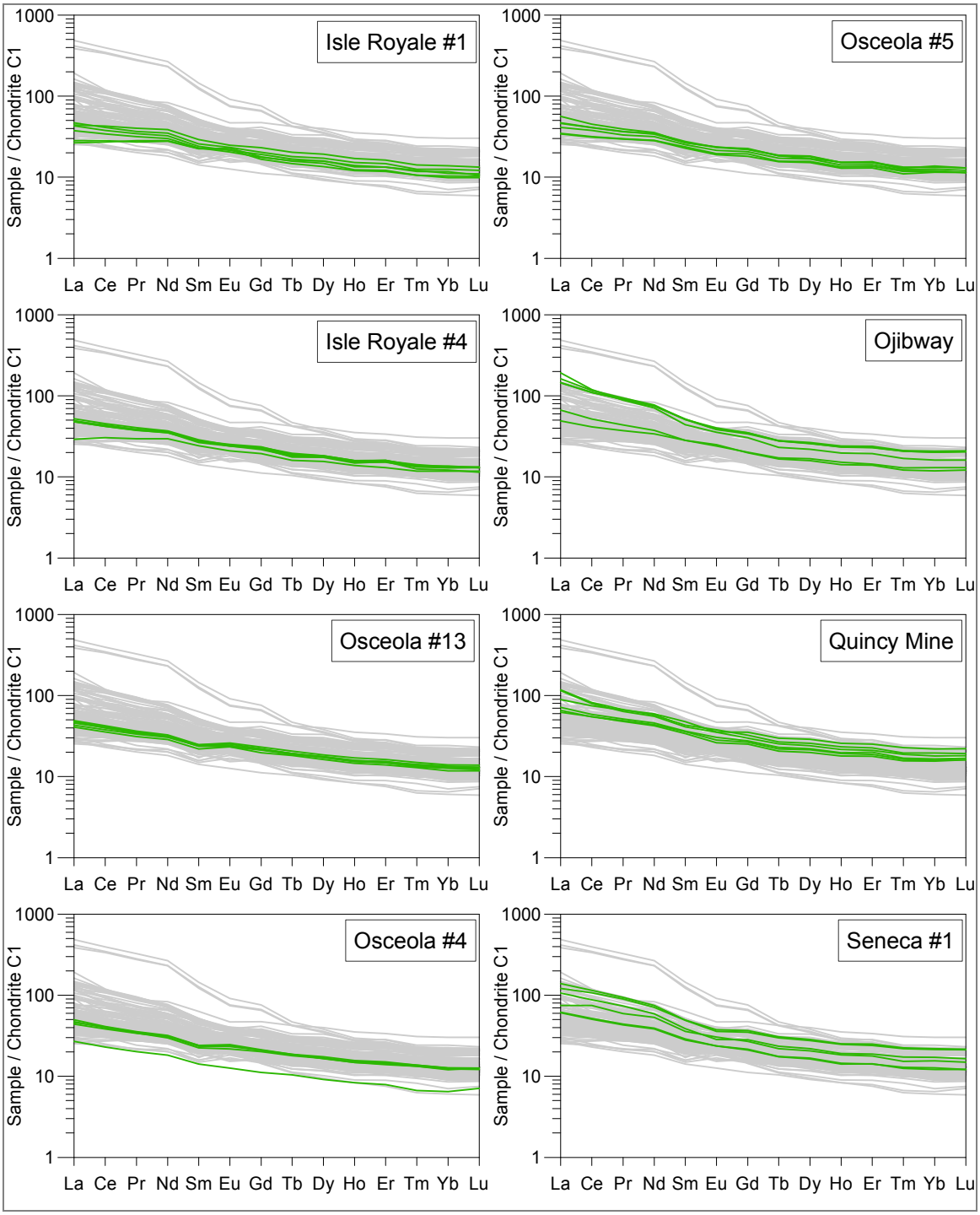

Figure H-2 (continued): REE diagrams by station for samples from the middle section. Sample stations are listed from north to south.

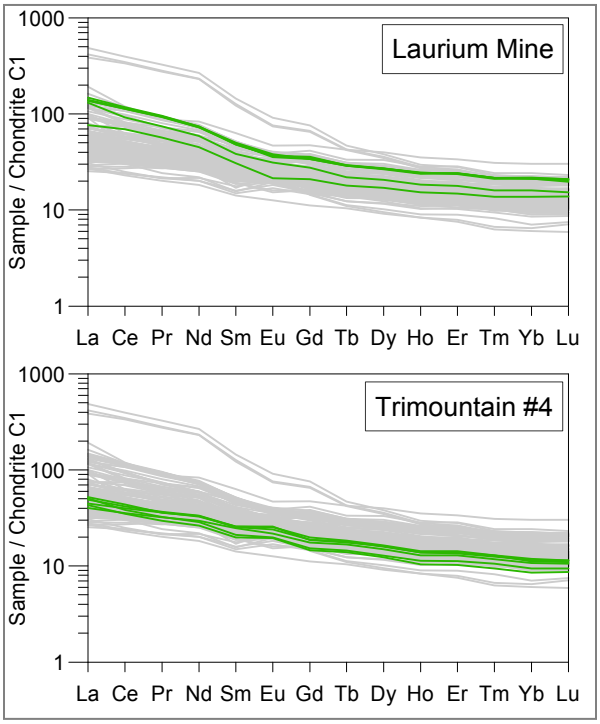

Figure H-2 (continued): REE diagrams by station for samples from the middle section. Sample stations are listed from north to south.

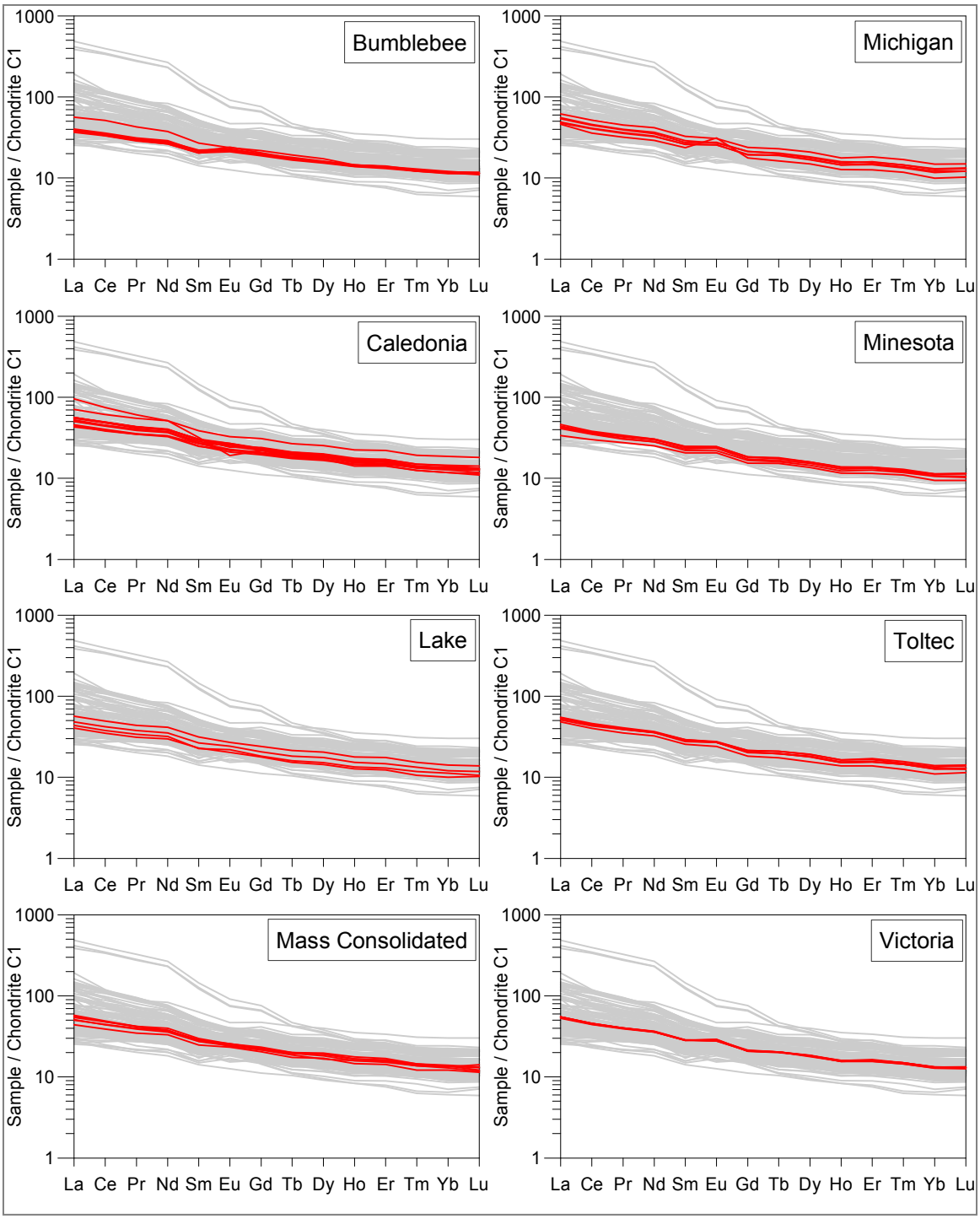

Figure H-3: REE diagrams by station for samples from the southern section. Sample stations are listed from north to south.

APPENDIX I: DATA USED FOR THERMODYNAMIC MODELING

Table I-1: Data used for modeling of forsterite decomposition products.

balanced equation (used for all equations)	$talc + 3\ CO_2 = H_2O + 3\ magnesite + 4\ quartz$
talc	$Mg_3Si_4O_{10}(OH)_2$
magnesite	$MgCO_3$
quartz	SiO_2
polynomial fit for equilibrium constant (K) at varying temperatures (T, in °C)	$\log K = 9.662 - 0.1238\,T + -04051\,T^2 - 8.85x10^{-7}\,T^3 + 8.772x10^{10}\,T^4$
equilibrium equation	$logK = \log a[H_2O] - 3\ \log f[CO_2(g)]$
fugacity of CO_2	$logf[CO_2(g)] = \frac{\log K}{-3}$

Table I-2: Equilibrium constants with temperature for forsterite decomposition products.

T (°C)	log K	T (°C)	log K
0	9.6686	150	-2.3335
25	6.7953	200	-4.5713
60	3.5165	250	-6.3518
100	0.5498	300	-7.7980

Table I-3: Data used for modeling of forsterite.

balanced equation (used for all equations)	$forsterite + 2\ CO_2(g) = 2\ magnesite + \ quartz$
forsterite	Mg_2SiO_4
magnesite	$MgCO_3$
quartz	SiO_2
polynomial fit for equilibrium constant (K) at varying temperatures (T, in °C)	$\log K = 14.37 - 0.1177\ T + -0377\ T^2 - 8.243x10^{-7}\ T^3 + 8.198x10^{10}\ T^4$
equilibrium equation	$logK = \ -2\ \log f[CO_2(g)]$
fugacity of CO_2	$logf[CO_2(g)] = \frac{\log K}{-2}$

Table I-4: Equilibrium constants with temperature for forsterite.

T (°C)	log K	T (°C)	log K
0	14.3739	150	2.8196
25	11.6359	200	0.6088
60	8.4951	250	-1.1741
100	5.6314	300	-2.6425

Table I-5: Data used for modeling of anorthite decomposition products.

balanced equation (used for all equations)	$laumontite + CO_2(g) = 2\,H_2O + calcite + kaolinite + 2\,quartz$
laumontite (zeolite)	$CaAl_2Si_4O_{12}{:}\,4H_2O$
calcite (carbonate)	$CaCO_3$
kaolinite (7A-clay)	$Al_2Si_2O_5(OH)_4$
quartz (silica)	SiO_2
polynomial fit for equilibrium constant (K) at varying temperatures (T, in °C)	$\log K = 6.528 - 0.05812\,T + -01943\,T^2 - 4.145x10^{-7}\,T^3 + 4.058x10^{-10}\,T^4$
equilibrium equation	$logK = 2\log a[H_2O] - \log f[CO_2(g)]$
fugacity of CO_2	$logf[CO_2(g)] = -logK$

Table I-6: Equilibrium constants with temperature for anorthite decomposition products.

T (°C)	log K	T (°C)	log K
0	6.5310	150	0.9866
25	5.1850	200	-45
60	3.6570	250	-0.7477
100	2.2897	300	-1.3295

Table I-7: Data used for modeling of anorthite.

balanced equation (used for all equations)	$anorthite + 2\ H_2O + CO_2(g) = calcite + kaolinite$
anorthite (zeolite)	$CaAl_2Si_2O_8$
calcite (carbonate)	$CaCO_3$
kaolinite (7A-clay)	$Al_2Si_2O_5(OH)_4$
polynomial fit for equilibrium constant (K) at varying temperatures (T, in °C)	$\log K = 12.26 - 0.09271\ T + -02744\ T^2 - 5.754x10^{-7}\ T^3 + 5.589x10^{-10}\ T^4$
equilibrium equation	$logK = -2 \log a[H_2O] - \log f[CO_2(g)]$
fugacity of CO_2	$logf[CO_2(g)] = -\log K$

Table I-8: Equilibrium constants with temperature for anorthite.

T (°C)	log K	T (°C)	log K
0	12.2683	150	2.8708
25	10.1020	200	0.9838
60	7.5735	250	-0.5656
100	5.2238	300	-1.8629

Table I-9: Data used for modeling of diopside.

balanced equation (used for all equations)	$diopside + 2\ CO_2(g) = dolomite + 2\ quartz$
diopside (pyroxene)	$CaMgSi_2O_6$
dolomite (carbonate)	$CaMg(CO_3)_2$
quartz	SiO_2
polynomial fit for equilibrium constant (K) at varying temperatures (T, in °C)	$\log K = 13.39 - 0.1111\ T + -03588\ T^2 - 7.881x10^{-7}T^3 + 7.856x10^{-10}T^4$
equilibrium equation	$logK = -2 \log f[CO_2(g)]$
fugacity of CO_2	$logf[CO_2(g)] = \frac{\log K}{-2}$

Table I-10: Equilibrium constants with temperature for diopside.

T (°C)	log K	T (°C)	log K
0	13.3931	150	2.5260
25	10.8106	200	0.4550
60	7.8546	250	-1.2144
100	5.1633	300	-2.5893

Table I-11: Data used for modeling of enstatite.

balanced equation (used for all equations)	$enstatite + CO_2(g) = magnesite + quartz$
enstatite (pyroxene)	$MgSiO_3$
magnesite (carbonate)	$MgCO_3$
quartz	SiO_2
polynomial fit for equilibrium constant (K) at varying temperatures (T, in °C)	$\log K = 6.522 - 0.05642\,T + -01812\,T^2 - 3.966x10^{-7}T^3 + 3.946x10^{-10}T^4$
equilibrium equation	$logK = -\log f[CO_2(g)]$
fugacity of CO_2	$logf[CO_2(g)] = -\log K$

Table I-12: Equilibrium constants with temperature for enstatite.

T (°C)	log K	T (°C)	log K
0	6.5250	150	0.9964
25	5.2132	200	-0.0586
60	3.7096	250	-0.9085
100	2.3400	300	-1.6078

Table I-13: Data used for modeling of clinochlore decomposition products.

balanced equation (used for all equations)	$saponite - Mg + 3.165\ CO_2(g) = 0.67H_2O + 3.165\ Magnesite + 0.165\ Kaolinite + 3.34\ Quartz$
saponite-Mg (smectite)	$Mg_{3.165}Al_{0.33}Si_{3.67}O_{10}(OH)_2$
magnesite (carbonate)	$MgCO_3$
kaolinite (clay)	$Al_2Si_2O_5(OH)_4$
quartz	SiO_2
polynomial fit for equilibrium constant (K) at varying temperatures (T, in °C)	$\log K = 9.501 - 0.1304\,T + -04228\,T^2 - 9.198x10^{-7}\,T^3 + 9.095x10^{-10}\,T^4$
equilibrium equation	$logK = 0.67 \log a[H_2O] - 3.165 \log f[CO_2(g)]$
fugacity of CO_2	$logf[CO_2(g)] = \frac{\log K}{-3.165}$

Table I-14: Equilibrium constants with temperature for clinochlore decomposition products.

T (°C)	log K	T (°C)	log K
0	9.5073	150	-3.1958
25	6.4778	200	-5.5820
60	3.0162	250	-7.4877
100	-0.1305	300	-9.0411

Table I-15: Data used for modeling of clinochlore.

balanced equation (used for all equations)	$clinochlore14A + 5CO_2(g) = 2H_2O + 5\,magnesite + kaolinite + quartz$
clinochlore-14A (chlorite)	$Mg_5Al_2Si_3O_{10}(OH)_8$
magnesite (carbonate)	$MgCO_3$
kaolinite (clay)	$Al_2Si_2O_5(OH)_4$
quartz	SiO_2
polynomial fit for equilibrium constant (K) at varying temperatures (T, in °C)	$\log K = 19.05 - 0.2241\,T + -07311\,T^2 - 1.605x10^{-6}\,T^3 + 1.599x10^{-9}\,T^4$
equilibrium equation	$logK = 2\log a[H_2O] - 5\log f[CO_2(g)]$
fugacity of CO_2	$logf[CO_2(g)] = \frac{\log K}{-5}$

Table I-16: Equilibrium constants with temperature for clinochlore.

T (°C)	log K	T (°C)	log K
0	19.0655	150	-2.7236
25	13.8610	200	-6.8181
60	7.9172	250	-10.0905
100	2.5290	300	-12.7598

Table I-17: Data used for modeling of ripidolite.

balanced equation (used for all equations)	$ripidolite14A + 3CO_2(g) + 5O_2(g) = 2H_2O + 3\,magnesite + kaolinite + hematite + quartz$
ripidolite-14A (chlorite)	$Fe_2Mg_3Al_2Si_3O_{10}(OH)_8$
magnesite (carbonate)	$MgCO_3$
kaolinite (clay)	$Al_2Si_2O_5(OH)_4$
hematite (oxide)	Fe_2O_3
quartz	SiO_2
polynomial fit for equilibrium constant (K) at varying temperatures (T, in °C)	$\log K = 50.01 - 0.2924\,T + -09467\,T^2 - 2.08x10^{-6}\,T^3 + 2.062x10^{-9}\,T^4$
assumption implicit in equilibrium equation	$fO_2(g) = 10^{-0.699}$
equilibrium equation	$logK = 0.345 + 2\log a[H_2O] - 3\log f[CO_2(g)]$
fugacity of CO_2	$logf[CO_2(g)] = \frac{\log K - 0.345}{-3}$

Table I-18: Equilibrium constants with temperature for ripidolite.

T (°C)	log K	T (°C)	log K
0	50.0287	150	21.4628
25	43.2298	200	16.0281
60	35.4569	250	11.6448
100	28.3867	300	8.0156

Table I-19: Data used for modeling of phengite.

balanced equation (used for all equations)	$phengite + CO_2(g) = magnesite + kspar + quartz + H_2O$
phengite (mica)	$KAlMgSi_4O_{10}(OH)_2$
magnesite (carbonate)	$MgCO_3$
kspar (clay)	$KAlSi_3O_8$
quartz	SiO_2
polynomial fit for equilibrium constant (K) at varying temperatures (T, in °C)	$\log K = 2.427 - 0.03535\,T + -01314\,T^2 - 2.825x10^{-7}\,T^3 + 2.738x10^{-10}\,T^4$
equilibrium equation	$logK = \log a[H_2O] - \log f[CO_2(g)]$
fugacity of CO_2	$logf[CO_2(g)] = -logK$

Table I-20: Equilibrium constants with temperature for phengite.

T (°C)	log K	T (°C)	log K
0	2.4292	150	-0.7354
25	1.6180	200	-1.2123
60	0.7220	250	-1.5417
100	-0.0459	300	-1.7647

Table I-21: Data used for modeling of epidote.

balanced equation (used for all equations)	$epidote + 1.5\ H_2O + 2\ CO_2(g) = 2\ calcite + kaolinite + 0.5\ Hematite + quartz$
epidote (epidote)	$Ca_2FeAl_2Si_3O_{12}OH$
calcite (carbonate)	$CaCO_3$
kaolinite (clay)	$Al_2Si_2O_5(OH)_4$
hematite (oxide)	Fe_2O_3
quartz (silica)	SiO_2
polynomial fit for equilibrium constant (K) at varying temperatures (T, in °C)	$\log K = 13.48 - 0.1184\ T + -03659\ T^2 - 7.888x10^{-7}T^3 + 7.673x10^{-10}T^4$
equilibrium equation	$logK = -1.5 \log a[H_2O] - 2 \log f[CO_2(g)]$
fugacity of CO_2	$logf[CO_2(g)] = \frac{\log K}{-2}$

Table I-22: Equilibrium constants with temperature for epidote.

T (°C)	log K	T (°C)	log K
0	13.4878	150	1.6823
25	10.7281	200	-0.6478
60	7.5382	250	-2.5631
100	4.6015	300	-4.1851

Table I-23: Data used for modeling of prehnite decomposition products.

balanced equation (used for all equations)	$laumontite + CO_2(g) = calcite + kaolinite + 2\ quartz + 2H_2O$
laumontite (zeolite)	$CaAl_2Si_4O_{12}{:}\,4H_2O$
calcite (carbonate)	$CaCO_3$
kaolinite (clay)	$Al_2Si_2O_5(OH)_4$
quartz (silica)	SiO_2
polynomial fit for equilibrium constant (K) at varying temperatures (T, in °C)	$\log K = 6.528 - 0.05812\ T + -01943\ T^2 - 4.145x10^{-7}T^3 + 4.058x10^{-10}T^4$
equilibrium equation	$logK = 2\log a[H_2O] - \log f[CO_2(g)]$
fugacity of CO_2	$logf[CO_2(g)] = -\log K$

Table I-24: Equilibrium constants with temperature for prehnite decomposition products.

T (°C)	log K	T (°C)	log K
0	6.5310	150	0.9866
25	5.1850	200	-45
60	3.6570	250	-0.7477
100	2.2897	300	-1.3295

Table I-25: Data used for modeling of prehnite.

balanced equation (used for all equations)	$prehnite + H_2O + 2\ CO_2(g) = 2\ calcite + kaolinite + quartz$
prehnite (mica)	$Ca_2Al_2Si_3O_{10}(OH)_2$
calcite (carbonate)	$CaCO_3$
kaolinite (clay)	$Al_2Si_2O_5(OH)_4$
quartz (silica)	SiO_2
polynomial fit for equilibrium constant (K) at varying temperatures (T, in °C)	$\log K = 13.38 - 0.1116\ T + -03455\ T^2 - 7.376x10^{-7}T^3 + 7.205x10^{-10}T^4$
equilibrium equation	$logK = -\log a[H_2O] - 2\log f[CO_2(g)]$
fugacity of CO_2	$logf[CO_2(g)] = \frac{\log K}{-2}$

Table I-26: Equilibrium constants with temperature for prehnite.

T (°C)	log K	T (°C)	log K
0	13.3856	150	2.2813
25	10.7847	200	0.1173
60	7.7775	250	-1.6402
100	5.0144	300	-3.0989

APPENDIX J: SUPPRESSING MINERALS IN THERMODYNAMIC MODELING

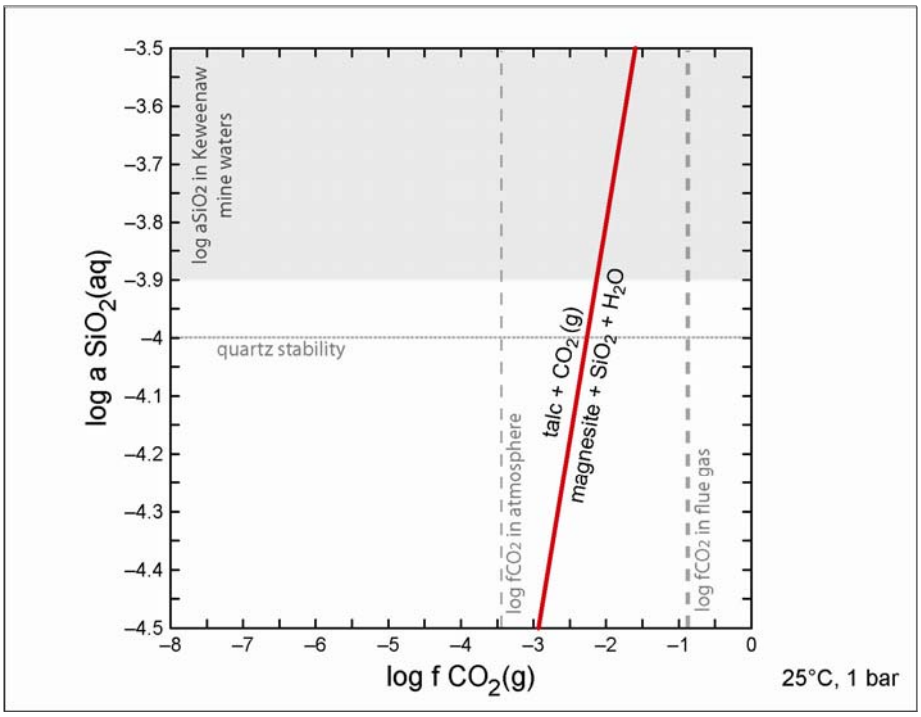

Figure J-1: Stability diagram of forsterite.

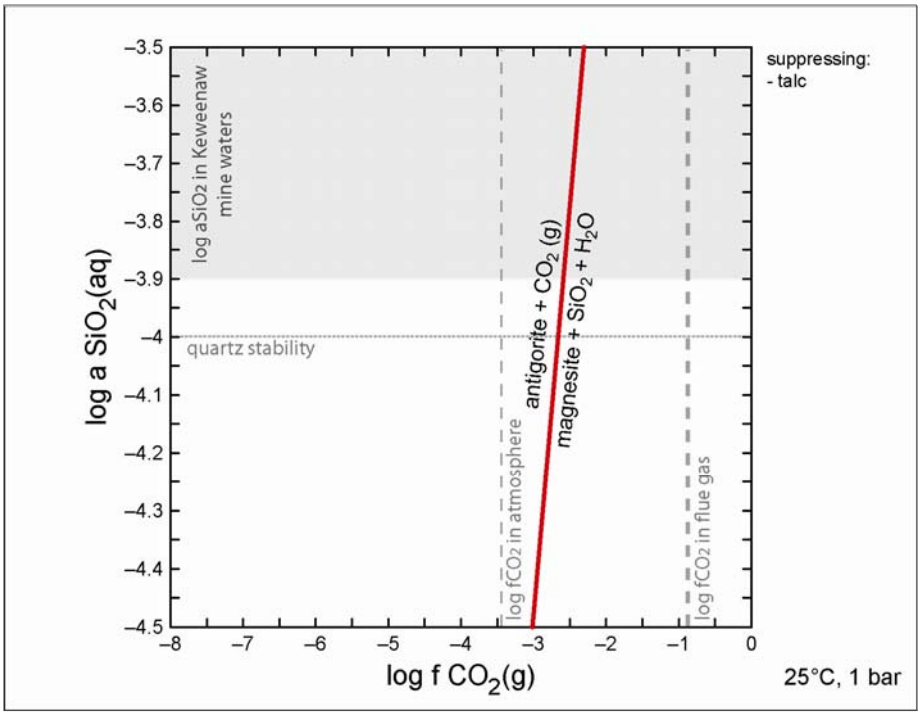

Figure J-2: Stability diagram of forsterite, suppressing one mineral. Mineral suppressed: Talc.

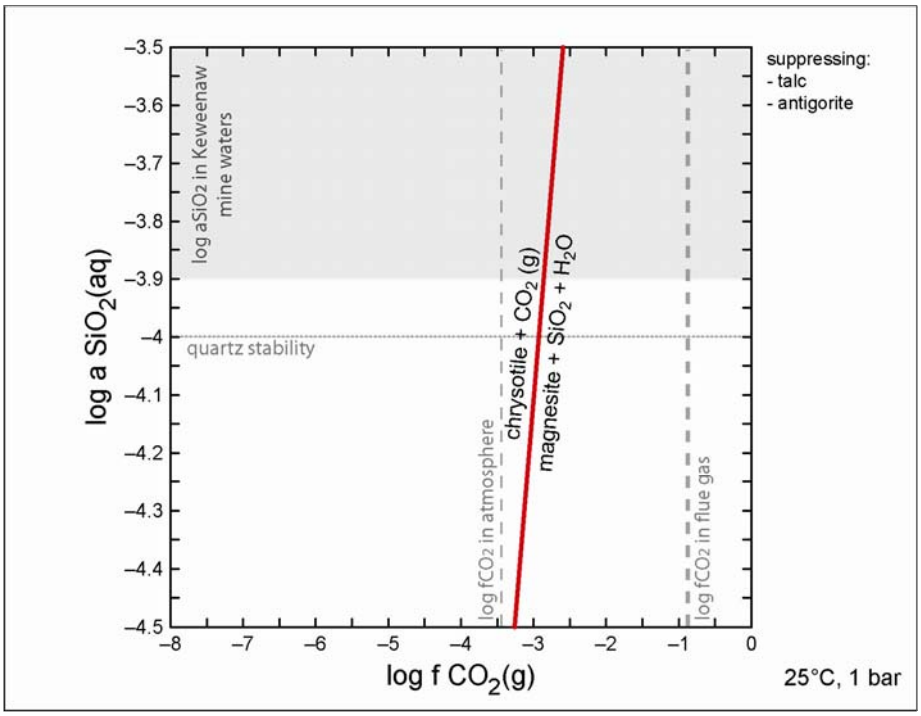

Figure J-3: Stability diagram of forsterite, suppressing two minerals. Minerals suppressed: Talc and antigorite.

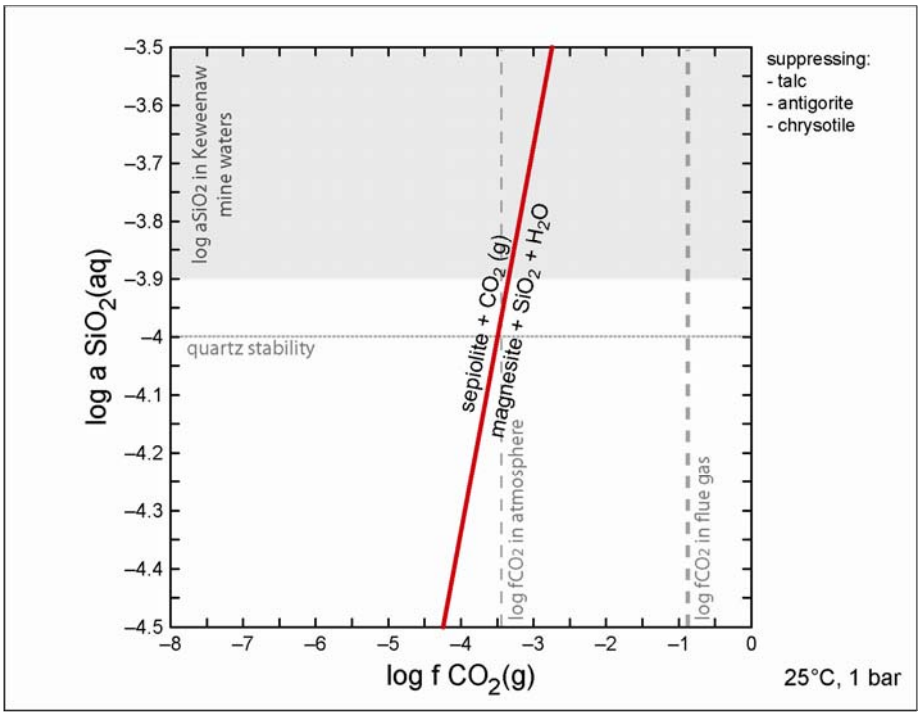

Figure J-4: Stability diagram of forsterite, suppressing three minerals. Minerals suppressed: Talc, antigorite, and chrysotile.

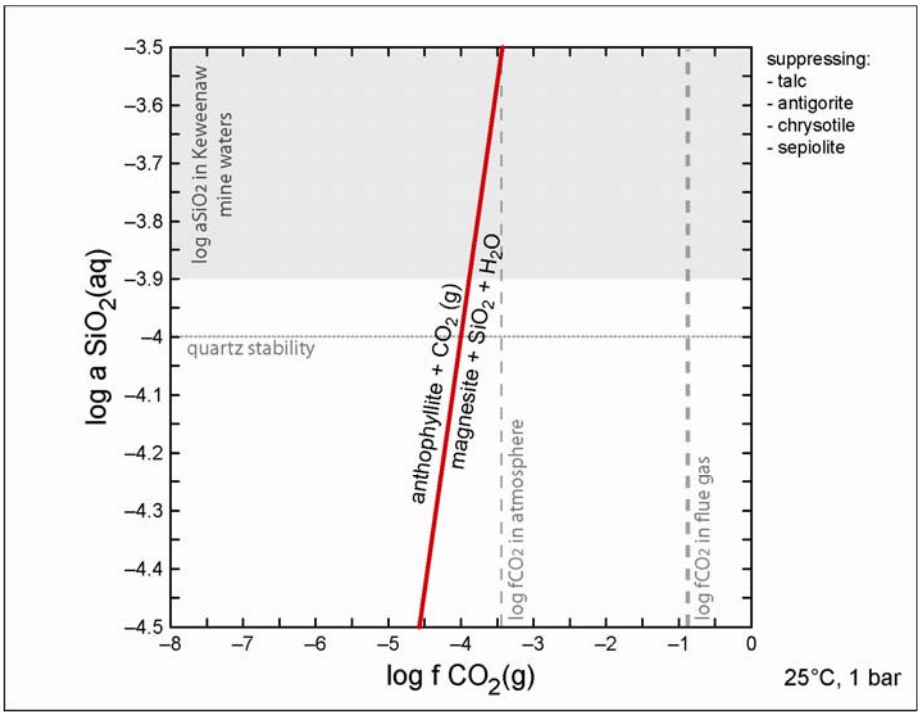

Figure J-5: Stability diagram of forsterite, suppressing four minerals. Minerals suppressed: Talc, antigorite, chrysotile, and sepiolite.

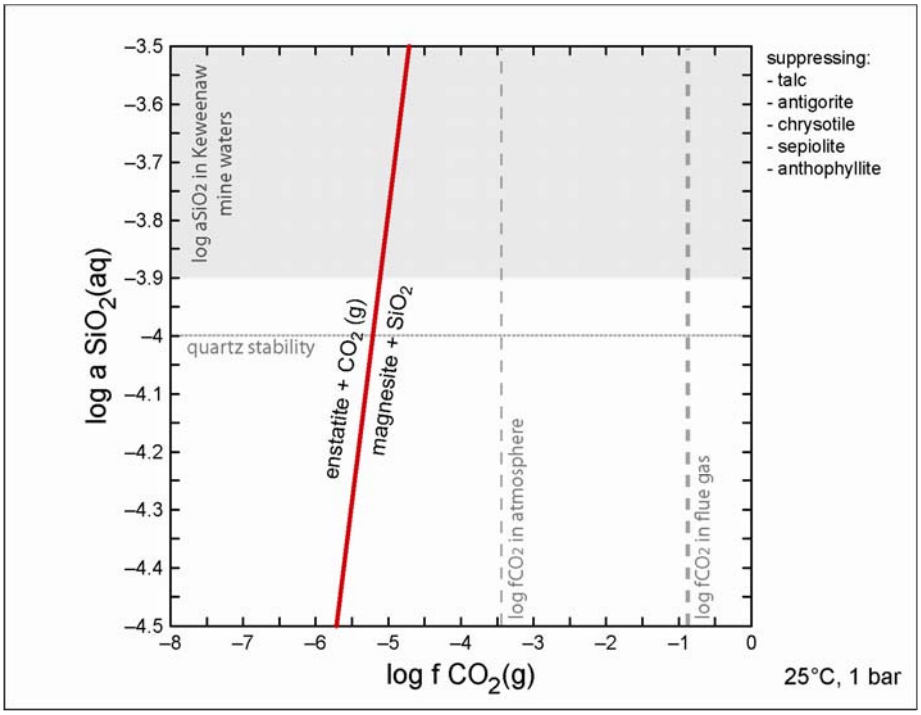

Figure J-6: Stability diagram of forsterite, suppressing five minerals. Minerals suppressed: Talc, antigorite, chrysotile, sepiolite, and anthophyllite.

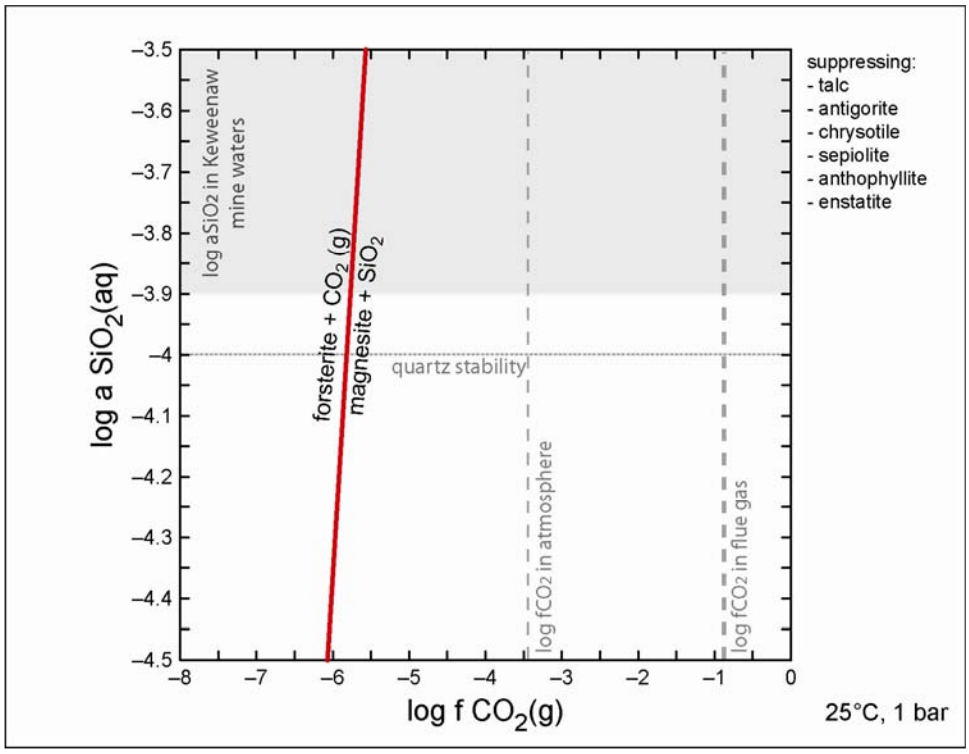

Figure J-7: Stability diagram of forsterite, suppressing six minerals.s.
Minerals suppressed: Talc, antigorite, chrysotile, sepiolite, anthophyllite, and enstatite.

APPENDIX K: REFERENCES USED IN APPENDIX

Armbruster, T., Bonazzi, P., Akasaka, M., Bermanec, V., Chopin, C., Gieré, R., Heuss-Assbichler, S., Liebscher, A., Menchetti, S., Pan, Y., and Pasero, M., 2006, Recommended nomenclature of epidote-group minerals: European Journal of Mineralogy, v. 18, no. 5, p. 551-567.

Blatt, H., Tracy, R.J., and Owens, B.E., 2006, Petrology. Igneous, Sedimentary, and Metamorphic (3rd ed.): New York, W.H. Freeman and Company.

Brooks, C.K., 1976, The Fe_2O_3/FeO ratio of basalt analyses: An appeal for a standardized procedure: Bull. geol. Soc. Denmark, v. 25, p. 117-120.

Deer, W.A., Howie, R.A., and Zussman, J., 1992, An Introduction to the Rock-Forming Minerals (2nd ed.), Pearson - Prentice Hall.

Hey, M.H., 1954, A new review of the chlorites: Journal of the Mineralogical Society, v. 30, no. 224, p. 277-292.

Irvine, T.N., and Barager, W.R.A., 1971, A guide to the chemical classification of the common volcanic rocks: Canadian Journal of Earth Sciences, v. 8, p. 523-548.

Leake, B.E., Wolley, A.R., Arps, C.E.S., Birch, W.D., GIlbert, M.C., Grice, J.D., Hawthorne, F.C., Kato, A., Kisch, H.J., Krivovichev, V.G., Linthout, K., Laird, J., Mandarino, J.A., Maresch, W.V., Nickel, E.H., Rock, N.M.S., Schumacher, J.C., Smith, D.C., Stephenson, N.C.N., Ungaretti, L., Whittaker, E.J.W., and Youzhi, G., 1997, Nomenclature of Amphiboles: Report of the Subcommittee on Amphiboles of the International Mineralogical Association, Commision on New Minerals and Mineral Names: The Canadian Mineralogist, v. 35, p. 219-246.

Morimoto, N., Fabries, J., Ferguson, A.K., Ginzburg, I.V., Ross, M., Seifert, F.A., Zussman, J., Aoki, K., and Gottardi, G., 1988, Nomenclature of pyroxenes: American Mineralogist, v. 73, no. 9-10, p. 1123-1133.

Passaglia, E., and Gottardi, G., 1973, Crystal chemistry and nomenclature of pumpellyites and julgoldites: The Canadian Mineralogist, v. 12, no. 3, p. 219-223.